Major faulting in London: Relating tectonic-scale processes to site-scale engineering geology

A thesis submitted to Imperial College London
in fulfilment of the requirements
for the degree of Doctor of Philosophy

Tom Owen Morgan

Supervised by Professor Richard Ghail, Doctor James Lawrence, and Doctor Philippa Mason

Department of Civil and Environmental Engineering

Imperial College London

London SW7 2AZ

May 2021

Abstract

Critical infrastructure projects in London increasingly encounter unexpected ground conditions caused by major faults in the near surface geology. Their presence challenges the traditional interpretation of minimal faulting, which stems from limited exposure and structural information, and historical misinterpretation. These major faults are now recognised as both a geological unknown and a geotechnical risk since their origins, extents and architectures are poorly constrained.

This research investigates major faults in London to characterise them structurally and determine their engineering geological impact. Direct observations and indirect evidence are coupled to overcome information deficiencies, provide fault analyses, generate geological models, map faults indirectly, and assess fault reactivation and inheritance mechanisms.

This investigation shows that Alpine reactivation of basement Variscan and post-Variscan faults caused propagation into overlying Late Cretaceous-Palaeogene cover through a series of *en échelon* Riedel shears and reversed faults. Fault compartmentalisation offset the ground into blocks and subtly influenced certain sedimentological and ongoing hydrogeological processes. Significant transpressive and transtensive shear zones developed where major faults interacted in the cover through linkage and/or confined block shearing. This research demonstrates that the London Basin is a structurally complex product of Alpine intraplate tectonism. The region is redefined here to reflect the differing Alpine responses of underlying basement domains, with the Variscan Front repositioned northward in light of London's Variscan fault network.

The identified local tectonism and regional partitioning cause lithological, mechanical, and hydrogeological properties to vary at the site-scale. Consequently, major faults inconsistently affect the ground across London to generate often unique local engineering geological impacts. Both a ground investigation workflow and fault zone categorisation criterion are proposed to improve their identification and engineering geology characterisation.

This research has revealed how Alpine-triggered widespread but locally complex fault propagation in London has contributed to subsurface geological complexity to the detriment of ground conditions.

Originality Declaration

This thesis comprises work that is my own except where due referencing and acknowledgement is made.

May 2021

Copyright declaration

Acknowledgements

This research was not produced in isolation and could not have been achieved without the help and support of many individuals. The investigation was not straightforward, and both it and I faced challenges along the way. I would like to take this opportunity to acknowledge the people who helped.

Firstly, I would like to thank my supervisors Prof Richard Ghail, Dr James Lawrence, and Dr Philippa Mason. Their belief, guidance and open-door attitude helped me throughout this. They encouraged my inquisitive nature and moulded my raw enthusiasm into a passion for research. I am so grateful.

I would like to thank members of the geotechnics section and the engineering geology scale research group at Imperial College London, who took the time to listen and discuss, especially Dr Jamie Standing and Dr JP Latham. I am grateful to have had the opportunity to work with and learn from Prof John Cosgrove and Dr Michael de Freitas; your help has been invaluable. Additionally, I would like to recognise both the historical and recent contributions to London geological research, I truly did stand on the shoulders of giants.

Much of the research could not have been achieved without support from both industry and certain leading members for their insights, discussions, and data. I would like to thank Dr Jackie Skipper and John Davis of GCG, Dr Tim Newman and Dr Neill Hadlow of Jacobs, Dr Ursula Lawrence of Capita, Mike Black of Transport for London, and Dr Jon Ford, Dr Don Aldiss, and Dr Richard Ellison of the BGS. I am grateful to the BGS, UKOGL, Thames Tideway, Crossrail, Silvertown Tunnel (TfL), and Thames Water for sharing data.

My research was generously funded at Imperial by EPSRC and the Skempton Scholarship, as part of the CDT in Sustainable Civil Engineering. I would like to thank Prof Chris Cheeseman for the CDT opportunity, and Sue Feller and Sarah Willis for administrative support throughout.

I would like to acknowledge PhD colleagues in my research group who provided open ears, put up with my nonsense and kept me sane with laughter; I will miss you all dearly. Especially, I would like to thank Stewart Agar for our many evenings solving engineering geology overs beers in the Beit, Justyna Edgar for her patience and encyclopaedic knowledge of London's lithologies, and Jenny Turner for listening when I needed to chat.

Finally, I would like to thank my family, Kate, Glynne and George, and my faith in God, for being there for me throughout this. This never could have happened without your love and support.

Table of contents

List of figures

List of tables

List of publications

MORGAN, T. O., GHAIL, R. G. & LAWRENCE, J. A. 2020. Major faulting in London: Evidence for inherited basement faults in the London Basin. *Quarterly Journal of Engineering Geology and Hydrogeology*. https://doi.org/10.1144/qjegh2018-193

SCOULAR, J., GHAIL, R., MASON, P., LAWRENCE, J., BELLHOUSE, M., HOLLEY, R. & **MORGAN**, T. 2020. Retrospective InSAR Analysis of East London during the Construction of the Lee Tunnel. *Remote Sensing*, 12, 849. https://doi.org/10.3390/rs12050849

COSGROVE, J. W., **MORGAN**, T.O., & GHAIL, R.C. 2021 The deformation history of southern England, and its implications for ground engineering in the London Basin. *Quarterly Journal of Engineering Geology and Hydrogeology*. https://doi.org/10.1144/qjegh2020-144

List of abbreviations

ABM	Anglo-Brabant Massif
BGS	British Geological Survey
DFH	Drift-filled hollow
GI	Ground Investigation
InSAR	Interferometric Synthetic Aperture Radar
OD	Ordnance Datum
NBF	Northern Boundary Fault
RHZ	Rhenohercynian Zone
SLF	Sticklepath-Lustleigh Fault
TBM	Tunnel Boring Machine
UCG	Unexpected Ground Conditions
WSG-Faults	Wimbledon-Streatham-Greenwich Faults

1. Introduction

London's near surface geology has long been viewed as a tectonically simple, undeformed 'layer cake' of Late Cretaceous-Palaeogene stratigraphy situated within the southern London Basin (e.g., Sumbler, 1996). However, there is growing consensus that it is more complex than recognised (Royse et al., 2012). Certain lithologies display extreme heterogeneity internally (Skipper and Edgar, 2020, Page and Skipper, 2000), and more generally, strata coverage and thicknesses are irregular (Mortimore et al., 2011, Ellison et al., 2004). Periglaciation has overprinted these with at-surface weathering (Culshaw et al., 2017) and the development of drift-filled hollows that can penetrate >60 m into the bedrock (Toms et al., 2016, Banks et al., 2015). Significant faulting (attributed to basement structures (Ellison et al., 2004)) is more widespread than mapped (Aldiss, 2013), has affected Late Cretaceous to Quaternary strata (Ghail et al., 2015a, Mortimore et al., 2011) and can be very complex locally (Newman, 2008, Carter and Hart, 1977).

These features are all detrimental to geotechnical engineering (Everett and Dewar, 2015) by introducing problematic ground conditions that deviate the geology and hydrogeology on-site from expected behaviours. To overcome this, the features require geological analysis to identify their engineering geological characteristics and reduce their geotechnical risks, as has been achieved for the complex lithologies (Edgar, 2021, Skipper, 2000) and periglacial features (Flynn, 2021).

Comparatively, major faults in London are poorly constrained and have caused problems for recent critical infrastructure projects (Bischoff et al., 2020b, Newman et al., 2016). At present their coverage, formation mechanisms, and direct and indirect alteration of near surface rockmasses in London are broadly unknown (Aldiss, 2013, de Freitas, 2009). Characterising major faults is critical to determining how they affect local ground conditions, and how to identify and mitigate them. This will become progressively more important as London's subsurface accommodates an ever-increasing proportion of its infrastructure and built environment to alleviate at-surface demands.

This investigation focuses on the geological characterisation of major faulting in London.

Defining 'major faulting'

Faulting occurs at multiple scales in London and is categorised into two groups for this investigation:

- Major faulting – Laterally extensive 'mappable' faults with metre-decimetre throws.
- Minor faulting – Short-lived metre-scale faults with <2 m throws.

1.1 Aims & Objectives

This research aims to analyse major faulting in London's subsurface to improve geological understanding and identify potential geotechnical problems. In doing so, this investigation asks the question: how do tectonic-scale processes affect site-scale engineering behaviour?

Three research objectives were outlined:

1. Origins and structure – How did major faults form and what are their internal architectures? How does this reflect the wider tectonic framework acting on the London Basin?
2. Location – Where are major faults in London and how can we improve their identification?
3. Geological and geotechnical impact – How have major faults influenced geological and hydrogeological processes in London? How does this affect local engineering geology?

By addressing these objectives, major faulting and its influence on subsurface geology were characterised and provide a basis for how faulting can cause problematic ground conditions in London. Recognition of these features can potentially minimise associated geotechnical uncertainty and risks for future engineering projects. Furthermore, the research outputs have implications for our tectonic understanding of London region.

1.2 Investigation Structure

A conventional structural geological investigation cannot be undertaken in detail in London because extensive urbanisation and superficial coverage prevent at-surface characterisation of faulting from mapping and exposure analysis. Similarly, sparse deep borehole coverage and minimal seismic data prevent analysis of basement-cover structural relationships. Furthermore, structural information for individual faults is consistently incomplete and they are often interpreted from only isolated exposures or during engineering investigations. Consequently, London's structural record is both incomplete and inconsistent.

To overcome this information deficiency, the investigation has collated multiple lines of direct and indirect evidence to develop structural interpretations. Fault observations in London are coupled with structural characterisation, a geological modelling programme, a novel fault mapping method, kinematic studies of basement fault reactivation, and inheritance evidence analyses. The investigation workflow is presented in figure 1.1, which links them with the research objectives in §1.1.

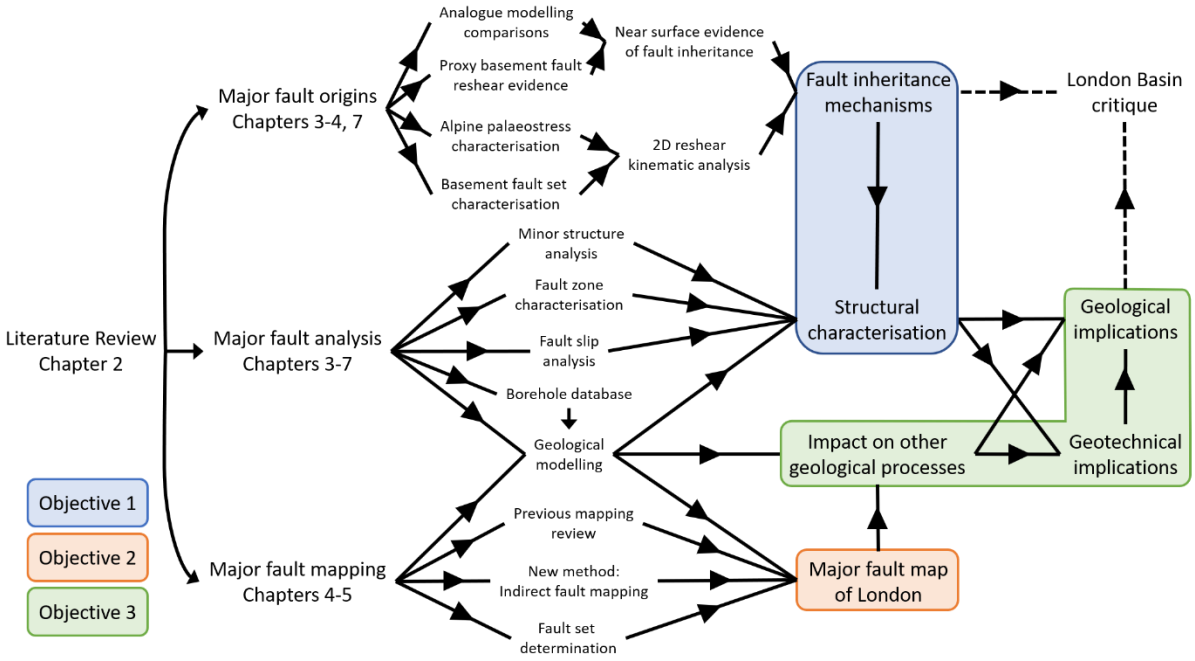

Figure 1.1 – Investigation workflow, outlining the analytical methods used to characterise London's major faults.

This thesis is structured into eight chapters. This first chapter introduces the motivations for this research, and the aims and objectives it seeks to address.

Chapter 2 presents the main literature review that addresses the geological and tectonic history of southeast England, and the geology of London.

Chapter 3 assesses the validity of a basement origin for major faults by kinematically analysing their Alpine reshear feasibility, and by comparing near surface faults with known propagation mechanisms.

Chapter 4 reviews the methodologies and limitations of previous fault mapping in London and develops a new technique that couples InSAR with subsurface topographic variation. It also interprets the major fault sets in London and outlines issues of strike-slip fault mapping.

Chapter 5 presents the East London geological modelling programme that characterises its subsurface and evaluates mapped faults. This includes the data acquisition and explicit-driven modelling methodologies, results, analysis, and method reviews.

Chapter 6 assesses the role of major faulting in compartmentalising geological processes and characterises complex shear zones (colloquially termed 'fault zones') produced by their interactions.

Chapter 7 discusses the implications of major faulting at various scales, from our regional tectonic understanding to how they affect site-scale engineering geology conducted near them, thereby addressing the overarching research question.

Finally, Chapter 8 concludes the thesis and the outcomes of this investigation.

1.3 Existing evidence for major faulting in London

London was historically perceived to be tectonically simplistic and dominated by minor faulting and very gentle folding. Significant structures were considered to be isolated occurrences, rather than widespread. This perspective stems partly from the challenges outlined in §1.2 (limited structural characterisation and information availability), and preconceived attitudes towards faulting in London.

These perceptions started changing in recent decades as major faults became increasingly identified by tunnelling and ground engineering projects. This has formed part of a larger transition to recognising that London's geology is complex (Royse et al., 2012), as the need to characterise the ground for civil engineering has progressively increased. Major faults are now considered to be under-represented in London and not absent (Aldiss, 2013).

The evidence base for major faulting in London and its geological implications are outlined below:

- Broader coverage of major faults is evidenced from regional and local variations in subsurface topography, linear features identified from river morphologies and InSAR displacement, and widespread interception of fault zones across London. Recurringly consistent lineament trend descriptions imply the presence of three sets.
- Greater structural complexity is evident from known major faults comprising multiple shears instead of individual shears. Both dip-slip and strike-slip dominant behaviour is documented for major faults and fault zones from high-quality ground investigations, shallow seismics and fieldwork. Similarly, structural behaviour appears to be regionalised into distinct domains.
- Regionalised processes, including present-day aquifer behaviour and at-surface displacement, and Late Cretaceous-Palaeogene sedimentological behaviour, have each been partly attributed to partitioning by faulting.
- Correspondence of near surface structures and/or inliers with basement structures and/or lineaments from geophysical analysis, deep borehole analysis and seismic profiles.

It is evident that we should expect major faults in London and more complex geology around them. But the existing knowledge base for analysing them is limited and requires pursuing multiple investigative avenues (fig. 1.1). The majority of information was publicly available and sourced from geological memoirs, academic literature, and online databases (BGS Geoindex and the UKOGL). Several private sources were also kindly made available and are outlined in Appendix A.

The research structure (§1.2) enabled interpretations to be progressively constructed and applied as the investigation developed. By determining major fault origins, their coverage and relationship to subsurface geology, causal links and structural mechanisms in the near surface could be characterised.

2. Literature Review

London is situated within the southern portion of the London Basin syncline, a product of Alpine compression that sits above the margin of an inverted Mesozoic basin and a stable Palaeozoic block. This literature review contextualises London's geology with regards to regional tectonism.

The first part (§2.1) reviews the regional geological history of southern Britain for two purposes. Firstly, to construct a representative tectonic framework for the southern London Basin and its underlying basement (§2.1.1). Pre-Alpine tectonic events were analysed to determine key structural domains in the basement and any fault sets underlying London. This is followed by a more focused analysis of Late Cretaceous-onwards tectonism, sea level changes and sedimentological processes specific to the development of the London Basin. Secondly, to characterise the evolution of the Alpine Orogeny and its broader interplay with epeirogenic and sea level processes in Southern Britain. From this, stress field axes and magnitudes of its phased compression are determined and related to the development of the southern London Basin (§2.1.2).

The second part (§2.2) reviews and describes the geology and structures present in London's near surface. It focusses solely on bedrock geology, and not superficial deposits or periglacial processes. Near-surface Late Cretaceous-Palaeogene lithologies are described (§2.2.1) to provide a basis for later analyses in the investigation. London's structural geological features are analysed (§2.2.2) to determine their relative scales, prevalence, and complexity; with the changing structural interpretation of region also reviewed. Finally, the debated origins of major faulting are discussed together with the limitations affecting their interpretation (§2.2.3).

2.1 Regional geological history: Palaeozoic to present

The regional tectonic evolution of southern Britain from the Palaeozoic to present is reviewed. Prior to the Cretaceous, this focuses on key tectonic events that may have generated the basement structures that are speculated to have influenced Alpine deformation in London. From the Cretaceous onwards, the geological processes specific to the London Platform and subsequent London Basin are also detailed.

The geological history begins with the Avalonian microcontinent since its internal crustal distinctions have regionalised tectonic behaviour in southern Britain since the Lower Palaeozoic (Pharaoh, 2018). This is important as the southern London Basin is situated above one of these crustal interfaces.

2.1.0.1 Pre-Variscan: Crustal accretion and terrane development

Southern Britain sits on the Avalonia microcontinent, a terrane assemblage of Neoproterozoic volcanic arcs and sedimentary basins (Pharaoh, 1999, Servais and Sintubin, 2009). During the Lower Palaeozoic, Avalonia migrated northwards as it progressively subducted the Iapetus Ocean (Woodcock, 2000b), with two 'core' terranes (the Charnwood & Fenland Terranes) of Avalonia remaining a shallow marine platform that accumulated Cambrian-to-Late Silurian sediments (Woodcock, 1991, Soper and Woodcock, 1990). Collision and crustal suturing during the Caledonian Orogeny (Woodcock, 2000a) caused distinct tectonic responses between the terranes. The Charnwood Terrane behaved as a "*rigid indenter*" becoming the Midland Microcraton (Soper et al., 1987), whilst the Fenland Terrane's cover (East Anglia) deformed as the concealed Eastern England Caledonides (fig. 2.1, Pharaoh et al., 1987). Terrane behaviour south of this core region (defined here as the 'Southern Province') is unclear due to its later Devonian coverage, Variscan tectonism and Mesozoic burial.

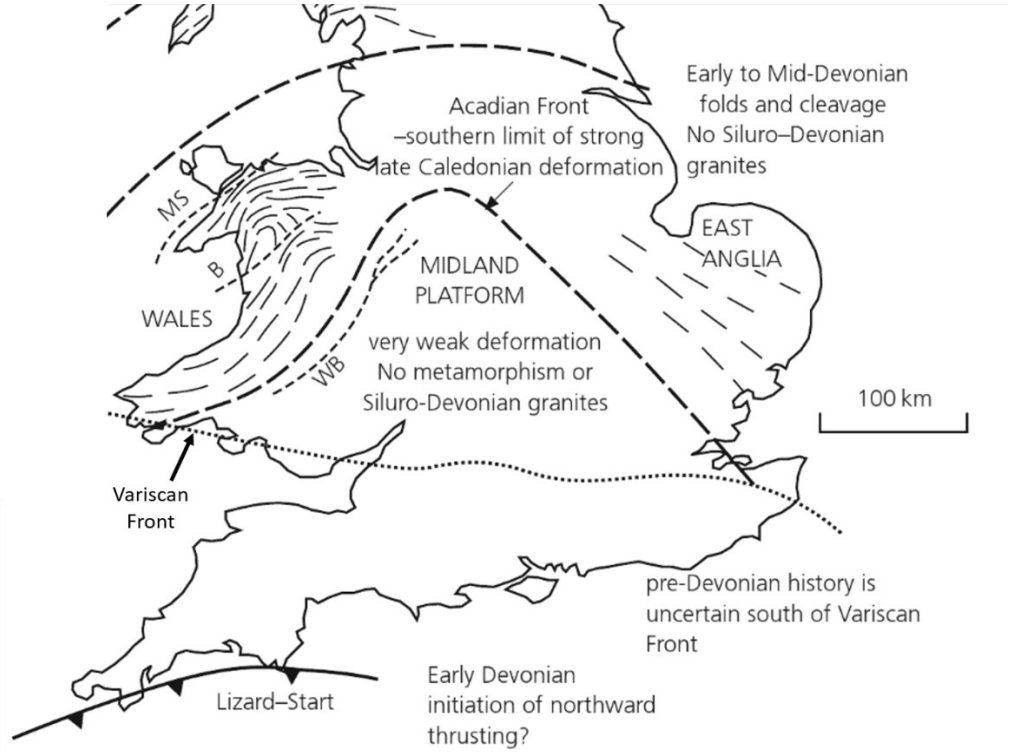

Figure 2.1 – Caledonian deformation of the Eastern Avalonian terranes in southern Britain. This tectonic framework (Pharaoh et al., 1987) is inferred primarily from geophysical lineaments (Lee et al., 1991) and analysis of borehole samples (Bullard et al., 1940, fig. 22, Merriman et al., 1993) beneath East Anglia and the east Midlands, with the terrane boundary originating from (Turner, 1949). The Charnwood and Fenland Terranes equate to the English portion of the Midland Platform and East Anglia, respectively. Modified from Woodcock and Strachan (2000a).

The two core Avalonian terranes maintained their tectonic stability following the Caledonian Orogeny. These have remained as a relatively high-standing, competent block since the Upper Palaeozoic and are collectively referred to as the Anglo-Brabant Massif (ABM) (fig. 2.2).

Caledonian compression waned by the Mid-Devonian. The ABM remained an exposed landmass throughout the Late Palaeozoic (fig. 2.2) with Mid-to-Late Devonian alluvial-shallow marine deposition along its southern and north flanks (Pharaoh, 2018, Lee et al., 2015, Butler, 1981, Chroston and Sola, 1975, Bullard et al., 1940). Comparatively, the Southern Province was uplifted in the Early Devonian by the Armorican collision[1] before undergoing extension and basin development from the Mid-Devonian to Upper Carboniferous (Woodcock and Strachan, 2000b).

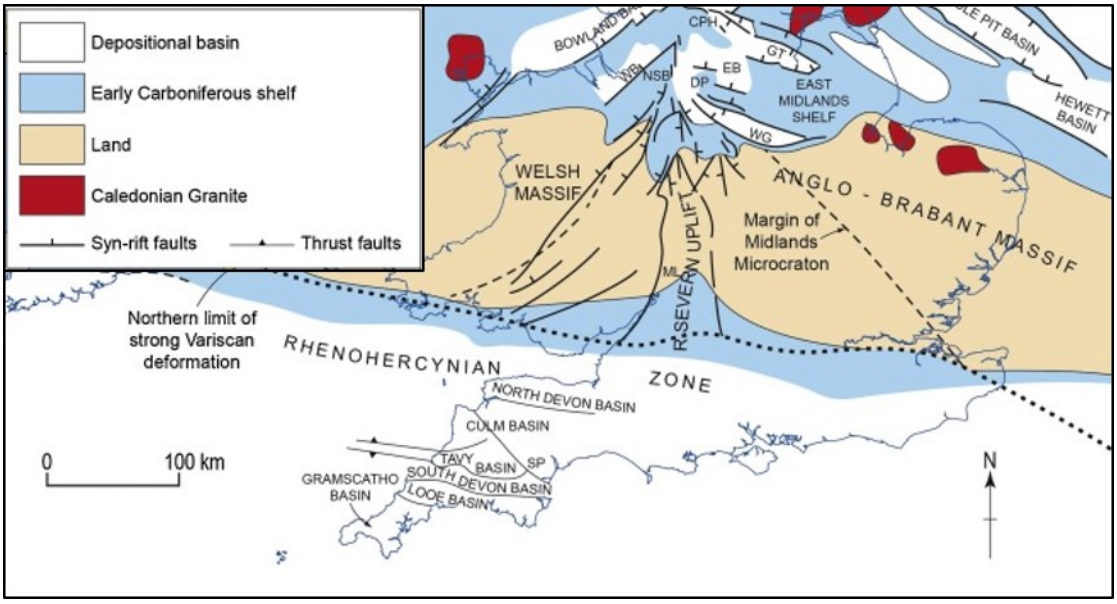

Figure 2.2 – Terrane behaviour during the Early Carboniferous. The Anglo-Brabant Massif (ABM) remained a tectonically stable exposed landmass unaffected by post-Caledonian extension, whilst the 'Southern Province' underwent basin development. Modified from Pharaoh (2018).

[1] An early phase of the Variscan Orogeny (prior to Gondwanan collision).

2.1.0.2 Variscan Orogeny: Heterogenous inversion of southern Britain

The Variscan Orogeny affected southern Britain from the Upper Carboniferous to earliest Permian, with Avalonia situated along the collision front between Laurussia and Gondwana (Warr, 2000).

The Southern Province was transpressively deformed between the rigid ABM and Armorican terranes, and tectonically altered into Rhenohercynian Zone (RHZ) to form part of the Variscan foreland. Thin-skinned thrusting developed a series of imbricated sheets in southern England (Coward and Smallwood, 1984, Lefort and Max, 1992) that thrusted onto the southern margin of the ABM (fig. 2.3) (Busby and Smith, 2001, Taylor, 1986). These sheets are internally characterised by thrust-fold deformation, and (predominantly dextral) strike-slip conjugate pairs (Woodcock et al., 2014, Royse et al., 2012). These fault sets strike East-West, NW (dextral) and NE-NNE (sinistral) respectively and are widespread under the southern England basins (fig. 2.4). Whilst thrusts accommodated shortening between sheets, strike-slip faults are present at varying scales, with several dextral strike-slip faults acting as major full-crustal shears causing extensive >100 km-scale displacement within the wider RHZ[2] (e.g. the Bristol-Bray Fault, Holder and Leveridge, 1986).

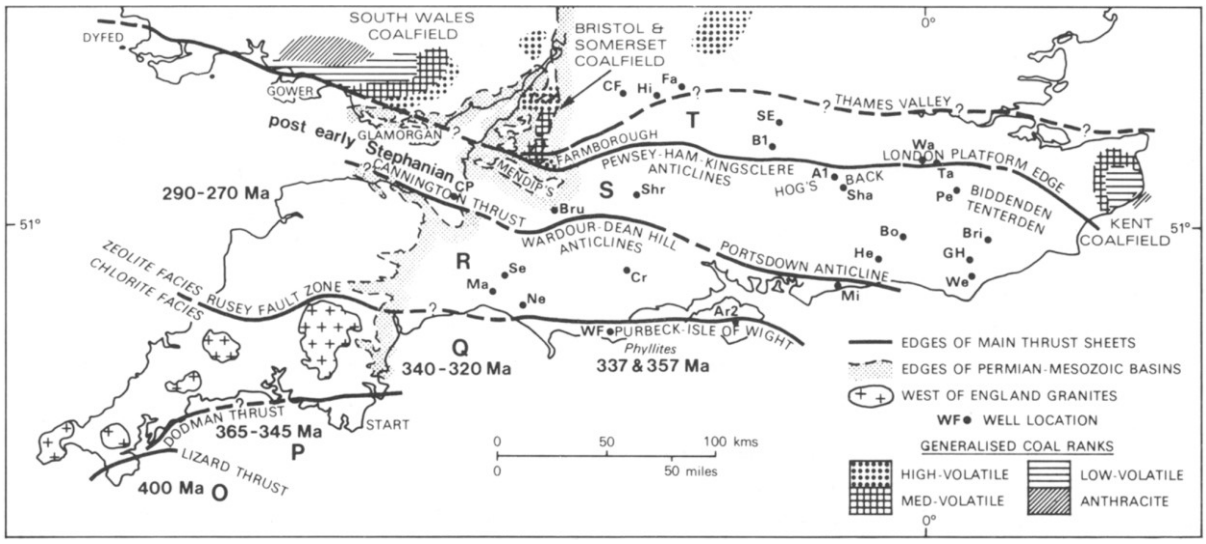

Figure 2.3 – Variscan thrust sheet boundaries on the Palaeozoic basement floor as inferred from topographic lineaments, regional geophysical and borehole analysis. Currently the 'London Platform Edge' sheet is interpreted to be the Variscan Front (VF), however, the Taylor (1986) postulated that a northward thrust sheet may exist also ('Thames Valley'). Sourced from Taylor (1986).

[2] Structures and stratigraphy between German, Belgian and Cornish Variscides are comparable, implying former continuity prior to major dextral full-crustal displacement along the Bristol Channel-Bray Fault.

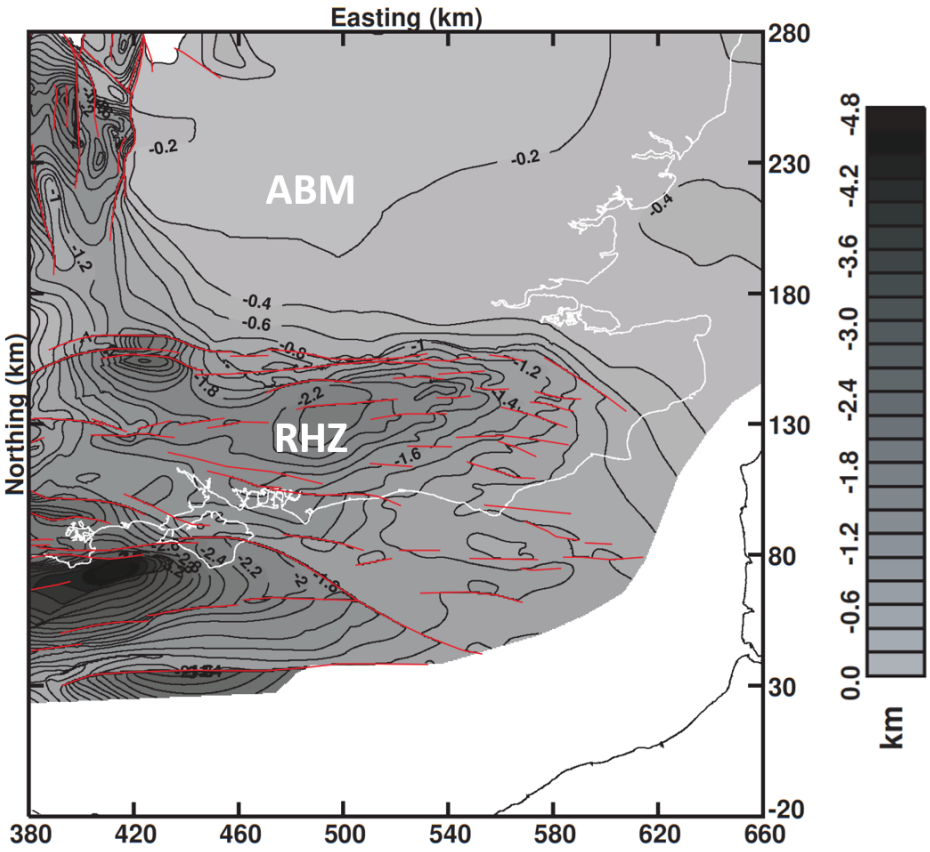

Figure 2.4 – Differential Variscan deformation of the ABM and RHZ terranes is apparent from structural and topographic distinctions in pre-Permian Palaeozoic basement floor underlying southeast England. Variscan thrusts and strike-slip faults are shown as red lines and were inferred from regional geophysical assessment, potential field, and structural contour analysis. Adapted from Busby & Smith (2001).

The Variscan Front (VF) marks the northernmost extent of direct Variscan tectonism in southern Britain; north of it compressive stresses were accommodated by pre-existing structures[3] (Warr, 2000, Chadwick et al., 1993). Shackleton (1984) defined the VF as "*the present northern limit of the* [Variscan] *décollement*" to reflect this and linked it directly with the northernmost thrust sheet that imbricated onto the southern margin of the ABM (Lefort and Max, 1992, Busby and Smith, 2001). This RHZ-ABM interface is suspected to underlie the North Downs where a crustal transition is implied from gravity, seismic and borehole data (Smalley and Westbrook, 1982, Kearey and Rabae, 1996) that is coincident with the northern limit of known Variscan faulting (fig. 2.4, Busby & Smith, 2001). Contrary to this, Taylor (1986) argued that the imbricated interface is further north with an additional thrust sheet subparallel to the Thames Valley due to a series of uplift structures along this axis. This has not been validated but would imply that Variscan faulting occurs deeper onto the ABM's southern margin than currently recognised (fig. 2.3, London Platform Edge vs. Thames Valley).

[3] Neoproterozoic, Caledonian, and early Carboniferous extensional faults.

Variscan-derived tectonism on the ABM was comparatively minimal (Pharaoh, 2018) and restricted to its southernmost margin (Pharaoh et al., 1996). Internally, Variscan stresses may have reactivated pre-existing faults but burial inhibits validation. Stresses were transmitted northwards beyond the ABM to reactivate faults in the main Caledonide belt (Chadwick et al., 1993) and cause inversion of the weak Carboniferous basements underlying the North Sea (Corfield et al., 1996). It is apparent that heterogeneous responses to Variscan compression reflect crustal variation between deeper terranes.

2.1.0.3 Early Permian-Early Cretaceous extension: Development of basin-platform dynamics

Variscan compression waned in the Early Permian and gave way to multiple episodes of extension in southern England (Chadwick, 1986, Warr, 2000, Ruffell and Shelton, 2000). These have been grouped into two extensional phases to distinguish when London's basement was not and was affected respectively: Permo-Triassic (ENE-WSW) and Jurassic-Early Cretaceous (N-S). Normal faults nucleated in the Palaeozoic basement by exploiting reactivated Variscan thrusts to develop basin structures during both phases (fig. 2.5, Brooks et al., 1988).

During this period, the ABM is referred to as the 'London Platform' to reflect its behaviour as a stable, exposed high that underwent minor episodes of partial submergence (Pharaoh, 2018). However, the term is also used to collectively describe the ABM and its cover prior to the London Basin's formation.

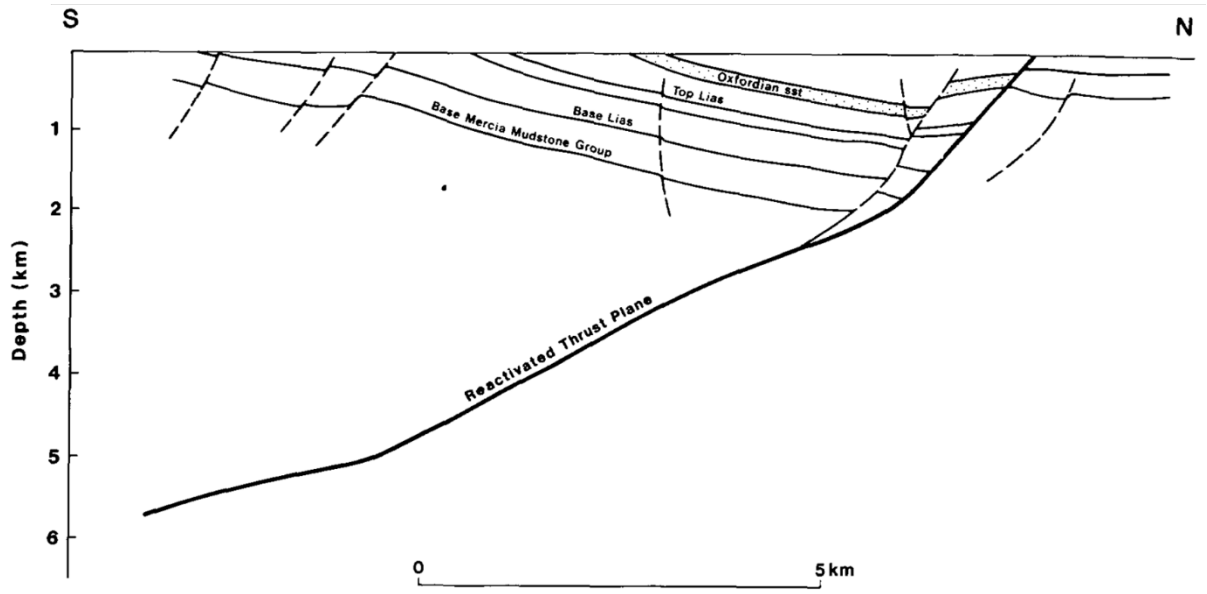

Figure 2.5 – Listric normal fault development in the Palaeozoic basement by extensional exploitation of a major Variscan thrust to form the Bristol Channel Basin. Adapted from Brooks et al. (1988).

ENE-WSW extension drove Permo-Triassic basin development (fig. 2.6) by causing minor reactivation of both Variscan thrusts in the western RHZ and a crustal suture along the ABM's western margin (Chadwick and Evans, 1995). The ABM and eastern RHZ remained as exposed highs (Ruffell and Shelton, 2000) with no significant fault reactivation evident, despite the ideal alignment of Caledonide

fabrics on the ABM (fig. 2.1, e.g., Glinton Thrust, Chadwick and Evans, 2005). The Variscan dextral strike-slip set underwent limited extensional reactivation in southwest England (Coward, 1990) and west Wales (Woodcock et al., 2014), implying potential reshearing in the eastern RHZ also. The Platform's northern margin was partially submerged during this episode (fig. 2.6, Scotney et al., 2012).

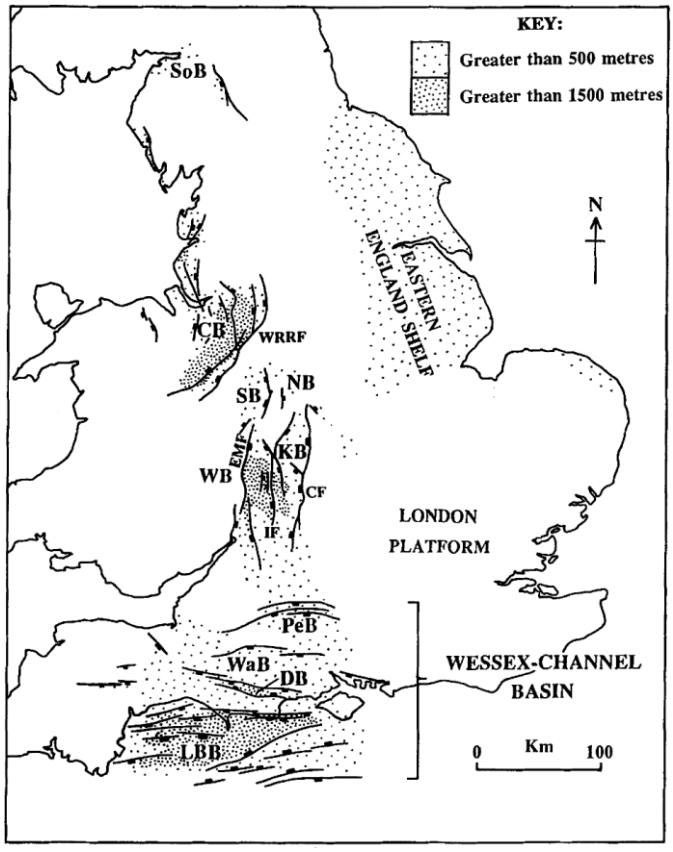

Figure 2.6 – Permo-Triassic normal faulting and sedimentation. From Chadwick & Evans (2005).

Pulsed Jurassic-Early Cretaceous N-S extension caused significant Variscan fault reactivation to develop a series of E-W fault-bounded basins across the RHZ (fig. 2.7, 2.5) (Brooks et al., 1988, Lake and Karner, 1987, Mansy et al., 2003, McMahon and Underhill, 1995). The development of the Weald Basin immediately south of the London Platform (fig. 2.7) formed as multiple listric normal faults exploited the northernmost thrust sheet (fig. 2.4) (Smith, 1985). The VF controlled the extent of basin development by restricting normal faulting to the ABM's southern margin (fig. 2.8). Jurassic sea level rise and fall caused partial submergence of, and onlapping onto, the Platform's southern and northern margins (Pharaoh, 2018; Lee et al., 2015).

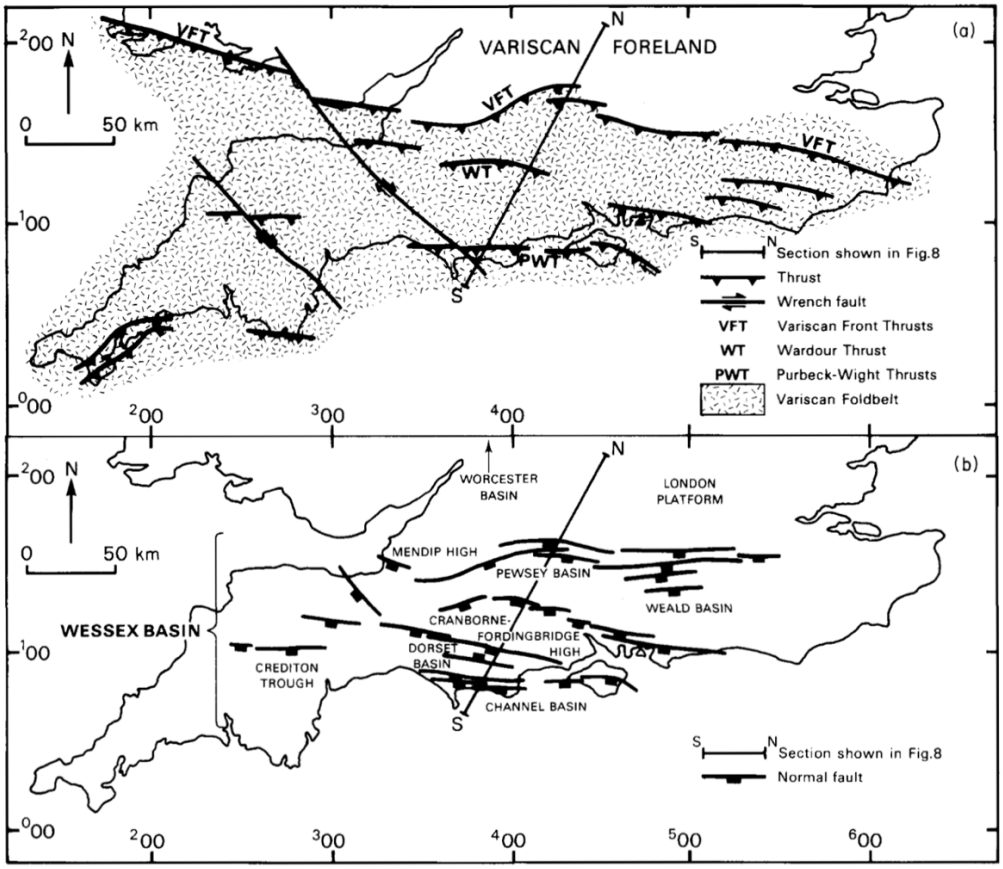

Figure 2.7 – Relationship between major Variscan thrusts and dextral strike-slip faults, and Permian-Early Cretaceous normal fault development in the RHZ basement of southern England. The associated basins are collectively referred to as the Wessex Basin. Adapted from Chadwick (1986).

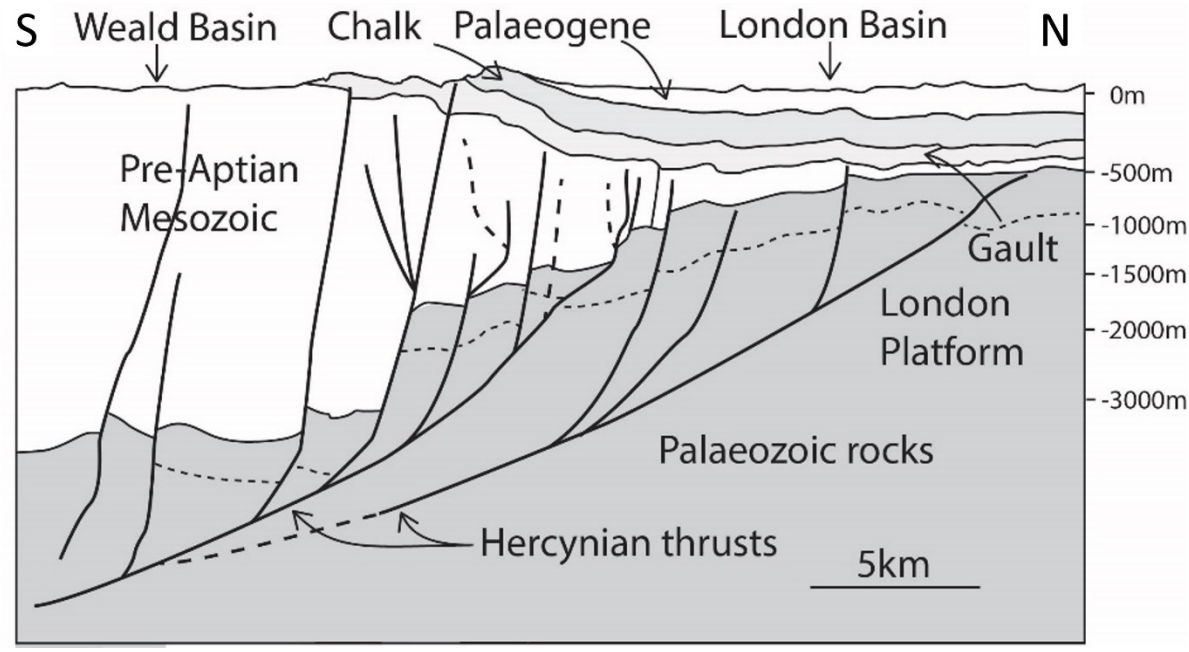

Figure 2.8 – The northernmost extent of Variscan thrusting and exploitative Mesozoic normal fault development in the pre-Permian basement along the (post-Alpine inversion) interface of the Weald Basin and the London Platform (now London Basin). Sourced from Cosgrove et al. (2021), adapted from seismic profile RG-001 (Butler and Jamieson, 2013). The seismic profile line is mapped on figure 3.23.

2.1.0.4 Early Cretaceous: Uplift, tectonic quiescence & complete submergence of the London Platform

The end-Jurassic was marked by regional uplift and regression (the 'Late Cimmerian Unconformity'; McMahon and Turner, 1998, Pharaoh, 2018). This caused erosion of the Platform's Palaeozoic centre and onlapped Jurassic margins to supply the adjacent Wessex and North Sea Basins (Lee et al., 2015, Allen, 1954). Some Late Jurassic sediments were structurally preserved along the Platform's southern margin in suspected grabens (Owen, 1971, Ellison et al., 2004). Extension waned throughout the Early Cretaceous (Mansy et al., 2003), causing a transition to terrestrial facies in the Weald Basin (Radley and Allen, 2012b, Radley and Allen, 2012a) as flexural subsidence drove post-rift Wessex Basin development (Chadwick, 1986, fig. 7).

The London Platform became an isolated landmass during the mid-Early Cretaceous. Renewed sea level rise (Chadwick, 1986) flooded the subsiding Wessex Basin and established marine connectivity with the North Sea Basin (Sumbler, 1996). During the Aptian, transgression caused progressive onlap onto the Platform (fig. 2.9; Ellison et al., 2004, Lee et al., 2015). Complete submergence was achieved during the Albian (Gallois et al., 2016) before regression and Platform exposure restricted deposition to its southern margin (Sumbler, 1996)

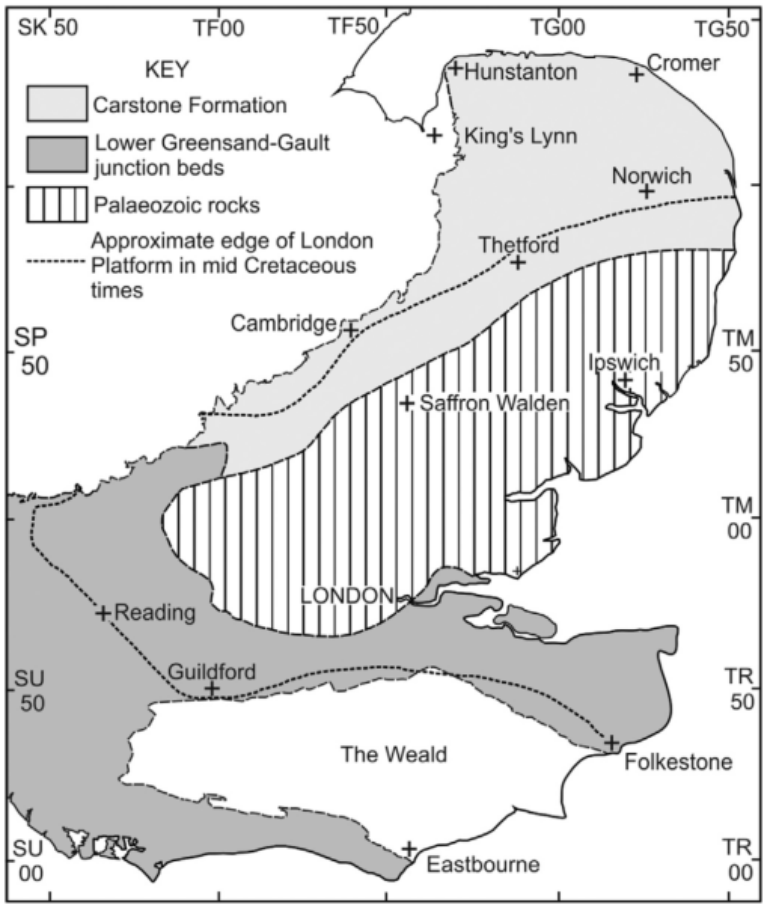

Figure 2.9 – Strata immediately underlying the Gault Formation in southeast England, illustrating the extent of Aptian onlap and later Albian submergence of the London Platform. Sourced from Gallois et al. (2016).

2.1.0.5 Late Cretaceous: Chalk blanketing and Alpine Orogeny onset

The London Platform's Early Cretaceous cover was partly denuded prior to mid-Cenomanian transgression and reburial (Gallois et al., 2016). Rising sea levels culminated in the mid-Late Cretaceous before gradually regressing (Mortimore, 2018, fig. 1). This submerged most of the British Isles, with no terrigenous supply (Chadwick, 1986) enabling a chalk sea to blanket (~500 m) the London Platform and the southern England basins (Mortimore et al., 1998). This formed part of the Anglo-Paris Basin (APB) depocentre (fig. 2.10) that extended to central France.

Far-field Alpine tectonism initiated during the Late Cretaceous with Europe-Iberia-Africa convergence (Kley, 2018, Kley and Voigt, 2008), beginning with the Subhercynian Phase (the first Alpine tectonic phase). Turonian onset is typically recognised (Kley, 2018), but earlier Cenomanian start is suspected in southern Britain (Vandycke, 2002). Tectonic responses were spatially inconsistent and reflect regional crustal and tectonic distinctions. Variscan basement faults reactivated in the Anglo-Paris Basin (APB) (Mortimore et al., 1998), inversion and salt diapirism occurred in the North Sea's Permian Basins (Kley, 2018), and Normandy underwent minor extension (Duperret et al., 2012). In the APB, Mortimore and Pomerol (1997) identified three distinct tectonic episodes within the Subhercynian Phase. These laterally resheared Variscan strike-slip and Mesozoic normal faults to generate local basins and inversion zones (Mortimore, 2011) that respectively rejuvenated and interrupted deposition (Newell et al., 2018). In the Wessex Basin there was widespread minor folding of the chalk (Ameen, 1995), with reactivated basement faults (Ameen and Cosgrove, 1990) generating *en échelon* periclinal folds (Mortimore, 2018). The Subhercynian Phase is recognised on the southern margin of the London Platform (Mortimore et al., 2011), but is less pronounced.

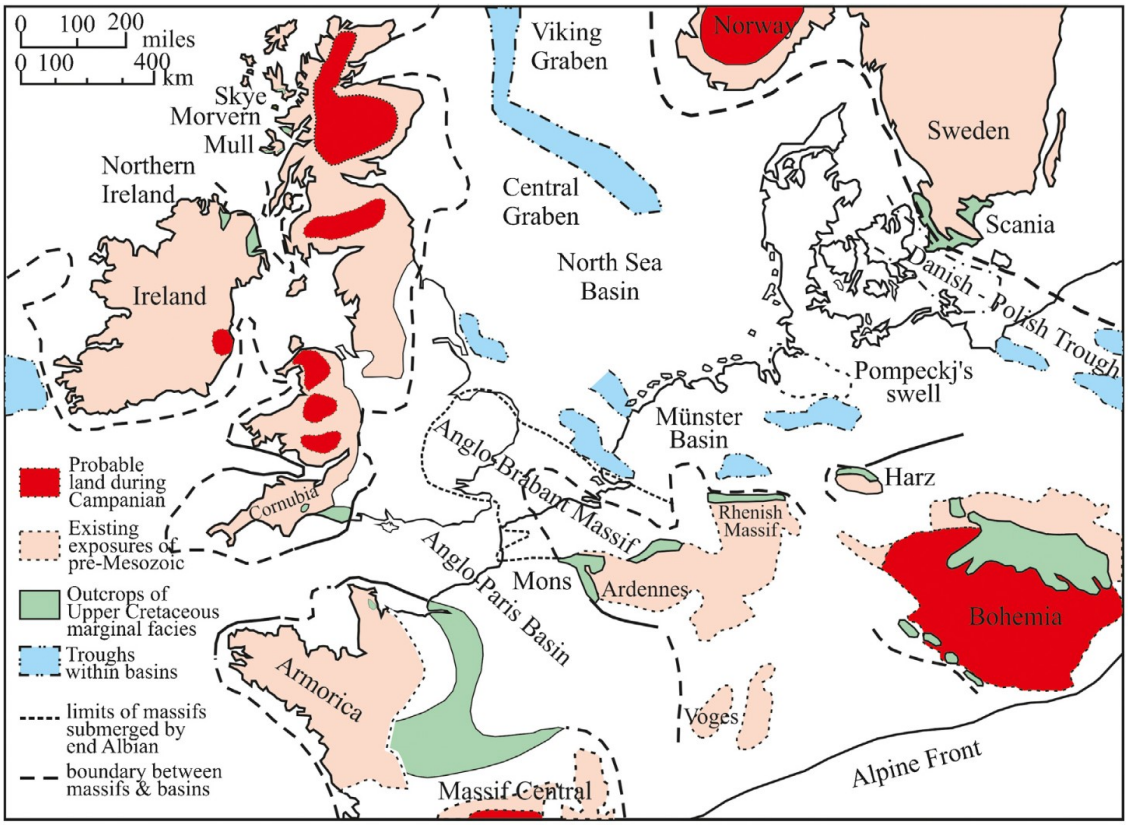

Figure 2.10 – Late Cretaceous palaeographic map of northwest Europe showing the extents of chalk seas and exposed landmasses. Sourced from Mortimore (2018). Note: the ABM forms part of the Late Cretaceous Anglo-Paris Basin (APB). The separate presence of the AMB in the figure refers to exposed landmasses during the end-Albian (i.e., its pre-Late Cretaceous outline, §2.1.0.4).

2.1.0.6 End Cretaceous-mid-Palaeocene: Regional uplift and denudation

Uplift of northwest Europe caused irregular denudation of the APB chalk blanket prior to Thanetian (late Palaeocene) reburial (fig. 2.11), with erosion most pronounced at subcrop on the southern margin of the Platform along a 'London axis'. Mortimore and Pomerol (1997) attributed this to the (end-Cretaceous-mid-Palaeocene) Laramide Phase of the Alpine Orogeny. Contrary to this, the main exhumation episode (Deckers and Matthijs, 2017) is contemporaneous with mid-Palaeocene epeirogenic uplift (Gale and Lovell, 2018, Knox, 1996) from the migrating Icelandic plume (Cogné et al., 2016, Lewis et al., 1992). Therefore, Alpine compression likely overprinted, rather than generated, this broader uplift to cause minor inversion and exhumation of the Weald Basin (Blundell, 2002, Jones, 1999). Denudational disparities between the Wessex Basin and the London Platform reflect crustal differences (fig. 2.2-3, 2.7) that affect their respective buoyancy and susceptibility to Alpine inversion. Similarly, the eastern offshore continuation of the Platform is recognised to have undergone domal uplift also (Deckers and van der Voet, 2018). The 'London axis' is situated near the basin-platform interface with faulting-controlled erosion speculated locally (Mortimore and Pomerol, 1997). This region of enhanced erosion may therefore reflect both mechanisms, with plume-driven uplift and tilting being locally complemented by fault-controlled block behaviour.

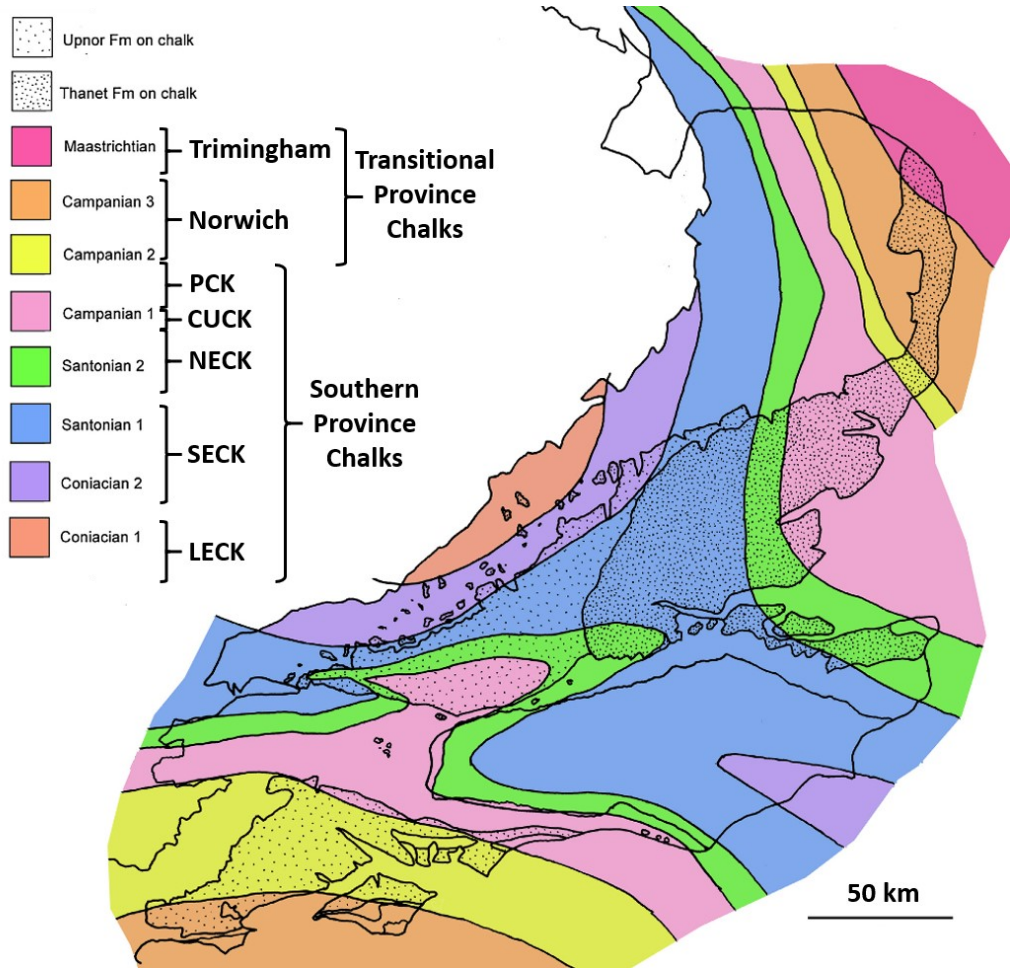

Figure 2.11 – Sub-Thanetian chalk surface map of southeast England showing irregular denudation across the uplifted London Platform and above the variably inverted Wessex Basins (i.e., Weald vs. Hampshire). Comparatively, chalk deposition continued into the Danian (early Palaeocene) in the North Sea Basin. Adapted from Gale and Lovell (2018) to assign stratigraphy to time markers.

2.1.0.7 Late Palaeocene-early Oligocene: Coastal-fluvial dynamics and Alpine escalation

By the Thanetian, southern Britain had thermally subsided (Knox, 1996) with the London Platform and its offshore extension reflooded to form part of a broad coastal plain (Deckers and van der Voet, 2018, Newell, 2014, King, 2006) along the southern margin of the North Sea Basin (fig. 2.12) .

Onlapping onto the eastern London Platform during an early Thanetian transgression (Deckers and Matthijs, 2017, Knox, 1996) deposited marine shelf sediments (Thanet Formation)[4] that were principally sourced from the uplifted Scottish Highlands (Jones et al., 2002, Morton, 1982). The Wessex Basin was exposed as restricted sediment coverage implies a southern palaeotopographic barrier (dense dots, fig. 2.11); however, more widespread deposition is debated (King, 2006). Tectonic quiescence is implied from a lack of syndepositional faulting. Mid-Thanetian regression and uplift re-exposed the Platform, causing a depositional hiatus, erosion, and leaching (Knox, 1996, Morton, 1982).

[4] And the Ormesby Clay Formation, its outer shelf lateral equivalent in East Anglia.

Figure 2.12 – Schematic interpretation of early Palaeogene palaeogeography in northwest Europe. London was situated within a coastal plain that was episodically submerged as a marine shelf throughout the late Palaeocene-Eocene. Sourced from Newell (2014).

Late Thanetian transgression resubmerged the Platform and connected it to southern England to form a broader coastal depocentre with the Wessex Basin[5] (fig. 2.12-13). Connectivity continued cyclically throughout the Eocene (fig. 2.14) between shallow marine and nonmarine fluvial conditions, and terrestrial hiatuses. Pulsed Alpine compression recommenced (Pyrenean Phase) causing syndepositional faulting along suspected basement lineaments (Ellison et al., 1996) and minor inversion of the Weald Basin causing Ypresian re-exposure of the "*Weald Island*" palaeotopographic barrier (King, 2006). Sediment supply was affected with Armorican and Scottish provenances (fig. 2.12) (Morton, 1982), and sequence reworking identified (Thomas, 2007, Huggett et al., 2017).

[5] The remnants of this broader depocentre are referred to as the Hampshire and London Basin (fig. 2.13-14) where sequences were partially preserved following Pyrenean inversion and Neogene erosion (fig. 2.16).

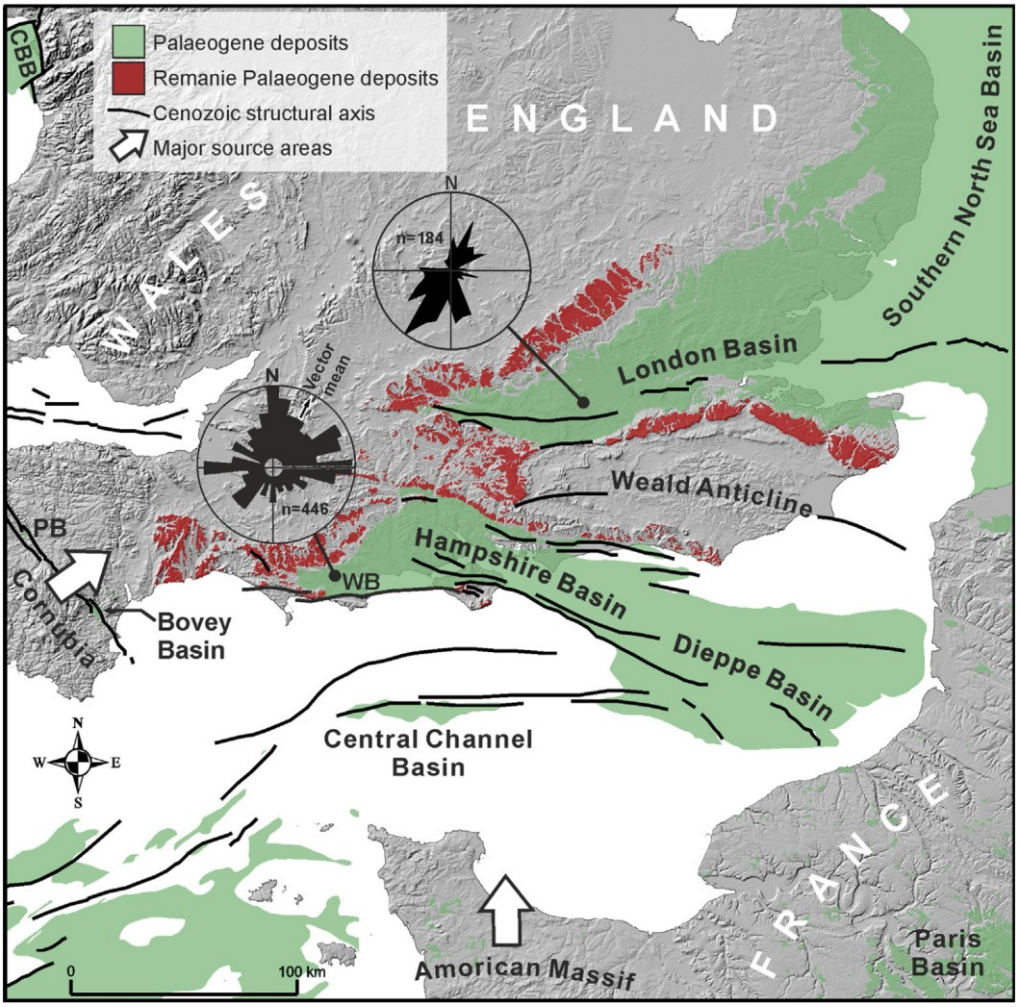

Figure 2.13 – Distribution of the former and current Palaeogene strata across onshore and offshore southern Britain. The depocentre was likely broader (fig. 2.12) as demonstrated by weathered Palaeogene remnants preserved beyond the Hampshire and London Basins. Palaeocurrent orientations of the Bracklesham Group (fig. 2.14) demonstrate flow direction from the fluvial Hampshire sequences to the estuarine London sequences. Sourced from Newell (2014).

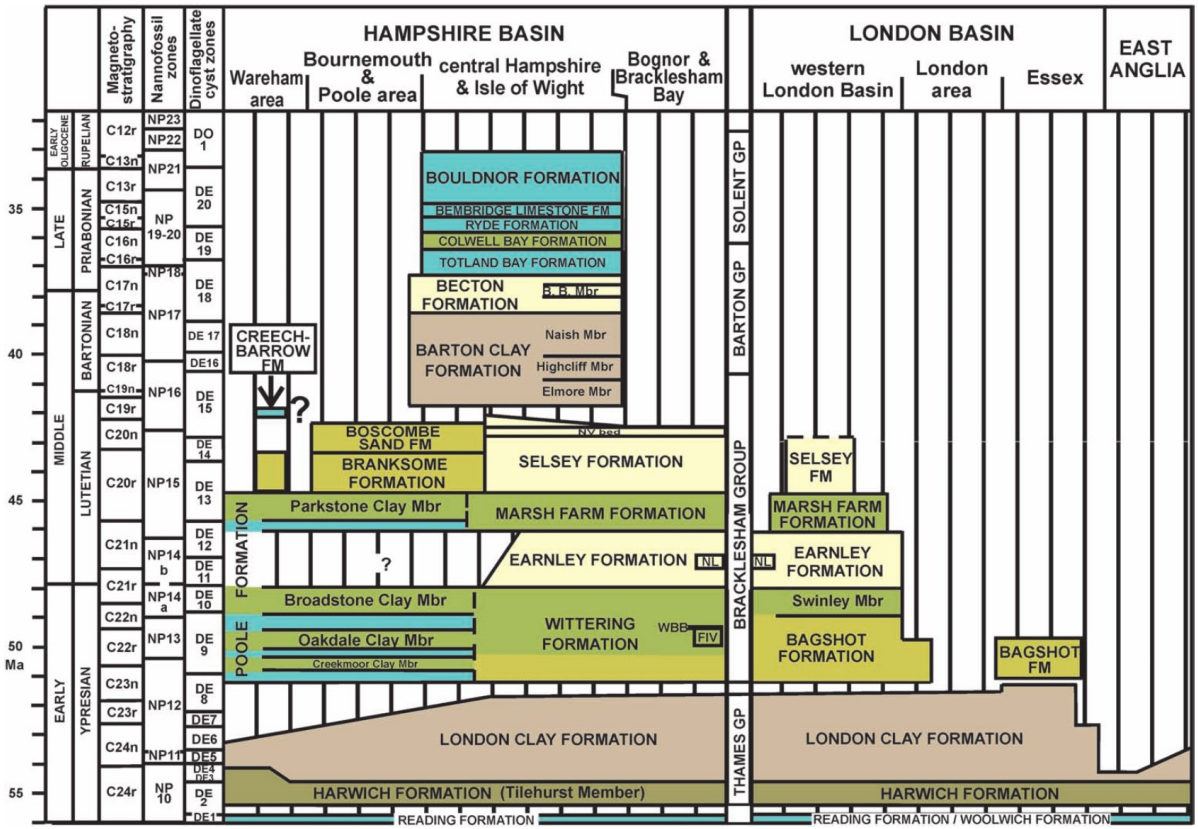

Figure 2.14 – Preserved Eocene stratigraphy in onshore southern Britain highlighting the connectivity of the Wessex Basin and London Platform coastal plains (fig. 2.12), depositional episodes and their lateral equivalents between regions. Sourced from King et al. (2016).

On the London Platform, deposition by a series of transgressive-regressive cycles during the Late Thanetian-earliest Ypresian are grouped into the Lambeth Group. The initial submergence deposited a series of glauconitic tidally-influenced estuarine/coastal to shallow marine shelf sequences (Upnor Formation) (Ellison et al., 1996, Aldiss, 2014). The depocentre transitioned to a coastal plain environment (Reading Formation) with London situated on the coastline (fig. 2.15) and was episodically onlapped by marginal marine conditions (Woolwich Formation) (Page and Skipper, 2000, King, 2006). This was interrupted by a major regressive episode (Mid-Lambeth Hiatus) during which the lower Reading and Upnor Formations in London were pedogenically altered (King et al., 2016) before onlapping resumed. Early Ypresian uplift terminated deposition and caused partial erosion (Ellison et al., 2004); this coincides with both far-field mantle pluming (Knox, 1996) and a probable Alpine tectonic pulse[6].

[6] Coincident inversion of the Weald Island is suspected as King (2006) notes that basal flints in the overlying Harwich Formation in London were likely derived from chalk on the Weald Basin, implying its exposed uplift.

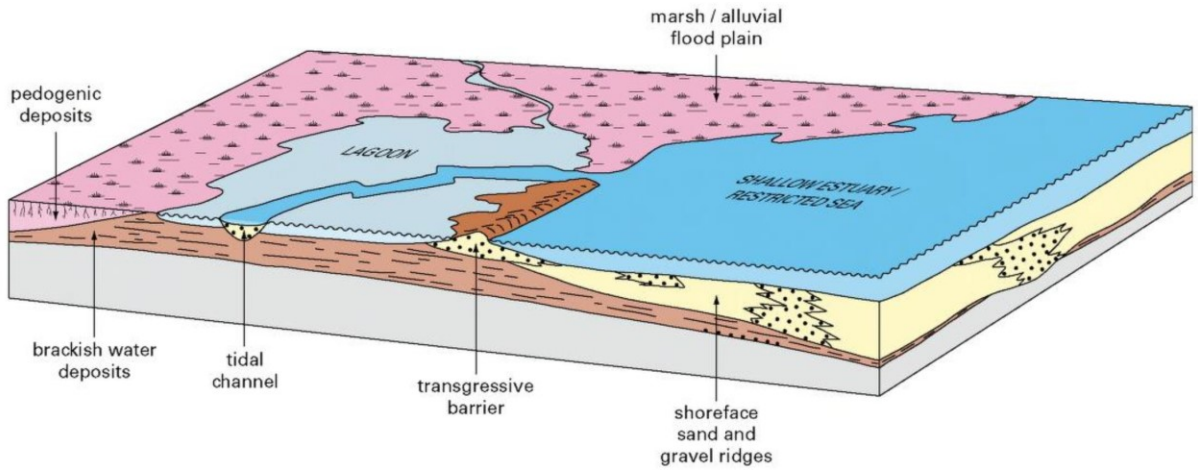

Figure 2.15 – Schematic overview of the coastal plain-marginal marine depositional environments that comprise the post-Upnor Formation portion of the Lambeth Group. Transgression-regression cycles caused episodic exposure and facies overlapping. Sourced from Ellison et al. (2004)

Early Ypresian sea level rise submerged the region, depositing laterally variable outer estuarine-to-tidal sediments that progressed to shallow marine shelf sequences (Harwich Formation) (Skipper and Edgar, 2020, Aldiss, 2014). Revived tectonism influenced local facies distribution (Edgar et al., 2021) and uplifted the Weald Island further (Jones, 1999). This disrupted depocentre connectivity and caused bidirectional flooding on the London Platform around the island (Edgar, 2021). Wealden uplift was ongoing, supplying flints for the basal Harwich sequences and raising their oversteps onto the Weald's exposed chalk along its northern margin (North Downs remanie, fig. 2.13) (King, 2006).

Continued sea level rise achieved its zenith in the Mid-Ypresian, submerging the entire coastal plain (inc. the Weald Island) and extending the North Sea Basin's shelf (King, 2006) to eventually connect with the North Atlantic (Knox, 1996). Deep marine neritic sequences were deposited across the region (London Clay Formation) (Aldiss, 2014, King, 2016) with minor regressive-transgressive cycles evident from lithostratigraphy (De Freitas and Mannion, 2007).

Major Late Ypresian regression caused north-westward shoreline retreat and reversion to transgressive-regressive cycles of shallow marine and non-marine sequences until a major sea fall in the early Oligocene (fig. 2.14) (Lee et al., 2015). Ongoing (yet minor) inversion of the Wessex Basin affected Eocene deposition south of the London Platform (Plint, 1982, Newell, 2014). Its progressive uplift restricted (fig. 2.13, palaeocurrents) and eventually disconnected these depocentres by the mid-late Eocene (King, 2006). Behaviour of the London Platform is broadly unknown due to limited preservation of post-Ypresian sequences (fig. 2.14).

2.1.0.8 Late Oligocene-early Miocene: Culmination of Alpine inversion

Pulsed Alpine compression culminated during the late Oligocene-early Miocene (Parrish et al., 2018). This caused widespread and variable tectonism across southern Britain (fig. 2.16) as basins inverted through bulk shortening of their fill, basin-bounding normal faults reversed (Bonini et al., 2012, Turner and Williams, 2004), and basement faults reactivated (Mansy et al., 2003, Chadwick et al., 1993).

The Weald Basin, and its thick fill, underwent significant inversion and uplift (Chadwick, 1993). The London Platform did not deform but its Late Cretaceous-Palaeogene cover has been interpreted to have undergone folding to produce the London Basin syncline (Ellison et al., 2004, Sumbler, 1996). This mechanism originates from geometrical interpretations in the early 1800s (Buckland, 1826, Martin, 1829), and predates the recognition of basin inversion in southern England (Stoneley, 1982).

Cover sediments on the Platform's interior underwent minimal deformation (Lee et al., 2015, Moorlock et al., 2003), with major faults and periclines restricted to the Thames Valley, North Downs and Thames Estuary[7] through suspected basement fault reactivation (Royse et al., 2012, Ford et al., 2010, Ellison et al., 2004, Blundell, 2002). This tectonic disparity in the southern London Basin likely reflects its proximity to the Platform's faulted southern interface with the RHZ (fig. 2.4; 2.8).

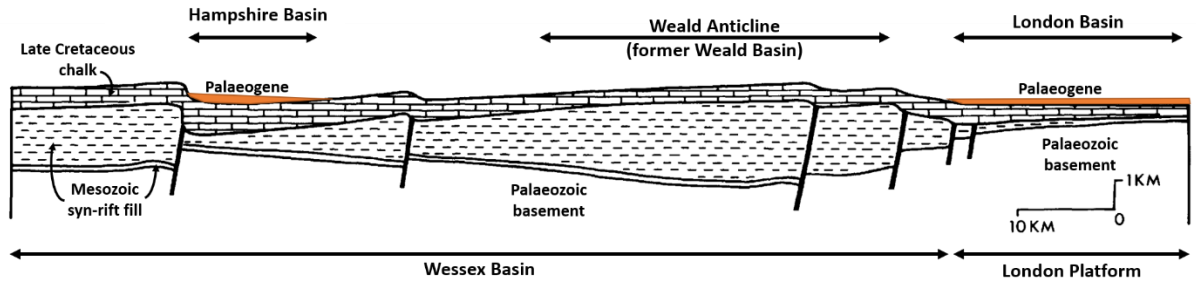

Figure 2.16 – Idealised post-inversion section of the Wessex Basin and London Platform following major late-Oligocene-early Miocene Alpine compression. This section intersects the western portion of the Weald Basin where the chalk was not fully denuded. Adapted from Chadwick (1993).

[7] These form the southern portions of the London Basin.

2.1.0.9 Miocene-Pliocene-Pleistocene: Regional denudation and minor depositional episodes

Alpine compression was ongoing (Helvetic Phase[8]) but waning (Ziegler, 1990, Parrish et al., 2018). Limited sediment preservation has inhibited Neogene tectonic analyses (Ellison et al., 2004) but continued exhumation of some inverting basins (including the Weald) is inferred (Hillis et al., 2008, Jones, 1999).

Southern Britain remained exposed throughout the Neogene, causing significant erosion of the former Palaeogene depocentres (remanie outlines, fig. 2.13) and the inverted Weald Basin (Jones, 1999, fig. 3). Denudation was enhanced in the London Basin and East Anglia (fig. 2.13) by the proto-Thames drainage pathway into the North Sea Basin (Gibbard & Lewin, 2016, 2003), with ≤200 m of erosion estimated in London[9] (Chandler, 2000). Two marine transgressions encroached onto them during the late Miocene (Sumbler, 1996) and late Pliocene-early Pleistocene (Davies et al., 2019, Lee et al., 2015) before being extensively eroded by terrestrial and glacial processes respectively.

2.1.0.10 Quaternary: Migration of the River Thames and periglaciation

Early Pleistocene regression caused a transition back to fluvial conditions and the deposition of river terrace deposits associated with the migrating River Thames (Lee et al., 2018). Quaternary uplift and southward tilting of the London Platform is suspected (Maddy, 1997, Blundell, 2002) as these sequences progressively young southwards to the present-day position of the Thames; but glacial-diversion may have contributed also (Bridgland and Gibbard, 1997). Quaternary glaciation affected North London only (Ellison et al., 2004, fig. 31), but periglacial processes have deteriorated lithologies at-surface and locally developed anomalous hollows (Flynn et al., 2020, Toms et al., 2016, Berry, 1979).

Neotectonism indicates that far-field Alpine compression is ongoing yet very minor (Baptie, 2010) with the ABM not considered to be a high strain region (Musson and Sargeant, 2007). However, there is evidence of Quaternary at-surface fault rupture in London from geological (Ghail et al., 2015a) and archaeological (Meddens, 1996, Meddens and Sidell, 1995) observations. This implies continued lateral confinement by Alpine compression and the North Atlantic.

[8] Multiple names are provided for the fourth Alpine compressive phase: 'Alpine' (e.g., Parrish et al., 2018), 'Helvetic' (e.g., Ellison et al., 2004), 'Savian' (e.g., Kley, 2018). Here Helvetic is used.

[9] Chandler (2000) conducted overconsolidation analysis on the London Clay Formation in west London. As glaciation did not occur locally (Ellison et al. 2004, fig. 31), this reflects 200 m of denuded lithological cover. These likely represent the Eocene-early Oligocene sequences preserved in the Hampshire Basin (fig. 2.14).

2.1.1 London's regional tectonic context

The southern London Basin is situated on an Avalonian crustal interface (fig. 2.1) that has demarcated contrasting mechanical responses to major tectonic events between the stable ABM block and the recurringly exploited RHZ terrane. This is reflected by their distinct stratigraphic coverage (fig. 2.17).

The interface is transitional with Mesozoic normal faults detaching from the northernmost RHZ Variscan thrust sheet emplaced onto the ABM's southern margin (fig. 2.8). Faulting derived from both the Variscan compression and Mesozoic extension (§2.1.0.2-3) should be anticipated in the Palaeozoic basement under London as it is situated directly above this transitional zone. Royse et al. (2012) argued similarly by using exposed Variscan faulting in southwest Wales as a proxy for basement conditions under London due to their comparable tectonic positioning; but their analogue lacks the Mesozoic extensional fabrics of southern England (fig. 2.5).

2.1.2 Alpine deformation in the southern London Basin

Stable Palaeozoic blocks, such as the London Platform, were less susceptible to Alpine inversion and exhumation than adjacent basins (Green et al., 2001), with internal deformation restricted to isolated features (e.g. Glinton Thrust, Woods and Chacksfield, 2012). Unlike adjacent regions, significant Alpine tectonism within the London Basin syncline is spatially restricted to its southern margin with several major faults and periclines attributed to suspected basement faults (Ellison et al., 2004, Royse et al., 2012). This implies that pre-existing basement faults along this underlying transitional interface (§2.1.1) reactivated and propagated during the Alpine Orogeny cover.

The ongoing Alpine Orogeny has progressively evolved since its Late Cretaceous inception, with four distinct phases recognised as the Eurasian-African collisional front rotated anticlockwise (Ziegler, 1989). Regional responses to Alpine tectonism in onshore and offshore southern Britain and across northwest Europe display considerable spatiotemporal variability (Mortimore, 2019, Parrish et al., 2018, Kley, 2018, Deckers and van der Voet, 2018, Green et al., 2018, Mortimore, 2018, Deckers and Matthijs, 2017, Green et al., 2001). This reflects their specific tectonic architectures and strengths, the evolving Alpine stress magnitudes and axis, and susceptibility to epeirogenic episodes.

These four phases introduced in §2.1 are outlined here. The Turonian-Campanian Subhercynian Phase caused minor inversion of southern England and Southern North Sea Basins, with faulting occurring along the London Platform's southern margin (Mortimore et al., 1998, Deckers and van der Voet, 2018). The Maastrichtian-mid-Palaeocene Laramide Phase was more significant in mainland Europe (Ziegler, 1989), but its impact in southern Britain is less clear due to contemporaneous migration of the Icelandic Plume. Associated minor tectonism occurred in the Wessex Basin region of the APB (Mortimore, 2018, Jones, 1999) but is absent from the London Platform and Southern North Sea Basin,

with both exhuming significantly during broader, mid-Palaeocene domal uplift (Deckers and van der Voet, 2018, Green et al., 2018, Green et al., 2001). Laramide compression may have initiated London Platform uplift, but pluming-related epeirogeny dwarfed it. The latest Palaeocene-early Miocene Pyrenean Phase was the main episode of Alpine compression in southern Britain (Parrish et al., 2018), causing major basin inversion (Chadwick, 1993), basement fault reactivation (Mansy et al., 2003) and syndepositional faulting along the Platform's margin. The phase's magnitude progressively increased and culminated during the late Oligocene. The Miocene-present Helvetic Phase appears to have been minor, however, regional Neogene and Quaternary uplift episodes (Japsen, 1997, Maddy, 1997) and fault reactivation (Lee et al., 2020) are recognised on the Platform.

The London Basin and its major faults are a product of polyphased Alpine compression, rather than a singular event. A full temporal appraisal of these Phases is critical for analysing fault behaviour within and beneath London. However, they have only been intermittently applied to the London Platform/Basin, despite near-ongoing tectonism implied by syndepositional faulting (Edgar, 2021, Mortimore et al., 2001, Skipper, 2000). Proxy observations from adjacent regions may be used to better characterise London's Alpine deformation, but this is considered inappropriate without contextualising their distinctive responses.

2.2 The geology of London

London's bedrock comprises approximately 300 m of Cretaceous-Palaeogene cover that rests directly on the shallow Palaeozoic basement along the ABM-Weald Basin interface (fig. 2.18). The shallow basement gently dips southwards before rapidly steepening as it approaches the North Downs (fig. 2.4), with several structures interpreted (fig. 2.19; Ellison et al., 2004). Sporadic preservation of onlapped Late Jurassic sediments in boreholes under London (e.g., Judd and Homersham, 1884, Prestwich, 1878) are attributed to basement normal faults (Owen, 1971).

London's near surface bedrock geology and structures are reviewed in §2.2.1 and §2.2.2, respectively. This is followed by an overview of the suspected origins of major faulting in §2.2.3. Since this work focuses on major faulting in the subsurface, the overlying Quaternary deposits and processes were not investigated; however, it is recognised that certain periglacial features may have exploited them (discussed in Chapter 7).

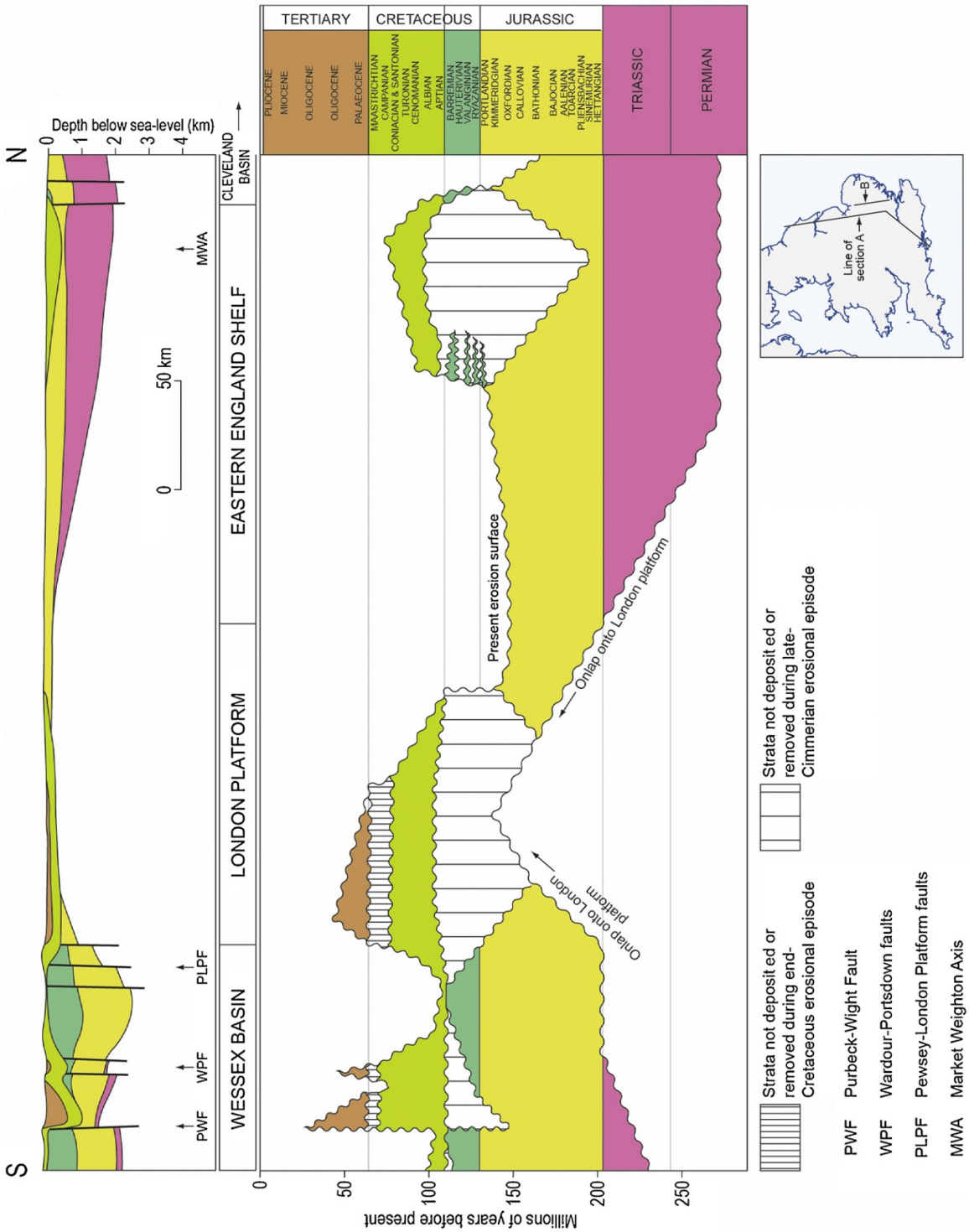

Figure 2.17 N-S cross-section and stratigraphic record through southeast England, highlighting stable block behaviour of the ABM/London Platform throughout the Mesozoic-Cenozoic to preventing basin formation and inversion, respectively. Sourced from Pharaoh (2018).

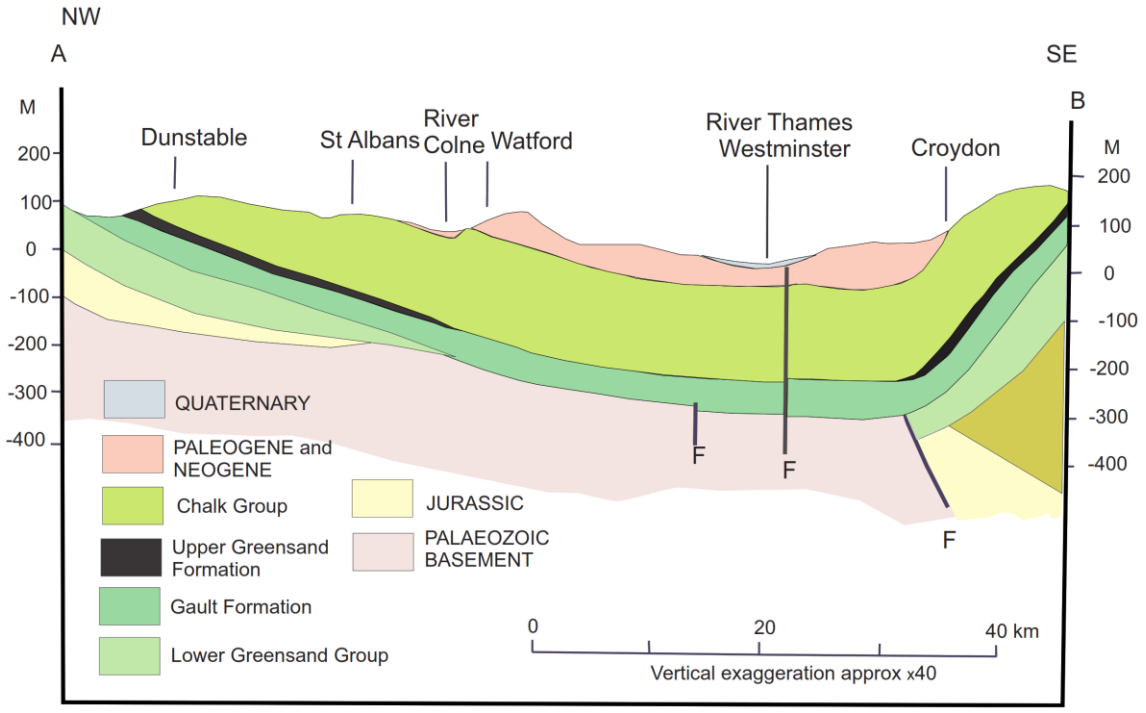

Figure 2.18 – Schematic cross-section through the London Basin syncline, its interface with the Weald Basin, and the shallow ABM. Sourced from Royse et al. (2012) who adapted from Sumbler (1996).

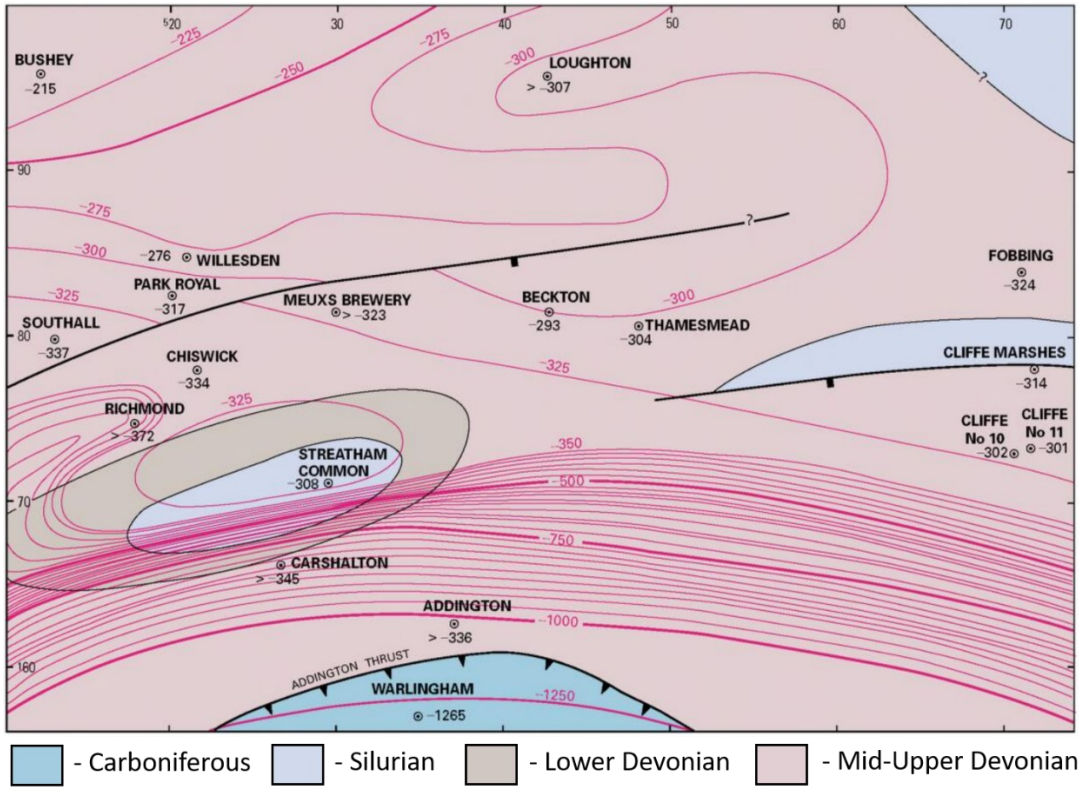

Figure 2.19 – Palaeozoic floor under London, interpreted from disparate boreholes (dots) and regional gravity data (and seismic surveys for the Addington Thrust only). Adapted from Ellison et al. (2004).

2.2.1 Near-surface geology of London

Key bedrock stratigraphy encountered in London's near surface (fig. 2.20) are described and summarised in table 2.1. These comprise the Late Cretaceous White Chalk Group (fig. 2.21), and the Late Palaeocene (Thanetian) Thanet Formation to Early Eocene (Ypresian) London Clay Formation (fig. 2.22). Later Eocene stratigraphy were not reviewed because the investigation did not encounter them. The lithology, depositional environment (refer to §2.1.0.5-7 for regional conditions), and coverage of each stratigraphic unit in London are described, together with evidence of syndepositional tectonism.

The London Clay Formation crops out across most of London (fig. 2.20) with inliers of older sequences present in east London and the Thames Estuary. Several major faults and anticlines are mapped but are recognised to be under-represented (Aldiss, 2013).

The review of Palaeogene strata relies heavily upon King et al. (2016), Aldiss (2014) and Ellison et al. (2004) for their lithological characterisation. These are referred only to here to avoid repetition.

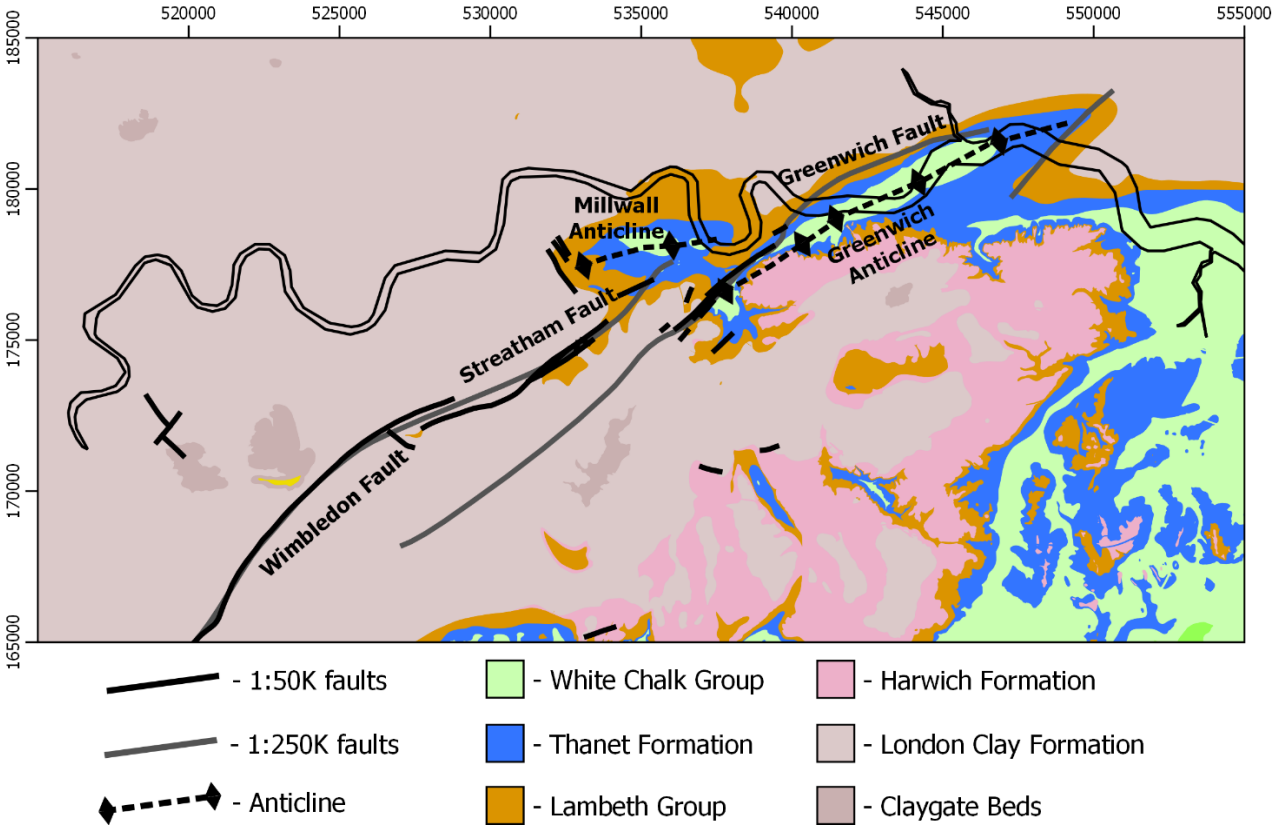

Figure 2.20 – 1:50K geological map of London and its major recognised structures (Ellison et al., 2018, Ellison et al., 2004). Faults are intentionally presented at 1:50K & 1:250K due to differing levels of detail and absence of some in higher resolution mapping. Faults and geology were sourced from the BGS (Geological Map Data BGS©UKRI 2020) with anticlines adapted from the BGS Lithoframe.

Table 2.1 – Lithostratigraphic summary of the near surface geology in London.

Sequence	Lithological Description	Thickness Range in London (m)	Depositional Environment	Syndepositional faulting		Sources	
				Activity	Depositional Influence		
White Chalk Group	Fine-grained white limestone with marl seams and flint bands.	~150-200 (approx.) (thins eastward)	Shallow marine shelf with little terrigenous supply	Yes	Suspected	Mortimore (2011); Mortimore et al. (2011); Ellison et al. (2004)	
Thanet Formation	Glauconitic silty fine sand becoming clayey with depth. Basal flint-rich conglomerate.	5-20 (thins westward)	Inner marine shelf above the fair-weather base	No	No	King et al. (2016); Aldiss (2014); Ellison et al. (2004)	–
Lambeth Group	Glauconitic sands and gravels overlain by interlayered mottled clay rich-horizons and marginal marine sediments.	10-20 (in London)	Marginal marine-lagoonal-estuarine-terrestrial mix.	Yes	Yes		Skipper (2000); Page and Skipper (2000); Entwisle et al. (2013); (Newman, 2021)
Harwich Formation	Highly heterogenous. Non-glauconitic sandy flint gravels to glauconitic silty fine sands and silty clays to clayey silts.	<1-12	Shallow marine proximal to nearshore to tidal to estuarine	Yes	Yes		Edgar (2021); Edgar et al. (2021); Skipper and Edgar (2020)
London Clay Formation	Homogeneous thinly laminated silty clay with partings-to-beds of glauconitic sandy silt and fine sands	<50 (Central London) 90-130 (Regional)	Deep, low energy marine shelf	Yes	Slumping only		King (1981); De Freitas and Mannion (2007); (Ghail and Standing, pers comms, 2021)

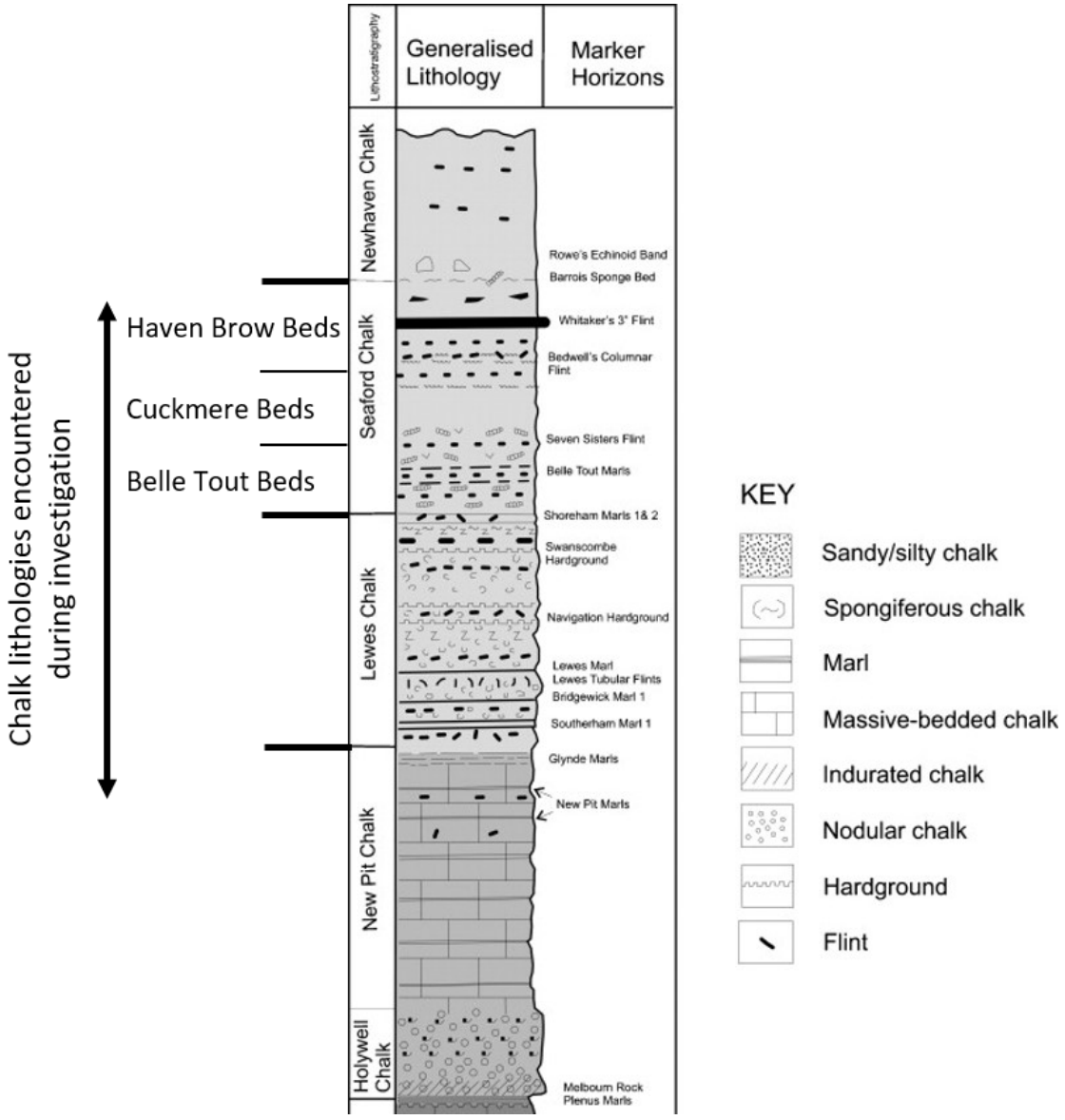

Figure 2.21 – Lithostratigraphic column of the White Chalk Group under London. Adapted from Royse et al. (2012), with Seaford Chalk Bed subdivisions extracted from Mortimore et al. (2011).

2.2.1.1 White Chalk Group

Chalk is a fine-grained biogenic limestone of accumulated coccoliths, marl seams and flints (Ellison et al., 2004). The White Chalk Group underlies all of London and is part of the Southern Province type deposited in the APB shallow marine shelf (fig. 2.10) (Mortimore et al., 2001, Mortimore, 2011). It is subdivided into formations and beds, with laterally consistent flint and marl seam marker beds present throughout (fig. 2.21). At least two denudation episodes are recognised: sub-Thanetian (fig. 2.11) and post-Oligocene (fig. 2.20). The erosional depth is irregular, but the Seaford Chalk Formation is typically the uppermost unit preserved (Mortimore et al., 2011). Both syn- and post-depositional faulting are recognised in the chalk (Mortimore et al., 2011, Carter and Hart, 1977).

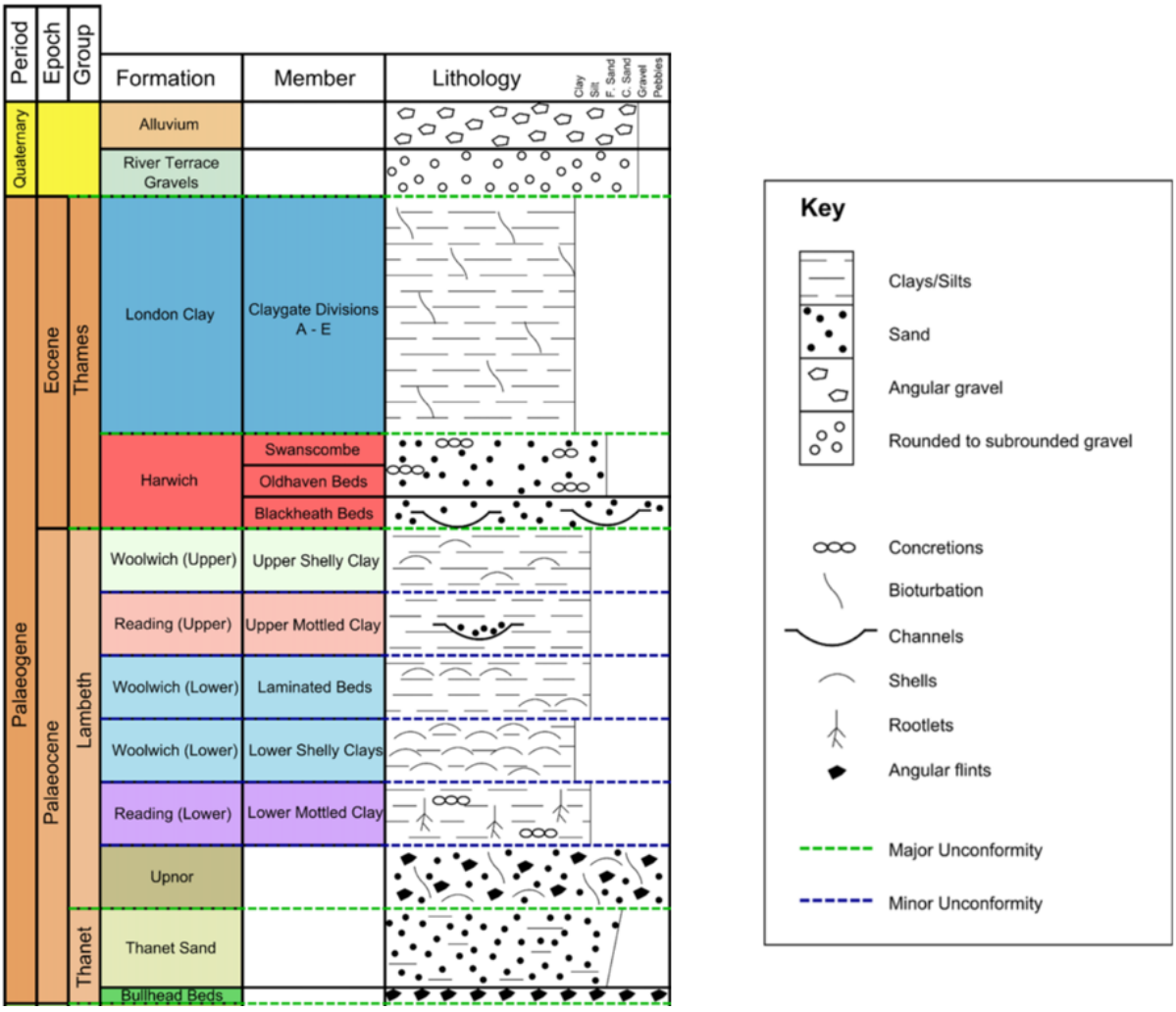

Figure 2.22 – Lithostratigraphic overview of the Palaeogene and Quaternary sequences in London. Adapted from Toms et al. (2016).

2.2.1.2 Thanet Formation

A well sorted glauconitic silty fine sand becoming progressively clayey with depth (Newman et al., 2016, fig. 9), deposited in an inner marine shelf (above the fair-weather base). The basal 0.5-1 m comprises the Bullhead Beds subunit, a conglomerate of rounded-angular flint gravel and pebbles in a glauconitic clayey fine-coarse sand matrix. The Thanet Formation covers the entirety of London but is absent from the western London Basin (fig. 2.11, dense dots). It rests unconformably on the irregular White Chalk Group surface and, following a major Thanetian depositional hiatus, was overlain by the Upnor Formation in London (fig. 2.22).

2.2.1.3 Lambeth Group

The Lambeth Group is comprised of the basal Upnor Formation that underlies all of London, and the laterally equivalent yet spatially restricted Reading-Woolwich Formations (fig. 2.23). Internally heterogeneous, Page and Skipper (2000) considered it to be the most diverse stratigraphy in the UK due to the degree of lithological variability present within its narrow stratigraphic thickness. The group was formally defined by Ellison et al. (1994) and has since been extensively characterised at the member-level (table 2.2), with Skipper's (2000) nomenclature used for this investigation. Its complexity reflects transgressive-regressive cycles onto the Platform: initial marine onlapping followed by episodic shoreline-coastal plain migration and terrestrial exposure.

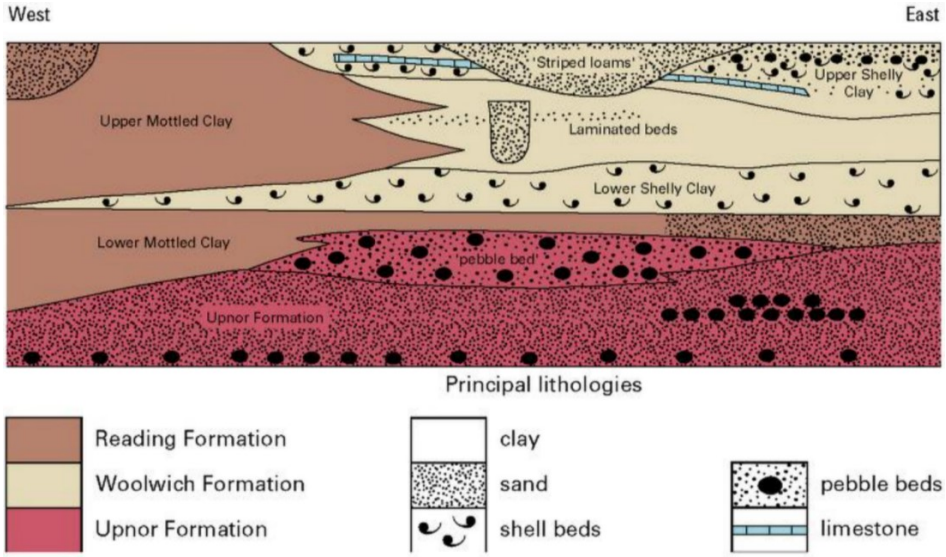

Figure 2.23 – Lithostratigraphic variation within the Lambeth Group across London. Note: Pedogenic alteration of the Upnor Formation (Mottled Upnor) is not displayed. Sourced from Ellison et al. (2004).

The Upnor Formation was deposited during two marine flooding events under tidal to near-shoreline conditions. It is a glauconitic fine-medium sand with well-rounded black flint pebbles in discrete layers and/or dispersed at the base that are overlain by a gravelly sand (fig. 2.23). Laminated silts-clays, channel fills and cross-bedding are also present (Entwisle et al., 2013, Page and Skipper, 2000).

Regression to coastal plain conditions (fig. 2.15) marked the depositional onset of the laterally equivalent alluvial floodplain (Reading Formation) and estuarine-marginal marine (Woolwich Formation) conditions that cyclically migrated across London (fig. 2.23). The clayey Reading Formation was initially deposited across London as the floodplain migrated eastwards. These, together with the uppermost Upnor, underwent significant tropical weathering during terrestrial exposure (the Mid-Lambeth Hiatus[10]) and were pedogenically altered to the Lower Mottled Beds and Mottled Upnor

[10] The Mid-Lambeth Hiatus is distinctly identifiable in London from its limestone nodules to bands.

(Skipper, 2000). Minor westward transgression caused lagoonal deposition of fossiliferous black clay (Lower Shelly Beds) and estuarine laminated silts, clays, and fine sand (Laminated Beds) with occasional sand channels. Contemporaneous floodplain conditions were maintained in west London (Upper Mottled Beds) with episodic shoreline migration causing interfingering (fig. 2.23). A final minor transgressive episode deposited further freshwater swamp-lagoonal fossiliferous black clay with silt-sand laminations (Upper Shelly Beds) (Newman, 2021) and sand channels before uplift and regression terminated Lambeth Group deposition. Many of the Lambeth Group's internal boundaries are unconformable (fig. 2.22) with the individual member coverage reduced by later denudation also.

Faulting is recognised in the Lambeth Group (Entwisle et al., 2013), with major fault-bounded blocks suspected of influencing palaeotopography and shoreline-coastal plain migration (Ford et al., 2010).

Table 2.2 – Lithostratigraphic nomenclature of the Lambeth Group in London that have replaced Prestwich's (1854) informal Reading and Woolwich Series classification.
[a] Skipper (2000) groups the Mottled Upnor with the Lower Mottled Beds.

Ellison et al. (1994)	Skipper (2000)	Aldiss (2014)	King et al. (2016)
Woolwich Formation	Upper Shelly Beds	Upper Shelly Clays	Brixton Member
Reading Formation	Upper Mottled Beds	Upper Mottled Clays	Bermondsey Member
Woolwich Formation	Lower Shelly Beds	Lower Shelly Clays	Charlton Member
	Laminated Beds	Laminated Beds	Laminated Beds
Reading Formation	Lower Mottled Beds	Lower Mottled Clays	Southwark Member
Upnor Formation	Mottled Upnor [a]	Upnor Formation	Upnor Formation
	Upnor Formation		

2.2.1.4 Harwich Formation

Situated between the Lambeth Group and the London Clay Formation, the Harwich Formation is a series of laterally discontinuous and extremely variable lithologies that were historically interpreted as a basal member of the London Clay Formation[11] (Prestwich, 1850, King, 1981). Ellison et al. (1994) redefined them as a distinct lithostratigraphic formation with three members in London (table 2.3). Ellison's nomenclature was used for this investigation, but Edgar (2021) and Edgar et al. (2021) have since reclassified them as facies to address member-level complexities. These were redefined from from lab and sedimentological testing, and independent borehole analysis. Harwich Formation lithological descriptions are based on Skipper and Edgar (2020) and Edgar et al. (2021).

[11] The London Clay Basal Beds and Unit A1, respectively.

Table 2.3 – Lithostratigraphic and facies nomenclature for the Harwich Formation present in London. These boundaries are not equivalent and prevent direct comparison.

Lithostratigraphic Members			Facies
Ellison et al. (1994)	**King et al. (2016)**		**Edgar (2021)**
Oldhaven Member Swanscombe Member			HWH1
			HWH2
			HWH3
Blackheath Member	Blackheath Formation		HWH4
			HWH5

Each member's distribution is spatially restricted in London (fig. 2.24) and rest unconformably on the irregularly denuded Lambeth Group in London (fig. 2.22). They are interpreted to represent onlapping transgression, progressively developing from outer estuarine to marginal marine conditions (Blackheath) to inner-mid marine shelf (Swanscombe), with facies analysis implying a structural influence on distribution. Calcareous hard bands (or concretions) are present throughout the formation, with a causal link with major faults suspected due to their spatially coincidence.

The Blackheath Member comprises rounded flint pebbles to gravels in a non-glauconitic sand-rich matrix with basal shells, but it is laterally heterogenous with clay-silt laminae, sand-dominant horizons and sand channels present also. The Oldhaven Member is a glauconitic silty fine sand with frequent shells and dispersed flint gravel towards it base. The Swanscombe Member is a glauconitic sandy silty clay-clayey silts with dispersed-to-thin horizons of shells, and occasional basal flints.

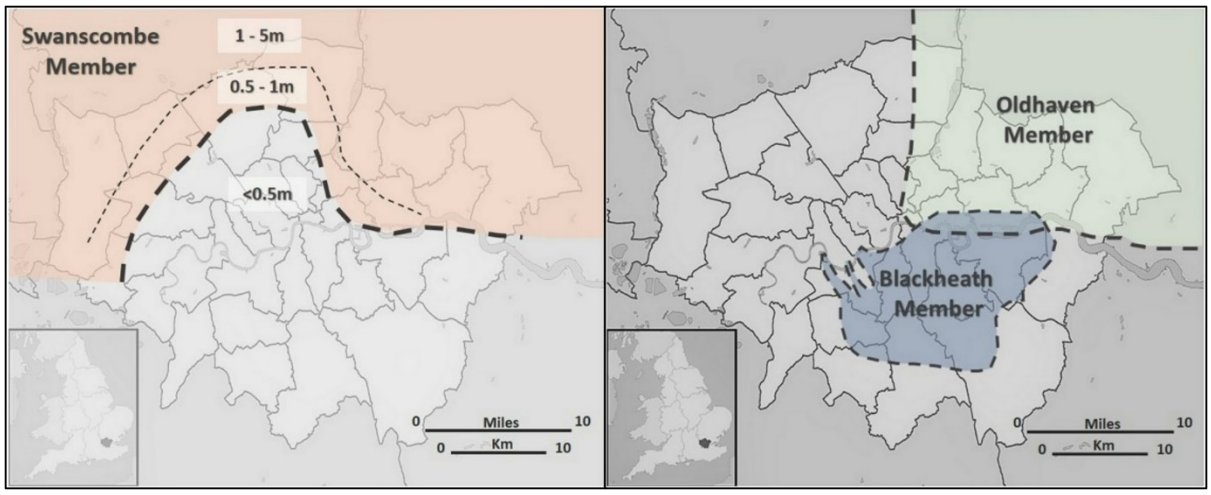

Figure 2.24 – Harwich Formation member distribution (table 2.3) in London.
Adapted from Skipper and Edgar (2020).

2.2.1.5 London Clay Formation

In London, the London Clay Formation (LCF) is comprised of homogeneous thinly laminated silty clay with partings-to-beds of glauconitic sandy silt and fine sands. Several coarsening-up sequences are internally recognised that represent minor transgressive-regressive cycles on an inner-to-outer marine shelf. Multiple classifications have been defined according to its lithostratigraphy and biostratigraphy (King et al., 2016, Ellison et al., 2004, King, 1981), with King's (1981) nomenclature used for this investigation due to its common usage used by London's geotechnical community (e.g., Standing, 2020, Sismondi et al., 2015, De Freitas and Mannion, 2007). This segregates the LCF along its coarsening up-sequences (Units A-E) and subdivides them into lithological groups (e.g., Units C1-C3). Confusingly, the basal LCF unit is A2 because the Harwich Formation was originally the A1 unit.

The majority of the LCF has been eroded in London with only units A2-B2 preserved (fig. 2.25) (Hight, 2003). It unconformably rests on the Harwich Formation and Lambeth Group, depending on the former's coverage (fig. 2.24). Faulting did not influence depositional behaviour of the LCF, but syndepositional activity is suspected from in-log observations of slumping (Ghail and Standing, pers comms, 2021).

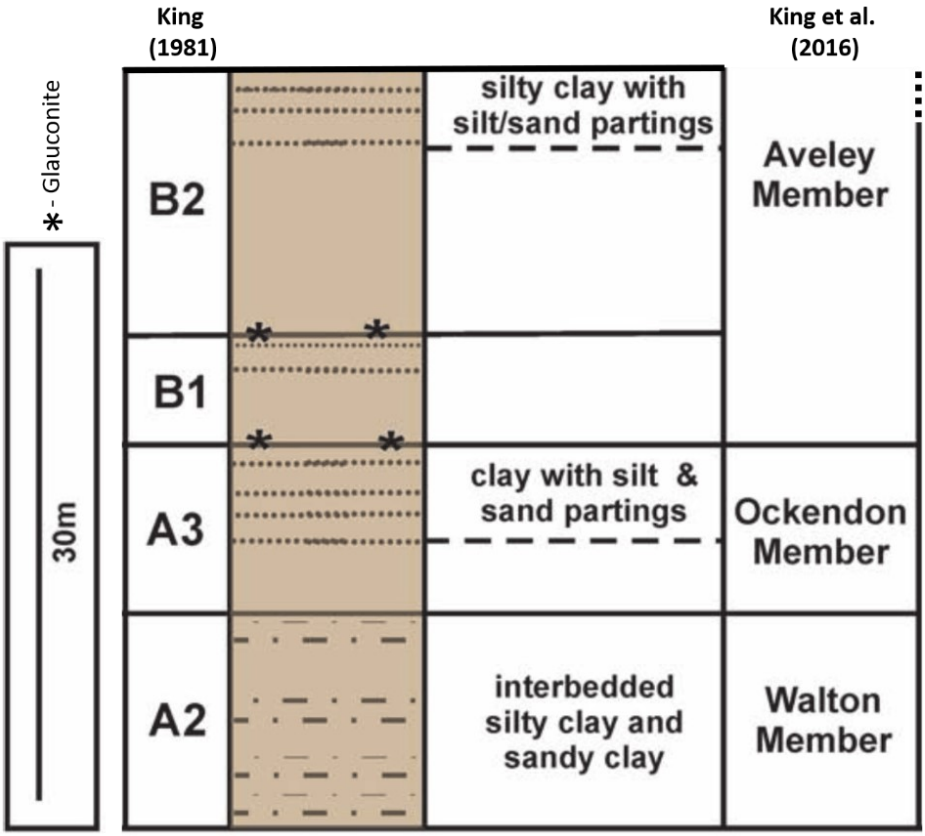

Figure 2.25 – London Clay Formation units preserved in central London. Predominantly a homogenous, thinly laminated silty clay with distinct lithological horizons markers. These are subdivided using lithostratigraphic interpretations from Kings (1981) and King et al. (2016). Adapted from King et al. (2016, fig. 133).

2.2.2 Structures in London

The review describes structural observations in London and the evolving interpretation of their prevalence. Faulting and folding are observed at multiple scales throughout London in all near-surface stratigraphy (§2.2.1). Only a few major structures are mapped in London (fig. 2.20), despite evidence of additional ones. Minor structures are prevalent across London yet unmapped due to their scale and confinement to individual exposures (Aldiss, 2013). Instead, they are restricted to exposure sketches and/or descriptions in memoirs, field excursions and academic papers (e.g., fig. 2.26).

2.2.2.1 Minor faulting

Ellison et al. (2004) notes that the majority of minor faults are normal with throws <2 m. This is supported by their prevalence in historical documentation (fig. 2.26) (Whitaker et al., 1872, Whitaker, 1889a) and recent engineering observations (e.g., Newman, pers comms, 2019a, Price et al., 2018). Thrust faults are comparatively rare[12] (fig. 2.27), yet local clustering of observations is apparent, with throws of ~0.15-0.3 m documented (De la Condamine, 1852, Whitaker, 1889b, Barrow, 1906, Crossrail, 2016). No minor strike-slip faulting has been documented yet lateral-slip slickensides are observed in the chalk in southeast London (Newman, pers comms, 2019b) and in northern Surrey (Woodward, 1909, Young, 1905). Thrust and strike-slip observations are typically proximal to larger faults, however, Crossrail outputs indicate that they are more frequent than recognised (Skipper et al., 2015, Crossrail, 2016).

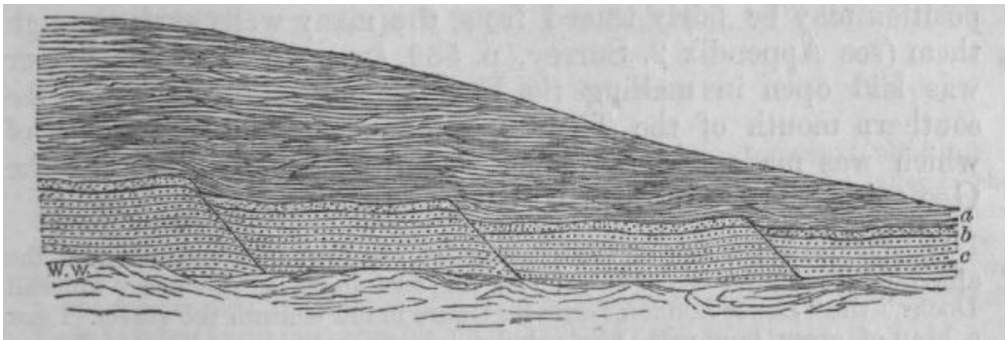

(*a.*) London Clay. Stiff brown roughly laminated and jointed (so as to break up into cuboidal pieces) rather sandy towards the base, where there are a few flint-pebbles, and some green grains.
(*b.*) Oldhaven Beds? Buff sand, with shells, 6 to 9 inches.
(*c.*) Woolwich Beds. Light-coloured sand, with many thin layers of clay, evenly bedded, 6 feet shown.

Figure 2.26 – Stepped normal faulting, observed near Dulwich, that have downthrown the Eocene sediments by <0.3 m. The London Clay has likely been displaced also but is masked by its near-homogeneous stratigraphy. Sourced from Whitaker et al. (1872).

[12] Many are documented as 'reverse' faults (e.g., fig. 2.27). Prior to standardisation (Reid et al. 1913), the term was historically used to describe any fault where the hanging wall block was upthrown (Prestwich and Morris, 1846, fig. 4, vs. De la Condamine, 1852, fig. 1) rather than solely normal fault reversal. In London, this is assumed to describe thrusting as reverse faults are absent from sketches.

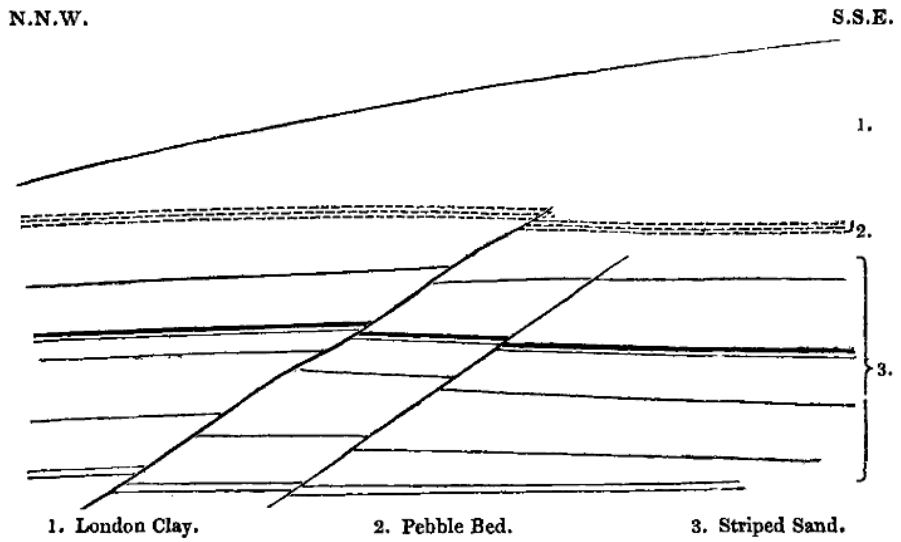

Figure 2.27 – Thrust fault at Loam Pit Hill, offsetting London Clay, Harwich, and Lambeth strata. Average fault angles of 30° with 0.15 m throws were documented. Sourced from De la Condamine (1852)

2.2.2.2 Major faulting

First documented by De la Condamine (1850), major faults have been progressively observed and mapped[13] in London (e.g., Mylne, 1858, Bristow et al., 1862, Whitaker et al., 1872). The review only describes the three named faults (fig. 2.20) recognised in Ellison et al. (2004, fig. 42)[14]. Major faulting is under-represented in London (Aldiss, 2013) with historical (e.g., Wood, 1866, Davis, 1928) and recent (e.g., Newman, 2009, Mortimore et al., 2011) observations demonstrating that they are more widespread than mapped. Additional faults are suspected from subsurface topographic variation but were not mapped due to a lack of verification (Ellison et al., 2004).

The *en échelon* Wimbledon–Streatham–Greenwich Faults (WSG-Faults) are three overlapping faults that trend NE-NNE in south and east London, with downthrows of 10-30 m to the north recorded (Ellison et al., 2004). The Greenwich Fault bounds the northern limb of the Greenwich Anticline, with a fourth unnamed fault recognised along its northeast margin (fig. 2.20) and referred to here as the 'Dagenham Fault'. Since they were mainly interpreted from former exposures and boreholes, their slip directions, dip, and azimuth are unknown, preventing structural characterisation. A sinistral slip component is inferred by this investigation due to their relative right-stepping arrangement being comparable with known *en échelon* behaviour (Mandl, 2000). Collectively, this implies that oblique-slip has occurred along them.

Comparisons of the WSG-Faults at 1:50K & 1:250K (fig. 2.20) locally demonstrate that they are comprised of multiple shears rather than single, contiguous planes. Royse (2010) commented that the

[13] Fault mapping in London, its techniques and interpretative credibility are reviewed separately in Chapter 4.
[14] Ellison et al. (2004) also extended the Cliffe Fault from the Thames Estuary into East London, but there is no published evidence to describe and confirm its extension. The Cliffe Fault is discussed in Chapter 3.

latter is an oversimplification with displacement likely distributed across many, smaller faults, however, descriptions in Ellison et al. (2004) indicate that some shears dominate overall.

Recent ground investigations (GIs) have also identified confined bands of extensive faulting and brittle deformation (fig. 2.28), termed 'fault zones' by Newman (2009). These are consistently idealised as vertical by ground investigations. Fault zones have been intercepted proximal to known major faults and away from them (Newman et al., 2016, Black, 2017), and appear to be complex structures internally. Fault zones are formally analysed in Chapter 6.

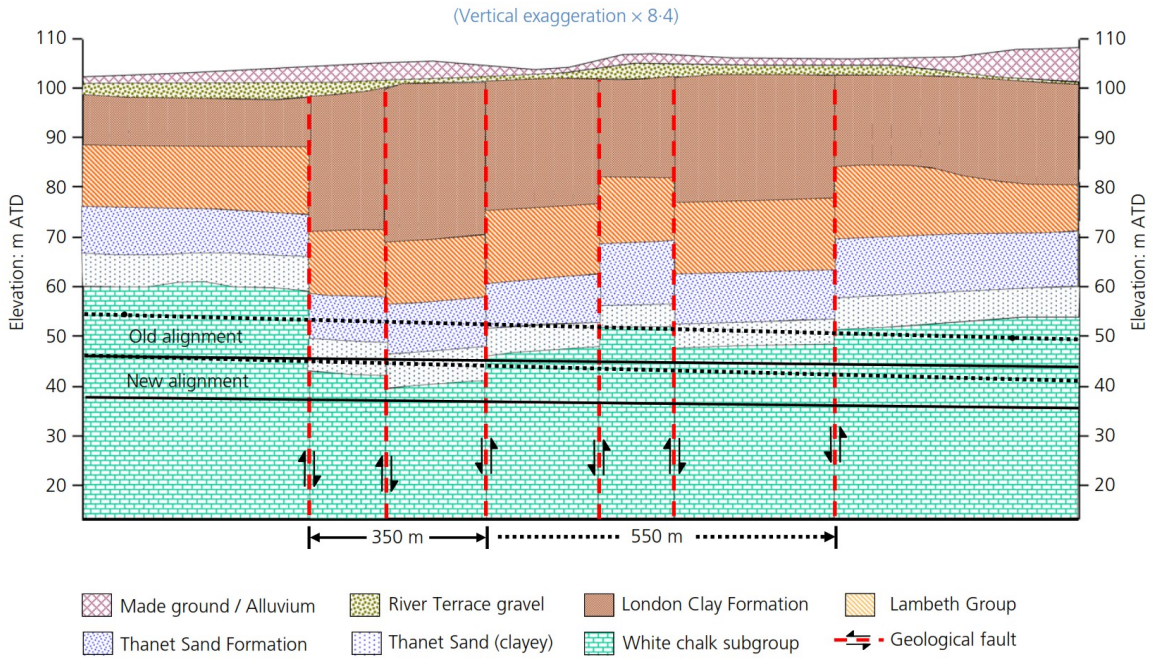

Figure 2.28 – The Plaistow Graben Fault Zone, a ~1.2 km-wide fault zone intersected by the Lee Tunnel in northeast London. Sourced from Newman et al. (2016, fig. 8). Refer to figure 6.21 for fault zone location.

2.2.2.3 Jointing and minor shear zones

Joint studies have been conducted on the LCF (southern London Basin only) (Skempton et al., 1969, Fookes and Parrish, 1969, Doherty, 2012) and the Chalk Supergroup (London Basin-wide) (Cawsey, 1977). Whilst noisy, regional joint sets are suspected by Bevan and Hancock (1986) in all near surface lithologies, with observations by Ellison et al. (2004) indicating potential local modification also.

Sub-horizontal shear zones have been identified near Heathrow that were attributed to flexural slip due to their proximity to a suspected anticline (Chandler et al., 1998, Skempton et al., 1969).

2.2.2.4 Folding

Minor folding is recognised throughout the London Basin (Woods and Farrant, pers comms, 2019, Ellison et al., 2004, Lake et al., 1986, Worssam, 1963) and is attributed to Alpine shortening. The majority are unmapped and restricted to memoirs. In the southern London Basin, the majority of folds are ENE-trending gentle folds with broad wavelengths and very low amplitudes (limb angles <2°), with steeper periclinal folds (limbs ≤7°) also documented south of the River Thames. Recent geological modelling (Ford et al., 2010) has since validated and mapped this regional difference.

Inliers and outliers in the London Basin were historically interpreted as anticlines and synclines respectively (Wooldridge, 1923), including a series of inliers parallel to the Thames Valley and the River Thames (Whitaker, 1875). Unlike the regional minor folding, these suspected folds are significant yet isolated. The two chalk inliers in southeast London are interpreted as the Millwall and Greenwich Anticlines (fig. 2.20). Both are proximal to major faulting. Ellison et al. (2004) attributed the latter to inversion of an underlying basement fault, with fault-capping folding similarly proposed for the Windsor Anticline (Blundell, 2002).

Very intense, short-lived folding has also been documented in the Lambeth Group (fig. 2.29) at two localities proximal to the WSG-Faults (Whitaker et al., 1872, Bromehead, 1922, Ellison et al., 2004). Bromehead attributed the folding to Quaternary slope failure, however, the cutting demonstrates that the overlying Harwich and LCF have maintained horizontality, implying an early Ypresian event.

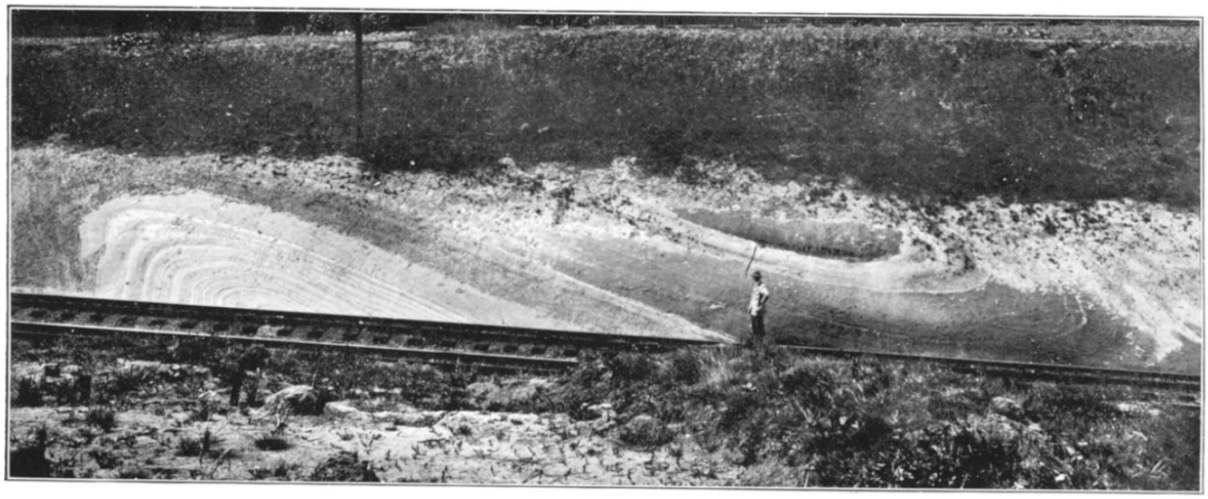

Figure 2.29 – Intense folding of the upper Lambeth Group in a railway cutting in southeast London, attributed to slope failure. Sourced from Bromehead (1922).

2.2.2.5 Structural interpretation

Characterisation of London's structures can be categorised into three distinct episodes of interpretation: 1800s-early 1900s geological research and recognition of structural anomalies; early-to-mid 1900s transition to oversimplified 'layer cake' model with minimal deformation; late 1990s-present rejuvenated efforts to analyse under-recognised structures intercepted by civil engineering.

The majority of structures were historically documented from the mid-1800s to early-1900s when Victorian-Edwardian infrastructure development and limited urbanisation provided numerous bedrock exposures. The small scale of most restricted them to memoirs and publications only, with the London Basin postulated to be the least tectonically disturbed region in Great Britain (Whitaker et al., 1872). However, attitudes did evolve throughout this period, with the prevalence of minor faulting changing from "*rare*" to "*numerous*" (Whitaker, 1875, Woodward et al., 1922). Comparatively, only two major faults were named in London. Firstly, the WSG-Faults (fig. 2.20) progressively developed, together with suspected anticlines, through extrapolation between exposures and well data (e.g., De la Condamine, 1850, Davis, 1928). Secondly, the larger, E-W striking "*Thames Valley Fault*" that was suspected from a series of "*disturbances*" (inliers) that extended from Windsor to the Thames Estuary (Woodward, 1909, Whitaker, 1889a). Major fault documentation is limited, however, others had been inferred also (Woodward et al., 1922).

Attitudes to structural interpretations became more conservative in the 1920s with previously inferred major faults redacted from maps due to insufficient evidence and an overreliance on extrapolation (Woodward et al., 1922). Only the WSG-Faults remained (Dewey and Bromehead, 1921) with significant elevation variations in London's sub-Palaeogene (chalk) floor (Barrow and Wills, 1913) attributed to folding instead (Bromehead et al., 1925). This redefined emphasis on broad regional folding is illustrated by Wooldridge's (1923) proposed structural interpretation of the Basin (fig. 2.30). Consequently, fault interpretations progressively fell out of favour with Sherlock (1947) describing the area as "*comparatively free from folding and faulting*". Fault documentation became confined to overlooked previous memoirs. Analyses focused on regional structures instead, such as the London Basin syncline, culminating in the 'layer cake' London model of minimally deformed sub-horizontal strata within a broad syncline (fig. 2.18), with no historical or new structures discussed in the most recent regional memoir (Sumbler, 1996). This change in attitude is also demonstrated by the progressive diminishing of structural discussions and analyses (table 2.4).

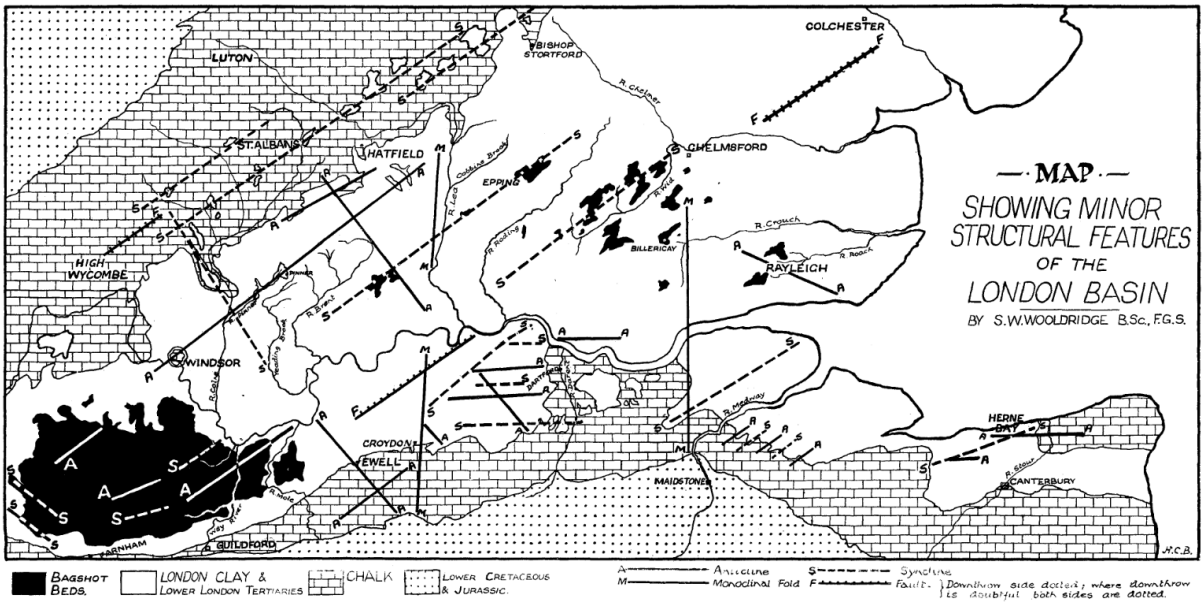

Figure 2.30 - Proposed structural map developed by Wooldridge (1923) who coupled discrete structural observations and inferences with geomorphological and geological data. This is reviewed in Chapter 4.

Table 2.4 – Progressive reduction in the documentation of geological structures in memoirs on London as illustrated by dedicated pages numbers. [a] Structures mentioned throughout also in relation to sediments.

Memoir	Memoir Coverage	Pages dedicated to structural analysis
Whitaker et al. (1872)	London Basin	11 [a]
Whitaker (1875)	London	5
Whitaker (1889a) & Whitaker (1889b)	London and part of the Thames Valley	5 [a]
Woodward (1909)	London	3.5
Woodward et al. (1922)		2.5
Bromehead et al. (1925)	North London	2.5
Dewey and Bromehead (1921)	South London	1
Sherlock (1947)	London & Thames Valley	2.5
Sumbler (1996)		1 [cross-section, not text]

Opinions began to change during the 1990s when significant faulting was increasingly identified during GIs for tunnelling and ground engineering projects (Newman, 2009, Page, 1995, Rainey and Rosenbaum, 1989, Carter and Hart, 1977). Coupled with outputs from early geological modelling (Ellison et al., 1993, Rosenbaum and Warren, 1986), it demonstrated that the then current geological interpretation (fig. 2.20) under-represented faulting in London (Aldiss, 2013, Ellison et al., 2004). Additional major faults and fault zones were identified once geotechnical projects began to anticipate faulting as a subsurface hazard (Black, 2017, Newman, 2017, Crossrail, 2012, Aldiss et al., 2012, Mortimore et al., 2011, Lenham et al., 2006, Newman, 2008); however, these represent intersections rather than fully mapped structures. Collectively these revived historical expectations of structures, with the geological community now advocating the prevalence of unmapped major faults across London that have likely compartmentalised the subsurface (Aldiss, 2013, Royse et al., 2012, de Freitas, 2009). This has rejuvenated new research into them and their potential geotechnical implications (Linde-Arias et al., 2018, Toms et al., 2016, Mason et al., 2015, Ghail et al., 2015a, Ghail et al., 2015b).

Renewed geological modelling interpreted widespread folding and major faulting, culminating in the BGS Lithoframe model (fig. 2.31) (Mathers et al., 2014, Burke et al., 2014, Royse, 2010, Ford et al., 2010, Royse et al., 2009, Ford et al., 2008). Ford et al. (2010) separated London into two distinct structural domains separated by a narrow graben. North and West London comprise large fault-bounded blocks with marginal monoclines and are minimally deformed internally. Southeast London is extensively folded and subdivided into a region of broad folds, and of periclinal ones associated with faulting. The model completely overhauls the former structural interpretation of London (fig. 2.20) but its recognition has been slow: uptake by infrastructure projects is limited but increasing (Ting et al., 2020, Price et al., 2018) yet it is absent from the most recent geological characterisation of London and the Thames Valley (Ellison et al., 2018). GIs have intercepted faults away from modelled structures (e.g., fig. 2.28) indicating London's structural characterisation is still incomplete.

2.2.3 The origin of major faulting in London

The comparative difference in scale between minor (fig. 2.26-27) and major faults (fig. 2.20) implies two distinct formation mechanisms. Major faults (and associated folds) have long been attributed to reactivated basement structures (Ellison et al., 2004, Sumbler, 1996, Wooldridge, 1923). The theory originates from Godwin-Austen (1856) and Whitaker et al. (1872) who suspected an underlying, faulted crustal interface. However, efforts to structurally characterise the underlying basement (Pharaoh, 2018, Pharaoh et al., 1987, Allsop and Smith, 1988, Chroston and Sola, 1975, Owen, 1971, Bullard et al., 1940) have been inhibited by sparse deep borehole coverage and minimal regional subsurface exploration. Bouguer gravity analyses have inferred basement structural lineaments

(Aldiss et al., 2014, Ellison et al., 2004) with Ford et al. (2010) noting spatial coincidence with modelled faults (fig. 2.31). Whilst deep structures are evidenced, their characterisation remains incomplete. This led Royse et al. (2012) to propose a Variscan fabric from proxy observations in southwest Wales due to its comparative positioning North of the Variscan Front. However, despite the geophysical evidence and tectonic analogies, an inheritance origin for London's major faults has yet to be validated.

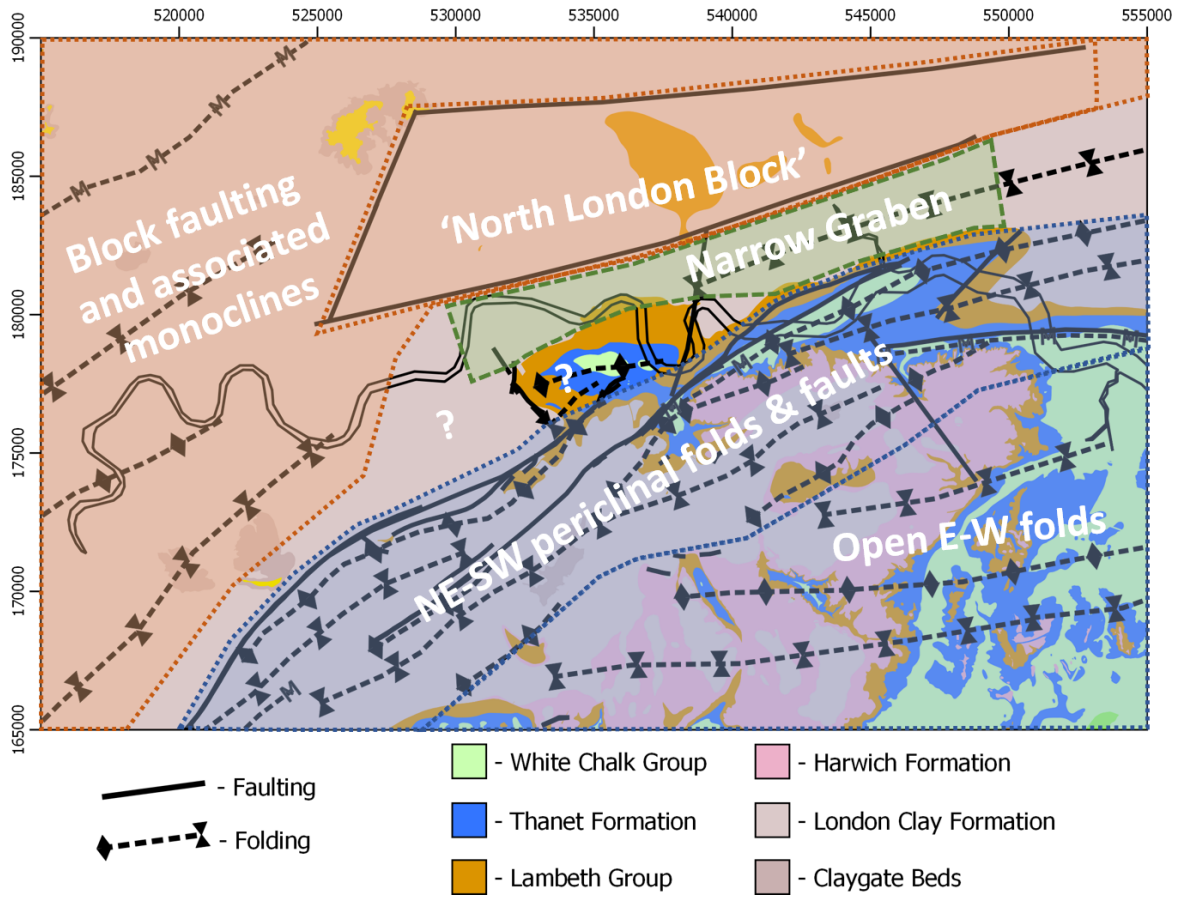

Figure 2.31 – BGS Lithoframe structural interpretation of London [accurate as of 12/05/2020]. Ford et al. (2010) divided the region into two distinct structural domains that are separated by a narrow graben structure. Additional block boundaries are evident in North and West London from subsurface topographic variation but were not mapped as faults in the Lithoframe. These have been (approximately) subdivided to highlight regional variation within each domain. Figure generated by overlaying BGS Lithoframe structures provided by Ford (pers comms, 2020) onto 1:50k BGS lithologies.

2.3 Conclusion

London is situated within the southern London Basin. Its near surface geology comprises an unconformable succession of Late Cretaceous-Palaeogene strata (fig. 2.21-22). These have been tectonised to varying degrees (§2.2.2), with the impact and behaviour of major faulting (together with folding) varying across London (fig 2.31).

The southern London Basin is situated above a crustal interface between the stable ABM/London Platform and the weak RHZ terrane (fig. 2.1-2.4). This has caused the underlying basement along this margin to be repeatedly tectonised, with both Variscan and post-Variscan faulting anticipated. Crucially, these terranes have regionalised mechanical responses to tectonism and, by extension, governed the distribution of both faulting (fig. 2.3-2.8) and deposition (fig. 2.17; 2.9-2.14).

From the Late Cretaceous-to-Palaeogene, southern England was subjected to an interplay between sea level change, deposition and denudation, episodic Alpine compressive phases and fault activity, and epeirogeny. The stable London Platform remained an intermittent depocentre whilst the Weald Basin progressively inverted. Alpine compression eventually culminated during the end-Pyrenean Phase with the overlying sedimentary cover being folded into the London Basin syncline.

The majority of London's structures are relatively minor and indicate low confining stresses in the Late Cretaceous-Palaeogene cover. The contrasting scale and complexity of its major faulting imply that these are basement faults that reactivated and propagated during the Alpine Orogeny but this has not been validated yet (§2.2.3). This inheritance mechanism is appraised in Chapter 3 to determine whether major faults represent reactivated basement structures or Alpine new shears.

3. The origin of major faulting in London

A rockmass accommodates compressive stresses by generating new brittle and/or plastic structures or exploiting pre-existing weaknesses. As shown in Chapter 2, London's major faults are a product of Alpine compression, but their origins are unclear. A tectonic framework was developed (fig. 3.1) from §2.1.1 for the southern London Platform and its cover prior to the main Pyrenean Phase to conceptualise the potential fault mechanisms (new shear vs. inheritance). It comprises a thin, weak sedimentary cover resting upon the shallow basin-platform interface, where four basement fault sets are anticipated.

A basement fault origin is suspected but not validated (§2.2.3). For this to occur, fault reshearing must be kinematically feasible and mechanically more preferential than Alpine new shear development. Comparisons with conventional Alpine inversion responses demonstrate that both mechanisms are plausible (fig. 3.2). However, it would be inappropriate to rely on this since London's tectonic framework is structurally distinct from extensional basins (§2.1.1).

Chapter 3 investigates the validity of an inheritance mechanism by firstly determining whether these basement faults could reactivate, and secondly identifying propagation evidence in the Cretaceous-Palaeogene cover. If both are invalid, then London's major faults must be new shears. The Alpine reshear feasibility of basement faults were assessed from case studies across the British Isles (§3.1) and kinematic analyses of anticipated fault sets (§3.2). Direct and indirect evidence of fault inheritance from within and around London were compared with known propagation mechanisms (§3.3). The outputs were discussed to assess how Alpine stresses were accommodated in the London Basin (§3.4).

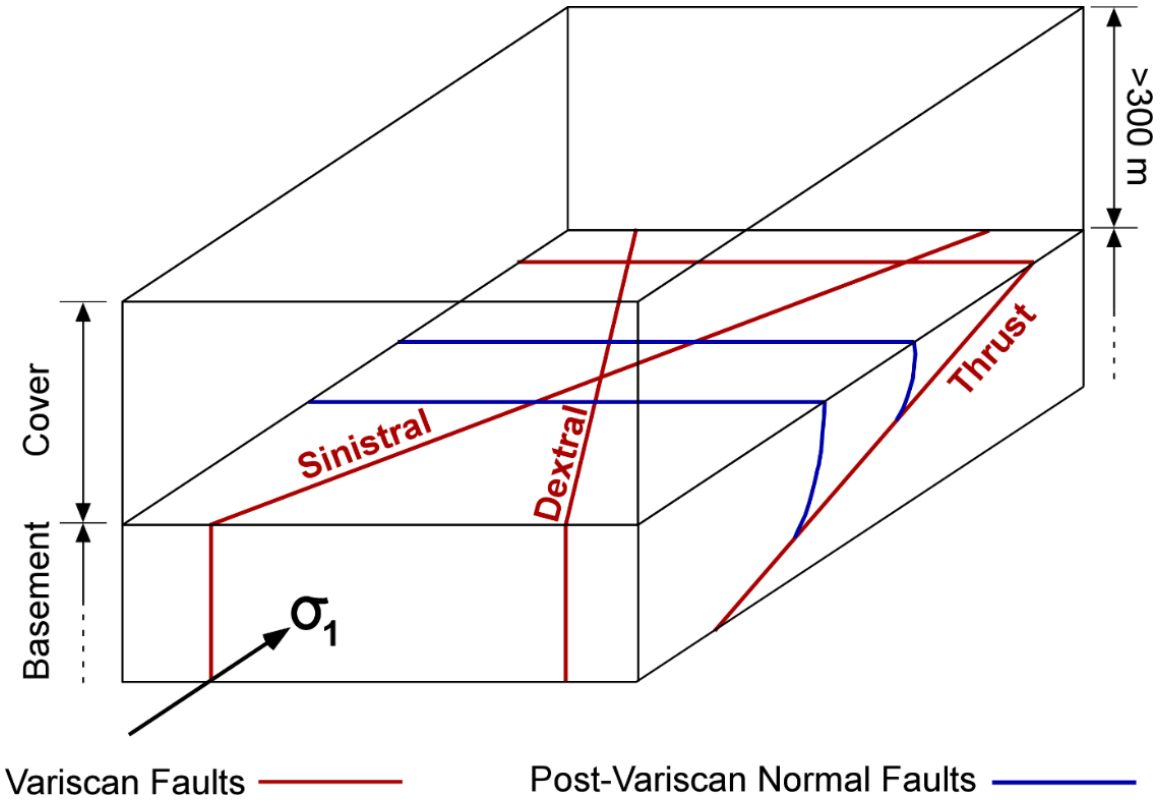

Figure 3.1 – Mechanical schematic of the key structural components that may control Alpine deformation along the southern London Platform margin: a Palaeozoic basement containing weak four fault sets, overlain by a cover of weak Late Cretaceous-Palaeogene sediments.

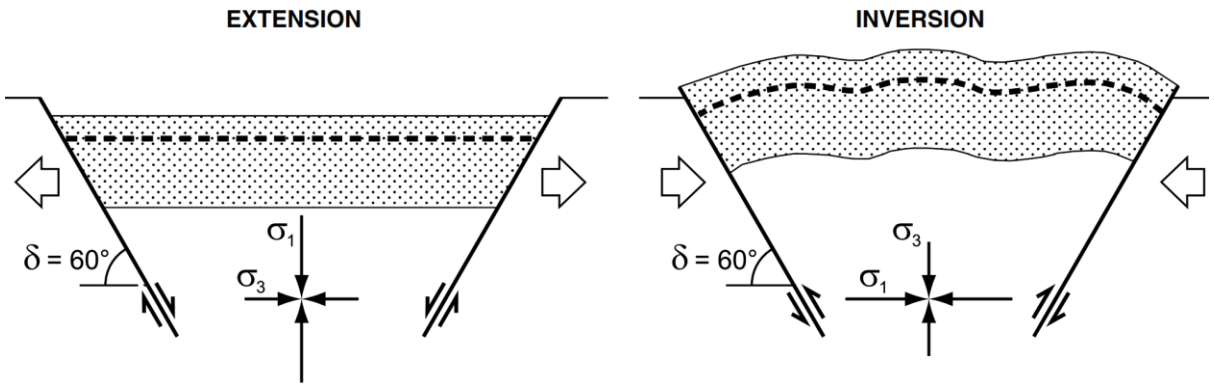

Figure 3.2 – Inversion of a formerly extensional basin. Compression is accommodated through reshearing and reversal of basin-bounding normal faults, and the bulk shortening of the internal fill through brittle and ductile mechanisms. Adapted from Bonini et al. (2012).

3.1 Evidence for Alpine reactivation of basement faulting across the British Isles

Published evidence of Alpine-induced reactivation of exposed and/or buried basement faults across the British Isles were collated to determine which pre-Alpine fault sets were susceptible. These are plotted in figure 3.3 with additional details about their tectonic fabrics and reactivation behaviour summarised in table 3.1. It demonstrates that fault sets from all compressional and extensional Palaeozoic-to-Mesozoic tectonic events (§2.1.0.2-3) could reactivate under Alpine compression.

The basement under London is anticipated to contain Variscan thrusting and strike-slip, and Mesozoic normal, fault sets (§2.1.1). Reshearing of these sets therefore provide proxy evidence for their reactivation under London (fig. 3.1). However, the transferability of these mechanical responses to London's basement is limited by two considerations.

Firstly, these do not account for the spatiotemporal evolution of the Alpine stress field imparted on the British Isles and regionalised susceptibility to it (§2.1.2). Aside from Wessex and Weald Basin structures (Parrish et al., 2018), it is unclear which compressive Phase(s) these reactivations are attributable too. Furthermore, plume-related associated uplift in the northern Britain would influence reshear conditions by increasing σ_V and reduce comparability with behaviour in southern Britain.

Secondly, elevated fluid pressures within inverting sedimentary basins (fig. 3.2) will make normal fault reshear and reversal kinematically efficient and favourable (Turner and Williams, 2004), reducing the applicability of these observations to structural domains that are not basins.

Consequently, it would be inappropriate to rely solely on these observations as they may reflect local tectonic conditions that could be absent from the southern margin of the London Platform (fig. 3.1).

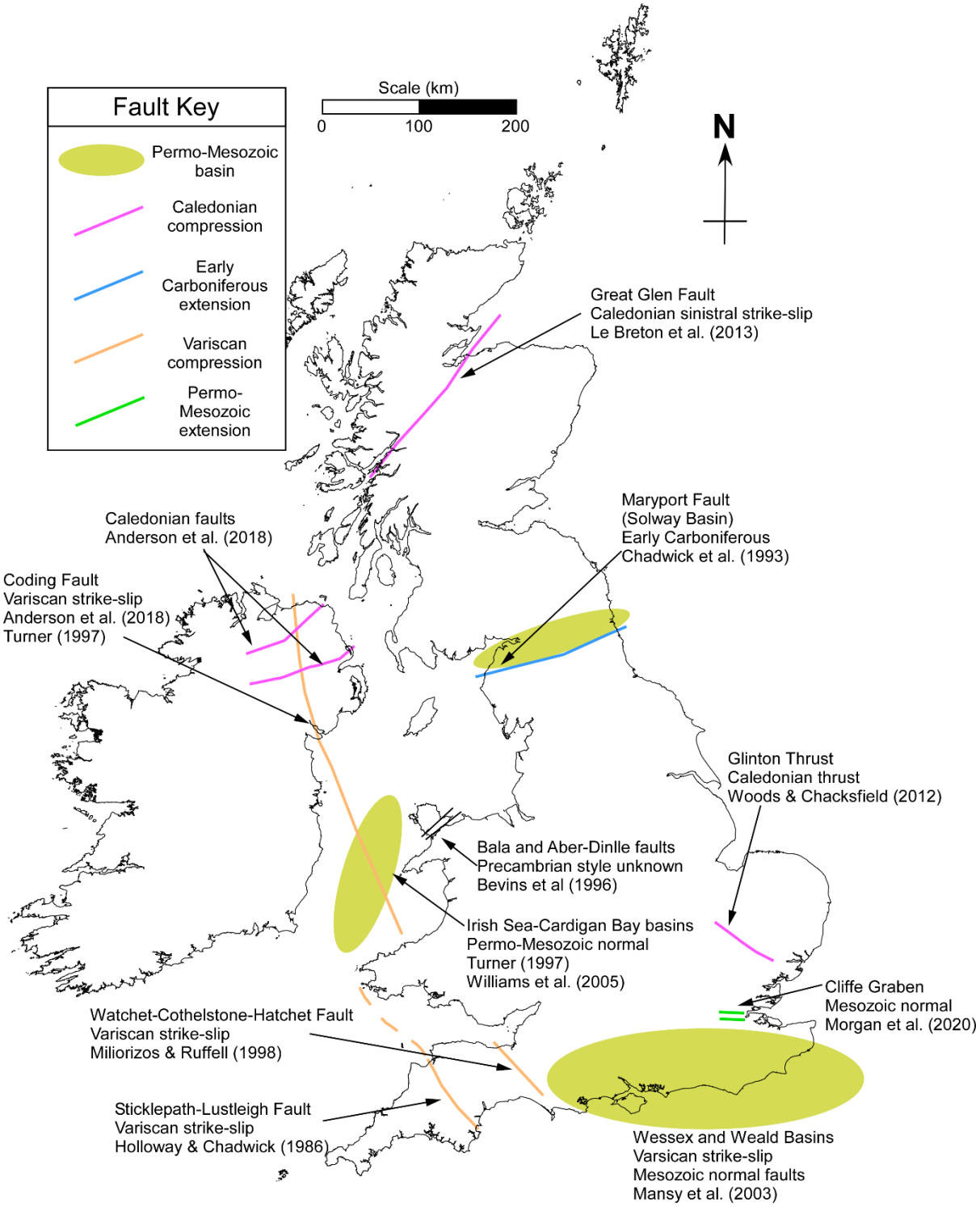

Figure 3.3 – Published evidence of Alpine reactivation of buried and/or exposed basement faults across the British Isles. Structures are coloured according to their originating tectonic event with additional information provided in table 3.1. Structure locations are approximate. British Isles base map extracted from the European Environment Agency's (2017) Europe coastline shapefile and transformed to British National grid.

Table 3-1 – Structural information about identified Alpine-reactivated basement faults across the British Isles (figure 3.3) from pre-Alpine tectonic events §2.1. Reshear style is approximate with oblique-slip components expected for all faults as coaxiality with the Alpine stress field(s) was highly unlikely. Nomenclature for fourth column: Precambrian – PC, Caledonian – C, Early Carboniferous extension – EC, Variscan – V, Permo-Triassic extension – PT, Jurassic-Early Cretaceous extension – JEC.

Source	Region (Approx.)	Tectonic fabric(s) present (§2.1)	Fault type(s) reactivated	Fault trends	Reactivation Style
Mansy et al. (2003)	Southern England basins	Variscan	Dextral Strike-slip (V)	NW-SE	Dextral
		Jurassic-Early Cretaceous	Normal (JEC)	E-W	Reversal
Chadwick et al. (1993)	Solway Basin (Northern England)	Caledonian Early Carboniferous Permo-Triassic Jurassic-Early Cretaceous	Normal (EC)	ENE-WSW	Reversal
Miliorizos and Ruffell (1998)	Southwest England	Variscan	Dextral Strike-slip (V) (postulated)	NW-SE	Sinistral (postulated)
Holloway and Chadwick (1986); Cosgrove et al. (2021)	Southwest England	Variscan	Dextral Strike-slip (V)	NW-SE	Sinistral
Bevins et al. (1996)	Northwest Wales	Late Precambrian	Unclear	NE-SW	Sinistral
Turner (1997); Williams et al. (2005)	Irish Sea-Cardigan Bay Basin	Caledonian Variscan Post-Variscan extension	Normal (PT or JEC)	NE-SW	Sinistral
			Dextral Strike-slip (V)	NW-SE	Dextral
Anderson et al. (2018)	Northern Ireland	Caledonian Variscan	Unknown Strike-slip (C)	NE-SW	Sinistral
			Dextral Strike-slip (V?)	NNW-SSE	Dextral
Le Breton et al. (2013)	Scottish Highlands	Caledonian (Great Glen Fault)	Sinistral Strike-slip (C)	NE-SW	Dextral
Woods and Chacksfield (2012)	East Anglia	Probable Caledonian	Thrust (C)	NW-SE	Original
Owen (1971); This study.	London	Jurassic-Early Cretaceous	Normal (JEC)	E-W	Reversal

3.2 Kinematic assessment of basement fault reshear feasibility during the Alpine orogeny

Only if reshearing was kinematically feasible can London's major faults be products of inheritance. Proxy evidence (fig. 3.3), despite their limitations, imply that Alpine reshearing was likely feasible. Kinematic analyses were undertaken to assess these inferences, with assumptions made to better represent local conditions. Two-dimensional reactivation studies were conducted under the three main Alpine Phases that affected London to determine how the evolving stress field affected reshear behaviour. §3.2 presents 2D fault reactivation theory, methodology and assumptions of their kinematic analyses, the results for each basement fault set, and the limitations of this assessment. The results were discussed and compared with basement fault reactivation in southern Britain to appraise the proposed Alpine reshear behaviour.

3.2.1 Fault reactivation theory

As brittle shear planes, the genesis and reshearing of faults can be idealised through Mohr-Coulomb theory. The section provides an overview of the mechanical principles of 2D fault reactivation theory under a Mohr-Coulomb framework, and the frictional properties of faulting.

3.2.1.1 Mechanical theory

A 2D schematic comparison between new shear development and the reactivation of a pre-existing one is present in figure 3.7. The generation of new brittle shear under Mohr-Coulomb conditions (fig. 3.4.a) will generate a shear plane inclined at θ_i to the σ_1, the orientation of which is dependent on the material's internal angle of friction (ϕ_i) and the applied differential stress (σ_1-σ_3) axis. The orientation of a pre-existing fault (θ) relative to a later σ_1-axis will dictate whether reshearing maintains the original slip sense or reverses it (fig. 3.4.b-c).

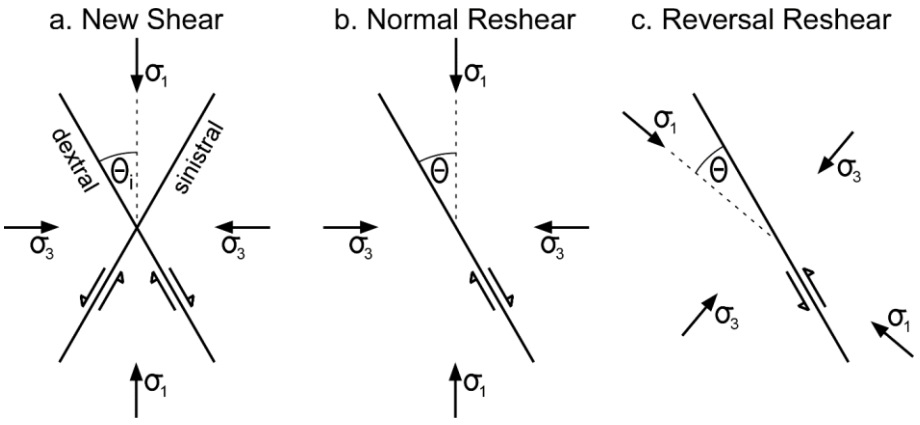

Figure 3.4 – New brittle shear development vs. reshear behaviour of a pre-existing plane inclined at θ to the applied stress field, the orientation of which will determine the style of reshear.
a. A shear developed under Mohr-Coulomb conditions will form at θ_i to the σ_1-axis.
b. Reshear of a pre-existing shear plane under the same shear sense as its initial formation.
c. Reverse shearing on the pre-existing plane due to the alignment of the stress axis.

Sibson (1974) mathematically analysed the stress and frictional requirements of Andersonian fault reaction under Mohr-Coulomb conditions. An optimal reactivation angle (θ*) was identified that is dependent upon the fault's frictional properties (μ, frictional sliding coefficient) and the acting fluid pressures. Sibson (1985, 1994) developed a 2D mathematical relationship for the reshearing of cohesionless fault plane inclined along the maxima (σ_1) and minima (σ_3) stress axis (eq. 3.1). Stress is expressed as a ratio (σ_1/σ_3), enabling the differential stress (σ_1-σ_3) to be quantified without *a priori* knowledge of their respective magnitudes. This produces a negative parabolic relationship between the acting stresses and the relative inclination of the fault plane, referred to as the reactivation profile (fig. 3.5). The minimum differential stress conditions for reshearing are achieved at the apex of the parabola, when θ fulfils θ* conditions (eq. 3.2). For sliding to occur at a specific θ, (σ_1/σ_3) must be greater than or equal to the profile. Reshear becomes progressively less efficient as θ deviates from θ*, with frictional lock-up achieved when θ = 0° or = 2θ*, as (σ_1/σ_3) → ∞.

$$\left(\frac{\sigma_1}{\sigma_3}\right) = \frac{(1 + \mu \cdot \cot\theta)}{(1 - \mu \cdot \tan\theta)} \qquad Equation\ 3.1$$

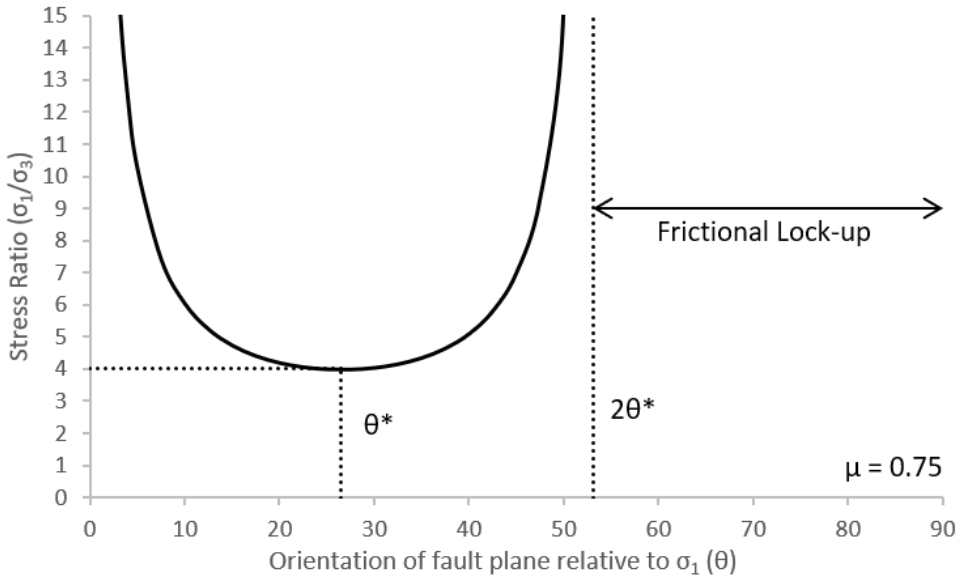

Figure 3.5 – Reactivation profile for a fault plane with a frictional sliding coefficient (μ) of 0.75. Reproduced from Sibson (1985).

$$\theta^* = 0.5 \cdot tan^{-1} \cdot \left(\frac{1}{\mu}\right) \qquad Equation\ 3.2$$

Sibson (1990b) revised the reactivation profile to allow direct determination of the required differential stress confitions (σ_1-σ_3) instead of the stress ratio (eq. 3.3). This also produces a negative parabolic relationship, but it requires *a priori* knowledge of the vertical stress axis (σ_V').

$$(\sigma_1 - \sigma_3) = \mu \cdot \left[\frac{(tan\,\theta + cot\,\theta)}{(1 - \mu \cdot tan\,\theta)}\right] \cdot \sigma_v' \qquad Equation\ 3.3$$

Sibson (1990a, 1990b) introduce nomenclature to describe fault plane's susceptibility for reshear depending upon θ. Sibson noted that at θ = ± 15° from θ*, reactivation requires a 50% increase in differential stress conditions from optimal conditions. Within this range faults are "*favourably oriented*"; beyond this they are "*unfavourably oriented*". Faults oriented at θ ≥ 2θ* undergo frictional lock-up and are "*severely misoriented*".

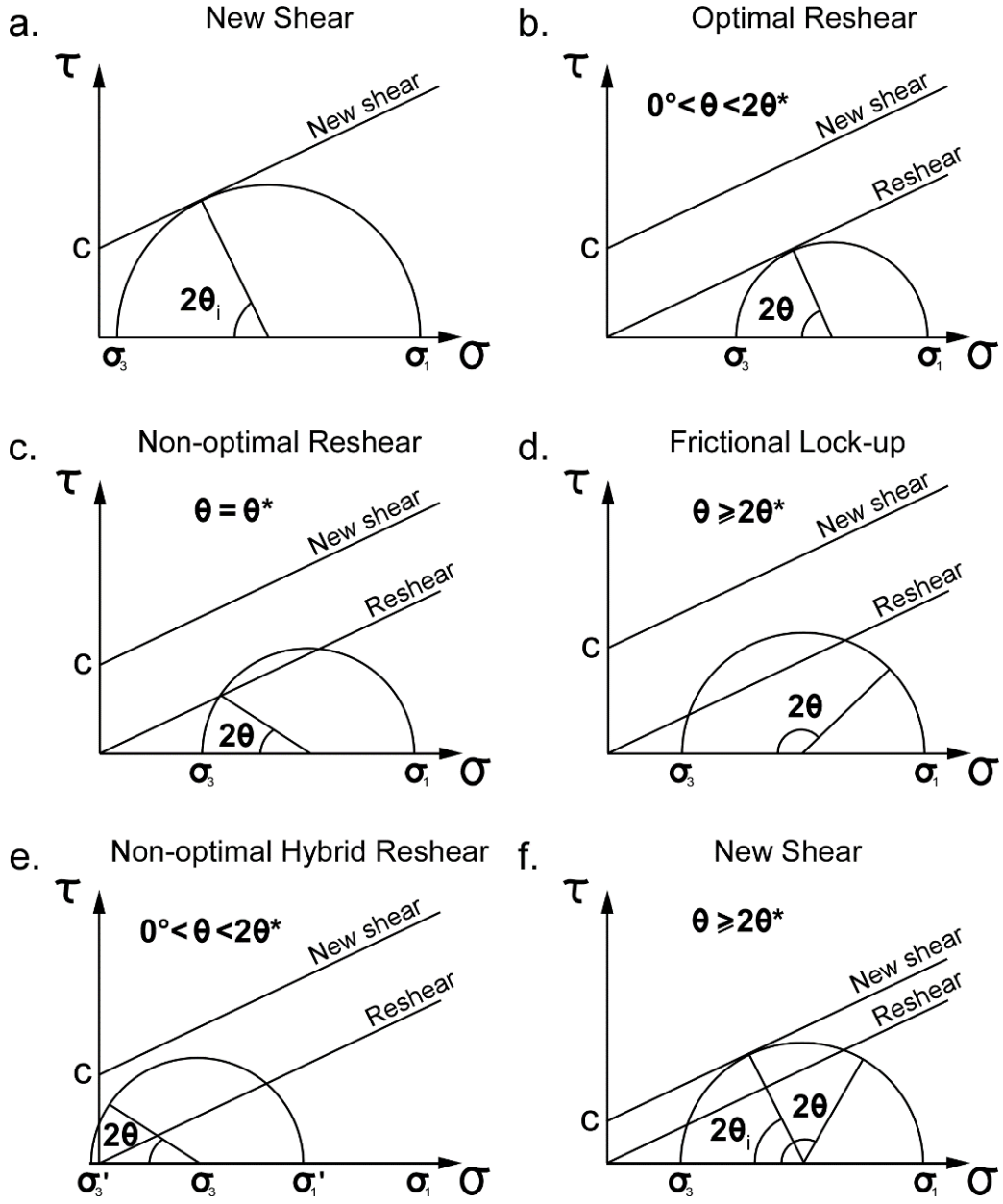

Figure 3.6 – The feasibility of new fault development vs. fault reshearing under an applied stress field in Mohr-Coulomb space is dependent upon the pre-existing plane's orientation (θ), and the respective shear strengths of both the fault and intact rock. Parts a-e adapted from Sibson (1985).
a. New shear development under Mohr-Coulomb conditions (fig. 3.4.a).
b. Optimal reactivation of the plane (θ = θ*), requiring the minimum (σ_1-σ_3) conditions.
c. Non-optimal reshearing when 0° > θ > 2θ* is achieved but not θ = θ*.
d. Frictional lock-up occurs when the fault plane is aligned at θ = 0° or θ ≥ 2θ*.
e. Elevated fluid pressures causing $\sigma_3' < 0$, enabling dilational hybrid reshearing of the fault plane.
f. Conditions when new shear development is mechanically more favourable than reshear.

For a fault to reactivate, it must be mechanically more favourable than new shear development. The stress conditions for various new shear and reshear scenarios have been plotted in Mohr-space in figure 3.6. Both the failure and reshear envelopes share the same friction angle ($\phi_i = \phi$), with the former being cohesive (c) also. In an unfaulted rock mass, a new brittle shear will develop at θ_i to the σ_1-axis (fig. 3.4.a) when the Mohr-circle intercepts the failure envelope with an arc ($2\theta_i$) normal to the line (fig. 3.6.a). The orientation of a pre-existing plane (θ; fig. 3.4.b-c) will dictate the positioning of the arc 2θ, with reactivation only feasible when it intercepts the reshear envelope. θ^* is achieved when this arc is normal to the envelope, with the required (σ_1-σ_3) to reshear increasing as θ deviates from θ^*. Eventually $\theta \geq 2\theta^*$ is achieved (fig. 3.6.d) and frictional lock-up occurs (fig. 3.5).

Elevated fluid pressures will improve reshear favourability by inducing effective stresses conditions (σ_1'-σ_3' < σ_1-σ_3), causing the Mohr-circle to laterally migrate towards the origin with the σ_3'-value dictating the reshearing style: normal reshear when ($\sigma_3' > 0$) (fig. 3.6.b), or dilational hybrid reshearing when ($\sigma_3' < 0$) (fig. 3.6.e). The latter enables locked faults ($\theta \geq 2\theta^*$) to reshear also (Sibson, 1990b). Sibson (2009) expressed fluid pressure in the reactivation profile using the pore fluid factor[15] (λ) (fig. 3.7). The profile flattens as $\lambda \rightarrow 1$: reductions in effective stresses cause reactivation to become more favourable across a broader θ-range at lower (σ_1'-σ_3').

Progressive deviation from θ^* will cause new shear development to become mechanically more efficient as unfavourably oriented faults will eventually require greater (σ_1-σ_3) conditions (fig. 3.6.f). Sibson (2009) incorporated new shear favourability into the reactivation profile by integrating intact shear strength (fig. 3.7). Referring initially to $\lambda = 0$, the reshear window has narrowed to within ± 20° of θ^*. Beyond this (σ_1-σ_3) will induce new shearing by satisfying the conditions of figure 3.6.f. This window progressively widens as $\lambda \rightarrow 1$.

[15] Hubbert & Rubey (1959) developed pore fluid factor (λ) to express the fluid pressure relative to the lithostatic pressure: λ = fluid pressure / σ_V

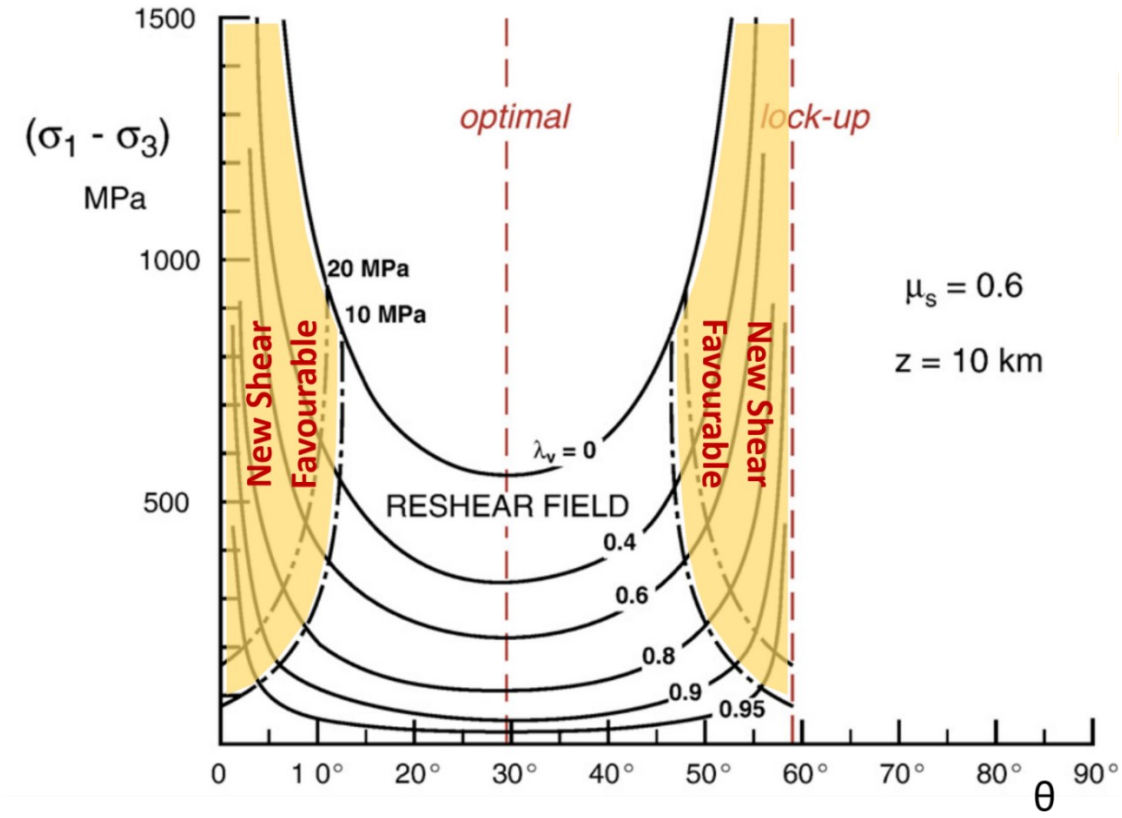

Figure 3.7 – Reactivation profile demonstrating the influence of fluid pressure as expressed by the pore fluid factor (λ) and the intact rock shear strength (yellow windows) upon reactivation behaviour and feasibility. The plot has been simplified from Sibson's initial assessment to assume the rock is of 'moderate competence' only, with T = 10 MPa. The differential stress conditions are expressed as (σ_1-σ_3) (eq. 3.3). Intact rock shear strength was determined using composite Griffith-Coulomb failure criterion developed by Sibson (1998). Adapted from Sibson (2009).

3.2.2.2 Frictional properties of faults

In brittle mechanics, friction is the component of shear strength affected by the applied stress field (Mandl, 2000). For a pre-existing shear plane this is governed by its frictional sliding angle (ϕ) and is expressed by Sibson as its coefficient (μ, eq. 3.4). The plane's frictional properties will dictate the reactivation profile's parabola (figure 3.8; table 3.1), and the positions of θ* and 2θ* (eq. 3.1, 3.3). Weaker faults reactivate more easily across a broader θ range as decreasing μ will flatten the profile, causing θ* to migrate towards 45° and require lower (σ_1/σ_3). Consequently, the selected μ-value will significantly affect the reactivation feasibility assessments. However, the frictional properties of faults are debated with multiple ranges proposed from lab testing and geophysical analyses. These were reviewed to inform the frictional coefficient value used for this investigation.

$$\mu = tan^{-1}\varphi \qquad Equation\ 3.4$$

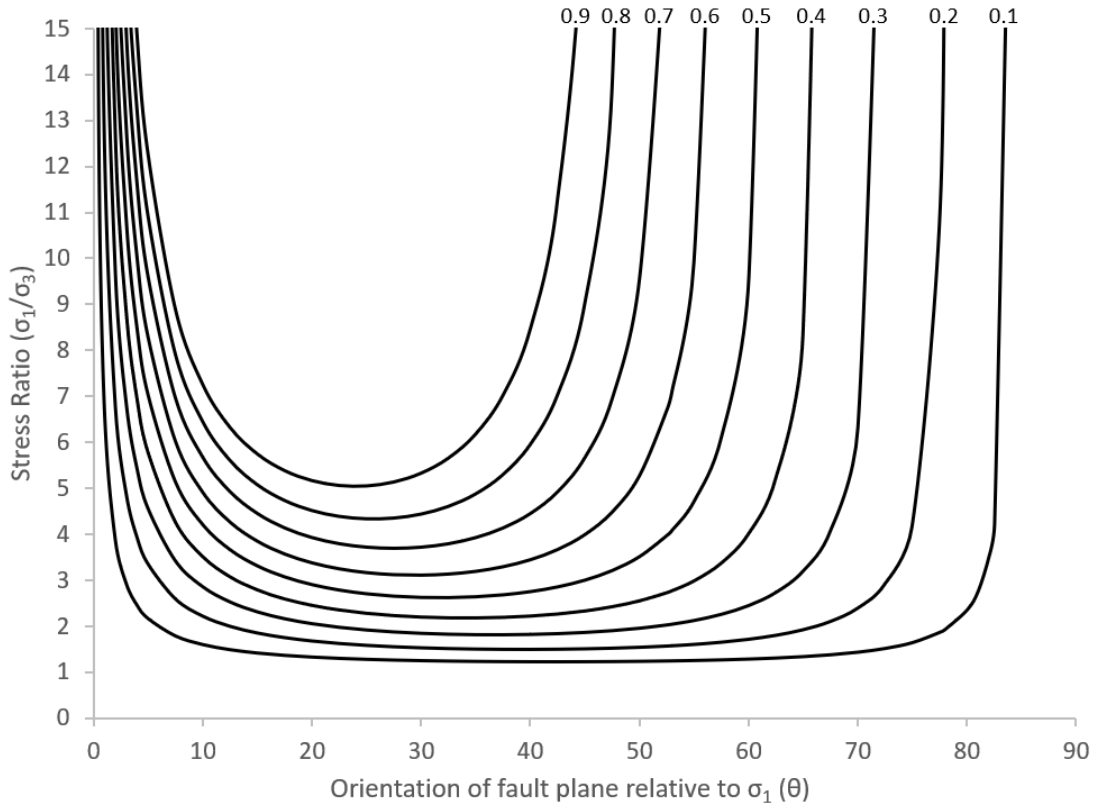

Figure 3.8 – The influence of friction (μ) on fault reshear feasibility. Weaker faults require lower (σ_1-σ_3) conditions to reshear across a broader range of θ. Refer to table 3.2 for values.

Table 3-2 – Implications of fault plane friction on the optimal reshear and lock-up conditions.

Frictional sliding parameters		**Optimal reactivation parameters**		**Frictional lock- up, 2θ* (°)**
Frictional sliding angle, ϕ (°)	**Frictional sliding coefficient, μ**	**Inclination of fault plane, θ* (°)**	**Stress ratio for reshearing (σ_1/σ_3)***	
5.7	0.1	42.1	1.2	84.3
11.6	0.2	394	1.5	78.7
17.7	0.3	36.7	1.8	73.3
24.2	0.4	34.1	2.2	68.2
31.3	0.5	31.7	2.6	63.4
39.2	0.6	29.5	3.1	59.0
48.3	0.7	27.5	3.7	55.0
59.0	0.8	25.7	4.3	51.3
72.2	0.9	24.0	5.0	48.0

Barton (1973) identified a broad frictional range for clean faults without any filling (ϕ = 20-80°) from surface roughness, whilst reviewing the shear strength of 'rock joints' (an all-encompassing term for "[clean] *mechanical discontinuities of geological origin"*). This range was associated with several mechanisms[16] that will affect the discontinuity plane's roughness and shear behaviour. The degree of strain accommodation was considered most significant for clean fault friction (fig. 3.9). Through continued shearing from peak strength, ϕ will progressively decrease until residual strength is achieved. This residual frictional angle window is significantly weaker (ϕ_r = 23-39°).

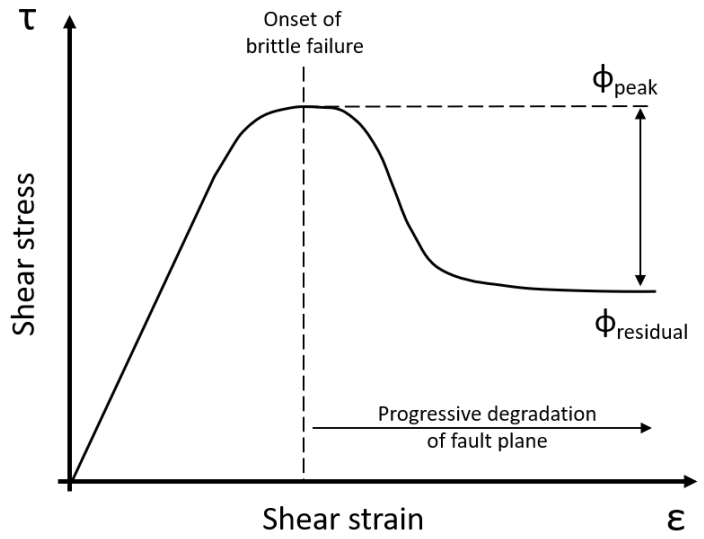

Figure 3.9 – Idealised stress-strain curve for the generation of a clean fault plane with no infilling. The initial brittle failure will form a rough surface with asperities at peak strength. Progressive shearing will cause asperite degradation and plane smoothening until residual strength is achieve.

Byerlee (1978) characterised clean fault surfaces to propose a frictional window of ($\phi \approx$ 40-65°) from published experiments[17], civil and mining engineering, and geophysical data. Friction was partly dependent on confining stresses as surface roughness becoming less influential with increased normal stress, and (in general) independent of lithology, and to a lesser extent, sliding velocity, roughness, and temperature. Byerlee's Law is widely applied in geology, particularly for estimating fault strength and seismicity (Scholz, 2002), with Sibson (1994) identifying agreement between the frictional window and lock-up conditions from field data[18] (fig. 3.6.d). Sibson concluded that the reshearing of unfavourably oriented faults reflected elevated fluid pressures (fig. 3.7, $\lambda > 0$) under Byerlee conditions, rather than "*anomalously low-friction material*" on the fault plane.

[16] Peak vs. residual strength, weathering, water, the diminishing influence of asperities at higher confining pressures, and very low normal stresses

[17] Tilt testing of sawed surfaces and natural clean discontinuity surfaces.

[18] Sibson applied structural data from all fault styles to the reactivation profile (fig. 3.5) and assumed that the faults were both cohesionless and had achieved frictional lock-up ($2\theta^*$).

The above analyses of frictional sliding of faults have focused on clean faults (fig. 3.10.a) through experimentation and mechanical assumptions, and do not account for plane degradation other than by smoothening. Instead, fault cores are likely to develop granular fault breccias and clay-rich gouges (fig. 3.10.b) through comminution and cataclasis, respectively. Consequently, the fault's frictional properties may be lower than Byerlee's window, reflecting their mechanically degraded interiors.

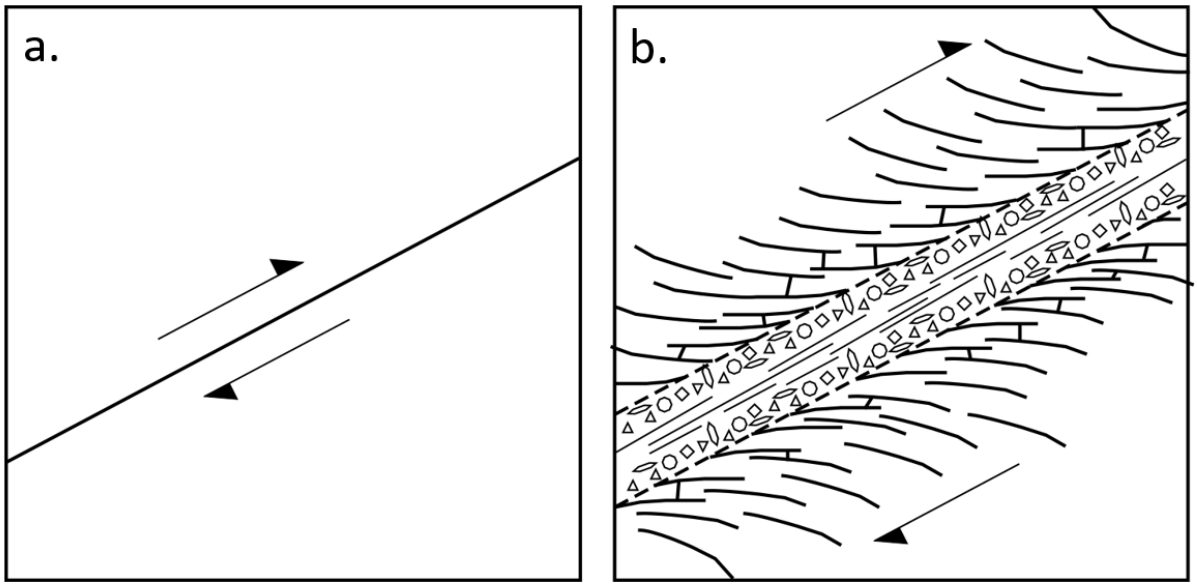

Figure 3.10 – End members of macroscopic fault textures observed within rock masses.
(Scales are intentionally avoided for both figures).
a. 'Clean' faults: Single shear plane with no degradation of the host rock.
b. Development of a brittle damage zone around the central fault core, comprised of a cataclasis breccia bands surrounding a central comminuted gouge.

Research on fault strength behaviour has progressively shifted to the geological and geophysical assessment of actual faults or representative tests to reflect the presence of weaker materials.

Lab testing demonstrates that clay-infillings and gouges are considerably weaker than clean planes, with strength partly dependent on mineralogy (Byerlee, 1978). Lockner and Beeler (2002) proposed a μ = 0.1-0.6 fault gouge window by crushing 15 different minerals and shearing between blocks. Variation between and within mineralogies was identified also, reflecting sensitivity to confining stresses, temperature, and water (for expandable clays). Lockner et al. (2011) demonstrated that natural faults are much weaker by testing clay-rich fault core ($\mu = 0.15$) extracted from the San Andreas Fault.

Copley narrowed this range through indirect analyses of actual faults. Middleton and Copley (2014) calculated $\mu < 0.3$ (and potentially ≤ 0.1) from seismic focal mechanisms of recently active continental faults globally. Copley and Woodcock (2016) inferred $0.24 > \mu > 0.02$ from numerical strength analysis of the Variscan inversion of Early Carboniferous normal faults. Copley (2017) finally proposed that 0.3

> μ > 0.05 was an appropriate frictional range for natural faults following a thorough comparison of indirect geophysical inferences, geological observations, and borehole and laboratory testing. He concluded a situation of "*weak faults embedded in strong surroundings*".

The debate has progressed from 'strong vs weak faults' (fig. 3.10.b) to recognise their complexity. Collettini et al. (2019) emphasised fault structural and frictional heterogeneity, and that fluids chemically deteriorate fault planes by locally replacing strong minerals with weaker phyllosilicates-rich zone[19]. They determined that these clay/mica-rich faults are weak (0.3 > μ > 0.1) (fig. 3.11).

The frictional properties of the fault will determine both the θ-range where reshear is favourable and the required (σ_1-σ_3) (fig. 3.8). Fault strength characterisation has progressed from idealised tests to the assessment of actual faults coupled with recognised internal complexities. The outputs are summarised here as two friction windows: Byerlee's high friction (0.85 > μ > 0.6) & Copley's low friction (0.3 > μ > 0.05). The latter is considered more representative of natural faults.

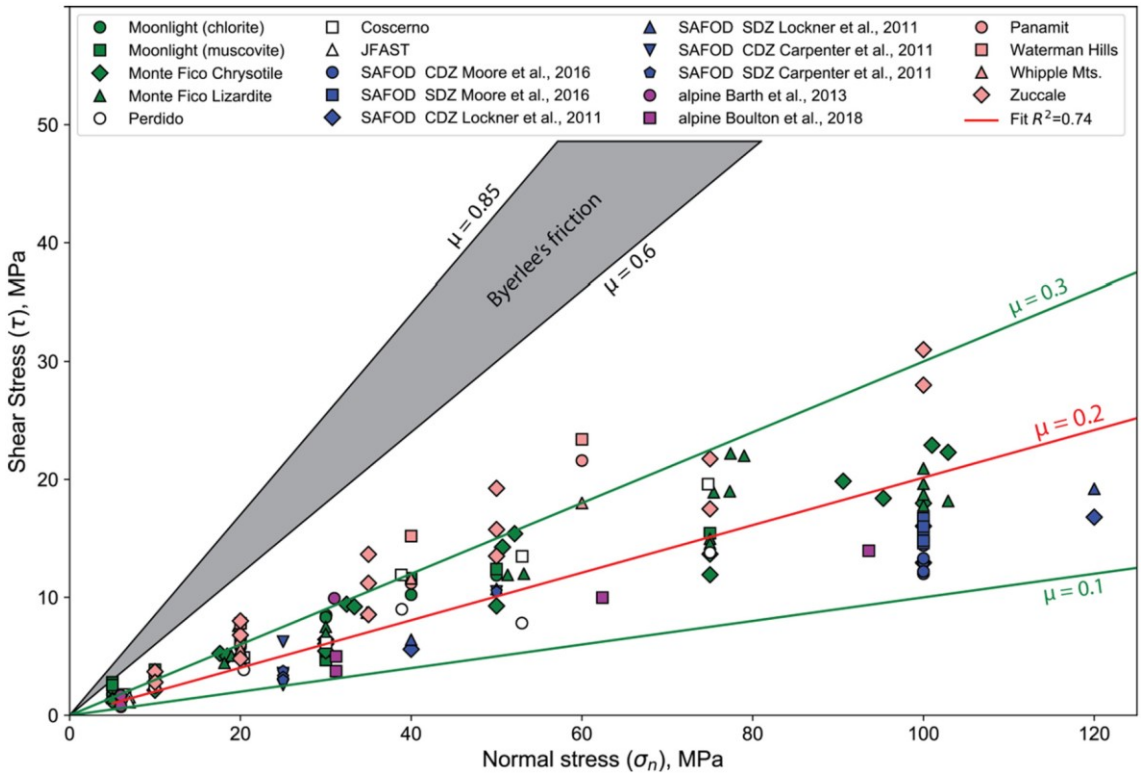

Figure 3.11 – Frictional coefficients of phyllosilicate-rich (micas & clays) faults determined from their laboratory testing, with a frictional window of 0.3 > μ > 0.1 proposed. From Collettini et al. (2019).

[19] Recent literature on fault strength avoids defining these clay-rich zones as gouge, emphasising heterogeneity rather than implying the interior of the fault core (e.g., fig. 3.10.b)

3.2.2 Methodology and analysis assumptions

Sibson's (1985) reactivation profile was used to assess the kinematic feasibility of Alpine reactivation of the basement fault sets (fig. 3.1). The strike-slip and dip-slip sets were assessed separately to satisfy their differing σ_1-σ_3 axis requirements under 2D analysis. These were conducted for the three Alpine Phases that affected London, with Laramide Phase ignored (§2.1.2).

The methodology is outlined below:

1. The reactivation profile was produced for the chosen coefficient of friction, $\mu = 0.3$.
2. For each fault set, determine θ from the intersection angle between the fault strike and the σ_1-axis of each Phase (fig. 3.4.b-c):
    a. For strike-slip faults, all three Phases were calculated for.
    b. For dip-slip, only a single 'hybrid' Subhercynian-Pyrenean Phase was assessed due to issues associated with fault-stress field axis coaxiality of the later Helvetic Phase.
3. Calculate the corresponding stress ratio (σ_1/σ_3) requirements (eq. 3.2) and tabulate.
4. Plot the results on the reactivation profiles and 2D mechanical slip schematics. The former assesses required stresses for shear, and the latter characterises the reshear style.

Several assumptions were required to satisfy the conditions for 2D mechanical reshear analysis: reactivation profile method, fault strength, fluid pressures, fault set geometries, Alpine Phase palaeostress axes, coaxiality idealisation.

3.2.2.1 Reshear analytical method

Two methods were outlined for calculating the reactivation profile: stress ratio (σ_1/σ_3, eq. 3.1) vs differential stress ($\sigma_1-\sigma_3$, eq. 3.3). The latter method is inappropriate as it requires the Alpine stress magnitudes, fluid pressures and depth of reshearing to be defined *a priori* (Sibson, 2009). As the analyses were retrospective these cannot be accurately quantified. The stress ratio method was selected, requiring the fault plane's friction (μ) and orientation (θ) to be defined only.

3.2.2.2 Fault strength

A frictional sliding coefficient of $\mu = 0.3$ was adopted following the fault strength review as weaker materials are anticipated for all basement fault sets due to their previous tectonic histories (§2.1). This value is conservative and represents the upper bound limit for natural fault strength (fig. 3.11); however, this was considered appropriate as fault inaccessibility prevents their direct testing.

3.2.2.3 Fluid pressures

The influence of fluid pressures was ignored as they could not be retrospectively constrained. However, elevated pressures above hydrostatic are anticipated.

3.2.2.4 Fault set geometries

Price (1966) defined a 'set' to be discontinuities of the same tectonic origin that follow planar, sub-parallel arrangements, thus forming a systematic orientation.

Four fault sets are anticipated in the basement: Variscan thrust set and conjugate strike-slip pair, and a Mesozoic normal fault set (fig. 3.1). Their geometries were inferred (table 3.3) by coupling published fault strikes from proxy regions with idealised dips dependent on their styles. The distinct geometries of each fault set will affect their respective reactivation feasibility and slip behaviour.

For analytical simplicity, all fault sets are assumed to follow constant planar geometries. From these trends, the palaeostress conditions of each pre-Alpine tectonic regime that affected the southern margin of the Anglo-Brabant Massif/London Platform were inferred (fig. 3.12).

Table 3-3 – Inferred basement fault sets geometries from published strikes in proxy regions that were affected by the same tectonic events, and idealised fault dips.

Tectonic origin	Fault set	Analysis group	Strike (°) (measured)	Dip (°) (ideal)	Proxy region	Sources
Late-stage Variscan	Dextral strike-slip	Strike-slip	160	Vertical	Pembrokeshire, Wales	Dixon and Strahan (1977), via Woodcock et al. (2014)
	Sinistral strike-slip		030	Vertical		
Early-stage Variscan	Thrust	Dip-slip	100	30	Gower, Wales	British Geological Survey (1977, 2002), via Wright et al. (2009)
Jurassic-Early Cretaceous extension	Normal		095	60	Southern England (unexposed)	(Chadwick, 1986)
					Bristol Channel Basin	Nemčok et al. (1995)

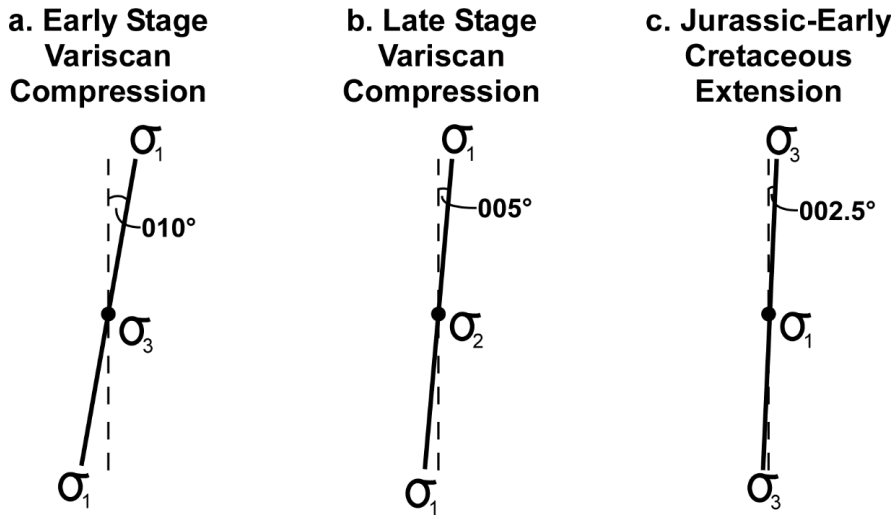

Figure 3.12 – Palaeostress orientations (± 10°) for pre-Alpine tectonic regimes in southeast England, as inferred from fault trends (table 3.3). Updated from Morgan et al. (2020, fig. 12) with data sources amended to be better reflect regional Jurassic-Early Cretaceous extension.
a. Thrust regime during early-stage Variscan orogeny.
b. Strike-slip regime during the late-stage Variscan orogeny.
c. Extensional regime during Jurassic-Early Cretaceous.

3.2.2.5 Alpine Phase palaeostress axes

Southern Britain was affected by four Phases of the Alpine Orogeny (§2.1.2), each with distinct stress axis alignments and magnitudes (table 3.4):

1. Subhercynian – Initiation of Alpine collision causing minor inversion in southern Britain.
2. Laramide – Unclear.
3. Pyrenean – Main Alpine tectonic phase in southern Britain, culminating in the Late Oligocene.
4. Helvetic – Minor compression and uplift.

Only three of the four Phases were assessed (Subhercynian, Pyrenean, and Helvetic), in addition to the current Neotectonic regime. The second, Laramide, Phase was not investigated due to the lack of palaeostress data, and its apparent dwarfing by contemporaneous plume-related epeirogenesis (§2.1.0.6). Calculation of θ for each fault set (fig. 3.3.b-c) throughout the evolving Alpine Orogeny required the σ_1-axis for each Phase to be determined (fig. 3.13). These were quantified from published structural and palaeostress data from southern Britain and the North Sea (table 3.4).

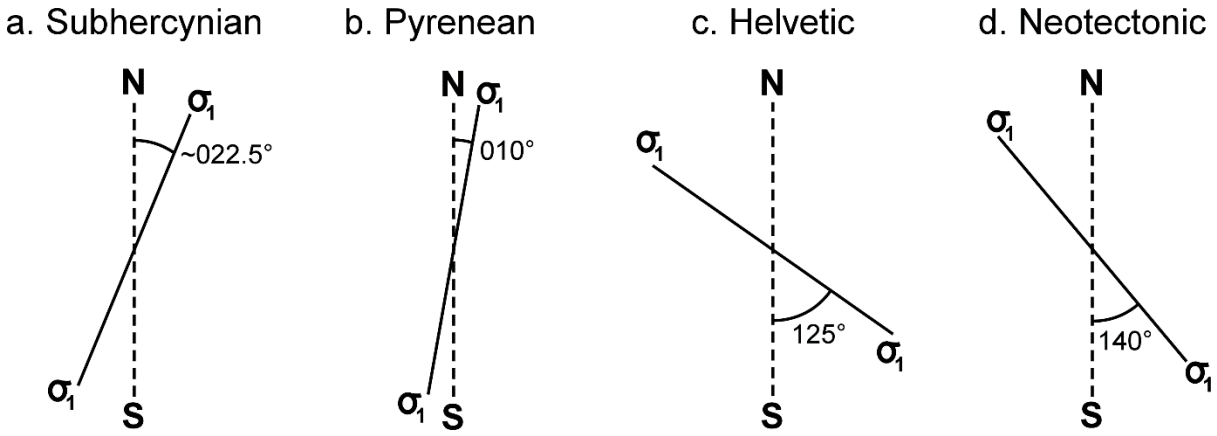

Figure 3.13 – Palaeostress for three of the four Alpine Phases and the Neotectonic regime acting on southern England. Refer to table 3.4 for the determination of these parameters.

Table 3-4 – σ_1-axis palaeostress assessment of the Alpine Phases and the Neotectonic regime, as determined from published literature. [Brackets] used to distinguish between sources.

Phase (Duration)	Orientation of σ_1 (°)	Method	Rationale	Sources
Subhercynian (Turonian – Maastrichtian)	~NNE-SWW 022.5-202.5° (approx.)	Qualitative descriptive data	• [a] NNE-SSW • [b] NNE-SSW	[a] Kley and Voigt (2008) [b] Kley (2018)
Laramide (Maastrichtian – Mid-Palaeocene)	-	-	No palaeostress data available	-
Pyrenean (Late Palaeocene – Late Oliogcene)	010-190°	Structural data	• Structurally data presented in paper is dated to the Pyrenean Phase	Parrish et al. (2018)
Helvetic (Late Oligocene – Miocene)	125-305°	Structural data	• Qualitatively described as NW-SE [b,c]. • 'Mesofractures' across southern England and northwest France [a] provided quantification.	[a] Bevan and Hancock (1986) [b] Kley and Voigt (2008) [c] Peacock (2009)
Neotectonic	140-320°	Seismic focal mechanisms	• England & Wales LSIB results used as it was geographically the most appropriate. • Approximated to Andersonian conditions.	Baptie (2010)

3.2.2.6 Fault coaxiality under 2D stress axes

The stress field and the fault geometries are restricted to the σ_1-σ_3 axis by Sibson's 2D method. This intrinsically assumes parallel alignment of the fault plane with the σ_2-axis to ignore any oblique-slip.

Strike-slip and dip-slip fault sets will require separate reactivation profiles to reflect their differing 2D slip behaviour. As the Alpine Phases were compressive regimes, $\sigma_1 = \sigma_H$ is inherent, with σ_3-axis alignment altered to accommodate the fault style being assessed (fig. 3.14, σ_1-$\sigma_3 = \sigma_H$-σ_h vs. σ_H-σ_V).

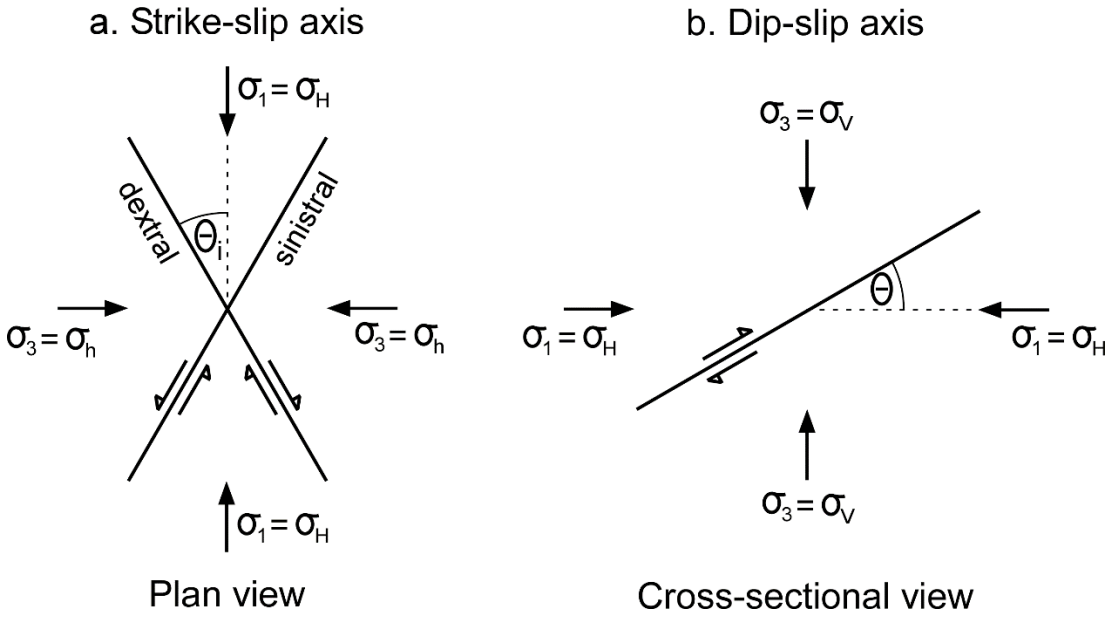

Figure 3.14 – Components of Andersonian stress axis required to achieve coaxial 2D reshear conditions for equation 3.1. In both schematics $\sigma_1 = \sigma_H$, with the σ_3-axis oriented with the minima stress for coaxial slip conditions of: a. Strike-slip ($\sigma_3 = \sigma_h$); b. Dip-slip ($\sigma_3 = \sigma_V$).

3.2.3 Strike-slip fault assessment

The results for strike-slip analyse of the Variscan strike-slip pair (table 3.5) have been presented in two forms for each Phase: the reactivation profile, and a mechanical schematic. For clarity, the members of the pair are described as the 'NW-set' and 'NNE-set', with each initially characterised by dextral and sinistral slip respectively during the Variscan.

The results describe the deviation between the Alpine Phases and the Late Variscan axis (table 3.4, 3.12.b) that generated the strike-slip conjugate pair, the kinematic feasibility of reactivating each set, and their slip sense upon reactivation.

Table 3-5 – θ and σ_1/σ_3 calculated for the Variscan strike-slip pair under each Phase of the Alpine Orogeny analysed. Negative notation is used to signify reverse reactivation of a fault.
[a] Frictional lock-up is achieved as $\theta > 2\theta^*$ for $\mu = 0.3$ (see table 3.2).

Phase	**σ_1 (°)**	**θ for Variscan strike-slip pair (°)**		**σ_1/σ_3 for Variscan strike-slip pair**	
		NW-set	**NNE-set**	**NW-set**	**NNE-set**
Subhercynian	022.5-202.5° (approx.)	42.5	7.5	1.83	3.41
Pyrenean	010-190°	30	20	1.84	2.05
Helvetic	125-305°	-35	85	1.81	∞ [a]
Neotectonic	140-320°	-20	70	2.05	6.31

3.2.3.1 Subhercynian Phase

The Subhercynian deviates ~15-20° from the Late Variscan axis, approaching coaxiality. The results are presented in figure 3.15.

Subhercynian reshear of both strike-slip faults was kinematically feasible, maintaining their original senses of shearing. The NW-set is near-optimally aligned (θ = 42.5°) for reshearing, with the NNE-set approaching frictional lock-up conditions (θ = 7.5°), with both maintaining their original Variscan sense of slip (fig. 3.15.b). The NW-set will be the preferentially exploited member of the pair, with the NNE-set requiring considerably greater differential stress conditions to reshear.

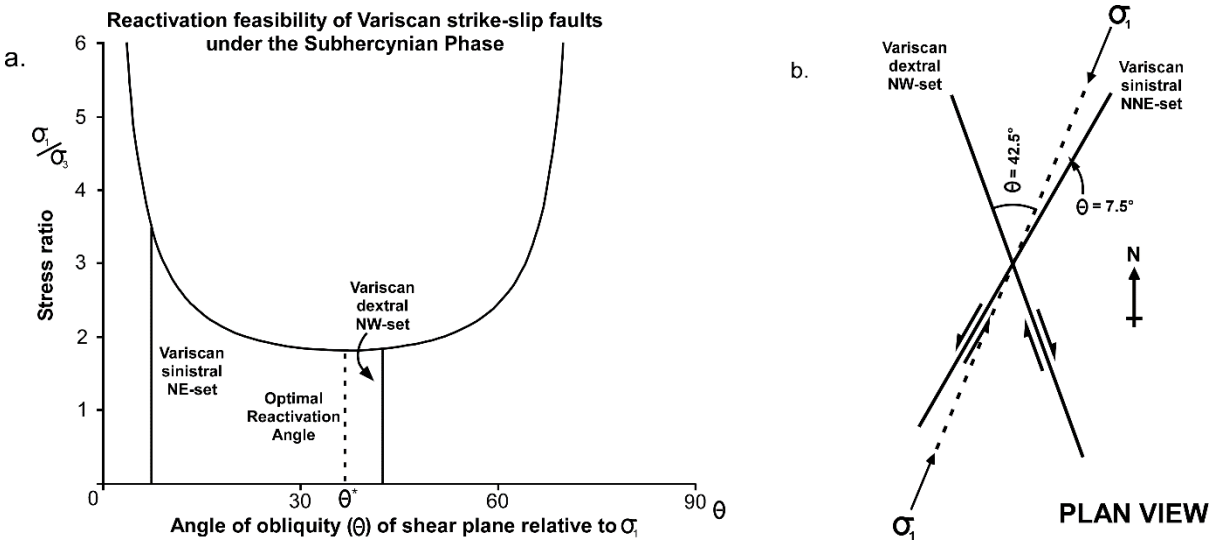

Figure 3.15 – Subhercynian Phase reactivation behaviour of the Variscan strike-slip conjugate pair. a. Reactivation profile analysing the stress conditions required to achieve reshear of each fault set. The near optimally aligned NW-set will be preferentially exploited over the unfavourable NNE-set. b. Reshear behaviour of the fault sets. Both faults undergo reshear with the same sense of slip.

3.2.3.2 Pyrenean Phase

The Pyrenean Phase deviates 005° from the Late Variscan compression regime and can be approximated to coaxial. The results are presented in figure 3.16.

The reshear of both strike-slip faults was kinematically feasible and would maintain their Variscan shear sense during Pyrenean Phase. The Variscan dextral NW-set (θ = 30°) is near-optimally aligned (table 3.2, θ* = 36.7°), with both sets requiring low differential stress conditions to reshear (table 3.5). Due to the comparable stress requirements, it is likely that preferential exploitation will be minor.

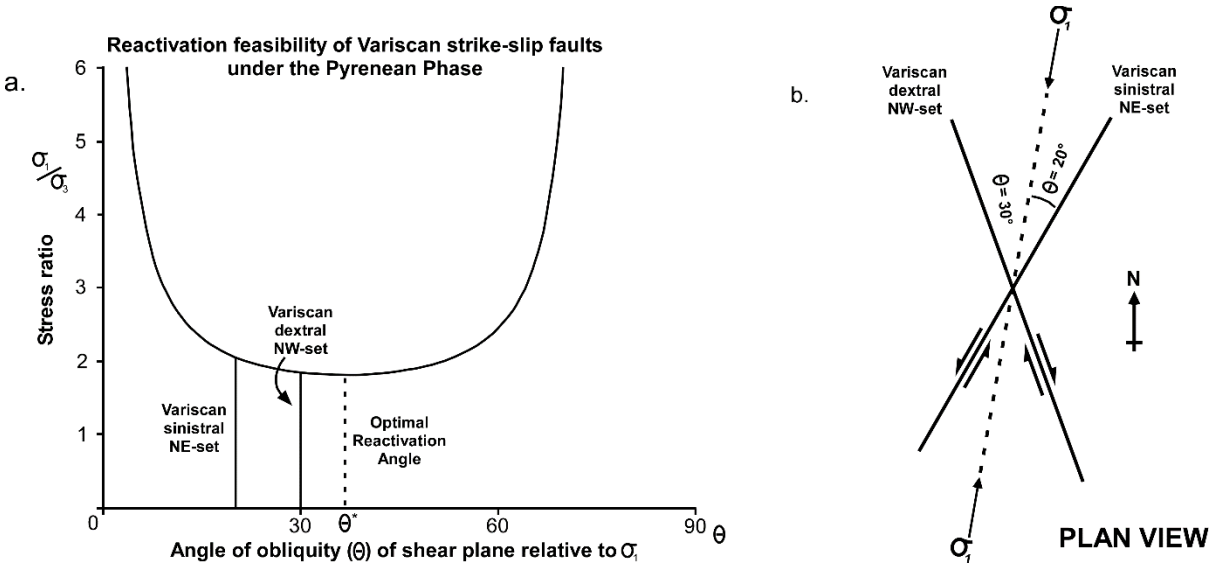

Figure 3.16 – Pyrenean Phase reactivation behaviour of the Variscan strike-slip conjugate pair. a. Reactivation profile analysing the stress conditions required to achieve reshear of each fault set. Both sets require low differential stresses to reshear, with the NW-set near optimally aligned. b. Under the Pyrenean stress field both strike-slip faults will undergo the same sense of slip.

3.2.3.3 Helvetic Phase

The Helvetic Phase is considerably misaligned with the Late Variscan axis, deviating by 120°. The results are presented in figure 3.17.

Reshear was only kinematically feasible for the NW-set (θ = 35°), being within 1.7° of θ*, with the NNE-set achieving frictional lock-up (θ = 85° > 2θ*). The severe misalignment of σ_1 will cause the NW-set to undergo sinistral reversal (fig. 3.17.b) in the opposing direction to its initial dextral sense.

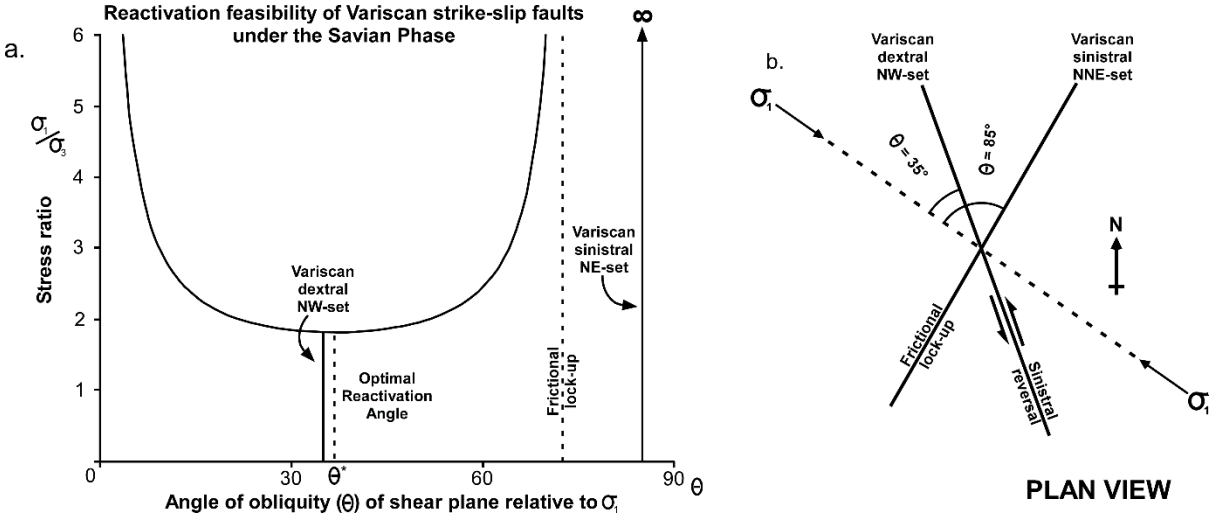

Figure 3.17 – Helvetic Phase reactivation behaviour of the Variscan strike-slip conjugate pair.
(a) Reactivation profile analysing the stress conditions required to achieve reshear of each fault set. The NW-set is near-optimally aligned, with NNE-set achieving frictional lock-up.
(b) Under the Helvetic stress field, the NW-set undergoes sinistral reversal.

3.2.3.4 Neotectonic Regime

The current Neotectonic regime deviates by 135° from the Late Variscan axis. The results are presented in figure 3.18.

Under the current Neotectonic regime the reshear of both fault sets is kinematically feasible, with the NW-set maintaining sinistral reversal and the NNE-set undergoing its original sinistral slip. However, the stress conditions required to reshear the NNE-set (σ_1/σ_3 = 6.31) are approximately triple the NW-set (σ_1/σ_3 = 2.05), making their reactivation unachievable under the current tectonic regime.

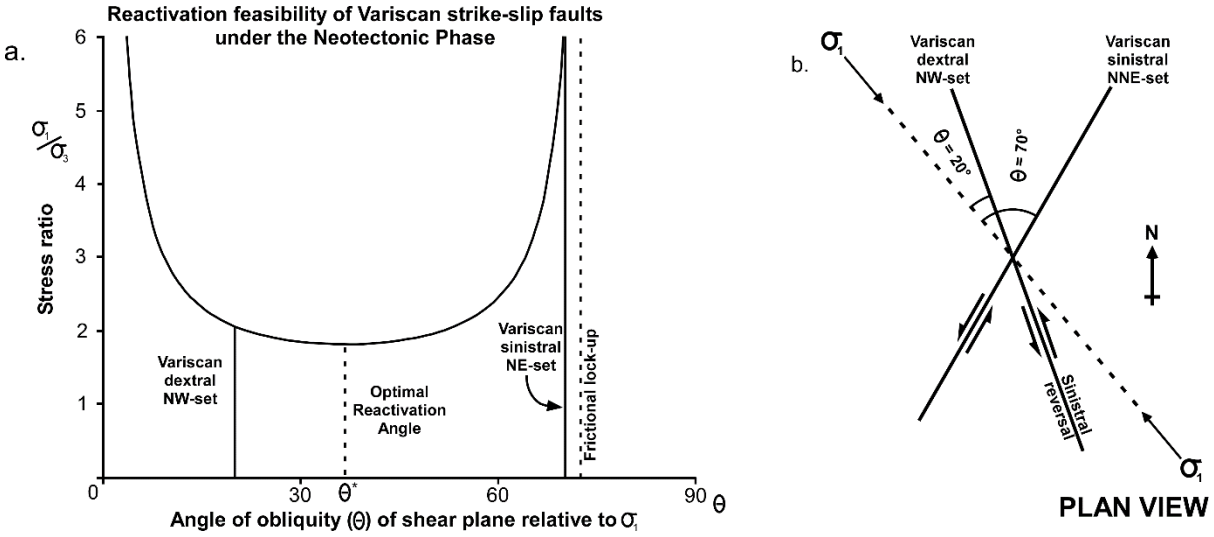

Figure 3.18 – Neotectonic reactivation behaviour of the Variscan strike-slip conjugate pair.
(a) Reactivation profile analysing the stress conditions required to achieve reshear of each fault set. The NW-set requires low differential stresses to achieve reshear, with the demands required for NNE-set to reactivate making it unfeasible.
(b) Under the Neotectonic stress field, reshear would induce sinistral slip on both fault sets.

3.2.3.5 Discussion

Alpine reshearing of the Variscan strike-slip conjugate pair was kinematically feasible, with their reactivation and respective slip behaviours varying between each Alpine Phase. However, the analyses do not provide any insight into the stress magnitudes as they assess reshear feasibility and not probability. Case studies were presented to validate whether reshearing did occur.

The NW-set is more favourably aligned than the NNE-set in all the Phases assessed (fig. 3.15-18). Only during the Pyrenean Phase do both faults have comparable stress requirements (table 3.5); this is coincident with the most significant period of tectonism in southern Britain (Parrish et al. 2018). Other Phases will preferentially exploit only the NW-set due to its lower stress requirements and/or frictional lock-up behaviour of the NNE-set; consequently, evidence of NNE-set reactivation will likely be more limited. This appears consistent with the lack of evidence for Alpine reshear of the Variscan sinistral NNE-set (fig. 3.3), and the prevalence of NW-set trends in the Mesozoic cover above the Variscides of southern England (fig. 2.7; Mansy et al., 2003). However, contrary to this deduction, both sets appear to have reactivated along the London Platform's southern margin as two fault sets were identified during this investigation (Chapter 4) that are parallel to their strikes. Both fault sets could feasibly reactivate under the Neotectonic regime, but a lack of seismic focal mechanisms (Baptie, 2010) comparable with the NNE-set implies that the required stress magnitudes are currently unachievable.

The most significant output was the identified sinistral reversal of the NW-trending (initially dextral) Variscan set during the Helvetic Phase (fig. 3.17.b). It is likely that this reversal did occur due to its low stress requirements (table 3.5). These inferences are validated by the Sticklepath-Lustleigh Fault (SLF) in exposed Palaeozoic basement (fig 3.19.a) in southwest England, which provides direct evidence of both Alpine reshear and slip behaviour evolution for the Variscan dextral NW-set. This series of Variscan left-stepping *en échelon* faults have dextrally offset both a Late Carboniferous granitic intrusive and the Permo-Triassic fill of the Crediton Trough. Two pull-apart basins, the Petrockstow and Bovey Basins, are situated at linkage points between the faults, implying sinistral slip also, and have been dated to the Eocene-Oligocene (Freshney et al., 1979) and Eocene-Oligocene(-Miocene) (Selwood et al., 1984) respectively. Holloway and Chadwick (1986) suggested at least four periods of shearing along these faults including two Alpine reshear episodes[20]: ~Eocene sinistral reversal and pull-apart basin generation, and ~Miocene dextral slip. Their timings, however, contradict kinematic behaviour of NW-set reactivation during the corresponding Alpine Phases (table 3.4). Pyrenean Phase

[20] Postulated Alpine reshears episodes of the SLF from Holloway & Chadwick (1986):

1. "Early Tertiary" (~Eocene) sinistral reversal to generate pull-apart basins filled with Eocene-Oligocene sediments. Interpreted as extension potentially associated with the Lundy Granite emplacement.
2. "Mid-Tertiary" (~Miocene) minor dextral Alpine reshearing inferred from postulated dextral Riedel shear zone in Bovey Basin and Palaeozoic sediments overlying pull-apart basin margins.

dextral slip (fig. 3.16.b) would cause transpressive linkage and not pull-apart basins (fig. 3.19.b). The sinistral slip is instead compatible with the later (Miocene) Helvetic Phase (fig. 3.19.c, 3.17.b). Either the sediments pre-date the pull-apart basins, or, that they are younger than dated. The former is suspected as the Eocene-Oligocene floodplain (with minor lacustrine) facies in both basins do not indicate accommodation space generation, implying post-depositional preservation during Helvetic Phase reversal within these pull-apart basins.

The net dextral displacement of the post-Variscan Crediton Trough is concordant with the dextral Pyrenean Phase (fig. 3.19.b) being the main episode of compression in southern Britain, with the pull-apart basins indicating minor Helvetic sinistral reversal (fig. 3.19.c).

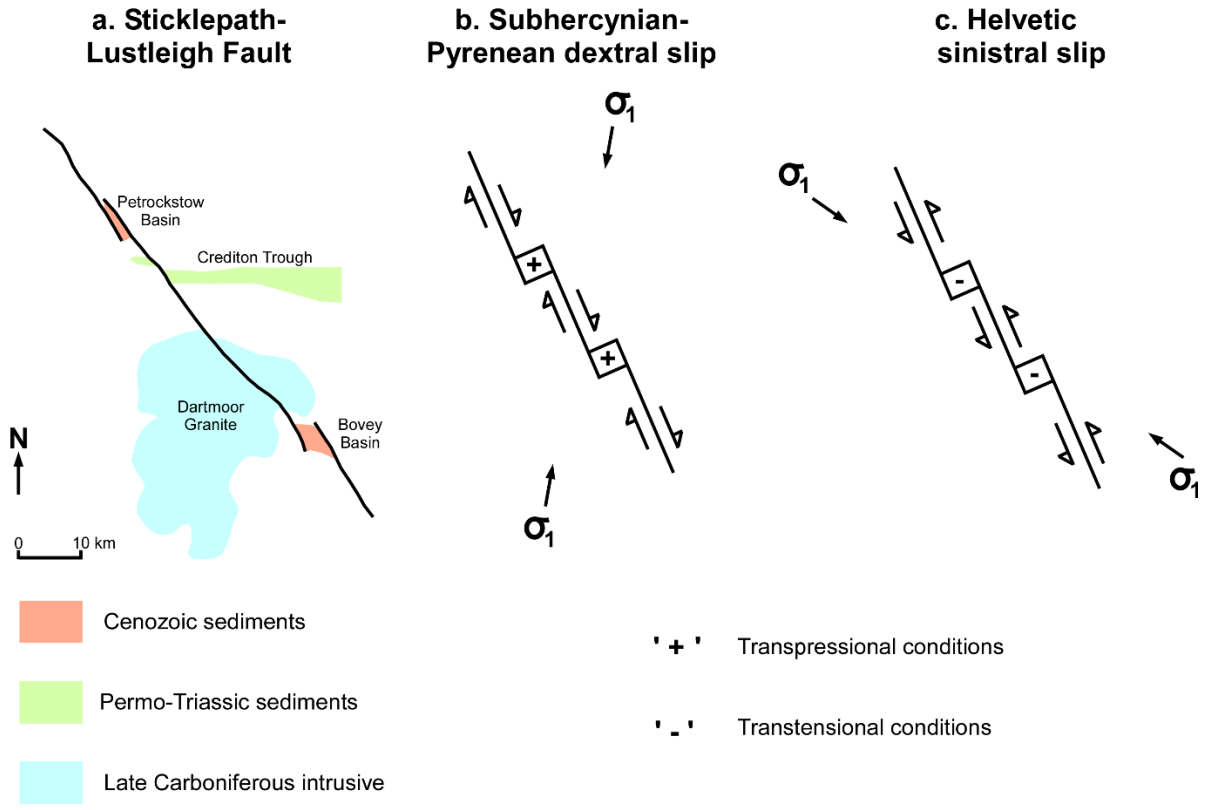

Figure 3.19 – Left-stepping *en échelon* Sticklepath-Lustleigh (SLF) Variscan dextral strike-slip faults.
a. Geological map of the SLF adapted from Holloway & Chadwick (1986). Net dextral offsetting of both a Late Carboniferous intrusive and a small Permo-Triassic basin, with Cenozoic pull-apart basins implying minor sinistral reversal also.
b. Idealised schematic for dextral reshear behaviour of NW-trending left-stepping *en échelon* faults under Subhercynian-Pyrenean stress conditions to cause transpression at linkage points.
c. Idealised schematic for sinistral reshear behaviour of NW-trending left-stepping *en échelon* faults under the Helvetic Phase, and the development of transtensional pull-apart basins at linkage points.

3.2.4 Dip-slip fault assessment

Reactivation feasibility assessment was only undertaken for a single hybrid Subhercynian-Pyrenean Phases scenario, where σ_H was sub-perpendicular to the strikes of each fault sets. This was idealised due to the sub-coaxial alignment of their stress axes with these fault geometries (fig. 3.13; table. 3.3). Comparatively, the Helvetic Phase's axes would make 2D reshear analysis inappropriate as the oblique-slip component would not be considered. For the post-Variscan normal fault set, a lower-bound range was prescribed to discuss the impact of listric geometries also. The results for dip-slip fault analyses are presented in table 3.6 and figure 3.20.

The findings imply that the reshear of both dip-slip fault sets is feasible, with the Variscan thrust set being more favourably aligned for reshear.

Table 3-6 – θ and σ_1/σ_3 calculated for the basement dip-slip fault sets under a hybrid scenario that idealises the Subhercynian and Pyrenean Phases to a coaxial alignment.

Dip-slip fault set	θ for dip-slip faults (relative to horizontal) (°)	σ_1/σ_3 for dip-slip faults
Variscan thrust	30	1.84
Post-Variscan normal fault	60	2.44

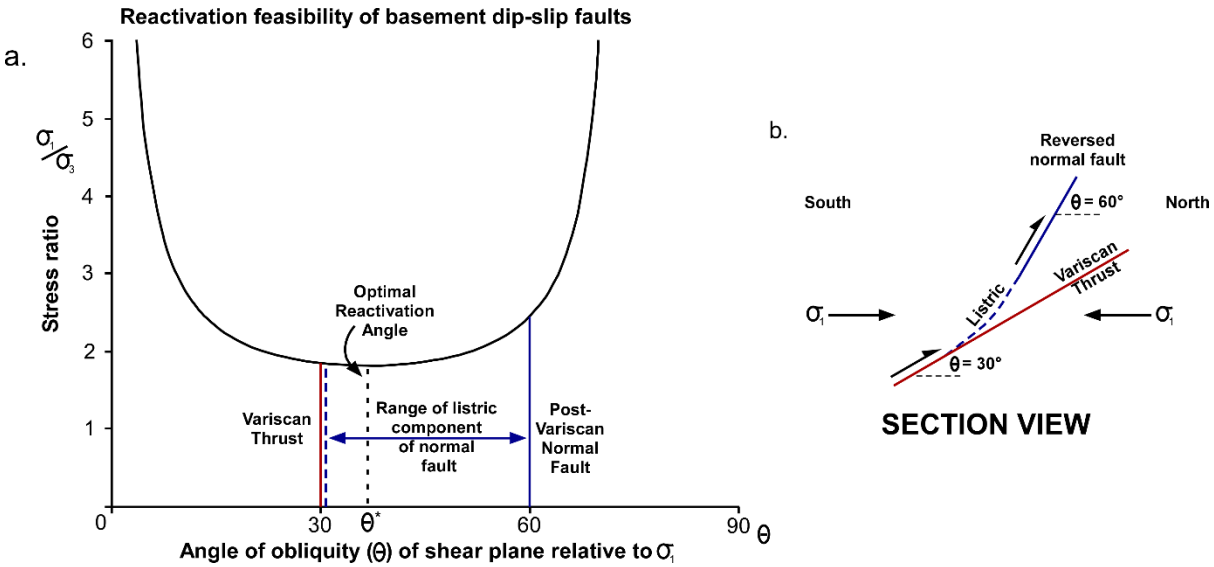

Figure 3.20 – Reactivation behaviour of the anticipated dip-slip fault sets under a hybrid Subhercynian-Pyrenean Phase where the stress axes were sub-coaxial with idealised fault strikes.

3.2.4.1 Discussion

Whilst mechanically valid, the preferential exploitation of Variscan thrusting contradicts published observations of normal fault susceptibility to inversion (Cooper and Williams, 1989, Buchanan and Buchanan, 1995, Turner and Williams, 2004). Alpine normal fault reversal in southern England basins is well-documented (fig. 2.16; Roberts, 1989, Chadwick, 1993, Westhead et al., 2018) with the bulk occurring during the Pyrenean Phase (Parrish et al., 2018); whilst Variscan thrusts across the Alpine foreland were comparatively less susceptible to compressional reshear (Ziegler, 1987).

The dip-slip fault analyses idealised normal faults to linear geometries and ignored their listric component (fig. 3.21). Their gentling dips will cause θ to progressively approach θ* with depth and eventually become more favourably aligned to reshear (fig. 3.20, dashed blue line) than the thrust set. Comparatively, Variscan thrust reshear feasibility will reduce as they progressively shallow towards their mid-crustal basal décollements (Lefort and Max, 1992), causing deviation from θ*. Listric faults normal faults expected under London would favourably reshear before thrusts.

Elevated fluid pressures have been attributed to stimulating normal fault reversal in sedimentary basins (Turner and Williams, 2004, Sibson, 1995) by reducing effective stress conditions (fig. 3.7). However, this would enhance the susceptibility of both fault sets and not solely normal faults.

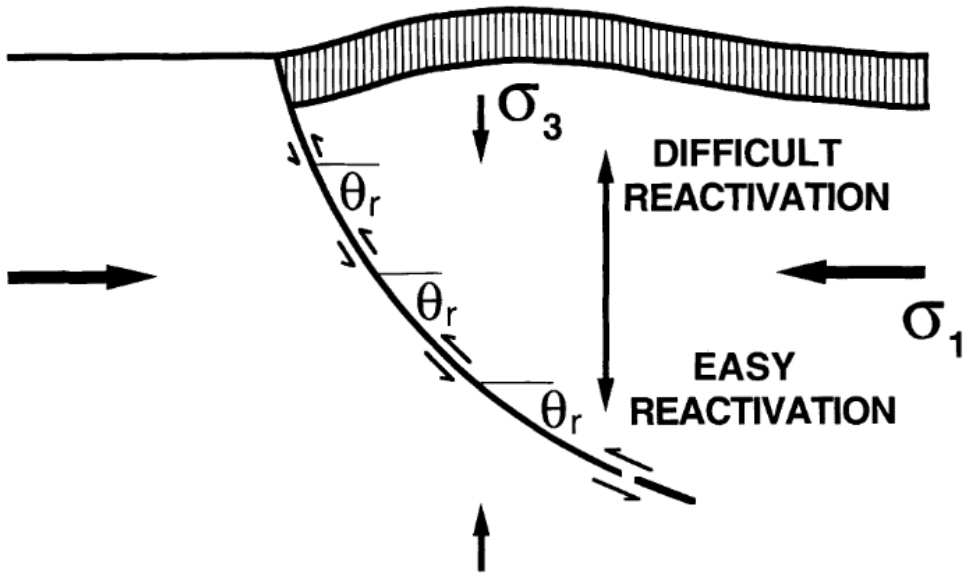

Figure 3.21 – Listric normal fault geometries progressively reduce the required differential stresses to reshear with depth. From Sibson (1995).

3.2.5 Outcomes of kinematic analysis

The feasibility analyses assessed whether basement fault reactivation could happen under Alpine compression and not if it happened. These were compared with observations from southern Britain for each fault set to appraise the results.

The Variscan conjugate strike-slip pair and the listric post-Variscan normal fault set could reactivate during the Alpine Orogeny, with reshear feasibility and behaviour varying between each Phase. The Variscan NW-set and the post-Variscan normal fault set were most favourably aligned with their reactivation validated from case studies (fig. 3.19; 2.16). Therefore, of the basement fault sets outlined in figure 3.1, these three fault sets could have reactivated and been inherited into the overlying Cretaceous-Palaeogene cover along the London Platform's southern margin.

3.2.6 Limitations of analytical methods

The analytical method and assumptions applied limit how representative the analyses are of actual Alpine reactivation behaviour of the basement faults. Several factors are outlined and discussed.

3.2.6.1 Limitations of 2D coaxiality requirements

Sibson's reshear feasibility assessment (eq. 3.1) is a 2D empirical relationship that assumes a linear-elastic brittle failure envelope along a σ_1-σ_3 plane with σ_2 ignored (fig. 3.4.b-c).

For σ_2 to be negligible, the pole of the fault plane must be parallel with the σ_1-σ_3 plane (Sibson, 1994). Reshear characterisation is reduced to movement along this axis only and cannot model oblique-slip behaviour. However, none of the Alpine Phases have stress axes (fig. 3.13) coaxially aligned with the modelled fault planes (fig. 3.12). Furthermore, the relative magnitude of the σ_V axis for each Phase was undetermined and idealised to strike-slip ($\sigma_V = \sigma_2$) or thrust ($\sigma_V = \sigma_3$) alignments for their respective analyses (fig. 3.14). Satisfying the required 2D conditions causes the analyses to become progressively less valid as the stress regime deviates further from coaxiality and introduces a larger 3D oblique-slip component (Del Ventisette et al., 2006, Bonini et al., 2012) that the analyses ignored. This was only considered an issue for the dip-slip faults under Helvetic and Neotectonic conditions.

To overcome this, a reactivation mechanism must be developed that addresses the implications of oblique-slip behaviour by considering the 3D fault geometry under the applied stress field. This 3D reactivation profile could potentially incorporate Bott's (1959) expression of oblique-slip into Sibson's reactivation profile, thereby incorporating the σ_2-axis absent from the 2D mechanical analysis of reshear (Sibson, 1985).

3.2.6.2 Alpine Phase palaeostress determination

The σ_1-axis orientation for each Phase will affect fault coaxiality (fig. 3.13) and reshear feasibility. These were determined from structural and/or qualitative data (table 3.4) across southern Britain or the North Sea and may not be representative of London's Alpine stress conditions. For example, nearby data from Kent (Vandycke, 2002, Bergerat and Vandycke, 1994) indicate a ~N-S Subhercynian σ_1-axis rather than NNE-SSW, producing reshear conditions comparative to the Pyrenean Phase. This will predominantly have implications for the θ-values used for strike-slip analyses (table 3.5).

Targeted palaeostress analyses are required to produce a more representative evolution of the Alpine stress field under the southern London Basin.

3.2.6.3 Mechanical parameters assumptions

Frictional strength significantly influences reshear capabilities (fig. 3.8). The upper bound value for natural fault frictional ranges ($\mu = 0.3$) was applied and assumed to be both consistent between fault sets and unaffected by progressive mechanical wearing (fig. 3.9). Whilst conservative, the actual friction cannot be reliably determined without direct testing of the buried fault planes themselves, but they could be as low as $\mu = 0.05$ (§3.2.2.2). Therefore, these faults may have reactivated over a broader range of θ and at lower σ_1/σ_3 conditions (fig. 3.8). Shear strength testing of exposed fault cores in southern Britain for each set may provide appropriate proxies for determining respective μ.

Fluid pressures were ignored as their magnitudes cannot be retrospectively determined. However, compression likely elevated them to make reshear more favourable than calculated (fig. 3.7, $\lambda > 0$).

3.2.6.4 Basement fault geometries inferences

Fault sets orientations (table 3.3) were inferred from published trends in proxy regions that shared the anticipated tectonic fabrics. Yet strike variability within each set should be anticipated under London as demonstrated by Variscan strike-slip trends across southwest Wales (fig. 3.22); this was not accounted for. Both within-set variation and potential geographical differences may be sufficient to alter θ and cause differing reshear behaviour of the Variscan strike-slip from that calculated (fig. 3.15-18). Future assessments should use a strike range (± 10°) instead of a single value to assess any within-set variation in reshear behaviour.

3.2.6.5 Impacts on kinematic analyses

Alpine basement fault reactivation could have occurred across a broader θ-range and under lower stress conditions than calculated for in §3.2. Upon review, the parameter assumptions are more impactful for the strike-slip sets since their θ-values depend upon both strike and palaeostress angle. Also, 3D reshear behaviour was ignored by idealising obliquely aligned dip-slip sets to 2D coaxiality.

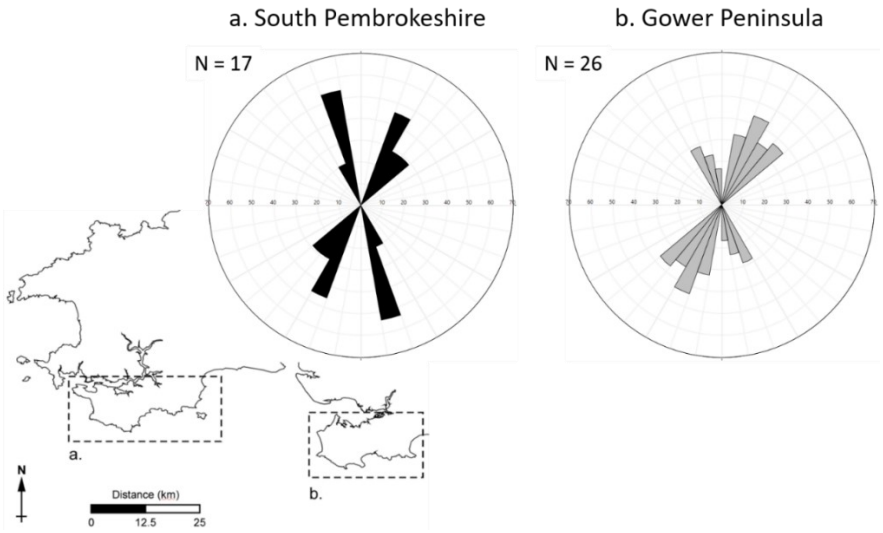

Figure 3.22– Comparison of Variscan strike-slip fault strikes from two proximal regions in southwest Wales. Strikes were measured from BGS maps and digitised using Stereonet 10 (Allmendinger et al., 2011, Cardozo and Allmendinger, 2013). Base map from Ordnance Survey data.
a. South Pembrokeshire, sourced from Dixon and Strahan (1977).
b. Gower Peninsula, sourced from the British Geological Survey (1977, 2002).

3.3 Evidence of fault inheritance in London and the Thames Estuary

Three of basement fault sets could reactivate under Alpine compression. However, kinematic analyses alone are insufficient to validate either an inheritance mechanism for London's major faulting nor the expected fault sets that underlie it. §3.3 presents fault inheritance evidence from across the southern London Basin. At-surface and basement fault strikes were initially assessed for their comparability (§3.3.1). Near surface and penetrative observations (fig. 3.23) were then compared with analogue modelling to develop inheritance case studies for each fault set (§3.3.2-3).

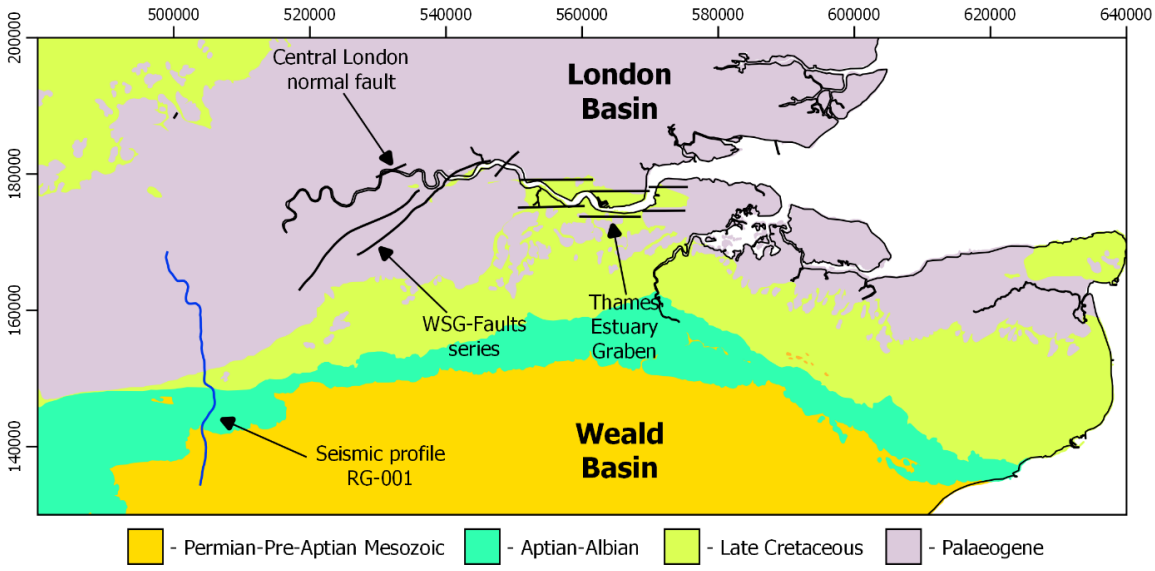

Figure 3.23 – Fault inheritance case study locations discussed in §3.3.

3.3.1 Basement-cover fault strike comparison

If major faulting in London is genetically related to underlying basement structures, then they are expected to share sub-parallel trends. The strikes of mapped faults and structural lineaments were compared with proxy basement fault set trends from across southern Britain.

3.3.1.1 At-surface fault strike collection

Two independent sources were collated from in and around London to characterise at-surface faults.

The strikes of mapped faults from across the southern London Basin in 1:50,000 BGS maps were measured and digitised (fig. 3.24) due to the similar basement-cover relationship across this area of the Basin (§2.1.1). This provided a representative sample size for London. Whilst scatter is present, three distinct trends were qualitatively defined: NE-NNE, E-ENE, and NNW.

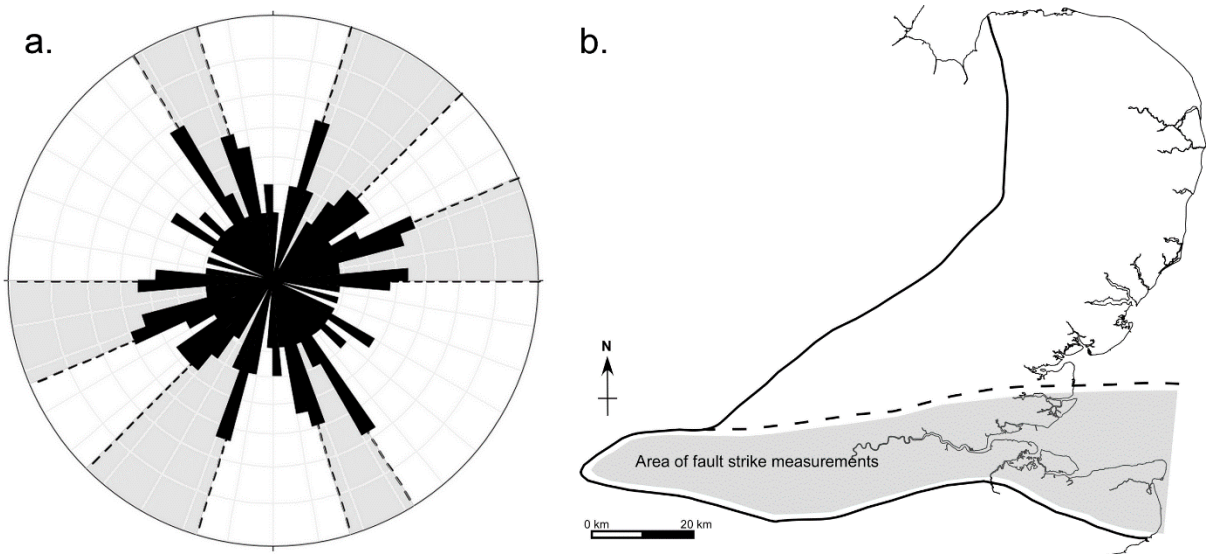

Figure 3.24 – Fault strikes from across the southern portion of the London Basin, measured from 1:50,000 BGS data. Geological Map Data BGS © NERC 2018.
a. Rose plot of measured fault strikes (N = 77). Any faults with mild curvature were linearised. Two lengthy and sinuous major faults were segmented into five consistent strikes. Constructed using Stereonet 10 (Allmendinger et al., 2011, Cardozo and Allmendinger, 2013).
b. Area of fault data collection (grey) from the southern London Basin.

A hidden fault network was identified in London during this investigation (discussed in Chapter 4). It comprises spatially coincident lineaments (fig. 4.22) between long-term InSAR displacement and subsurface topographic changes in the White Chalk Group. Three sets are present that strike approximately NE, ENE and NNW, and are consistent with mapped fault trends (fig. 3.24).

3.3.1.2 Fault strike comparison

The strikes of the two at-surface fault datasets, and proxy trends for the basement fault sets from across southern Britain are presented in figure 3.25.

The comparable trends between the two at-surface datasets (fig 3.25.a-b) indicates the presence of three fault sets within London's near-surface. Variation in scatter between the two datasets likely reflects the differing fault scales between them: fault lengths in the BGS vary from hectometres to kilometres with the scatter present in the former scale, whilst the lineaments are all km-scale. Two different modes of fault generation are inferred from this difference, with the longer faults forming these three fault sets.

If these major fault sets represent inherited basement faults they will be sub-parallel with their trends (fig 3.25.c,d) and associated palaeostresses (fig. 3.12). Comparatively, if they are new Alpine shears, they would be aligned with one of its Phases (fig. 3.13), most likely the main Pyrenean Phase.

The NE-NNE and NNW faults are compatible with the Late Variscan strike-slip conjugate pair (fig. 3.25.c). However, this is insufficient alone to validate inheritance as their acute bisector of ~005-to-180° is comparable with both Late Variscan (3.12.b) and Alpine (fig. 3.13.a-b) stress axes.

The E-ENE set is misaligned with both Variscan thrust and Jurassic-Early Cretaceous extensional regimes (fig. 3.25.c-d; 3.12.a,c) and the main compressive Alpine Phases (fig. 3.13.a-b) by ~10-20°. This disparity may reflect spatial differences in orientation of the Early Variscan stress field (and later Mesozoic extensional axis) along the Anglo-Brabant Massif's southern margin as the proxy faults are from southern England's inverted basins (§3.2.6).

The three major at-surface fault sets are broadly concordant with basement fault orientations, with the shorter, scattered faults being Alpine new shears. However, the findings are inconclusive as fault geometry is insufficient to confirm compatibility with either Alpine new shear or reshear inheritance.

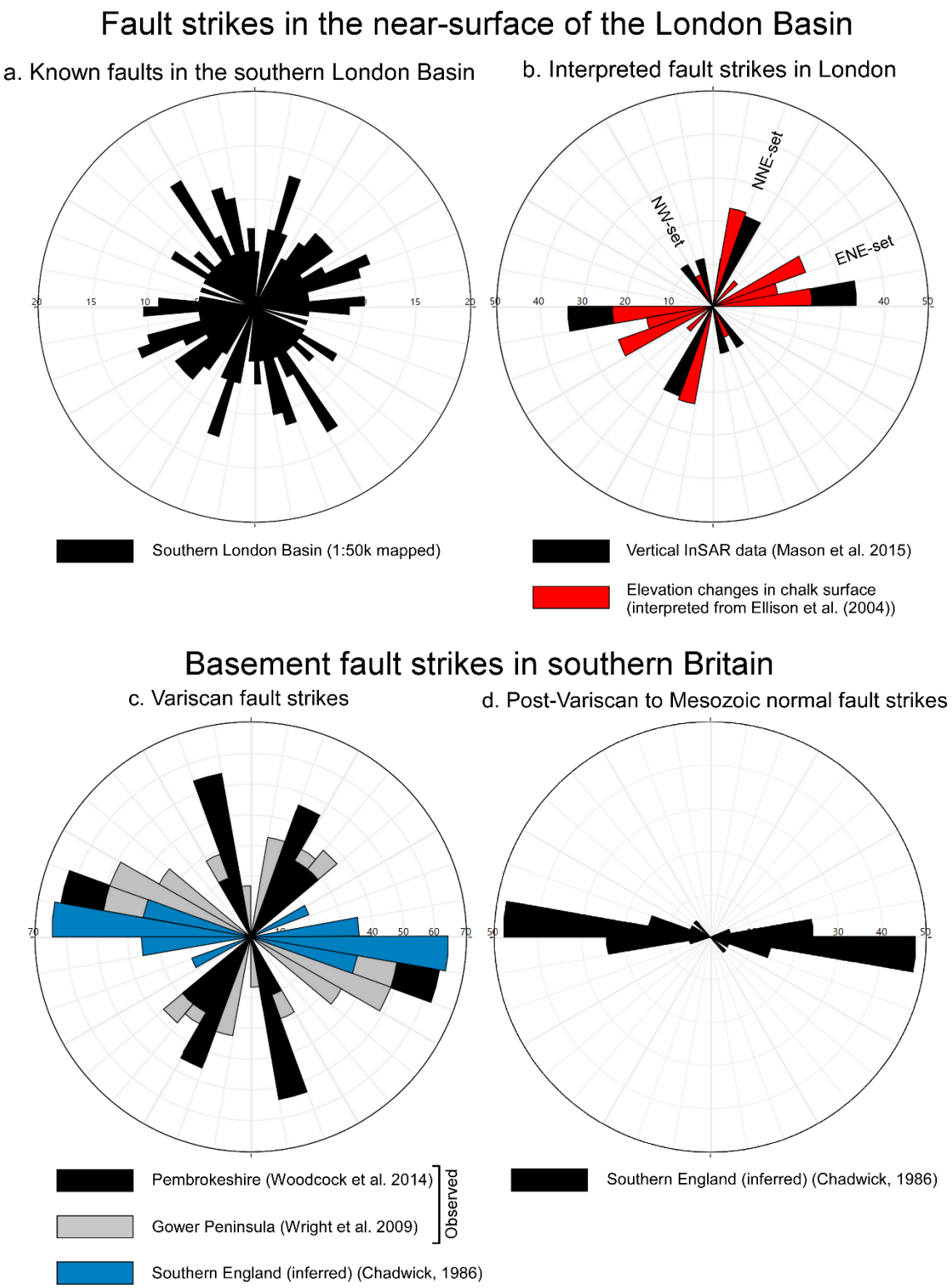

Figure 3.25 – Cross-comparison between published and inferred fault strikes within the southern London Basin's near-surface with published trends from across southern Britain providing proxies for basement fault sets. Rose plots constructed using Stereonet 10 (Allmendinger et al., 2011, Cardozo and Allmendinger, 2013).
a. Mapped faults from across the southern London Basin (fig. 3.24).
b. Inferred fault lineaments (fig. 4.22) from the indirect mapping methodology outlined in Chapter 4.
c. Exposed (Wright et al., 2009, Woodcock et al., 2014) and inferred (Chadwick, 1986) Variscan thrust and strike-slip fault trends from across southern Britain.
d. Inferred (Chadwick, 1986) Jurassic-Early Cretaceous normal fault set beneath southern England.

3.3.2 Reversed normal fault inheritance in London and the Thames Estuary

Post-Variscan normal faults are anticipated in the basement under London that may have reversed and propagated during Alpine compression. Three case studies (fig. 3.23) are presented that independently support reversed normal fault inheritance from three different analytical methods: seismic profile, basement-cover analysis, and shallow structural analysis coupled with gravity data.

3.3.2.1 Seismic profile RG-001: Interface of the Weald Basin and London Basin

RG-001 is a basement-penetrating seismic profile through the Hampshire and Weald Basins and the southern margin of the London Basin. It was interpreted by Butler and Jamieson (2013) and is publicly available in the UK Onshore Geophysical Library (UKOGL). The section along the Weald Basin-London Basin interface was analysed (fig. 3.26) as a proxy for the Alpine behaviour of post-Variscan normal faults and Variscan thrusts under London.

The Weald Basin-London Platform transition is illustrated by the rapid northward shallowing of the basement that is controlled by normal faults that attach onto an underlying Variscan thrust. (Their listric geometries also support the discussion in §3.2.4). The uplifted Cretaceous flank of the North Downs provides direct evidence of basement-derived normal fault inversion, despite a net-downthrow slip being maintained. Inversion is also demonstrated by bulk shortening of the pre-Aptian Mesozoic fill, that progressively thins as it onlaps onto the London Platform.

Propagation into the London Basin is less obvious in the seismic profile as offsetting of its post-rift cover is comparatively minimal. However, cover undulations are coincident with underlying normal faults (fig. 3.26). Within the original seismic profile there is evidence of offsetting and localised uplift of Cretaceous sequences immediately above these faults that is compatible with analogue modelling of reversed propagation into a sedimentary cover (fig. 3.27). These are interpreted to be propagated fault zones, with comparative offsetting observed above basement normal faults elsewhere in the southern London Basin.

The reversal and propagation of post-Variscan normal faults into the southern London Basin's cover is demonstrated in seismic profile RG-001 and supports an inheritance mechanism for London also. The profile provides two other critical observations regarding the London Basin and its relationship with underlying structural domains. Firstly, the northward change in the London Basin's synclinal geometry from inclined to flat interior is coincident with the underlying transition from the inverted Weald Basin to the London Platform (fig. 3.26). Secondly, Variscan thrust sheet continuation beneath the London Basin contradicts the termination of the Variscan Front under the North Downs. Both points are beyond the scope of this chapter's objective and are discussed in Chapter 7.

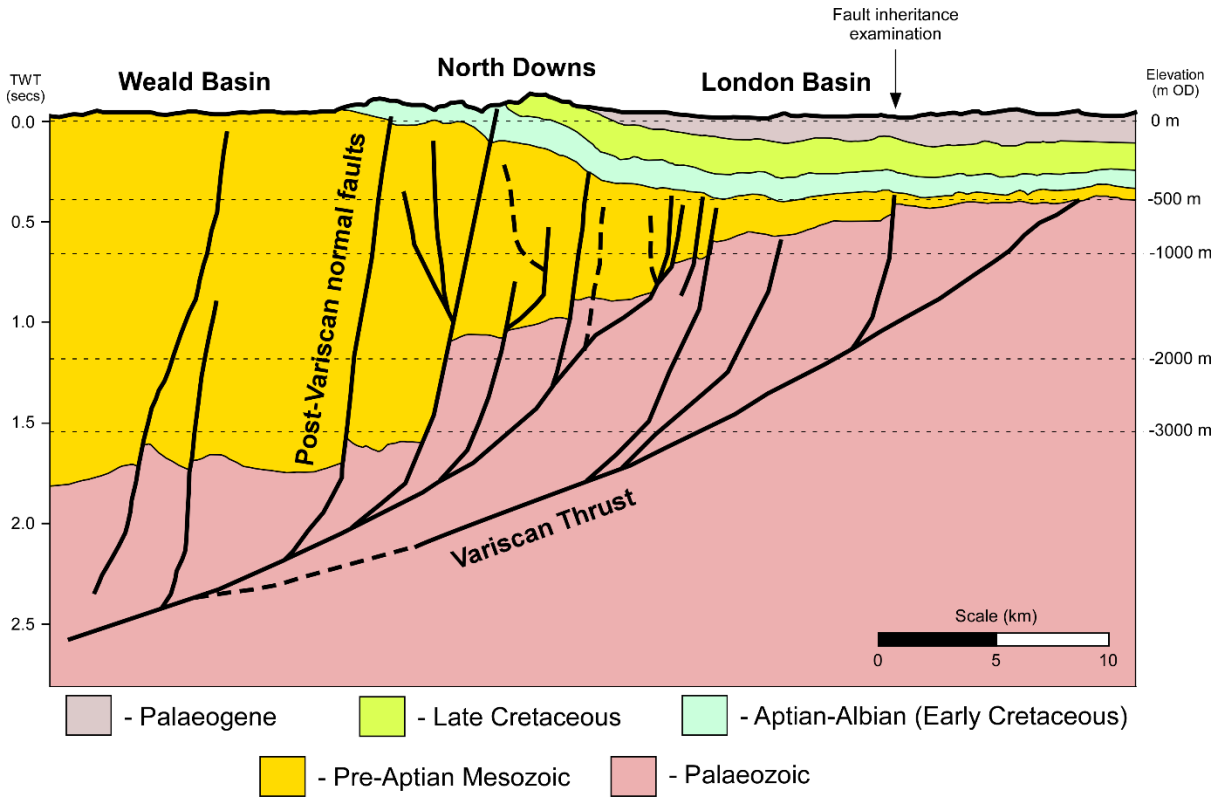

Figure 3.26 – Geological adaptation of the Weald-London Basins interface in seismic profile RG-001 (fig. 3.23), with depth in two-way time. The section confirms the continuation of both Variscan thrusting and post-Variscan normal faulting under the London Basin, with Alpine reversal of the latter demonstrated by post-rift uplift. Adapted from Butler and Jamieson (2013).

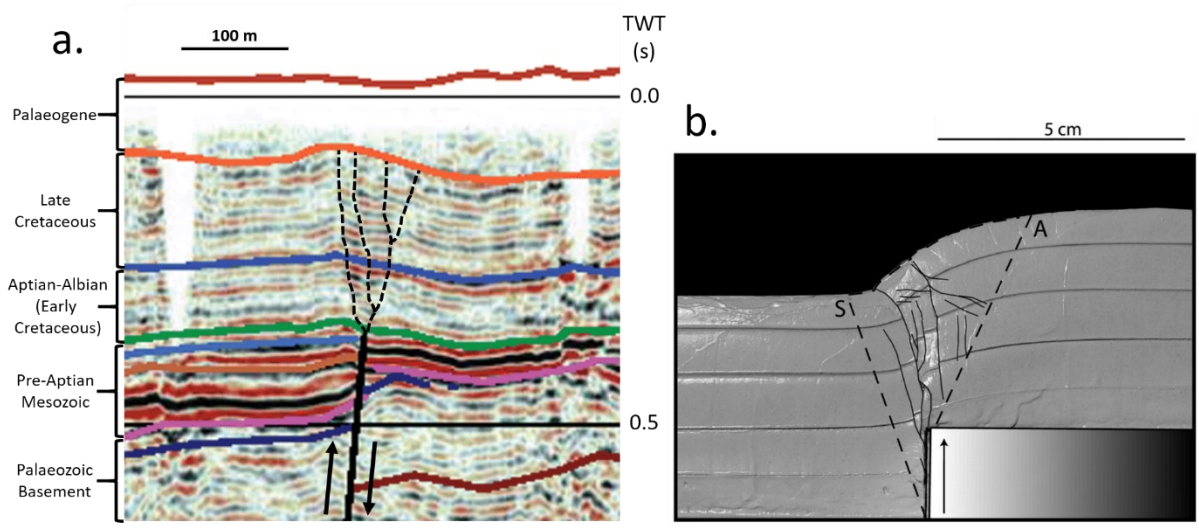

Figure 3.27 – Cover offsetting in the London Basin above a basement normal fault is compatible with modelled propagation behaviour of reversed normal fault inheritance.
a. Interpreted offsetting and uplift of Cretaceous sequences (interpreted here as dashed line) above a reversed post-Variscan normal fault in RG-001 (marked on fig. 3.26). Adapted from Butler and Jamieson (2013).
b. Wet clay analogue modelling of cover deformation above an uplifting vertical basement faulting. Inheritance behaviour is characterised by localised development of a fault zone and deflection of stratigraphy immediately above the basement fault. Adapted from Miller and Mitra (2011).

3.3.2.2 Thames Estuary Graben: Localised Alpine inversion within the London Basin

Owen (1971) identified a confined band of Oxford Clay from deep boreholes in the Thames Estuary and proposed preservation within a graben in the Palaeozoic basement: the Cliffe Graben (fig. 3.28). This structure is compatible with the basement-derived normal fault set (fig. 3.1). However, Owen only analysed the graben's Late Jurassic-Early Cretaceous tectonic activity. Its Alpine inversion behaviour has been deduced by this investigation.

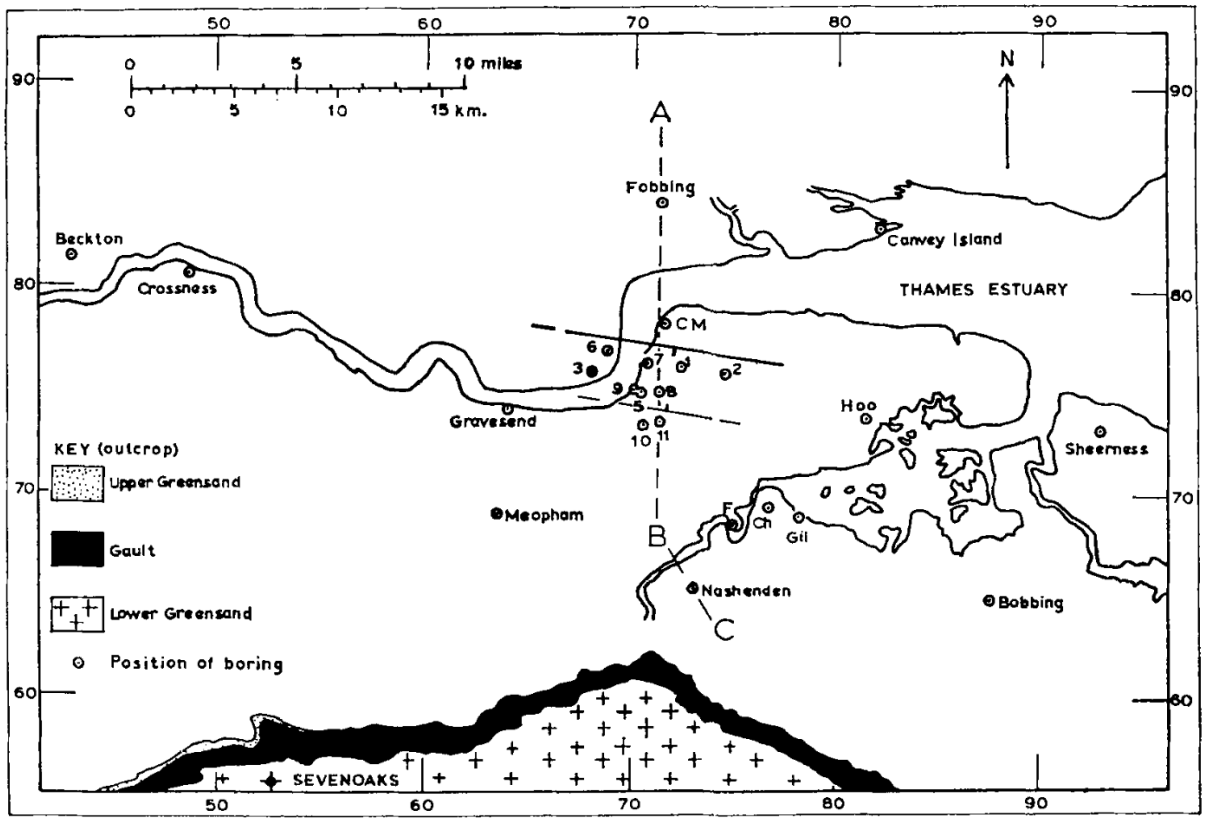

Figure 3.28 – ESE-trending Cliffe Graben proposed by Owen (1971) from the restricted coverage of Oxford Clay in sub-Aptian penetrating boreholes. Owen determined the basement structure to be a graben in the London Platform's southern margin that was active during the Early Cretaceous, locally preserving onlapped Jurassic strata and affecting Albian sedimentation. Sourced from Owen (1971).

The Cliffe Graben is coincident with a ~20 km E-W trending chalk inlier that is continuous across the Thames Estuary, implying localised Alpine-related uplift. Sub-Aptian penetrating boreholes from across the Thames Estuary (table 3.7) were interpreted to reconstruct the Cliffe Graben and determine the broader extent of Oxford Clay preservation (fig. 3.29). This was undertaken to validate Owen's proposed structure and to constrain the cause of broader uplift. The findings demonstrate that the Cliffe Graben is part of a larger basement structure that reversed and propagated into overly Late Cretaceous-Palaeogene cover: the Thames Estuary Graben.

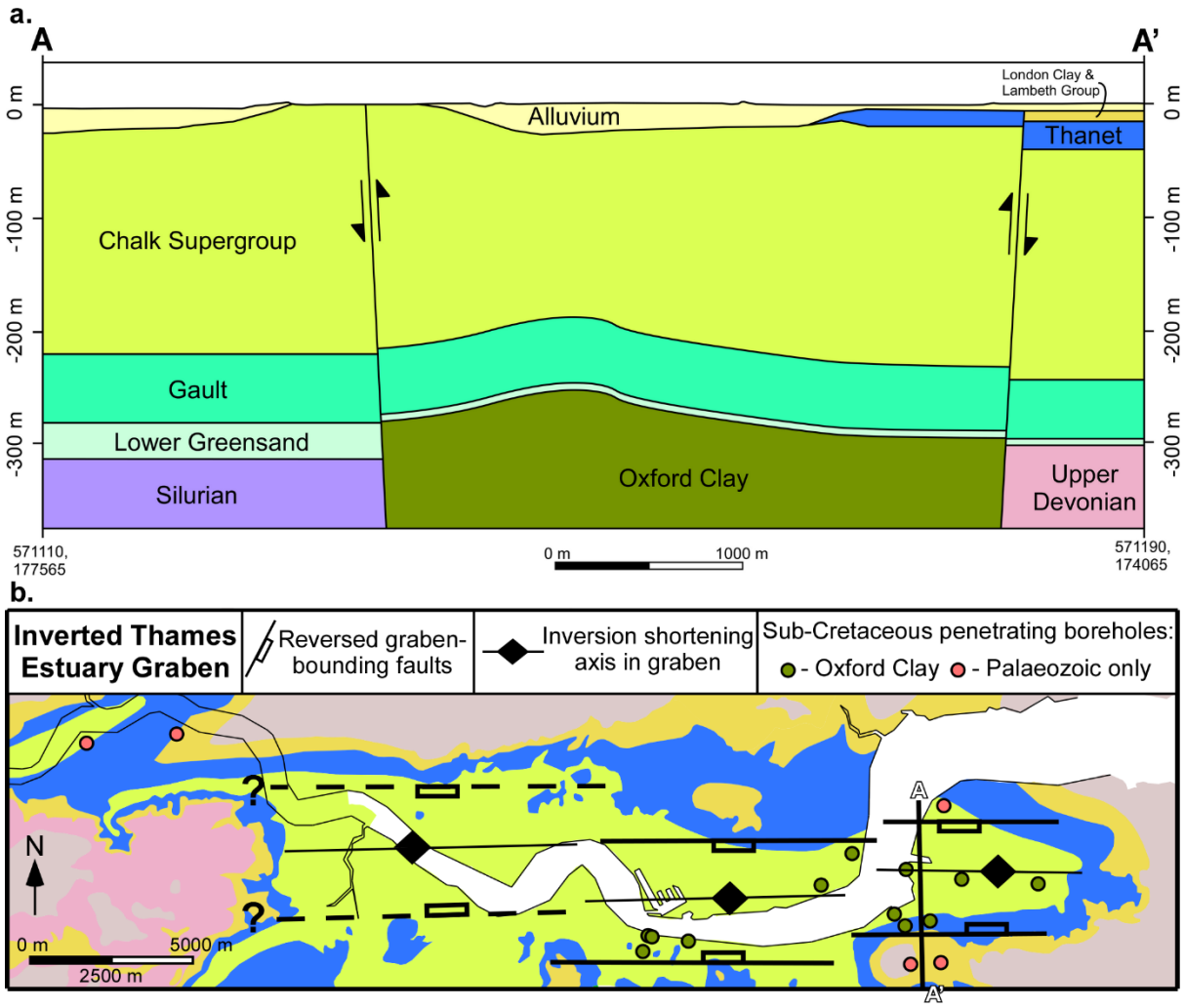

Figure 3.29 – Proposed inverted Thames Estuary Graben.
a. Cliffe Graben cross-section (line A-A') reinterpreted from 12 boreholes (table 3.7).
b. Proposed westward extension of the inverted Thames Estuary Graben, with the Cliffe Graben being the easternmost member. This was interpreted from additional Oxford Clay-intercepting boreholes (table 3.7) and the westward continuation of the chalk inlier. It is unclear if these graben-bounded reversed faults are *en échelon* or have been laterally displace.

The inlier at Cliffe is a product of graben inversion through normal fault reversal and propagation, and internal shortening of its Jurassic fill, causing localised uplift of the cover (fig. 3.29.a). Pyrenean Phase timing is inferred from Palaeogene offsetting and partial truncation, agreeing with kinematic analyses (fig. 3.20) and Alpine Phase analyses (§2.1.2). Minor Subhercynian tectonism is also suspected, but in-log chalk stratigraphic detail was insufficient to distinguish this.

The western extent of this graben system is unclear and varies between publication. Eastward it is reasonably constrained, with its termination evidenced by cessation of the chalk inlier and the lack of Jurassic strata in basement-penetrating borehole [TQ87SW46] beyond this map's extent. Owen's (1971) ESE-striking structure was based on borehole coverage and geophysical anomalies (Falcon and Kent, 1960); but he postulated a westward continuation from a Gravesend borehole [TQ67SW15] (fig.

3.28). Ellison et al. (2004, fig. 42) proposed that the Cliffe Graben continued westward along an E-ENE axis that tapered in east London from parallel linear Bouguer gravity gradients that they attributed to graben-bounded pre-Aptian Mesozoic strata. An alternative model is proposed here from at-surface geology and borehole analyses (fig. 3.29.b). Westward continuation is supported by Oxford Clay interception in Gravesend (table 3.7) that is coincident with the chalk inlier. Offsets in this inlier indicate that it is not a continuous structure but composed of several *en échelon* or potentially laterally displaced grabens. This Thames Estuary Graben system is formed of (at least) three grabens, with the Cliffe Graben being the easternmost member. The graben likely terminates with the chalk inlier, with its truncation at Erith forming the western boundary. The uplifted pre-London Clay flanks likely reflect propagation behaviour in figure 3.27, to develop its internally inclined geometry.

The Thames Estuary Graben confirms the presence of post-Variscan normal faulting in London's basement, and its inversion and inheritance during the Alpine orogeny, validating kinematic analysis. Further analyses are required to characterise its geometry, offsetting, and internal architecture.

Table 3-7 – Publicly available boreholes utilised to develop the Thames Estuary Graben model (fig. 3.29), including boreholes used by Owen (1971). [a] TQ77SW11/B constrained Palaeogene offsets.

BGS Reference Number	Location Groupings	Palaeozoic floor elevation (m OD)	Oxford Clay elevation (m OD)	Purpose
TQ77NW43/B	Cliffe	-312.42 (Silurian)	-	Cliffe Graben cross-section development (fig. 3.29.a)
TQ77NW24		-	-248.76	
TQ77NW37		-	-265.42	
TQ67NE10		-	-265.58	
TQ77SW1		-	-292.47	
TQ67NE6		-	-272.82	
TQ77NW20		-	-249.29	
TQ77NW30		-	-285.46	
TQ77NW27		-	-287.88	
TQ77SW2		-300.84 (U. Devonian)	-	
TQ77SW3		-299.78 (U. Devonian)	-	
TQ77SW11/B [a]		-	-	
TQ67SW561	Gravesend	-	-274.07	Westward graben constraining (fig. 3.29.b)
TQ67SW18		-	-261.67	
TQ67SW12		-	-268.23	
TQ67SW11		-	-266.84	
TQ48SE756	East London	-281.9	-	
TQ48SE74		-306.14	-	

3.3.2.3 Central London graben: Syndepositional inheritance and transtension

The interception of the Great Oolite Group (Jurassic) strata by the basement-penetrating Meux's Brewery Well (Prestwich, 1878, Moore, 1878) [TQ28SE156] is coincident with an ENE-WSW trending negative gravity anomaly (fig. 3.30). Ellison et al. (2004) attributed this anomaly to localised Jurassic sediment preservation within a basement graben structure.

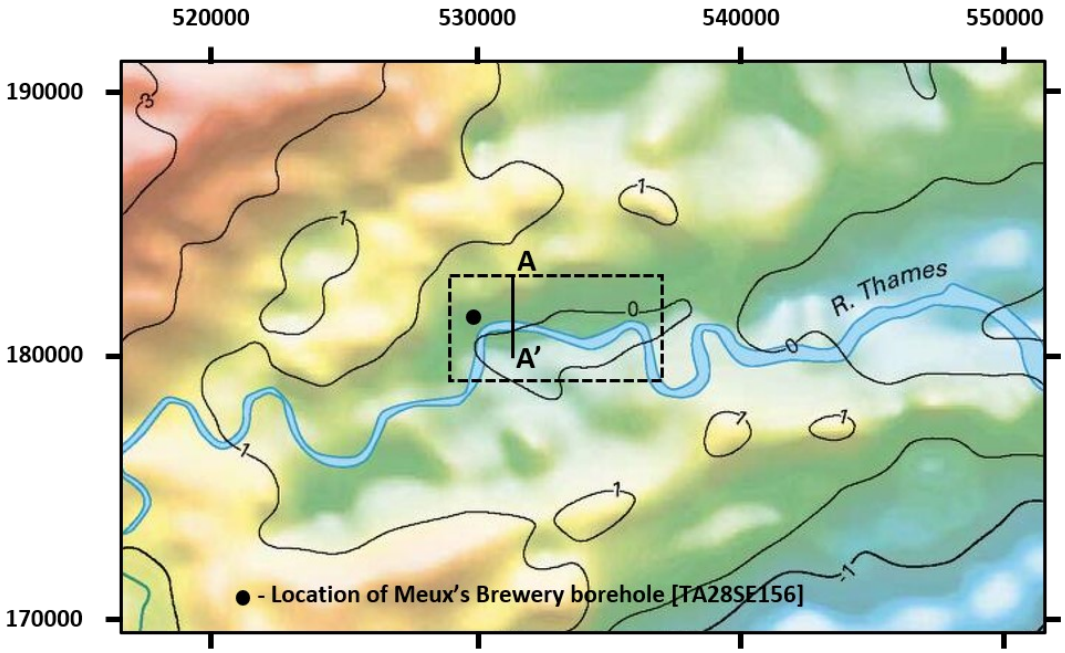

Figure 3.30 – Colour-shaded Bouguer gravity relief map of London overlain with (approximate) positions of the near surface cross-section trace (fig. 3.31, A-A') and Meux's Brewery well. The near surface trough (fig. 3.31) is parallel with this feature. Base map adapted from Ellison et al. (2004).

A shallow ENE-trending trough in the near surface is spatially coincident with this basement graben. This was initially identified by Meyer (2018) from geological modelling[21], and developed further for this research (fig. 3.31). Bounding faults are indicated from rapid elevation changes parallel to the margins of this internal depression and are verified by the indirect fault map in Chapter 4. Section A-A' intercepts the northern bounding fault, highlighting both the offsetting of Chalk-Palaeogene sequences and the restricted internal coverage of the Harwich Formation. Comparisons with Edgar et al. (2021) imply that this graben provided syndepositional accommodation space. Similar across-fault lithological variation within the Lambeth Group was undetermined due to its limited subdivision.

Independent validation for this trough and its approximate geometry is provided by both the BGS Lithoframe (narrow graben, fig. 2.31) and the Thames Tideway Tunnel (TTT). Additionally, TTT also identified that it is highly faulted internally and downthrown towards the trough's centre (London Bridge Fault Zone, Newman, 2017). This structure is revisited during fault zone analyses in Chapter 6.

[21] Implicit-driven geological modelling with bedding surfaces developed by Ordinary Kriging of borehole data.

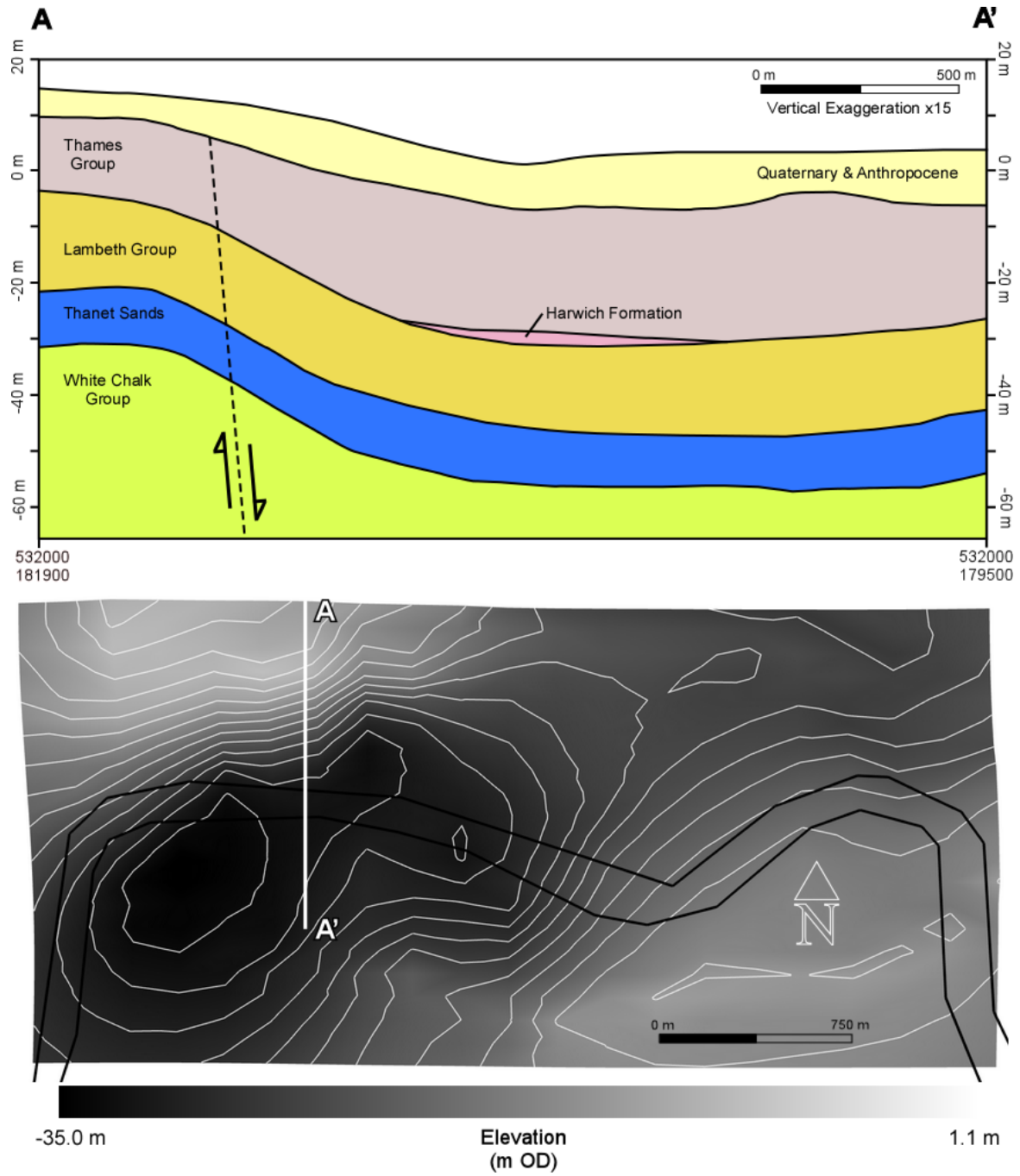

Figure 3.31 – Fault-controlled depression beneath central London. This is spatially coincident and geometrically consistent with the negative gravity anomaly in figure 3.30. Figures and modelling developed by Morgan, T. from initial analyses by Meyer (2018) in MOVE.
a. Section A-A' through the trough's northern margin. Normal faulting was inferred from rapid elevation changes. Restricted Harwich Formation coverage implies syndepositional accommodation space generation.
b. Lambeth Group surface topography demonstrating an internal depression bounded by two parallel ENE-trending margins, interpreted to be faults.

The near surface trough is interpreted to be causally linked with the suspected basement graben underlying central London, representing the inheritance of two reversed post-Variscan normal faults. Syndepositional activity is consistent with the Pyrenean Phase (fig. 3.20). (The other Phases are undetermined, but recent activity may be implied by downthrown Quaternary sediments.)

The inherited structure's internally depressed geometry implies extension and normal faulting (fig. 3.31.a), contradicting both Alpine compression and comparative inheritance behaviour above the inverting basement graben in the Thames Estuary (fig. 3.29). This contradictory structure likely reflects localised transtensional conditions generated by fault interaction that can attributed to basement structure- and/or inheritance-related mechanisms. These basement normal faults could generate deeper transtension if a relay ramp or releasing bend is present immediately below and reactivated with an oblique-slip component (as expected, §3.2.6.1). Alternatively, observations from the North Downs (Sherlock et al., 1962) indicate that reversed normal faults propagate as *en échelon* faults in the cover. During the main Pyrenean Phase, these propagated faults would obliquely reverse with a sinistral component (fig. 3.32.a) as they were not coaxial to the stress axis (fig. 3.13.b). If they are *en échelon*, their overlap (left- vs. right-stepping) will dictate how they interact under this regime (fig. 3.32.b-c). Left-stepping will induce transpression and uplift at the linkage point, whilst right-stepping will cause transtension and localised depression. This transtensional trough may be caused by either mechanism, but requires further investigation to define its extent and interior architecture.

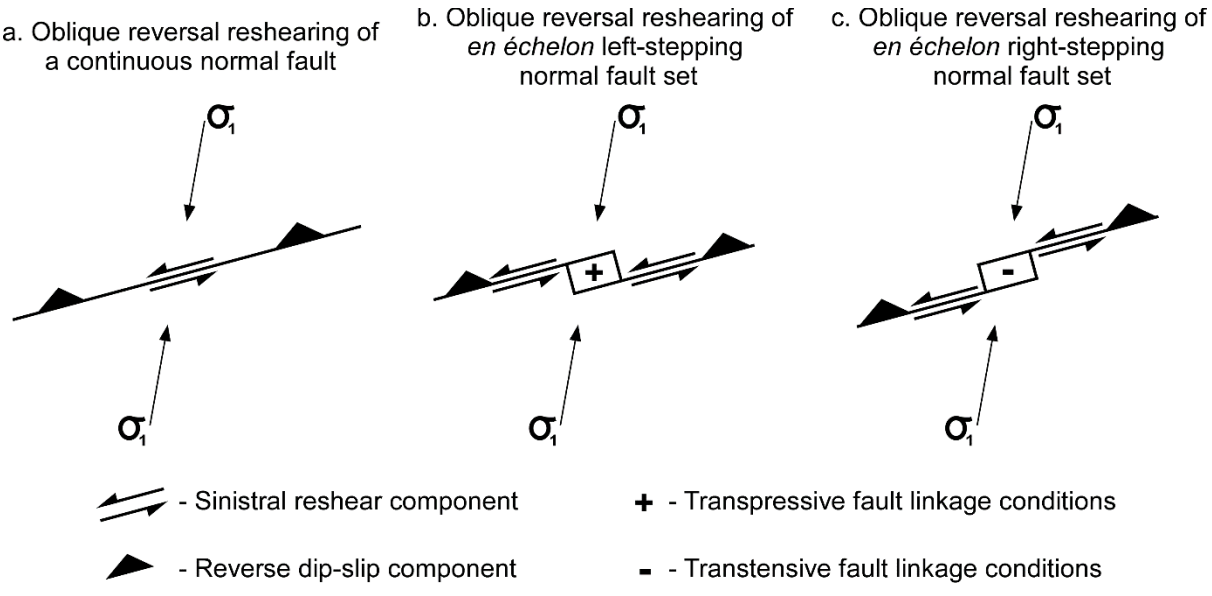

Figure 3.32 – Plan view of oblique reverse reshear behaviour of a normal fault, and the role continuous vs. *en échelon* fault geometries on localised deformation. Fault strike (075°) idealised from figure 3.31, with the 010° σ_1 alignment from the Pyrenean stress axis (fig. 3.13).

3.3.3 Variscan strike-slip fault inheritance in London

Two Variscan strike-slip fault sets are anticipated in the basement under London that may have reactivated and propagated during Alpine compression, with their reshear behaviour evolving between each Phases (fig. 3.15-19). However, their inheritance may not be apparent in the near surface as their vertical offsets are likely minor, preventing analyses similar to those used for the reversed normal fault set (§3.3.2). To overcome this, strike-slip inheritance behaviour was initially characterised from published analogue modelling and then compared with structural observations from the Wimbledon-Streatham-Greenwich Faults (WSG-Faults).

3.3.3.1 Strike-slip fault inheritance insights from analogue modelling

Analogue modelling enables tectonic processes to be replicated under specific scenarios in the lab to analyse their deformation behaviour. It has developed significantly from initial shear zone development (Cloos, 1928, Riedel, 1929) to a quantitative discipline (Koyi, 1997) using granular and cohesive media (Reber et al., 2020) to analyse the strain (e.g. Krézsek et al., 2007), temporal evolution (e.g. Wu et al., 2009), and complex structural architectures (e.g. Bonini et al., 2015). Here propagation behaviour is summarised from analogue modelling outputs of the strike-slip reactivation of a sub-vertical fault beneath an unsheared sedimentary mass. This is summarised schematically in figure 3.33, with the reader referred to Dooley and Schreurs (2012) for a comprehensive review.

Strike-slip faults do not propagate as a single shear. Instead their reactivation locally disrupts the acting stress field by causing basal shearing along the cover-basement interface (Naylor et al., 1986). This distortion locally generates sufficient shear stresses to propagate by splaying into multiple *en échelon* Riedel shears that are oblique to the basement fault trend (fig. 3.34) (Mandl, 2000). As they propagate upwards, they become less influenced by this deep stress distortion, causing their shear planes to progressively realign with the acting stress field to develop helicoidal geometries (fig. 3.33) (Mandl, 1988, Dooley and Schreurs, 2012). Progressive shearing causes the *en échelon* Riedel shears to eventually link and develop a continuous shear zone in the cover (fig. 3.34.b) (Naylor et al., 1986).

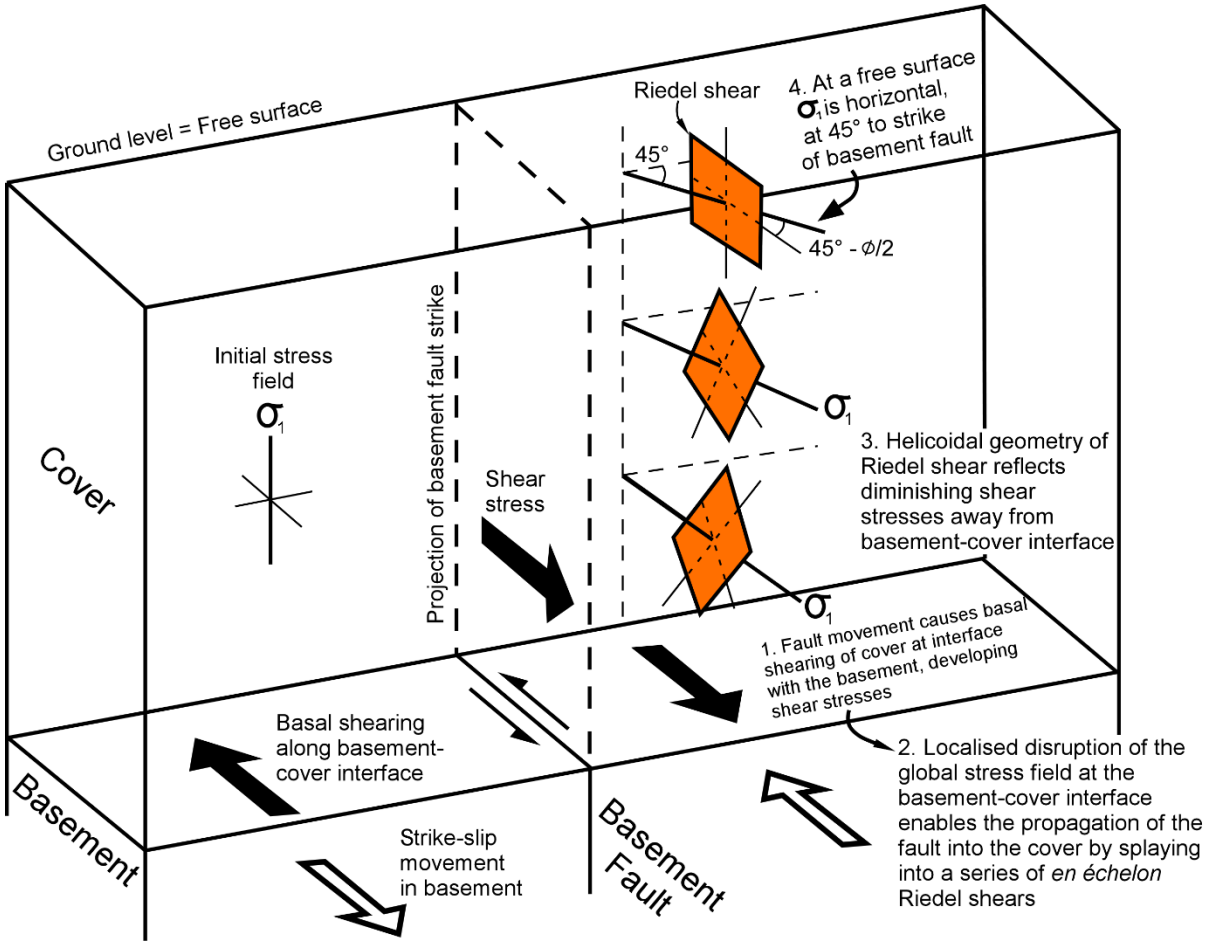

Figure 3.33 – Inheritance mechanism for a reactivated vertical strike-slip basement fault into the overlying cover by the localised disruption of the stress field and the development of *en échelon* Riedel shears. The solid bold lines represent the σ_1-axis. The orange planes reflect helicoidal Riedel shear geometries. Adapted and annotated from Dooley and Schreurs (2012) and Mandl (1988).

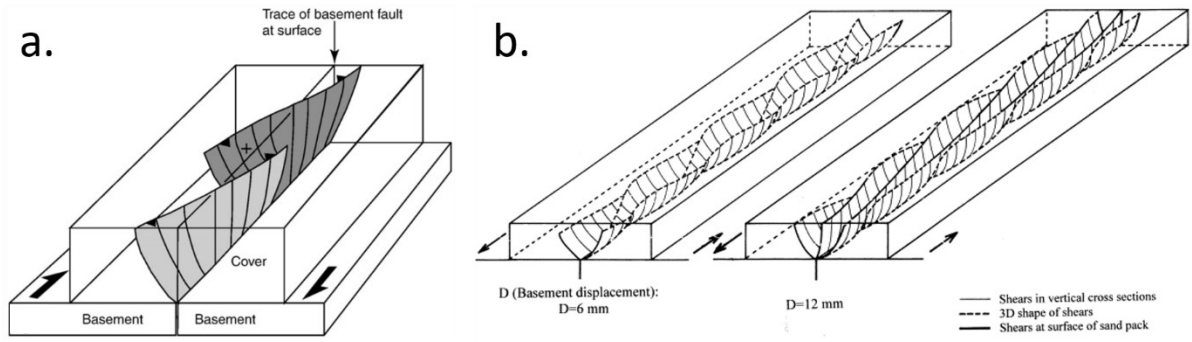

Figure 3.34 – Riedel shear propagation from dry sand experiments. Multiple splaying *en échelon* Riedel shears collectively root from a single strike-slip fault at depth.
a. Helicoidal geometry of two propagated *en échelon* Riedel shears. Adapted from Dooley and Schreurs (2012), originally from Mandl (1988).
b. Three-dimensional evolution of individual Riedel shear into a continuous shear zone above the basement strike-slip fault through its progressive shearing. From Ueta et al. (2000).

Propagated *en échelon* Riedel shears locally rotate the stress field in the cover to develop secondary faults within these linkage zones to form the continuous shear (fig. 3.35). Inter-connectivity through 2nd order shear development is required as isolated Riedel shears are unable to fully accommodate strains induced by basement shearing (Naylor et al. 1986). This singular 'throughgoing' shear zone is parallel to the basement fault trend (fig. 3.34.b) and progressively develops with further shearing.

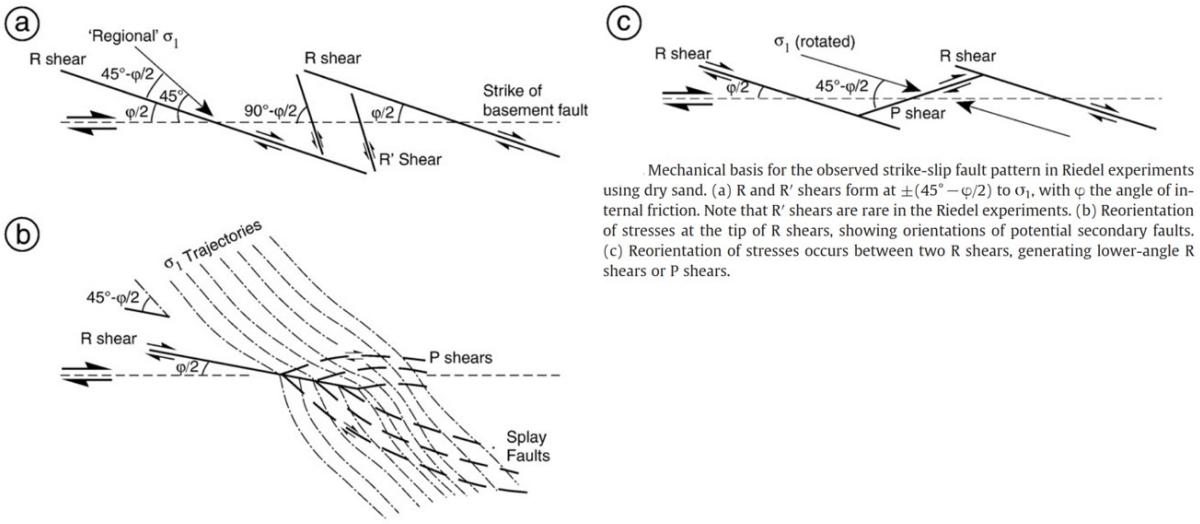

Mechanical basis for the observed strike-slip fault pattern in Riedel experiments using dry sand. (a) R and R′ shears form at $\pm(45^\circ - \varphi/2)$ to σ_1, with φ the angle of internal friction. Note that R′ shears are rare in the Riedel experiments. (b) Reorientation of stresses at the tip of R shears, showing orientations of potential secondary faults. (c) Reorientation of stresses occurs between two R shears, generating lower-angle R shears or P shears.

Figure 3.35 – Plan view of inherited *en échelon* Riedel shear zone development at the free surface (fig. 3.33) above a resheared dextral strike-slip fault. Localised stress distortion causes secondary fault generation that connect Riedel shears to develop a continuous shear zone. Adapted from Dooley and Schreurs (2012), originally from Naylor et al. (1986).
a. Riedel shears (R) are oriented at (45°- ϕ/2) to σ_1 at the free surface, as the stress axis is unaffected by basal shear distortion (fig. 3.33). When overlap is sufficient, antithetic Riedel shears (R') may form with opposing shear senses that link Riedel shears.
b. The stress axis is locally reoriented at Riedel shear tips and can produce secondary shears within the developing shear zone. The compressive side develops P-shears, and extensive side develops short-lived splays. The stress regime reverts to global conditions away from the shear tip.
c. P shear generation link *en échelon* Riedel shears with the same slip sense. They favour underlap.

Connectivity of inherited Riedel shears causes localised strain accommodation and increased deformation within the linkage zones. The style may reflect basement fault architecture and/or the shearing direction (fig. 3.36) and will affecting the products of inherited strike-slip faulting observed in London. Transpression is the de facto product of interaction and linkage (fig. 3.34.a), reflecting localised convergence (fig. 3.35) as the lateral-slip component becomes obstructed within linkage zones (Mandl, 2000) to generate push-up structures (3.36.b). Restraining bends along the underlying strike-slip will also induce transpression upward from the basement (fig. 3.36.a) (Fossen, 2016). In London, push-up structures would appear as localised syndepositional palaeotopographic and denudational influences, and by the development of post-depositional inliers.

Transtension and pull-apart basin generation (e.g., fig. 3.19.c) at inherited fault linkage points are induced by releasing steps in the basement strike-slip fault (McClay and Dooley, 1995) and/or σ_1 being aligned sub-parallel to the fault strike (Mandl, 2000), or reversal of the initial propagation slip sense. In London, transtension may lead to localised sediment accumulation within pull-apart basins.

Additionally, the sense of *en échelon* stepping may be used to infer basement fault slip style during the initial inheritance (Mandl, 2000) and potentially provide a tool to validate expected shear behaviour (fig. 3.15-17): Dextral shearing induces left-stepping, and sinistral shearing right-stepping. For the Variscan NW-set, it is unclear how Helvetic sinistral reversal (3.17.b) will affect the initially dextral inheritance.

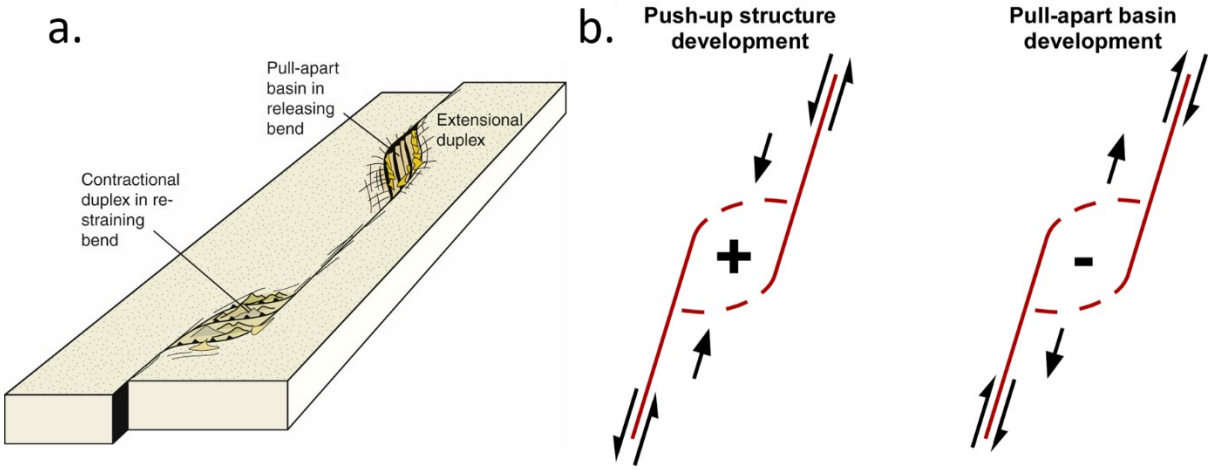

Figure 3.36 – Linkage style of *en échelon* Riedel shears is dependent on basement fault architecture and shear behaviour of its inherited products.
a. Fault bends will cause local convergence (transpression) and release (transtension). This is unaccounted for by idealised vertical planar basement fault models. Sourced from Fossen (2016).
b. Riedel shear linkage behaviour in the cover and the style of stress localisation through continued shearing (fig. 3.35) will be dependent on their slip sense. Push-up structures develop where converging *en échelon* shears generate transpressive conditions internally. Pull-apart basins form where diverging *en échelon* shears generate transtensive conditions internally, causing localised extension and depression.

3.3.3.2 Wimbledon-Streatham-Greenwich Faults: NNE-set Variscan strike-slip inheritance

The right-stepping *en échelon* Wimbledon-Streatham-Greenwich Faults (WSG-Faults) and the 'Dagenham' Fault are four overlapping NE-NNE trending faults (fig. 3.37) that intersect southern and east London. They are oblique slip with a significant sinistral component, and bound elevated stratigraphy, such as the 'Greenwich Anticline' inlier (§2.2.2.2). Collectively this is comparable to propagated *en échelon* fault linkage and transpressive push-up structure development (fig. 3.34). The structures are analysed below with independent observations to assess whether this is valid.

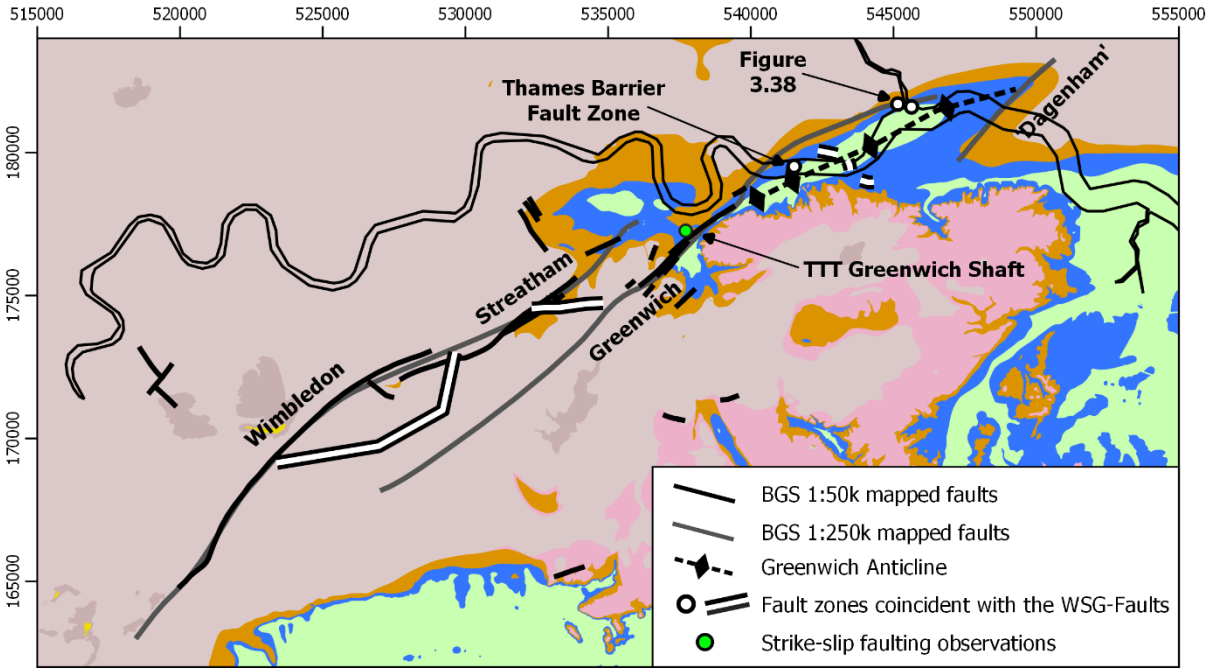

Figure 3.37 – The right-stepping *en échelon* Wimbledon–Streatham–Greenwich Faults and the 'Dagenham' Fault mapped by the BGS at 1:50k and 1:250k resolutions. Structurally analysed from fault zones, subsurface topography, and site observations to determine its tectonic origin under Alpine compression, together with the Greenwich Anticline.

The elliptical Greenwich Anticline chalk inlier is interpreted to cap an inverted basement fault (Ellison et al., 2004). The majority is bounded by the mapped Greenwich and Dagenham Faults, with stratigraphic elevations abruptly changing across the former and rising towards its centre (fig. 3.38). The Dagenham Fault likely continues south-westward to link and fully bound the inlier since strata suddenly becomes sub-horizontal away from it in the Crossrail post-construction section (Crossrail, 2016). Internally uplift is fault-controlled and rises towards the centre, as multiple fault zones have been identified within and along the inlier's margins (fig. 3.37-38) during recent and historical GIs (Conway and McCann, 1972, Carter and Hart, 1977, Newman, 2009, Newman et al., 2016, Black, 2017). This contradicts a fold capping/bending mechanism. Structural characterisation from the Thames Barrier site demonstrates lateral-slip dominance internally with a minor reverse dip-slip component (Carter and Hart, 1977). This indicates a confined transpressive, brittle push-up structure caused by

Dagenham-Greenwich Fault linkage, with its anticlinal-like geometry causing misinterpretation. The Greenwich Anticline is revisited in Chapter 6 to further characterise this transpressive structure.

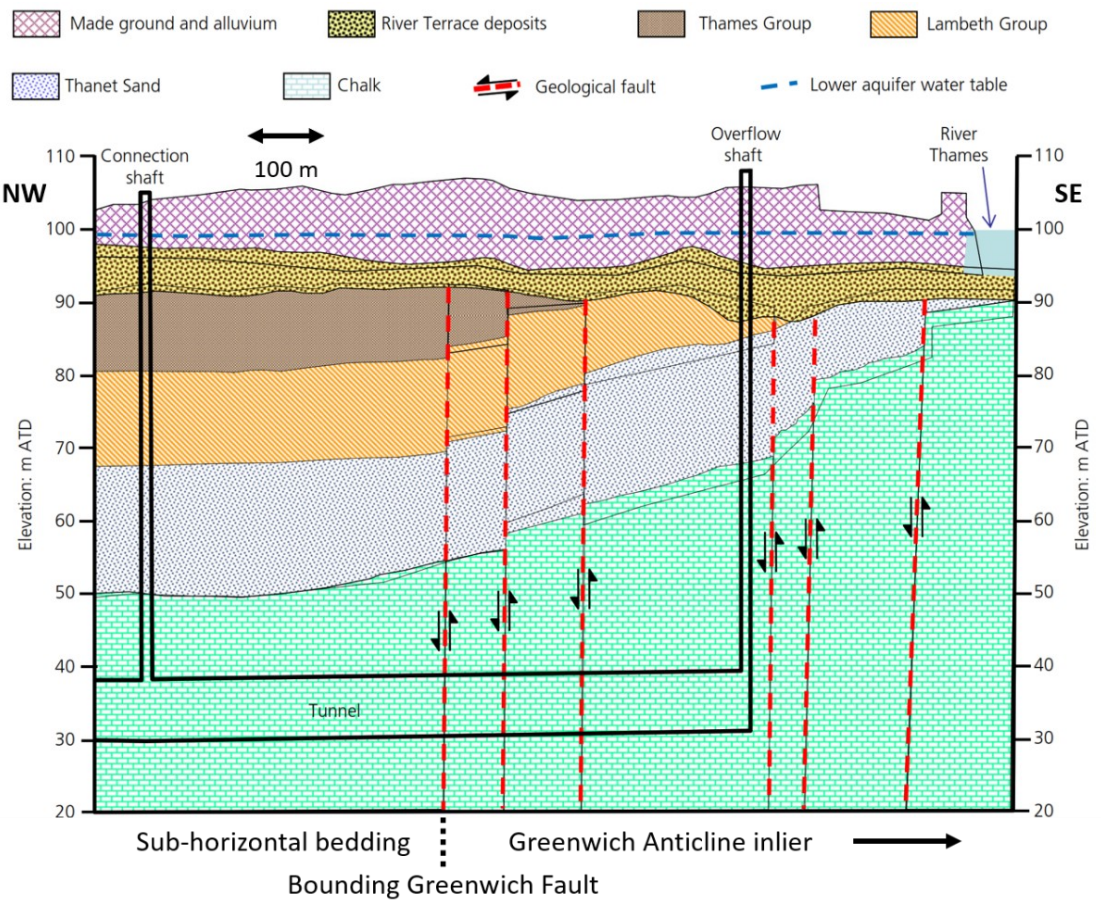

Figure 3.38 – Beckton Outflow Shaft Fault Zone. Transition from sub-horizontal bedding to abrupt internally fault-controlled uplift and inclination within the bounded Greenwich Anticline inlier. This fault zone's extent is undetermined; Newman et al. (2016) linked it to the Greenwich Fault however, it is likely part of a larger brittle transpressive structure within the inlier (fig. 3.37). Adapted from Newman et al. (2016).

Transpressive fault linkage is evident elsewhere along the WSG-Faults as unexposed elevated blocks are spatially coincident with other *en échelon* overlaps (fig. 3.39). Like the Greenwich Anticline, these overlaps are extensively faulted internally (fig. 3.37) with strike-slip faulting observed in chalk exposures at the TTT Greenwich Shaft site (Newman, pers comms, 2019b). Overall, the major fault geometries and linkage zones indicate full Riedel shear connectivity (fig. 3.37, 3.39). This is supported by the indirect fault map in Chapter 4, which bounds it with two lineaments parallel to the overall trend. Collectively, this implies the development of a continuous throughgoing shear zone (fig. 3.34)

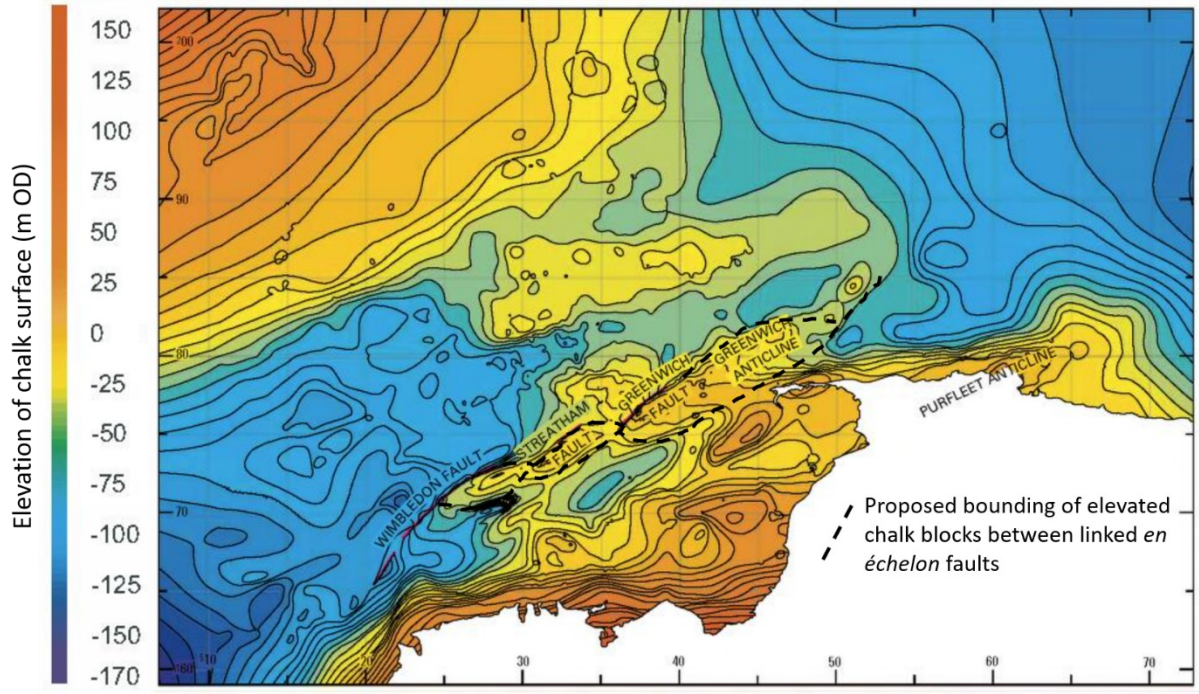

Figure 3.39 – Proposed linkage of the *en échelon* WSG-Faults linkage as projected overlapping fault members enclosing elevated, rhomboidal chalk regions. Base map adapted from Ellison et al. (2004).

Carter and Hart (1977) subdivided displacement at the Thames Barrier Fault Zone (fig. 3.37) into Pre- and Post-Thanetian (Late Palaeocene) episodes. The two episodes likely correspond with the Subherycian and Pyrenean Phases respectively, but any Helvetic Phase activity cannot be discounted due to the lack of Neogene sediments.

The WSG-Faults are either a product of direct Alpine compression, or inheritance of a reshear NNE-striking Variscan sinistral fault (fig. 3.1). The analyses indicate that these sinistral-slip dominant *en échelon* faults have connected to develop a continuous shear zone, with confined transpressive uplift where they overlap and link. A new shear mechanism is unlikely due to both its scale relative to minor structures attributed to direct Alpine compression, and misalignment with Alpine stress axes (fig. 3.13); furthermore, a mechanism that induces significant strike-slip faulting in thin cover yet a different method of strain accommodation in the basement is likely impossible.

The WSG-Faults are interpreted to be Riedel shears inherited from an underlying NNE-striking Variscan strike-slip fault (fig. 3.40). Their *en échelon* architecture and transpressive linkage zone development are compatible with inheritance behaviour of a sinistral shearing basement fault (fig. 3.34-36.b) that have connected into a throughgoing shear zone. Their Late Cretaceous-Palaeogene activity and slip sense are consistent with this set's Subhercynian-Pyrenean kinematic analyses (fig. 3.15-16). The findings support the basement origin suspected by Ellison et al., 2004.

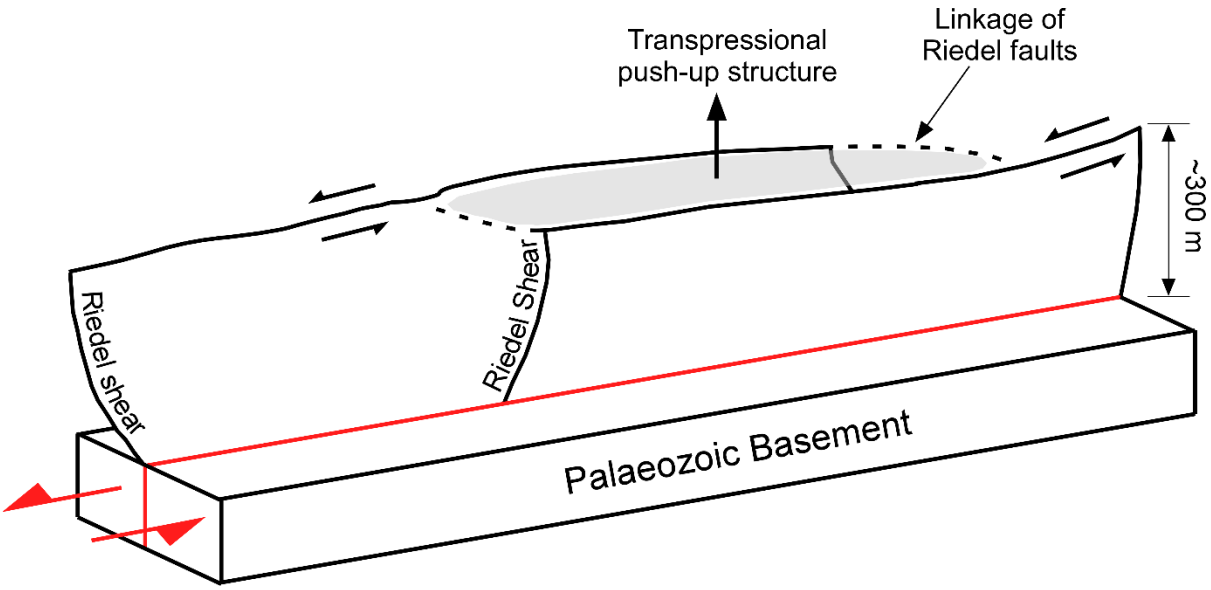

Figure 3.40 – Schematic interpretation of two of the WSG-Faults formed by Subhercynian-Pyrenean sinistral reshearing and *en échelon* Riedel shear propagation into the cover of a basement Variscan strike-slip fault. Connection of individual shears causes transpressive conditions within the linkage zones.

3.3.3.3 NW-striking Variscan dextral set inheritance in London

Subhercynian-Pyrenean kinematic analyses (fig. 3.15-16) and structural analyses (§3.2.3) imply that reshearing of the dextral NW-set was preferentially favoured over the sinistral NNE-set. However, this is contradicted by the lack of obvious evidence for the NW-set in London, yet apparent inheritance of the latter. This is attributed to the near-optimal alignment of the NW-set causing reshear with minimal oblique-slip. Hence resultant elevational offsetting in the cover would be restricted to linkage zones between individual *en échelon* dextral Riedel shears, preventing obvious detection in London's near surface. To contrast, the more oblique WSG-Faults has 10-30 m vertical offsets along individual Riedel shears and substantial push-up structures. The argument is supported further by parallel lineaments in the indirect fault map (fig. 3.25.b; Chapter 4) and lateral displacement observed by InSAR (Mason et al., 2015), yet minimal topographic presence (fig. 3.39).

Alpine inheritance of the Variscan dextral set is expected in London as kinematic and proxy analyses both demonstrate its suitability for reactivation. This is supported as the less favourable sinistral set is also present in the cover.

3.4 Alpine stress accommodation in the southern London Basin

Identifying whether London's major faults are new Alpine shears or basement reshears determines how stresses were relatively distributed between the basement and cover along the southern margin of the London Platform (fig. 3.1). This crustal interface demarcates between the competent shallow Anglo-Brabant Massif (ABM), and the weak Rhenohercynian Zone (RHZ) and its overlying extensional basins, as outlined in §2.1.1, making comparisons with conventional inversion behaviour (fig. 3.2) inappropriate for characterising its Alpine deformation.

Alpine compressive stresses in London were accommodated by a combination of brittle and ductile processes (§2.2.2). The contrasting scale between the minor and major faulting implies that they are products of two separate mechanisms. Major faulting in London represents the Alpine reactivation and inheritance of three basement fault sets according to direct and indirect propagation evidence, kinematic analyses, and proxy case studies: the Variscan conjugate strike-slip pair and post-Variscan normal fault set. Minor faults are likely direct Alpine products, however, stress distortion around major faults may also play a role for some (discussed in §7.4.3).

The spatial extent of structural inheritance across the Basin remains unknown due to comparative subsurface data sparsity and fault identification issues (discussed in Chapter 4). It appears to cease north of London as indicated by structural contour and faulting data (Lake et al., 1986, Bristow et al., 1985, Ellison et al., 1986, Pattison et al., 1993). Two basement-derived faults are suspected within the London Basin's interior: the Lilley Bottom Structure (Hopson et al., 1996, Mortimore et al., 2001) and the Glinton Thrust (Woods and Chacksfield, 2012). Despite an anticipated Caledonian fabric within the ABM (Pharaoh et al., 1987), these structures are likely older crustal weaknesses within the ABM as they are isolated phenomena. The restriction of inheritance to the ABM's southern (and probably northern) margins implies that the platform was relatively rigid with Alpine strains concentrated along its faulted boundaries with weaker structural domains, behaving consistently with its responses to previous tectonic events (§2.1).

The findings restrict direct tectonism of London's cover to the pervasive minor faulting, broad open folding, and tensile and shear jointing observed throughout the southern London Basin. Their scale, variable strikes (fig. 3.24), and normal fault prevalence imply that lateral confinement and burial of the cover were limited ($\sigma_V = \sigma_1$ or $\sigma_V = \sigma_1 = \sigma_2$), even during the main Pyrenean Phase. This implies that the underlying platform effectively 'shadowed' (or protected) its overlying cover to reduce acting Alpine stresses, as adjacent inverting basins demonstrate that compressive magnitudes were relatively high ($\sigma_V = \sigma_3$).

The mechanical favourability of basement fault reactivation over new shear development along the platform margin should be anticipated. Rock mechanics contextualises this since pre-existing discontinuities (i.e., faults) can significantly weaken the rock mass overall (fig. 3.41). In the Alpine framework of London (fig. 3.1) this amounts to shear strains being localised through reshearing in the shallow faulted basement to minimise deformation in the overlying weak yet unfaulted cover. This is recognised by Copley's (2017) concept of "*weak faults embedded in* [relatively] *strong surroundings*", with only severe misalignment to the stress field allowing new shear to become favourable (fig. 3.7). When coupled with the cover's protection from straining by the London Platform, the origin of major faulting becomes obvious.

The analyses provide new insights into how shallow Palaeozoic platforms and their overlying cover mechanically respond to intraplate compression. 'Platform inversion' of a compressed shallow rigid block is characterised by shear strain concentration along its margins to favourably exploit pre-existing faults rather than develop new structures in either the basement or its covering sediments.

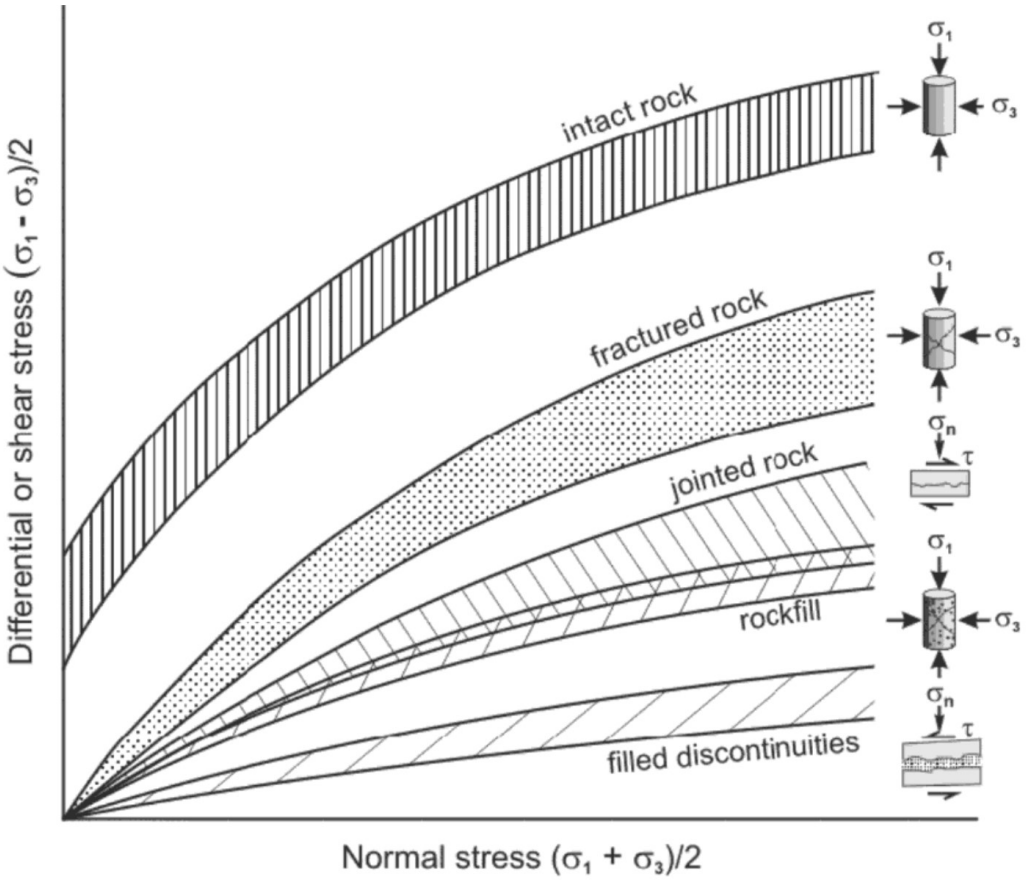

Figure 3.41 – The impact of a discontinuity and its frictional properties on the shear strength of a rock mass. Sourced from Cosgrove and Hudson (2016), who adapted from Barton (2006).

3.5 Conclusion

The origin of major faulting observed in and around London was investigated to determine whether they were inherited from the underlying basement, or new products of Alpine compression. This was achieved by assessing the feasibility of the former mechanism through kinematic reactivation and proxy analyses, and fault propagation evidence in the southern London Basin.

The findings imply that, like elsewhere in the British Isles (fig. 3.3, 3.19), Alpine compression caused Variscan strike-slip and Mesozoic listric normal fault sets to reshear along the southern margin of the Anglo-Brabant Massif. Fault set-specific reshear feasibility evolved between the Alpine Phases (fig. 3.15-21), with the Variscan dextral fault set reversing during the later Helvetic Phase. Major faults in the near surface can be directly linked with basement faulting (fig. 3.26-29), and, indirectly through compatibility with expected propagation behaviour (fig. 3.37-40 vs. 3.33-36) and geophysics (fig. 3.30-31). This validates suspicions of basement influence in London's near surface (Royse et al., 2012, Ellison et al., 2004).

Major faults in London are interpreted to be inherited basement faults, with their reshearing and propagation being the principal accommodator of Alpine stress. Their restriction to the southern London Basin implies that strains were concentrated along the ABM's margins, rather than distributed within it. New Alpine structure development played a comparatively minor role, implying that cover material on platforms was 'shadowed' from lateral compression by stress accommodation in the basement. Lower confining stresses in the cover are evidenced by the scale of minor faults and the broad, open folds (§2.2.2).

Platform inversion is proposed as a mechanism for how competent, shallow basement influences the structural response of its overlying cover to compression through the exploitation of pre-existing structures as strains are concentrated along its margins.

The basement origin of major faulting in London provides a basis for characterising their behaviours and architectures in later chapters (Chapters 6-7). However, their presence and coverage in London must first be analysed. Chapter 4 investigates the identification and mapping of major faulting, challenges encountered and potential options for overcoming them, and characterises their sets.

"*The general law seems to be, that when any band of earthy crust has been greatly folded or fractured, each subsequent disturbance follows the very same lines - and that, simply because they are the lines of least resistance*"
Godwin-Austen (1856)

4. Fault mapping in London

Analysis from Chapter 3 implies that London's major faults are inherited from underlying basement faults that reactivated under Alpine compression. But observations of fault zones (fig. 4.1) away from known structures demonstrates that many inherited faults are unmapped. This under-representation is now recognised (§2.2.2.5) with major faulting expected but broadly unidentified in London.

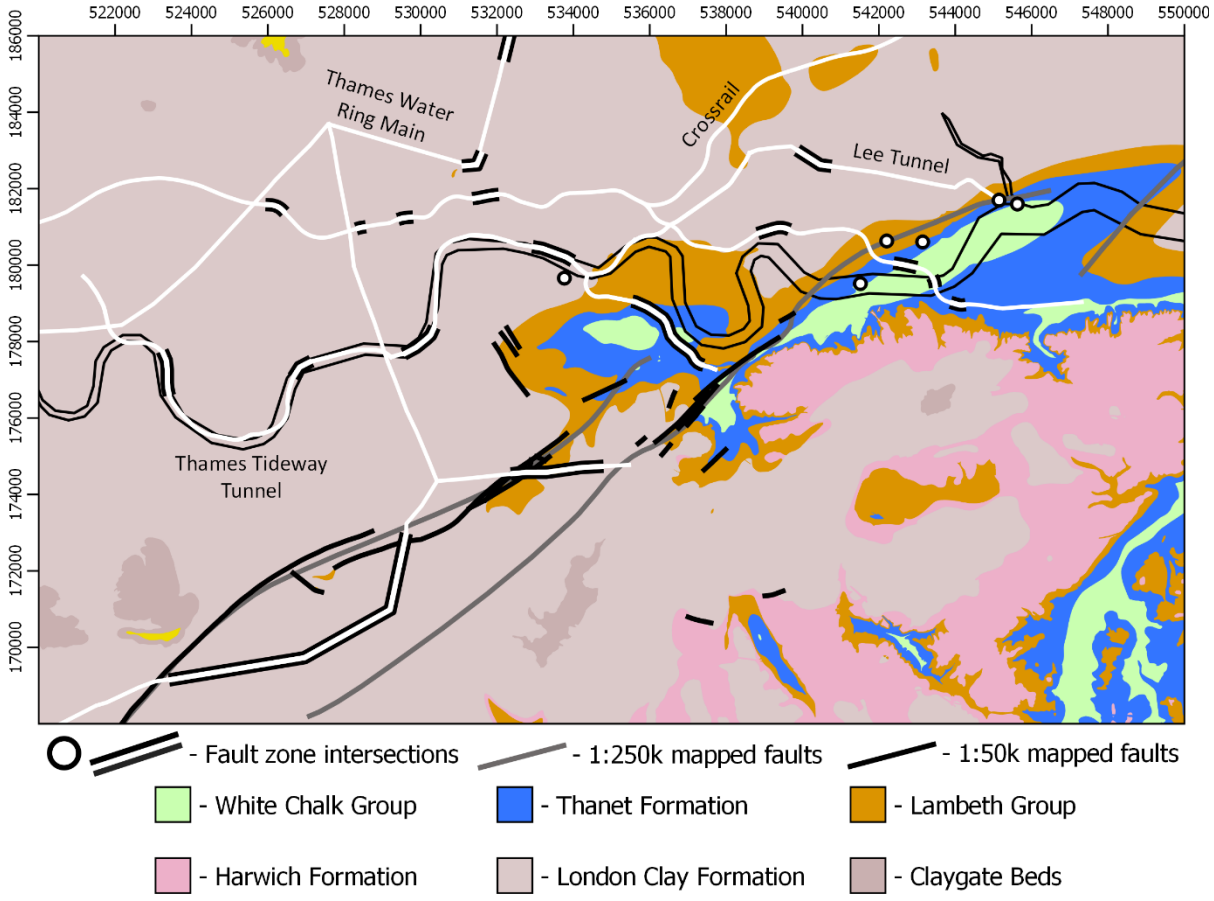

Figure 4.1 – Geological map of London overlain with BGS mapped faults at 1:50,000 and 1:250,000 resolution, and fault zone positions identified by major infrastructure projects. Tunnel alignments are marked in white.

Chapter 4 investigates fault identification in London and its challenges. Mapping methods and previous contributions are reviewed (§4.1). Following this, a new indirect technique is introduced together with fault set trend analyses (§4.2). The outputs of both are presented (§4.3) and discussed (§4.4) through critiquing against published maps, analysing discrepancies, and defining fault sets and their specific behaviour. Please refer to the lithology key in figure 4.1 for all maps in this chapter.

The outcome is a hidden fault network under London and the characterisation of its three major (inherited) fault sets in the near surface.

4.1 Fault mapping and identification in London

Fault mapping has been undertaken in London since at least 1850 (De la Condamine, 1850). Multiple contributions have since been made as lithological understanding, subsurface data, and technology have improved over time. But map accuracy and/or validity varies, and reflects the methods, assumptions, and analytical conservativeness specific to each. Consequently, multiple fault maps exist for London that contain inconsistent structural interpretations.

These contributions are reviewed in §4.1 according to their overarching methods to determine the best technique for major fault identification in London. These are summarised in table 4.1, and are split into three groups according to methodology:

- §4.1.1 Geological mapping – Primarily at-surface structural observations coupled with geological and geomorphological mapping and limited reliance on localised subsurface data.
- §4.1.2 Geological modelling – Primary reliance on subsurface data, coupled with surface features, to provide three-dimensional (3D) structural analyses.
- InSAR – Identifying spatiotemporal variations in at-surface ground movement to infer the positioning of structures in the near-surface.

4.1.1 Geological Mapping

Near surface structure identification is typically achieved through mapping of exposures coupled with indirect evidence from lithological offsets and geomorphological features (Lisle et al., 2011). Subsurface data has a limited role and is typically used to locally constrain structures. Four geological mapping contributions (table 4.1) are summarised and have been grouped here according to whether they undertook conventional or geomorphologically-driven mapping.

4.1.1.1 Conventional geological mapping

Faulting in London was first identified during the Victorian era from exposures in railway cuttings and brickyards, gravel pits and tunnel excavations (e.g., fig. 2.26, 2.29). But the scale of most made mapping impracticable (Whitaker et al., 1872, De la Condamine, 1852) and restricted fault observations to memoirs/field reports instead. De la Condamine (1850) undertook the first structural mapping of southeast London (fig. 4.2) by correlating abrupt lithological changes with fault exposures to form the basis for the Greenwich and Streatham Faults (fig. 2.20). Mylne (1856, 1858) extended these and identified new faults that were further constrained by Bauerman et al. (1885) and Whitaker and Dawkins (1892).

Table 4.1 – Overview of previous contributions to inferring and mapping faults in and around London

Group			Overview	Sources
4.1.1	Geological Mapping	Historical Mapping	Collates limited exposure observations with mapped, abrupt lithological changes (and limited borehole analysis) to identify several faults in southeast London.	De la Condamine (1850); Mylne (1856, 1858)
		Wooldridge Structure Map	Locally constrained structures from limited exposures, inliers and outliers, and geomorphology also. Over-extrapolation from initial local interpretations without validation severely limits the validity of this interpretation	Wooldridge (1923)
		BGS 1:50,000 Mapping and Digitisation	Coupled mapping with improved lithological understanding and borehole data to refine known faults and identify new ones. Digitisation enabled communication of mapping confidence and progressive updating of features.	British Geological Survey (1996), British Geological Survey (1998b), British
		River Morphology Mapping	Geometries of river valleys used to infer the positioning of underlying faulting, as they preferentially exploit pre-existing weaknesses associated with structures.	de Freitas (2009)
4.1.2	Geological modelling	Roads in Tunnels Study	Geostatistical interpolation of 2,500 boreholes with an embedded algorithm for inferring faulting from anomalous gradients. No new faults were proposed.	West (1983), Rosenbaum and Warren (1986)
		The Reading Report	Extensive fault network proposed from geostatistical highlighting of areas with elevational variation of >5 m. Map questioned, with over-extrapolation present.	Andrews et al. (1995)
		BGS LOCUS Modelling	Generation of the subsurface from geostatistical interpolation between 22,000 boreholes in London. No new faults identified, but postulated with folding also.	Ellison et al. (1993); Strange et al. (1998)
		BGS Lithoframe Modelling	Construction of informed cross sections and resultant fence diagram that constrained the later interpolation process. Rigorous identification of new faults and folding in London.	Ford et al. (2008), Ford et al. (2010), Mathers et al. (2014), Burke et al. (2014)
		Localised modelling	Several separate models are presented to highlight inconsistency in the approach to structural analysis in London. One proposed new faults, another reinterprets the Greenwich Fault as a syncline, with others ignoring the potential for faulting.	Howland (1989), Howland (1991); Paul (2016); Price et al. (2018);Burke et al. (2018)
4.1.3	InSAR	BGS Remote Sensing	Coupled PSI with GPS and absolute gravity readings to identify near-surface geological, tectonic, and anthropogenic processes, and the possible presence of underlying basement structures.	Aldiss et al. (2006), Aldiss et al. (2014)
		Imperial College InSAR	Long timeframe analysis has identified block-like movement in the near-surface but lack ground truthing. Short timeframes have indirectly inferred faulting from both dewatering behaviour and coupling with multiple lines of evidence.	Mason et al. (2015); Bischoff et al. (2020b); Scoular et al. (2020a)

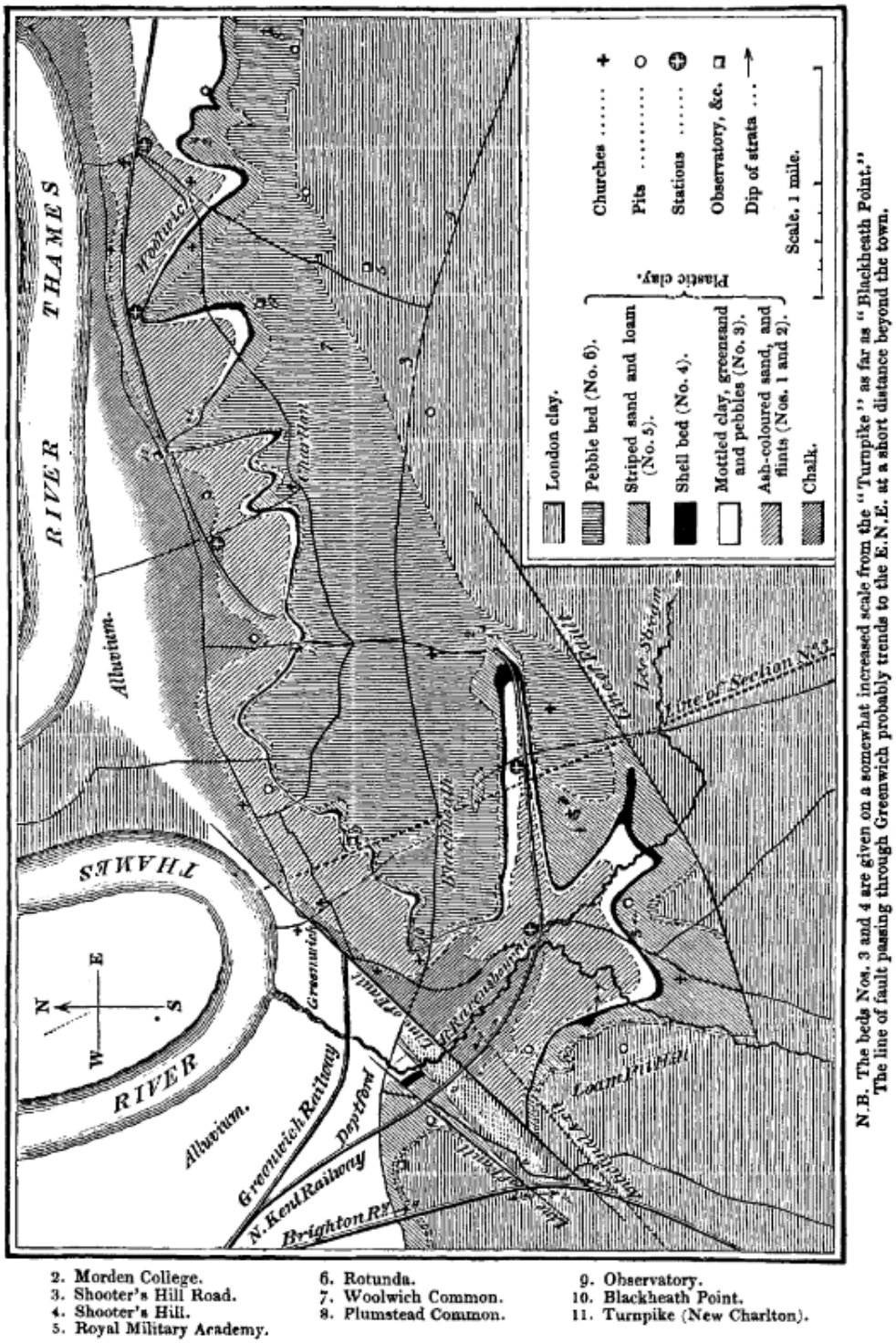

Figure 4.2 – Geological map of southeast London produced by De la Condamine (1850), who first mapped major faulting in London from exposures and abrupt changes in geology.

Progressive understanding of Palaeogene lithologies (fig. 2.22) coupled with increasing availability of subsurface data from bored wells aided fault identification. This is illustrated by the Wimbledon Fault's determination by Davis (1928) in figure 4.3. By the end of this period, three major faults were recognised in London that formed the basis for the BGS' 1:250,000 map (fig. 2.20): the NE-trending *en échelon* Wimbledon-Streatham-Greenwich Faults (WSG-Faults).

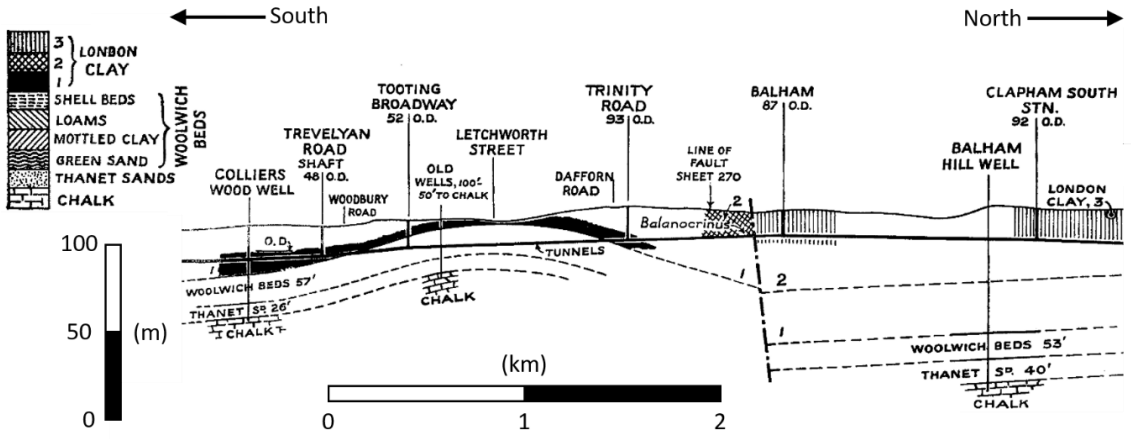

Figure 4.3 – Constraining of the Wimbledon Fault by coupling tunnel and at-surface exposures with biostratigraphic subdivisions of the London Clay and subsurface elevational variation from boreholes. Adapted from Davis (1928).

Higher resolution (1:50K) mapping (fig. 4.4) has been achieved (British Geological Survey, 1996, British Geological Survey, 1998b, British Geological Survey, 1998a, British Geological Survey, 2006) by recent advances in London's lithostratigraphy (King, 1981, Ellison et al., 1994, Skipper, 2000, Mortimore et al., 2001), increased subsurface data availability, and the advent of digitisation (Smith, 2009b, Jordan and Napier, 2016). The majority are associated with the WSG-Faults rather than separate major faults, with no new faults identified in North London (Map Sheets 256-257). Most are 'inferred' (fig. 4.4) according to their digitised metadata, which grades interpretative confidence: Observed > Inferred > Conjectural (Smith, 2009a). Further faults are likely to be identified through higher resolution remapping and lithostratigraphical advances (e.g., Aldiss et al., 2018). Notably much of the Greenwich Fault and the 'Dagenham' Fault, mapped at 1:250K (fig. 2.20), are absent at this resolution.

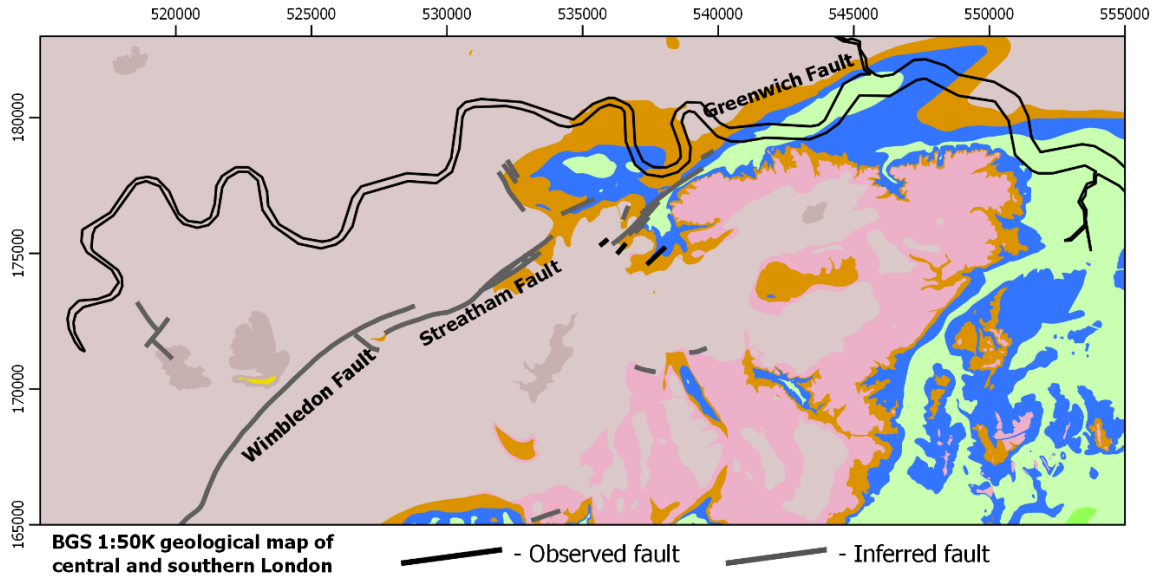

Figure 4.4 – 1:50,000 BGS geological mapping of central and southern London. The 24 faults interpreted in the map area are graded according to the interpretative confidence in their associated metadata.

The reliance upon predominantly direct structural evidence provides confidence in the conventional mapping method. But it has also led to an under-recording of faulting across London (fig. 4.1) as the accessibility to at-surface geology is challenged in London by four restrictions (Aldiss, 2013):

- Extensive urbanisation inhibits the ability to undertake field mapping due to developed anthropogenic cover across London.
- Superficial coverage masking underlying spatial changes in bedrock subcrop.
- Lithological homogeneity of both the London Clay and the Chalk Supergroup, inhibiting offset identification.
- Limited topographic expressions (particularly where London Clay is crops out).

Outliers and heterogeneous lithologies in southeast London (fig. 4.4) favour fault identification by overcoming several of these issues. This relative abundance locally may misleadingly cause a perception of minimal faulting elsewhere in London, but this is incorrect (i.e., fault zones, fig. 4.1). Additionally, Aldiss (2013) noted that conservative mapping rationales may have contributed to this under-recording of faults by historically favouring in-field observations and not including structures without sufficient evidence. But this does provide considerable confidence in BGS mapped faults.

4.1.1.2 Geomorphological-driven mapping

The potential for underlying geological structures to influence at-surface processes led two mapping exercises to use geomorphological evidence to infer fault positions in London.

Wooldridge (1923) produced a structural map of the London Basin (fig 2.30) by extrapolating between disparate geological and structural observations using alignments inferred from both outcrops and geomorphological (e.g., valley) trends. Four structural trends were proposed: N-, NW-, NE-, and E-sets. General structure types were inferred from boreholes, with inliers and outliers used to propose anticlines and synclines, respectively. Most were interpreted to be folding (§2.2.2.5).

De Freitas (2009) proposed that the morphology of the River Thames and its tributaries may reflect an underlying fault fabric (fig. 4.5.a) since weaker tectonised ground can locally influence river morphology and linearise their alignments through preferential erosion. They were identified to follow consistent sub-linear trends (fig. 4.5.b): NW-to-NNW, NE-to-NNE, & East. This method is distinct from other mapping exercises (table 4.1) as it relies solely upon river trends. The trends spatially correlate with several features indicative of underlying structures: bounding both elevated chalk ‘domes’ in the subsurface and rectangular anthropogenic cones of depression, coincidence with deep rockhead anomalies, and fractal length relationships comparable to fault-controlled river patterns.

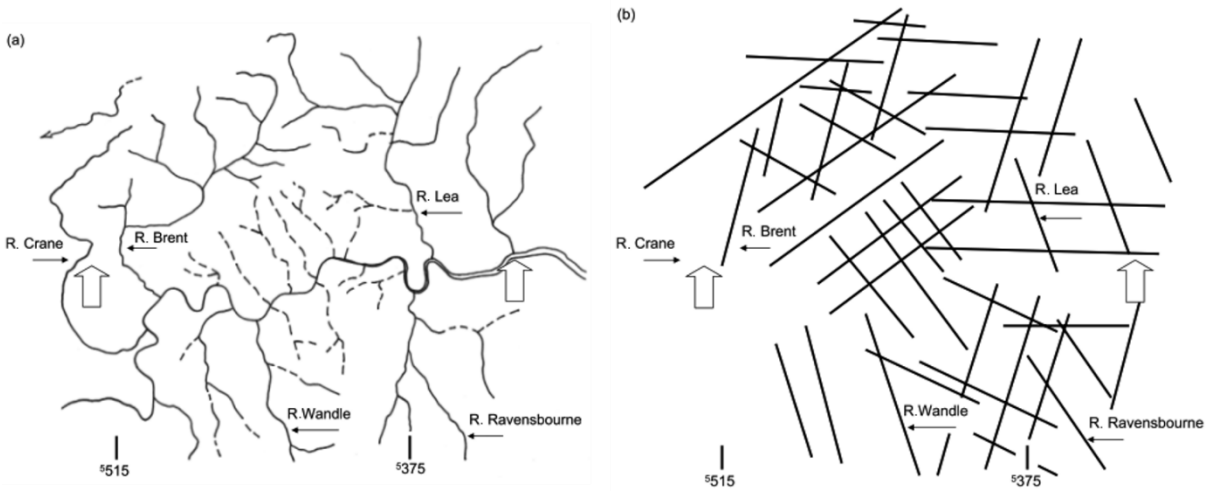

Figure 4.5 – Fault map proposed by De Freitas (2009) by mapping highly-linear river trends in the London Basin. Adapted from De Freitas (2009).
a. Morphology of the River Thames and its tributaries, comprising both at-surface and 'lost' (buried) rivers.
b. Lineament map developed from river trends in and around London.

Geomorphological evidence provides an alternative to conventional fault mapping where exposures are limited. Both contributions are locally validated by structural evidence, but the majority of inferred lineaments lack verification and may reflect other processes also. For example, Wooldridge interpreted hills capped by the sandier Bagshot Formation as synclinal inliers rather than geomorphological features more resistant to erosion than the underlying London Clay Formation.

De Freitas's contribution requires analysis to confirm the coincidence of each river with faulting since drainage patterns are potentially unreliable in isolation (Aldiss, 2013). This has already been achieved locally by De Freitas and independently for the Lea Valley Fault (e.g. Ghail et al., 2015a, Linde-Arias et al., 2018). Comparatively, Wooldridge's map is considered inconclusive given it extrapolated between distal, isolated exposures without validation in-between on a London Basin-wide scale.

4.1.2 Geological modelling

London is data-poor in at-surface observations but data-rich in subsurface geological information due to its extensive borehole coverage (fig. 4.6). Faulting offsets can be identified by abrupt lithological changes between proximal boreholes, overcoming the geological mapping issues outlined in §4.1.1.1. Three dimensional (3D) models of these faults and the geological units they bound can be developed by analysing a collated network of subsurface and at-surface data. Geological modelling is categorised here into two branches:

- Explicit Modelling – Where interpretations are defined manually from informed geological reasoning and incorporated into the model.
- Implicit Modelling – Where geostatistical methods interpolate between data points to construct geological surfaces and undertake probabilistic analyses for the presence of faults.

Modelling workflows typically combine both branches, but the ordering is critical to the generated model's outputs and interpretative rationale: explicit- vs. implicit-driven. London-wide modelling programmes have been grouped according to dominant modelling technique (§4.1.2.1-2), with localised modelling reviewed separately (§4.1.2.3).

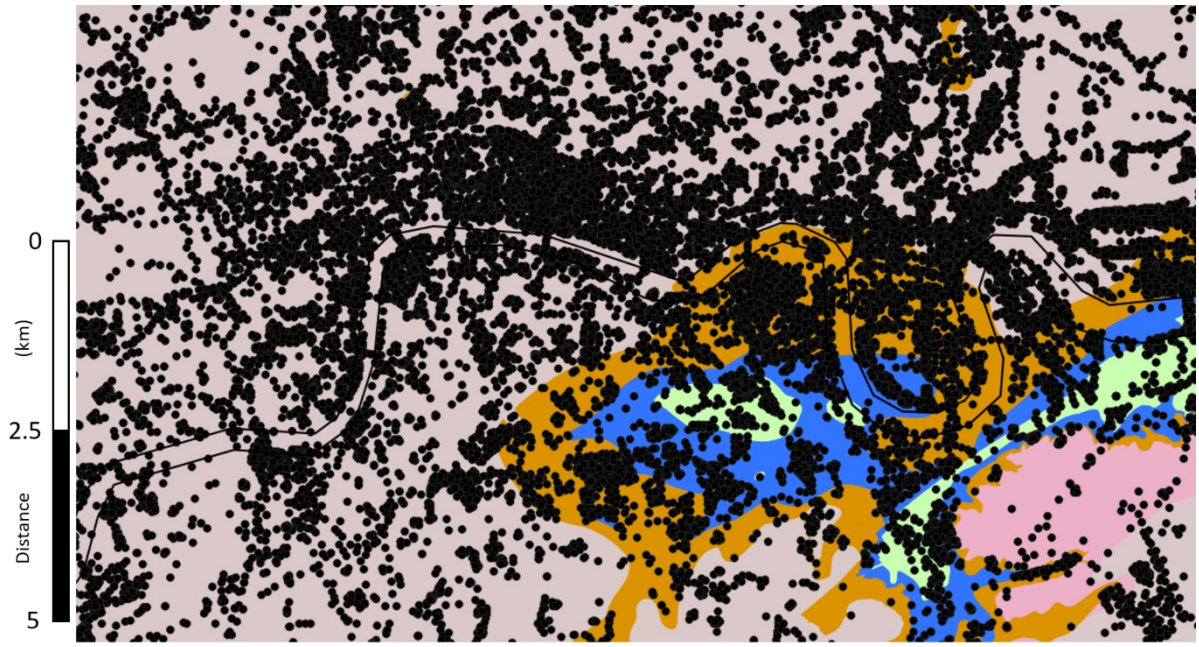

Figure 4.6 – Borehole coverage of London (approximately 24,200 presented). Extracted from the BGS' Single Online Borehole Index (SOBI) of Great Britain and Northern Island.

4.1.2.1 Implicit-driven modelling

Barrow and Wills (1913), and later Buchan (1938), undertook the first modelling programme of London. They produced contoured elevation maps of the Chalk surface (fig. 4.7) from water wells to hydrogeologically characterise the Lower Aquifer. The model was implicit with structures pre-determined from historical geological mapping to influence the interpolation process. They comprised the WSG-Fault and an unverified N-trending fault at the mouth of the River Roding[22]. Considerable elevational variation and localised areas of steepening are present. Despite not being intended for structural mapping, Buchan did postulate the presence of folding, interpreting ENE-trending depressions (green) and uplifted flanks (white) to be synclines and anticlines, respectively.

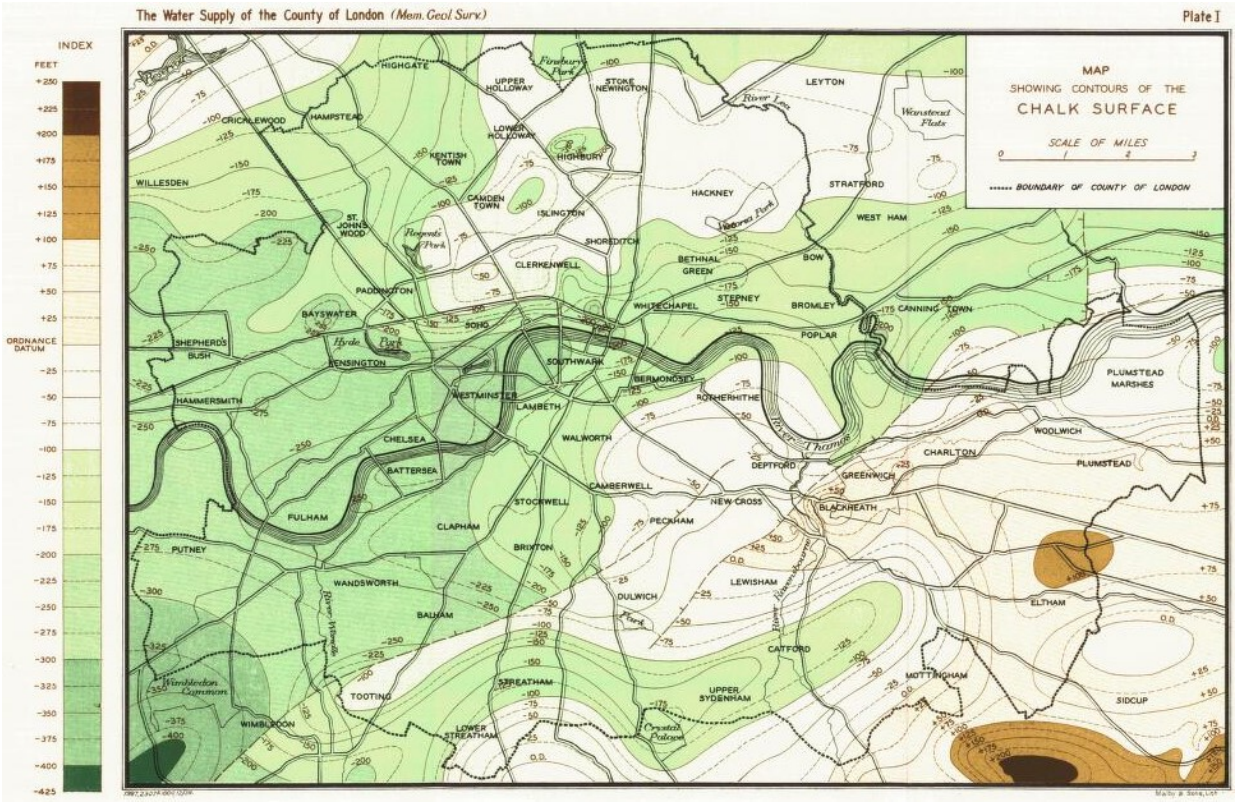

Figure 4.7 – Contoured elevation map of the Chalk surface under London. No new faults were mapped, despite localised areas of steepening contours. Anticlines and synclines were inferred from the continuous surface generated. Sourced from Buchan (1938).

The Roads in Tunnels Study was conducted to aid ground investigations by anticipating troublesome lithologies along tunnel alignments and is documented in West (1983) and Rosenbaum and Warren (1986). They used an implicit modelling-driven workflow to develop contoured surfaces for each defined layer[23] (fig. 4.8.a) by interpolating between boreholes containing them, from which unit thicknesses were also determined (fig. 4.8.b). To identify the location of faults, an algorithm was

[22] The rationale behind this new fault is unclear and it is not present in future works nor validated by them.
[23] Quaternary Deposits, London Clay Formation, Lower London Tertiaries, and the Chalk. The 'Lower London Tertiaries' is an outdated term for grouping of the Thanet Formation, Lambeth Group and Harwich Formation.

included that detected anomalous gradient changes within a surface and inserted a steeper gradient to signify the offset portions of the surface. No new faults were proposed.

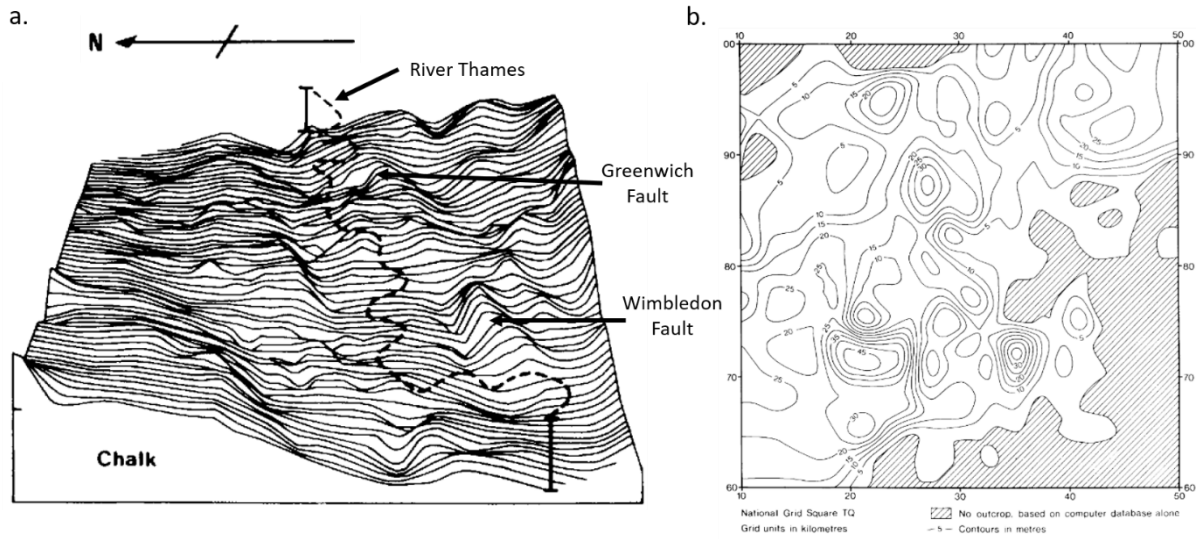

Figure 4.8 – Outputs of geological modelling from the Roads in Tunnels Study conducted for Greater London Council. Adapted from Rosenbaum and Warren (1986).
a. Elevation of the Chalk surface under London. Only the Greenwich and Wimbledon Faults were marked on the model, despite the methodology used to increase gradients along suspected faults.
b. Thickness plot of the London Clay Formation determined from surface interpolation of its upper surface and the surface of the underlying 'Lower London Tertiaries' (see footnote 23).

In the early 1990s, Thames Water Limited funded a research project at the University of Reading to hydrogeologically characterise and structurally reassess the Lower Aquifer[24] of the London Basin from water wells and boreholes. The output (Andrews et al., 1995) is colloquially referred to as the 'Reading Report'. They developed an algorithm to aid fault identification that assessed datapoints within a 250 m radius for elevational variations. If <5 m of variation was achieved, the data was grouped and outputted as an "*intermediate*" value, rather than rely on all available subsurface data. Faulting was locally assumed if >5 m variation occurred, preventing the statistical method being undertaken. There is limited information regarding the decision-making process behind fault interpretation in the report. Elevational and derived thickness data were also extracted to construct contour maps from which geological structures were interpreted. The proposed faults (fig. 4.9) consistently follow NW- and NE-strikes, being idealised to straight lines (apart from the known WSG-Faults). Andrews et al. (1995) respectively termed these 'strike' and 'dip' faults; this outdated terminology describes orientation relative to the London Basin's axis (Buchan, 1938) and does not reflect slip behaviour.

[24] The Lower Aquifer is comprised of the Chalk Supergroup, the Thanet Formation, and the sand-dominant portions of the Upnor Formation (fig. 2.21-22). Within the report, the latter two formations are referred to as 'the Basal Sands of the Lower London Tertiaries'.

In central and east London, faults broadly correlate with uplifted inliers, and imply the presence of structures where London Clay coverage has previously inhibited fault identification (fig. 4.9, 4.4). The intersection of these two fault sets has generated fault blocks that confine internally up- and down-warped lithologies that Andrews et al. (1995) attributed to folding.

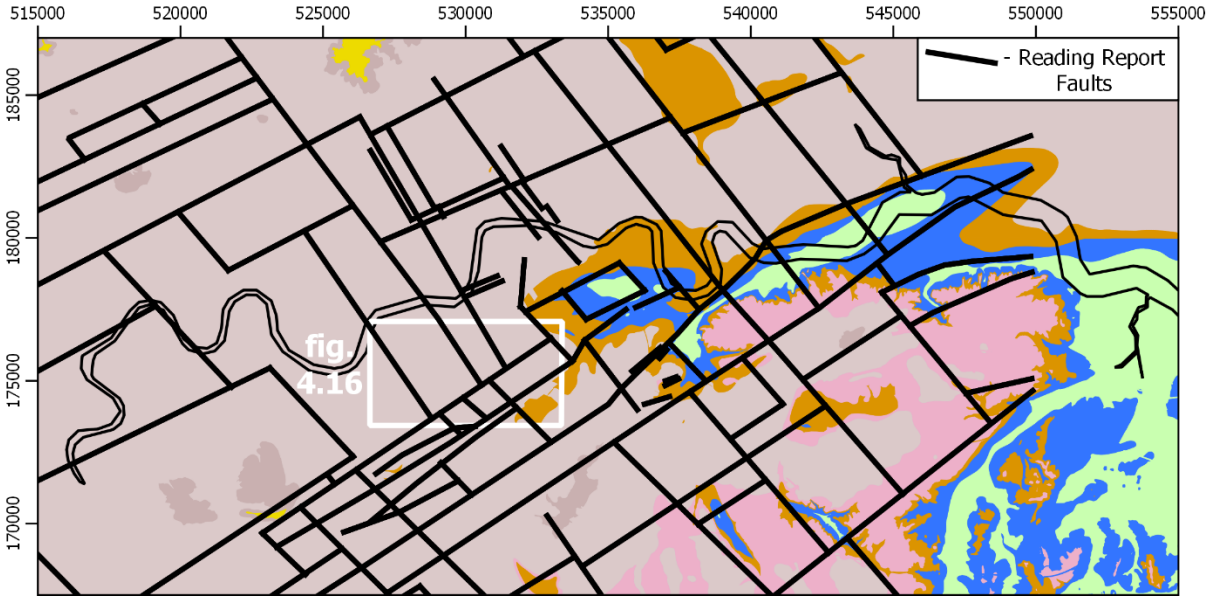

Figure 4.9 – Faults inferred from geological modelling by Andrews et al. (1995) whom interpreted their positions from hand-drawn contour maps generated from subsurface data statistically generated from both idealised and actual borehole/well data. Faults were georeferenced by Jennifer Scoular, PhD Researcher from the Geotechnics Section, Imperial College London, in January 2020.

The LOCUS (LOndon Computerised Underground and Surface) Project, documented in Ellison et al. (1993) and Strange et al. (1998), was the BGS' first regional geological model of London. Layers were grouped according to geological and hydrogeological properties to maintain the manageability of the 22,000-borehole database: bases of the anthropogenic layer, superficial deposits, and the London Clay Formation, and the top of the Chalk. Their surfaces were constructed using an implicit-only workflow, being constrained locally by the predetermined WSG-Faults (fig. 4.10). The chalk surface rapidly steepens along linear boundaries that separate abrupt changes in elevation across them. Analysis of these delineated features indicate NE-, ENE- and (to a lesser extent) NW-trends. No new faults were modelled but Ellison et al. (2004) did postulate the presence of unrecorded faults and/or folds.

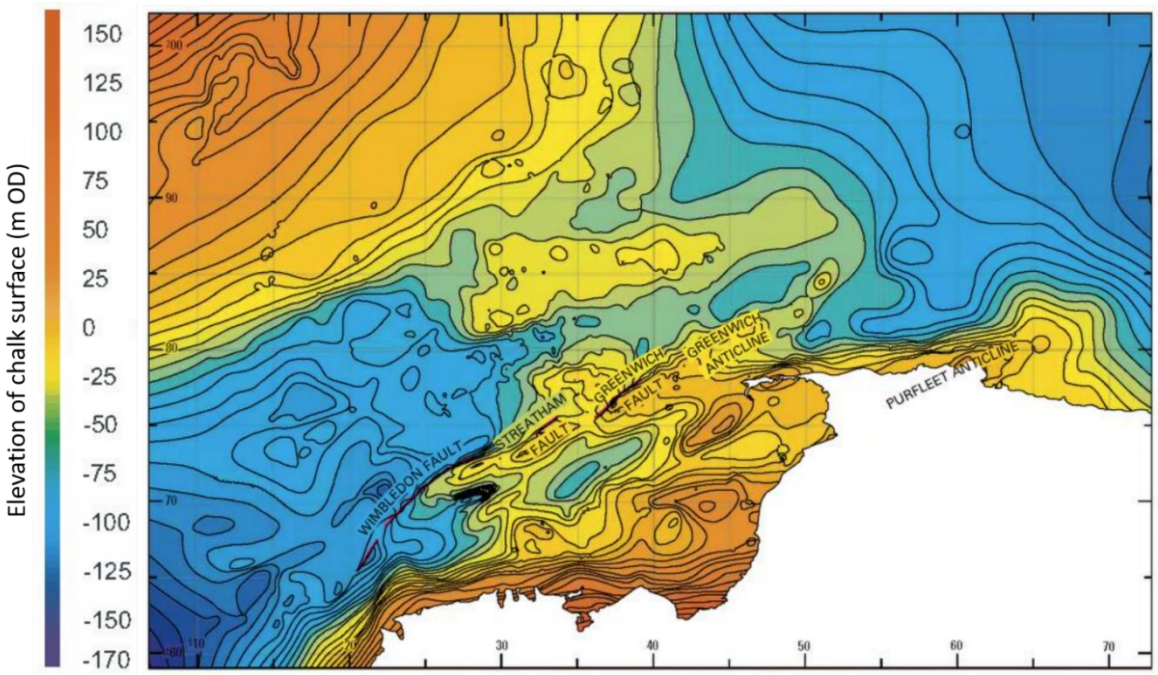

Figure 4.10 – Elevational contour map of the White Chalk Group surface generated by the LOCUS Project. Interpolation was locally constrained by known fault positions. Adapted from Ellison et al. (2004).

4.1.2.2 Explicit-driven modelling

The BGS Lithoframe is the only regional model in London that can be considered explicit-driven, and forms part of a nationwide programme to model Great Britain's subsurface that employed the GSI3D (Geological Surveying and Investigation in 3D) workflow. This is summarised here (fig. 4.11) from Kessler and Mathers (2004) and Kessler et al. (2009). Explicit modelling is initially undertaken through cross-section generation between strategically selected boreholes. These are coupled with DTM and mapped outcrop data to produce a fence diagram. Intrinsic modelling is then undertaken to generate the 3D surface of a stratigraphic unit that is constrained from known outcrop and inferred subcrop positionings in the fence diagram. These surfaces and fences are then collated into a geological model. Fault identification is embedded into the initial explicit phase and controls the later implicit modelling.

The Lithoframe model has progressively developed from 2006 onwards for London and (part of) the Thames Estuary (Ford et al., 2008, Ford et al., 2010) and now encompasses a significant portion of the London Basin (Mathers et al., 2014, Burke et al., 2014). New faults and folds were identified under London (fig. 4.12.a) that complement previous fault mapping conducted by the BGS (fig. 4.4). The folds consistently follow NE-ENE trends, progressively aligning towards E-W in the southeast (fig. 4.14). The faults follow three trends: NNE-NE, and ENE-E, and NW.

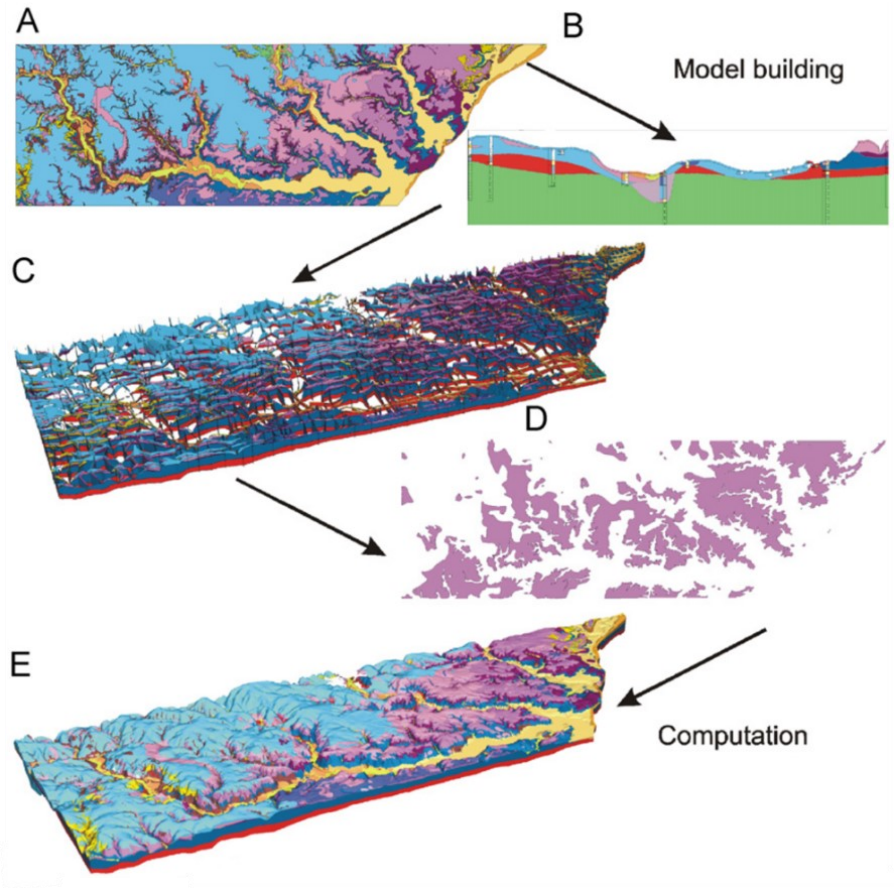

Figure 4.11 – The GSI3D workflow employed for the Lithoframe modelling of Great Britain. Current geological knowledge (A) is used to inform the construction of cross-section between strategically selected boreholes (B) to develop a fence diagram (C). This is used to construct a unit's 3D surface by coupling known outcrop with inferred subcrop positioning through geostatistical interpolation (D). The 3D geological model is constructed by compiling the surfaces and fence diagram into a block model (E). Adapted from Kessler et al. (2009).

Ford et al. (2010) divided these structures into two distinct domains that are each characterised by distinct structural styles and elevational variations in the near surface lithologies (fig, 4.12.b). The 'North London Block' is characterised by fault-bounded blocks and monoclinal folding along their margins; internally they appear to be comparatively undeformed. The 'Southern London Fold Belt' is dominated by NE-trending periclinal folds and some synclines and faulting aligned with their axes. The two domains are separated by a narrow 'graben' (fig. 4.12b). These are explained in detail in §2.2.2.5.

Mathers et al. (2014) outlined several limitations with the model, with the majority relating to the resolution of the input data. Crucially for subsurface analysis, not all available boreholes (fig. 4.6) were utilised since the borehole selection criteria (outlined in Burke et al. (2014)) favoured depth, log detail and evenly distributed coverage. Regardless, the borehole density used was clearly sufficient to interpret new structures and characterise London's subsurface geology with the BGS grading the model as Lithoframe50 (equivalent to 1:50k map resolution).

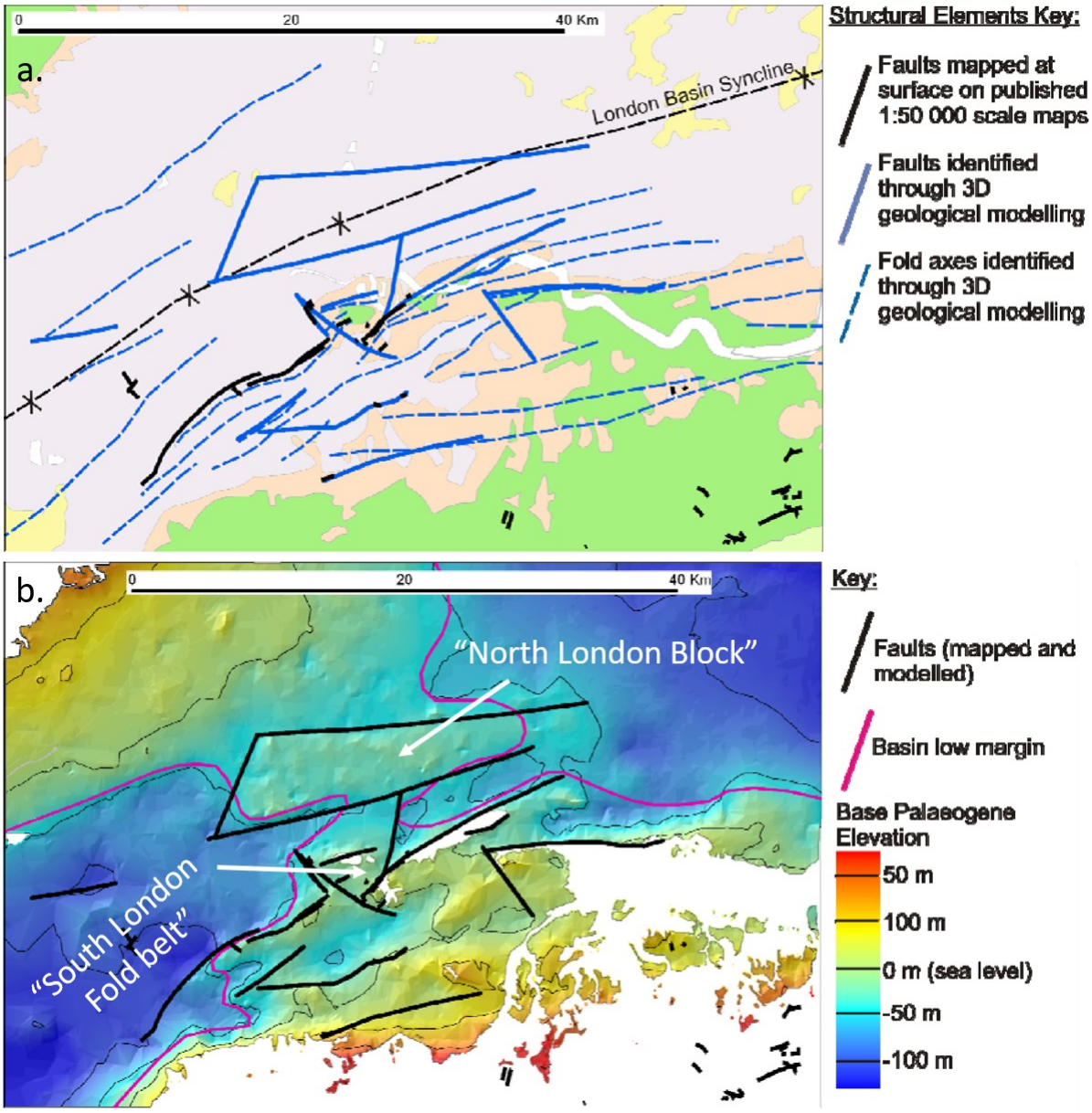

Figure 4.12 – Faulting identified under London by the BGS' Lithoframe. Figures adapted from Ford et al. (2010).
a. Geological map of London comparing faulting and folding identified from geological modelling with published at-surface inferences and observations of faulting from 1:50,000 map (fig. 4.4).
b. Mapped and modelled faulting superimposed onto a topographic map for the base of the Palaeogene sediments. Compare with the LOCUS surface in figure 4.10 (Ellison et al., 2004).

4.1.2.3 Localised geological modelling

Smaller programmes conducted in London have been separately reviewed due to their scale. The majority did not identify faulting despite having higher borehole densities within a smaller area.

Howland (1989, 1991) modelled East London from ~4,500 local boreholes to aid the London Docklands Development Scheme. The workflow was implicit-driven with no apparent incorporation of offset identification into its workflow. Howland argued that the Greenwich Fault (fig. 4.1) does not exist and instead attributed elevation variation across it to both the Greenwich Anticline and a newly proposed 'Greenwich Syncline'.

Farringdon Station underwent two phases of explicit modelling to constrain a suspected faulting. A local fault zone comprised of dip-slip faults (fig. 4.13) was interpreted by the initial 2009 BGS model using the GSI3D workflow (Aldiss et al., 2012) (fig. 4.11). These faults were further constrained by new borehole data in 2015 using a similar explicitly-driven workflow (Gakis et al., 2016).

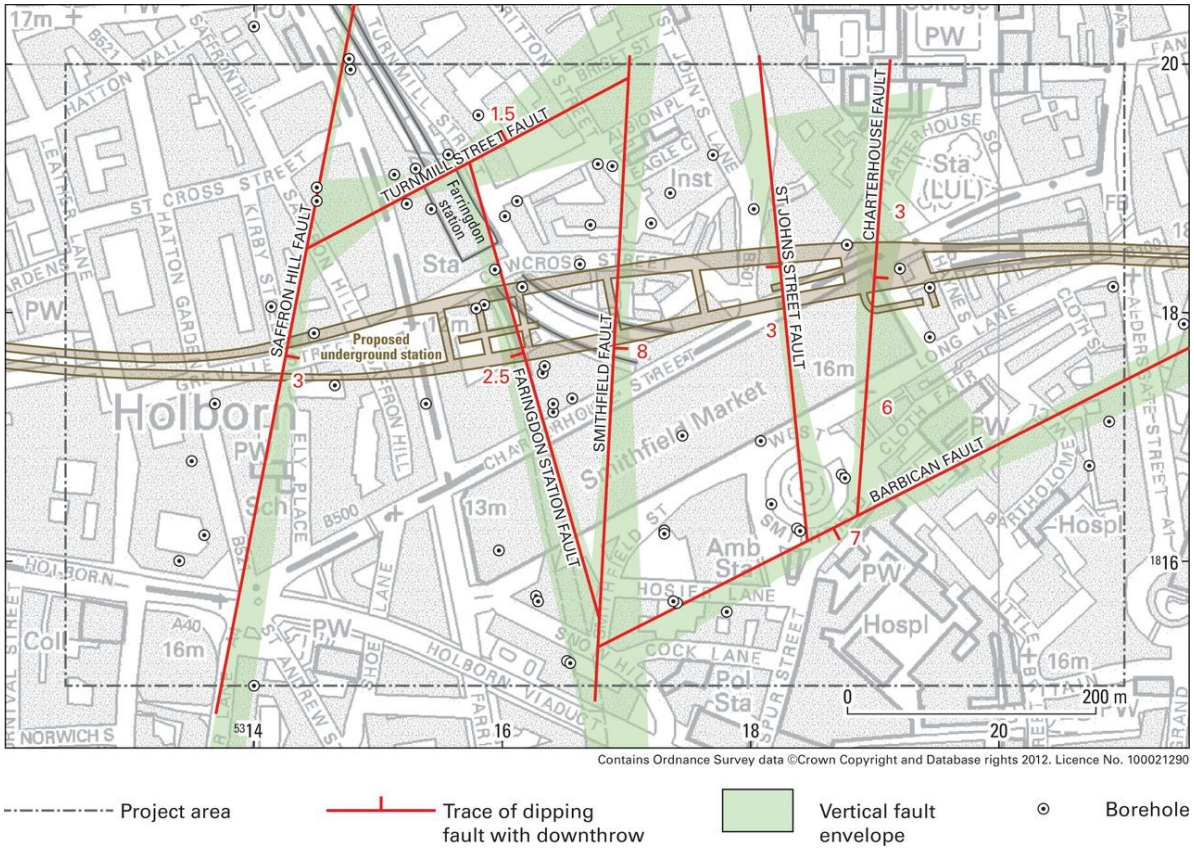

Figure 4.13 – Inferred fault positions from 2009 BGS explicit modelling programme for Farringdon Station. Green envelopes illustrate potential fault positions if idealised to vertical structures. Sourced from Aldiss et al. (2012).

Paul (2016) implicitly modelled central London from 1,122 boreholes. ENE- and NNW-trending linear offsets are present (fig. 4.14) but structural analysis was intentionally not undertaken, despite Paul's own recognition of unmapped faulting in London.

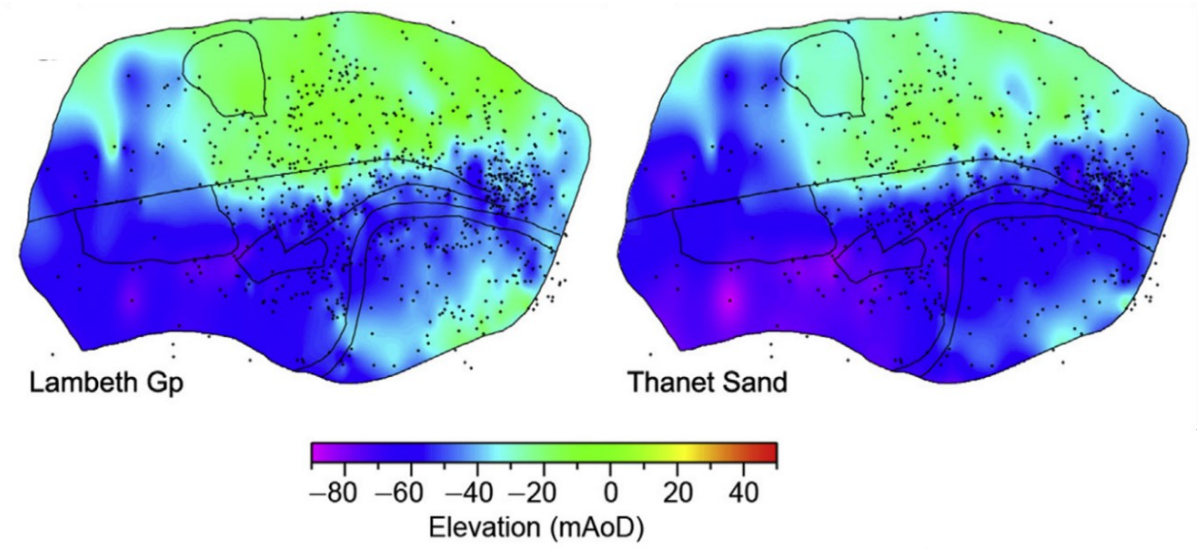

Figure 4.14 – Bases of the Lambeth Group and Thanet Sand Formation in central London, generated by implicit modelling in a workflow that intentionally did not undertake structural analysis. Despite this, abrupt, linear elevational changes are present in all generated surfaces. Adapted from Paul (2016).

The City of London area was modelled from 303 boreholes using the GSI3D workflow (fig. 4.14), as part of a collaboration between the BGS and the University of Birmingham (Burke et al., 2018). Faults were intentionally not modelled by this investigation.

Price et al. (2018) explicitly modelled around Earls Court from 96 boreholes. They identified two faults on the site, but they highlighted uncertainties of one due to reliance on a single deep yet poor quality borehole to locally characterise the Chalk depth.

4.1.2.4 Review of geological modelling

The utilisation of both at-surface and subsurface data enables this method to develop a more informed view of near-surface structures. Despite this, regional fault identification in London is extremely inconsistent between the modelling programmes reviewed (fig. 4.7-10, 4.12-14). Analysis of these models indicates that this variation is due to the workflows used, both general and specific, data quality and coverage, and potentially preconceived biases affecting structural analysis.

Implicit-driven workflows are considered detrimental to fault identification in London. The method can mask and smooth offsets into continuous planes interrupted by steepened areas (fig. 4.15.a) that can be interpreted as faulting or folding. This is evident as none of these programmes (except the Reading Report) inferred new faults in London, but several did postulate their presence from the elevational variation. Comparatively, the Reading Report did propose new faults in London, however, a manual review of its statistically selected data by this investigation points did not identify consistent elevations differences across them (fig. 4.16). Additionally, the implicit method has also led to

proposed revisions of established faults as folds from surface geometries (i.e., 'Greenwich Syncline'). These factors all demonstrate that geospatial interpolation without geological constraint is ineffective for fault mapping in London.

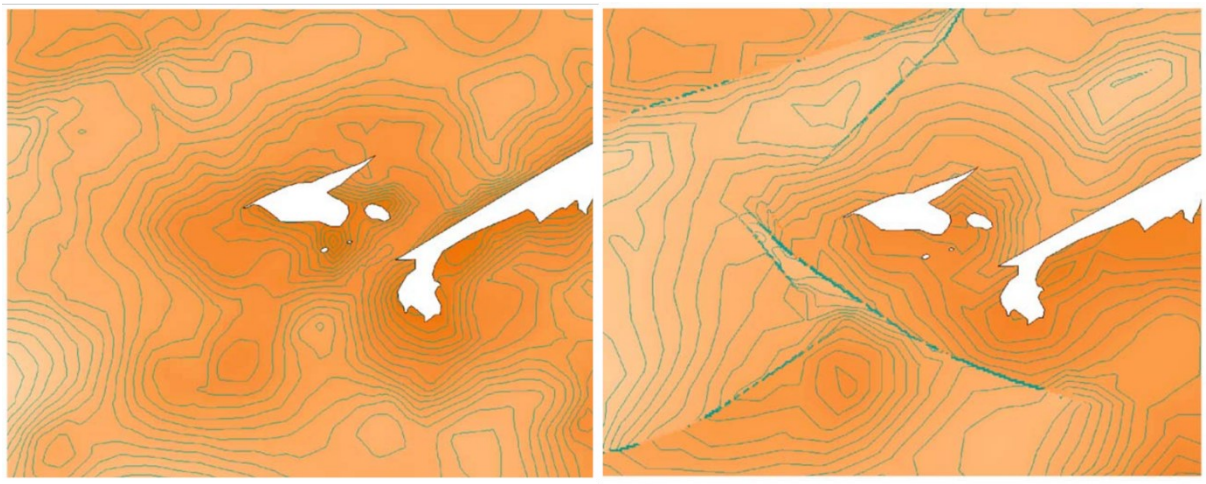

a. Geostatistical interpolation only (Implicit Modelling)

b. Geological analysis and geostatistical interpolation (Explicit informing implicit modelling)

Figure 4.15 – Differences in structural features of surfaces generated by implicit (a) and explicit (b) driven modelling workflows for the Palaeogene strata base in central London from boreholes. Faulting is masked by the implicit workflow (a) but identified through explicit modelling (b), enabling constraint of surface offsetting in latter. Adapted from Royse (2010).

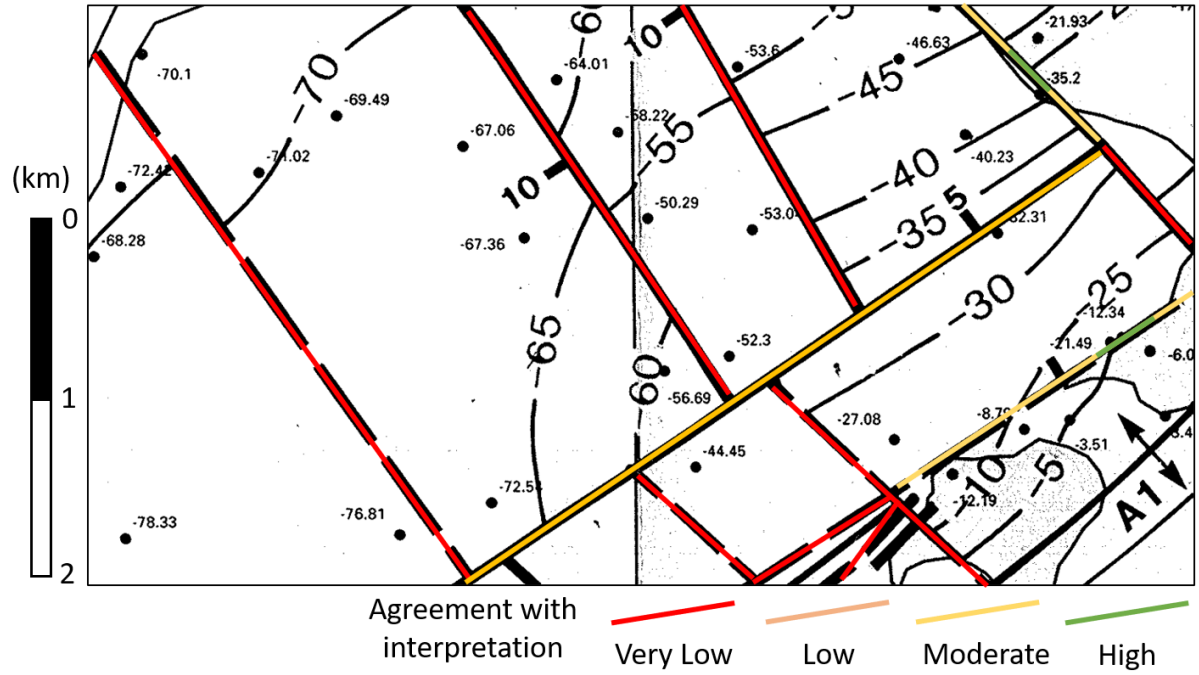

Figure 4.16 – Comparison of inferred fault positions with statistically selected borehole elevation data for the Chalk. The extent of agreement with the Reading Report interpretation has been colour coded, based on both borehole spacing and elevational differences between them. Adapted from Andrews et al. (1995).

Explicit-driven workflows, in comparison, encourage the *a priori* identification of structures by incorporating them into the model before surface generation (4.11). At both the regional- and local-scale (fig. 4.12-13) the workflows identified new faults and structural complexity that cannot be discerned from geological mapping alone (fig. 4.4). The method is time consuming, encouraging preferential selection of borehole data to maximise coverage and depth. This potentially risks shadowing highly localised geological features and elevational changes to influence interpretations.

Preconceived assumptions about London's subsurface is an unappreciated potential bias that will affect the investigator's rationale for fault identification in London and their chosen modelling workflow. This is apparent from the localised programmes (§4.1.2.3), where structural identification was variable despite having higher borehole densities than the regional modelling exercises. Paul (2016) and Howland (1989, 1991) did not identify any faults, despite both having evidence of them in their respective implicit models and recognising under-recording of faulting in London. Comparatively, Price et al. (2018) expected faulting and adopted an appropriate explicit workflow.

If faulting is not expected by the investigator, it will influence the modelling techniques used, thereby favouring implicit workflows and the further masking of faulting. This bias may stem from historical interpretations of minimal faulting (§2.2.2.5). Equally, this may also cause a bias for fault interpretations if only faults are expected. A holistic approach to characterising geological variation must be appreciated that considers the multiple processes that generated London's geology.

Geological modelling relies upon subsurface data to develop and map structures in 3D. London has considerable borehole coverage (fig. 4.6), but both their coverage and quality are inconsistent. Reduced coverage will affect offset deduction through both implicit and explicit modelling workflows. Poor data quality may cause locally erroneous features to appear in the model, as noted by Price et al. (2018). Both issues affect the quality of the generated model and the reliability of its structural representation, regardless of whether the model is implicit or explicit.

4.1.3 InSAR

Remote sensing may be a valuable alternative for fault mapping where exposures and/or accessibility are inhibited. Interferometric Synthetic Aperture Rader (InSAR) can infer underlying faults by identifying lineations that bound differential displacement behaviour across them. This satellite-based technique can measure point movements of the Earth surfaces by temporally analysing positional variations between multiple flyovers (fig. 4.18) and express them in terms of both displacement and velocity. Identification of mm-scale displacements can be achieved but is dependent upon the flyover recurrence time, analytical timeframe, processing methodology and type of radar data used.

InSAR was first applied in London by Boyle et al. (2000) for the generation of DEMs, and has since been used for engineering (Bischoff et al., 2020b, Scoular et al., 2020a, Scoular et al., 2020b) and more general geological applications (Aldiss et al., 2006, Cigna et al., 2015, Bonì et al., 2016).

The purpose of an InSAR investigation will affect its effectiveness for fault interpretation, reflecting project specific workflows. The applicability of this method for structural analysis will be influenced by four key factors that affect InSAR processing:

- Timeframe range: The temporal period covered by the analyses will affect the style and mechanism of surface movement identifiable in the data. For simplicity, InSAR analyses will be described as either long- or short-timeframe analysis depending upon the temporal range undertaken by each study. Long-timeframe analysis enables 'deeper', slower natural processes to be observable by eliminating temporal signatures associated with seasonal meteoric and anthropogenic processes. Short-timeframe analysis will cause shallower and ephemeral displacement to be more pronounced and mask longer term processes.
- Reference point: Displacement is relative to a point of reference on the master scene (fig. 4.17). Consequently, the location of this point will affect the displacement measured. If situated within an area of 'deformation', that process's movement will not be recorded.
- Processing and filtering: At-surface displacement is a product of multiple interacting phenomena, e.g., soil moisture (Agar et al., 2018), that can mask the desired process being investigated. Statistical processing is required to filter and remove these features.
- Line of sight: The orbital direction of the satellite will affect the displacement measured. Ascending can detect vertical and Eastward movement, whilst descending can detect vertical and Westward motion. Either type can be used for vertical analyses, but they must be combined to measure E-W lateral. The orbit prevents N-S lateral measurement.

Multiple investigations have identified linear trends in London from InSAR analysis that are indicative of near surface faulting. These are grouped here according to their timeframe range.

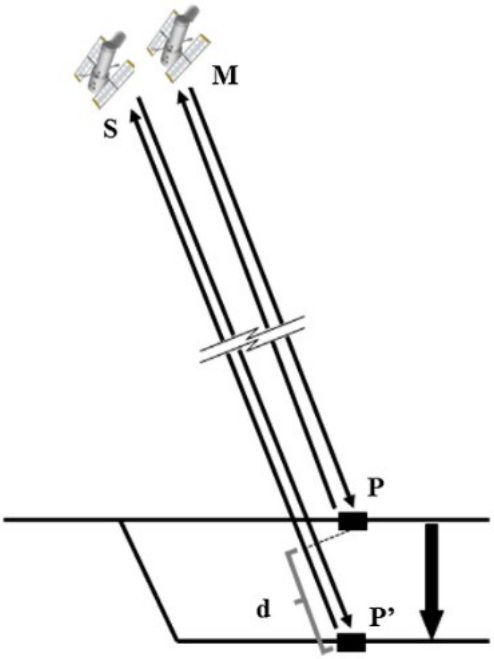

Figure 4.17 – Overview of InSAR measurements of changes in the positioning of an at-surface point. Changes are determined by comparing the initial 'Master' (M) measurements with later 'Slave' (S) flyovers (Point P vs. P'). Sourced from Crosetto et al. (2016).

4.1.3.1 Long-timeframe analysis

Aldiss et al. (2006, 2014) combined Persistent Scatterer Interferometry[25] (PSI) with GPS and absolute gravity data to assess land level changes in London and the Thames Estuary. Long-timeframe analysis was undertaken using 60 descending SAR scenes from 1997 to 2005 and grouped into domains of comparative displacement (fig. 4.18). Identified NE-trending boundaries in at-surface displacement were coincident with gravity anomalies attributed to basement fault. Additionally, displacement was also identified to correspond with near-surface geological and anthropogenic processes. These NE-striking lineaments were attributed to near-surface major faults due to the subparallel alignment of the western one with the WSG-Faults (fig. 4.18 vs. 4.4). It is unclear if the eastern lineament was also verified with geological/structural evidence.

Mason et al. (2015) demonstrated that the surface of London is moving in a block-like manner (fig. 4.19) from long-timeframe PSI analysis. They collated 18 years of PSI data from two satellite missions between 1992 and 2010 (ERS, 1992-2001, and ENVISAT, 2002-2010) and produced continuous velocity surfaces for each scene to enable comparison between the two datasets. Descending data was available throughout the time period enabling vertical displacement to be combined over the 18-year

[25] A form of Differential InSAR analysis that analyses the displacement of points that are consistently present across multiple temporal 'scenes' of a region.

period (fig. 4.19.a). But E-W lateral displacement analysis was restricted to the 1992-2001 period as the required combination with ascending data was available for the ERS dataset only. Block-like regions were identified with vertical and E-W lateral displacements of ≤ 2 mm.a^{-1} internally that are bounded by consistent linear trends, across which opposing senses of motion are observed. Together with Ghail et al. (2015a), they inferred that these linear boundaries represented a fault network comprised of three fault sets.

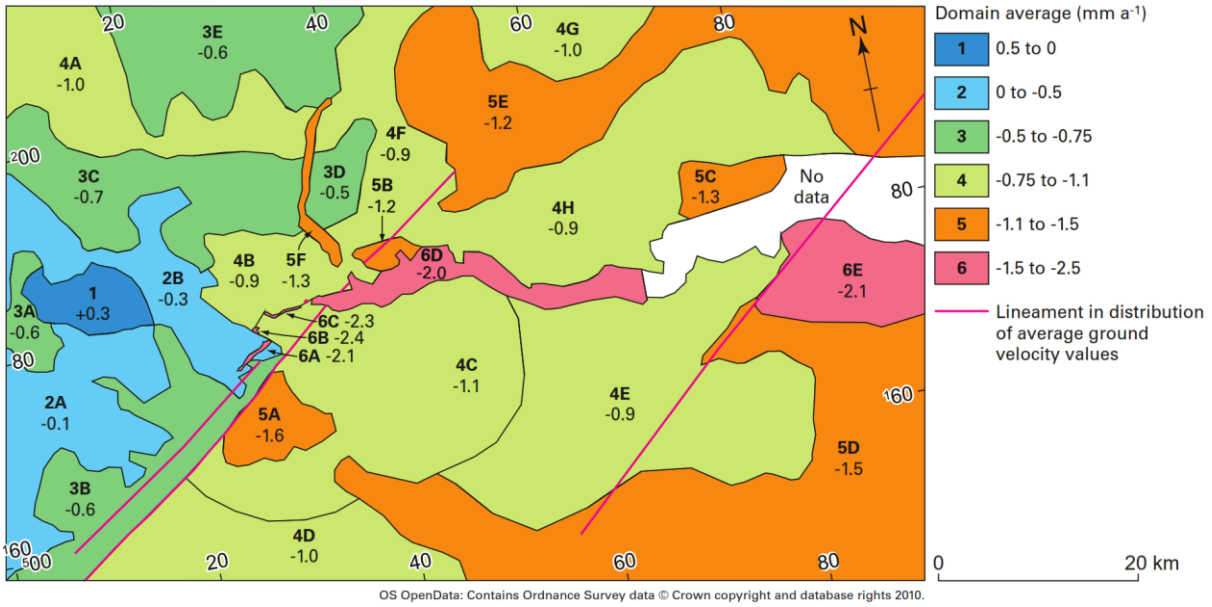

Figure 4.18 – Average vertical ground velocity domains and lineaments inferred from PSI analysis by processing 60 descending scenes taken between March 1997 to December 2005. Sourced from Aldiss et al. (2014).

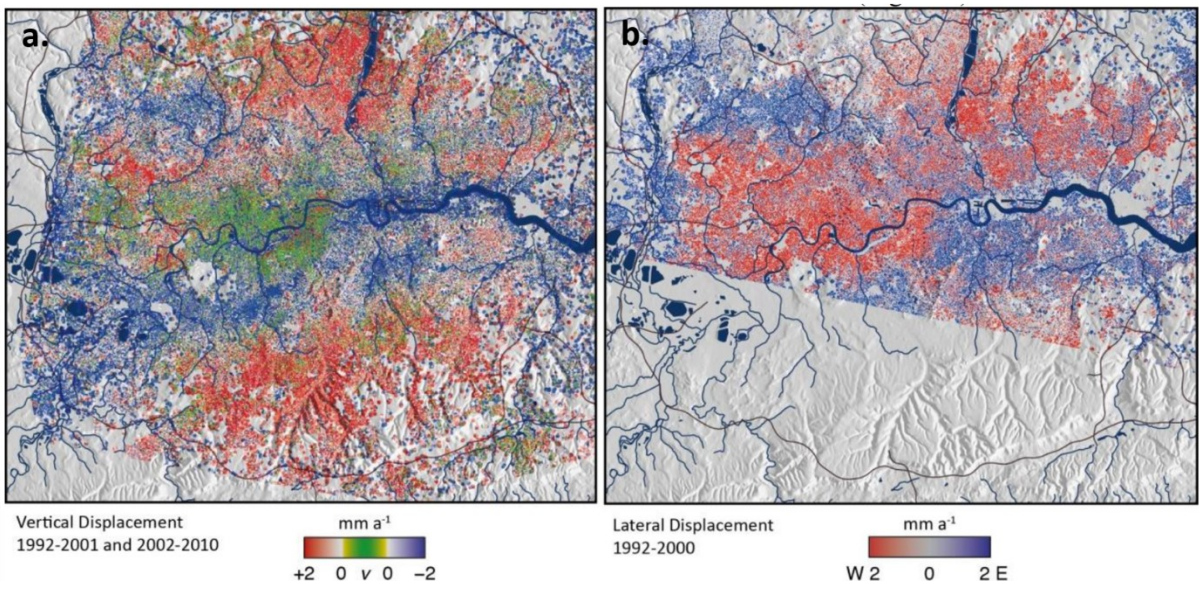

Figure 4.19 – Long-timeframe PSI analysis of London. Surface displacement is characterised into block-like regions of consistent velocity behaviour. Linear boundaries between these regions indicate the presence of near-surface faulting. Adapted from Mason et al. (2015).
a. Vertical displacement of combined descending PSI data from 1992-2001 and 2002-2010.
b. Lateral E-W displacement of combined ascending and descending PSI data from 1992-2001 (ERS only).

4.1.3.2 Short-timeframe analysis

Short-time frame analysis can also provide indirect evidence of near surface faulting. Bischoff et al. (2020b, 2020a) identified an irregular cone of depression in response to Crossrail dewatering and later recharge of the Lower Aquifer in the Limmo Peninsula (fig. 4.20). The linear geometry of the cone's western margin is coincident with the strike of the Lea Valley Fault, indicating the presence of a low permeability fault core within the Lower Aquifer that impedes flow across it. Here InSAR indirectly identified a fault due to its hydrogeological influence being accentuated by anthropogenic dewatering.

The presence of a NE-striking faulting in Newham, East London was postulated by Scoular et al. (2020a) due to differential subsidence behaviour observed across this trend and its proximity to both the Plaistow Graben and structures inferred by this investigation (§4.3-4).

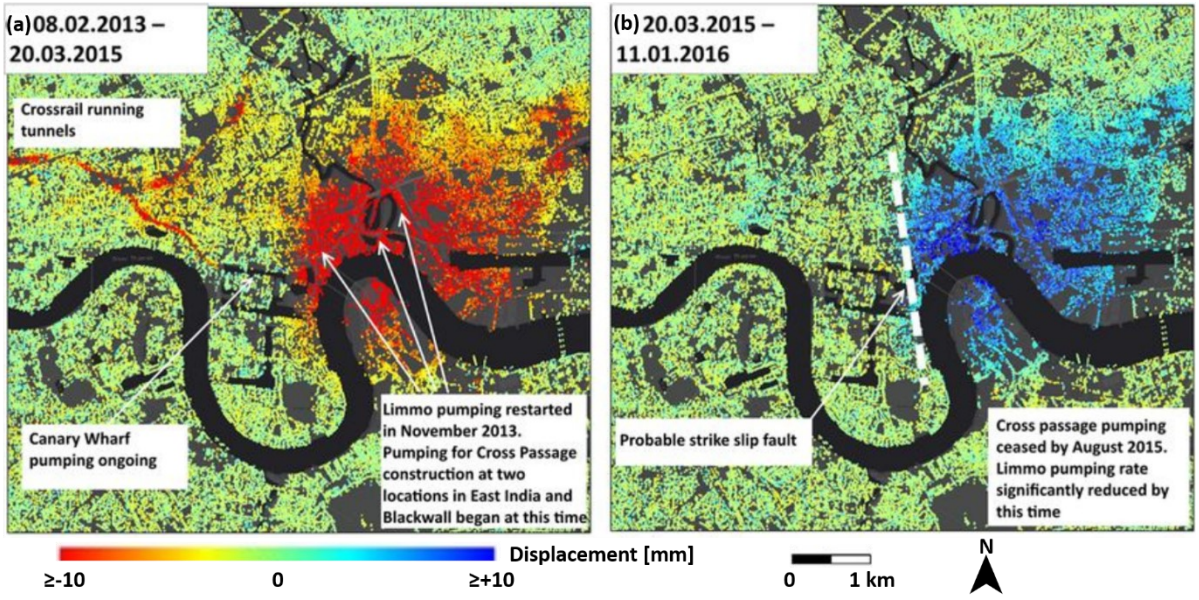

Figure 4.20 – InSAR measurements of episodic ground subsidence and rebound in response to artificial dewatering and natural recharging of the Lower Aquifer in the Limmo Peninsula for the Crossrail tunnelling project. The irregular geometry of the cone of the depression is a product of the low permeability NW-trending Lea Valley Fault inhibiting hydrogeological continuity of the Lower Aquifer. Adapted from Bischoff et al. (2020b). a. Ground subsidence associated with a second episode of artificial dewatering for the Crossrail tunnel. b. Ground rebound due to cessation of pumping, and subsequent recharging of the Lower Aquifer.

4.1.3.3 Limitations of InSAR analysis for fault mapping

In London, InSAR has identified distinct block-like ground movement delineated by linear boundaries. These are evident in long-timeframe analysis (fig. 4.18-19), and indirectly observable in short-timeframes under specific circumstances (fig. 4.20). The coincidence of some boundaries with known faults (WSG-Faults and the Lea Valley Fault) demonstrates that these movements can correspond with geological structures due to the processes they influence, e.g., hydrogeology. But the majority of lineaments are inconclusive of fault positions without further validation and subsurface ground truthing. InSAR should not be used in isolation for faulting mapping but as a line of evidence.

At-surface ground deformation is a complex phenomenon controlled by multiple interacting processes. This may cause fault-related displacement signatures to be masked or even completely absent, with the outputs of InSAR analysis depending upon the investigation's workflow.

Observed surface displacement is relative to the selected point of reference on the initial 'Master' scene (fig. 4.17). Ongoing deformation simultaneous to this scene will be less pronounced than if a 'Master' was selected prior to this specific displacement beginning, being exacerbated further if the reference point is inappropriately positioned. The observations by Bischoff et al. (2020) (fig. 4.20) were achieved because the 'Master' scene was taken prior to dewatering beginning, enabling faulting to be inferred from distinct ground subsidence and resurgence observed relative to this initial reference.

4.1.4 Review of methods

Three distinct methods for fault identification in London were reviewed from their case studies (table 4.1): geological mapping and modelling define faulting from observed and/or inferred offsetting, whilst InSAR can identify differential displacement behaviour across them. Interpretations were inconsistent between projects, with each presenting a different structural arrangement. But three sub-linear trends are consistently defined across the majority of the analyses reviewed: NE-NNE, ENE-E, and NW-NNW striking. This implies that three major fault sets are present in London that are independently identifiable from structural (fig. 4.4, 4.12), fluvial (fig 4.5) and displacement data (fig. 4.19). Crucially, these trends agree with expected basement faults strikes (fig. 3.25).

The methods themselves each have limitations for fault identification. Some are intrinsic to the technique itself, whilst others are specific to the project, London's mapping restrictions, or structural preconceptions of the investigator. Geological mapping (§4.1.1) is reliant on at-surface evidence and provides confident constraint where structures are locally identified but is limited in London by minimal exposure and homogenous lithologies. Geological modelling (§4.1.2) combines at- and sub-

surface data to develop an informed 3D conceptualisation of the ground, including fault offsets, but it is impacted by modelling workflows and data coverage and quality. Long timeframe InSAR (§4.1.3.2) displays grid-like displacement attributable to faulting, but the technique must be targeted and requires cross-comparisons to validate interpretations. Finally, preconceived attitudes were identified as a key factor for the interpretation of faulting in London, independent of the methodology. The traditional perspective that London is tectonically simplistic (§2.2.2.5) may introduce unintended biases to structural interpretation.

Upon review, explicit-driven geological modelling is considered the most appropriate method for fault mapping in London because of the reliance on manual structural interpretation coupled with the substantial borehole database in London (fig. 4.6). Faulting is defined early-on from cross-sectional offsetting rather than by potentially unreliable geostatistical methods or disparate exposures. The BGS Lithoframe (fig. 4.12) supports this by providing the most informed and spatially extensive structural interpretation of London to date. However, the presence of fault zones away from Lithoframe faults (fig. 4.21) demonstrates that major faults are still under-recorded, and that mapping is incomplete.

The presence of regional variations in both subsurface topography (fig. 4.10) and at-surface displacement behaviour (fig. 4.19) indicate additional faulting but are inconclusive in isolation. If demarcated boundaries from both were coupled, would this provide an alternative method for indirectly defining faulting? This is explored in §4.2-4.3.

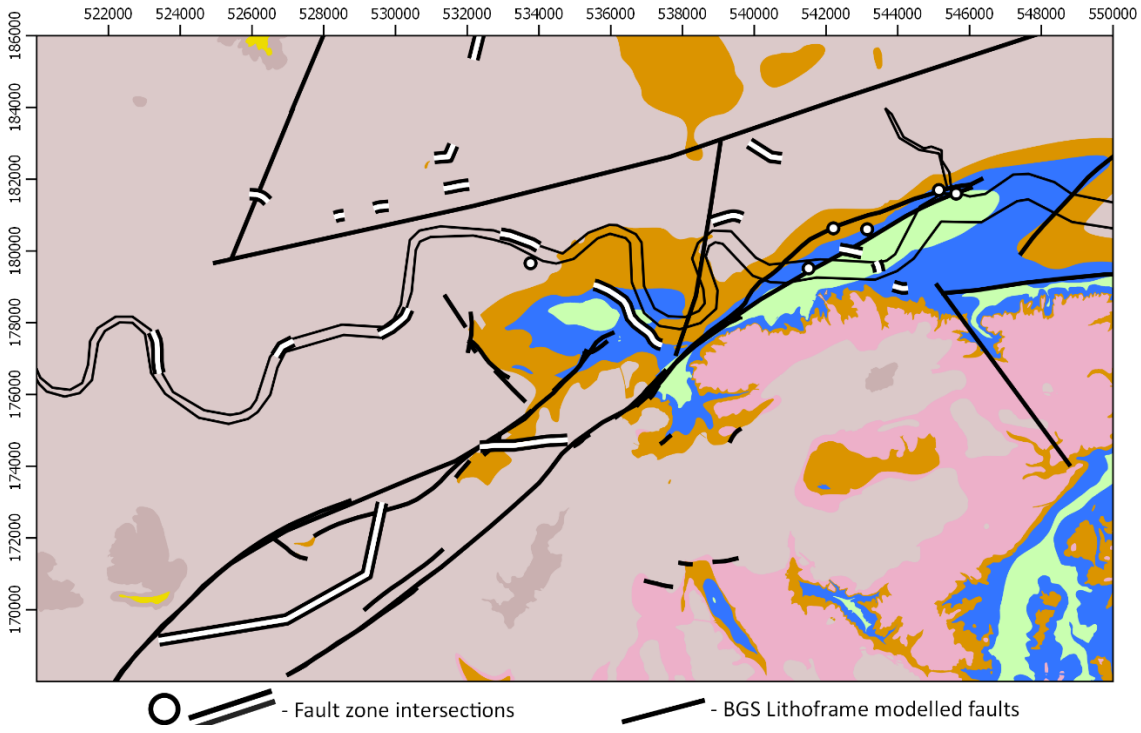

Figure 4.21 – Comparison of fault zones locations (table 6.4) with BGS Lithoframe faults. The presence of fault zones away from inferred structures demonstrates that additional major faults are present under London.

4.2 Methodologies

The section describes the rationales and methodologies for a newly developed indirect fault mapping technique (§4.2.1) and fault trend analysis (§4.2.2).

4.2.1 Indirect fault mapping

Fault mapping is affected by limited exposure in London, modelling methodologies and subsurface data coverage. Consistent sublinear trends can be identified from river morphology (fig. 4.7), InSAR (fig. 4.21) and elevational changes in subsurface lithologies (fig. 4.12; 5.14). In isolation these observations are insufficient to infer the positioning of faulting. But if these lineaments are spatially coincident, they indirectly demonstrate the presence of a hidden fault network beneath London.

4.2.1.1 Methodology

The positioning of sublinear trends from vertical displacement InSAR and subsurface chalk topography were spatially compared for positional commonalities, and locally appraised with mapped faults and fault zones for a more rigorous comparison. The datasets and their sources are presented in table 4.2.

Lineaments were interpreted from significant steepening of the BGS LOCUS-modelled White Chalk surface (fig. 4.10, Ellison et al., 2004). These were superimposed onto vertical long-timeframe InSAR analysis from Mason et al. (2015), which was selected since it reveals geological significant delineated block-like displacement (fig. 4.19) by removing anthropogenic and seasonal masking. These were plotted against mapped faults and fault zone. The BGS 1:250K faults were considered appropriate given the resolution of both the InSAR and modelling data used. Fault zones were collated from published observations (table 6.4) and georeferenced for analyses in §6.2.

Table 4.2 – Data used for indirect fault mapping (fig. 4.22). This is updated from Morgan et al. (2020) to include additional fault zones.

Data	Dataset Type	Interpreted for this investigation	Data Source(s)
Vertical displacement InSAR	GeoTIFF	N/A	Mason et al. (2015) (provided by Ghail (co-author) in 2018)
Topographic data	Structural contour map	N/A	Ellison et al. (2004)
	Topographic boundary lineaments (polylines)	Manually interpreted for Morgan et al. (2020)	
BGS 1:250K faults	Polylines	N/A	Geological Map Data BGS © UKRI 2018
Fault Zones	Combination of polylines and points	Collated from tunnel alignments and sites observations	Refer to table 6.4

4.2.2 Fault set orientation analysis

Three consistent trends are recurringly defined in published structural, geomorphological and InSAR analyses (NE-NNE, ENE-E, & NW-NNW) that imply three major fault sets present in London's near surface. To assess the validity of this, the distributions of linearised trends from three independent fault mapping exercises (including §4.2.1) and river morphologies were qualitatively interpreted. Rose plots and frequency distribution plots were constructed to assess these lineament trends and identify commonalities between them that may be indicative of an underlying fabric.

Directional statistics were explored to provide quantitative rigour to the analysis but were not feasible. The reasonings for this and implications are discussed in §4.4.7.

4.2.2.1 Methodology

The four datasets utilised are summarised in table 4.3. Their strikes were digitised. Faults in the BGS Lithoframe (fig. 4.12) were linearised to representative trends by measuring the orientation between the endpoints of each fault, however, several longer, curving faults were separated into multiple segments to prevent extreme distortion. The extracted lineaments for each dataset were grouped into 10° bins for constructing the rose plots and the frequency distribution plots. Rose plots were constructed using Stereonet 10 (Allmendinger et al., 2011, Cardozo and Allmendinger, 2013).

Table 4.3 – Datasets utilised for lineament trends analysis. Data sourced from mapped and suspected faults, and river morphology. [a] The analyses required datasets to be linearised. Only the BGS Lithoframe faults required linearising, as described in the methodology.

Lineament	Lineament Type	Linearised trends	Required linearising [a]	Source
Indirect fault map	Structural	Yes	No	§4.2.1
River lineations	Geomorphological	Yes	No	De Freitas (2009)
BGS Lithoframe faults	Structural	Yes	Yes	Provided by Ford (pers comms, 2020)
Reading Report faults	Structural	Yes	No	Andrews et al. (1995)

4.3 Results

The indirect fault mapping aims to overcome some of the issues identified for mapping in London. The fault set analysis aims to characterises major fault geometries and define their sets. Their results are presented in §4.3.1 and §4.3.2, respectively.

4.3.1 Indirect fault mapping

The results of indirect fault mapping are presented in figure 4.22, with 12 lineaments interpreted from the chalk surface. It is updated from Morgan et al. (2020) with additional fault zone positions. There is spatial agreement between the lineations interpreted from the subsurface topography and the vertical InSAR data. The majority of fault zone observations intersect or occur proximal to the lineaments; but no boundaries were identifiable in West London from either dataset.

Three lineament sets are interpreted from the geometries of both datasets (fig. 4.23.a) that strike approximately NNE, ENE, and NW.

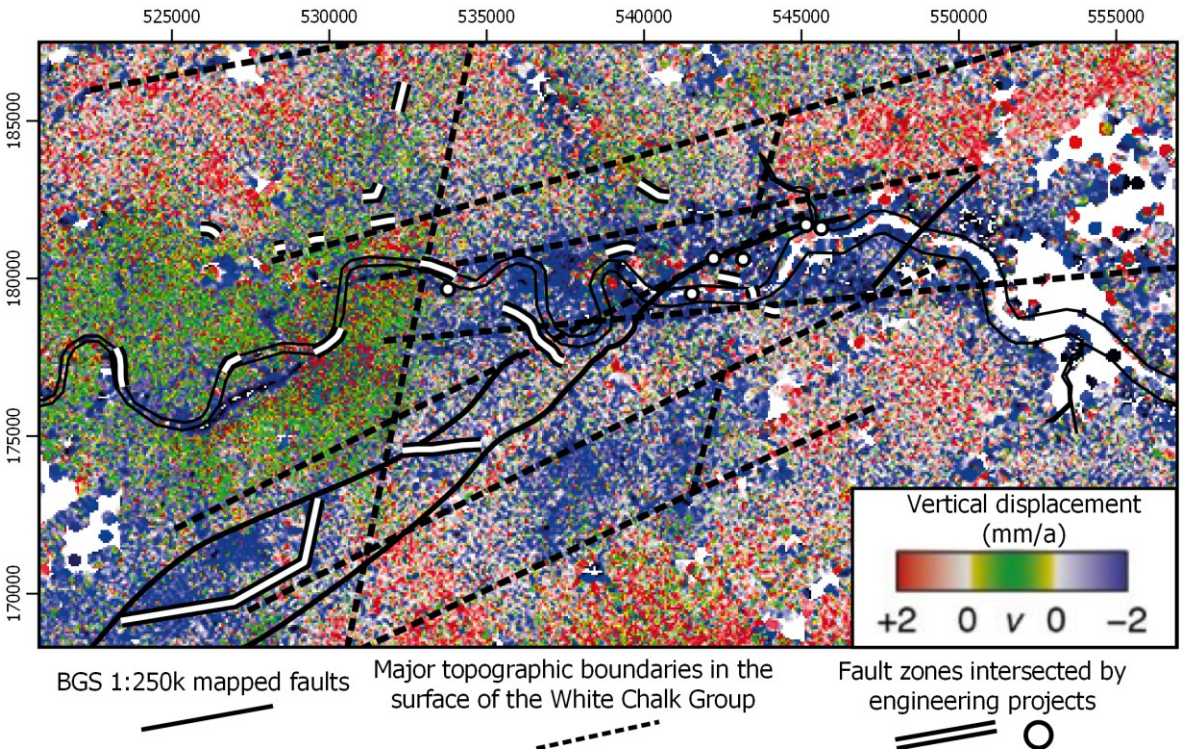

Figure 4.22 – Indirect fault map of London constructed by coupling lineaments interpreted from steepening of subsurface topography with differential vertical displacement behaviour from long-timeframe InSAR (table 4.2) and compared with significant fault observations. Linear block-like boundaries identified by InSAR correlate with both known faults and elevational changes in the White Chalk Group surface. Updated from Morgan et al. (2020).

4.3.2 Lineament set orientation analysis

The results of the orientation analysis are presented as rose diagrams (fig. 4.23) and frequency distribution plots (fig. 4.24). Considerable variation exists between the datasets, with the InSAR/chalk lineaments and the BGS Lithoframe faults being the most comparable overall. Multiple sets are definable in most datasets; but the Reading Report contains only 2. When individual trends are qualitatively assessed from their frequency distributions, clusters do emerge. An NNE-set is evident, with a weaker NE-component also. A NW-trend centred around 140-150° is also apparent. There are multiple overlapping trends situated between 60-120°, limiting separation into discrete sets.

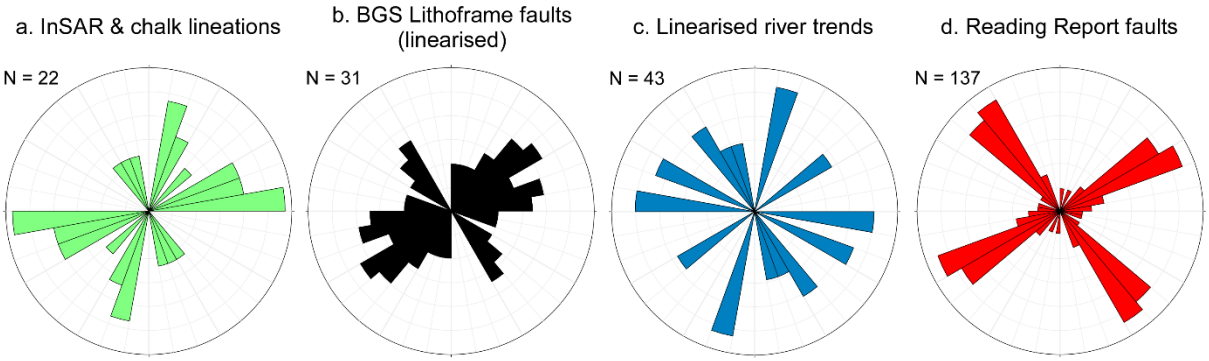

Figure 4.23 – Rose plots generated from published lineations of inferred faulting and river trends (table 4.3). Data have been grouped into 10° bins and scaled by area.
a. Lineations interpreted from long timeframe InSAR and chalk topography.
b. BGS Lithoframe faults (Ford, pers comms, 2020). These faults have been linearised and separated into sections of sublinear trends where faults were too long and irregular to reliably measure.
c. Linearised river trends from de Freitas (2009).
d. The Reading Report faults (Andrews et al., 1995)

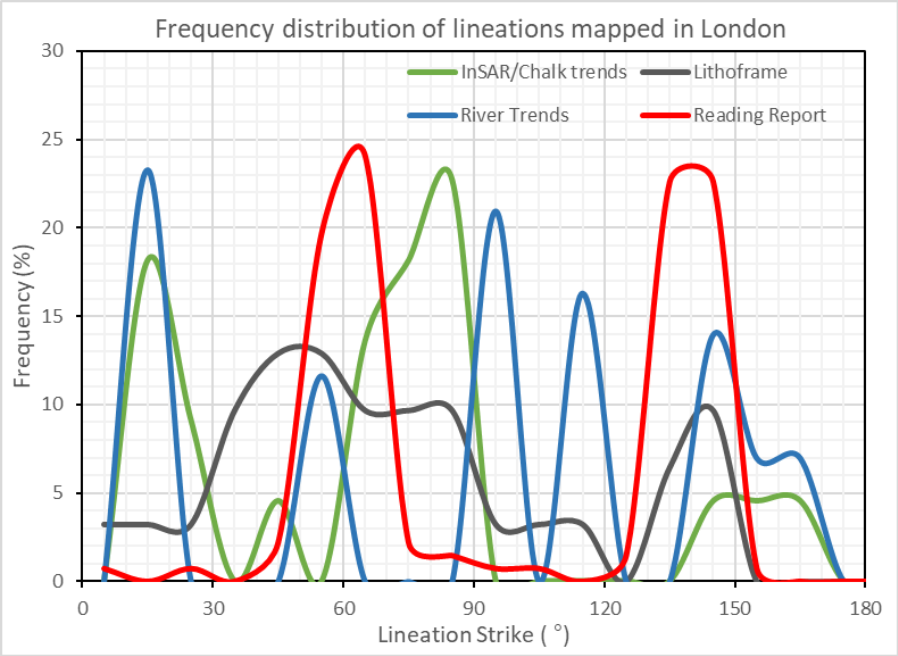

Figure 4.24 – Frequency distribution plot of lineations strikes (table 4.3), grouped into 10° bins to identify consistent trends within them.

4.4 Discussion

The indirect method is distinct from the techniques discussed in §4.1 as it couples subsurface topographic trends with at-surface displacement to identify spatial commonalities indicative of faults. Boundaries in subsurface topography and vertical displacement behaviour from InSAR are spatially coincident and show good correlation with direct evidence of faulting. The mapped lineaments are interpreted to represent an underlying hidden fault network in London comprised of three fault sets.

Comparisons with the positioning of BGS Lithoframe faults and inlier geometries (fig. 4.25) provide further validity to the indirect fault mapping method. Both maps are dominated by the ENE-E trending set, with the indirect method identifying further members to the south. There is limited representation of the other two sets (~NNE & NW) in either model, with both containing faults that are not present in the other. Differences likely reflect the respective methods employed and distinct types and resolutions of their data (table 4.2 vs. fig. 4.11). The Lithoframe model (fig 4.12) is considered to be more representative of the subsurface than the LOCUS model (fig. 4.10) used for this analysis, potentially affecting structural lineation inferences in §4.2.1.

Confidence in the proposed lineaments is further supported by their intersection with and/or proximity to fault zones (fig. 4.22) and notably achieves greater spatial coincidence than the BGS Lithoframe (fig. 4.21). But fault mapping is incomplete still as some fault zones are isolated.

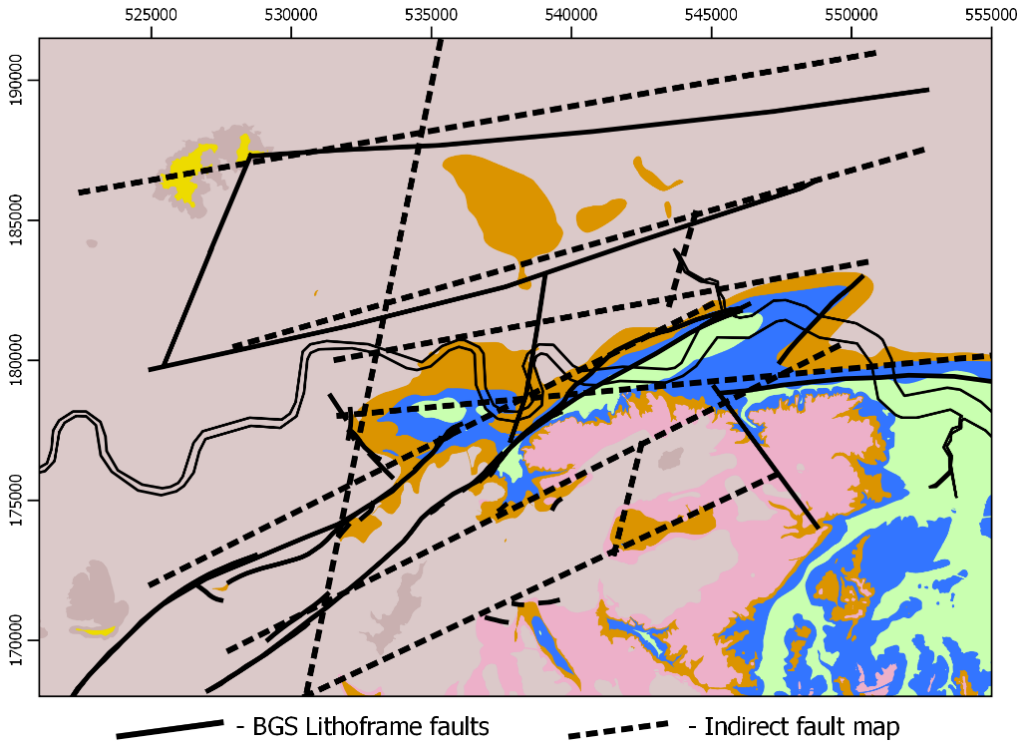

Figure 4.25 – Comparison of the indirect fault lineaments with BGS Lithoframe faults and inlier geometries. Some faults are spatially comparable; however, both have distinct faults also. Others that have been independently verified (e.g., the Lea Valley Fault) are absent from both.

4.4.1 Fault set interpretation

Three lineament trends are discernible from qualitative orientation analysis of the indirect mapping method, BGS Lithoframe faults and river trends: NNE-NE, ENE-E, and NW (fig. 4.23.a-c, 4.24). These are broadly compatible with basement fault trends (§3.3.1.2) and support associated fault inheritance.

Strike variation both within and between datasets may limit this interpretation. For example, there are two peaks in Lithoframe trends at broadly ~40-50° and ~80-90° but considerable overlap exists between 30-100°, limiting confidence in their definition. This variability is principally attributed to linearising irregular, sinuous features, and the narrow 10° bin widths. The former will cause divergence dependent on how the trend is measured, and the latter will cause natural variability within a set to become divided into separate bins. This is likely to be most impactful for the indirect method (§4.2.1), which interpreted implicit modelling derived structural contours, and the fluvial morphologies (fig. 4.5) as they be influenced by non-structural processes also. The lack of noise and incomparability in the Reading Report dataset (fig. 4.23.d, 4.24) implies that their interpretations (fig. 4.9) are overly idealised and potentially unrepresentative.

The investigation centres on mapping and characterising major faulting in London attributed to inheritance. But the BGS Lithoframe also contains shorter faults that may be unrelated. To distinguish between them, the 31 Lithoframe faults were divided by a selected length of 1 km (fig. 4.26.c) to assess differences in strike distributions (fig. 4.26.a-b). Faults >1 km contain less noise with three sets becoming more evident: NNE-NE, ENE, and NW. Shorter faults also contain three sets, but these are more oblique to the major trends. They may be associated with direct Alpine compression and/or linkage zone interiors instead (§3.3.2-3, §3.4), with the positioning of some relative to major faults (fig. 4.26.c) implying that both interpretations are valid. Additionally, the interaction of overlapping faults may introduce a further complication as localised stress distortion will curve them away from expected trends (Fossen, 2010).

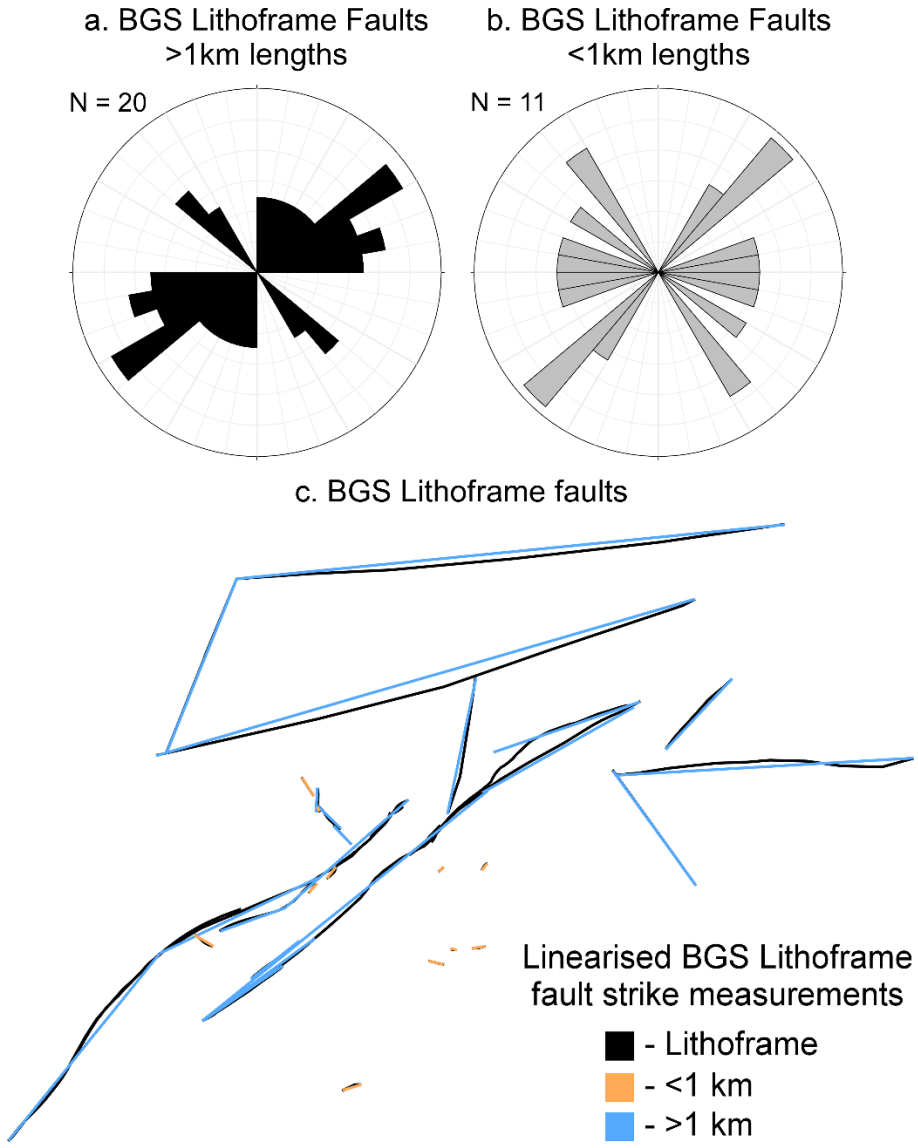

Figure 4.26 – Dividing of the linearised BGS Lithoframe fault data using a selected length of 1 km. a. Strikes of linearised Lithoframe faults >1 km. b. Strikes of linearised Lithoframe faults < 1 km. c. Categorisation of linearised faults by length, superimposed on actual Lithoframe data.

4.4.2 Fault map discrepancies and refinement

There are discrepancies between the indirect fault map and known faults in London (fig. 4.22, 4.25). Some faults are absent, whilst other's trends diverge from expected strikes. To illustrate both, the Lea and Rodding Valleys are respectively analysed against the indirect fault map (fig. 4.27).

The NNW-trending Lea Valley Fault is evident from multiple investigations and is suspected to be a strike-slip fault (Linde-Arias et al., 2018, Ghail et al., 2015a, de Freitas, 2009, Wooldridge, 1923, Wood, 1882). No fault was defined because a boundary was only loosely present in the vertical InSAR data (fig. 4.27) and not the LOCUS model's topography (fig. 4.10). This highlight's issues with the method for identifying faults with minimal vertical offset.

The parallel geometry of the Roding Valley with the Lea Valley implies that a NW-trending fault is present there also. An NNE-trending fault was wrongly inferred locally instead of this (fig. 4.27) and may reflect structural contour misinterpretation (fig. 4.10). Faulting is present at the Roding Valley-River Thames confluence (Kirkpatrick and McCann, 1984, Newman et al., 2016) but it is unclear if it is associated with the Greenwich Fault (fig. 4.1) or a 'Roding Valley Fault'.

The extent of misinterpretation is considered to be limited since the lineaments overall correlate with both inlier geometries and known faults (fig. 4.22, 4.25). The minor positional disparities present are attributed to linearising elevation boundaries instead. However, the issues associated with potential misinterpretation and assumed linearity highlight the necessity for 'ground truthing' these lineaments to confirm their presence and constrain their positioning.

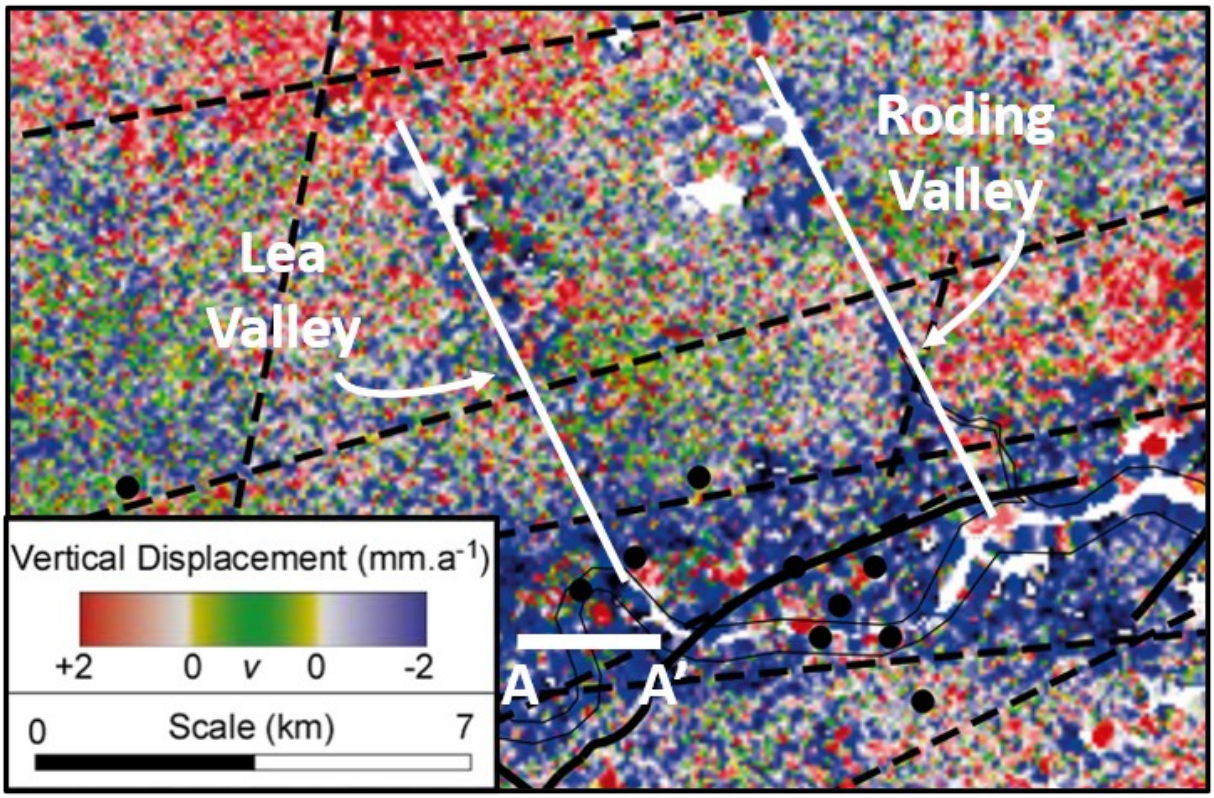

Figure 4.27 – The positions of the Lea and Roding Valleys (white lines) superimposed onto the indirect fault map (fig. 4.22). The Lea Valley follows a suspected underlying fault but was not defined. The Roding Valley likely follows a NW-trending fault also, but a NE-trending lineation was misinterpreted from the chalk surface.

4.4.2.1 Fault map refinement

The fault network was refined to account for recognised positional discrepancies and absentee faults. This coupled inlier geometries with suspected faults, InSAR lineations and the morphologies of certain river valleys. Broader geomorphological evidence was also explored but was considered inappropriate without further verification of their structural influences. Three faults were refined (fig. 4.28):

- Inclusion of the Lea Valley Fault.
- Reorientation of the Roding Valley Fault to NW-trending, parallel to the valley alignment.
- Reorientation of the labelled ENE fault (fig. 4.28) to bound the northern margin of the Millwall Anticline (fig. 2.20) instead of intersecting its interior (compare with fig. 4.25)

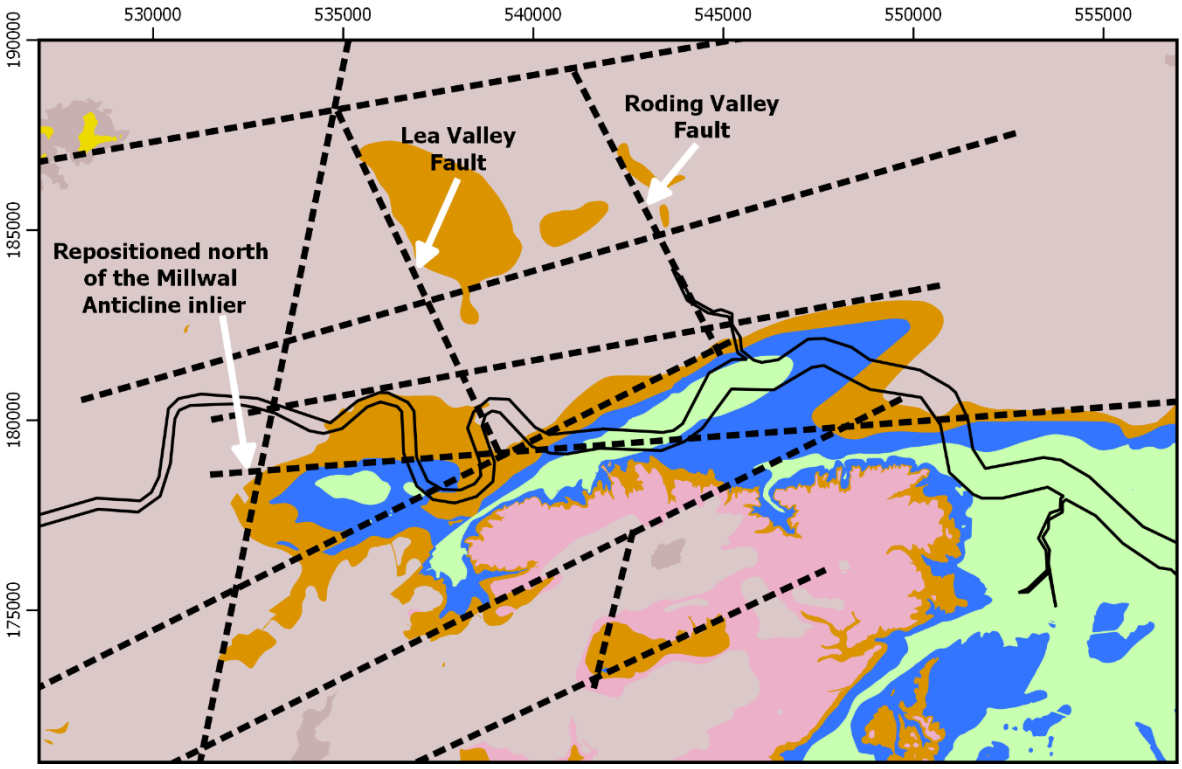

Figure 4.28 – Refinement of indirect fault map from geological evidence to include the Lea Valley Fault, and to re-orientate the Roding Valley Fault and an unnamed ENE-striking fault.

4.4.3 Paradoxical observations and challenges for strike-slip fault mapping

The NW-trending fault set is less prevalent than the NNE-set in the indirect fault map (fig. 4.24, green). This contradicts expected behaviour for the inherited major faults, since kinematic analyses indicated that the former set was preferentially aligned for reactivation (§3.2.3). If these are inherited faults, then the observations may reflect a combination of 3D reactivation behaviour of each set and the indirect mapping methodology's reliance on only vertical displacements.

The obliquity of the acting stress field will affect the slip distribution between vertical and lateral slip components (§3.2.6.1; Mandl, 2000, Bonini et al., 2012). Progressive divergence from coaxiality will cause more obliquely-resheared strike-slip faults to contain a larger dip-slip component. Pyrenean reshearing (fig. 3.16) would introduce a dip-slip component to the misaligned (sinistral) NNE-set, whilst vertical offsetting would be restricted to linkage zones along the inherited (dextral) NW-set instead.

The indirect fault mapping method interpreted lineations from solely vertical data: topographic changes in the Chalk and vertical displacement InSAR behaviour. This will favourably identify the comparatively oblique-slip NNE-set and cause the minimally dip-slip NW-set to be less apparent. To assess this, the indirect fault lineaments were superimposed onto long-timeframe lateral E-W InSAR by Mason et al. (2015) to identify lineations characterised by lateral-slip behaviour (fig. 4.29). Lateral displacement behaviour is evident along both NW- and NNE-sets, but only inferable for one ENE-fault. Comparatively, the former two sets' outlines are significantly noisier and less obvious in vertical InSAR.

The comparison demonstrates that the 3D slip behaviour of each fault set will determine how perceptible they are from vertical data. This has likely contributed to under-representation of lateral-slip dominant faults in London's near surface since most mapping methods rely upon vertical offsetting (§4.1) as exposures are absent. However, InSAR does not capture lateral N-S displacement and may miss strike-slip faults that oriented this way.

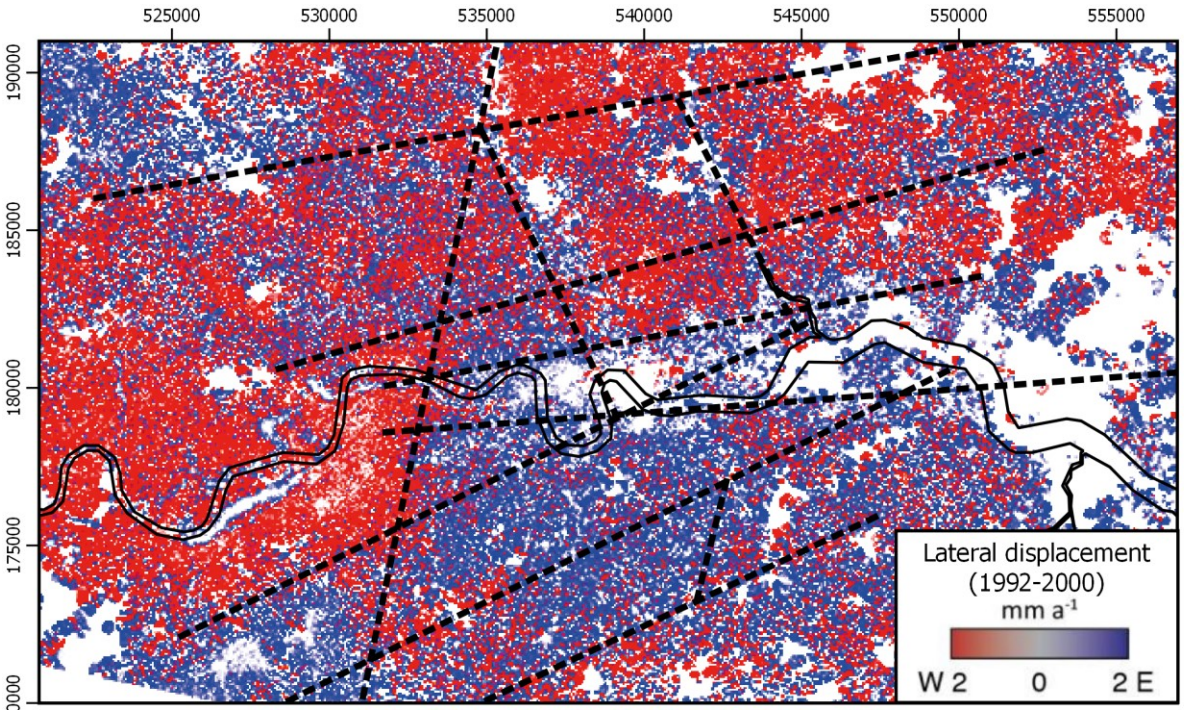

Figure 4.29 – Comparison of refined indirect fault map (fig. 4.28) with long-timeframe (1992-2000) E-W lateral displacement InSAR (fig. 4.19.b) from Mason et al. (2015).

4.4.3.1 Potential methods for identifying strike-slip faults in London

To fully characterise structures in London, future fault identification workflows must incorporate methods that can detect strike-slip faults. Three techniques below are proposed:

- Lateral E-W InSAR: Long timeframe analysis can reveal laterally displacing regions separated by linear boundaries (fig. 4.29). But to map strike-slip faults this method requires specific processing techniques, sufficiently long data windows and an undeforming reference point. This potentially restricts further lineation identification beyond findings already in Mason et al. (2015). Additionally, it will not identify lateral-slip on faults aligned ~N-S.
- Inlier offset identification: The geometry of inliers in London (fig. 4.1) reflects their bounding structures. Strike-slip faults can be inferred from consistent boundaries that trend NW-NNW and/or NE-NNE and from lateral offsets across them.
- Linkage zone interpolating: Strike-slip inheritance mechanisms (fig. 3.33-34) cause the development of *en échelon* Riedel shear zone in the cover that interact and link at points of overlap (fig 3.35-36). If linkage zones can be mapped along NW-NNW or NE-NNE corridors, then the approximate position of an inherited strike-slip fault may be inferred.

Applicability and interpretation confidence vary between each method. Inlier offsets are considered the most rigorous yet are only applicable in certain situations. Interpolating between linkage zones is dubious as they can be generated by multiple mechanisms and requires multiple linkage zones to be first mapped. The lateral E-W InSAR is widely applicable but requires validation with geological data.

4.4.4 Fault-partitioned blocks and compartmentalisation in London

The indirect fault lineaments delineate abrupt block-like changes in the subsurface topography of Late Cretaceous-Paleogene sequences that spatially correlate with differential grid-like at-surface displacement (fig. 4.10, 4.12 vs. 4.19) and inlier geometries (fig. 4.1). Similarly, block geometries are also interpreted by the BGS Lithoframe (fig. 2.31; §2.2.2.5) (Ford et al., 2010). Collectively, these imply that London's near surface has been compartmentalised into a series of discrete fault-bounded blocks by the inheritance of three basement fault sets.

Fault-bounded partitioning supports de Freitas' (2009) proposal that London's subsurface is geologically and hydrogeologically discontinuous. This implies that fault inheritance may have influenced inter- and intra-block behaviour since their Alpine reactivation and propagation, as lithological, denudational and hydrogeological variation are observed between them. The impact of fault compartmentalisation on geological processes is assessed in §6.1.

4.4.5 Major fault set interpretation in London

Three major fault sets have been identified in London that trend NW-NNW, NE-NNE, and ENE-E. The former two sets are interpreted to be predominantly strike-slip, being more prevalent in lateral InSAR and less apparent from chalk topography. The latter ENE-E set are dip-slip dominant, being obvious from both vertical InSAR and chalk topography but less discernible from lateral InSAR.

Major faults in London were determined to be inherited from three basement faults (§3.2-3): Variscan strike-slip conjugate pair and reversed Mesozoic normal fault set. The sets from structural lineaments and mapped near surface faults are interpreted to represent these inherited structures as they display comparative trends (fig. 4.23.a-c vs. 3.25.c-d) and slip behaviour. This is further supported by Ford et al. (2010), who identified that the Lithoframe faults spatially correlated with steepened gradients in Bouguer residual gravity data that was 'gravity-stripped' of its post-Palaeozoic cover. Minor deviation does exist between near-surface and basement fault trends. Given the evidence supporting inheritance, this divergence may imply differences in basement fault orientations along the Anglo-Brabant Massif's southern margin and/or fault realignment with the Alpine stress field in the cover (fig. 3.33). From these analyses the three major fault sets in London are interpreted as:

- NW-NNW: Inherited Variscan dextral strike-slip faults
- NE-NNE: Inherited Variscan sinistral strike-slip faults
- ENE-E: Inherited reversed post-Variscan normal faults

4.4.6 Mechanisms for at-surface displacement

Opposing senses of vertical and E-W lateral at-surface movement are observed across fault lineaments that produce differential block displacement (fig. 4.22, 4.29). This behaviour is attributed to an interplay between discontinuous groundwater behaviour in the Lower Aquifer and neotectonism.

Both historical and recent changes in Lower Aquifer water levels demonstrate block-like variations (Aldiss et al., 2014, Buchan, 1938, de Freitas, 2009) that mirror fault positions (fig. 4.28) and imply across-fault flow impedance. The Lower Aquifer has been naturally (and locally artificially) recharging since the 1970s (Ellison et al., 2004). Where confined, recharge will cause the aquifer to expand vertically due to its lateral confinement and be observed as differential displacement between fault-bounded blocks (fig. 4.22). Variation between blocks likely reflects the impacts of their specific recharge behaviour, aquifer confinement and overburden thickness.

The E-W lateral movement is predominantly coincident with inherited strike-slip fault sets (fig. 4.29). It is unlikely to be a hydrogeological response since the Lower Aquifer is laterally confined. Instead, it

is attributed to neotectonic lateral fault creep since far-field compression is still acting on southern Britain (Baptie, 2010). Intriguingly this includes movement along the kinematically inefficient NNE-set (fig. 3.18) and may imply that the set is weaker than modelled (§3.2.2.2) or that coaxiality is different through stress or fault set misalignment (fig. 3.13.d; table 3.3). Alternatively, it may represent motion of the bounded blocks themselves as their displacements are uniform internally and imply fault confinement. Neotectonic creep may have contributed to vertical displacement also given the prevalence of the ENE-E reverse normal fault set in vertical InSAR.

4.4.7 Limitations of lineament set orientation analysis and directional statistics applicability

The three distinct fault lineament trends interpreted in §4.4.1 and §4.3.2 are based on qualitative analysis of rose diagrams and frequency distribution plots (fig. 4.23-24, 4.26), with similar inferences made in §3.3.1.1 also (fig. 3.23). These lacks quantitative rigour, making the interpretations subjective and risks the potential for interpretative biases.

Directional statistical analyses could provide the necessary rigour by determining whether the lineament tends within these four datasets (table 4.3) are significantly different. This was determined to be unfeasible since no directional statistical method was identified that could separate and compare between individual trends within a broader dataset (fig. 4.24). These tests treated the datasets collectively and treated them as a broad spectrum between 0-180° instead, making trends quantitatively indiscernible despite being present (fig. 4.23). For example, the nonparametric Watson U^2 test, which assess whether two sets of azimuths are significantly different, returned all the datasets as not different to 1% confidence.

The potential for discretising each dataset into defined bins to perform the tests was also explored. But this was also considered inappropriate since it would introduce interpretative biases and potentially reduce certain sets below statistical significance.

The interpretations in §4.4.1 are limited by their qualitative analyses, but the potential to provide rigour and quantify this is unfeasible since. Despite this, there are visually obvious trend groups shared between three of the datasets (fig. 4.23.a,c vs. 4.26.a, 4.24) that support published inferences of three major fault sets (§4.4.5).

4.5 Conclusion

Major fault identification in London was investigated by reviewing potential techniques and their associated contributions, developing a new mapping method, and characterising fault set geometries.

Fault under-representation in London reflects minimal at-surface exposure and homogeneous lithologies in London (Aldiss, 2013). Historical expectations of minimal faulting (§2.2.2.5) have likely contributed to this also that introduce structural preconceptions independent of mapping method. Explicit-driven geological modelling (§4.1.2.2) is the most appropriate fault identification method because it utilises London's data-rich subsurface in a geologically constrained manner. The BGS Lithoframe is considered to be the most representative structural map at present.

A hidden fault network was identified under London by comparing linear boundaries in subsurface topography and at-surface displacement (fig. 4.22, 4.29), and is partly verified by fault zones, 1:250k mapping and the BGS Lithoframe (fig. 4.25). This indirect method (§4.2.1) is a novel alternative that may overcome mapping issues where fault exposures are minimal and/or inaccessible.

Three major fault sets are evident from structural, InSAR and fluvial evidence that correspond with expected inherited fault orientations (§4.4.5, §4.3.2). But the reliance on vertical offsetting by most mapping techniques has further downplayed the identification of both strike-slip fault sets (§4.4.3) and is difficult to overcome without exposures.

The indirect fault map, together with the BGS Lithoframe, demonstrates that faulting is more widespread than recognised and that fault inheritance has compartmentalised the ground into a series of discrete blocks. But fault mapping is incomplete since isolated fault zones still exist (fig. 4.21-22).

The proposed fault lineaments require 'ground truthing' with subsurface data to confirm and constrain their positionings. Chapter 5 outlines the geological modelling programme conducted in East London to validate this indirect fault map and investigate the potential impact of fault compartmentalisation.

5. Geological modelling of East London

A hidden fault network identified in London (fig. 4.28) separates geologically and hydrogeologically distinct areas (§4.4.4). This implies that the subsurface has been compartmentalised into discrete blocks through the intersection and offsetting of inherited faults.

An explicit-driven geological modelling programme was undertaken for East London (fig. 5.1) to identify major faulting and characterise the subsurface, and to validate the inferred fault lineaments in Chapter 4. East London was selected for structural analysis due to prevalence of major faulting locally (fig. 5.1), numerous inliers and subsurface topographic variation (fig. 3.39), and excellent borehole coverage (fig. 4.8). Collectively, these factors will improve fault offset identification.

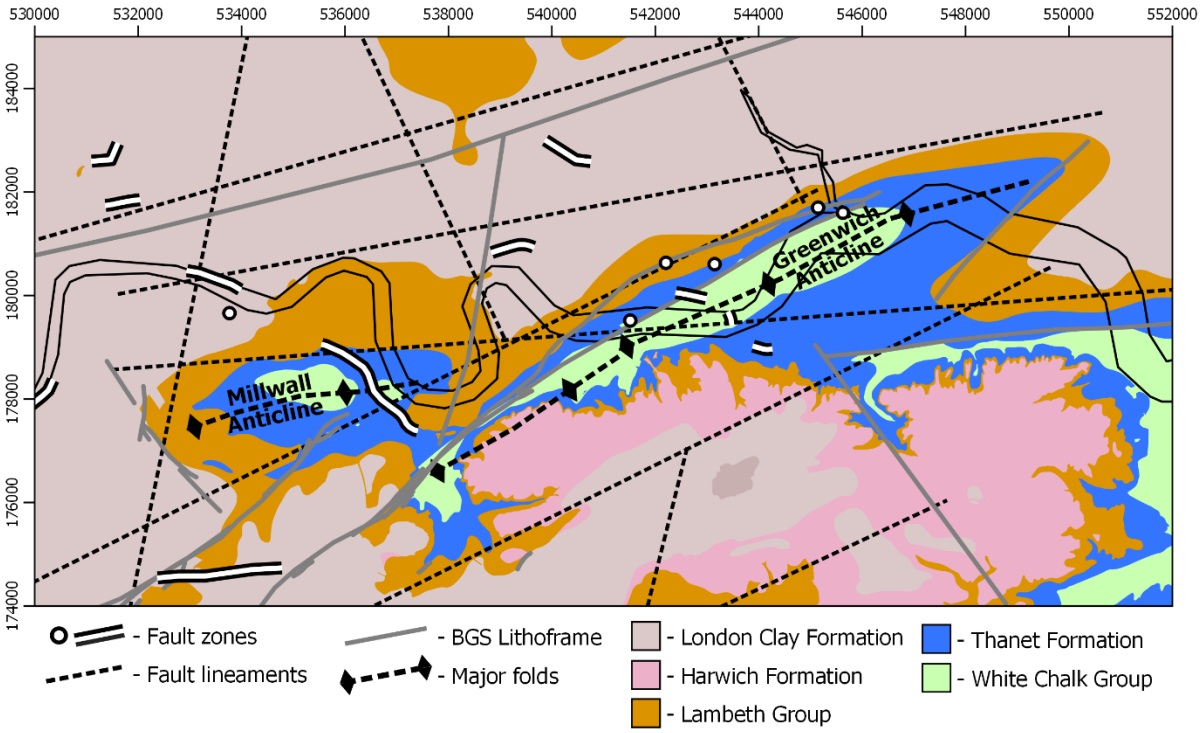

Figure 5.1 – Geological map of the investigation area in East London. Structural analysis was conducted here due to its complex near-surface geology and data availability.

This chapter presents the East London geological modelling programme. The methodology workflow, outlined in figure 5.2, is separated into borehole data preparation (§5.1) and modelling (§5.2). The outputs of both phases are presented (§5.3) and analysed (§5.4) through comparisons with published models and discussions on fault interpretation. Finally, the programme's methodology and analytical issues are reviewed (§5.5).

The outcome is a model of East London's subsurface, constructed from 761 boreholes and 47 cross-sections, that constrains major fault positions and the lithologies they bound.

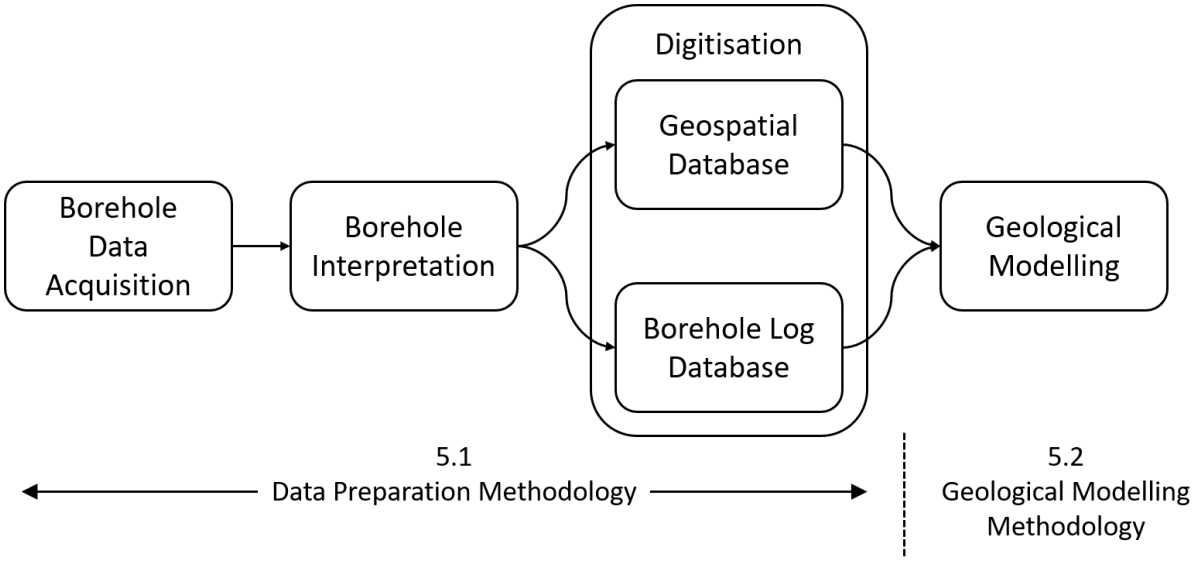

Figure 5.2 – Overview workflow for geological modelling programme of East London.

5.1 Data preparation methodology

Geological modelling interprets the ground from a combination of at-surface and subsurface data (§4.1.2), with this investigation utilising existing borehole data to model the latter component. Borehole logs were analysed to extract the lithologies intercepted and any in-borehole faulting evidence. The former enabled lithology coverage and fault offsetting to be characterised, whilst the latter provide spatial evidence of faulting locally.

The section outlines the development of the log and geospatial databases from boreholes. The methodology is broken down into three parts (fig. 5.2):

- §5.1.1 – Data Acquisition

  The selection process developed to prioritise linear borehole datasets that maximise coverage and extractable information.
- §5.1.2 – Data interpretation

  The interpretation rationale of key lithological and tectonic features in borehole logs.
- §5.1.3 – Data Digitisation

  The development of two databases and a hierarchical recording system to maximise the information extracted and to ensure their communicability in appropriate formats.

5.1.1 Data acquisition

London is rich in subsurface information due to density of boreholes (fig. 4.8) from historical well drilling and recent geotechnical investigations. However, not all boreholes can be confidently utilised as their quality and extractable geological information are highly inconsistent. This is illustrated by lithological descriptions of the Mid-Lambeth Hiatus[26] in figure 5.3, limiting their input into the generated database. Consequently, the rationale behind borehole selection will affect both how informative the generated database is and the effectiveness of the geological modelling itself.

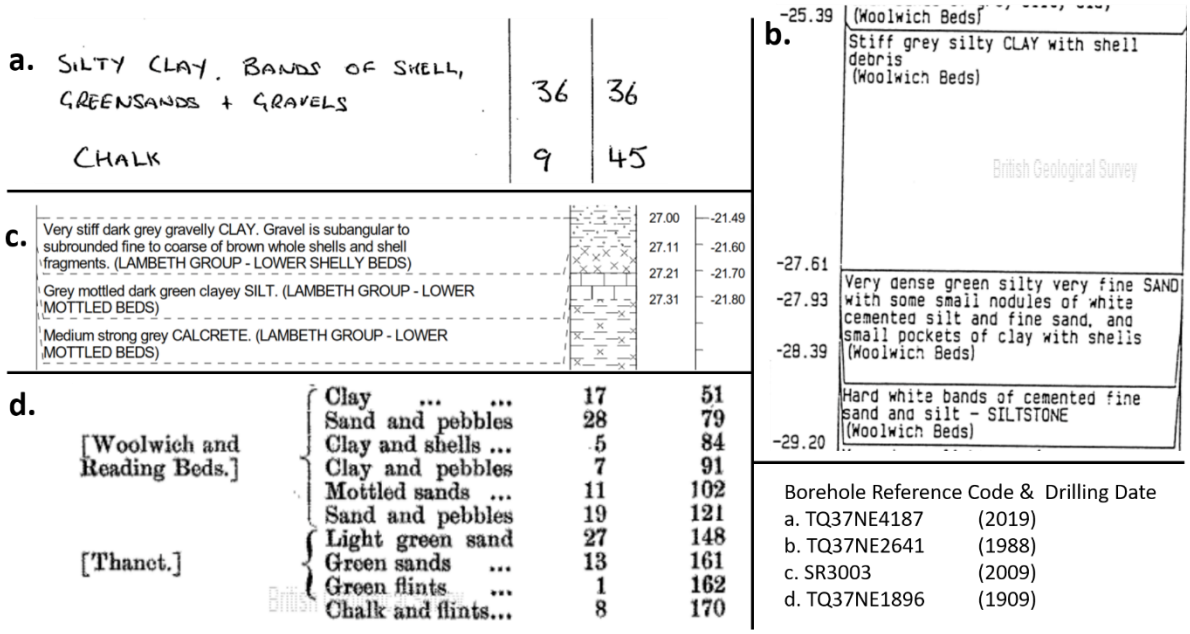

Figure 5.3 Inconsistent lithological descriptions of the Mid-Lambeth Hiatus (MLH) and surrounding lithologies, reflecting both the lithological knowledge at the time and their specific drilling purposes (will affect the logged information quality). Boreholes a, b, & d are publicly available; log c is sourced from Thames Tideway.
a. a. Grouping of the Lambeth Group and Thanet Formation. MLH positioning is unextractable.
b. Broad transition present in description, despite wrongly interpreting it all as Woolwich Formation.
c. Highly detailed sub-formational breakdown of the MLH transition.
d. Bulk description of the Lambeth Group. Relative positioning of the MLH inferred between "clay and shells" and "clay and pebbles" rather than through direct interpretation.

To overcome this, a targeted approach to borehole acquisition was adopted to prioritise borehole datasets[27] that maximised extractable information and coverage, with the intention to generate an overlapping grid-like data array. A tiered system was developed to score and identify appropriate datasets using this rationale (fig. 5.4). This targeted approach favoured ground investigations (GIs) from major infrastructure projects as they are typically laterally extensive datasets comprised of high-

[26] The hard band transition between the Lower Mottled Beds (Reading Formation) and the Lower Shelly Clays & Laminated Beds (Woolwich Formation) forms a distinct marker in the Lambeth Group (§2.2.1.3).
[27] A 'borehole dataset' is defined here as a group of boreholes drilled for a specific project, e.g., Crossrail.

quality information (grades 1-2). From these datasets, boreholes with penetrative depths typically greater than 10 m were selected to ensure bedrock penetration.

Following this initial database development, a secondary acquisition phase was undertaken to target and improve data coverage in structurally and/or geologically complex areas. Here lower scoring datasets (grades 3-4) were also utilised.

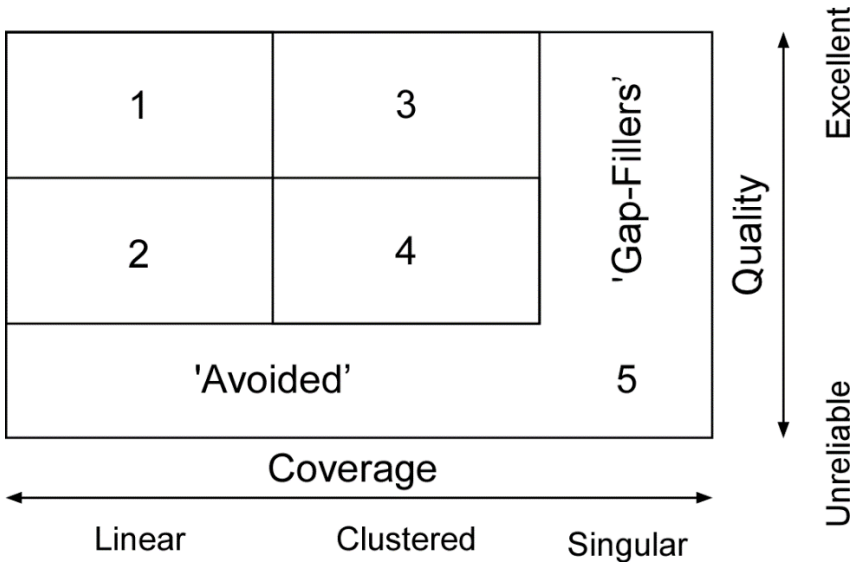

Figure 5.4 – Tiered data acquisition hierarchy devised for grading borehole datasets that prioritises both coverage and quality.

5.1.2 Data interpretation

The rationale for extracting lithological and tectonic interpretations from borehole log descriptions are discussed. Both were dependent upon borehole log quality (fig. 5.3).

5.1.2.1 Lithological interpretation

London's near surface comprises a sequence of episodically deposited shallow marine to deltaic Paleogene sequences (fig. 2.22) unconformably resting on the eroded White Chalk Group (fig. 2.21).

The interpretation phase aimed to define these lithologies to their lowest lithostratigraphic subdivisions in each log. This principally relied upon their description in the log sheets (e.g., fig. 5.3.c), which generally adhered to BS5930[28] (BSI, 2015) or its previous versions. This was typically sufficient for lithological interpretation as it describes grain sizes, colour, and their along-tract variability, and provides drilling information that could further indicate material changes[29]. Where available, core photographs were also used to aid interpretations, however, these were only available for some privately sourced datasets. Where material complexity was apparent and/or information limited, cross-comparisons were undertaken with adjacent boreholes.

Log descriptions are typically accompanied by in-log interpretations. These were not relied upon for Palaeogene strata as their nomenclature is typically outdated and/or do not subdivide lithologies; or were erroneous. They may introduce uncertainties into the database and, by extension, the model, if not validated and reinterpreted by this investigation. In contrast, in-log subdivisions of the White Chalk Group were relied upon if present (Thames Tideway dataset only[30]) as log descriptions were insufficient to subdivide it to its Formation and Bed levels (fig. 2.21).

Lithological interpretations and subdivision of the Palaeogene strata were achieved by comparing in-log descriptions with type standards for each lithology (King et al., 2016, Aldiss, 2014, Entwisle et al., 2013). This was complemented by Lambeth and Thames Groups courses to develop interpretative experience and lithological knowledge of these sequences. An additional unpublished Harwich Formation basal sequence[31] was also included to improve its definition in East London. Borehole interpretation is an iterative process, with problematic areas requiring multiple revisions as further logs were locally collated.

[28] British Standard 5930 details the methods of recording lithologies for geotechnical investigations. This requires a thorough description of lithologies (including discrete horizons internally) and their interpretation.
[29] For example, the cohesiveness of a sand-dominant interval can be inferred from total core recovery (TCR), helping to distinguish between the clayey sands of the Upnor Fm. and the silty sands of the upper Thanet Fm.
[30] These were logged independently by Rory Mortimore, who developed the modern chalk lithostratigraphy.
[31] This silty fine SAND was first documented in the study area by J. Skipper (Crossrail, 2016).

5.1.2.2 Tectonism interpretation

In-borehole direct and indirect evidence of brittle tectonism (faulting and jointing) can provide proxy confirmation of nearby faulting. Furthermore, these features may be useful for geotechnical analysis and indicate the impact of faulting on the local rockmass, e.g., material-specific brittle damaging and/or repetition. Interpretations were primarily based upon in-log descriptions (fig. 5.5-6) and drilling information, with discontinuity logs and core photographs used if available.

A general criterion of descriptive features indicative of faulting was developed. Direct evidence was based on observations of repetition (fig. 5.5.b), slickensides, comminution (fig. 5.5.a), and enhanced jointing and/or fissuring[32]. Indirect evidence provided a proxy for faulting, with features such as considerable core loss[33] in cohesive clay-rich lithologies (fig. 5.6) or dense sands recorded. However, the applicability of the general criterion was dependent upon the material properties of each layer (e.g., the low-cohesive sand-rich Thanet Formation is unlikely to shear as joints).

Lithology-specific criterion were also developed from relevant literature and collaborative efforts with colleagues[34]. The most extensive was the White Chalk Group criterion to reflect its greater susceptibility to alteration following brittle tectonism (fig. 5.5.a):

- Weathering depth: Increased fracturing locally enhances weathering.
- Fracture spacing: Decreased fracture spacing may imply borehole proximity to faulting.
- Structureless chalk: Disaggregation caused by either poor drilling practice or faulting.
- Separation of jointing style: Jointing varies between chalk formations (Mortimore, 2012), with unexpected changes and/or concentrations potentially implying faulting locally.
- Joint staining: Orange-staining of chalk surfaces reflects groundwater flow (Mortimore et al., 2011) and may have preferentially exploited both jointing and faulting as conduits.

In isolation, many of these ‘direct’ and ‘indirect’’ observations are insufficient to confirm faulting. For example, brittle fabrics may be generated by periglacial processes and poor drilling practices also. However, they can provide multiple lines of evidence for local tectonism and its geotechnical impact when cross-compared with other indicative features (within and between boreholes). When sufficient evidence was identified in the log, a shear zone was recorded with an accompanying summary.

[32] Jointing is most prevalent in the brittle chalk; however, it is also recognised in certain clay-rich Palaeogene lithologies where it is typically misinterpreted as fissuring. Therefore, extensive fissuring was also recorded.
[33] Core loss can be triggered by both poor drilling technique and the disaggregation of rock mass. Its occurrence in competent materials may imply local brittle tectonism and fragmentation. Core loss was not recorded for gravel-rich lithologies (Upnor Formation) nor logs with evidence of cable percussion malpractice.
[34] For example, discussions with Justyna Edgar highlighted that cemented bands in the Harwich Formation may be an indicator of major faulting. Assessed in §7.4.4.

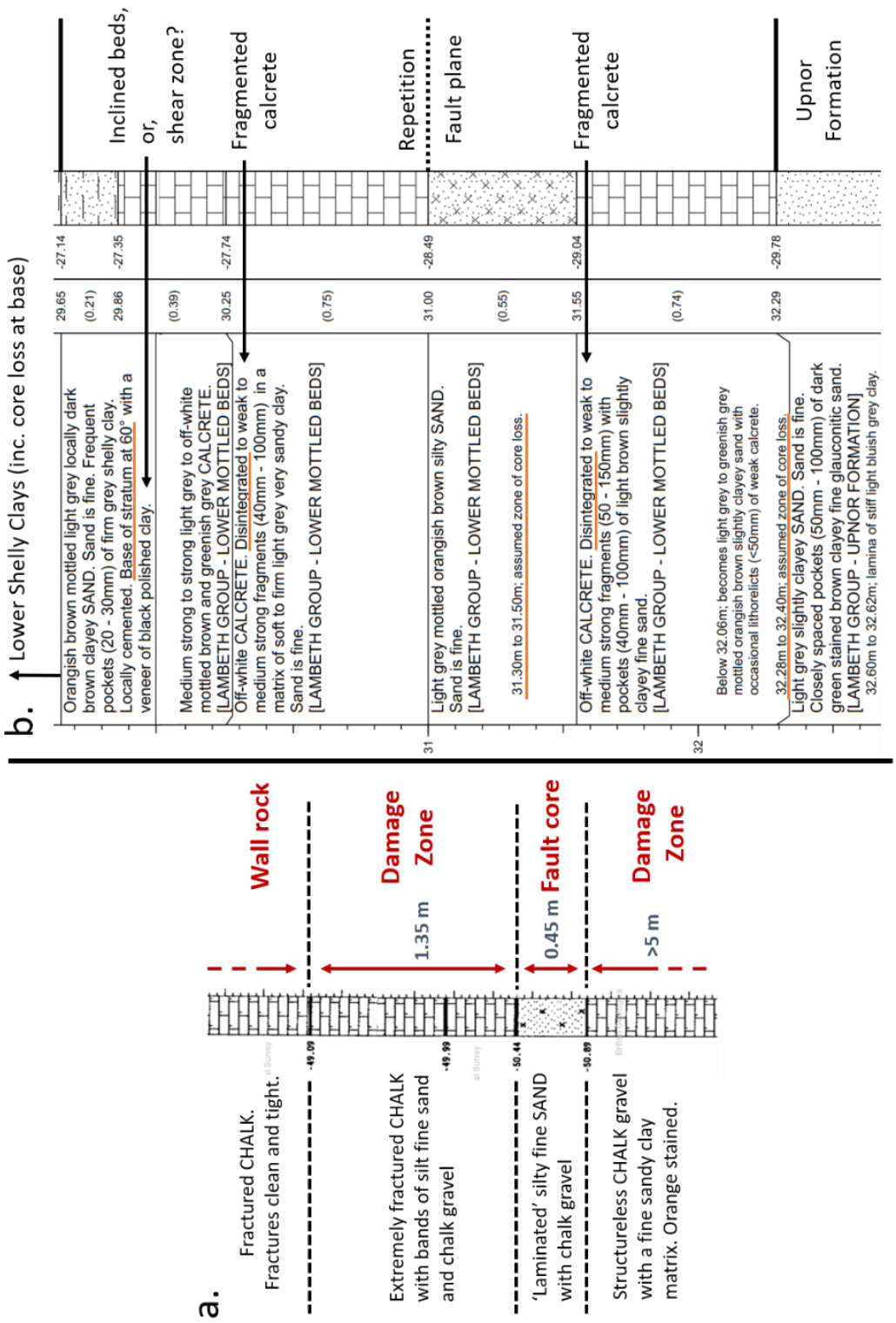

Figure 5.5 – In-borehole evidence of faulting in the Chalk and Lambeth Group.
a. Fault core in the White Chalk Group – Borehole TQ38SE1425 [BGS].
Log transitions from 'normal' fractured chalk to a heavily fragmented and structureless orange strained mass surrounding a laminated sandy band. This is comparable to brittle damage zone development surrounding a comminuted, sheared fault core (fig. 3.10.b).
b. Faulting and repetition of the Lower Mottled Clay – Borehole GPB-04 [Silvertown].
Repeated sequence of mottled clayey-silty sand and calcrete horizons. Tectonism also evidenced by calcrete 'disintegration', core loss, inclined bedding, and clayey polished interfaces.

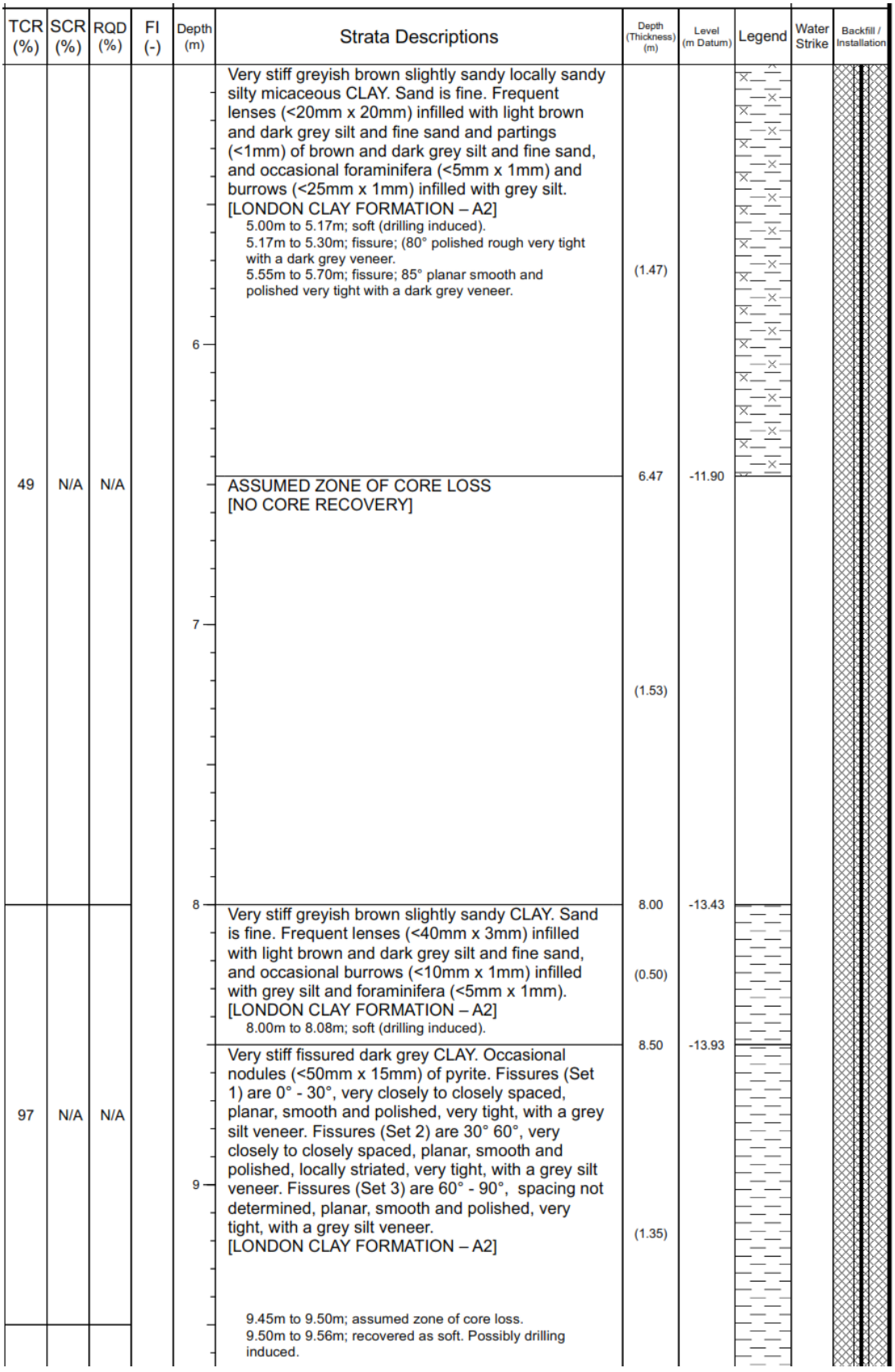

Figure 5.6 – In-borehole fault evidence in the London Clay. Borehole RTB-24 [Silvertown Tunnel]. Brittle degradation of the cohesive near-homogenous London Clay into a sheared, locally loose blocky mass, as evidenced by multiple polished and locally striated fissure sets (likely joints), soft horizons and a band of substantial core loss (despite rotary coring).

5.1.3 Data digitisation

The extracted lithological and tectonic information required digitising. However, the specific formatting requirements of the geological modelling software (MOVE) for inputting boreholes restricted the accessibility and utilisation of this data once digitised. Additionally, MOVE does not recognise the AGS format, preventing a direct reprocessing of already digitised GI data.

To overcome this, two databases were developed to maximise the usage of these data in appropriate formats. The 'log database' adhered to the MOVE's format for inputting borehole logs. The 'geospatial database' recorded information that is not readily extractable from the log database. For example, tectonic evidence documented in the log database cannot be easily manipulated in a single consistent format, requiring separate recording in the geospatial database also.

The development of these two databases to format extracted information are discussed.

5.1.3.1 Log database formatting

MOVE requires an ASCII format for importing log data (fig. 5.7). An 'input sheet' was produced to digitise each borehole dataset (footnote 27). These were later collated into a 'master input sheet' for importing into the model.

Lithostratigraphic interpretations are recorded as 'horizons' with an accompanying justification and summary of key lithological and tectonic information in the 'remarks'. These are inputted along with that horizon's elevation, XY coordinates, and the unique code of the borehole[35].

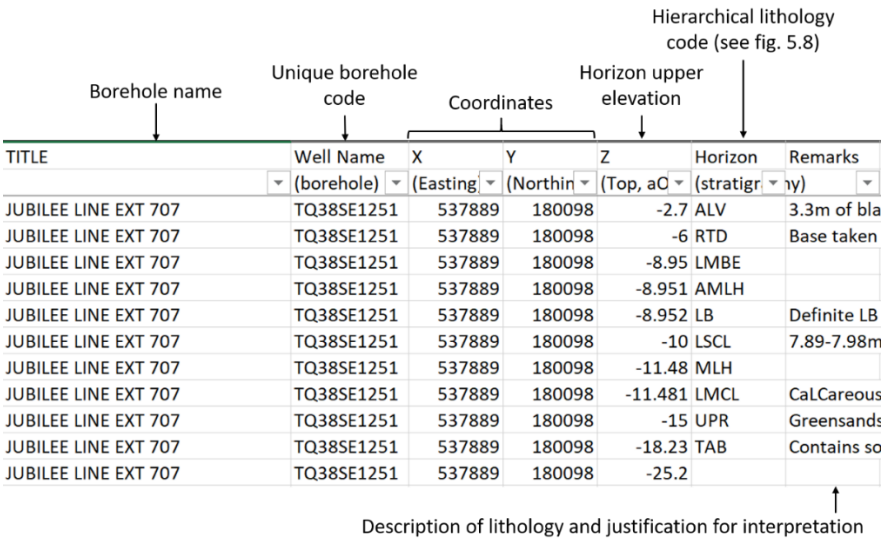

TITLE	Well Name (borehole)	X (Easting	Y (Northin	Z (Top, aC	Horizon (stratigr	Remarks ıy)
JUBILEE LINE EXT 707	TQ38SE1251	537889	180098	-2.7	ALV	3.3m of bla
JUBILEE LINE EXT 707	TQ38SE1251	537889	180098	-6	RTD	Base taken
JUBILEE LINE EXT 707	TQ38SE1251	537889	180098	-8.95	LMBE	
JUBILEE LINE EXT 707	TQ38SE1251	537889	180098	-8.951	AMLH	
JUBILEE LINE EXT 707	TQ38SE1251	537889	180098	-8.952	LB	Definite LB
JUBILEE LINE EXT 707	TQ38SE1251	537889	180098	-10	LSCL	7.89-7.98m
JUBILEE LINE EXT 707	TQ38SE1251	537889	180098	-11.48	MLH	
JUBILEE LINE EXT 707	TQ38SE1251	537889	180098	-11.481	LMCL	CaLCareous
JUBILEE LINE EXT 707	TQ38SE1251	537889	180098	-15	UPR	Greensands
JUBILEE LINE EXT 707	TQ38SE1251	537889	180098	-18.23	TAB	Contains so
JUBILEE LINE EXT 707	TQ38SE1251	537889	180098	-25.2		

Figure 5.7 – Borehole log ASCII formatting for input into MOVE. The XYZ coordinates define the 3D position of a specific lithological horizon as markers along the borehole tract when imported.

[35] The unique borehole code was relied on for modelling to avoid potential repetition of names (typically based on location). Their nomenclature is source-dependent, originating from either BGS or privately held database.

These horizons represent the upper boundary of a lithostratigraphic unit, with the lower boundary defined by the underlying layer. A basal boundary was defined for the London Clay also as it has an irregular basal interface with the Harwich Formation and the Lambeth Group (fig. 2.23-24) that prevented its lower boundary from being consistently defined.

5.1.3.2 Hierarchical lithostratigraphic system

Each lithostratigraphic unit was allocated a specific code (table 5.1), allowing corresponding horizons in other boreholes to be linked across the database. A hierarchical coding system was developed to prevent the database being restricted by the least-detailed log. Lithostratigraphy was defined at multiple levels, overcoming inconsistencies in the level of lithological breakdown interpretable between borehole logs. This hierarchy maximised lithological detail where available and linked boreholes that had contrasting levels of information for the same material. Every lithostratigraphical group was broken down into its lowest definable constituents along with other key marker horizons[36], with a unique code assigned at each level: Group > Formation > Member.

The application of the hierarchical system is illustrated in figure 5.7 by the Laminated Beds: LMBE > AMLH > LB. When a Group is entered for the first time, the elevation is recorded. If sufficient detail is present for further breakdown, then this will progress to the member-level. When the log transitions to a distinct lithology within that group only its code and elevation will be recorded.

The hierarchical system minimises the impact of inconsistent borehole quality by digitising each log to the lowest lithological level achievable. All boreholes containing the same lithology are linked at least at the Group level, with lower tiers recorded where logs are sufficiently detailed. Cross-comparison with adjacent boreholes is thus enabled regardless of how detailed they are. This is illustrated in figure 5.8, where breakdown of the “Blue Formation” has enabled identification of a normal fault, rather than being restricted by the least informative borehole log present.

[36] Key markers bands included the LC-Base and Lambeth Group non-layer horizons: Mid-Lambeth Hiatus (MLH), and above (AMLH) or below (BMLH) Mid-Lambeth Hiatus. The two latter markers address spatial variability in post-depositional erosion of the Lambeth Group, with BMLH only used when the AMLH and MLH are absent.

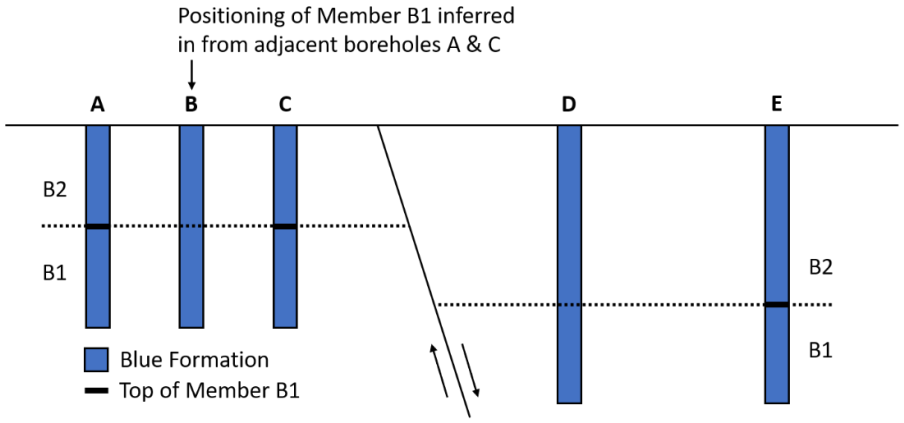

Figure 5.8 – Cross-section interpretation from boreholes with inconsistent lithological details. The member-level boreholes (A, C, & E) confirm offsetting and are not impeded by poor quality logs.

Table 5.1 – Hierarchical lithostratigraphic codes for sequences encountered during East London modelling. Colour scheme adapted from the BGS to replace the laterally equivalent Reading and Woolwich Formation with positionings relative to MLH. Major unconformities marked with solid dashed lines.

Time			Group		Formation		Member	
Period	Epoch	Age	Name	Code	Name	Code	Name	Code
Palaeogene	Eocene	Ypresian	Thames	THAM	London Clay	LC	B unit	LC-B
							A3 unit	LC-A3
							A3ii subunit	LC-A3ii
							A3i subunit	LC-A3i
							A2 unit	LC-A2
							Base of LC	LC-Base
					Harwich	HWH	Swanscombe	SWCB
							Oldhaven	OH
							Blackheath	BLB
							Harwich Basal Sand Unit	HBSU
			Lambeth	LMBE	Above MLH	AMLH	Upper Shelly Clay	USB
							Upper Mottled Clay	UMCL
							Laminated Beds	LB
							Lower	LSCL
					Mid-Lambeth Hiatus	MLH		
					Below MLH	BMLH	Lower Mottled Clay	LMCL
							Mottled Upnor	MUPR
	Palaeo-cene	Thanetian			Upnor	UPR		
			Thanet	TAB	Thanet	TAB	Bullhead Beds	BLHB
Cretaceous	Late Cretaceous	Turonian-Campanian	White Chalk	WHCK	Seaford	SECK	Haven Brow Beds	SECK-HBB
							Cuckmere Beds	SECK-CB
							Belle Tout Beds	SECK-BTB
					Lewes Nodular	LECK	Beach Head Beds	LECK-BHB
					New Pit	NPCH		

5.1.3.3 Geospatial Database

The geospatial database was developed to collate layer-specific lithological and tectonic features with their coordinates into an extractable format for geospatial analysis. It also had a secondary purpose for monitoring interpretation progress and summarising borehole features[37] and their metadata[38]. This allows spatial analysis in a manner that cannot be achieved by the log database format (fig. 5.7) since many features are embodied within descriptions, e.g., atypical core loss. The database structure is presented in figure 5.9, where key borehole information and layer-specific features associated with the Harwich Formation (as an example) are presented.

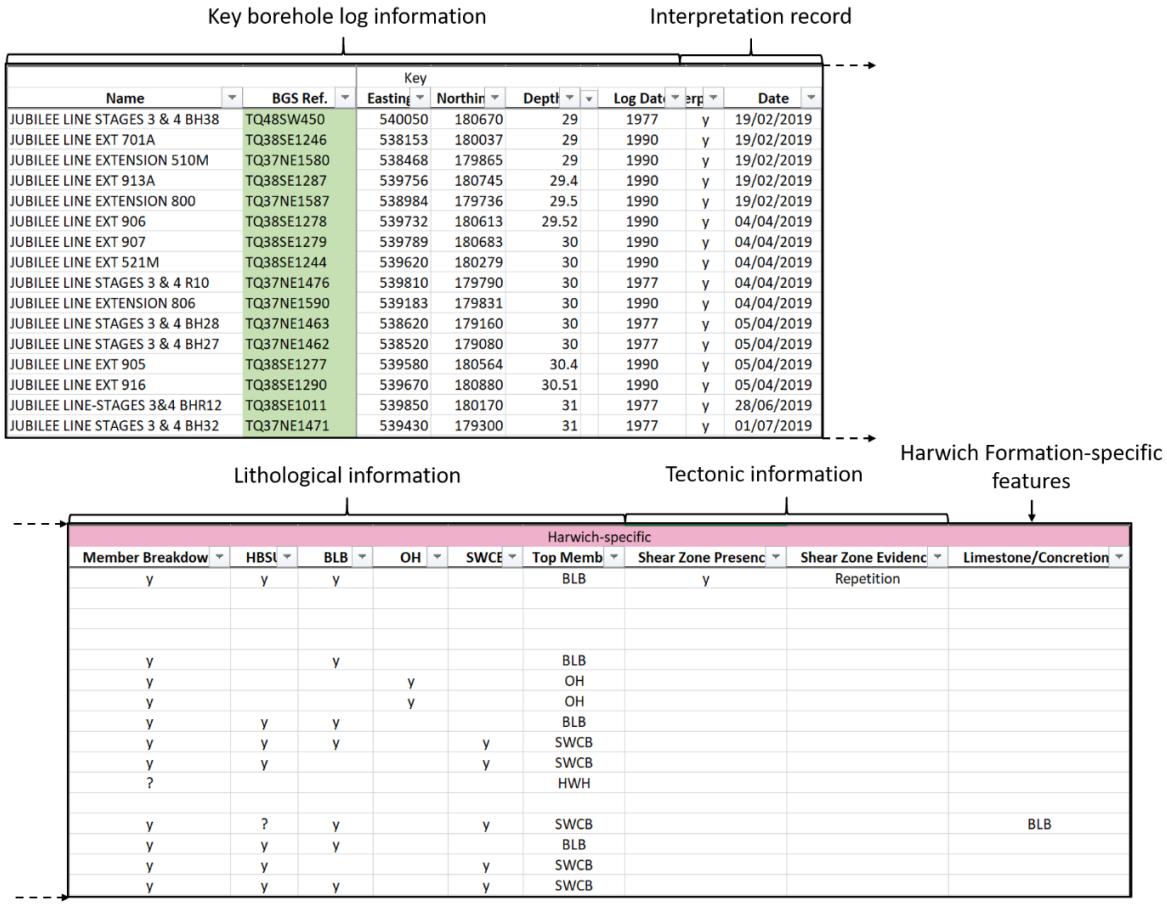

Name	BGS Ref.	Key Easting	Northing	Depth	Log Date	erp	Date
JUBILEE LINE STAGES 3 & 4 BH38	TQ48SW450	540050	180670	29	1977	y	19/02/2019
JUBILEE LINE EXT 701A	TQ38SE1246	538153	180037	29	1990	y	19/02/2019
JUBILEE LINE EXTENSION 510M	TQ37NE1580	538468	179865	29	1990	y	19/02/2019
JUBILEE LINE EXT 913A	TQ38SE1287	539756	180745	29.4	1990	y	19/02/2019
JUBILEE LINE EXTENSION 800	TQ37NE1587	538984	179736	29.5	1990	y	19/02/2019
JUBILEE LINE EXT 906	TQ38SE1278	539732	180613	29.52	1990	y	04/04/2019
JUBILEE LINE EXT 907	TQ38SE1279	539789	180683	30	1990	y	04/04/2019
JUBILEE LINE EXT 521M	TQ38SE1244	539620	180279	30	1990	y	04/04/2019
JUBILEE LINE STAGES 3 & 4 R10	TQ37NE1476	539810	179790	30	1977	y	04/04/2019
JUBILEE LINE EXTENSION 806	TQ37NE1590	539183	179831	30	1990	y	04/04/2019
JUBILEE LINE STAGES 3 & 4 BH28	TQ37NE1463	538620	179160	30	1977	y	05/04/2019
JUBILEE LINE STAGES 3 & 4 BH27	TQ37NE1462	538520	179080	30	1977	y	05/04/2019
JUBILEE LINE EXT 905	TQ38SE1277	539580	180564	30.4	1990	y	05/04/2019
JUBILEE LINE EXT 916	TQ38SE1290	539670	180880	30.51	1990	y	05/04/2019
JUBILEE LINE-STAGES 3&4 BHR12	TQ38SE1011	539850	180170	31	1977	y	28/06/2019
JUBILEE LINE STAGES 3 & 4 BH32	TQ37NE1471	539430	179300	31	1977	y	01/07/2019

Harwich-specific								
Member Breakdow	HBSt	BLB	OH	SWCB	Top Memb	Shear Zone Presenc	Shear Zone Evidenc	Limestone/Concretion
y	y	y			BLB	y	Repetition	
y		y			BLB			
y			y		OH			
y			y		OH			
y	y	y			BLB			
y	y	y		y	SWCB			
y	y			y	SWCB			
?					HWH			
y	?	y		y	SWCB			BLB
y	y	y			BLB			
y	y			y	SWCB			
y	y	y		y	SWCB			

Figure 5.9 – Example of the geospatial database highlighting key borehole information and Harwich Formation-specific lithological and tectonic features for several Jubilee Line Extension boreholes.

[37] Coordinates, unique reference codes, penetration depth, log date, major lithologies encountered.
[38] Borehole source, log quality (fig. 5.4), GI project (and specific phases), geophysical data and drilling method.

5.2 Geological modelling methodology

An explicit-driven workflow was developed for this investigation following its identification as the most appropriate method for fault mapping and subsurface characterisation in Chapter 4: Interpretations are manually defined by geological reasoning to constrain modelled surfaces.

The geological modelling workflow (fig. 5.10) is schematically visualised in figure 5.11. Following the initial model setup (§5.2.1), digitised boreholes were imported. Targeted cross-sections were constructed to define fault positions and lithologies as a series of polylines that outline perceived block boundaries and their interiors (explicit modelling, §5.2.2). Major fault planes were then generated that constrained the lithological surfaces they bound (implicit modelling, §5.2.3). Surface geometrical properties were then extracted to finalise the model.

Fault blocks were defined from inferred fault lineaments and coded (fig. 5.12) to categorise cross-sectional analyses and surface generation. The exception is Block G, which was kept whole despite a major fault intersection, as it bounds the WSG-Faults shear zone interpreted in §3.3.3.2. The primary acquisition phase's borehole distribution controlled which blocks were codified.

The geological modelling software MOVE (version 2019.1) (Petroleum Experts, 2020) was chosen due to its licensed availability, modelling flexibilities, in-built GIS functionalities and structural analysis features, and previous experience with this software. Other packages, such as Leapfrog and the open-source Gempy were also considered but they unfavourably emphasised implicit modelling workflows.

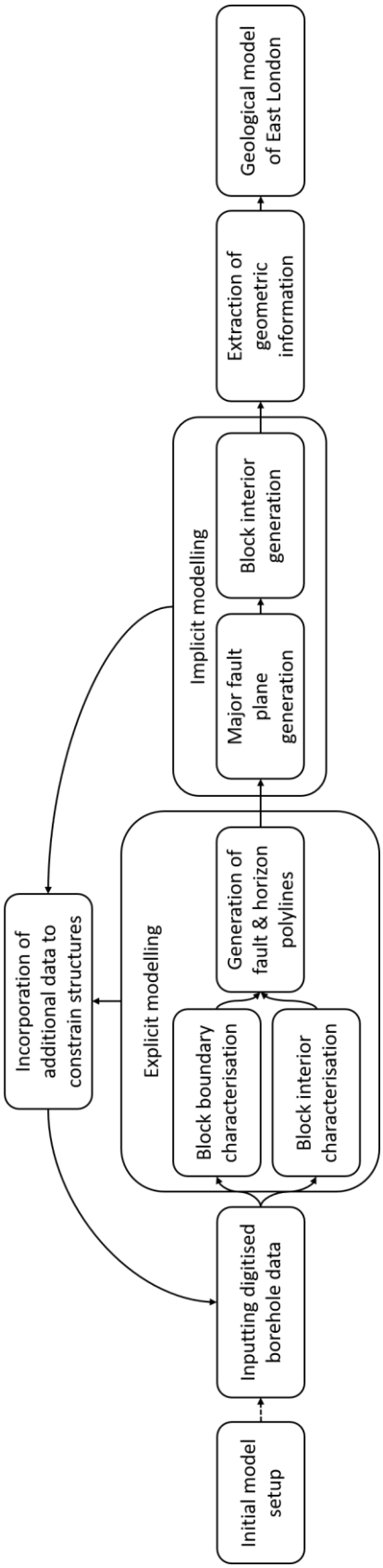

Figure 5.10 – Geological modelling workflow developed for subsurface analysis of East London. The programme is explicitly driven with the positions of major faults and their bounded lithological surfaces constrained by cross-sectional analysis. New borehole data can be iteratively incorporated at any stage in the investigation to improve coverage and/or counter anomalies.

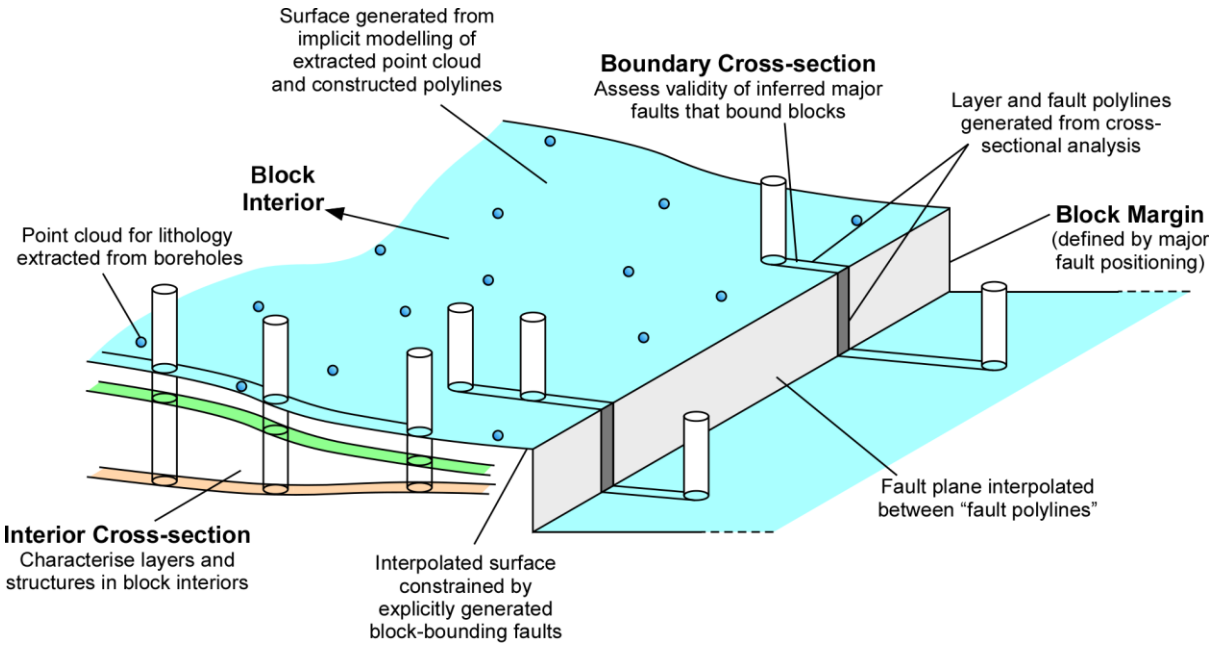

Figure 5.11 – Schematic of geological modelling programme, demonstrating how the block-bounding faults and the lithological surfaces they compartmentalise are generated from cross-sectional analysis in the initial explicit modelling phase. Refer to figure 5.10 for workflow structure.

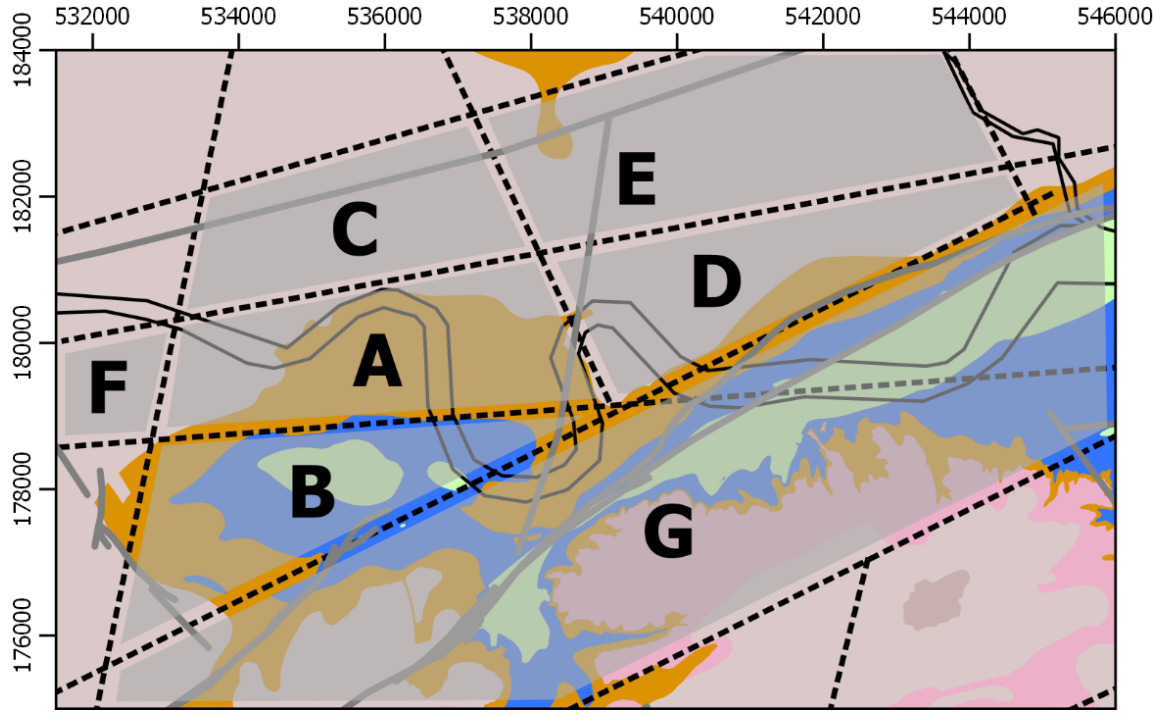

Figure 5.12 – Fault block positions inferred from indirect fault lineaments intersections (Chapter 4).

5.2.1 Initial model setup

The model was set up using OSGB1936/British National Grid coordinate system. Outlined are the processes undertaken prior to geological modelling.

5.2.1.1 Preliminary data importation

Seven datasets were imported into MOVE (table 5.2): model stratigraphy, borehole input sheets, rockhead data, the refined indirect fault map, BGS 1:50,000 geological map, BGS Lithoframe faults, and the DTM of East London. The purposes of each dataset are outlined in table 5.3.

5.2.1.2 East London stratigraphic codes

The hierarchical lithological system (table 5.1) was restructured into a stratigraphic ASCII format specific to MOVE to enable horizons (imported or generated) to be correctly recognised. Additional features, such as sequence age and mechanical properties, could have been attached also, but were considered unnecessary for this investigation.

5.2.1.3 Borehole error and quality assessment

The entirety of the borehole database is then manually assessed for errors once imported into MOVE to check for correct lithological linkages, typos, and the misplaced commas. Mistakes were rectified in the corresponding input sheets, before reimporting into MOVE.

5.2.1.4 Rockhead surface development

The rockhead was used to define the bedrock-superficial interface during explicit modelling and required defining prior to cross-sectional analyses. The rockhead point cloud was interpolated to produce the preliminary surface before cross-section analysis. This was projected into sections as intersecting polyline and revised during explicit modelling, with a finalised rockhead surface refined during the implicit modelling phase. The rockhead was assumed to be continuous and unaffected by tectonism and ignored evidence of fault offsetting (e.g., Ghail et al., 2015a).

Table 5.2 – Overview of datasets imported into MOVE prior to geological modelling. [a] – Format specific to MOVE.

Imported data	Data type	Data Format	Data Owner	Source
East London stratigraphic codes	ASCII Stratigraphy Format [a]	.csv	Tom Morgan	§5.2.1.2
Borehole input sheets	ASCII Well Format [a]			Log database (§5.1.3.1)
Rockhead elevation and lithology	Point cloud			Geospatial database (§5.1.3.3)
Refined indirect fault map	Polylines	Shapefile		Indirect fault mapping (Chapter 4, fig. 4.28)
BGS 1:50,000 geological map	Polygons		British Geological Survey (BGS)	Edina Digimap
BGS Lithoframe fault map	Polylines			Provided by Jon Ford (pers comms, 2020), (Chief Geologist of England, BGS)
OS Terrain 5 DTM	GeoTIFF (Originally ASC)	Raster	Ordnance Survey	Edina Digimap

Table 5.3 – Purposes of imported datasets for the initial model setup.

Imported Data	Purpose
East London stratigraphic codes	Enables MOVE to recognise the lithostratigraphic horizon codes (table 5.1) and assign their correct colours.
Borehole input sheets	To import the digitised boreholes (fig. 5.7) into the model. These were collated into a master input sheet for each data acquisition phase.
Rockhead elevation and lithology	To develop a preliminary bedrock-superficial interface (rockhead) during cross-sectional analysis.
Refined indirect fault map	To provide preliminary block boundaries to aid cross-section targeting.
BGS 1:50,000 geological map	To provide near surface bedrock stratigraphy.
BGS Lithoframe fault map	To provide complimentary, higher resolution positionings of major faults.
OS Terrain 5 DTM	To provide at-surface topography for both 3D and cross-sectional analysis.

5.2.2 Explicit modelling phase

Cross-sections constructed during the explicit modelling phase (fig. 5.11) to characterise East London's subsurface have three purposes, to:

- Identify fault offsets both at perceived block boundaries and within their interiors,
- Characterise lithological behaviour both within and across perceived blocks,
- Generate polylines for these features to constrain interpolation between boreholes.

Boreholes are selected along sub-linear distributions to generate these cross-sections. Sinuous fits were used to align the section with the selected boreholes and prevent linear traces. Intersecting polylines for the DTM and initial rockhead surface were extracted along their alignments.

Three types of cross-section are defined based on their alignments relative to the inferred blocks, each with their own unique nomenclature using the block codes outlined in figure 5.12:

- Interior sections - Characterise block interiors only.
  BLOCK_interior_# (e.g., A_interior_1)
- Boundary sections - Intersect the boundary of two blocks.
  BLOCK1_BLOCK2_boundary_# (e.g,. A_D_boundary_4)
- Across sections - Intersect the entirety of a block and its boundaries with two neighbours.
  BLOCK_across_BLOCKBOUNDARY1_BLOCKBOUNDARY2_# (e.g., B_across_A_G_2)

The same interpretation process is used for all section types, preventing structural biases being introduced where fault interpretations are incorrectly restricted to perceived block boundaries only: A fault is interpreted only where a fault is interpreted.

5.2.2.1 Rockhead polyline refinement

The morphology of the preliminary rockhead surface (§5.2.1.4) is broadly unrepresentative as it relied upon a disparate point cloud. Its intersected polylines are revised and constrained against boreholes in-section to produce a more geologically accurate version (fig. 5.13).

Rockhead positions in boreholes are ignored where they are identified as erroneous, reflecting two causes: misinterpretation of bedrock sediments as alluvium and/or river terrace deposits[39]; and over-projection of distal boreholes that are locally unrepresentative. These are identified by cross-comparisons with neighbouring boreholes and their logs (fig. 5.13), with erroneous horizons ignored during rockhead polyline revisions.

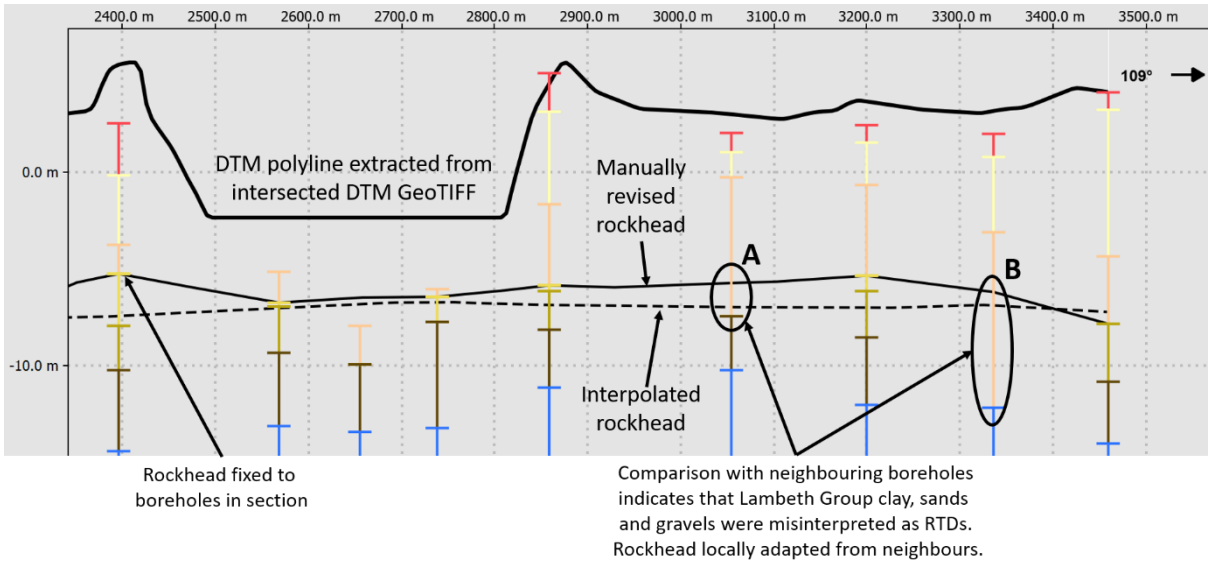

Figure 5.13 – In-section refinement of the rockhead polyline from boreholes. Where rockhead discrepancies are attributed to an erroneous borehole, the polyline is refined by its neighbouring boreholes instead. Two examples are provided:
A – Sandy Laminated Beds and clayey Lower Mottled Clays portions of the Lambeth Group were misinterpreted as river-terrace deposits (RTDs) in log.
B – Misinterpretation of the Upnor Formation as RTDs. This is not an over-projected borehole as the geological map shows that Lambeth Group crops out here.

[39] Misinterpretations are attributed to poor in-log descriptions and/or indivisible groupings as London's superficial and bedrock sequences are comparatively distinct. This may cause sandy and gravelly bedrock horizons (e.g., Upnor Fm.) to be misinterpreted as alluvium and/or river terrace deposits.

5.2.2.2 Cross-section interpretation

Lithological and faults polylines (fig. 5.14) are explicitly constructed during cross-sectional analysis.

Lithological polylines, like horizons (fig. 5.7), represent the layer's upper surface and adhere to the hierarchical coding system (table 5.1). Polylines are defined by linking between boreholes (fig. 5.14.b), with irregular horizons reviewed to determine whether they are erroneous.

Faults are interpreted where offsetting is apparent between boreholes (fig. 5.14.b). These are idealised to vertical and drawn at the midpoint. Additional evidence is provided by lateral changes in lithologies and/or thicknesses, variation in horizon morphologies, and in-log faulting indicators.

Borehole spacing and penetrative depth are typically inconsistent across sections, causing issues for both layer and fault defining. Lithological polylines are projected using the morphology of overlying strata, with thickness assumed from known lengths in adjacent boreholes (fig. 5.14.a). Fault defining is intentionally conservative to prevent misinterpretation of inclined strata when borehole spacing is poor; challenges were identified and are discussed in §5.5.3.

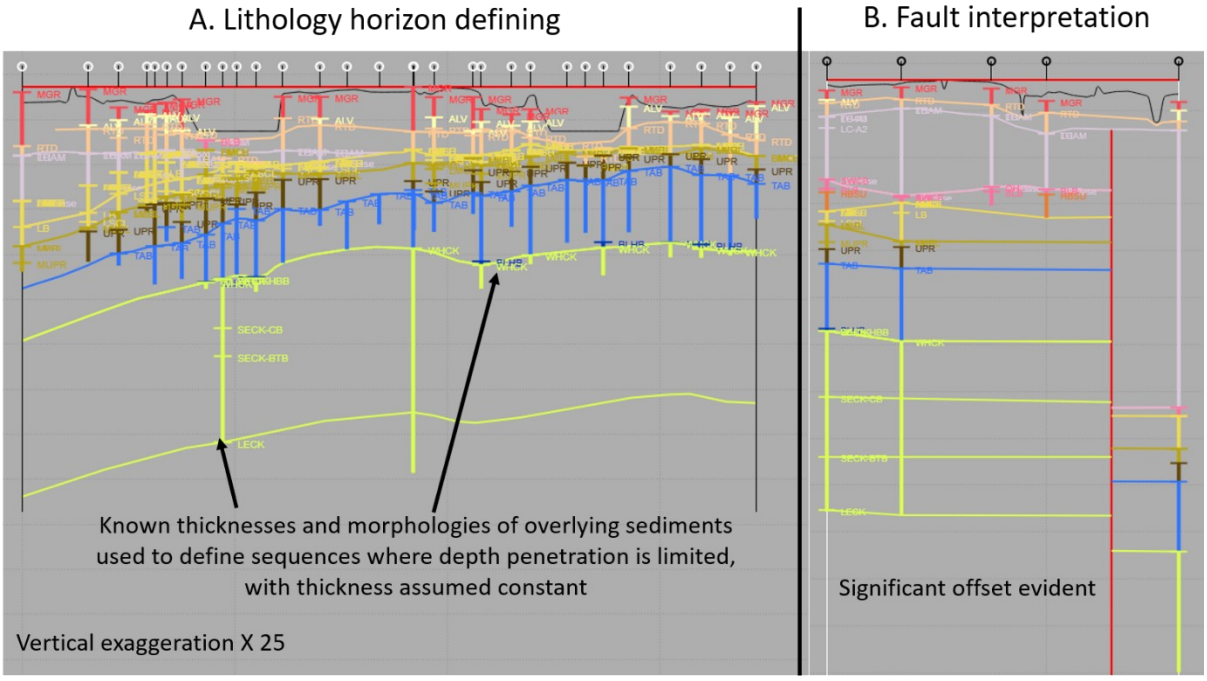

Figure 5.14 – Examples of horizon and fault polyline interpretation during cross-sectional analysis. Scales and orientations are ignored as sections are for illustrative purposes only.
A – Lithological 'horizons' are defined by linkage of boreholes.
B – Faults are interpreted from offsets and changes in horizons geometries across them.

5.2.2.3 In-model revisions of boreholes and section uncertainties

Neighbouring boreholes occasionally displayed conflicting information, in terms of elevational and/or lithological discrepancies. Where recognised, analysis generally showed that the cause reflected lithological misinterpretations based on the available descriptions provided (fig. 5.3).

Erroneous boreholes are revised in both MOVE and the log database, supported with comments justifying the amendment. Rarely, a borehole is intentionally ignored in section if it is identified to be completely discordant with surrounding boreholes. Comments are added to sections to highlight uncertainties and justify decisions.

5.2.2.4 Defining major fault

Block-bounding faults are selected from the interpreted faults based on whether they separated distinct regional differences in horizon elevation, thickness, geometry, and presence. This analysis is conducted in sections and by cross-comparison of extracted polylines in 3D model view.

Selected faults are copied and named according to the blocks they bound (e.g., FAULT_AB). Their Z-coordinates are modified to range from +10 to -90 mOD to provide consistent lengths during the major fault surface generation (§5.2.3.1) and to ensure that all horizons at depth are intercepted.

Major fault definition is difficult where regional boundaries are complex and comprised of multiple faults. This will be revisited in the §5.5.3.

5.2.3 Implicit modelling phase

Fault planes and geological layers are generated as 3D polygons (fig. 5.11) by interpolating between the explicitly modelled lithological and fault polylines, and lithological point clouds.

5.2.3.1 Major fault plane generation

Major fault planes are inferred from major fault polylines that are collectively considered to represent a single block boundary, based on their consistent and distinct geological behaviour across all the cross-sections in 3D model view.

There are two scenarios in which major faults require idealising to prevent them from intersecting unfaulted areas or generating surface artefacts[40], requiring the adaptation of fault planes and/or the generation of additional ones.

- Erroneous intersections

  One interpolated fault plane intersected an unfaulted interior cross-section (D_interior_6), indicating that the fault instead curved around it. A fault polyline was added to the edge of this section, with the major fault plane revised to prevent the erroneous intersection.

- Artefact wrapping

  The interpolation process stitched lithological surfaces to the faults that bound them. However, the surface was locally unconstrained where horizon data extended beyond the fault plane length, causing the surface to wrap around the fault plane's edge. To prevent this, additional fault planes were locally constructed in two situations to prevent artefact wrapping (fig. 5.15). These idealised faults are coloured green to distinguish them from modelled major faults and are only used to constrain surface interpolation.

5.2.3.2 Lithological surface generation

The surface of a specific lithology is interpolated from the explicitly modelled horizon polylines and borehole point clouds. Surfaces are modelled as discrete meshes bounded by the interpreted major faults, rather than as a continuous surface, because block-like compartmentalisation behaviour was apparent from fault offsets during the explicit phase.

[40] Artefacts are an erroneous by-product of the interpolation process and are typically generated where the surface is unconstrained due to minimal data coverage. These are overcome by maximising data coverage and targeting the processing conditions.

Discrete surfaces are generated by clustering polylines and point clouds within a specific block, stitched to major fault planes (cut to generate an enclosed block perimeter) (fig. 5.15) and interpolated. These were intentionally not stitched to the entireties of confining faults as extensions beyond data coverage exacerbated artefact risks.

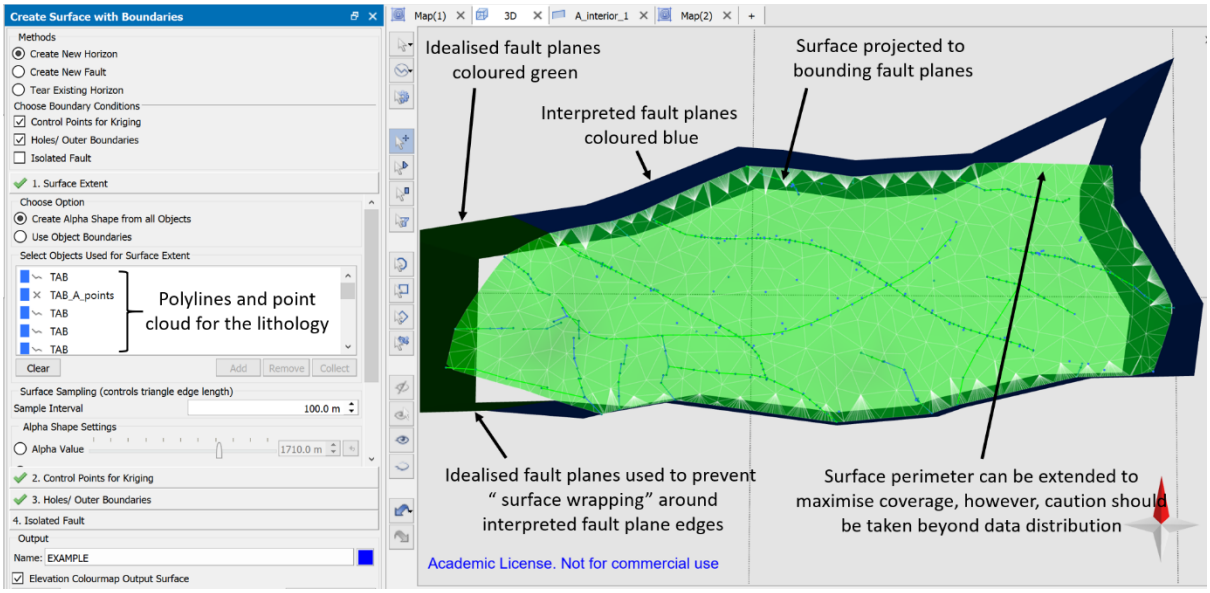

Figure 5.15 – Generation of block-bounded lithological horizons by collating lithological polylines and point clouds confined by major fault planes. Surfaces are named by their lithology and block code.

5.2.3.3 Rockhead refinement and lithological surface revision

The interpolated lithological surfaces do not account for recognised deep rockhead anomalies that penetrate into the subsurface and so incorrectly continue through them. To overcome this, the rockhead surface was revised from the rockhead polylines (fig. 5.13) and point cloud (table 5.2). This new surface is used to cut surfaces that intersect significantly deep anomalies and delete the erroneous portions within the depression. This was only conducted for the Blackwall anomaly due to its relative scale (where rockhead penetrates to > -65 mOD [borehole TQ38SE1395]).

5.3 Results

The outputs of borehole data preparation (§5.1) and lithological and structural analysis from geological modelling (§5.2) in East London are presented. The respective coordinates of maps and surfaces outlined in figure 5.16, and a key of the bedrock geology in the geological modelling is presented in figure 5.17.

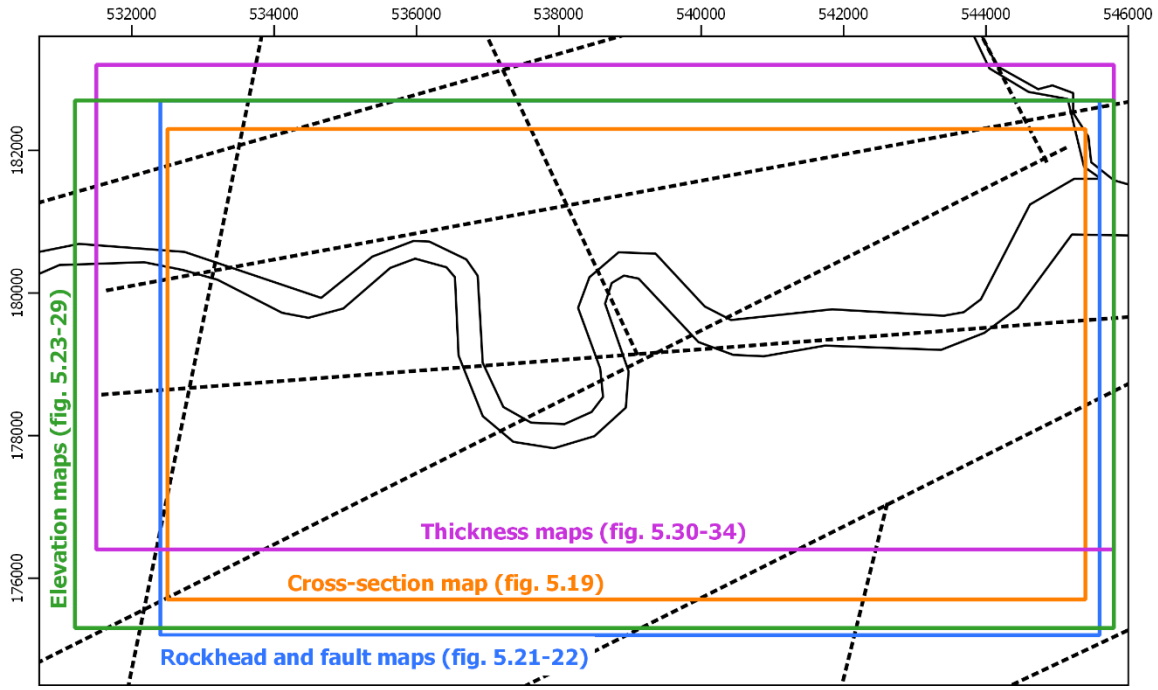

Figure 5.16 – Coordinates for map and surface figures in §5.3. The original grid references provided by the modelling software were illegible and removed post-modelling.

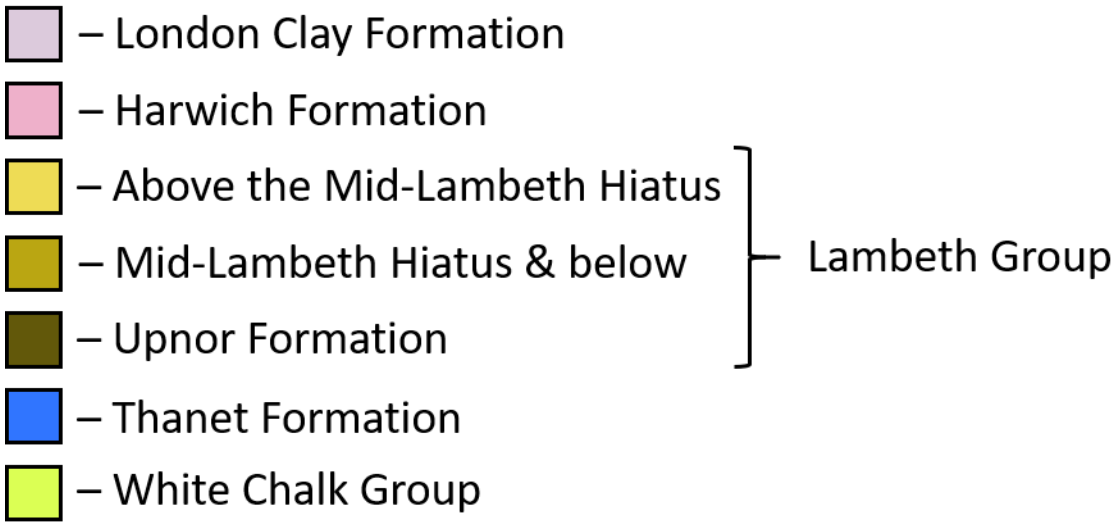

Figure 5.17 – Key of major lithological horizons used for geological modelling in East London (table 5.1). The Lambeth Group was subdivided and does not follow the conventional BGS colour scheme.

5.3.1 Borehole Interpretation

The model interpreted and digitised 761 boreholes during two phases of acquisition (fig. 5.18). Initially, 676 boreholes were acquired from linear engineering projects, followed by a further 85 obtained from a broader range of sources (table 5.4). The second phase improved borehole coverage overall but primarily targeted the margins between suspected fault blocks A, C, F & D.

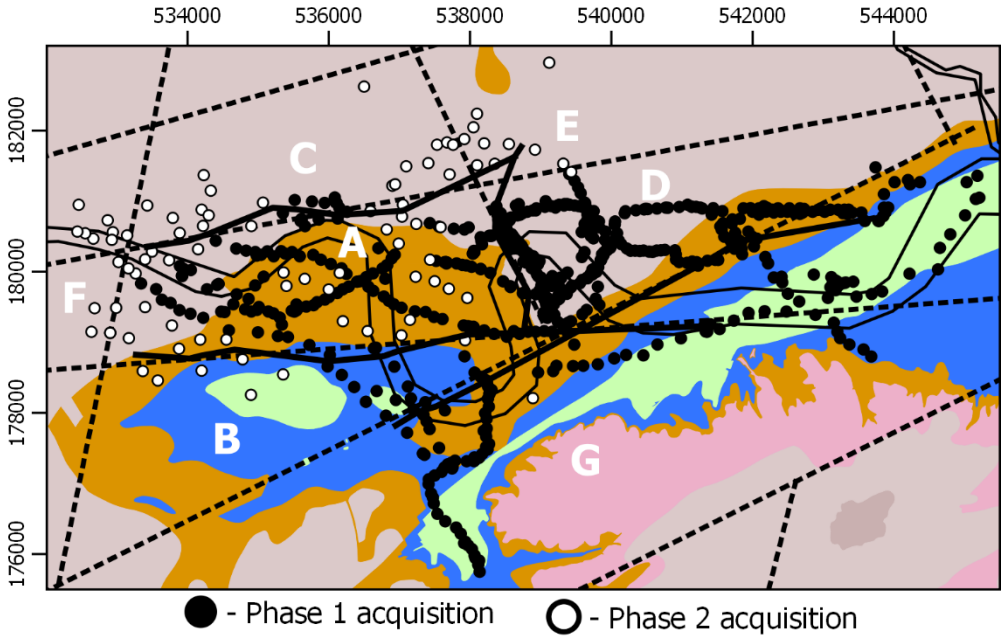

Figure 5.18 – Borehole coverage (761 logs) in East London following two phases of data acquisition (table 5.4). This includes 6 boreholes where only the deeper stratigraphy was digitised due to complications with shallower sequences preventing reliable categorisation.

Table 5.4 – List of boreholes datasets interpreted and digitised, refer to Appendix A for private datasets. [a] Isolated refers to boreholes that were collated from a range of project types and qualities.

Infrastructure Project	Project Type	Total [761]	Phase 1 [676]	Phase 2 [85]	Source	Availability
Jubilee Line Extension	Linear	184	178	6	BGS	Public
Blackwall Tunnel	Linear	109	109	-	BGS	Public
Canary Wharf Eastern Access	Cluster	17	17	-	BGS	Public
Silvertown Tunnel	Linear	39	39	-	Transport for London (TfL)	Private
Thames Tideway Tunnel	Linear	115	100	15	Thames Water	Private
DLR Lewisham Extension	Linear	52	52	-	BGS	Public
DLR Beckton Extension	Linear	63	63	-	BGS	Public
Royal Docks Drainage	Linear	118	118	-	BGS	Public
Isolated [a]	Isolated	64	-	64	BGS	Public

5.3.2 Cross-sectional analysis

The boreholes form multiple curvilinear alignments within and across suspected blocks. From these alignments, 47 cross-sections were constructed (fig. 5.19) and explicitly modelled (Appendix B). Refer to figure B.1 for a location map of all the sections, with the naming nomenclature outlined in §5.2.2.

Several sections are presented for analysis in §5.4-5. These are outlined below in figure 5.20.

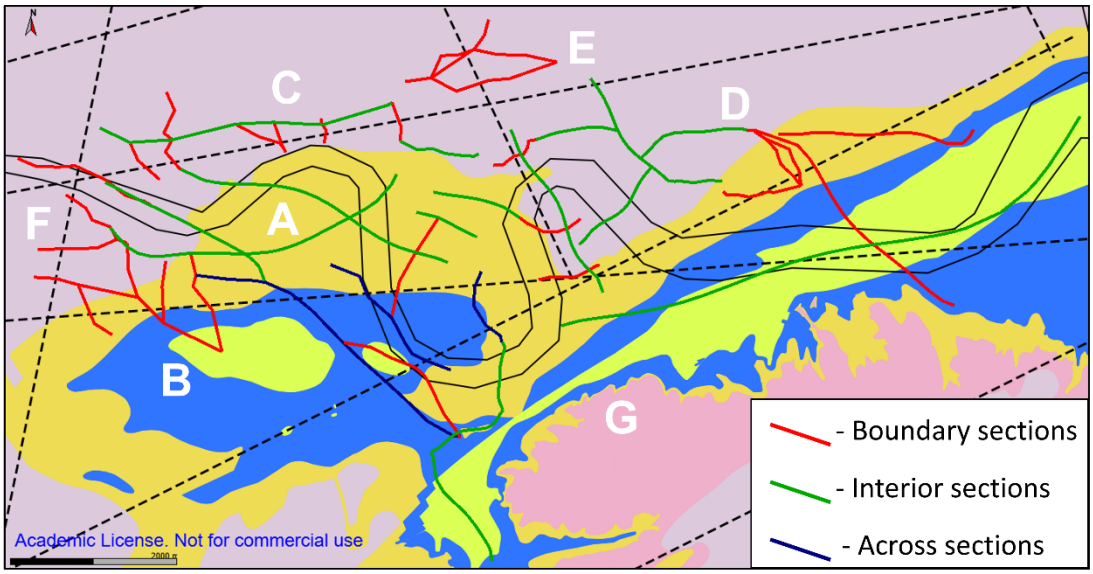

Figure 5.19 – Positions of 47 cross-sections from the explicit modelling phase (Appendix B). These are categorised into three types (outlined in §5.2.2): Boundary (27), Interior (17) & Across (3).

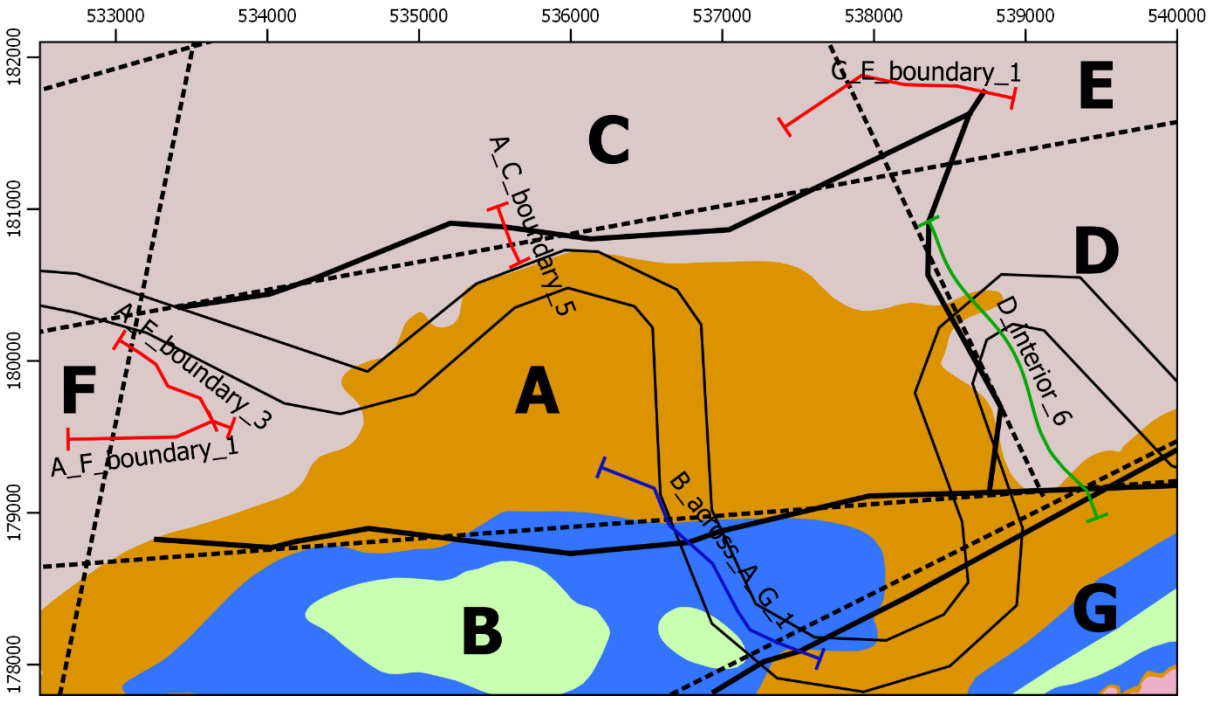

Figure 5.20 – Sections analysed in §5.4-5.

5.3.3 Rockhead surface

The bedrock-superficial interface was intercepted in 733 boreholes and refined with 47 polylines during explicit modelling (fig. 5.13) to constrain the surface (fig. 5.21).

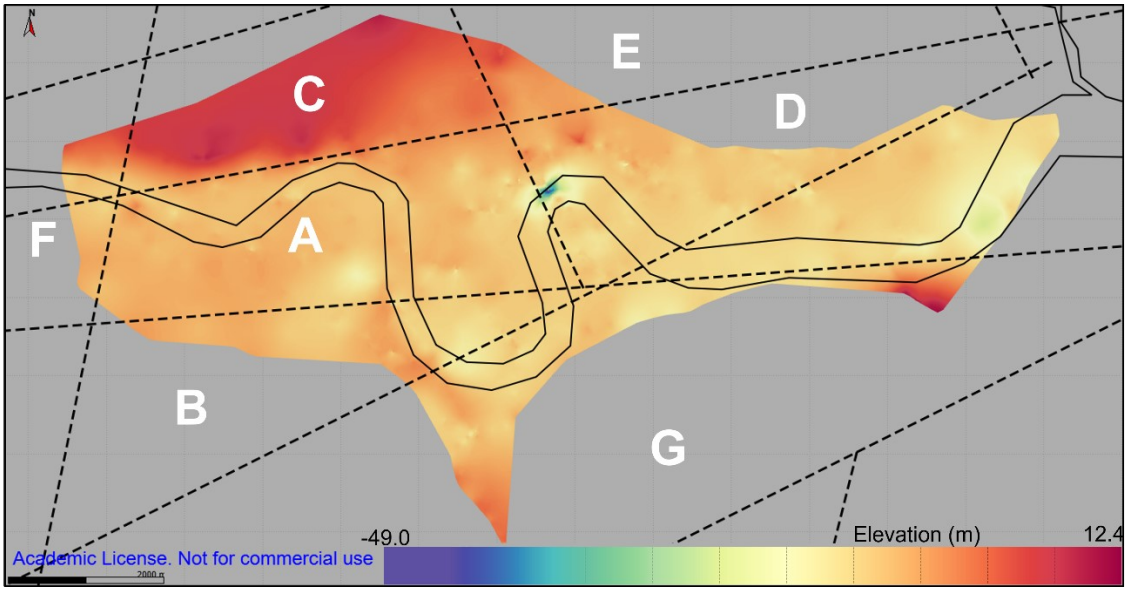

Figure 5.21 – Rockhead topographic surface implicitly modelled from rockhead point cloud and polylines. The deep anomaly at Blackwall corresponds with the recognised drift-filled hollow there.

5.3.4 Faulting

Explicit modelling interpreted 61 faults in East London, plotted in figure 5.22 with several in-log indicators (§5.1.2.2). The majority of observations are spatially coincident with indirect fault lineaments (Chapter 4) and BGS Lithoframe faults, but some are situated within block interiors.

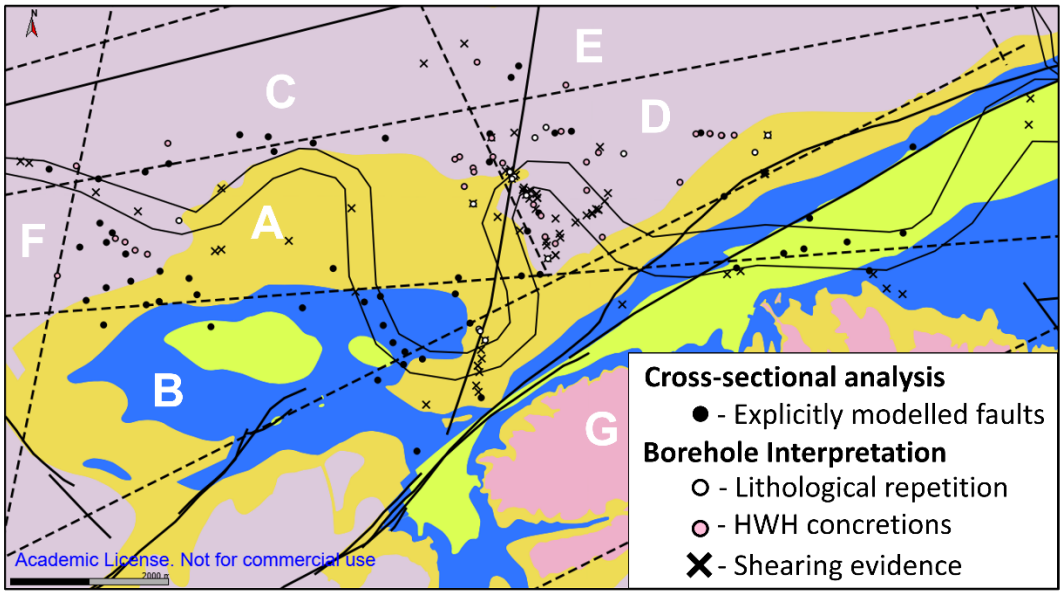

Figure 5.22 – Positions of explicitly modelled faults from cross-sectional analysis (fig. 5.19), and some direct and indirect in-borehole indicators of localised tectonism in East London.

5.3.5 Major faults

Four major faults were interpreted (fig. 5.23) from consistent and distinct topographic behaviour across them. Their lateral extents are confined by the positions of explicitly modelled faults and are not extrapolated beyond these limits (fig. 5.15).

The boundary between Blocks A and F (fig. 5.12) was not defined despite the localised abundance of explicitly modelled faults (fig. 5.23). The structure is unclear and likely comprises multiple faults, but its interpretation is limited by local data coverage. An idealised fault boundary was instead created to prevent artefact wrapping (fig. 5.15).

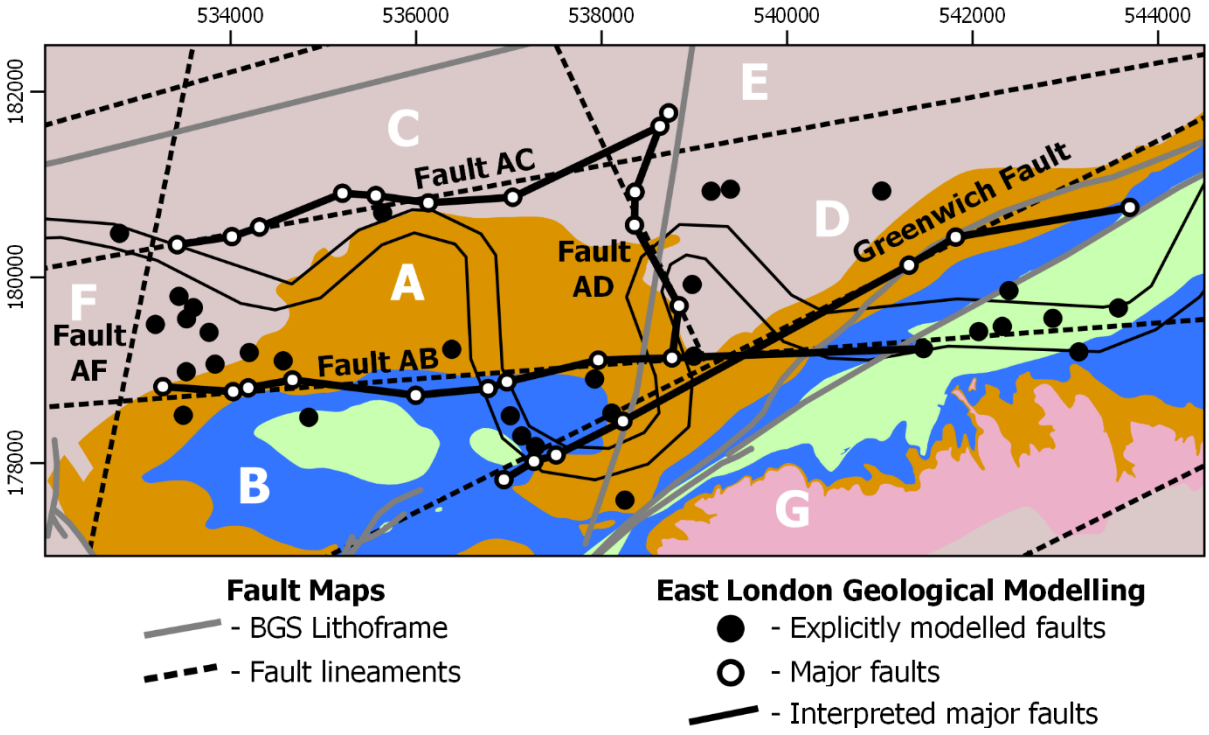

Figure 5.23 – Interpreted major faults, compared with indirect fault lineaments and the BGS Lithoframe. Blue dots represent explicitly modelled faults selected to generate major fault planes.

5.3.6 Lithological surfaces

Surfaces for the upper boundary of the White Chalk Group, Thanet Formation, Mid-Lambeth Hiatus, Lambeth Group, and the upper and lower boundaries of the London Clay Formation (fig. 5.24-29) were constructed from extracted lithological point clouds and polylines. No surface was constructed for the Harwich Formation because of its irregular and sporadic coverage.

All lithological surfaces display distinct topographic behaviour between fault-bounded blocks.

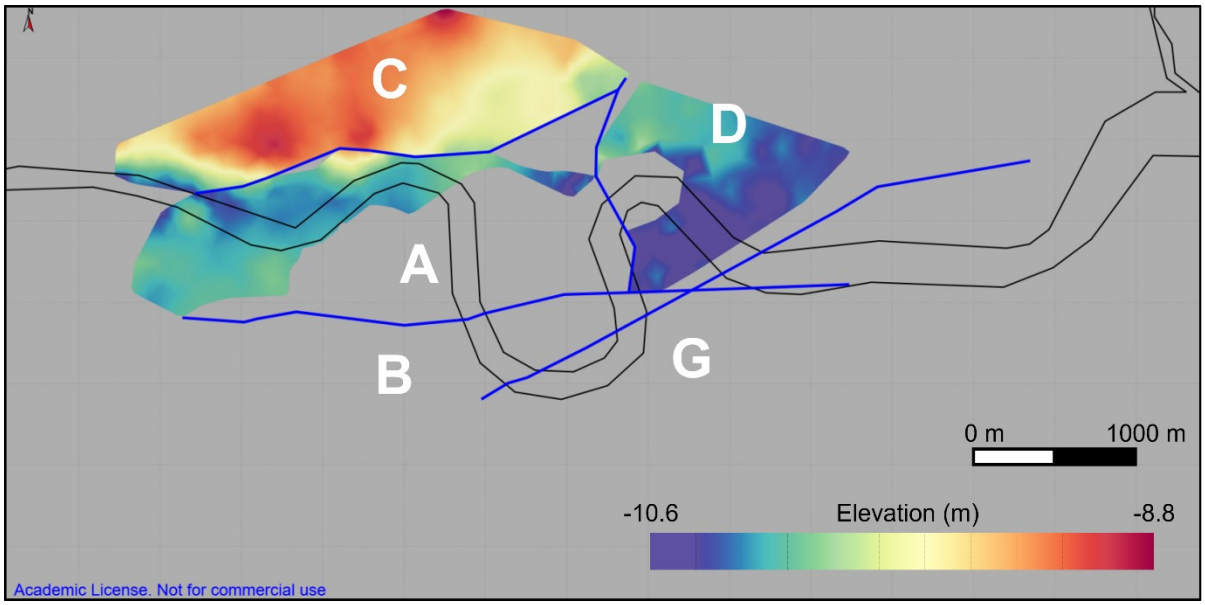

Figure 5.24 – Elevational surface for the upper boundary of the London Clay Formation.

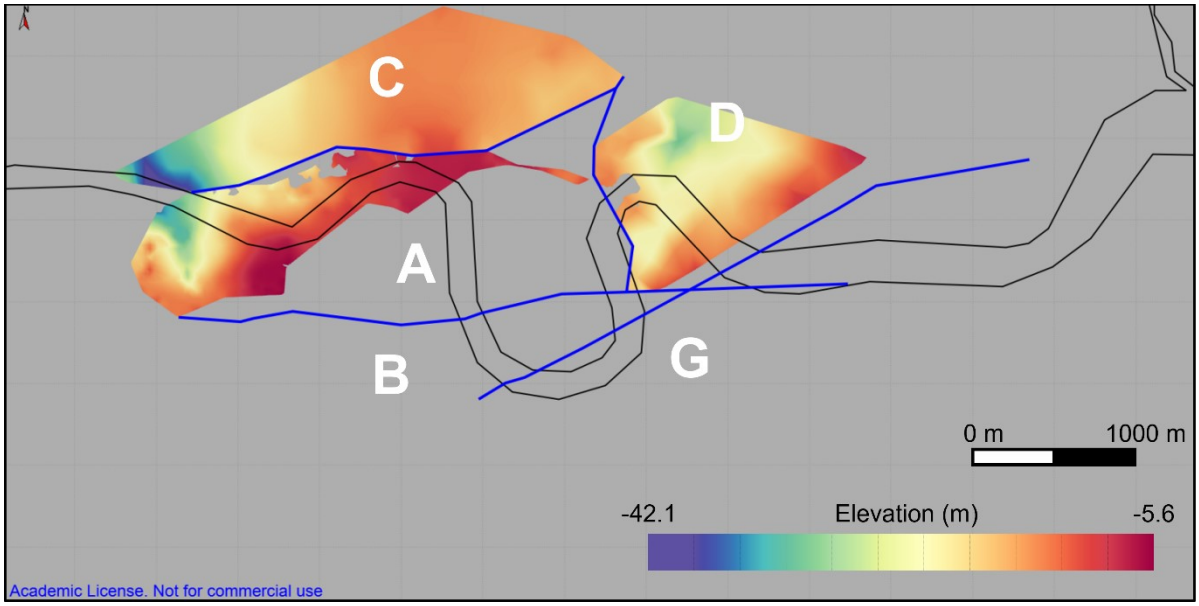

Figure 5.25 – Elevational surface for the lower boundary of the London Clay Formation.

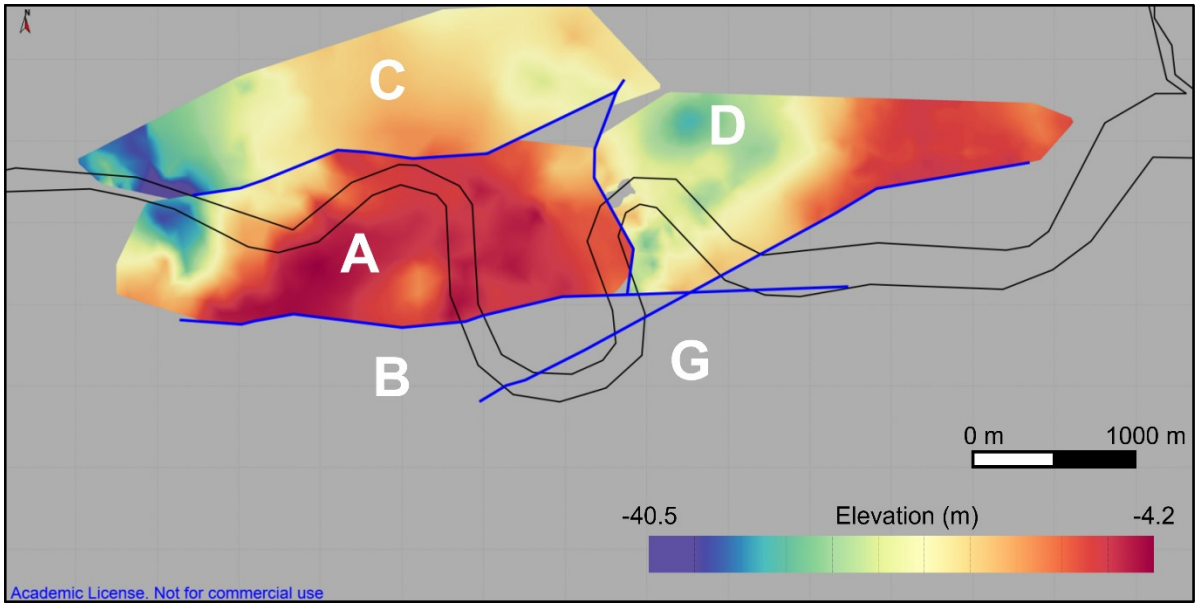

Figure 5.26 – Elevational surface for the Lambeth Group.

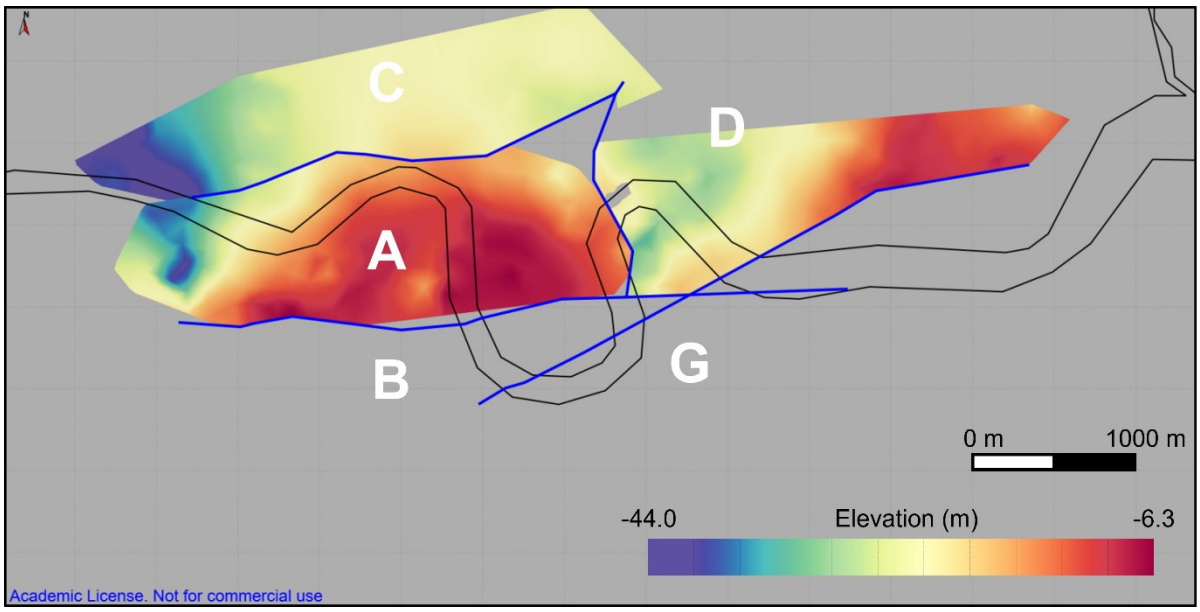

Figure 5.27 – Elevational surface for the Mid-Lambeth Hiatus.

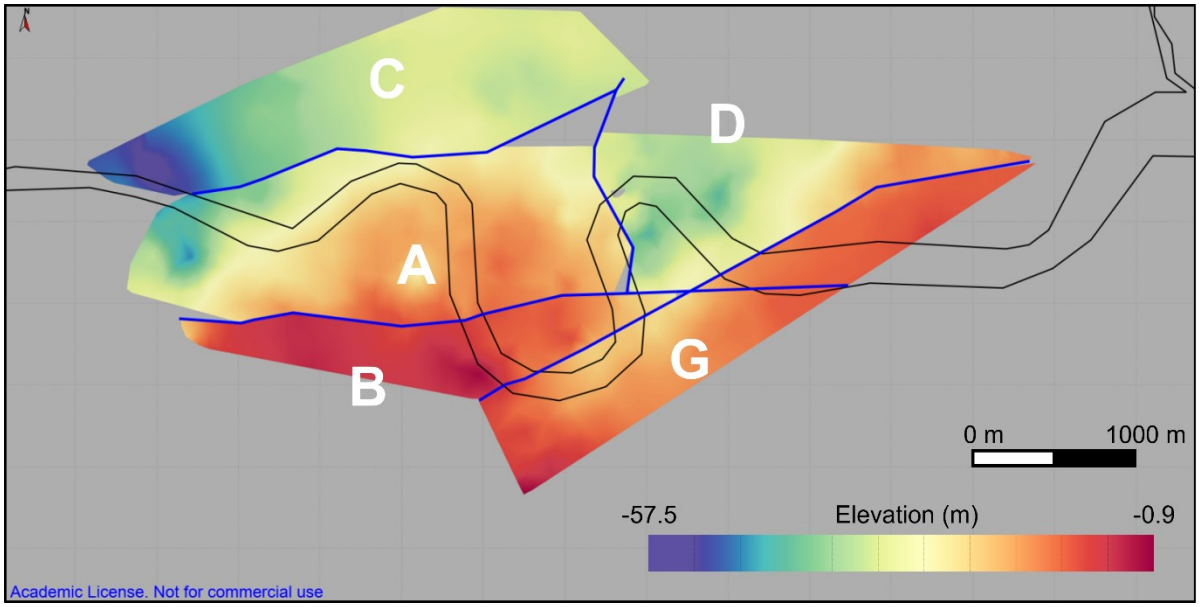

Figure 5.28 – Elevational surface for the Thanet Formation.

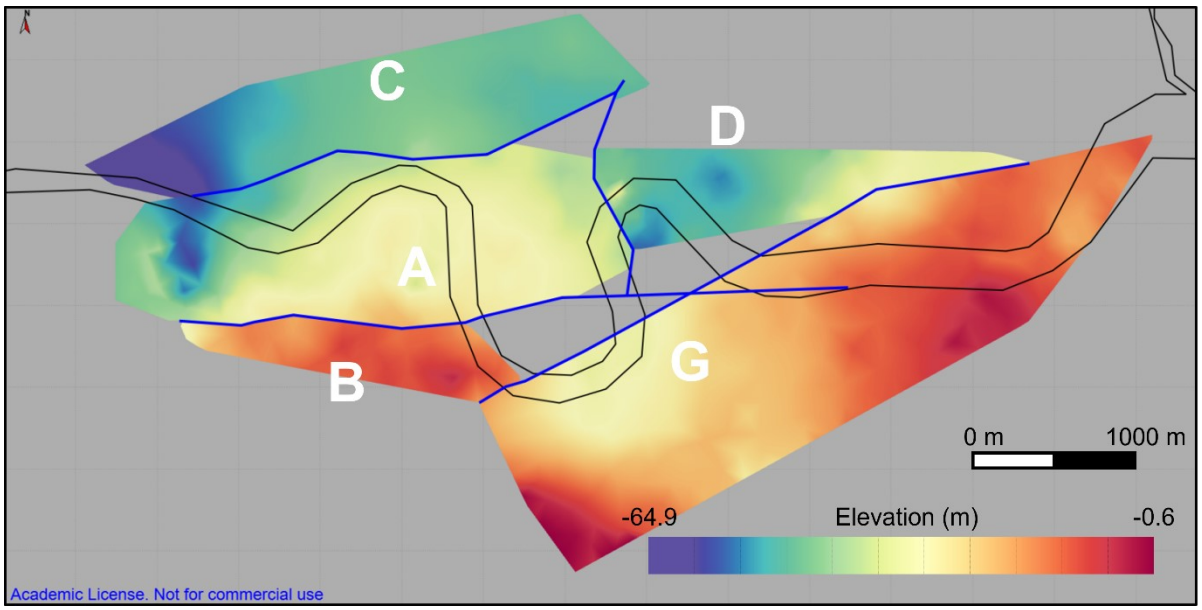

Figure 5.29 – Elevational surface for the White Chalk Group.

5.3.7 Lithological thicknesses

Thickness calculations were conducted for the Thanet Formation, Lambeth Group (both as a whole and separated into Above and Below the Mid-Lambeth Hiatus), and the London Clay Formation. These are presented in figures 5.30-34 with the upper surface of each layer colourised; white areas represent a lack of thickness calculations due to basal layer being locally absent.

Thickness variations are evident both within and between blocks; however, it is most significant where a specific lithology is exposed at rockhead. For example, rapid thinning of the London Clay Formation within Block A (fig. 5.30) corresponds with the Lambeth Group inlier in the centre, which itself thins towards the south (fig. 5.31).

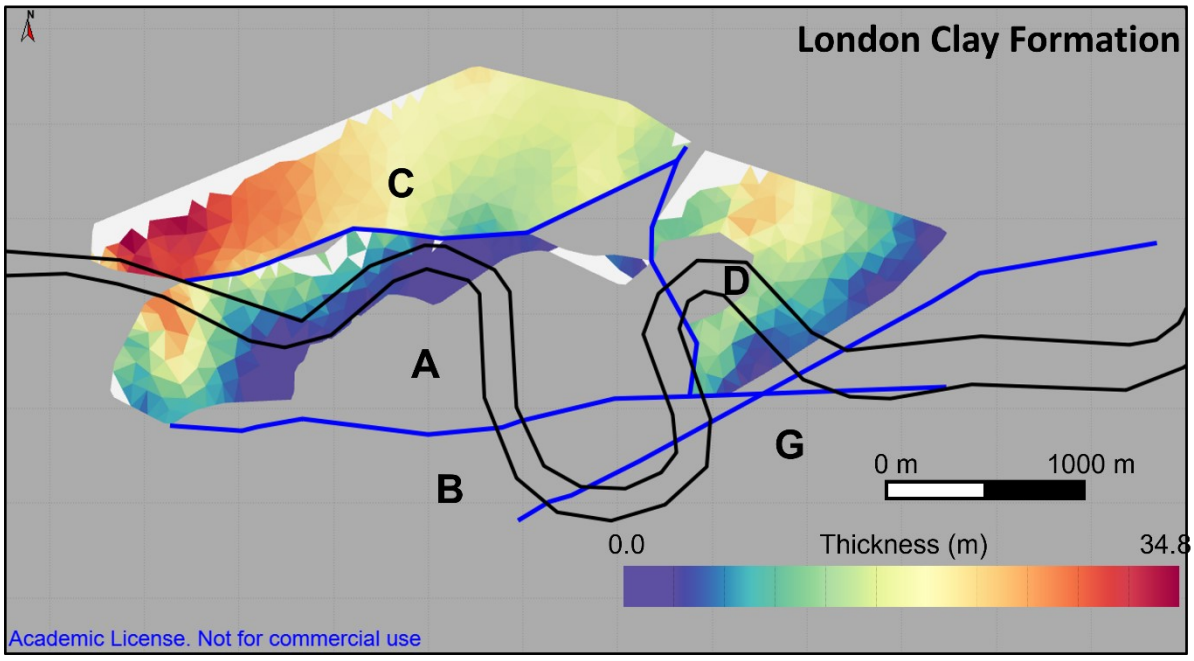

Figure 5.30 – Thickness map of the London Clay Formation, constructed from its upper and lower surfaces (fig. 5.24-25).

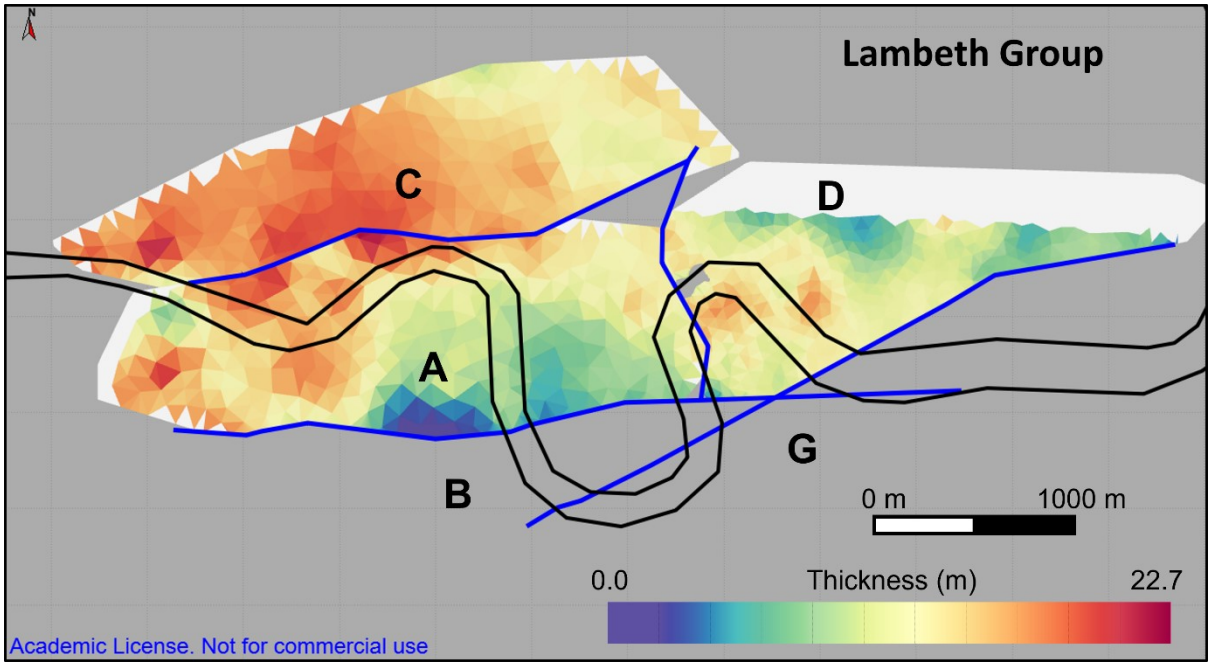

Figure 5.31 – Thickness map for the entirety of the Lambeth Group, constructed from the surfaces of the Lambeth Group and Thanet Formation (fig. 5.26, 5.28).

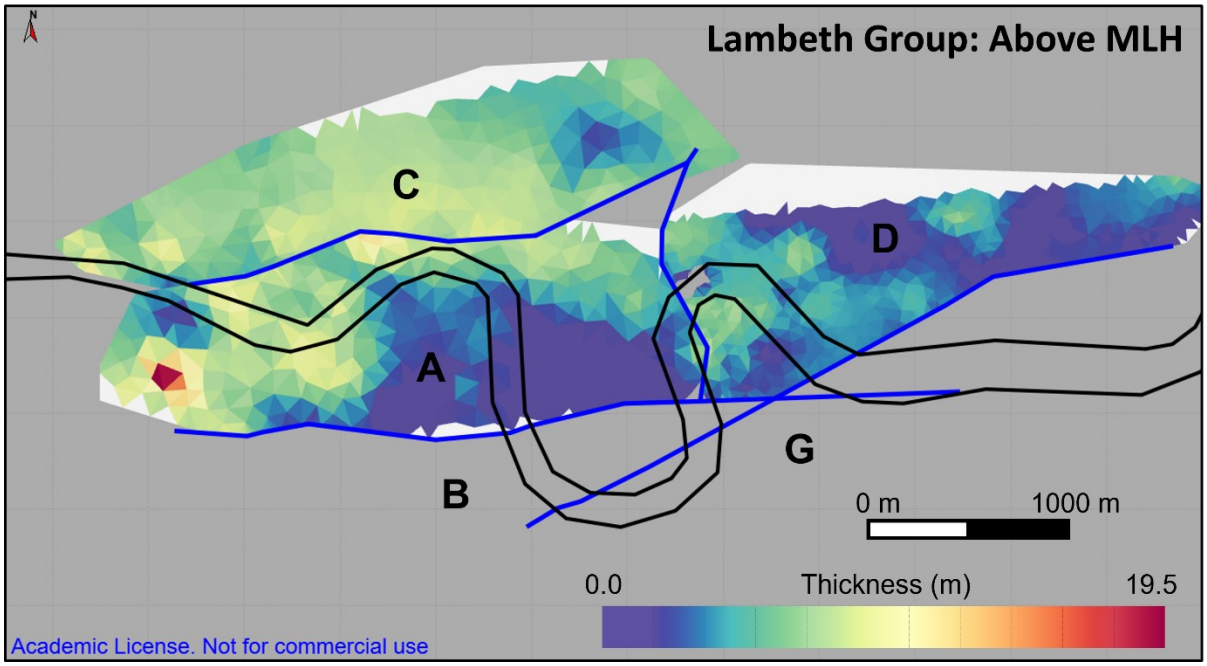

Figure 5.32 – Thickness map for the portion of the Lambeth Group above the Mid-Lambeth Hiatus, constructed from the surfaces of the Lambeth Group and Mid-Lambeth Hiatus (fig. 5.26-27).

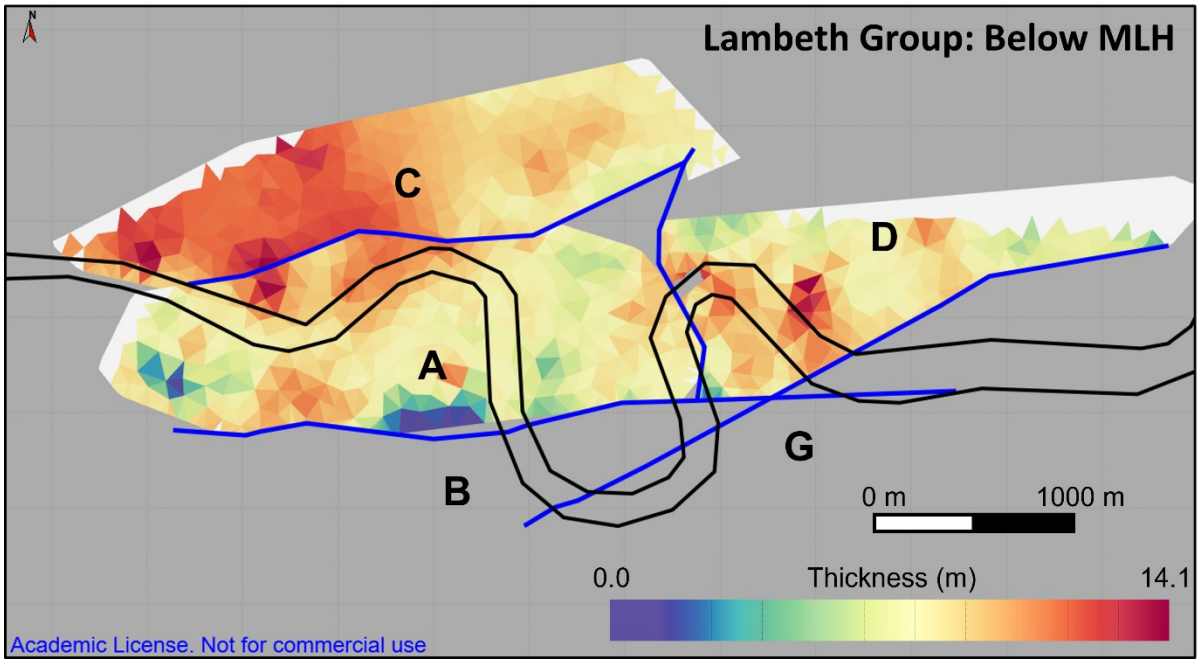

Figure 5.33 – Thickness map for the portion of the Lambeth Group below the Mid-Lambeth Hiatus, constructed from the surfaces of the Lambeth Group and Mid-Lambeth Hiatus (fig. 5.27-28).

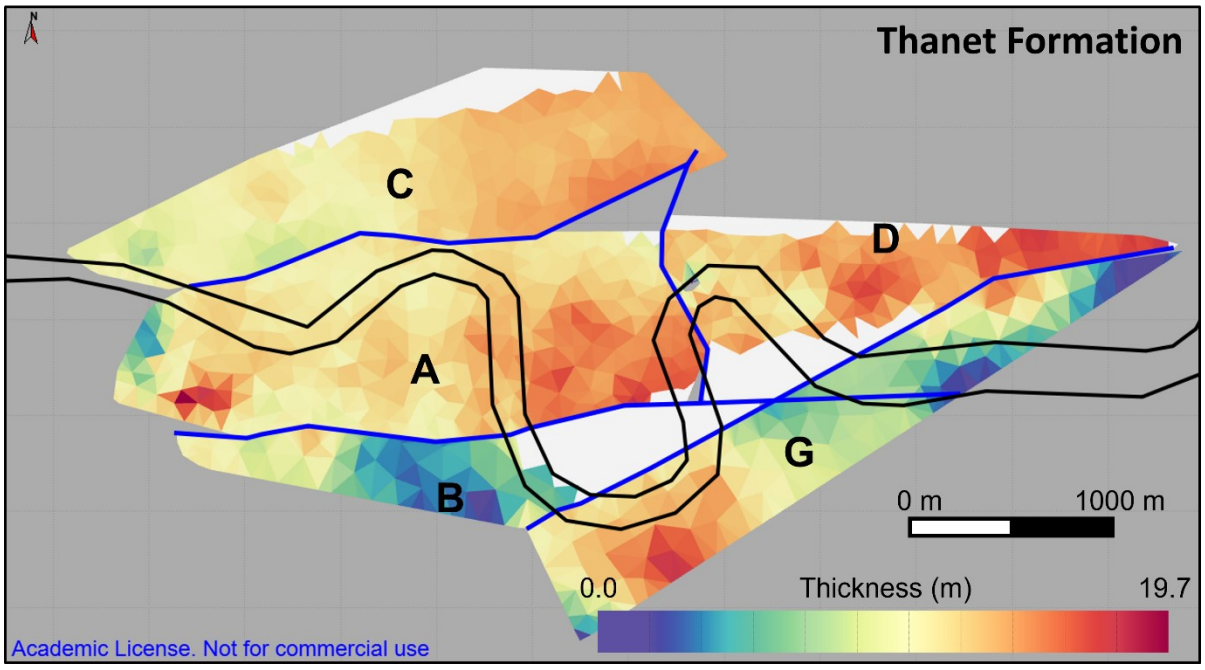

Figure 5.34 – Thickness map for the Thanet Formation, constructed from the surfaces of the Thanet Formation and White Chalk Group (fig. 5.28-29).

5.4 Model interpretation and discussion

The programme identified an irregular subsurface in East London, with major faults offsetting and compartmentalising the geology into a series of discrete blocks. Explicit modelling identified 61 faults in total, with four major fault planes interpreted. Data coverage restricts the assessment of complete block-bounding behaviour to Block A only, however, it is likely widespread, as indicated by lithological surfaces (fig. 5.24-29; 4.12) and fault lineaments (fig. 5.1).

The modelled faults are presented in figure 5.35 with their vertical offsets. Major faults are named according to the blocks they separate, except the Greenwich Fault which is labelled (see fig. 5.23). The ENE-striking Fault AC downthrows to the North, with narrow branching indicated where borehole coverage is high (fig. 5.18). Fault AD curves from NNW- to NNE-striking and is characterised by relatively large offsets that downthrows to the East. The E-striking Fault AB downthrows to the North and possibly intersects the Greenwich Fault; its exact positioning is uncertain as multiple faults were modelled locally. The NE-striking Greenwich Fault upthrows Block G relative to D and downthrows it relative to Block B. Fault AF is undefined due to the complexity of local structures and is represented by fault clustering instead; its geometry is unclear. The remaining modelled faults are likely fault zones and/or diffuse branching of major faults[41].

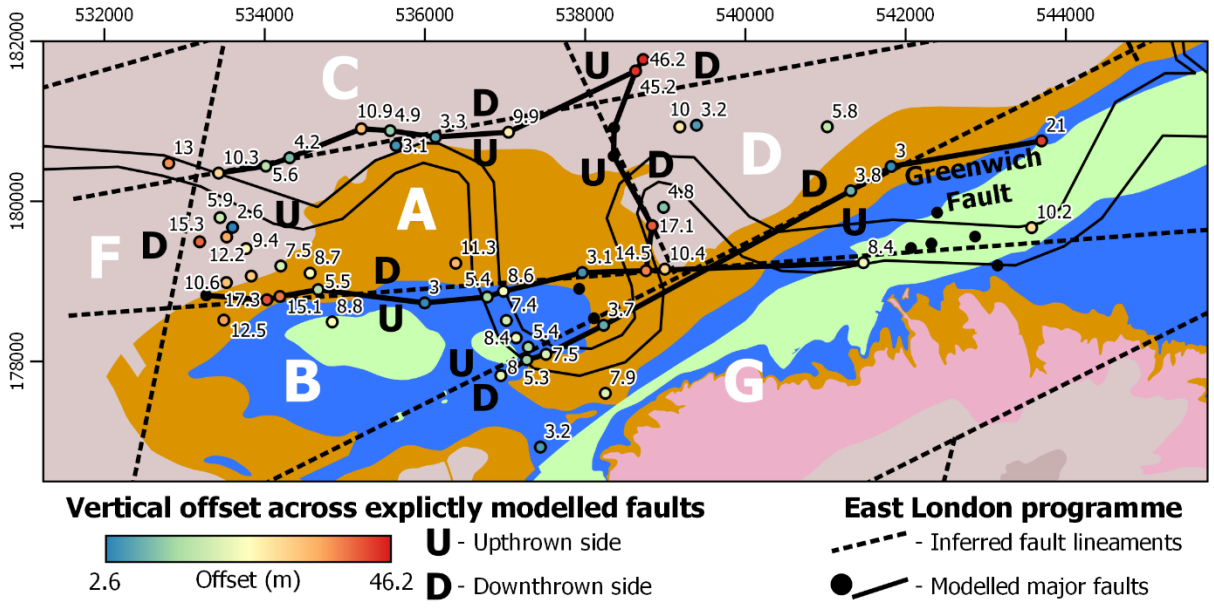

Figure 5.35 – Vertical offsets from explicitly modelled faults. Maximum offsets were measured in section. These were prevented for certain faults by absent horizon markers and/or erosive surfaces.

[41] These would traditionally be described as 'fault zones', however, this term is used colloquially in London geology to describe larger faulted bands (analysed in Chapter 6) rather than conventional branching within a single fault (e.g., Schultz & Fossen, 2008).

The four major faults are spatially coincident with the indirect fault map, demonstrating that these lineaments are indeed faults, and that inherited faults bound and regionalise distinct subsurface topography and at-surface displacement behaviour observed across London. Furthermore, the modelled faults also validate the indirect mapping method (§4.2.1).

The structural interpretation of each block couples in-borehole fault indicators, cross-sections, and surface geometries to characterise them. Block A is internally undeformed and inclined northwards, causing irregular preservation of its Thames and Lambeth Group strata. The position of its western border is unclear but is likely a band of faults rather than a single fault plane. Block C has a thick cover of London Clay and is internally undeformed and sub-horizontal. Block B is itself a fault zone, with displacement increasing towards its centre and is upthrown relative to Blocks A and G, in agreement with independent observations (Newman, 2017). Block D is downthrown relative to A and G with localised tectonism suggested internally by faulting (fig. 5.35), in-log evidence, and fault zone localities (§6.2). Block G corresponds with the WSG-Faults, with irregular inlier topography and internal faulting supporting the proposed linkage structures (fig. 3.37-40), however, poor data coverage prevents broader characterisation and surface generation. Borehole coverage also prevents definition of the Block D and E transition. Elevational, structural, and lithological differences between blocks indicate that major faulting has compartmentalised the subsurface.

5.4.1 Comparisons with the BGS Lithoframe and published fault observations

Comparison of the East London model and the indirect fault lineaments (beyond the model's study area) with the BGS Lithoframe (fig. 5.36) and other published faults (fig. 5.37), supports these faults.

Comparable positionings and trends for the Northern Boundary Fault, the Wimbledon-Streatham-Greenwich Fault System (WSG-Faults) and the Lea Valley Fault (fig. 5.36) are observed in the Lithoframe model, but the two ENE-E striking faults (Faults AC & AB) are not recognised. The discrepancies of Faults AC and AB likely reflect the more targeted nature of the East London programme, the (probable) greater data density locally, and access to data that postdate the Lithoframe model. Limited representation of individual WSG-Fault members by this programme is attributed to sparser borehole coverage in Block G (fig. 5.18).

Published East London fault are from two sources: fault zones analysed by this investigation (table 6.4); and faults proposed by Mortimore et al. (2011)[42] from infrastructure observations. Higher

[42] Mortimore et al. proposed two new faults (fig. 5.37). The NNE-trending Plaistow Graben from multiple downthrown fault zones (e.g., fig. 2.28). The NW-striking Rotherhithe Fault was proposed to explain perceived lateral-offsetting of the Streatham and Wimbledon members of the WSG-Faults.

densities of explicitly modelled faults (dots) correspond with fault zone interceptions, highlighting regional contrasts between areas of discrete major faulting and extensive brittle shearing.

The Plaistow Graben corresponds with localised London Clay Formation thickening (fig. 5.30) and two modelled fault polylines, with Fault AD curving parallel to the structure (fig. 5.37). However, it was not identified fully within the study area despite a locally high borehole density (fig. 5.18-19). This likely reflects the lack of Crossrail borehole data in the model from which this fault zone was proposed (table 5.4; Crossrail, 2012). No comparative offset with the Rotherhithe Fault exists in the model (fig. 5.37), nor are offset inliers apparent beyond the WSG-Faults. This investigation attributes this perceived lateral offsetting to *en échelon* Riedel shear overlap instead, as interpreted in §3.3.3.2.

There is good structural agreement overall with independent modelling, and published observations and interpretations in East London. This model identifies both block-bounding faults and areas of extensive faulting/fault zones. Where disagreements exist, these are attributed to localised data coverage, differing methods and model resolutions.

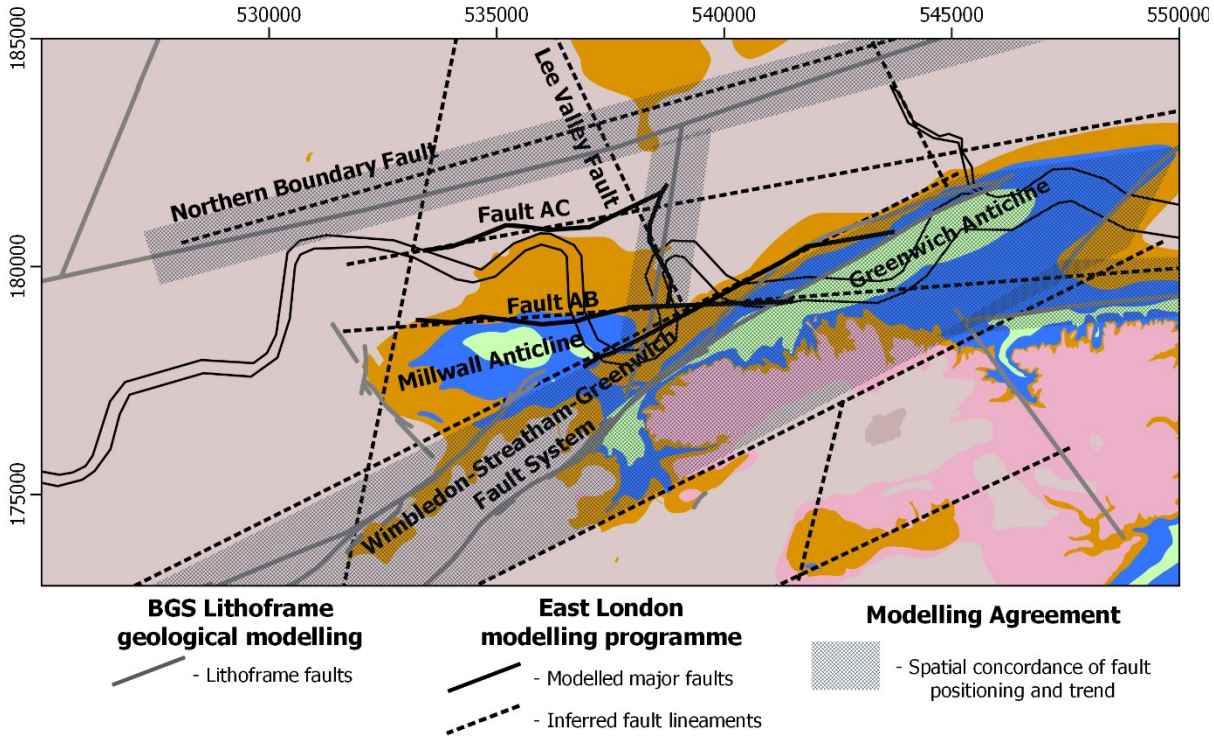

Figure 5.36 – East London programme modelled fault comparison with the BGS Lithoframe. Spatial concordance between fault positions and trends are highlighted by the dark blue overlays, with the indirect fault lineaments relied on where not confirmed by the East London programme.

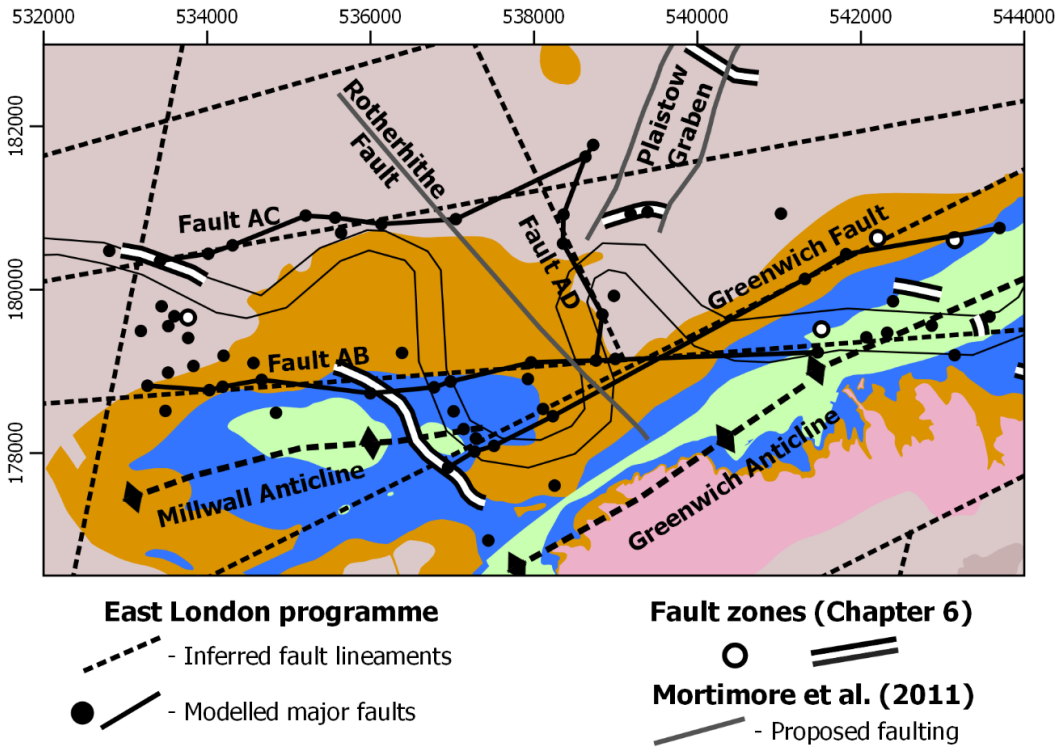

Figure 5.37 – East London programme modelled faults comparison with published fault zone (table 6.4) and faults proposed in Mortimore et al. (2011, georeferenced from fig. 14).

5.4.2 Positioning of faulting in the Lea Valley

The north-eastward continuation and intersection of Fault AC and Fault AD in the Lower Lea Valley, an area of poor data coverage (fig. 5.18), are defined by two cross-sections [C_E_boundary_1, C_E_boundary_2]. Their associated offsets are unexpectedly large (fig. 5.35) and attributed to a significant fault (fig. 5.38.a); whose local presence in this area is supported by lineaments (fig. 5.1), published faults (fig. 5.36-37), and geological analyses (Linde-Arias et al., 2018, Ghail et al., 2015a).

Retrospective analyses identified that this offset was misinterpreted from an erroneous borehole [TQ38SE2022], caused by MOVE's importation process. Comparisons between the log database and the model's equivalent database show it to be an internal error (fig. 5.38.b-c) that would not have been identifiable during §5.2.1.3. The isolated borehole led to an interpretation of downthrow along a fault that cannot be substantiated within the model, but this was not apparent during modelling due to limited local data coverage (fig. 5.18) and was only recognised during post-modelling analysis.

The error affects the model but not the structural interpretation since there is compelling evidence for a major fault here (fig. 5.36; Linde-Arias et al., 2018, Ghail et al., 2015a, de Freitas, 2009, Wooldridge, 1923, Wood, 1882). The erroneous offset and poor data coverage cause mispositioning in the model and highlights the risk of inferring across-fault displacement from an isolated borehole.

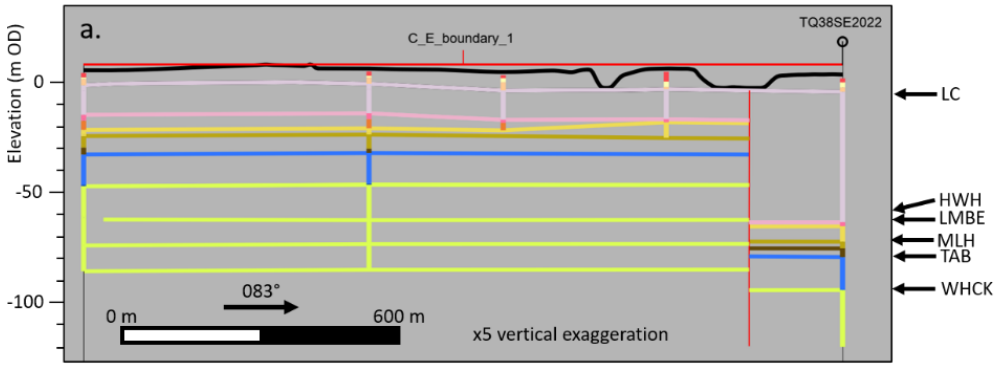

b. Log database

TITLE	Well Name	X	Y	Z	Horizon
QUADRANT S1	TQ38SE2022	538920	181730	2.04	MGR
QUADRANT S1	TQ38SE2022	538920	181730	0.21	ALV
QUADRANT S1	TQ38SE2022	538920	181730	-2.11	RTD
QUADRANT S1	TQ38SE2022	538920	181730	-4.06	THAM
QUADRANT S1	TQ38SE2022	538920	181730	-4.061	LC
QUADRANT S1	TQ38SE2022	538920	181730	-18.379	LC-Base
QUADRANT S1	TQ38SE2022	538920	181730	-18.38	HWH
QUADRANT S1	TQ38SE2022	538920	181730	-18.381	BLB
QUADRANT S1	TQ38SE2022	538920	181730	-20.21	LMBE
QUADRANT S1	TQ38SE2022	538920	181730	-20.211	AMLH
QUADRANT S1	TQ38SE2022	538920	181730	-20.212	LB
QUADRANT S1	TQ38SE2022	538920	181730	-27.22	MLH
QUADRANT S1	TQ38SE2022	538920	181730	-27.221	LMCL
QUADRANT S1	TQ38SE2022	538920	181730	-30.27	UPR
QUADRANT S1	TQ38SE2022	538920	181730	-34.23	TAB
QUADRANT S1	TQ38SE2022	538920	181730	-49.17	WHCK
QUADRANT S1	TQ38SE2022	538920	181730	-119.88	

c. Model database

1: X(East)	2: Y(North)	3: Z	4: Horizon	5: Colour	6: Well Name
538920.0	181730.0	2.0	MGR		TQ38SE2022
538920.0	181730.0	0.2	ALV		TQ38SE2022
538920.0	181730.0	-2.1	RTD		TQ38SE2022
538920.0	181730.0	-4.1	THAM		TQ38SE2022
538920.0	181730.0	-4.1	LC		TQ38SE2022
538920.0	181730.0	-63.3	LC-Base		TQ38SE2022
538920.0	181730.0	-63.3	HWH		TQ38SE2022
538920.0	181730.0	-63.3	BLB		TQ38SE2022
538920.0	181730.0	-65.1	LMBE		TQ38SE2022
538920.0	181730.0	-65.1	AMLH		TQ38SE2022
538920.0	181730.0	-65.1	LB		TQ38SE2022
538920.0	181730.0	-72.1	MLH		TQ38SE2022
538920.0	181730.0	-72.1	LMCL		TQ38SE2022
538920.0	181730.0	-75.2	UPR		TQ38SE2022
538920.0	181730.0	-79.1	TAB		TQ38SE2022
538920.0	181730.0	-94.0	WHCK		TQ38SE2022

Figure 5.38 – Fault misinterpretation caused by erroneous importation of log TQ38SE2022.
a. Section C_E_boundary_1. Post-Ypresian downthrowing to the East was originally interpreted, causing thicker preservation of the London Clay Formation across the fault. Refer to figure 5.20 for section position.
b. Interpreted elevations of sub-London Clay strata in the log database for TQ38SE2022.
c. Erroneous elevations of the sub-London Clay strata in the model database for TQ38SE2022.

5.4.3 Credibility of in-borehole fault evidence

Four features were outlined as potential in-borehole fault indicators: lithological repetition, enhanced brittle shearing, Harwich Formation concretions, and significant core loss (specifically in the London Clay and Thanet Formations). The former two are direct evidence of brittle tectonism locally, whilst the latter are indirect and may be attributed to other mechanisms also (footnotes 33-34).

These were extracted from the geospatial database and compared with explicitly modelled fault positions (fig. 5.39) from the East London and Lithoframe programmes. There is good correlation between major faults and internally faulted blocks (D & G) with shearing evidence, lithological repetition, Harwich Formation concretions and London Clay core loss, confirming their reliability as in-borehole indicators of local faulting. Variable deformation behaviour between fault sets is implied by the inconsistent coverage of indicators. The findings demonstrate that rockmass alteration is not restricted to the immediate vicinity around the fault but can affect geotechnical behaviour over a wider area instead.

Not all indicators correspond with suspected major structures. Direct indicators within unfaulted blocks (e.g., A) may represent products of minor faulting, independent of inherited faulting. However, both periglacial processes and/or poor drilling practices may also induce brittle shearing and/or enhanced core loss that could falsely imply faulting locally. This is apparent in Thanet Formation core loss which does not reliably correlate with any interpreted structures. Consequently, the geological and anthropogenic processes that acted on the extracted material must be considered when trying to distinguish tectonic evidence.

In-borehole indicators should be used as part of a 'multiple lines of evidence' approach to identifying faulting on or near site.

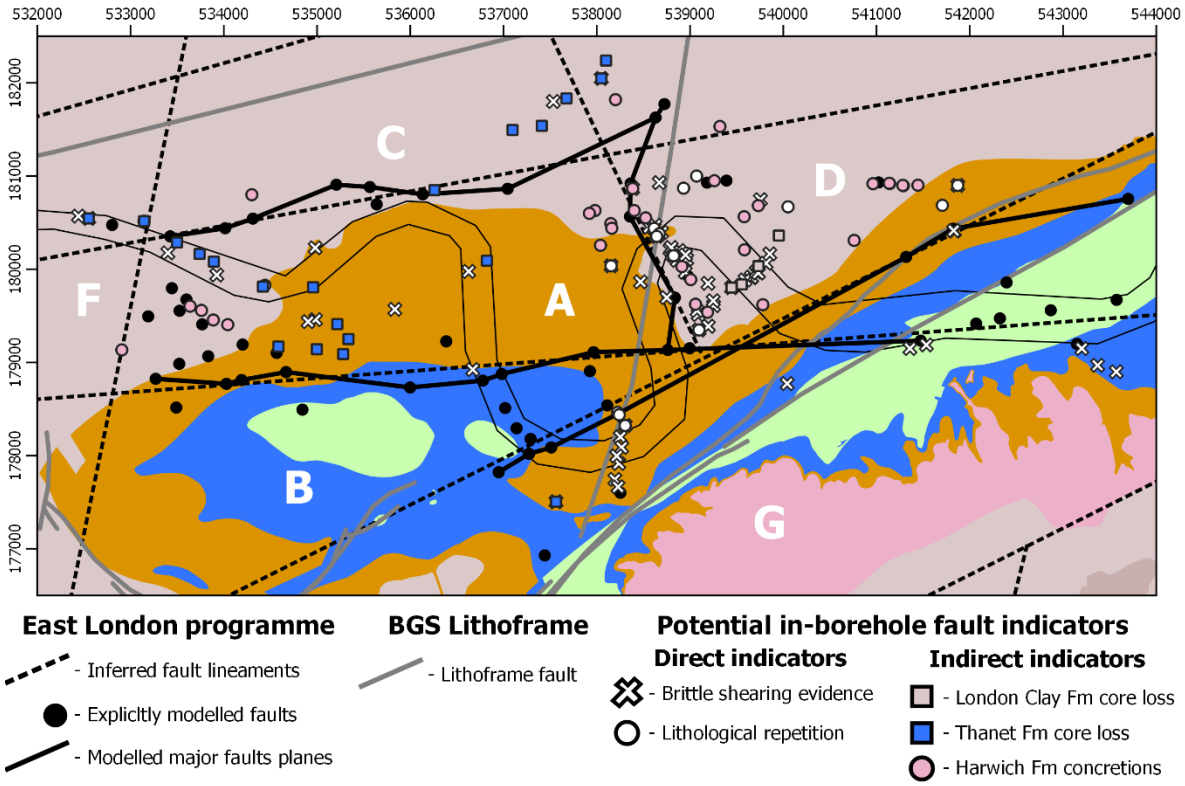

Figure 5.39 – Comparison of potential in-borehole fault indicators with explicitly modelled fault positions. Most indicators correspond with major faults or faulted blocks, supporting the proposed variation in block interior deformation.

5.4.4 Major fault characterisation

Major faults mapped in London are typically portrayed as single lines. However, it is unlikely that inherited faults will be individual, discrete planes due to their propagation behaviour (§3.3.3) and progressive development through episodic reactivation. This is evidenced by many sections identifying multiple faults rather than single offsets (fig. 5.40), agreeing with previous analyses (Royse, 2010). Three major faults in East London are identified to be wholly or in part diffuse and characterised by multiple faults (fig. 5.16): Fault AB, Fault AC and Fault AF. Their interpreted widths vary from a singular plane to up to ≤ 500 m wide bands.

Similarly, intersected portions of the WSG-Faults are characterised by multiple faults or 'fault complexes' (Newman et al., 2013, Mortimore et al., 2011, Newman, 2009), although it is unclear if these represent individual Riedel shears or their linkage products (§3.3.3).

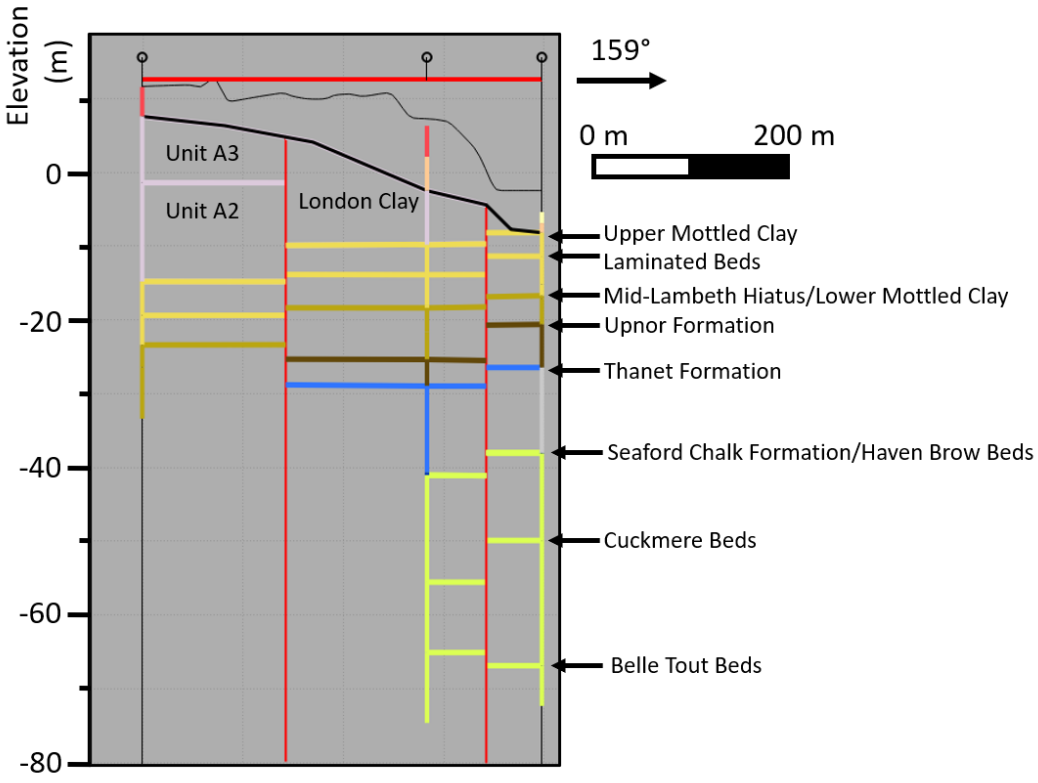

Figure 5.40 – Fault AC characterised by two faults in section A_C_boundary_5. Refer to figure 5.20 for section position.

5.4.4.1 Characterising Fault AF

Interpretative difficulties arise where major faults are structurally complex. The border of Blocks A & F is complex with a significant structural interface being apparent from local fault clustering (fig. 5.35). However, confidence in defining Fault AF is affected by contradictory structural behaviour observed internally and is compounded by limited data coverage (fig. 5.18). The interface is typically banded but its style varies from graben (fig. 5.41) to stepdown (fig. 5.42) to a single fault in section A_F_boundary_2. Complicating matters, the western interior of Block A warps down towards this interface (fig 5.24-29) apparently without any internal faulting.

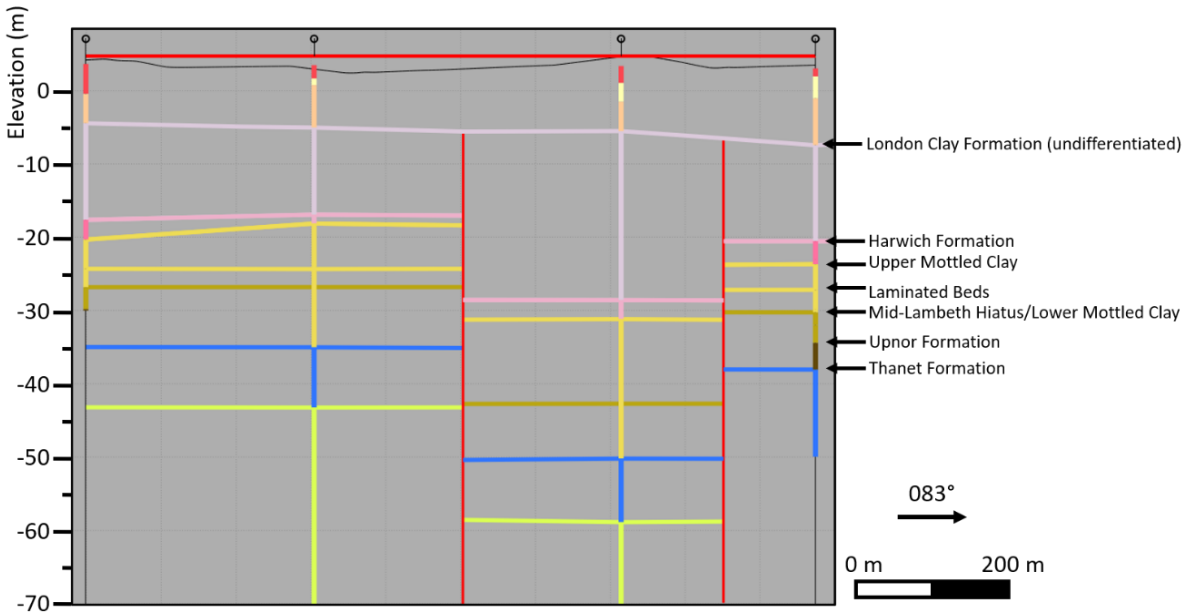

Figure 5.41 – Graben-like structure in Fault AF in section A_F_boundary_1. Refer to figure 5.20 for section position.

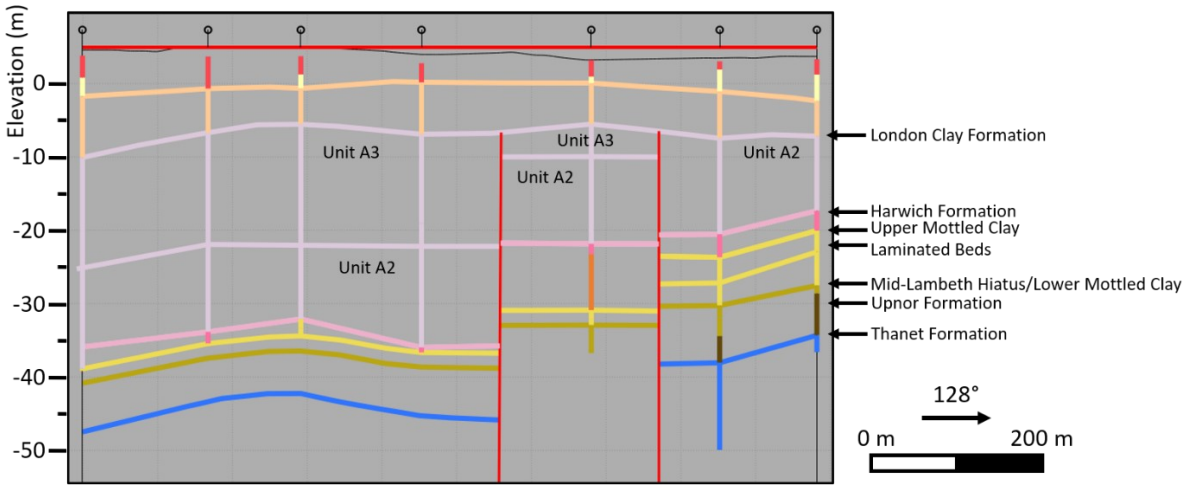

Figure 5.42 – Step-down interface along Fault AF downthrowing Block F in section A_F_boundary_3. Refer to figure 5.20 for section position.

Fault AF was reassessed post-modelling from fault positions, other modelling outputs (table 5.5) and local structural evidence. It was initially postulated to comprise two NNW-striking faults bounding a downthrown interior (fig. 5.43). But this is incorrect since western, northern, and southern extents are not characterised by the model, nor does it account for the internally conflicting slip behaviour.

Instead, broader strata depression (London Clay bases, fig. 5.43) northwards corresponds with a graben proposed in both §3.3.2.3 and the BGS Lithoframe (fig. 2.31), and the internally downthrown London Bridge Fault Zone identified by the Thames Tideway GI (fig. 6.16.a). Collectively, these imply that the interface is wide and complex and part of a larger ENE-striking structure (Central London Graben) rather than an individual major fault as indicated by structural lineaments.

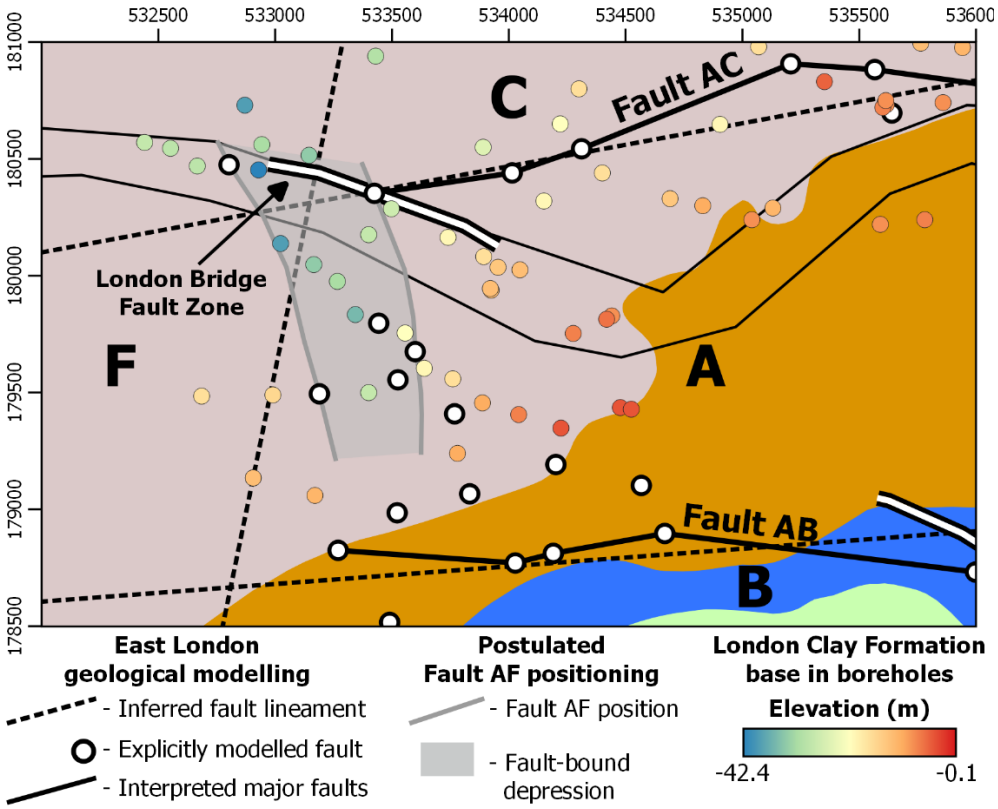

Figure 5.43 – Post-modelling analysis of Fault AF from geological modelling outputs (table 5.5).

Table 5.5 – East London geological modelling outputs used to reanalyse the position of fault AF.

Modelling outputs	Data Types	Data Origin
ACROSS_AF_1	Cross-sections (boreholes, explicitly modelled fault & stratigraphy polylines)	Digitised borehole logs.
ACROSS_AF_2		
ACROSS_AF_3		
ACROSS_AF_4		
ACROSS_AB_2		
Fault positions	(Vertical) Fault polylines	Explicit modelling & cross-sectional analysis
Base of London Clay Formation	Surfaces	Implicit modelling of point clouds and polylines
Top of the White Chalk Group		
Base of London Clay Formation	Point cloud	Digitised borehole logs

5.4.4.2 Distinguishing between major faults and fault zones

Major fault widths vary both along and between faults (fig. 5.44), likely reflecting differences between the specific inheritance mechanisms, general fault branching, and relative position along the fault (i.e., individual shear vs overlap, fig. 3.32, 3.36). However, they may also represent causally associated fault zones (fig. 2.28). These are distinct from major faults in being their interaction by-products rather than directly inherited shears (discussed in §6.2), adding to the uncertainty in characterising fault widths.

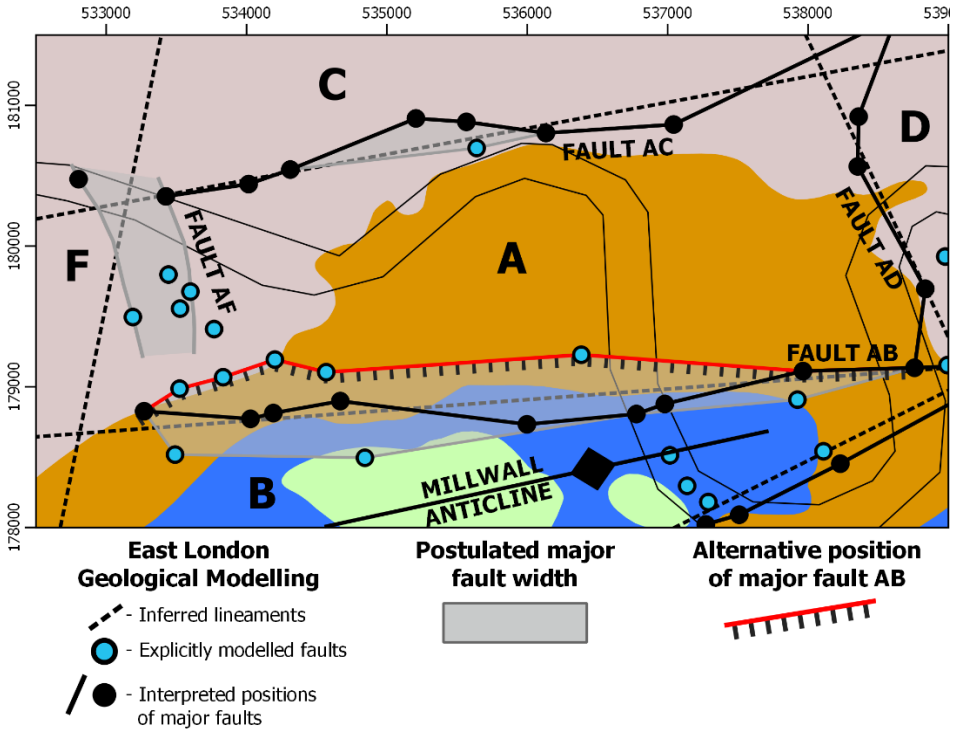

Figure 5.44 – Potential widths of major faults (solid black) based on relative positioning of explicitly modelled faults (blue) with concordant slip behaviour. Fault AB highlights issues with differentiating between faulting associated with a major fault and the fault zone it bounds.

It may be difficult to differentiate between faulting associated with a major fault and an adjacent fault zone. Block B, coincident with the Millwall Anticline inlier (fig. 5.1), was interpreted as a continuous, internally uplifted fault zone (fig. 5.45) and is independently identified in the Thames Tideway GI (Greenwich Conneciton Tunnel Fault Zone, Newman, 2017). Originally its bounding fault, Fault AB (fig. 5.45, marked with 'M'), was interpreted to be a 'wide' major fault (fig. 5.44) with the northernmost fault considered too distal to be associated with the internal structure of Block B. However, comparisons with the Thames Tideway GI imply that the fault zone extends further North (fig. 6.21). This discrepancy likely reflects poor borehole coverage and the lack of chalk stratigraphic breakdown locally, making the positioning of Fault AB uncertain. It is now suspected to be situated further north and bounds the wide fault zone (fig. 5.44, red line) associated with the Millwall Anticline.

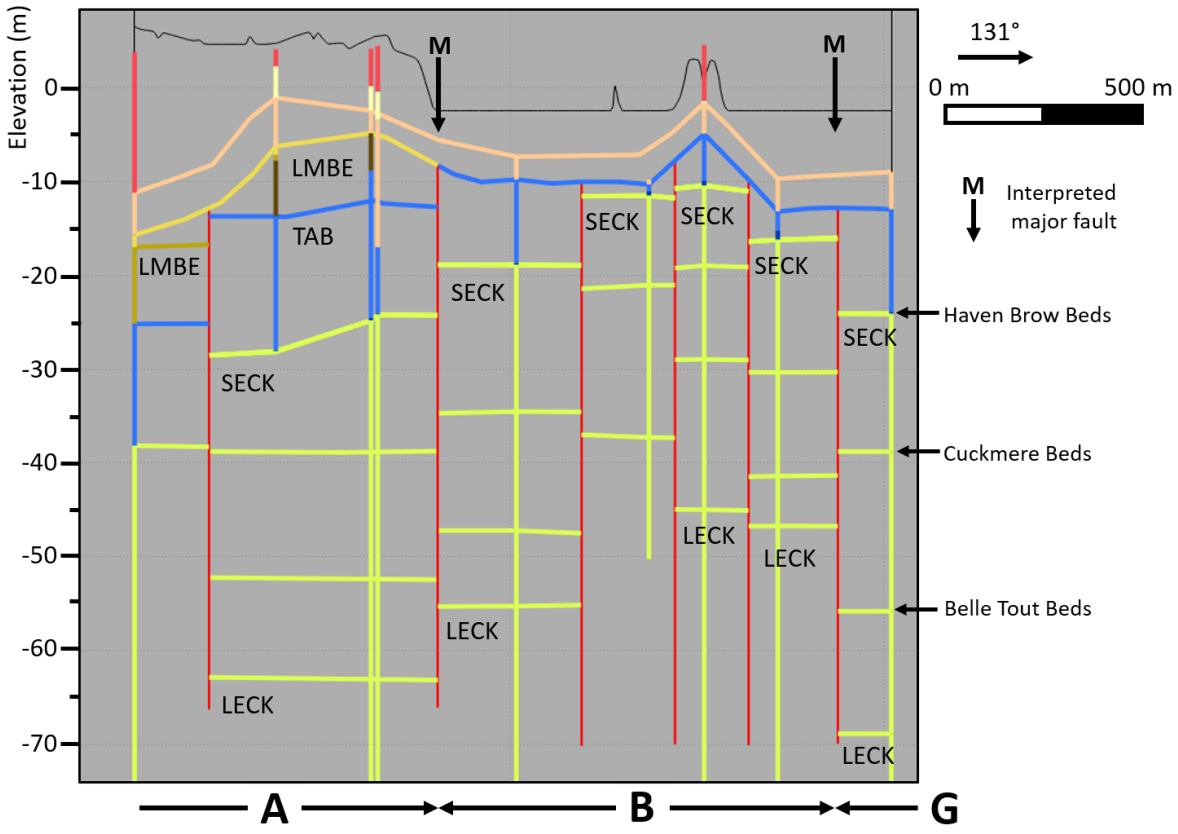

Figure 5.45 – Continuous fault band interpreted in section B_across_A_G_1 causing difficulties for distinguishing between major faults (Faults AB & BG) and the Block B fault zone they bound. Refer to figure 5.20 for section position.

5.4.4.3 Strike-slip fault identification in London

Vertical offset analysis is ineffective at identifying faults with minimal dip-slip components (§4.4.3). The NW- and NNE-trending fault lineaments (fig. 5.1) are likely inherited strike-slip faults (§4.4.5). The Lea Valley Fault, demarcating the A-D Block interface, was originally inferred to be a NW-set member, however, this research and the Lithoframe (fig. 5.36) both indicate that it c is part of the NNE-striking set instead. Its identification by modelling demonstrates a dip-slip component, agreeing with analysis in Chapter 3 that this fault set would have an oblique-slip component.

5.5 Modelling programme review

The outputs of this investigation validate that explicit-driven geological modelling with high data coverage is the most appropriate method for dip-slip fault analysis in London (§4.1.4). However, limitations are identified, as well as challenges affecting lithological and fault analyses.

5.5.1 Methodological review

The programme methodology (fig. 5.2, 5.10) developed upon previous modelling investigations conducted during this research and by related MSc student-driven projects (e.g., Meyer, 2018, Dimosthenous, 2018, Marriott, 2019). A review of these, coupled with relevant modelling literature, highlighted issues associated with acquired data quality, and inconsistencies in the interpretation and digitisation processes. Aspects of the programme's methodology are reviewed here.

5.5.5.1 Borehole coverage and acquisition strategies

Model data distribution is intrinsically controlled by whether a borehole is present in a specific location (fig. 4.8) and if its data are accessible (e.g., sensitivity or company data sharing policies). Consequently, the model's data coverage is spatially inconsistent (fig. 5.18) but is sufficient to identify major faulting. But coverage likely affected their positioning and subdivision into multiple faults, and lithological characterisation. This is reflected by the uncharacterised Fault AF (fig. 5.43), Fault AD positioning (fig. 5.38), incomplete surfaces within blocks (e.g., northeast quadrant of Block A), and the ignoring of distal boreholes to minimise interpolation artefacts. Additional linear datasets are identified to improve coverage; however, their incorporation was inhibited by time constraints, data formats (below) and accessibility issues. Comparatively, the second phase's more targeted nature highlights the benefit of acquiring individual boreholes to improve local data density.

Future data acquisitions should have three defined phases. The first maximises coverage and defines the positions of major structures, similar to §5.1.1. The second phase is targeted to improve fault characterisations. The third stage targets general areas of poor coverage to improve lithological and block interiors analyses. These two latter phases should be iterative. All phases should prioritise high quality logs unless coverage is particularly poor.

5.5.5.2 Data digitisation

Two databases were constructed as the formatting requirements for MOVE (§5.1.3) restricted data extractability and usage. The geospatial database documented key lithological and tectonic information and provided a progress tracking system, successfully enabling these features to be expressed in the model (e.g., rockhead) and during post-modelling analysis (e.g., fig. 5.39). No issues were identified regarding database structuring.

The majority of recent GI data are stored in AGS format[43], due to its prevalence in the geotechnical engineering industry. Because AGS is a complex, almost bespoke format, requiring specialist software, it is not recognised by MOVE, preventing the direct transfer of AGS-held borehole logs. This limited the usage of major datasets, such as Crossrail, and primarily restricted data acquisition to log report formats (i.e., fig. 5.5-5.6). Manual AGS extraction using SQL was trialled for the Thames Tideway dataset. Whilst successful, this workaround is not viable in practice due to the additional time required and software complexities introduced.

5.5.5.3 Geological modelling workflow

The explicit-driven modelling workflow (fig. 5.10) was developed following a review of geological modelling in Chapter 4, and was influenced by the GSI3D methodology (fig. 4.14; Kessler et al., 2009). No issues were identified with the modelling workflow.

5.5.5.4 Geological modelling software and data transferring

The modelling software, MOVE, was used because it favours explicit-driven workflows. No issues were identified with the software.

Future projects should incorporate AGS data by integrating an AGS-reading software into the workflow (fig. 5.46) to convert it into a format recognisable by MOVE. However, if unavailable then the modelling software could be replaced by Leapfrog which accepts AGS formatting (whilst its developers favour an implicit modelling, explicit-driven workflows can still be used).

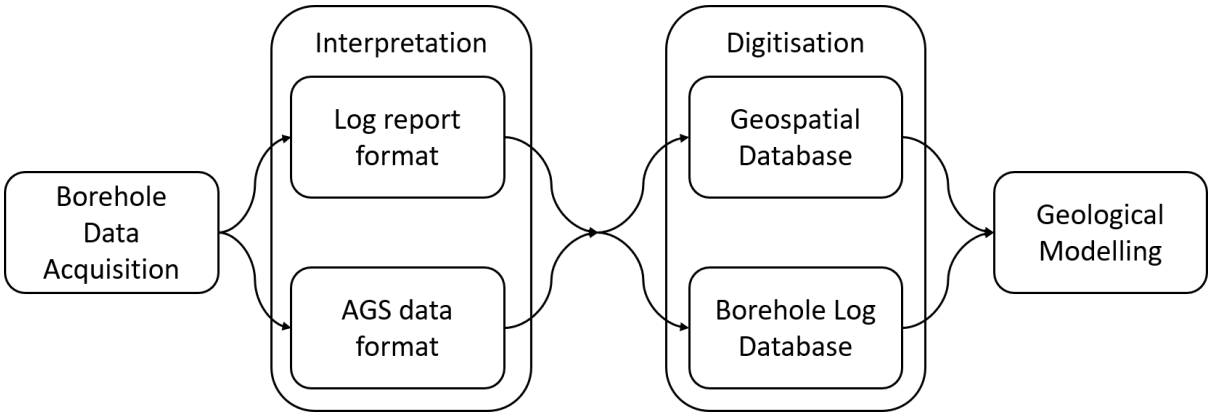

Figure 5.46 – Proposed revision to programme workflow (fig. 5.2) to incorporate both AGS and log report formats into the borehole interpretation process to improve data accessibility and coverage.

[43] A standardised format for collating and linking data from ground investigations, laboratory testing and monitoring data produced by the Association of Geotechnical & Geoenvironmental Specialists.

5.5.2 Lithological analyses and interpretative difficulties

Correct determination of lithologies in boreholes improves fault offset identification and lithological characterisation of East London's subsurface. The methodology aims to maximise lithological detail (where available) by developing a hierarchical system that captures any variation (§5.1.3.2; table 5.1). However, difficulties and uncertainty are introduced through poor log quality and lithological complexities intrinsic to specific stratigraphic units.

5.5.2.1 Borehole log quality and uncertainty

The acquisition strategy assumes that log quality would be relatively consistent within a dataset. However, these are typically inconsistent for a specific project because they comprise multiple GIs whose qualities are affected by the drilling technique used[44], their specific purposes[45], and the quality of the original logging and interpretation[46].

Poor log quality (fig. 5.a,d) affects the interpretation phase by reducing the extractable lithological details and heightening the risk of misinterpretation. For example, the London Clay was misinterpreted in some logs in Block A as the Upper Mottled Beds due to poor log descriptions. Despite the two sequences having distinct colourations, their grain sizes are comparable, causing in-log descriptions of 'purple and blue' to be misinterpreted as mottling. This was recognised from anomalous thickening and/or isolated occurrences of the latter during modelling and rectified in the model (§5.2.2.3).

Core photographs are rarely provided but referred to whenever available. On several occasions they contradicted the log descriptions, leading to revised interpretations.

[44] Poor drilling techniques (i.e., cable percussion) and/or practice can destroy subtle lithological features (e.g., laminations) and mix separate horizons together.
[45] For example, GI targetting the White Chalk Group may devote limited attention to Palaeogene strata.
[46] This reflects individual experiences and allocated time to conducted descriptions and interpretations.

5.5.2.2 Differentiating lithologically similar sequences

The Harwich Formation and Lambeth Group can be difficult to interpret because they are heterogeneous, laterally discontinuous, and complex. Yet both contain lithologically similar members that are difficult to differentiate. This is further compounded by the former resting unconformably on the latter's irregular upper surface.

Silty fine SAND can be attributed to both the Blackwall Facies[47], a recently identified basal unit of the Harwich Formation (Crossrail, 2016), and sand channels associated with the Upper Mottled Beds and Laminated Beds of the Lambeth Group (§2.2.1.3). These sand channels may be present along the upper interface of the Lambeth Group as the Laminated Beds are commonly be the uppermost unit preserved locally. Collectively this introduces uncertainty where these lithologically similar units are in contact, potentially causing grouping or interface misinterpretation that result in irregular thicknesses and topography.

A laterally continuous silty fine (occasionally laminated) SAND horizon was identified in Block D during explicit modelling. However, this was allocated between the HBSU and the Laminated Beds during log interpretation on the basis of when laminations occurred in the log, with recurrences of silty fine SAND attributed to sand channels. Portions of section D_interior_6 containing this sand unit are presented in figure 5.47, with selected logs broken down according to their (simplified) material composition and colour instead of their interpreted lithostratigraphic unit. Three distinct lithologies are distinguishable[48] from these subtle differences, which define a more consistent interface between the Harwich Formation and Lambeth Group. Arguably, the sand horizon could be debated as a Lambeth Group sand channel instead, but it is consistent with Blackwall Facies characterisation by Edgar et al. (2021) and Marriott (2019). This misallocation caused localised thickening of the Lambeth Group (fig. 5.30-31). Notes were attached to aid future analysis, as with other areas of uncertainty.

The findings highlight that stratigraphic errors may only become apparent through cross-section analysis despite critical efforts to correctly interpret them during the borehole interpretation phase.

[47] Referred to as the Harwich Basal Sand Unit (HBSU) in the model. This has since been updated to Blackwall Facies (Edgar et al., 2021; Skipper, pers comms, 2019) as it is unclear if it is a Blackheath facies or a separate unit. Its coverage is broadly restricted to within Block D.

[48] The brown silty fine SAND of the Blackwall Facies, the grey Laminated Beds, and the dark grey Lower Shelly Clays. The sand horizon could be debated as a Lambeth Group sand channel instead, however, that is beyond the scope of this investigation.

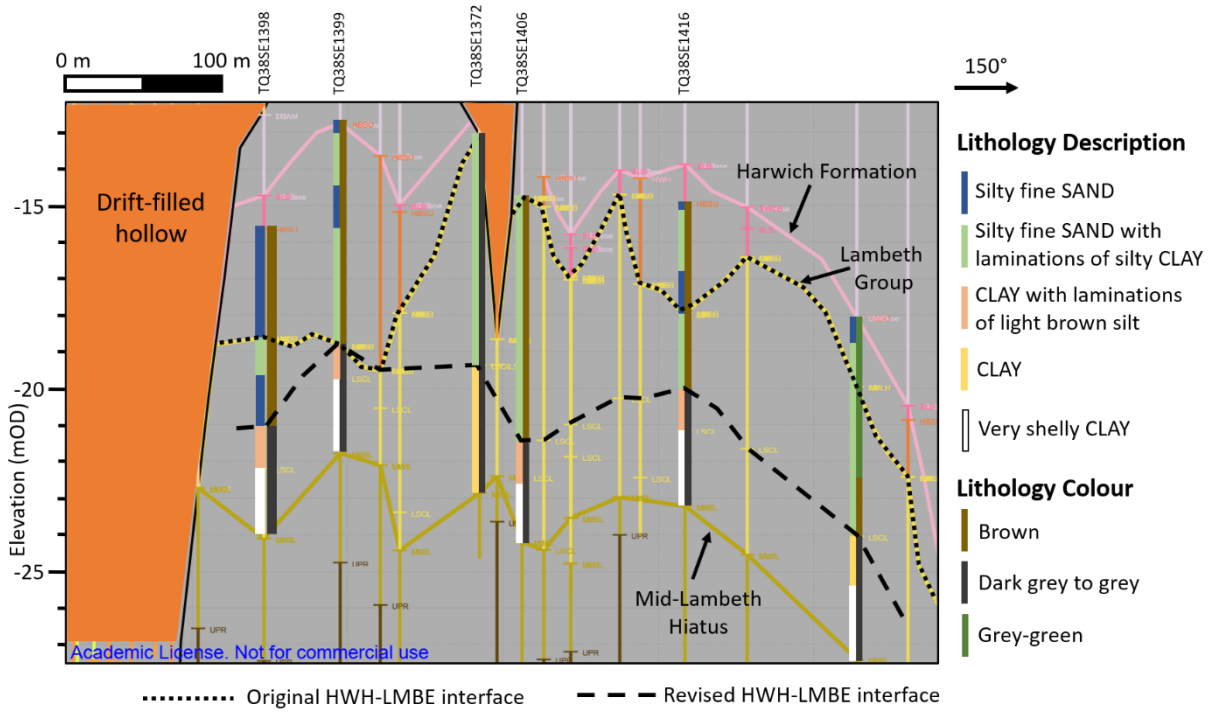

Figure 5.47 – Portion of section D_interior_6 containing laterally continuous silty fine (occasionally laminated) SAND horizon of unclear lithostratigraphy. The original interpretation segregated the horizon between the Harwich Basal Sand Unit/Blackwall Facies and the Laminated Beds on the basis of laminations occurring (regardless of their continuity). This led to an irregular boundary between the Harwich Formation and Lambeth Group (dotted line). Selected boreholes were reviewed according to their lithology and colour to produce a more consistent interface (dashed line). Refer to figure 5.20 for section position.

5.5.2.3 Categorising pedogenically altered sequences

The Lambeth Group was deposited in a tropical terrestrial-to-lagoonal environment characterised by cyclical sea level change. During the low stands, exposed sediments were tropically weathered and pedogenically altered to the Lower and Upper Mottled Clays. The former event was deep acting and partially altered the underlying Upnor Formation (Aldiss, 2014). Within this 'Mottled Upnor' the flint pebbles are discoloured and the glauconite oxidised to produce a less green, mottled sandy matrix. It is grouped into the 'Lower Mottled Beds' along with the 'Lower Mottled Clays' to reflect this alteration (Page and Skipper, 2000), despite their lithological distinctions. However, its exact boundaries with both the unaltered Upnor and the Lower Mottled Clay is difficult to identify (King et al., 2016).

The categorisation is logical; however, the partial separation of the overall Upnor Formation by post-depositional processes limits its usage as a single unit for lithological and tectonic characterisation. It is unclear whether to define the occurrence of Mottled Upnor as the top of the Upnor Formation or not. This is also affected by poor log quality that prevents separation between them and/or with the Lower Mottled Clays. Neither polylines nor lithological surfaces were produced for the Upnor units.

5.5.2.4 Geometrically characterising lower level lithostratigraphy

Most of the lower lithostratigraphic levels within the London Clay Formation, Harwich Formation and Lambeth Group (fig. 2.22) are not modelled as polylines and surfaces, despite the resolution achieved by borehole interpretation (table 5.1). This reflected uncertainties specific to each layer during explicit modelling caused by irregular stratigraphic positionings (fig. 5.46), inconsistent coverage, indivisible groupings in descriptions, pedogenic alteration, and confidence in their interpretation. For example, the London Clay subunit polyline coverage was limited and not defined in all boreholes, making surface generation inappropriate. Comparatively, the distinct Mid-Lambeth Hiatus (fig. 5.3) is consistently defined, enabling the Lambeth Group to be characterised as above or below this key marker (fig. 5.26).

The members of the Lambeth Group have previously been assigned to the Reading and Woolwich Formations (fig. 2.23). This was not undertaken here because they are interfingering, laterally equivalent units and would introduce surface generation complications.

5.5.2.5 Lithostratigraphic vs lithological horizon interpretation

Specific lithostratigraphic horizons are interpreted from in-log lithological descriptions. Overall, this was successful but, as outlined above, complexities within and similarities between specific stratigraphic units may lead to misinterpretation.

This can be avoided if lithological variability is also divided into specific horizons (fig. 5.47), allowing material characteristics to independently verify lithostratigraphic interpretations during cross-sectional analysis. The AGS data format enables material breakdowns to be presented and characterised, however, it could not be integrated into MOVE. Instead, a third ‘materials’ database would be required to define changes in grain size, textures, and colour.

5.5.3 Fault analyses

The explicit definition of faults from offset identification is considered robust as an existing method (§4.1.2.4) and not disputed in this review. However, the decision to demarcate a fault in section is not always straightforward and reflects uncertainties intrinsic to structural analysis through geological modelling that are not considered to be investigation specific.

Fault interpretation was intentionally conservative, and it is likely that multiple faults were missed during the explicit modelling phase. Difficulties associated with explicitly modelling faults where data coverage is poor or strata is inclined, and defining major fault, are identified and discussed.

5.5.3.1 Impact of borehole coverage on offset definition

The research relied solely on boreholes to characterise the subsurface by providing arrays of vertical snapshots of the immediate surrounding geology in cross-sections. Whether or not a fault-induced offset is explicitly identifiable in section is dependent on relative borehole spacing. This is highly inconsistent, being a product of the data acquisition phase (fig. 5.18), cross-section positioning (fig. 5.19), and data availability (fig. 4.8). The impact of borehole spacing on fault definition is illustrated in figure 5.48: poor spacing in section can misinterpret actual fault offsets as inclined bedding.

Where offsets are apparent between two boreholes, a fault is interpreted at the midpoint between them. This is sufficiently accurate when the borehole spacing is high but as the borehole spacing increases, the accuracy of the fault position(s) decreases markedly.

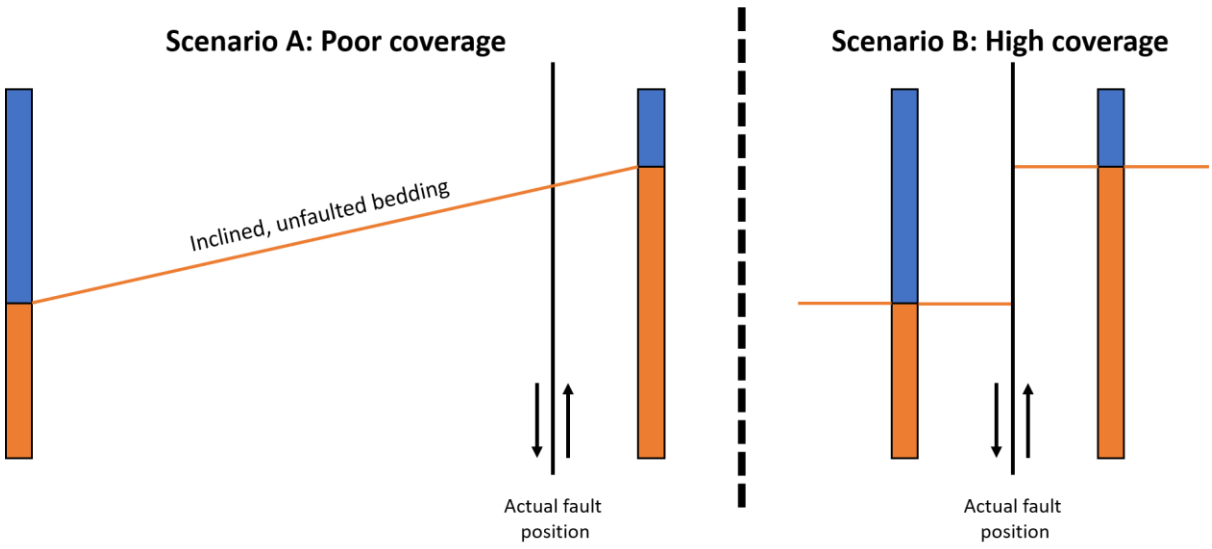

Figure 5.48 – The impact of borehole spacing on fault identification during cross-sectional analysis.

5.5.3.2 Differentiating inclined strata from faulting

London's subsurface is known to undulate through a combination of faulting, folding and block behaviour (Ellison et al., 2004, Ford et al., 2010). During modelling, conservative fault appraisal prevented any potential investigative biases that might falsely attribute topographic changes to faulting. However, where data coverage is poor, distinguishing fault offsets from inclined layers is challenging (fig. 5.48), with the former only interpreted where confidently apparent from evidence.

The London Clay locally thickens (fig 5.30) between inclined strata in the eastern portion of section D_interior_6 (fig. 5.49) and appears to be downthrown. The two borders of this feature are labelled A and B but were each interpreted from degrees of differing borehole coverage and penetrative depths. These boundaries are discussed and 'groundtruthed' individually against comparable structural observations. Rapid steepening of Boundary A implies a fault offset, with a single fault modelled at its base. However, it is likely that multiple faults (dotted lines) are present since the high borehole density contradicts a single offset. It is unclear if this boundary corresponds with localised thinning of the Harwich Formation or a misinterpreted lithological interface (fig. 5.47) as borehole coverage diminishes East of this fault. Comparatively, whether Boundary B comprises tilted strata or multiple minor offsets is unclear due to poor borehole coverage and depth penetration over more-gently inclined horizons (fig. 5.49). Possibly this represents part of the Greenwich Fault along the margin of the Greenwich Anticline linkage zone since its progressive shallowing is concordant with wider behaviour along this interface (fig. 5.24-29). This is comparable to the Greenwich Fault's interface at Beckton which separates sub-horizontal bedding from stepped faulting within the Greenwich Anticline inlier (fig. 3.38). Alternatively, this and the adjacent depression may form the 'Greenwich Syncline' proposed by Howland (1991), although this is considered unlikely due to the proximal faulting. The feature is likely fault-controlled, reflecting sub-horizontal strata between two independent structures: a fault within Block D's interior (Boundary A), and branches of the Greenwich Fault (Boundary B).

Greater borehole density is required to define the broader structure of the Greenwich Fault interface; the London Clay was not subdivided here but may help to assess this in-section. The case study highlights the issues associated with fault interpretation and reinforces the impact of borehole spacing and coverage discussed above.

Similar issues occur when defining fault positions within Block B, a continuous fault zone (Newman, 2017) coincident with the Millwall Anticline (fig. 5.1). Some sections define internal faulting (fig. 5.45), whilst others [B_across_A_G_3] only interpret the bounding faults, since borehole spacing and detail is insufficient internally to confidently determine them. Comparatively, the Thames Tideway GI could define these faults by coupling borehole data with seismic profiles.

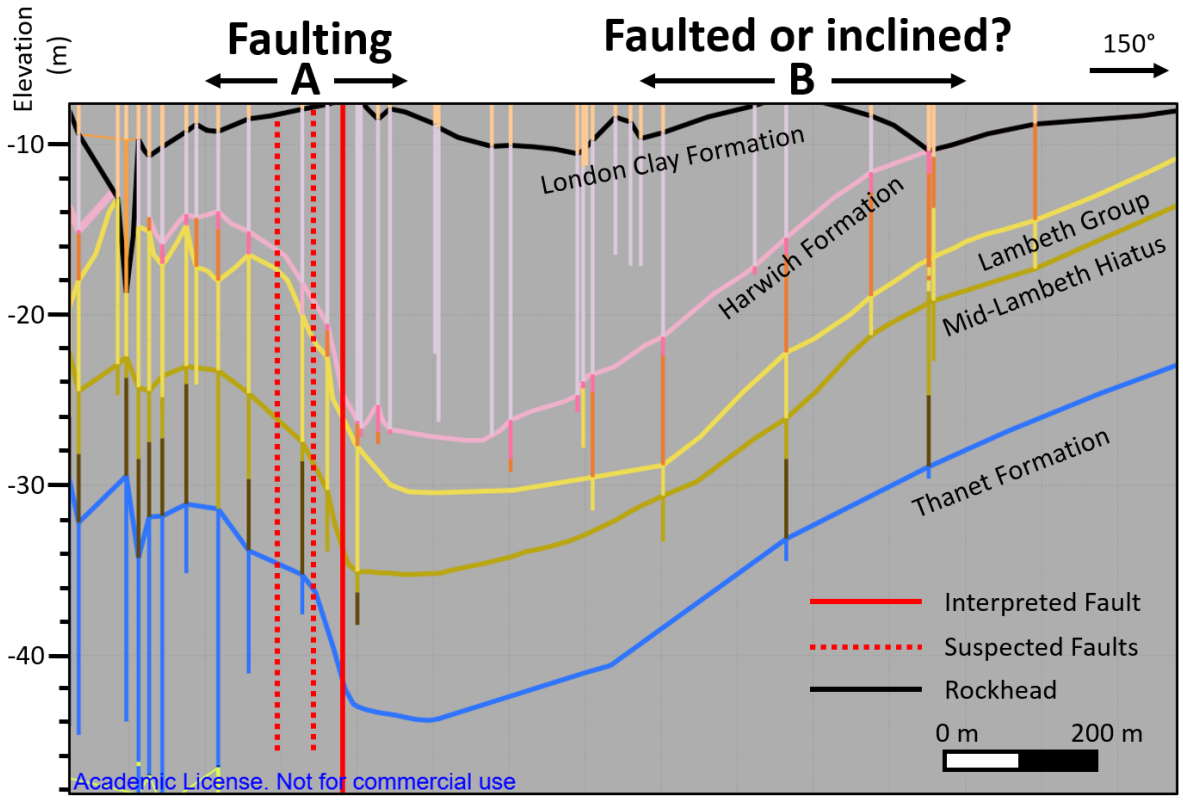

Figure 5.49 – Localised thickening of London Clay Formation in D_interior_6 is suspected to be fault-controlled. However, the structural analysis of both boundaries is unclear. Boundary A appears to comprise a diffuse, narrow band of faulting. Boundary B is unclear and impacted by poor borehole coverage. It may be associated with a nearby inherited fault and linkage structure. Refer to figure 5.20 for section position.

5.5.3.3 Major fault definition

Structural analyses in London are constrained by the lack of exposure and overreliance on spatially restricted borehole data. Their interpretation and characterisation will always be an imperfect approximation. Defining these structures is, however, crucial for communicating risk to the geotechnical community. This was not achieved for Fault AF despite local faulting being identified because the research aimed to model only complete structures. Instead, partial definition should be undertaken to communicate the structure's presence and provide a basis for future investigations.

5.5.4 Future directions for the modelling programme

Further investigations are needed to constrain the structures and subsurface stratigraphy proposed here and extend the model to characterise the wider, regional structural geology by increasing data density and coverage, and by integrating new features into the model.

A review of the investigation and its methodologies has highlighted several areas that could be developed and/or improved to aid the lithological and tectonic analysis of East London:

- Development of a three phased acquisition data system to improve borehole targeting.
- Incorporation of AGS data using format-reading softwares (fig. 5.46).
- Development of a third database to characterise in-log descriptions according to material properties. This will complement the lithostratigraphical input sheets (log database).
- Assigning geotechnical properties to horizons in the log and material databases.
- Incorporation of other types of subsurface data (e.g., seismic profiles) where available.
- Increased explicit and implicit characterisation of lower-level sequences of the London Clay and Harwich Formations, and the Lambeth Group.
- Longer investigative time period.
- Revision of the borehole grading system (fig. 5.4) to improve retrospective grading.

5.5.4.1 Transitioning to an engineering geological model

Major infrastructure projects are planned in East London, providing a solid justification for the expansion of this model to characterise its subsurface. However, it must incorporate engineering geology to better facilitate geotechnical appraisal and risk identification. This could be achieved by both incorporating the proposed material database and the assignment of geotechnical properties to specific horizons. This would enable a single geological material to be spatially parameterised and allow the geotechnical implications of tectonism and depositional features to be assessed for a specific lithology. A preliminary trial of this was undertaken for the Upnor Formation to assess spatial variation in shear strength by superimposing and interpolating the internal angle of friction (ϕ) data onto its surface (fig. 5.50). The outcome does not account for internal lithological variation but provides a proof of concept for future research.

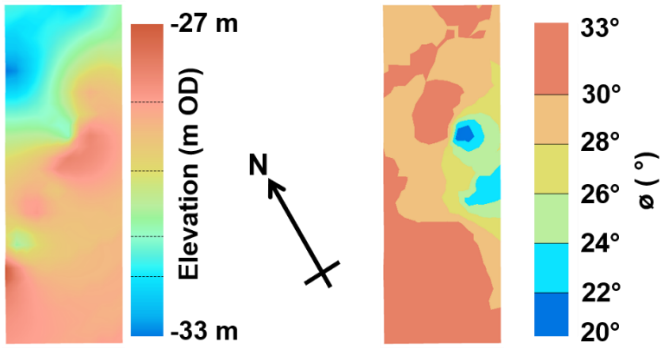

Figure 5.50 – Spatial variation in Upnor Formation shear strength in a small portion of East London. Internal angle of friction (ϕ) values were interpolated across the layer's predefined surface. ϕ-values were sourced from laboratory testing conducted as part of the Silvertown Tunnel GI (Appendix A).

5.6 Conclusion

The East London geological modelling programme was undertaken to characterise its subsurface structures and lithologies, and to validate suspected fault lineaments (fig. 5.1). Boreholes (table 5.4) were acquired and interpreted using a hierarchical system that maximised data extraction and were digitised into two databases. These were explicitly modelled to produce polylines of faults and the layers they bound, which were implicitly modelled to generate fault planes and surfaces, respectively.

Five major faults were interpreted that separate distinct subsurface blocks, four of which were modelled as planes (fig. 5.23, 5.43). These show good agreement with published models and fault analyses and confirm several proposed fault lineaments; with two new major faults proposed.

Explicitly modelled faults (fig. 5.35) demonstrate that major fault architectures and complexity are variable along and between faults (fig. 5.40-45). This is attributed to differing fault set inheritance behaviour, causing both variable and complex architecture (§5.4.4), and under-definition by section-specific borehole coverage (fig. 5.48). Fault-controlled compartmentalisation is apparent as lithological elevations, coverage and thicknesses are irregular both within and between blocks (fig. 5.24-34). Variable internal block deformation indicates that inheritance has inconsistently tectonised the subsurface through within-set linkage (Block G) and broader interaction (Block B). The geological impact of compartmentalisation, and the development and characterisation of fault zones are assessed in Chapter 6.

Post-modelling analysis led to structural and stratigraphic revisions following a review of the model, its surfaces, and cross-sections. These critiques were groundtruthed against other model outputs and published evidence of the same structure and/or strata, and highlight issues associated with data coverage and quality, and London's geological complexity in general. The reinterpretations emphasise greater structural complexity (§5.4.4.1-2) and difficulties associated with differentiating both lithological similar strata (§5.5.2.2) and faulting from inclined strata (§5.5.3.2). Some of these revised outputs are inconclusive (e.g., Fault AF) and demonstrate that the geological characterisation of East London remains incomplete.

The programme demonstrates greater structural and lithological complexity in East London than recognised. However, limitations (primarily related to data coverage) introduced challenges for fault and lithological analyses during explicit modelling. These may be overcome by improving the data acquisition strategy, and by incorporating both AGS data (fig. 5.46) and material information.

6. Geological impact of major faulting in London

Explicit geological modelling identified a fault network in east London (fig. 6.1) and locally confirmed inferred fault lineaments from indirect mapping (fig. 4.28). These have partitioned and offset the bedrock into a series of blocks that have distinct elevations and strata thicknesses internally. Major fault architectures were identified to be complex and variable, both along and between major faults.

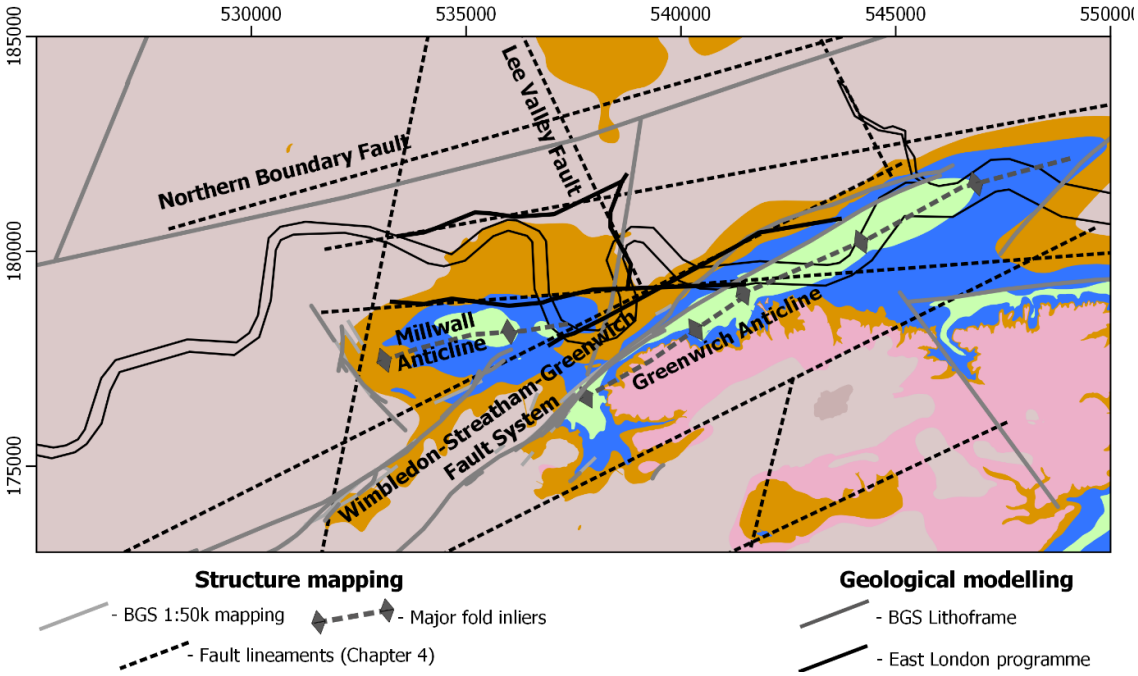

Figure 6.1 – Positions of major faults and folds interpreted by this investigation and the BGS.

The geological impact of major faulting in London extends beyond the faults themselves and the strata they offset. An influence on sedimentological and current hydrogeological processes is suspected as laterally variable lithological coverage and discontinuous aquifer behaviour correspond with changes in subsurface elevations attributable to faulting. A causal link is suspected with fault zones (poorly understood yet complex faulted bands) due to their spatial correlation and comparative similarities with fault linkage behaviour. Both features introduce unknown structural and geological complexities to the near surface that may be detrimental for geotechnical projects.

Chapter 6 assesses the direct and indirect impacts of fault inheritance on London's geology by assessing causal relationships with both compartmentalisation (§6.1) and fault zones (§6.2). The evolving Alpine slip behaviour of these three inherited fault sets is summarised:

- NW-set (strike-slip): Dextral becoming sinistral reshearing with a minimal dip-slip component.
- NNE-set (strike-slip): Sinistral reshearing with a minor dip slip component.
- ENE-set (reversed normal fault): Dip-slip dominant with a minor sinistral slip component.

6.1 Fault-controlled compartmentalisation

De Freitas (2009) argued that structural partitioning of London's subsurface has caused it to be geologically and hydrogeologically discontinuous. Major faults have since been demonstrated to segregate topographically distinct areas at both regional (fig. 4.12) and local (fig. 5.24-29) scales. Observations also indicate that fault partitioned block-like geometries correspond with thickness variability (fig. 5.30-34), at-surface displacement (fig. 4.19, Mason et al., 2015), and Lower Aquifer behaviour (Buchan, 1938). Faulting is suspected to have influenced Lambeth Group, Harwich Formation and White Chalk Group depositional behaviour (Aldiss, 2014, Edgar et al., 2021, Mortimore and Pomerol, 1997). These observations raise two questions:

1. Has fault-controlled compartmentalisation also influenced geological processes?
2. At what scale are faults influencing processes? Regional and driven by specific faults or localised into discrete blocks?

The relationship of major faults with depositional, denudational and hydrogeological behaviour in London was assessed by coupling outputs from East London model and the geospatial database (§ 5.1.3) with private data and published observations. The analyses used major fault positions (fig. 6.1) from the East London programme, indirect fault mapping, and the BGS Lithoframe to provide the differing scales required. Local-scale analyses focused on East London and its modelled fault-bounded blocks (fig. 6.2). Regional analyses compared spatial variation across London with fault lineaments and the BGS Lithoframe faults (fig. 6.3).

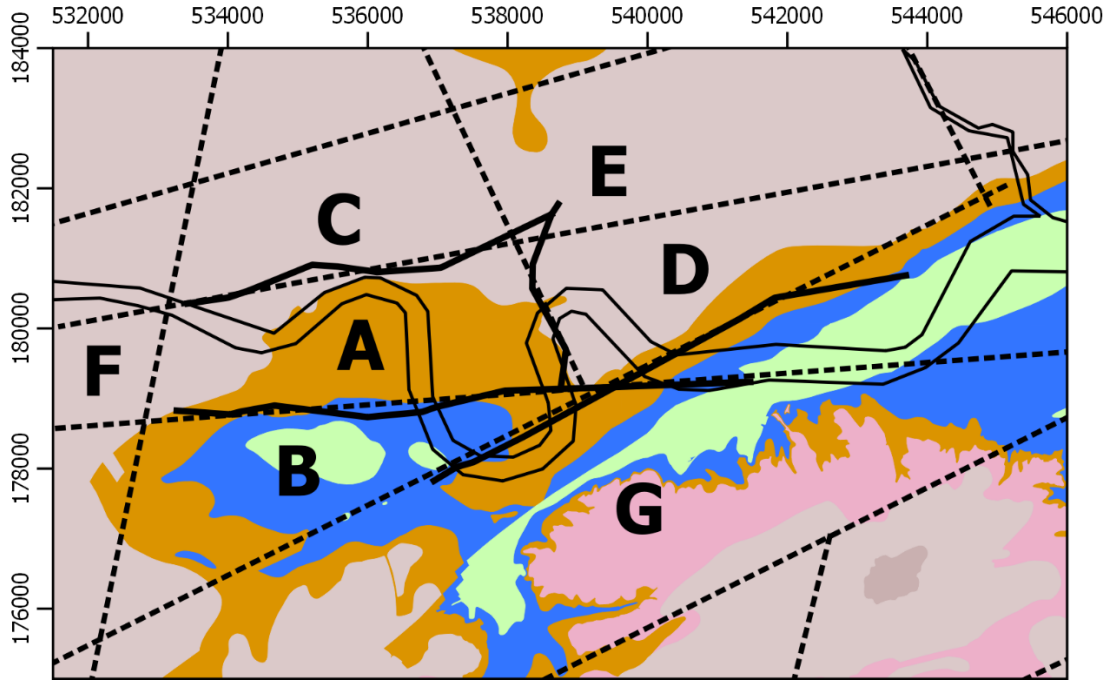

Figure 6.2 – Local-scale compartmentalisation analysis using fault block positions in East London.

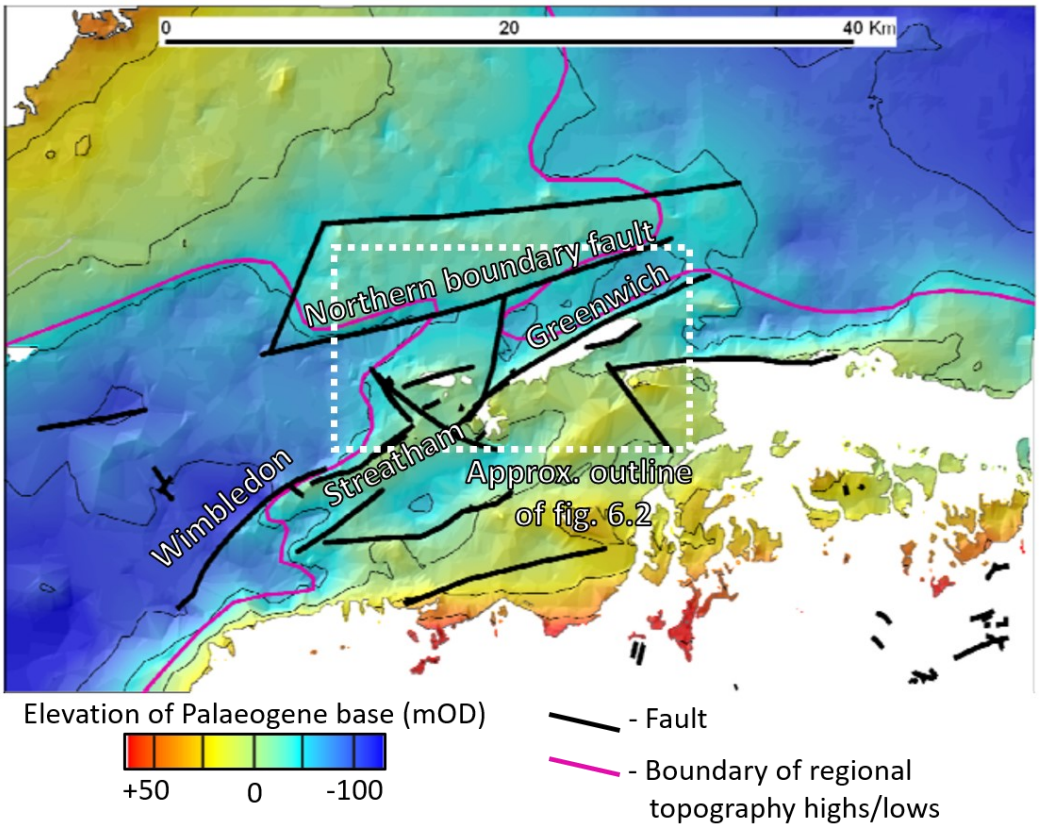

Figure 6.3 – Regionalised partitioning of London's bedrock by major faulting. Topographic variation of the Palaeogene base corresponds with BGS Lithoframe faulting. Adapted from Ford et al. (2010).

6.1.1 Depositional Analysis

Suspected Late Cretaceous and post-Thanetian Palaeogene syndepositional fault activity is coincident with the Subhercynian and Pyrenean Phases of Alpine compression (§2.1.2). Ellison et al. (1996) suspected that this activity was associated with basement faulting. All three inherited fault sets could reactivate during these Phases (fig. 3.15-16, 3.20) and influence depositional behaviour through topographic alteration. Three case studies are analysed for evidence of structural influences, followed by an assessment of their respective depositional environment sensitivities to faulting:

- §6.1.1.1. Lambeth Group
- §6.1.1.2. Harwich Formation
- §6.1.1.3. White Chalk Group
- §6.1.1.4. Depositional environment sensitivity

6.1.1.1 Lambeth Group: member distribution

BGS Lithoframe analysis (Ford et al., 2010) proposed that London's bedrock was deformed into fault-bounded blocks to the north and periclinal folds (and faults) to the south (fig. 2.31). They identified a "*structural culmination*"[49] (fig. 6.3, pink lines) that separated topographically lower regions based on elevational and structural outputs. This axial highpoint likely acted as barrier that influenced connectivity and depositional conditions based on Lambeth Group member distributions (fig. 6.4).

Cross-comparison within member facies distributions (Ellison et al., 2004, fig. 17, 19) also identifies broad correspondence with regional subsurface topography, and individual faults. Clay- and sand-dominated portions of the Upper Shelly Beds respectively correspond with regional 'lows' and the axial high, implying a contrast between lagoonal and tidal conditions. The sandier coverage is only coincident with WSG-Faults (fig. 6.1) part of the high. The Lower Shelly Bed's sand-dominant is restricted to Block E (fig. 6.2), similarly implying partitioned uplift.

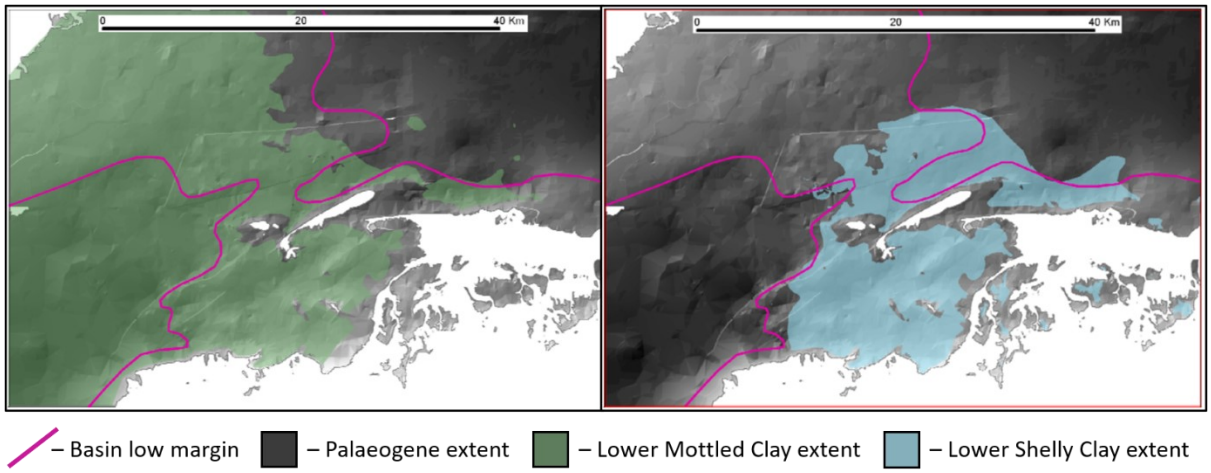

Figure 6.4 – BGS Lithoframe distribution of the Lower Mottled Clay and Lower Shelly Clay members of the Lambeth Group relative to inferred palaeotopography along London Basin synclinal axis. The former sequence is restricted to the western depression and structural highpoint, becoming sand-dominated east of this; the latter member is restricted to the axial highpoint. Adapted from Ford et al. (2010).

[49] "*The highest point along a structural axis or fold system*" Lageson (1984). Ford et al. (2010) used this term as they interpreted the raised area to be an axial highpoint along the London Basin synclinal axis.

6.1.1.2 Harwich Formation: members and facies distribution

The laterally discontinuous Harwich Formation's members reflect progressive westward transgression from outer estuarine to shallow marine conditions (table 2.1). Their distributions (fig. 2.24) were assessed as members in East London (fig. 6.5) and facies across London (fig. 6.6) from Edgar (2021).

Harwich Formation's members and the Blackwall Facies distributions in East London were extracted from the geospatial database. Swanscombe and Blackheath Members coverage does not correlate with block behaviour. Comparatively, the Oldhaven Member and Blackwall Facies are predominantly restricted eastward in Block D. However, analyses are spatially restricted by Harwich denudation and poor data coverage where not.

Edgar (2021) redefined these sequences as five distinct facies (table 2.3). Edgar proposed that faulting caused topographic overprinting, from comparisons with the indirect fault lineaments (Chapter 4), to provide both syndepositional barriers and accommodation space, and to influence channel development. The HWH2 facies (equivalent to the Blackwall Facies) are restricted to discrete blocks (Block D and possibly C), whilst HWH5 is regionally partitioned by a single fault. Other facies appear to be less influenced by major faulting overall.

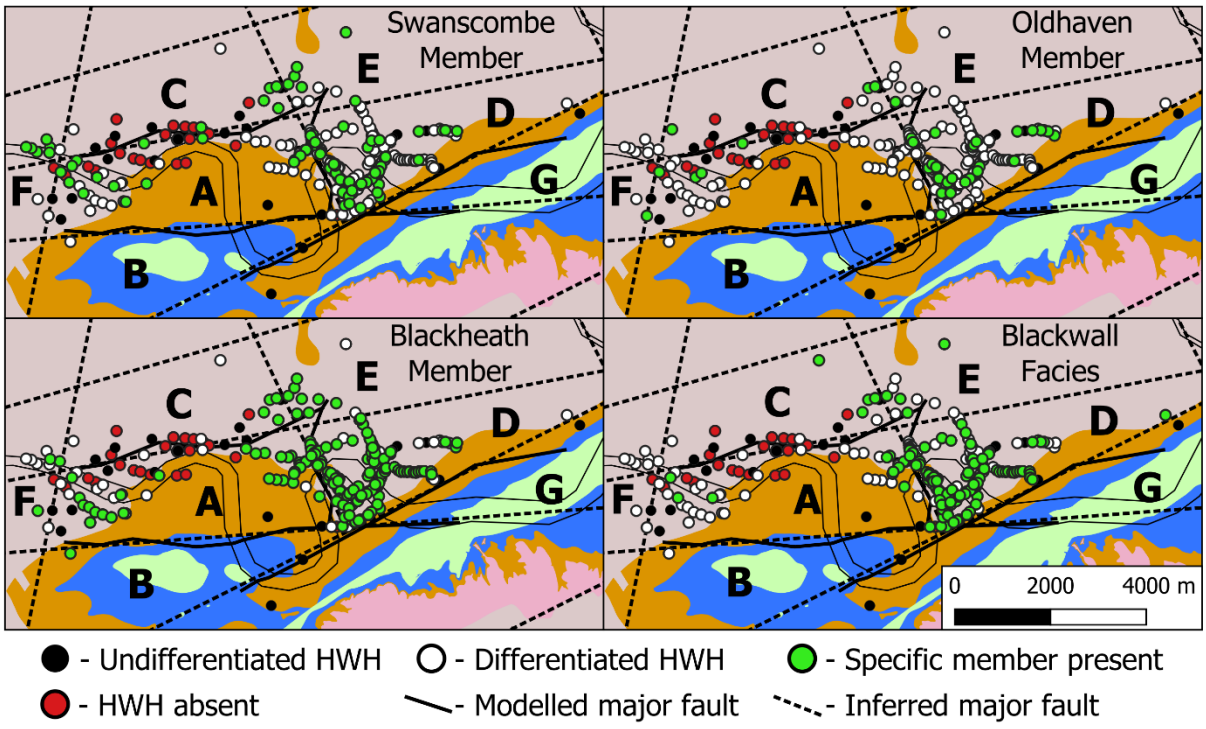

Figure 6.5 – Harwich Formation unit distributions in East London relative to major faulting.

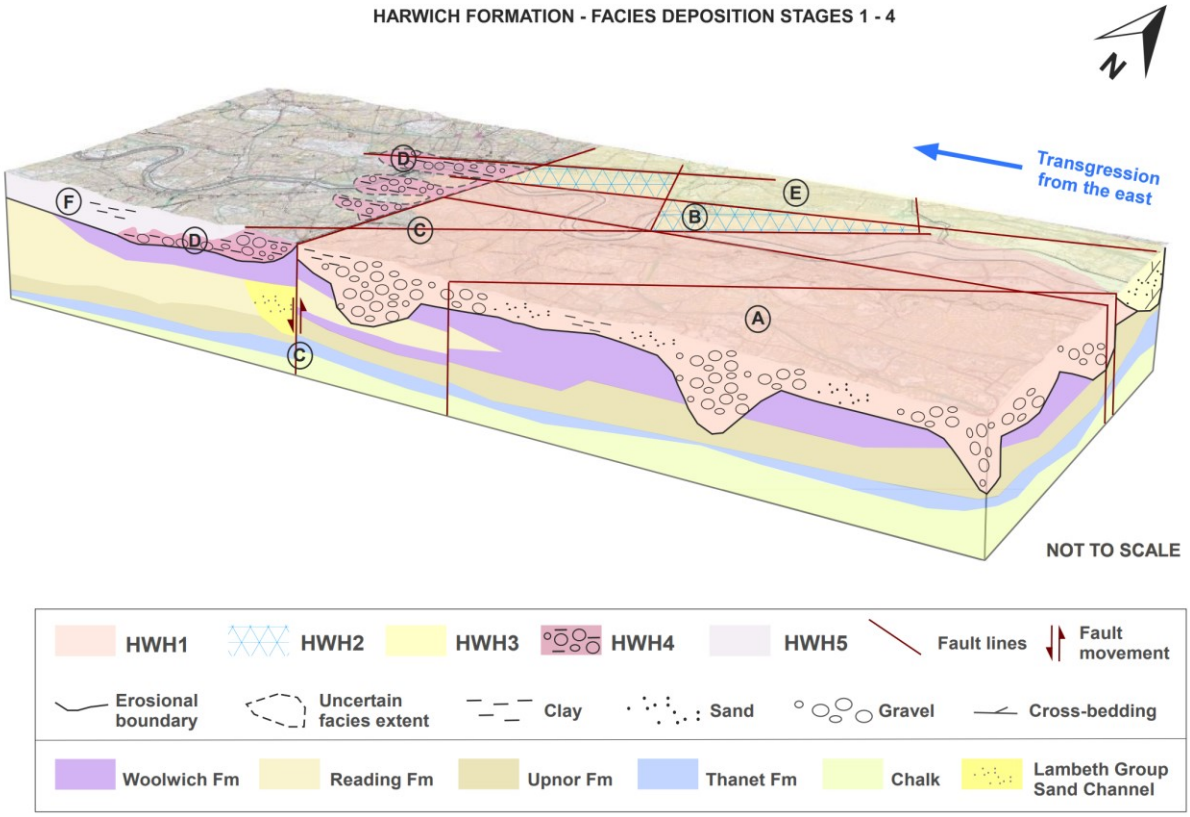

Figure 6.6 – Idealised depositional model of Harwich Formation facies across London, comparing individual facies coverage with fault lineaments and depositional conditions. Sourced from Edgar (2021).

6.1.1.3 White Chalk Group: thickness variability

Depositional behaviour of conformable White Chalk Group Formations can be determined from thickness variations. The Seaford Chalk (SECK) and Lewes Nodular Chalk (LECK) formations are thicker in East London than in the North Downs, which Mortimore and Pomerol (1997) attributed to differential tectonic responses to Alpine inversion between the London Platform and Weald Basin.

Thickness variability of these units in East London was assessed from across-fault measurements (fig. 6.7, table 6.1) and borehole analyses (fig. 6.8) (of Thames Tideway logs) to determine whether syndepositional faulting is overprinted onto this broader tectonic response. Partial denudation of the uppermost Haven Brow Beds (Mortimore et al., 2011) restricted SECK analysis to only the Cuckmere and Belle Tout Beds (fig. 2.21), whilst the LECK is presented undivided. Thickness variations are observed across several faults (>4 m in SECK beds, table 6.1) but do not align with block positions (fig. 6.8). Only the Greenwich Anticline (Block G) corresponds with Belle Tout Bed thickening (fig. 6.8) and LECK hardground development[50] (Mortimore et al., 2011; fig. 10), respectively implying tectonically driven lowering and uplift of this block during the Late Cretaceous.

Data analyses also identified that isolated thicker points that do not correspond with known fault positions (fig. 6.8; 5.35-36), and that net displacement did not increase with age as expected (table 6.1, fault #1). Both indicate that certain datapoints may be erroneous, highlighting difficulties associated with defining chalk lithostratigraphic boundaries during logging.

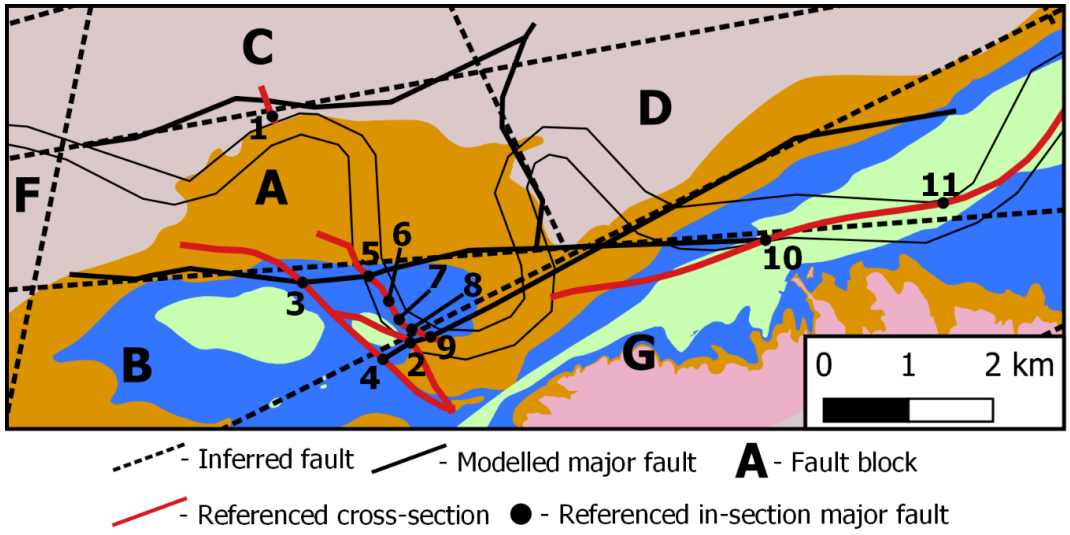

Figure 6.7 – Positions of major faults utilised for across fault thickness and offset cross-sectional analyses (table 6.1) of SECK members and LECK formation.

[50] Episodes of chalk 'non-deposition', indicative of uplift (Mortimore et al., 2011; Mortimore, 2018).

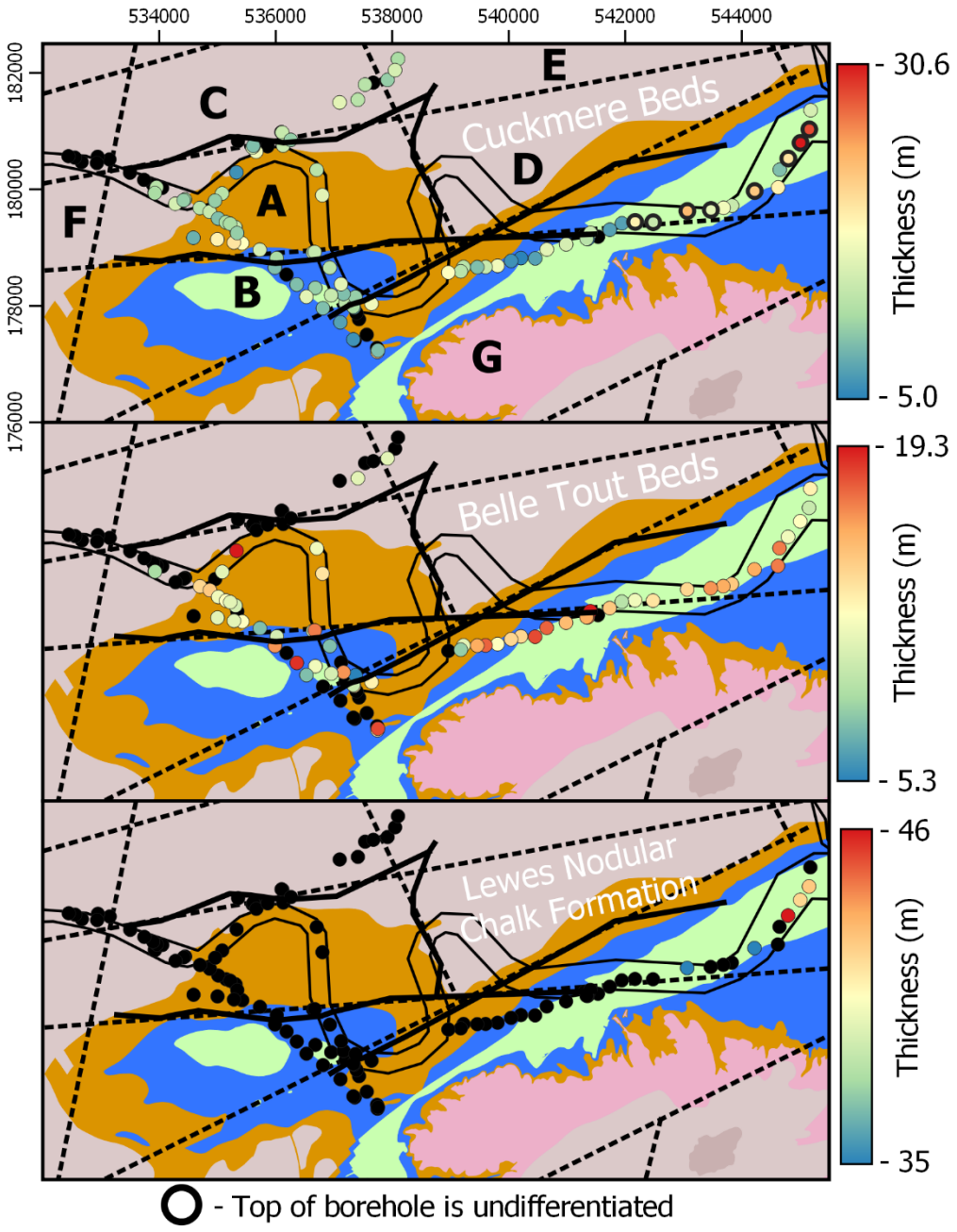

Figure 6.8 – Thicknesses of the Cuckmere Bed and Belle Tout Bed members of the SECK, and LECK, intercepted by Thames Tideway boreholes digitised for the East London model. Several Cuckmere Beds datapoints (ringed) have anomalous thicknesses as their logs did not define its upper boundary.

Table 6.1 (next page) – Across-fault thickness variability and offsets of subdivisions of White Chalk Group measured from cross-sectional analysis conducted in Chapter 6. See figure 6.7 for positions of referenced in-section faults and cross-sections relative to interpreted and inferred major faults.

[a] 'Relative fault positions' is defined by whether an in-section fault is situated on a major fault boundary or the interior of a fault zone.

[b] The Haven Brow Beds have been partly-denuded under London and are used in §6.1.3.

[c] The uplift of the Belle Tout Beds implies that the fault underwent reversal causing Block A to be upthrown. This is considered to be erroneous.

Fault #	Section	Relative fault position [a]	Across fault thickness difference (m)				Fault offset of downthrown side (m)				Down-thrown block
			Seaford Chalk Formation			Lewes Nodular Formation	Seaford Chalk Formation			Lewes Nodular Formation	
			Haven Brow Beds [b]	Cuckmere Beds	Belle Tout Beds		Haven Brow Beds	Cuckmere Beds	Belle Tout Bed		
1	A_C_boundary_5	AC	2.7	7.5			3.1	5.5	-1.8 [c]		A
2	B_G_boundary_1	BG	1.5	4.2	3.5		5.3	6.8	3.9	7.1	G
3	B_across_A_G_3	AB	4.3	2.4	5.8		3.2	6.9	9.5	3.6	A
4		GB	5.7	2.3	2.1		N/A – Explicitly modelled polylines not offset				G
5	B_G_across-1	AB	0.6	0.8	2.3		5.4	4	5.2	7.8	A
6		FZ Interior	6.1	3.5			7.4	13.1	10.5		Uplifted Interior
7		FZ Interior	1	6.2			1	1.8	8.4		
8		FZ Interior	5.6	1.1	10.7		5.4	12.2	12.4	1.7	
9		GB	0.6	5.9	7.8		8	8.5	14.5	22.2	G
10	G_interior_1	FZ Interior	0.9	0.7	6.7			1.4	1.6	8.4	Uplifted Interior
11		FZ Interior		1.7	0.6	1.1		12.4	14.5	13.9	

6.1.1.4 Depositional environment sensitivity

Individual faults and/or block partitioning have affected the distribution of certain units within the Lambeth Group and Harwich Formation. Comparatively, inconclusive analysis of the White Chalk Group (§6.1.1.3) and consistent London Clay Formation sub-unit thicknesses and facies across London (King et al., 2016) may suggest a lack of compartmentalisation. These differential responses demonstrate their respective sensitivities to syndepositional faulting and relief generation as it contrasts lithologies deposited under shallow marine-estuarine conditions (fig. 2.15) with deeper marine shelf settings (table 6.2). Therefore, Eocene estuarine-to-nearshore conditions were most receptive to accommodation space and topographic barriers generated by major fault activity.

Table 6.2 – Fault depositional fault evidence and depositional environments of London's strata.
[a] Refer to table 2.1 for depositional environment sources.
[b] Evidenced at regional or local scale in London only.

Sequence	Depositional environment [a]	Syn-depositional fault activity [Alpine Phase]	Fault depositional influence evidence [b]
White Chalk Group	Marine shelf	Yes [Subhercynian]	Inconclusive
Thanet Formation	Inner-to-outer shelf	No [N/A]	No
Lambeth Group	Fluvial-estuarine to marginal marine	Yes [Pyrenean]	Yes
Harwich Formation	Estuarine to nearshore to shallow marine		
London Clay Formation	Inner-to-outer shelf		No

6.1.2 Denudational Analysis

The majority of London's post-Chalk stratigraphic boundaries are unconformable (fig. 2.22) due to episodic sea level changes (Knox, 1996) and exposure throughout the Palaeogene (§2.2.1, 2.1.0.7). Alpine Phases concurrent with the end-Cretaceous and Eocene may have affected post-depositional erosion by locally elevating strata and/or influencing fluvial processes.

The denudation behaviour of the White Chalk Group, Lambeth Group, and London Clay Formation were characterised to determine syn-denudational tectonism. This focused on denudation prior to reburial by later Palaeocene-Eocene sediments as post-Eocene denudation (§2.1.0.8) was evidently fault-controlled as present-day inliers correspond with major fault positions (fig. 6.1) and likely reflects the Oligocene culmination of the Pyrenean Phase. Where possible, denudation attributable to post-Eocene and recent erosion was distinguished.

The required stratigraphic resolution restricted this assessment to East London only (fig. 6.2).

6.1.2.1 White Chalk Group: denudation analysis

End-Cretaceous-mid-Palaeocene denudation of the White Chalk Group prior to Thanetian burial is more pronounced on the London Platform than elsewhere in onshore southern Britain (fig. 2.11) due to its susceptibility to epeirogenic uplift (§2.1.2). Compartmentalised overprinting in East London is implied as chalk erosion is "*stepped, controlled by faults and/or fault blocks*" (Mortimore and Pomerol, 1997), indicating possible (Maastrichtian–Mid-Palaeocene) Laramide Phase reactivation.

Spatial variation in the uppermost preserved members of the White Chalk Group were analysed (fig. 6.9). The sub-Thanetian surface is consistently comprised of the Haven Brow Beds (HBB) (fig. 2.21), however, the logs lacked the stratigraphical resolution utilised by Mortimore and Pomerol (1997; fig. 16-17) to differentiate this ~30 m thick unit. To overcome this, HBB thickness was also analysed (fig. 6.9). Thinner HBB in Blocks A & B than G, C, & E imply between-block variation; however, within-block variation is potentially more significant. The HBB is thickest in the Greenwich Anticline inlier (even where at rockhead). This implies that Block G was then lower relative to neighbouring blocks to enable greater preservation (with uplift and inlier generation likely post-dating Palaeogene sedimentation). Aside from the WSG-Faults, faulting had minimal influence on pre-Thanetian chalk denudation, agreeing with expected Laramide Phase quiescence (§2.1.2).

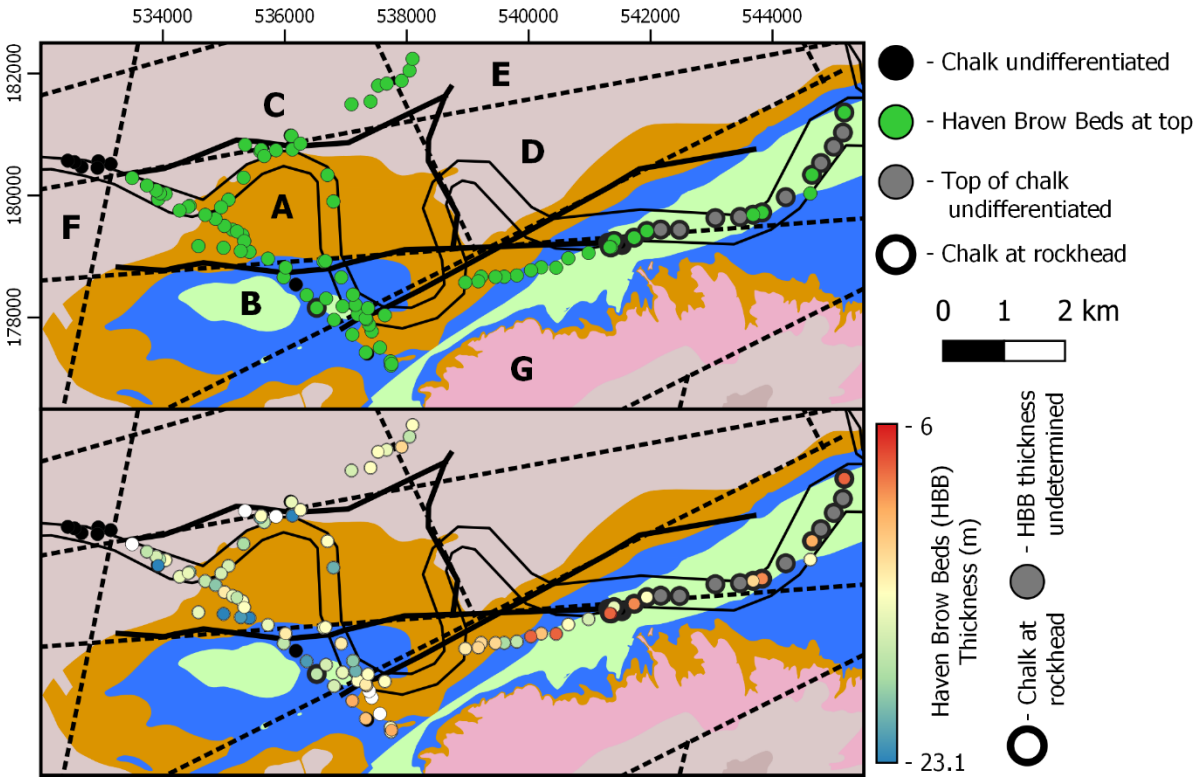

Figure 6.9 – Denundation analysis of the White Chalk Group in Thames Tideway boreholes (digitised for the East London model, table 5.4). The Haven Brow Beds (HBB) are consistently the uppermost preserved chalk member with irregular thickness evident within- and between-blocks.

6.1.2.2 Lambeth Group: irregular erosion depth

Spatial variation in the uppermost preserved member of the Lambeth Group can indicate the extent of erosion prior to Harwich/London Clay Formation burial. These were extracted from the geospatial database to assess this (fig. 6.10), with rockhead exposure and depositional coverage accounted for.

No structural influence on Lambeth Group denudation is evident due to the lack of across fault or between block variation. Upper Mottled Clay absence in Block D likely reflects its restricted depositional coverage (Ellison et al. 2004, fig. 20) rather than structurally controlled denudation. Differential within-block erosion is observed in Block A as the uppermost member differs between unexposed Lambeth Group and exposed inlier. This likely reflects the blocks northward tilt (fig. 5.28), and possibly the complex wide graben/Fault-AF (fig. 3.30-31, 2.31, 5.43) along its western interface.

Major unconformities also exist within the Lambeth Group (fig. 2.22) with thickness variations below the mid-Lambeth Hiatus (MLH) analysed (fig. 5.33) to assess the denudational interplay between regression and faulting. There are minor differences between block's (C vs. A), however, within-block variability is more pronounced. This implies that a subtle structural influence overprinted more dominant subaerial processes, prior to submergence and burial.

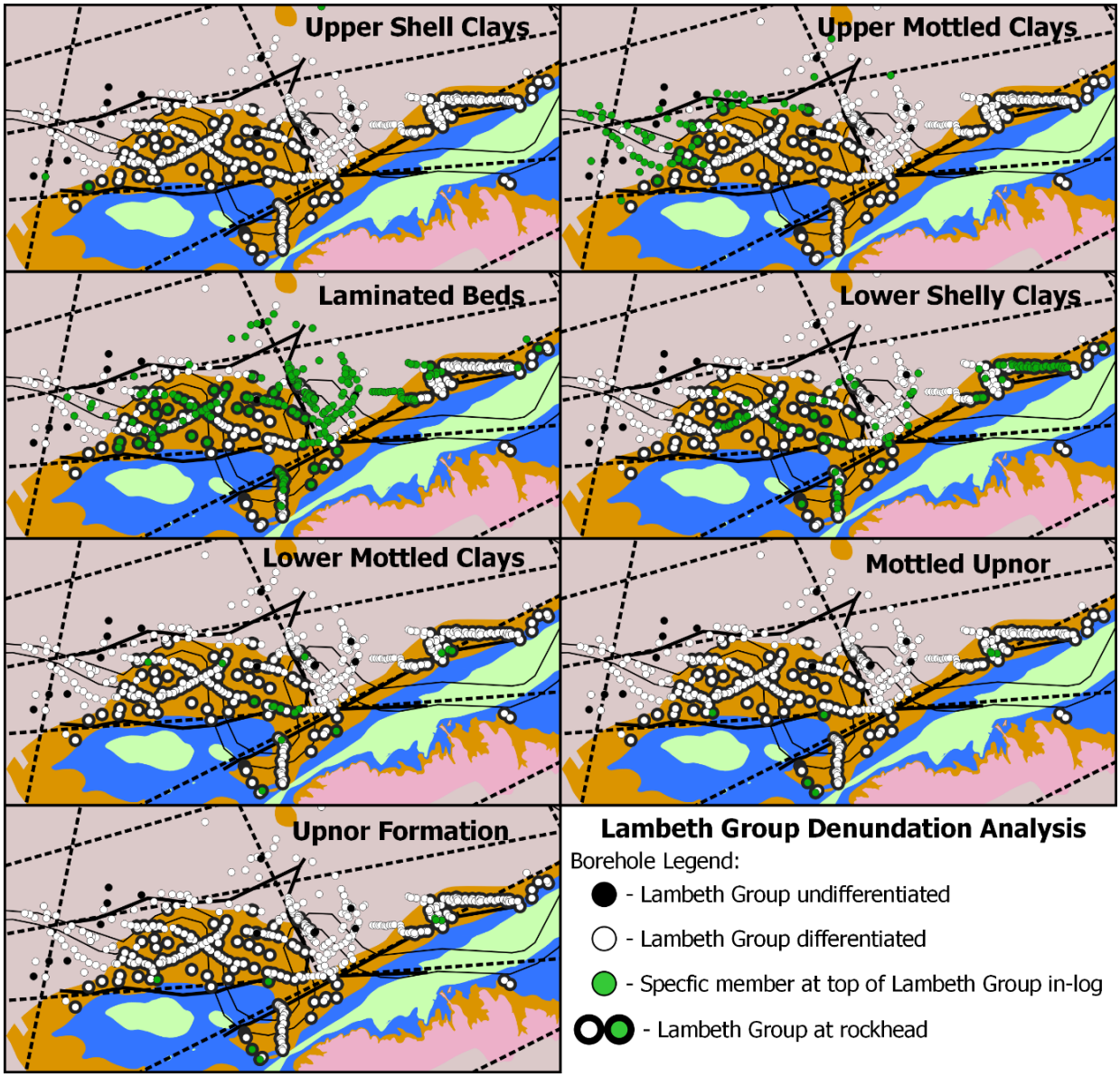

Figure 6.10 – Denudational analysis of the Lambeth Group intersected in boreholes. The uppermost member of the Lambeth Group indicates the extent of local denudation, with rockhead (black rings) highlighted to indicate where pre-burial and recent erosion cannot be distinguished.

6.1.2.3 London Clay Formation: thickness variability

The London Clay Formation is the youngest Palaeogene sequence preserved in the East London model, preventing comparative pre-burial analyses. However, a structural influence may be discernible that reflects post-Eocene and recent erosional behaviours combined since Alpine tectonism has been ongoing to present.

Thickness variations were analysed from borehole coverage (fig. 6.11) and modelled surfaces (fig. 5.30). The findings demonstrate variation both within- (Block D) and between-blocks (Blocks A vs. C). Westward thickening corresponds with the suspected (downthrown) central London graben (fig. 3.30-31; 2.31) or 'Fault AF' to locally inhibit denudation and preserve Unit B. Thickening within Block D is coincident with the Plaistow Graben and internally downthrown fault zones (fig. 5.37; 2.28). This implies that the majority of denudation occurred prior to the pre-Helvetic waning of Alpine compression, or, that fault activity is more recent than currently recognised. Both may be valid.

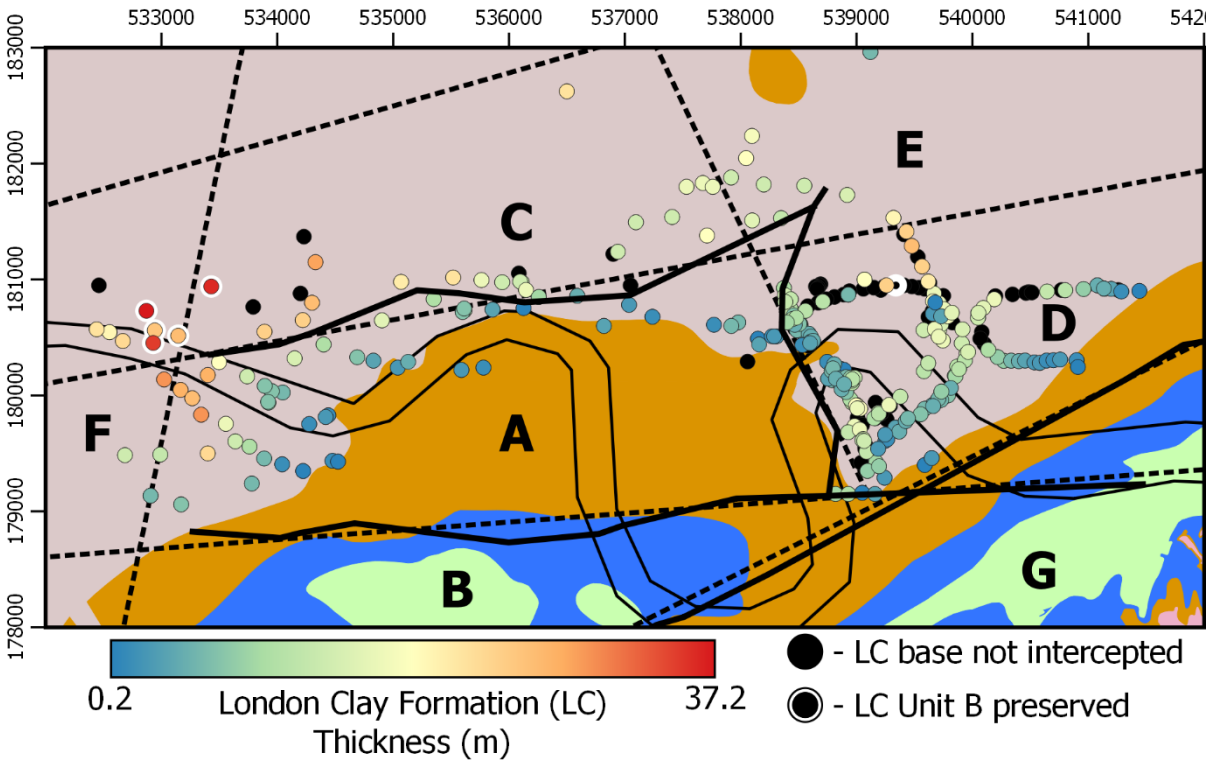

Figure 6.11 – London Clay thickness in borehole logs overlain onto inferred and modelled major faults. White rings locate where Unit B has been locally preserved and identified in borehole logs.

6.1.3 Hydrogeological Analysis

London's Lower Aquifer is situated within the White Chalk Group and the sand-dominant Thanet and Upnor Formations. Discontinuous aquifer behaviour is recognised (Environment Agency, 2018), with historical standing water levels (Buchan, 1938, plate II) mirroring fault positions (fig. 6.1). Certain faults likely have lower permeabilities that impede across-fault Lower Aquifer connectivity. For example, the WSG-Faults affects flow (Buchan, 1938, fig. 4) and the Lea Valley Fault caused delayed responses to Crossrail dewatering across it (fig. 4.22; Bischoff et al., 2020b).

Published groundwater data and modelling outputs for the Lower Aquifer (table 6.3) were compared against fault positions to analyse their impact on its discontinuous hydrogeological behaviour.

Table 6.3 – Published Lower Aquifer hydrogeological outputs used for fault impact analyses.

Data	Data type	Source(s)
Water table readings from observation wells	Point cloud/CSV	Environment Agency (EA), provided by Lack (pers comms, 2020).
Regional groundwater level changes from 1997-2006	Map GeoTIFF georeferenced from Aldiss et al. (2014)	Environment Agency (EA) groundwater surfaces analysed by Aldiss et al. (2014)
Modelled low permeability barriers in the Lower Aquifer	Map GeoTIFF georeferenced from Lawrence and Black (2019)	Crossrail Environmental Statement (Crossrail, 2005); Lawrence and Black (2019)

6.1.3.1 Lower Aquifer groundwater changes: Observation water well analysis

Temporal changes in Lower Aquifer groundwater levels were analysed across East London (fig. 6.12) from 27 Environment Agency (EA) observation wells. These were undertaken relative to 2015 over 10-year and 25-year periods to minimise anthropogenic influences acting on the Aquifer.

Variation is inconsistently observed across faults and within blocks. Data analysis identified several wells undergoing artificial discharging simultaneous to the dates selected, undermining the long-term rationale. This assessment is considered inappropriate given overall well sparsity and unknown dewatering episodes conducted in London.

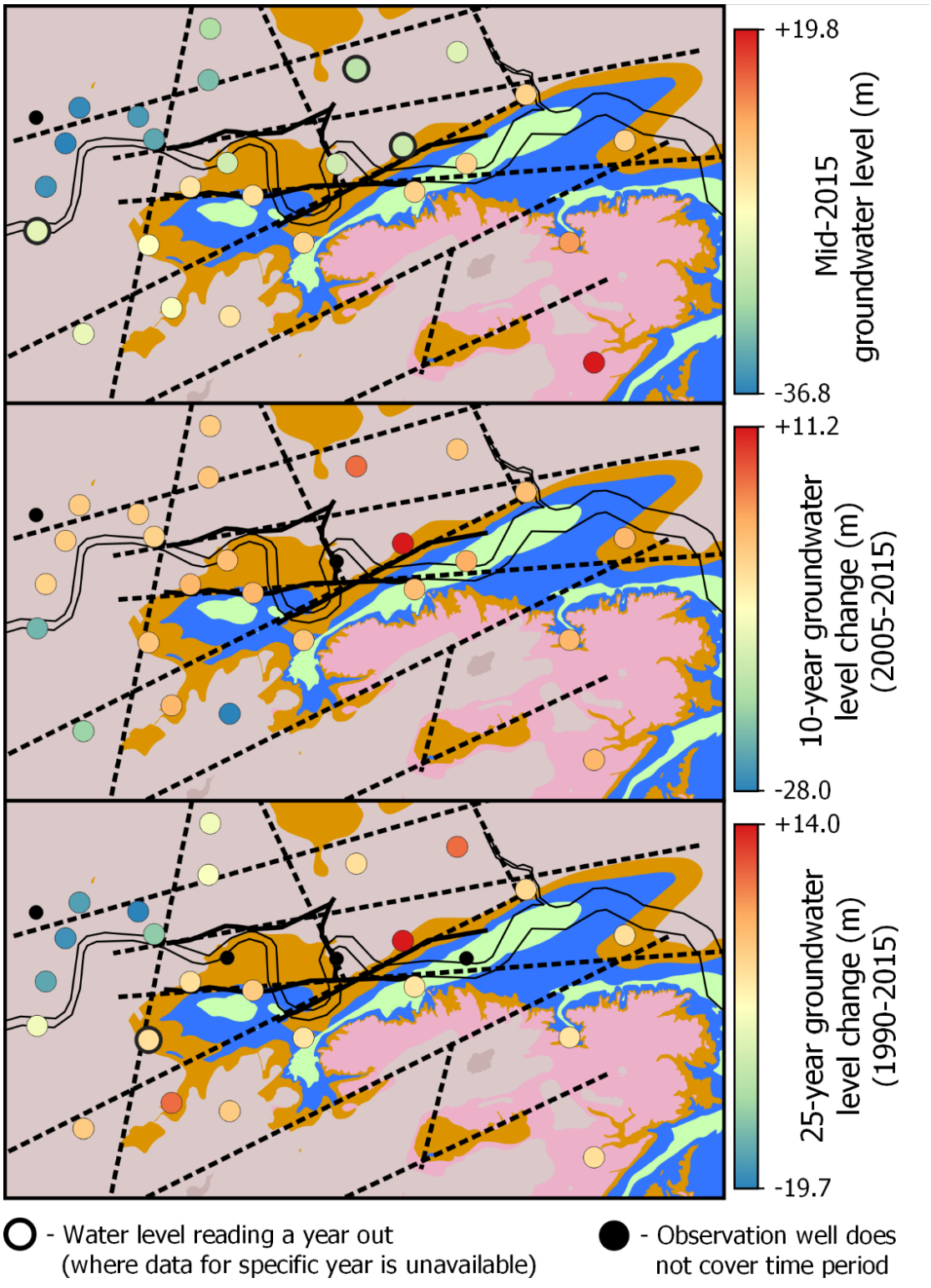

Figure 6.12 – Temporal analysis of Lower Aquifer groundwater level changes in 27 EA observation wells over 10- & 25-year periods were assessed relative to 2015. Measurement dates were selected as close to June 1st of each year as possible to minimise seasonal fluctuation, however, monitoring frequencies were inconsistent. When a specific year was unavailable, the nearest measurement was selected instead ('year out' readings have thicker rings).

6.1.3.2 Lower Aquifer ground water changes: Regional analysis

Aldiss et al. (2014) compared regional changes in the Lower Aquifer water table over a nine-year period (1997-2006) as part of their at-surface displacement analyses in London. They compared these with BGS 1:50k faults, suspected basement lineaments and known anthropogenic extraction[51] (fig. 6.13).

Faulting from this investigation was superimposed onto their results (fig. 6.13). The positions of several major faults correspond with differential groundwater level changes: an unnamed NNE-striking fault separates a major discharge-recharge contrast to the south and bounds an unchanged triangular region with the Lea Valley Fault. This fault and the Roding Valley Fault also partition the Stratford-East Ham depression (green ring). The ENE-striking faults that confine Block A (fig. 6.1) appear to bound a corresponding recharge zone. These demonstrate that certain major faults reduce Lower Aquifer connectivity to influence both natural and anthropogenic behaviour.

The coarseness of each pixel (~600 x 600 m) will amalgamate neighbouring readings into a grid, with Aldiss et al. (2014) considering the data resolution to be low. This may cause significant differences to be misaligned with faults and/or masked entirely.

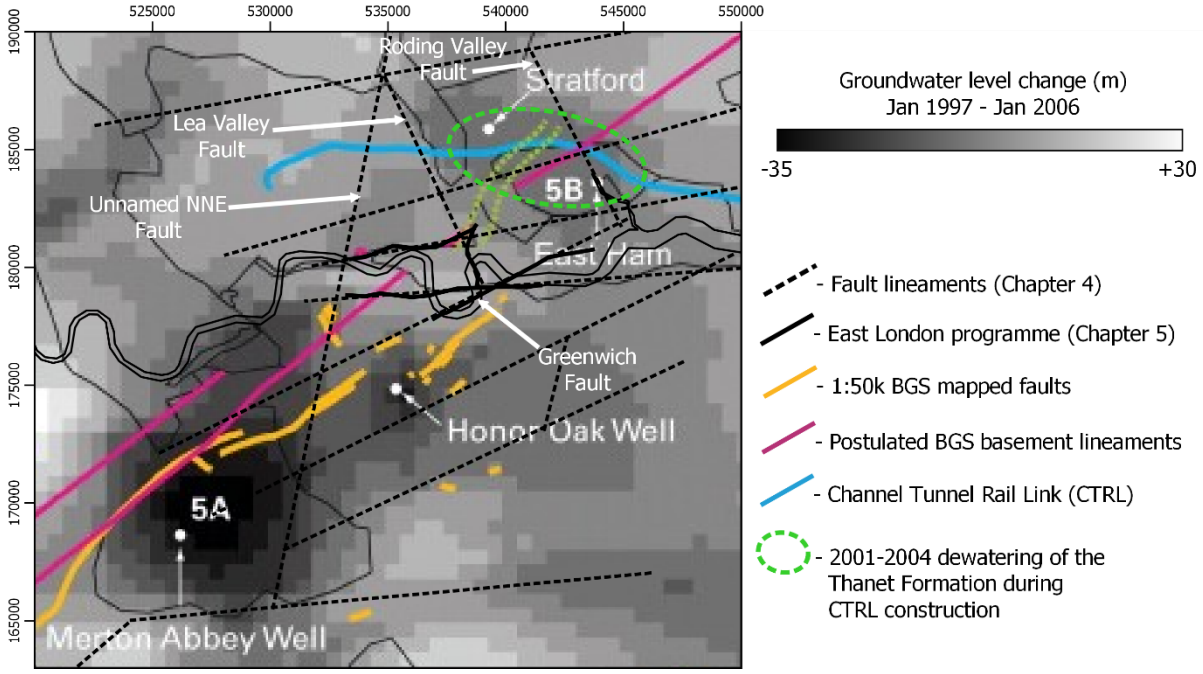

Figure 6.13 - Changes in regional Lower Aquifer groundwater levels from 1997-2006 by Aldiss et al. (2014) using EA groundwater data. The figure was georeferenced, with faults from this investigation (and the River Thames) superimposed. They determined that the Wimbledon Fault had a low permeability as it bounded and constrained dewatering in Merton, agreeing with Buchan (1938).

[51] Unlike the previous analysis, the BGS and EA were aware of artificial extraction occurring in London: irregular dewatering cones were identified in the Chalk in Merton and the Thanet Formation in Stratford-East Ham area.

6.1.3.3 Low permeability barriers: Groundwater flow modelling

Crossrail (2005) interpreted sublinear low permeability barriers in the Lower Aquifer that impede internal flow and connectivity using a modified version of the London Basin Groundwater Model (LBGM)[52]. Their trends are compatible with the major fault sets (§4.4.5): ENE, NNE, and NNW.

Barrier trends and positionings are spatially concordant with four major faults (fig. 6.14): the Greenwich Fault, the Northern Boundary Fault, an unnamed ENE-fault, and more tenuously it is coincident with either short BGS Lithoframe faults or an unnamed NNE-fault lineament. The latter barrier highlights the issues associated with interpreting gridded data.

The NNW barriers are likely unmapped members of the NNW-fault set due to their approximate coincidence[53] with the strike-slip Lea Valley and Roding Valley Fault lineaments. This implies that Lower Aquifer groundwater modelling may be a viable method for strike-slip fault identification in London.

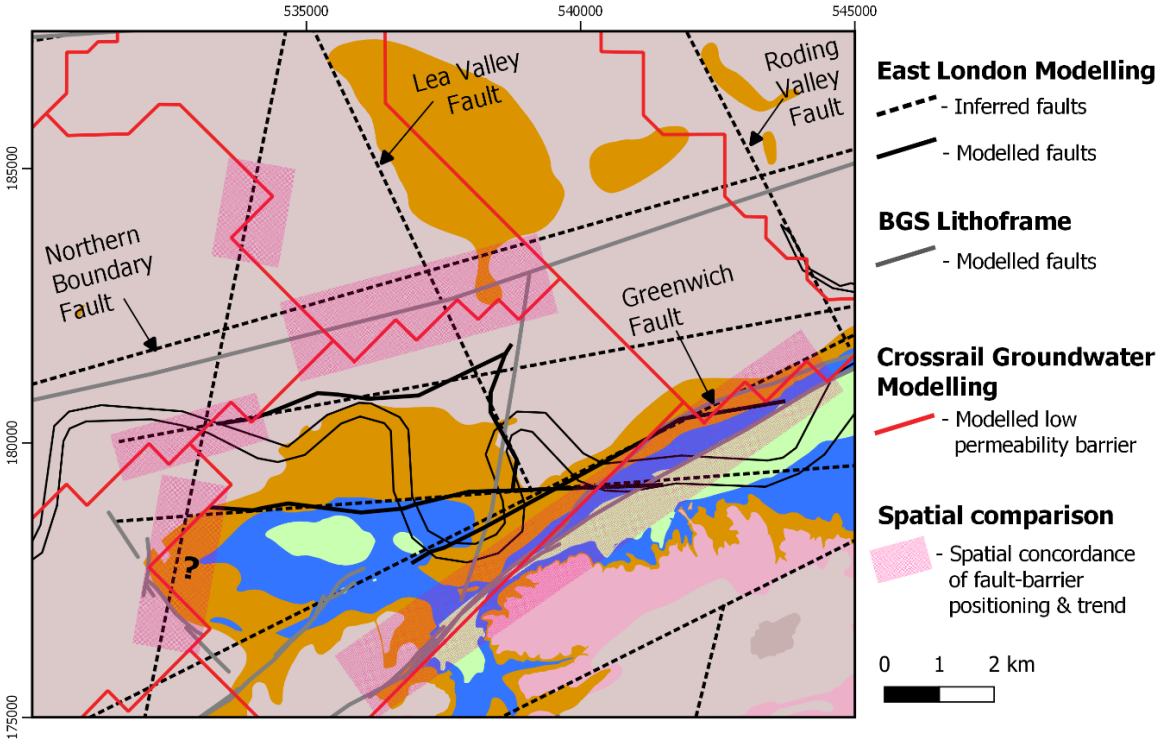

Figure 6.14 – Comparison of Lower Aquifer low permeability barriers with major faults in London. These barriers were georeferenced from Lawrence and Black (2019; fig. 6).

[52] The LBGM is gridded cell model for simulating ground water behaviour that was developed for Thames Water and the EA in 2000 and refined up to 2004. For Crossrail, it was coupled with new EA and Crossrail data.
[53] Poor correlation may reflect the model's actual data coverage locally, similar to figure 6.13.

6.1.3.4 The impact of aquifer lithologies and fault development on across-fault flow behaviour

The hydrogeological impact of major faults is highly inconsistent, some impede flow whilst others lack groundwater variation across them. This individualised impact on aquifer connectivity reflects three factors: materials-specific responses to faulting, differential shear behaviour between fault sets, and irregular aquifer water levels.

Groundwater flow and permeability in the Lower Aquifer depends on stratigraphical positioning between the fracture-driven chalk and the pore-driven Palaeogene sand (Thanet & Upnor Formations) portions. Both material groups respond differently to faulting to cause distinct across-fault flow behaviour. The chalk (a brittle weak rock) will develop a fault core. But their internal textures are inconsistent with both breccia- and gouge-dominated cores observed during borehole analysis (Chapter 5) and in proxy fault exposures (Tudor, 2019). These will cause distinct hydrogeological properties in the chalk: disaggregation will increase fault permeability by generating blocky textures, whilst comminution will decrease it by developing a fine-grained gouge. Comparatively, faulting in the Palaeogene portion will likely enhance permeability as dense sand shearing favours dilational grain reorganisation. However, reorganisation in the Thanet's lower clayey parts may favour gouge development instead to reduce flow. Both appear to be plausible as highly variable permeabilities have been documented within the Thanet Formation (Linney and Withers, 1998) proximal to major faults in East London.

Hydrogeological analyses indicate that the ENE- and NNW-striking fault sets broadly impede across-fault flow in the Lower Aquifer whilst the NNE-set have limited impact (excluding the WSG-Faults). The difference implies enhanced fault core development of the former two sets that likely reflects their specific propagation behaviours, architectures, and relative Alpine reshear favourability (§3.2, 3.3.2-3.3.3). Associated fault zones, (analysed in §6.2), indicate that both transpressive and transtensive stress conditions can locally occur around major faults. The former will confine voids to reduce flow, whilst the latter will cause dilational and open fractures and/or pore space; this may also explain variable fault core textures in the chalk.

The elevation of the Lower Aquifer water table is inconsistent (Environment Agency, 2018) causing variable stratigraphical positioning across London (chalk vs Palaeogene sands). When coupled with their differing shear responses, it is likely that higher water tables may locally mask the hydrogeological impact of faulting on aquifer connectivity in the chalk.

6.1.4 Assessing compartmentalisation

The spatial analyses demonstrate that inherited faults had regionalised influences on Palaeogene sedimentological and current aquifer behaviour to varying degrees. Localised block partitioning is less apparent overall but did influence some processes. Upon review, the influence of major faults on these processes was too minor to be described as 'compartmentalisation' since it did not control them.

The impact of syndepositional faulting was restricted to specific Eocene depositional environments (table 7.2) that were highly sensitive to topographic changes and caused variable thicknesses and facies distributions. This influence was principally regional and driven by individual faults (fig. 6.4) with localised block behaviour restricted to certain facies (fig. 6.6). The preferential influence on sensitive processes likely reflects their minor offsets (fig. 5.35) to overprint dominant sea level changes.

Fault-controlled denudation, attributed to the end-Pyrenean culmination, is evident as faults bound significant inliers (fig. 6.1) and between-block variation of London Clay Formation thicknesses (fig. 6.11). But the degree of structural influence prior to initial burial by later Eocene sediments was likely minor as denudation behaviour appears to be more variable within blocks than between them.

Discontinuous groundwater behaviour in the Lower Aquifer corresponds with some major faults. These impede across fault flow and aquifer connectivity whilst others do not, with block behaviour less apparent. This difference likely reflects both how faulting alters hydrogeological properties locally within different parts of the aquifer and the local water table relative to stratigraphy. The ENE- and NNW-striking fault sets are considered to have the most impact on aquifer connectivity.

6.1.4.1 The role of faulting: Regional vs. block behaviour

Inherited faults have caused discontinuous subsurface topography that varies at the regional-scale (fig. 6.3) and between individual blocks (e.g., fig. 5.28). The analyses demonstrate that major faults have also partitioned geological and hydrogeological processes. Fault compartmentalisation was and is primarily regionalised by several major faults. It is unclear if discrete block behaviour observed in East London is broadly representative as it is coincident with the complex, blocky 'structural culmination' (fig. 6.3 vs. 6.2) that demarcates distinct structural domains under London (fig. 2.31).

6.1.4.2 Validity of the analyses

The comparability of individual case studies may be questioned. Some were limited by coarse data granularity and/or coverage. Others were restricted by study area size, preventing scaled cross-comparisons of regional and localised behaviour. Despite this, the presence of demonstrable fault influences across a diverse range of evidence reinforces the argument rather than invalidating it.

6.2 Fault Zones

Kilometre-wide bands of extensive faulting that separate sub-horizontal, comparatively undeformed strata have been encountered across London by geotechnical and tunnelling projects (fig. 6.15, 2.28). These were termed as 'fault zones' by Newman (2009), and have been documented (table 6.4) since at least the 1970s (e.g., Thames Barrier site; Carter and Hart, 1977). Occasionally, they have also been referred to as 'fault complexes' when coincident with major faults.

The tectonic architectures, spatial coverage and origins of fault zones are unclear. Internal uplift and depression are both documented (fig. 6.16), with a lateral-slip component indicated from limited observations (table 6.4). A causal link with fault inheritance is suspected as many are spatially coincident with major faults and anticlinal inliers (fig. 6.1). Determination of 3D geometries and slip behaviour is however impeded by the majority of observations being restricted to cross-sections only.

The internal architecture(s) and spatial distribution of fault zones were characterised in §6.2 to assess their association with major faulting and to determine their formation mechanisms; with several case studies developed. A fault zone categorisation method was also proposed to improve their defining during ground investigations (GIs). Individual fault zones are referred to by their acronyms in §6.2, as outlined in table 6.4.

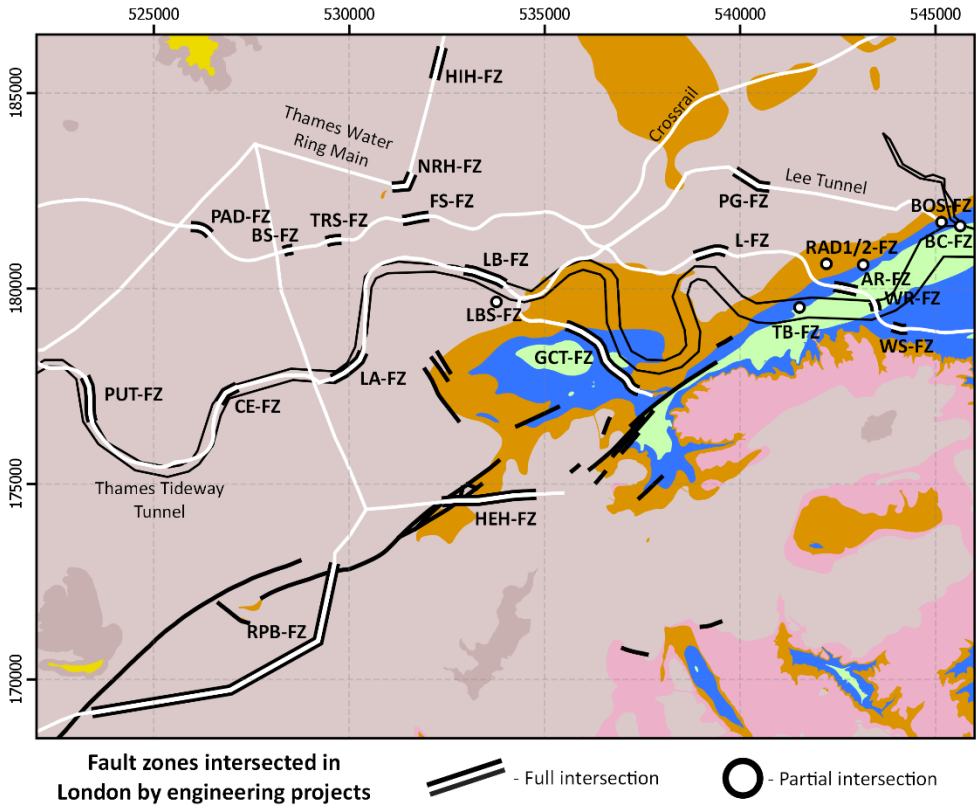

Figure 6.15 – Fault zones in London, partly or fully, intersected by engineering projects (table 6.4), overlain onto BGS 1:50k geological map. Recent major tunnelling projects are presented as white lines. Fault zone positions were georeferenced and are approximate.

Fault Zone	Code	Proximal major structures	Internal Displacement		Project	Source
			Vertical [e]	Lateral		
Thames Barrier	TB-FZ	Greenwich Anticline	Ascending [I]	Y	Thames Barrier	Carter and Hart (1977)
Barking Creek	BC-FZ	Greenwich Fault	Ascending or Stepped [B]	-	Barking Creek Tidal Barrier	Kirkpatrick and McCann (1984)
London Bridge Station	LBS-FZ	Fault AF	Descending [C]	-	Jubilee Line Extension	Page (1995), Black (2017)
Herne Hill	HEH-FZ	Wimbledon-Streatham Faults	Ascending [C]	-	Thames Water Ring Main (TWRM)	Newman (2009), Newman et al. (2010), Newman and Wong (2011)
Raynes Park-Brixton [a,b]	RPB-FZ		Unclear [B]			
New River Head	NRH-FZ	-	Descending [C]			
Highbury Hill	HIH-FZ	-	Descending [C]			
Plaistow Graben	LG-FZ	Plaistow Graben	Descending [C]	-	Lee Tunnel	Newman (2008), Mortimore et al. (2011), Bellhouse et al. (2015), Newman et al. (2016),
Beckton Overflow Shaft [d]	BOS-FZ	Greenwich Fault	Ascending or Stepped [B]	Y [f]		
Paddington	PAD-FZ	Unnamed NNE-fault (Lithoframe)	Stepped [C]	-	Crossrail	General: Lawrence and Black (2019), Black (2017), Crossrail (2016, 2012) WR-FZ: Lenham et al. (2006), L-FZ: Linde-Arias et al. (2018) FS-FZ: Aldiss et al. (2012)
Bond Street	BS-FZ	Northern Boundary Fault	Unclear [C]	-		
Tottenham Court Road	TCR-FZ		Neutral [C]	-		
Farringdon Station	FS-FZ		Stepped [C]	-		
Limmo	L-FZ	Plaistow Graben. Fault DE.	Descending [C]	-		
Albert Road	AR-FZ	Greenwich Fault	Stepped [B]	-		
Woolwich Reach	WR-FZ	Greenwich Anticline	Unclear. [C]	-		
Woolwich Station	WS-FZ		Neutral [C]	-		
Greenwich Connection Tunnel	GCT-FZ	Millwall Anticline /Greenwich Fault	Ascending [C]	Y [c]	Thames Tideway Tunnel (TTT)	Newman (2017) GCT-FZ: Newman (2017), East London modelling programme.
London Bridge	LB-FZ	Fault AF	Descending [C]	-		
Putney	PUT-FZ	-	Stepped [C]	-		
Lambeth Anticline	LA-FZ	-	Ascending [C]	-		
Chelsea Embankment	CE-FZ	-	Ascending [C]	-		

Table 6.4 (previous page) – Overview of fault zones (FZ) in London, including internal characterisation, proximity to major structures, and their associated sources. Additional fault zones have not been documented as their positions are unknown (such as those in Newman et al. (2013)).
[a] Published interpretations of the RPB-FZ do not display faulting throughout. However, it is interpreted to be a fault zone due to significant elevation changes internally and the presence of extensive faulting at Tooting Bec (Newman, 2009, fig. 12) along the tunnel alignment.
[b] Analysis of the RPB-FZ is limited by both the intersecting doglegged tunnel alignment providing an inconsistent orientation of its internal geometry, and the separation of this FZ across two sections with inconsistent vertical exaggerations. However, it appears to be ascending.
[c] Lateral shearing was observed during excavation of the Greenwich Shaft for the TTT project and is situated immediately south of the GCT-FZ.
[d] In literature, the BOS-FZ is referred to as the 'Greenwich Fault Zone' as it is coincident with the Greenwich Fault. It has been renamed according to its location instead to avoid confusion as other fault zones have also been identified proximal to the Greenwich Fault and/or within the Greenwich Anticline. The Greenwich Fault Zone may be a more appropriate term for the "anticline" itself.
[e] Refer to §6.2.1.3 for categorisation of fault zones according to their vertical displacement.
[f] Oblique striations were observed in chalk core extracted near the BOS-FZ (Mortimore et al., 2011, fig. 12).

6.2.1 Structural characterisation

Schultz and Fossen (2008) define 'fault zones' as a series of sub-parallel or anastomosing shears confining deformation between two bounding planes within a fault core. In London, Newman (2009) introduced the term to describe a "*a series of* [faulted] *blocks over a zone several hundred metres in width*" following multiple intersections by TWRM tunnelling. The applicability of this term was reviewed following characterisation.

Characterisation of individual fault zones is limited by the structural information available from their respective ground investigations. The majority of fault zones observations are restricted to vertical cross-sections only (fig. 6.16), with very limited information available (and accessible) regarding fault strikes and lateral-slip behaviour internally (table 6.5). Furthermore, most fault zone observations represent incomplete intersections of only interiors and/or a single bounding fault.

To overcome this, disparate fault zone observations were collated (§6.2.1.1, table 6.4) and analysed in unison to determine characteristic features of their internal architecture(s) and slip behaviour (§6.2.1.2). These were mainly sourced from pre-defined fault zones, but several additional ones were identified by this investigation based on:

- Observations of characteristic fault zone features that predate the term's introduction in London (BC-FZ & TB-FZ) were updated.
- Structures identified by Crossrail (2012) that were originally described as "*zones of faulting/folding*". Black (2017) updated most to fault zone, however, these were individually re-assessed as this analysis primarily relied upon the former source.

Following this characterisation, a new nomenclature was developed for the geotechnical community to categorise them from the minimal information typically available (§6.2.1.3).

6.2.1.1 Fault zone internal observations

Cross-sectional analysis consistently demonstrates that fault zones are comprised of multiple faults and their blocked strata confined between two bounding faults (fig. 6.16). Zones up to 3 km wide have been identified, yet these may not have been measured normal to the bounding faults.

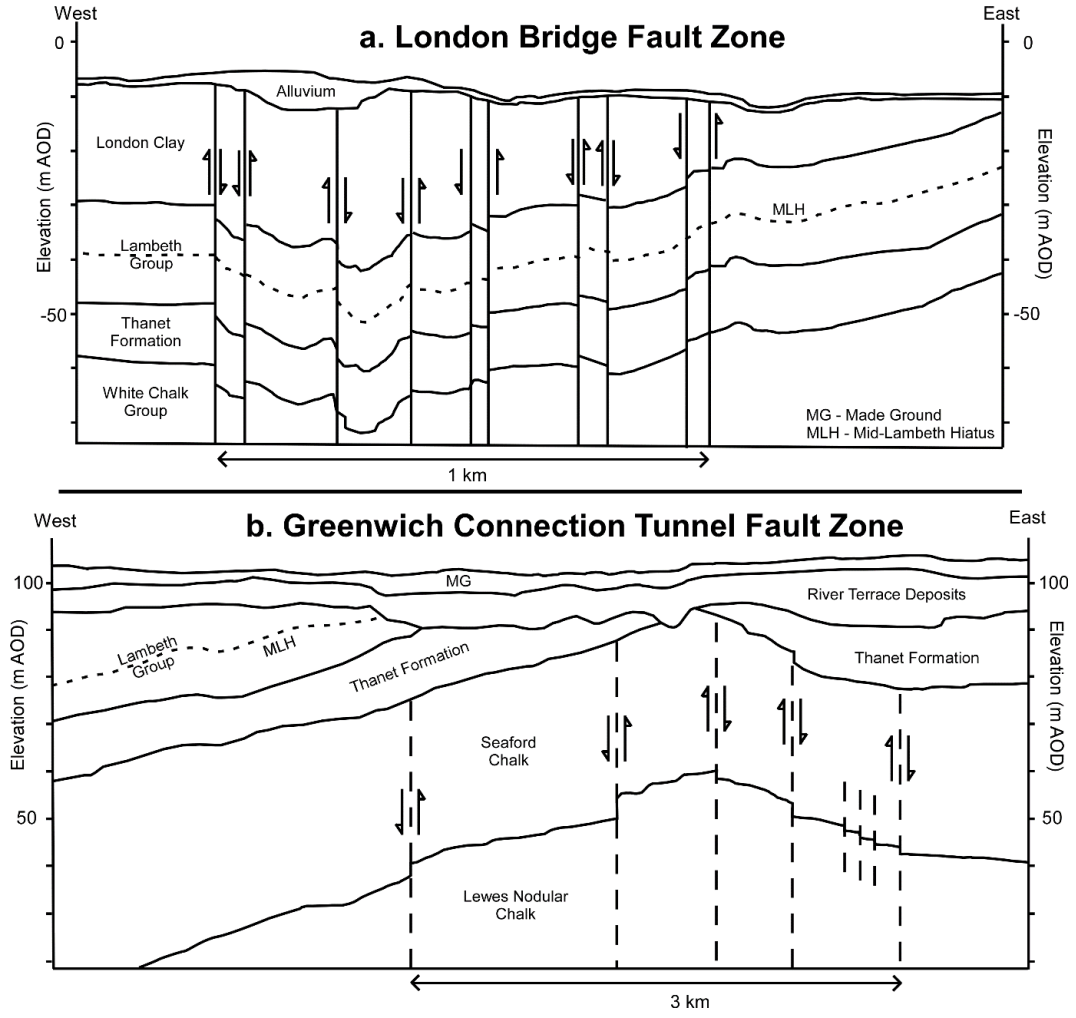

Figure 6.16 – Examples of the dominant types of fault zones observed where displacement increases towards their centres. Refer to figure 6.15 for their locations. Adapted from Newman (2017).
a. The London Bridge Fault Zone (LB-FZ), characterised by progressive downthrowing internally.
b. The Greenwich Connect Tunnel Fault Zone (GCT-FZ) which uplifts towards its centre.

The bounding and internal faults of fault zones have subvertical to steeply inclined dips according to limited exposures (Newman, pers comms, 2019b) and seismic surveying[54] along the Thames Tunnel alignment (Thames Water, 2009). However, they are consistently idealised as vertical in-section by ground investigations. Fault zone interiors are comprised of multiple fault sets (table 6.5; fig. 6.17, 4.13) rather than shears parallel to the bounding faults, with no consistent sets determinable between them from the limited data available.

[54] Based on visual analysis of a 1:20 vertically exaggerated seismic section, as inclinations were not quantified.

All fault zones display vertical displacement internally with the majority characterised by net uplift or downthrow towards their centres (fig. 6.16; table 6.4). However, additional in-section geometries are also documented. Some fault zones have increased displacement directed from one bounding fault to the other ('stepped', fig. 3.38, 6.18), and (where coincident with major faults) straddle the margins of differently elevated blocks. Others are 'neutral' and have no net vertical displacement internally[55]; it is unclear if these are natural or caused by oblique fault zone intersections during GIs.

Evidence of lateral-slip behaviour is limited to two fault zones (table 6.5) but where observed it implies transpressive stress conditions internally. The TB-FZ is a fault zone interior comprised of EEN- and *en échelon* NNE-trending fault sets (fig. 6.17). Carter and Hart (1977) identified that the latter *en échelon* faults were lateral-slip dominant and characterised as dextral following a highly detailed site investigation, with two very minor folding axes observed oblique to their trend.

Table 6.5 – Fault zones where strikes and lateral-slip behaviour were determined during this analysis. Refer to table 6.4 and figure 6.15 for names, locations, and sources of specific fault zones. Thames Tideway may have analysed lateral slip also (Hadlow, pers comms, 2020), but this was not accessible during the investigation. [a] Fault strikes were measured from maps specific to each fault zone and are approximate (±10°). [b] Exposure at the Greenwich Shaft (fig. 6.19; Newman, pers comms, 2019b), within Streatham-Greenwich Faults overlap.

Fault Zone Code	Fault strikes		Lateral slip	Vertical slip internally
	Observations	Measured (°) [a]		
TB-FZ	Yes	078 010-018 (curving to 176 once)	Yes	Uplift towards centre
FS-FZ	Yes	063 162 355-010	-	Uplift towards the West
WR-FZ	Yes	120-140 080-096	-	Unclear
WSG-Faults [b]	Yes	020-025 358-006	Yes	-
BOS-FZ	Yes	-	Oblique striations in core	

Strike-slip, reverse and normal faulting were documented in chalk exposures (fig. 6.19) at the TTT Greenwich and Deptford Shafts. Both sites are situated within the overlap of the Streatham-Greenwich Faults (fig. 6.1) and are proximal to the GCT-FZ (fig. 6.16.b). The former two fault styles have pronounced slickensided surfaces with the strike-slip fault most developed, whilst normal faults were comparatively under-developed yet more frequent. Tectonic and syndepositional origins are interpreted respectively from comparative fault plane development (fig. 6.19), indicating oblique stress conditions locally. No thrusting was observed. Oblique stress conditions are also indicated near the BOS-FZ by oblique striations observed in chalk core (Mortimore et al., 2011, fig. 12).

[55] No neutral fault zones are presented due to confidentiality reasons. For reference example, see figure 6.20.

Bounded strata within fault zones have also undergone extensive brittle deformation, with increased jointing and mechanical degradation both observed (Linde-Arias et al., 2018, Newman, 2009). These blocks vary from sub-horizontal to inclined strata in-section (fig. 6.16), with minor fold axes observed sub-perpendicular to fault strikes (fig. 6.17). Collectively, these imply differential degrees of oblique-slip behaviour between faults to induce variable lateral shortening and block rotation internally.

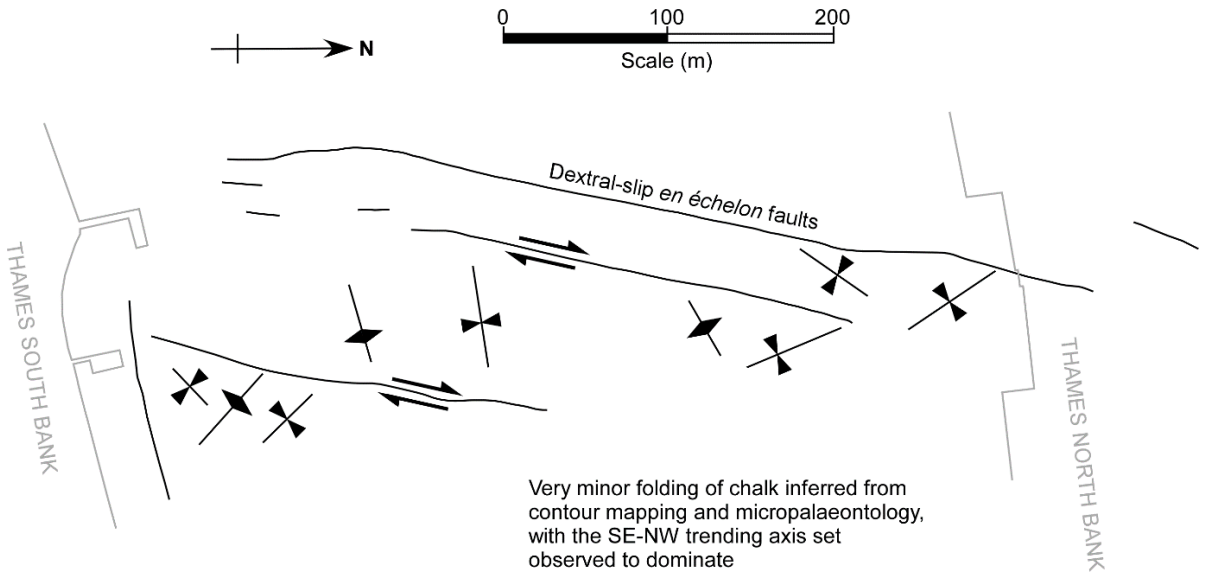

Figure 6.17 - Plan view of Thames Barrier Fault Zone (TB-FZ), adapted from Carter and Hart (1977), who identified a series of dextral slip NNE-trending *en échelon* faults and two minor folding sets onsite through a combination of contour mapping, micropalaeontology and geophysics. The geometric arrangement is comparable with a shear zone, with evidence of lateral shortening between the dextral-slip dominant *en échelon* faults and minor folding imply transpressive stress conditions internally.

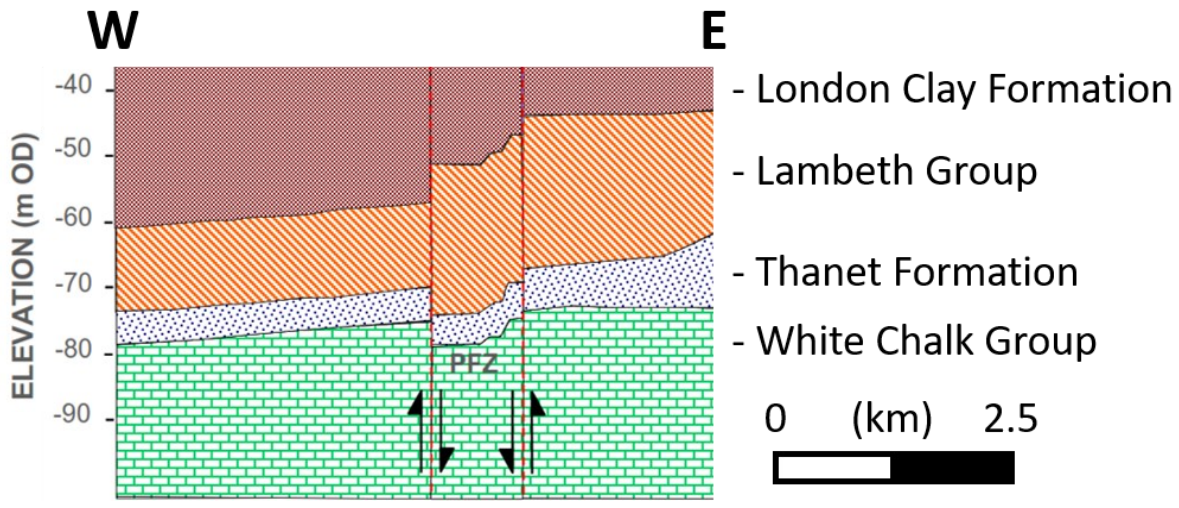

Figure 6.18 – Putney Fault Zone (PUT-FZ), an example of stepped displacement across the fault zone, bounded by strata of differing elevations (internal faults undefined). Adapted from Newman (2017).

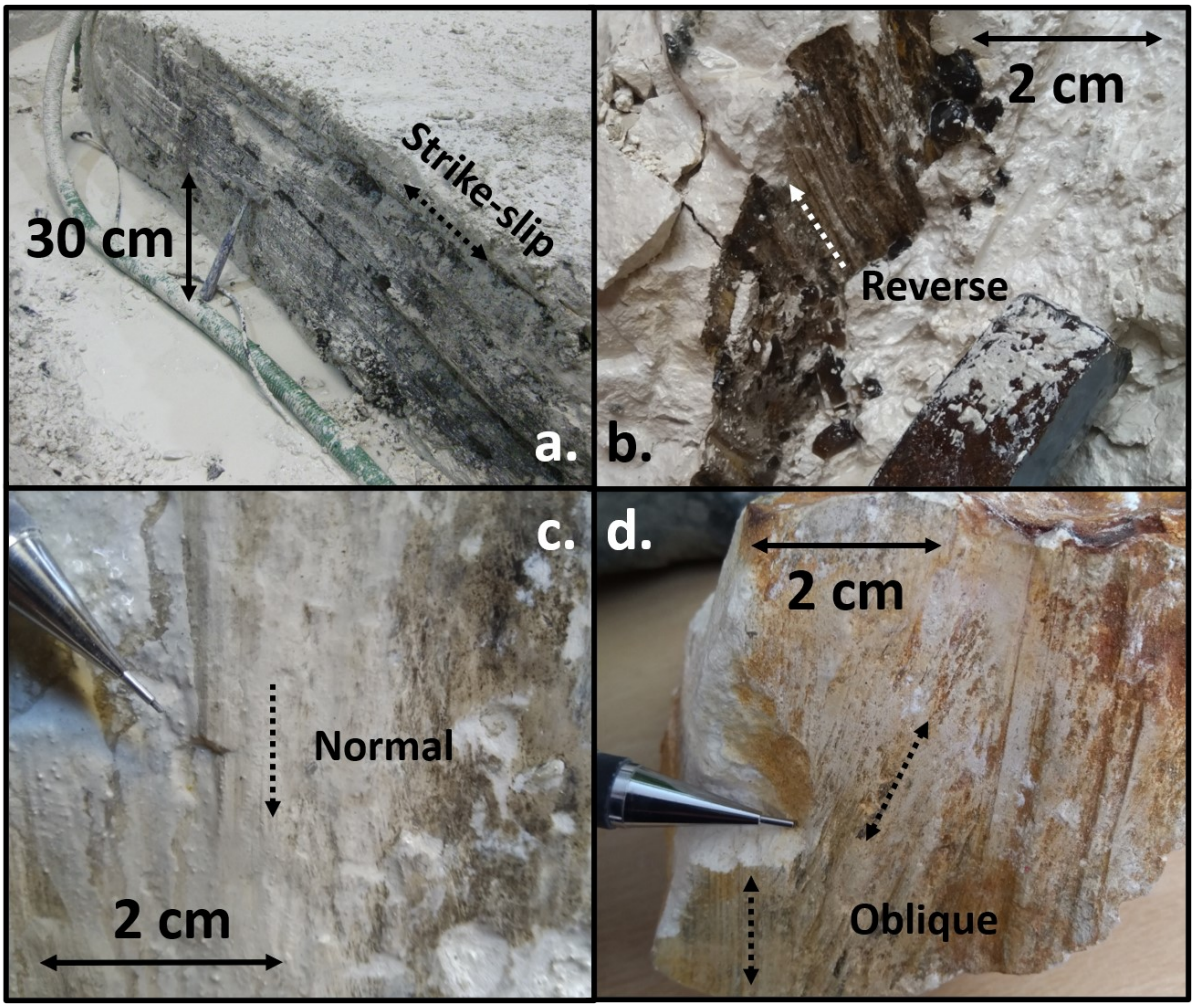

Figure 6.19 – Slickensided fault planes observed within the chalk at the TTT Greenwich and Deptford Shafts (table 6.5). These shafts are situated within the Streatham-Greenwich Fault overlap, and are proximal to the GCT-FZ. Dip-slip styles were determined from slickenside steps. Comparative analysis of fault plane development demonstrates that strike- and reverse-slip faults are both well-developed, with normal faults under-developed (yet more frequent). (Dip/Dip Azimuth)
a) Clay-smeared strike-slip fault (68°/098°). Greenwich Shaft (19/09/2019): Newman (2019b, pers comms).
b) Corrugated reversed fault (85°/289°). Deptford Shaft (03/04/2019): Tom Morgan
c) Normal fault (45° (likely steeper)/156°). Deptford Shaft (20/06/2019): Tom Morgan
d) Evidence of oblique- and dip-slip on a corrugated fault plane. Sample from the Deptford Shaft collected by Tim Newman, photo by Tom Morgan (20/06/2019).

6.2.1.2 Fault zone characterisation

London's fault zones are comprised of multiple subvertical-to-steeply inclined fault sets and brittlely deformed strata within a confined band. All fault zones display vertical displacement of varying styles and magnitudes, indicative of compressional or extensional conditions internally. However, these represent a minor component of the stress axis. Internal displacement is characterised by lateral-dominant oblique-slip according to site-scale analysis (fig. 6.17), relative slickenside development (fig. 6.19) and a lack of shortening or extensional features parallel to bounding faults. This oblique stress axes must be confined by the bounding faults to cause both these shearing arrangements and discretised block deformation. Therefore, both transpressive and transtensive stress axes must have been achievable internally to respectively cause uplift and downthrow (fig. 6.16).

Collectively, these features are characteristic of confined Riedel shear zones where stresses are locally concentrated oblique to the acting stress axis by shearing of the bounding faults (Mandl, 2000, fig. 8.19). Fault zones cannot be attributed to a single shear zone mechanism as their internal architectures and associated stress conditions (transtensive vs. transpressive) are too variable. But the prerequisite of bounding shears implies a genetic association with London's major faults.

Upon review, Newman's (2009) usage of 'fault zone' may be applicable for describing these shear zones as they geometrically represent confined bands of brittle shearing between two bounding planes. This is loosely compatible with Schultz and Fossen's (2008) definition, but the differences in scale (fault core vs. km-wide zones), lack of sub-parallel shearing internally and differing formation mechanisms should be recognised. The term should only be used descriptively to highlight shear zone intersection (and prevent misinterpretation as an individual fault interior as originally intended (i.e., fig. 3.10)). Alternatively, it may be appropriate to define them as 'fault complexes' to avoid any potential ambiguity.

6.2.1.3 Categorisation of fault zones

The degree of characterisation in §6.2.1 is unlikely to be achieved during an individual GI as their analyses are generally restricted to cross-sections. A categorisation system for fault zones (or 'complexes') is introduced that defines them according to their internal vertical displacement (fig. 6.20). This will allow the geotechnical community to characterise and communicate them without knowing their internal 3D architectures. Fault zones have been categorised into four types[56]:

- Ascending fault zone – Characterised by internal uplift relative to unfaulted surroundings. Example: GCT-FZ (fig. 6.16.b)
- Descending fault zone – Characterised by internal downthrow relative to unfaulted surroundings. Example: PG-FZ (fig. 3.28); LB-FZ (fig. 6.16.a)
- Neutral fault zone – Characterised a lack of dominating vertical slip behaviour internally.
- Stepped fault zone – Characterised by progressive change in elevation across the structure. Example: BOS-FZ (fig. 3.38); PUT-FZ (fig. 6.18)

A secondary code was developed to clarify the extent of the fault zone analysed (fig. 6.20) to prevent potential structural misinterpretation, as most were not fully intersected: 'Complete' [C] or partial intersection, with the latter subdivided into 'Border' [B] or 'Interior only' [I] to reflect whether this incomplete assessment includes a bounding fault or not.

The terms were retroactively applied to all fault zones analysed (table 6.4). Given the limited perspective, the terms should not be treated as structural terminology representative of the structure but provides a basis for future analysis, e.g., distinguishing transpressive and transtensive conditions.

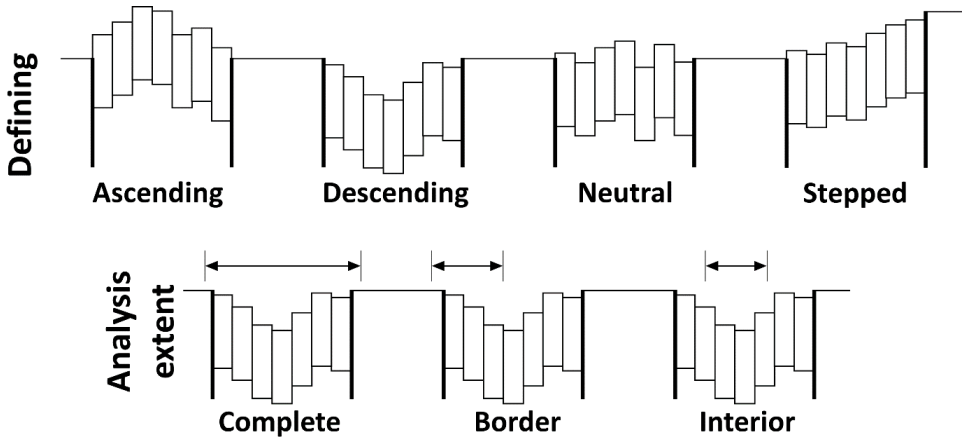

Figure 6.20 – Fault zone categorisation according to internal vertical offset and the proportion of the structure analysed. The former provides a method to define fault zones in section, whilst the latter highlights whether the interpretation reflects complete or incomplete assessment of the zone. Refer to table 6.4 for its application.

[56] 'Ascending' and 'descending' have replaced 'positive' and 'negative' used in Morgan et al. (2020) to avoid potential confusion and association with flower structures, a specific type of inherited shear zone structure.

6.2.2 Spatial distribution and relationship to major faults

The spatial geometries and extents of individual fault zones are unknown as they have been incompletely defined from linear intersections and/or localised surveys (fig. 6.15). Some are likely part of the same shear zone due to proximity (e.g., LB-FZ & LBS-FZ), whilst others are solitary. However, this lacks consideration of London's structural fabric.

A causal association with major faults is indicated when compared (fig. 6.22) as fault zones are spatially coincident where mapped. Several fault zones are also coincident with elongate, fault-bounded inliers historically interpreted as anticlines (e.g., Millwall Anticline, fig. 6.1, vs. GCT-FZ, fig. 6.16.b) and indicate that some shear zones are laterally extensive and misinterpreted.

The coincidence implies that isolated fault zones may therefore provide evidence of unmapped major faults in London. For example, westward extrapolation of the ENE-striking fault (that bounds the Millwall Anticline) will be proximal to the PUT-FZ, CE-FZ and LA-FZ.

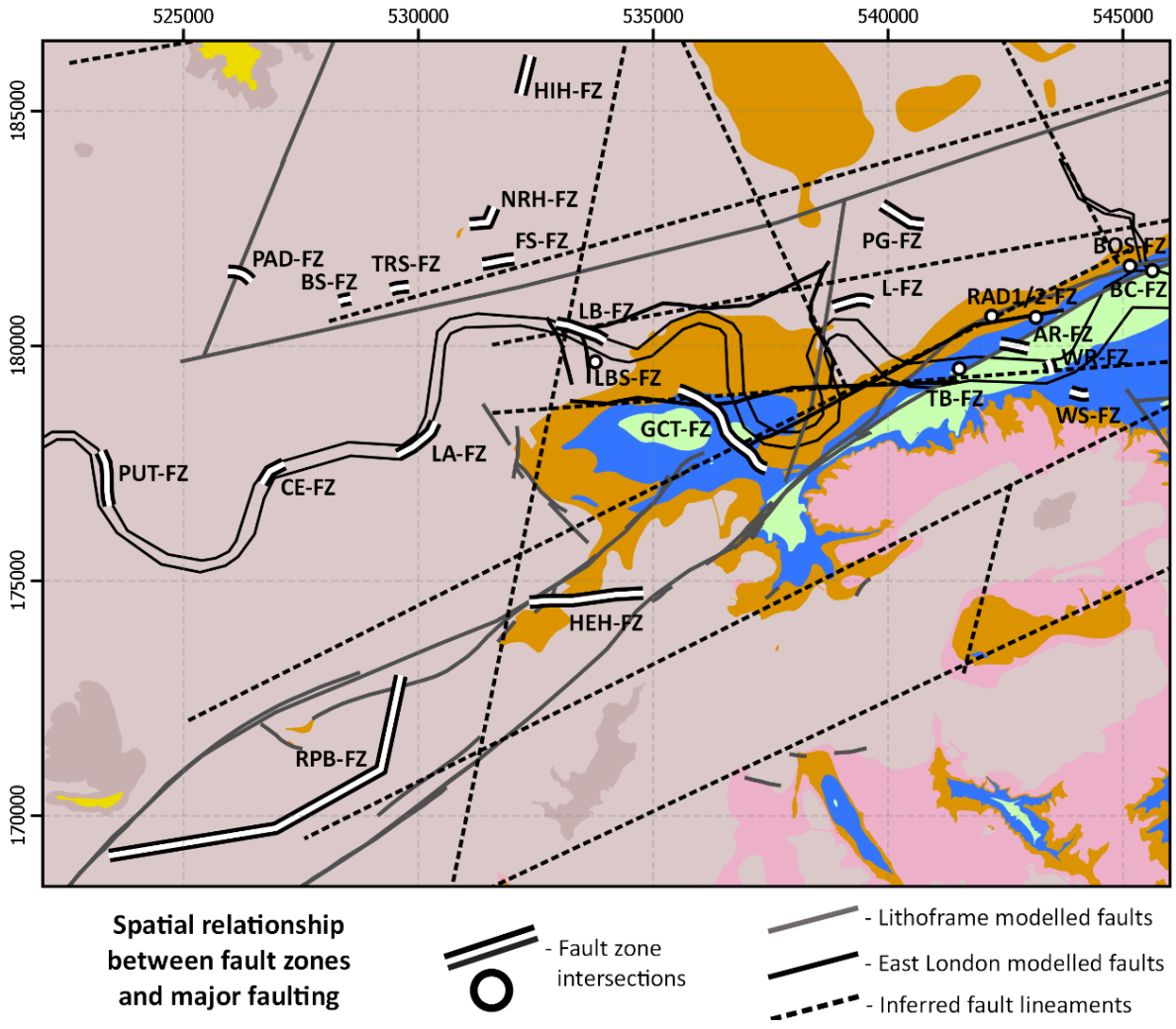

Figure 6.21 – Spatial comparison of documented fault zone positions (table 6.4) and major faulting from the BGS Lithoframe and this investigation. Refer to figure 6.1 for named major faults.

6.2.3 Formation mechanisms

A confined brittle shear zone internally characterised by oblique stress conditions may be generated in multiple ways, with fault zones reflecting their intersections. Direct Alpine stress magnitudes were likely insufficient (§3.4) to generate these fault zones since their scales and internal architectures imply significant shear stress concentration. Instead, brittle shear zones are associated with fault inheritance in London since spatially coincident major faults provide the prerequisite confining shears and are already recognised to produce them (§3.3).

Major faults are interpreted to generate shear zones in London through two processes: Firstly, through interaction and linkage of proximal faults to locally distort and concentrate the stress axis; secondly, by concentrating shear stresses within blocks they bound, causing internalised deformation through confined rotation and progressive shearing. Three mechanisms are proposed to induce these processes through the interaction and/or intersection London's three *en échelon* inherited fault sets:

- Within-set linkage
  Interaction and linkage of inherited *en échelon* shears from the same fault set will develop secondary Riedel shears between them and form linkage zones (fig. 3.32, 3.34). Dominant slip behaviour of the major faults will control the internal architectures: Lateral-slip will favour transpressive or transtensive interiors (fig. 3.36) whilst relay structures will develop along dip-slip dominant faults (fig. 3.32).
- Between-set linkage
  Stresses will become locally distorted and concentrate where London's three fault sets intersect to generate structures to accommodate this. Local stress conditions will be unpredictable as each interaction will be unique, depending upon the relative orientations and slip behaviour of the faults interacting.
- Confined block rotation
  Differential shear behaviour between block-bounding faults will cause internalised shear strains to develop as confinement inhibits translational and/or rigid rotational responses.

Structural analyses of the WSG-Faults and the Millwall Anticline provide respective case studies of within-set linkage (§6.2.3.1) and confined block rotation (§6.2.3.2) mechanisms. These are followed by a discussion regarding the applicability of these mechanisms to minor shear zones in London (§6.2.3.3), potential causes of transtension (§6.2.3.4) and the prevalence of block rotation (§6.2.3.5).

6.2.3.1 Within-set linkage: Wimbledon-Streatham-Greenwich Fault System

The Wimbledon-Streatham-Greenwich Fault System (WSG-Faults) were determined to be a series of overlapping *en échelon* sinistral-slip Riedel shears inherited from an underlying NNE-striking Variscan sinistral strike-slip fault (§3.3.3). Transpressive linkage was interpreted where they overlapped since multiple fault zones (fig. 3.37) are coincident with confined chalk uplift (fig. 3.39). The WSG-Faults were compared with fault zone characterisation (§6.2.1.2), the East London programme (Chapter 5), the indirect fault map (Chapter 4), and kinematic analyses to appraise this interpretation (table 6.6).

These linkage products are shown to have fault-controlled, uplifted interiors since fault zones consistently rise towards the centres of the *en échelon* overlaps (fig. 6.22). This is further evidenced by Section G_INTERIOR_1, which intersects the Greenwich Anticline sub-perpendicular to its perceived axial trace (fig. 6.23), with uplift towards the centre of the inlier along its elongate axis also.

Transpressive stress conditions are evidenced within two linkage zones along the WSG-Faults (table 6.6), with the TB-FZ demonstrating Riedel shear zone development within the Greenwich Anticline. Its *en échelon* geometries and dextral-slip dominant oblique shearing (fig. 6.17) are compatible with confined Riedel shear development within a sinistral shear zone (fig. 6.24.a-b) (Mandl, 2000). Both bounding and internal shear behaviours are consistent with the respective WSG-Faults and TB-FZ Riedel shears when realigned parallel to them (fig. 6.24.c). This confirms that these linkage zones are confined transpressive brittle shear zones comprised of second-order Riedel shears generated by linkage of *en échelon* inherited faults of the same (first-order Riedel shear) set.

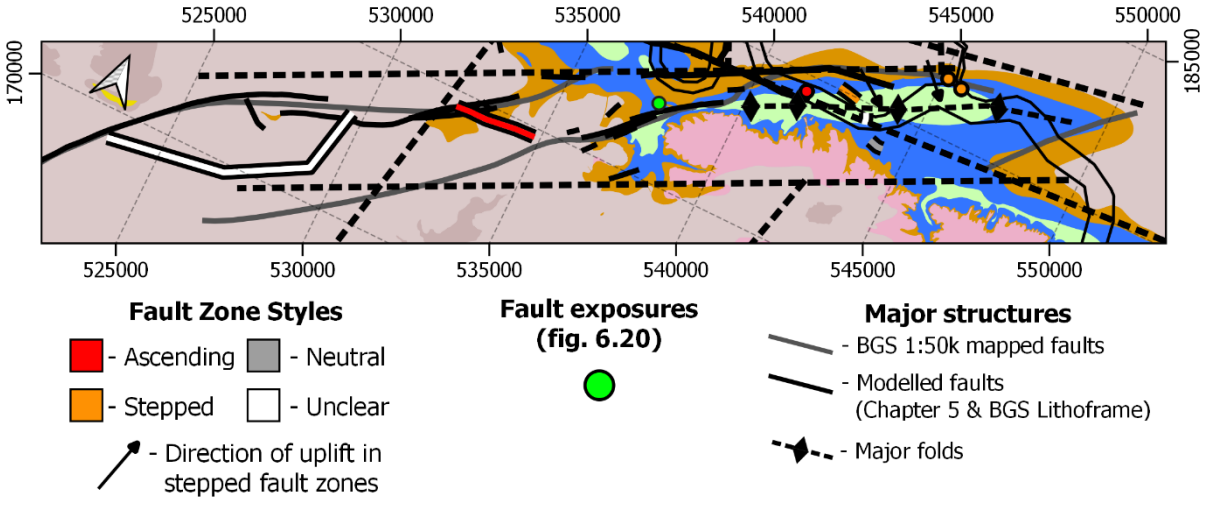

Figure 6.22 – Fault zone (colourised by style, fig. 6.20) coincident with the overlapping of the *en échelon* Wimbledon-Streatham-Greenwich Fault System (WSG-Faults) imply that linkage zones are characterised by brittle deformation and uplift internally.

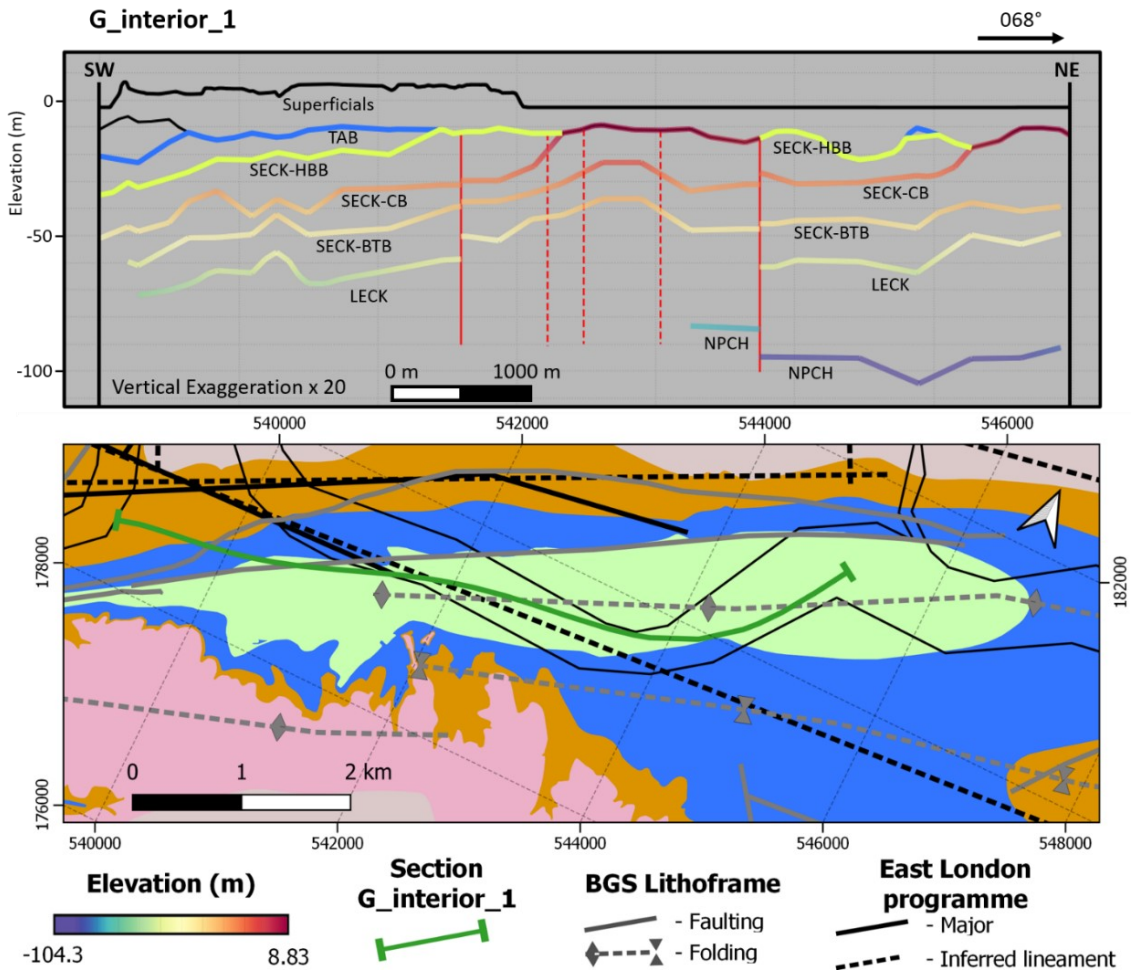

Figure 6.23 – Section G_interior_1 intersects the Greenwich Anticline parallel to its elongate axis. Elevational analysis of the lower members of the Seaford, Lewes Nodular and New Pit Chalk Formations demonstrate fault-controlled uplift internally (this was only part-defined during explicit modelling due to data coverage).

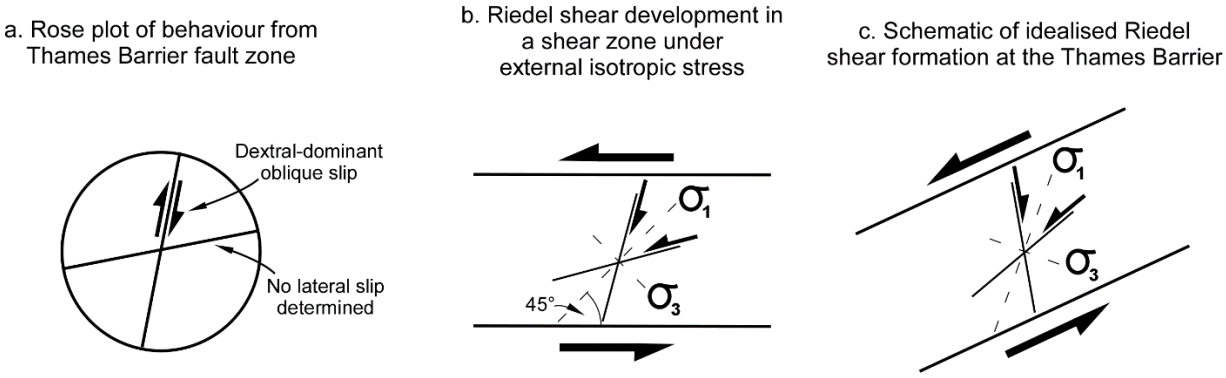

Figure 6.24 – Comparison of fault geometry and slip behaviour at the TB-FZ with known Riedel shear development under sinistral shearing (as determined for the right-stepping WSG-Faults). The comparability implies that linkage zones between the WSG-Faults are Riedel shear zones generated by sinistral shearing of these confining major *en échelon* faults.
a. Rose plot and slip behaviour of fault sets at the TB-FZ (fig. 6.17).
b. Idealised Riedel shear development within a sinistral shear zone when exerted to an external isotropic stress axis aligned parallel and perpendicular to the structure. Adapted from Mandl (2000).
c. Realignment of the sinistral shear zone parallel to the Greenwich Fault strike (~065°) produces comparable Riedel shear orientations and slip behaviour to the TB-FZ.

Table 6.6 – Structural observations and interpretations at points of overlap between individual faults along the *en échelon* WSG-Faults used to appraise transpressive shear zone development through Riedel shear linkage. [a] Assigned in §2.2.2.2 to the unnamed BGS 1:250k fault that bounds the inlier's eastern margin.

Fault overlaps along the WSG-Faults	Fault zones (fig. 7.31)	Internal uplift evidence		Internal stress conditions
Dagenham [a]-Greenwich Faults (Greenwich Anticline)	TB-FZ, AR-FZ, WR-FZ, WS-FZ, BOS-FZ, BC-FZ	Fault zone styles (fig. 6.22)	Section G_interior_1 (fig. 6.23)	Transpressive (TB-FZ; fig. 6.17, 6.24)
Greenwich-Streatham Faults	HEH-FZ		Chalk surface elevation (fig. 3.39)	Transpressive (TTT shafts; fig. 6.19)
Streatham-Wimbledon Faults	RPB-FZ	Davis (1928) (fig. 4.3)		Undetermined

6.2.3.2 Fault-bounded block deformation: Millwall Anticline

The triangular Millwall Anticline inlier (fig. 6.1) was historically attributed to folding despite its geometry and short-lived axis. Fault-driven uplift internally is interpreted by both the East London programme (fig. 5.45) and TTT (GCT-FZ, fig. 6.16.b). Transpressive stress conditions are indicated by proximal shaft exposures (fig. 6.19) but are unvalidated internally. The inlier is bounded by three faults: Fault AB, the WSG-Faults, and an unnamed NE-striking fault lineament (fig. 6.25.a).

The Millwall Anticline likely deformed internally as a discrete block since its fault-bounded geometry invalidates both within- and between-fault linkage. Prior to deformation, the block's lateral confinement inhibited rigid block translation or rotation to accommodate strains generated by Alpine reshearing of its bounding faults. Instead, differential oblique shearing of its bounding faults (fig. 6.25.b; table 6.7) caused internalised clockwise-rotation and shear strain development to produce a confined and uplifted transpressive shear zone.

Table 6.7 – Slip behaviour of the major faults bounding the Millwall Anticline inlier (fig. 6.25.b).

Fault	Subhercynian & Pyrenean Phase Slip Behaviour		Lateral slip evidence
	Vertical (relative to inlier)	Lateral	
WSG-Faults System	Inlier upthrown	Sinistral	Right-stepping of *en échelon* Riedel shears
Fault AB	Inlier upthrown	Undetermined. (minimal anticipated)	Kinematic analysis (Chapter 3, §3.2)
Unnamed-NE fault	Inlier upthrown	Sinistral	

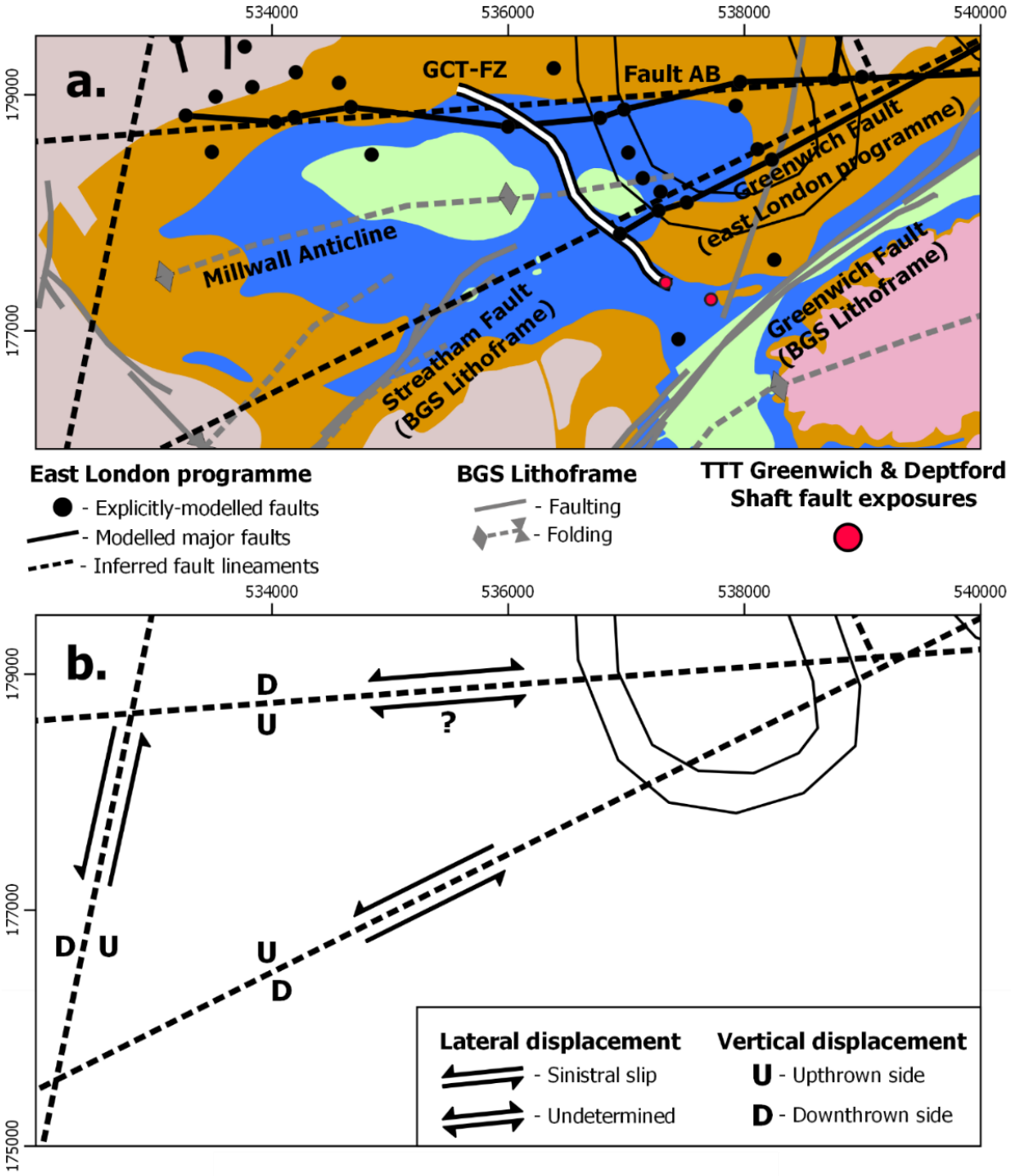

Figure 6.25 – Structural analysis of the Millwall Anticline inlier and its bounding major faults. a. Three major faults bound the inlier, which is characterised by fault-controlled uplift internally. b. Kinematic analysis of the inlier's bounding faults during the main Alpine compressive phases (table 6.7) indicates that significant shear strains would have generated internally due to confined clockwise rotation along faults with sinistral-slip components.

6.2.3.3 Minor fault zone mechanisms: Applicability and limitations

Most fault zones analysed are associated with the WSG-Faults and Millwall Anticline (table 6.4). Their shear zones are laterally expansive and have significant vertical displacement internally. Other fault zone intersections are comparatively narrow and more disparate (fig. 6.21). This contrasting scale suggests that it is unrealistic to characterise all fault zones using the above mechanisms since they reflect an overreliance on structural observations from two (potentially unique) structures. Therefore, narrower fault zones may represent minor linkage shear zones or major fault branching; and will likely depend upon the inherited fault set.

The ENE-striking Northern Boundary Fault (NBF) (fig. 6.1) has a relative vertical displacement of 20 m across it (that downthrows to the South (Ford et al., 2010)) and is interpreted to be an inherited reversed post-Variscan normal fault by this investigation. It is coincident with several fault zones (fig. 6.21) that were interpreted as 'stepped' or 'neutral' (table 6.4; fig. 6.20) that uplift internally towards the north[57] (FS-FZ in Aldiss et al., 2012, fig. 6). These are not continuous features of the NBF as the subparallel alignment of the Crossrail tunnel (fig. 6.15 vs. 6.21) only intersected them episodically; and are comparable with wider portions modelled along Fault AC (fig. 5.40, 5.44), another suspected inherited reversed normal fault. These fault zones may be minor relay ramp structures that have undergone internal shearing (fig. 3.32) since they are episodically situated along dip-slip dominant *en échelon* faults. Alternatively, these may reflect branching as dip-slip fault inheritance in the London Basin is recognised to bifurcate (fig. 3.27).

[57] The 'neutral' interpretations likely reflect oblique intersection of these fault zones.

6.2.3.4 Transtensional shear zones

Negative fault zones (fig. 6.16.a, 2.28) are likely transtensional structures since the Alpine stress field would inhibit direct extension. However, transtension is unvalidated since their internal characterisation was limited to cross-sections only (table 6.4). All negative fault zone observations are all proximal to major faults (fig. 6.26).

In central London and Southwark, the LB-FZ & LBS-FZ are coincident with the ENE-striking graben structure (fig. 3.30-31, 2.31), the unconstrained modelled Blocks A-F interface (fig. 5.41-43), and the intersection of NW- and ENE-striking fault lineaments. In northeast London, both the L-FZ and PG-FZ are coincident with two major fault intersections (ENE-striking fault (probable Lea Valley Fault) with the eastward continuations of the NBF and Fault AC)), and a continuous fault-bounded trough, the Plaistow Graben[58] (named after the PG-FZ (fig. 2.28; table 6.4) by Mortimore et al. (2011)).

Two previously discussed linkage mechanisms may cause localised transtension along a major fault: Oblique linkage of *en échelon* reversed faults (fig. 3.32), and Helvetic reversal of the strike-slip NW-set (fig. 3.17, 3.19). However, these structures are unlikely to be minor linkage products since they are laterally extensive features and relatively wide (LB-FZ is ~1 km wide, fig. 6.16.a). It is more likely that transtensional shear zones are either continuous within broader graben structures, or intersection products between inherited reversed and strike-slip fault sets. The former mechanism is considered more likely, but it contradicts Alpine compression and may indicate more complicated inheritance behaviour than recognised (§3.3).

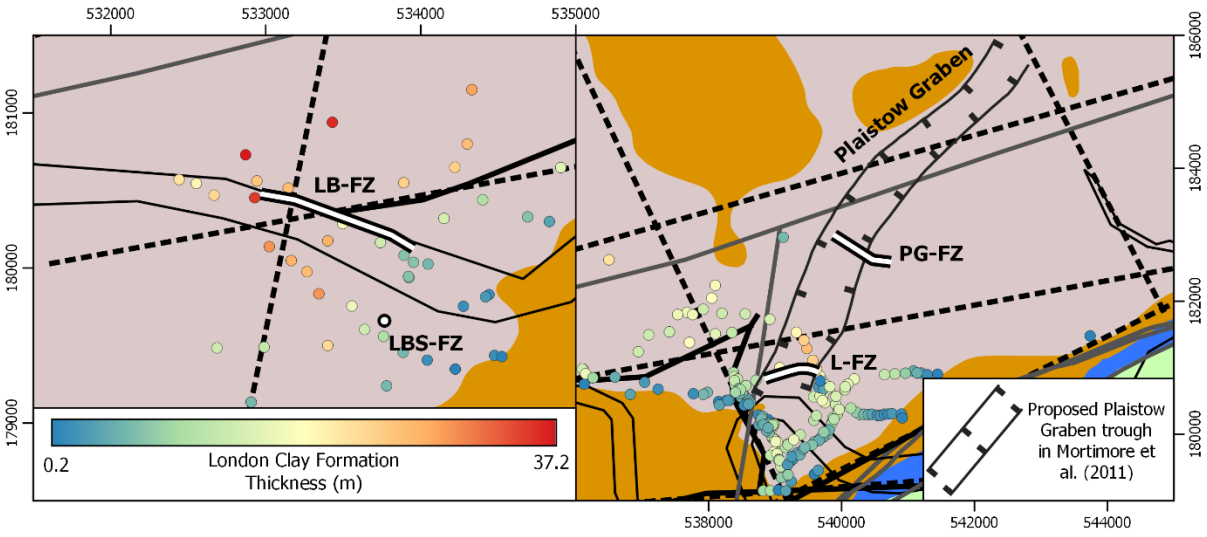

Figure 6.26 – Negative fault zones positions in central and northeast London in relation to major faulting (white lines/dots) interpreted by the East London programme, BGS Lithoframe and analysis by Mortimore et al. (2011).

[58] Mortimore et al. (2011) used a third negative fault zone intersected by Channel Tunnel Rail Link (Mortimore, 1996) to define the north eastern extension of trough. This fault zone was not analysed by this investigation.

6.2.3.5 Prevalence of confined block rotation

The orientations of London's three major fault sets will produce triangular and rhomboidal block geometries (fig. 6.27). Yet the isolated observation of 'confined block rotation' (fig. 6.25) implies that specific conditions are required to induce this form of rotational shear zones. The Millwall Anticline implies that this mechanism favours triangular blocks whose bounding faults have concordant lateral slip behaviour to encourage internalised rotational shearing. This implies that block susceptibility is a function of its geometry and size, and the slip behaviours of its intersecting fault sets. The Millwall Anticline may therefore be a unique shear zone because no other lateral-shear dominant triangular fault blocks have been identified in London (so far) (fig. 6.1).

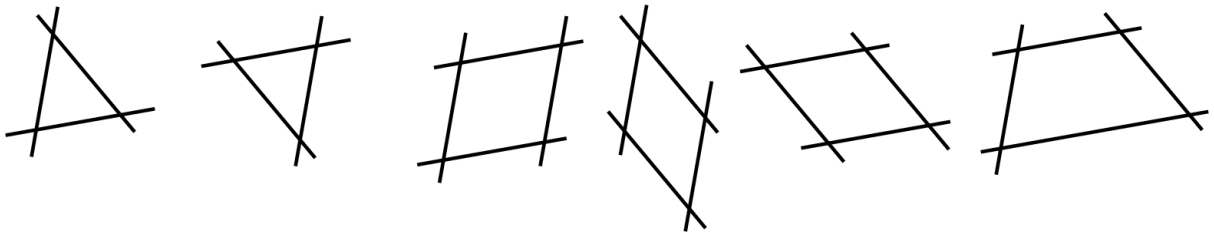

Figure 6.27 – Schematic of potential geometrical arrangements that could arise from the intersection of the three fault sets observed in London. Trends are idealised from outputs of Chapter 4.

6.2.4 Evaluation of fault zone analysis

A causal link with London's major faults has been determined, with fault zones representing various shear zone mechanisms and/or branching. However, the internal characterisation and genetic interpretation(s) of fault zones remains incomplete; this reflects the limited structural information available. Consequently, the analyses may be unrepresentative of minor fault zones because analyses overly relied upon observations from significant shear zones due to their comparative availability and broader data range. Further structural analysis is required to improve the characterisation of both minor fault zones and transtensional structures, ideally through an explicit modelling programme that couples localised, high density borehole coverage with shallow seismic profiles and structural analysis of site exposures.

'Fault zone' may continue to be used within London's geotechnical community as a descriptive term to characterise these structures without *a priori* knowledge of their internal architectures.

6.3 The impact of major faulting in London

The role of London's major faults in partitioning geological and hydrogeological processes and developing structurally complex features was characterised.

Major faulting has influenced Late Cretaceous-Palaeogene sedimentological processes and present-day connectivity of the Lower Aquifer. The extents varied, reflecting environmental sensitivities to topographic change in the former and the degree of low permeability fault core development in the latter. This partitioning is regionalised and driven by discrete inherited faults, with minimal localised block behaviour evident except under specific circumstances (e.g., fig. 6.6). Whilst discontinuous, London's geology is a product of faulting interplaying with other (generally more dominant) processes.

Fault zones were identified as intersections of complex brittle shear zones through collated analysis of disparate and limited structural observations from geotechnical projects. They are causally linked with London's major faults through their localised interaction and/or internalised deformation of the blocks they bound to produce transpressive or transtensive conditions. Their characterisation caused two major folds in London to be reinterpreted as shear zones. Linkage of the *en échelon* WSG-Faults produced transpressive push-up structures within overlap zones (e.g., Greenwich Anticline, fig. 6.23-24), the interiors of which are comparable to confined shear zone development (fig. 6.25). The Millwall Anticline is a transpressive product of sinistral slip-driven clockwise rotation and shear strain development within a confined triangular fault-bounded block (fig. 6.26). Limited information inhibited the genetic interpretation of other fault zones (minor and/or transtensive), yet fault zone analyses collectively highlight how localised and structurally complex some areas of London may be.

The analyses demonstrate that basement fault inheritance has directly contributed to London's subsurface complexity, more so than recognised. By extension, their impact on material properties and distribution, mechanical degradation and pore pressures will have significant geotechnical implications. However, the structural characterisation of the subsurface remains incomplete, preventing a thorough engineering appraisal. The outputs of this investigation provide a basis for further analyses when the availability and diversity of data improves and site exposure opportunities arise, enabling better characterisation of London's faults. The remainder of this thesis will discuss how major faulting can affect geotechnical engineering in London by linking Alpine tectonism exerted on the London Basin with present-day observations at the site-scale.

7. Discussion

This investigation has produced new structural insights into London and raised new questions, at various scales, which have implications for both regional tectonic understanding, and engineering geology in London. There are considered at four scales:

- §7.1 Tectonic-scale – Discussing London in the context of the London Basin and Alpine tectonism.
- §7.2 Fault-scale – Discussing the structural interpretations of major faults in London.
- §7.3 How do tectonic-scale processes affect site-scale engineering behaviour? – Discussing how fault inheritances deviates ground conditions from expected behaviour.
- §7.4 Site-scale engineering geology – Examples of how these manifest onsite, including the introduction of uncertainty and risk, and associated complications.

These address the research objectives and question in §1.1 and are accompanied by an outline for onsite characterisation of major faulting in London (§7.5) to reduce associated geotechnical risks.

7.1 Tectonic-scale processes

The presence of extensive fault inheritance in London is not accounted for by the synclinal model, nor the positioning of the Variscan Front beneath the North Downs. This discussion focuses on the tectonic framework along the southern London Basin to analyse why major faulting is present in London.

7.1.1 London's tectonic positioning

Alpine stresses were principally accommodated by basement fault reactivation and inheritance along the London Basin's southern margin (Chapter 3). Lateral confining stresses in the cover were comparatively negligible with normal faults dominant. The minor scale of compressive structures present implies that the underlying Platform shadowed the cover to minimise its confinement (§3.4).

London overlies a crustal interface between deeper Avalonian terrane assemblages that have recurringly controlled the stress distributions of Phanerozoic tectonic events between mechanically contrasting crustal blocks: the Rhenohercynian Zone (RHZ) was repeatedly tectonised whilst the Anglo-Brabant Massif (ABM) remained competent throughout (fig. 2.1-8, 2.16-17). By the Alpine Orogeny, this interface had developed into a transitional zone (fig. 3.26) as a Variscan thrust sheet had imbricated onto the southern margin of the ABM (§2.1.0.2) and subsequently been exploited by post-Variscan normal faulting to separate the Wessex Basins from the London Platform (§2.1.0.3). Alpine stresses were concentrated within this zone, preferentially reactivating its weak Variscan and post-Variscan faults to propagate instead of directly deforming its Cretaceous-Palaeogene cover (§3.4).

7.1.2 The positioning of the Variscan Front

The presence of Variscan faulting under London contradicts the 'Variscan Front' being situated beneath the North Downs (§2.1.0.2). This was previously indicated by seismic evidence of the Variscan thrust sheet continuing beyond the North Downs in §3.3.2.1. The exact positioning of the northernmost Variscan thrust sheet is unclear, but it must be further north than its exploitative post-Variscan normal faults (fig. 2.5). On this basis, the Variscan Front must underlie St. Albans-Harlow, immediately North of London (fig. 7.1). This is supported by an initial estimation of inheritance extent into the London Basin in §3.4 from published structural contour and fault data. Seismic line RG-001 (fig. 3.26) has enabled its westward identification also, indicating that the Variscan Front is sinuous. This supports Taylor's (1986) suspicion that a thrust sheet underlies the southern London Basin instead (fig. 2.3).

The revised Variscan Front is proposed at two isolated locations (VF in fig. 7.1). It is likely sub-parallel with the Basin's perceived synclinal axis since Whitaker (1872) noted that the axis formed the northern limit of major faulting. This implies that the Basin's geometry corresponds with changing basement domains and their respective Alpine behaviours instead of a fold mechanism.

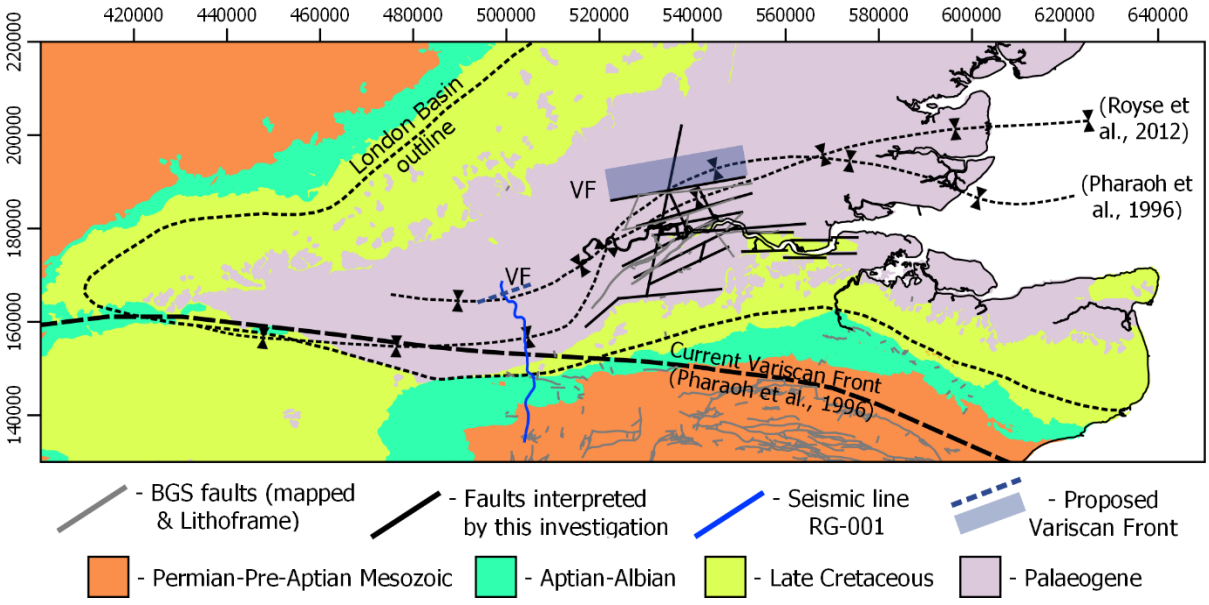

Figure 7.1 – Proposed repositioning of the Variscan Front (VF) under the southern London Basin based on the northernmost post-Variscan normal faults in the underlying basement. These are identified in two locations: Near Ascot in seismic profile RG-001 (fig. 3.26), and north of London from the northernmost ENE-trending fault (inherited normal fault set). These are both coincident with the Basin's inferred synclinal axis. Comparisons of the VF interpreted by Pharaoh et al. (1996) under the North Downs (dashed black line) with RG-001 indicate that it is a separate imbricated thrust sheet (fig. 2.3).

7.1.3 The nature of the London Basin

The London Basin is considered to be an asymmetrical Alpine syncline (fig. 2.18) that is internally minimally deformed. Its sub-horizontal northern limb dips SSE and the steeper (~3°) southern limb dips northwards (Ellison et al., 2018). The investigation has focused on London, yet fault inheritance and the presence of an underlying thrust sheet has implications for this broader tectonic interpretation also. The structure of the London Basin was reviewed by critiquing the synclinal model and comparing its geometry with new Palaeozoic basement modelling.

The 'London Basin' originated as a geomorphological description of a depressed trough of Palaeogene sediments situated between the North Downs and Chilterns chalk hills (Webster, 1814, Phillips, 1818). This geometry was structurally redefined as a syncline (Buckland, 1826) that formed a flexural continuation of regional folds in southern England (fig. 2.16; Martin, 1829) that were formerly connected as a depocentre (Prestwich, 1847, Prestwich, 1850, Prestwich, 1854). Its asymmetrical synclinal axis is parallel to the Thames Valley in the West (Whitaker et al., 1872) and diverts northwards above the Thames Estuary (fig. 7.1). Flexure of the London Basin, together with the Weald[59], progressively developed throughout the Cenozoic before Oligocene culmination (Woodward, 1909, Stamp, 1921, Stamp, 1924, Wooldridge, 1926). Its interior transitioned to undeformed (Sherlock, 1947) as previously inferred faults were downplayed (§2.2.2) (however, faulted monoclines were recognised along its interface with the Weald Anticline). The Hampshire and Weald Basins were structurally redefined following basin inversion recognition (Chadwick, 1993), yet the London Basin's synclinal model is still maintained (fig. 2.18; Sumbler, 1996, Ellison et al., 2018) as it was not a former basin. The interior is still interpreted as undeformed overall, but local structural complexities and major faults are now recognised in the southern portion (Ellison et al., 2004, Royse et al., 2012, Aldiss, 2013).

The synclinal model originates from its geometry but does not agree with structural observations. Firstly, lateral buckling also requires vertical confining stresses, yet the Late-Cretaceous-Palaeogene strata were not deeply buried. This mechanism has been maintained despite regional flexure of the neighbouring regions being superseded by inversion. Secondly, there is an in-built contradiction between its tectonic origin and minimally deformed interior as Whitaker et al. (1872) noted: "*The London Basin is perhaps the least disturbed of all the great geological tracts of our island, and yet its existence is in great measure owing to disturbance*". Thirdly, the presence of fault inheritance conflicts with an isolated buckling mechanism unaffected by the basement. Fourthly, and most importantly,

[59] Despite comparable timings, there were interpretative conflicts: Stamp argued for synchronous flexural development of both, whilst Wooldridge argued for isolated down warping of the London Basin's synclinal hinge.

the mechanism does not account for the implications of strata straddling both a basin and platform during inversion. This is despite a structural interface being suspected in the basement (Whitaker et al., 1872) from deep boreholes (e.g. Judd, 1882, Prestwich, 1858, Judd and Homersham, 1884) whilst the synclinal model was being developed.

The London Basin was generated by a mechanism that did not require vertical confinement nor significant lateral stresses in the cover. Instead, its formation and asymmetrical geometry must relate to its positioning above the London Platform and Weald Basin (§3.3.2.1), and their differing responses to inversion. The Pre-Permian[60] Palaeozoic basement and the base of the London Basin were implicitly modelled (fig. 7.2-3) to assess the relationship between the London Basin's geometry and its underlying structural domains (Weald Basin – Variscan transitional zone – London Platform).

The topographic disparity between the shallow Platform and the deep basement underlying the Weald are apparent, with the near-horizontal Platform dipping SSE. The London Basin's geometry mirrors the Palaeozoic floor along its southern margin (fig. 7.2) and rises as the basement abruptly deepens. This also corresponds with the London Basin's outline changing to follow the basement's sinuous interface (fig. 7.3). Its northern limb is controlled by the ABM's southeastward tilt whilst its steeper southern limb overlies and has been uplifted by the inverted Weald Basin. Both the basement and London Basin dips change direction at approximately 10 km north of the River Thames (fig. 7.2-3). This marks the transition from ABM to Variscan thrust sheet, corresponding with both the Variscan Front and changing bedding inclinations in the cover (~'synclinal axis', fig. 7.1).

Figure 7.2 – NNE-SSW cross-section of the Palaeozoic floor underlying the London Basin and its adjacent regions (fig. 7.3, line A). Proxy London Basin geometry provided by Chalk Supergroup baseline, generated by implicit modelling of 151 sub-chalk penetrating boreholes.

[60] Permian strata were ignored as they post-date the Variscan Orogeny (§2.1.0.3). They were primarily encountered in the model's western portions and do not reflect the basement underlying the London Basin.

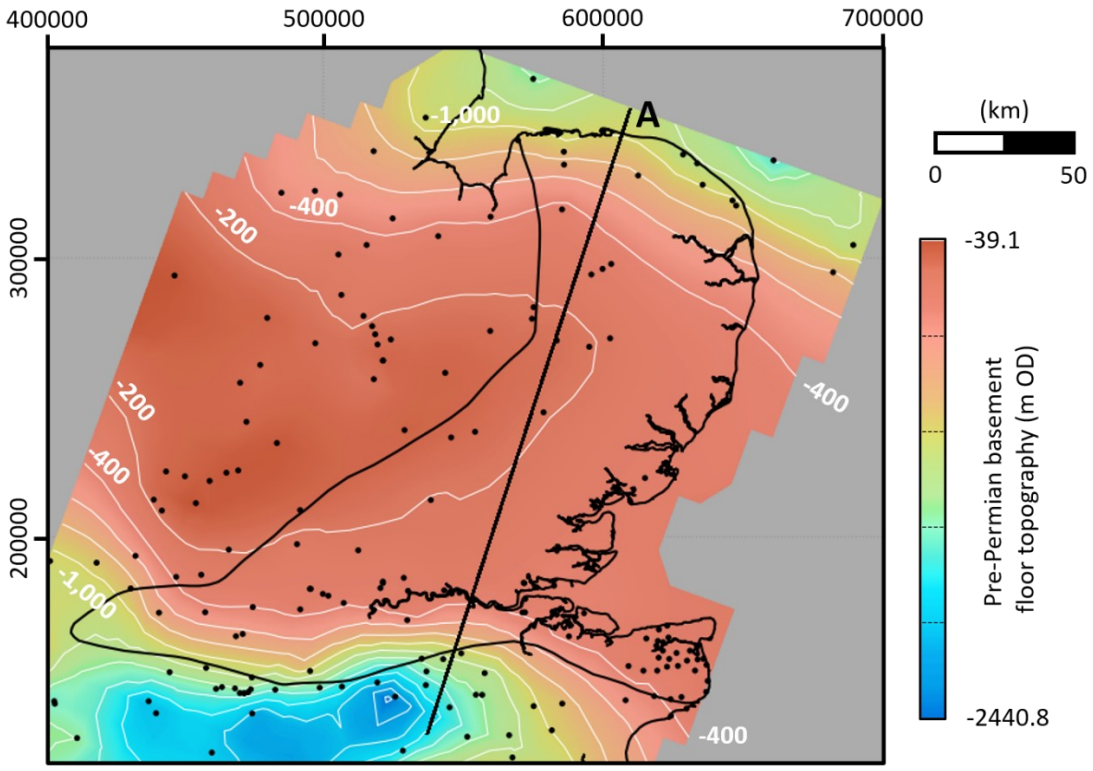

Figure 7.3 – Pre-Permian Palaeozoic basement topography underlying southeast England, with the chalk hills of the London Basin and East Anglia outlined. Surface constructed by implicit modelling of 190 boreholes interpreted and digitised from BGS and UKOGL databases. The model shows good agreement with published models and seismic profiles (fig. 2.4, 3.26), but lacks the resolution to model faulting along the ABM-Weald Basin boundary. Refer to figure 7.2 for cross-section A.

How the underlying structural domain responded to Alpine compression controlled and regionalised the formation of the London Basin. Inversion of the Weald Basin's fill uplifted its southern flank to generate the North Downs and caused reversed normal fault inheritance. The ABM did not deform as stresses concentrated along its margins but was instead susceptible to epeirogeny (§2.1.2). This protected its Late Cretaceous-Palaeogene blanket from compression (§3.4) and collectively they gently tilted to dip SSE. Isolated basement fault reactivation did occur in the ABM's interior (Lee et al., 2020, Woods and Chacksfield, 2012) but these local crustal weaknesses do not reflect its overall behaviour. The tilting is recent and occurred in multiple episodes. The confined former coverage of the Pliocene Crag Formation is coincident with Late Neogene uplift of the north-western British Isles (Japsen and Chalmers, 2000), implying that far-field intraplate uplift of Avalonia produced chalk hill topographic barriers. Southeastward Late Pleistocene (<450 ka) tilting is also evident from drainage migration and staircasing of river terrace deposits in the London Basin (Maddy, 1997) and on the Midland Platform[61] (Watts et al., 2000). This is attributed to rapid denudational unloading of Jurassic strata in the Midlands, causing flexural uplift of the ABM's north western flank (Lane et al., 2008, Watts

[61] The western portion of the ABM covered by Jurassic strata. Like London Basin stratigraphy, these are also tilted very gently towards the southeast (Lane et al. 2008, fig. 1.b).

et al., 2000). It is likely that the Platform's cover also extended further northwest prior to recent retreat. Finally, the Variscan thrust sheet situated between these structural domains underwent fault reactivation as the rigid ABM caused Alpine stresses to accumulate here. This transitional zone demarcates between the basin- and platform-controlled responses to Alpine inversion to produce the London Basin's asymmetrical fold-like structure (fig. 7.4). Therefore, the presence of major, inherited faults in London is a direct consequence of its crustal positioning above this transitional zone.

7.1.3.1 Redefining the 'London Basin'

The current title and geometric description are both misnomers that need updating. This has likely affected structural assumptions within the region as major faulting would be unexpected within an internally undeformed synclinal basin, despite evidence to the contrary. Similarly, Whitaker (1875) stressed that the London 'Basin' was a geomorphological description to prevent its misinterpretation.

The London Basin has a syncline-like geometry; but it is not a fold nor a basin. Its structure is an indirect product of polyphased Alpine tectonism and epeirogeny caused by straddling both an inverting basin and shallow basement platform. Categorising this structure is, therefore, not straightforward. It is proposed that the 'London Basin' be redefined as the 'London Blanket' to recognise the various structural domains it overlies and the role of multiple underlying tectonic mechanisms in its formation. Its alternative as a continuation of the 'London Platform' is contradicted by it partly overlying both the Weald and an imbricated Variscan thrust sheet.

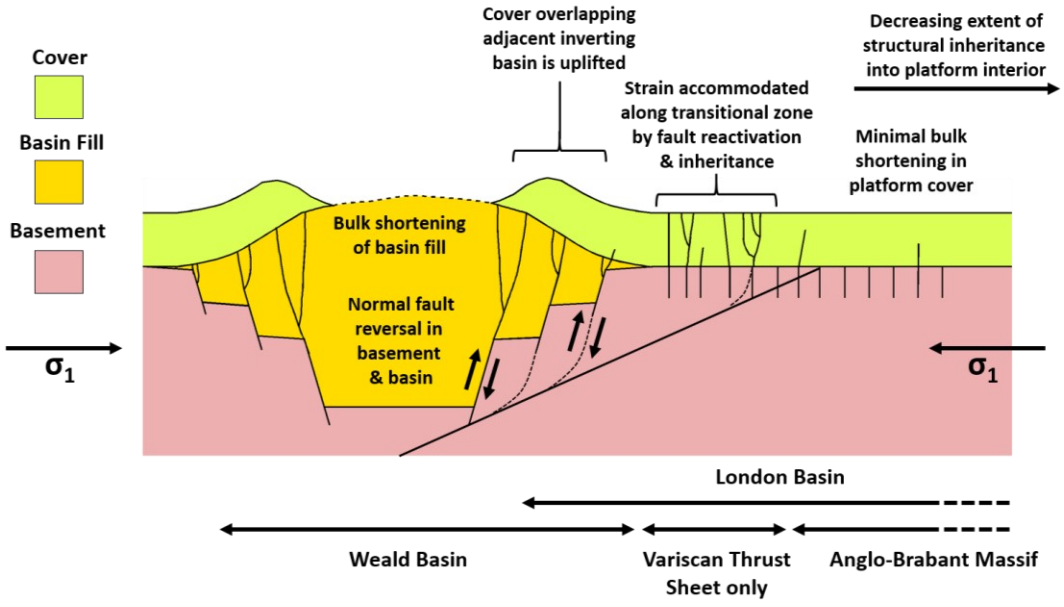

Figure 7.4 – Tectonic schematic of the differing mechanical responses to inversion of basins and shallow basement platforms, and its implications for the overlying cover. The style of deformation is dependent upon the relative positioning of the cover: Uplift on inverting basin flank; Basement fault reactivation and inheritance along the transition zone; Minimal deformation within the platform's interior. The contrasting behaviours of these regions generated the London Basin instead of a folding mechanism.

7.1.3.2 Further structural characterisation of the London Basin or Blanket

The above analyses identified that the region cannot be explained using an active folding mechanism. Instead, its trough geometry is basement-driven through a combination of basin inversion and platform tilting. This proposed mechanism requires critiquing and must also incorporate the region's progressive development. Further research is required to fully characterise its structure, formation, and basement-cover relationships. Outlined below are four research steps that require addressing.

Spatial variation of the region's structures and cover geometry must be further investigated to better assess the cover's tectonic arrangement. This should focus on both its interior and along its margins.

The region's spatiotemporal evolution is incomplete, both in terms of polyphased Alpine compression and epeirogenic events. This is most apparent during the End Cretaceous-Palaeocene and Neogene unconformities. Filling these gaps will improve the region's tectonic history, linkage to the behaviour responses of underlying structural domains, and the former extent(s) of this Palaeogene depocentre.

Basement structural domains under the whole London Blanket region must be characterised to relate Alpine-epeirogenic evolution to regionalised tectonic behaviour internally. Three structural domains are outlined by this investigation in the southern London Basin or Blanket (§7.1.2), but the tectonic fabrics underlying the Basin's interior, the Chilterns, and its interface with East Anglia require identifying. This 'northern' London Basin or Blanket, defined here as the area north of the Variscan Front, rests upon the ABM. This enigmatic basement requires further geodynamic characterisation (Pharaoh, 2018) to understand both its epeirogenic-susceptibility and the structural fabric(s) present, thereby defining any structural domains internally. Both a Caledonian fabric (Pharaoh et al., 1987) and crustal weaknesses (Pharaoh et al., 2006) are anticipated, and have caused localised inheritance (e.g., Mortimore et al., 2001, Woods & Chacklesfield, 2012). It is unclear why the portion of the ABM underlying the region has distinctly remained a relative highpoint throughout the Mesozoic-Cenozoic (fig. 2.9, 2.11, 2.17). Is it simply the centre of a tilting cratonic block, or is it relatively more buoyant?

Basement-cover relationships for both the whole region can be regionally characterised by coupling the cover's spatiotemporal evolution with improved tectonic characterisation of the basement and its Alpine-epeirogenic responses. From this the London Blanket can be geodynamically analysed to critique whether it is a single definable structure driven by regionalised basement mechanisms. For example, the London Basin's more distinctive synclinal western arm may be distinct from the proposed mechanism since it straddles the Vale of Pewsey instead of the inverted Weald Basin.

The research areas overlap but are all challenged by basement accessibility, penetrative geological and geophysical information, and the availability of cover structural data, regionally.

7.1.4 Spatiotemporal variation in polyphased Alpine deformation

Southern Britain is a product of polyphased Alpine compression from the Late Cretaceous to present day, and its interaction with sea level changes and epeirogeny. Spatial variation between differing structural domains is evident. However, a temporal component is also apparent as stress magnitudes and axes changed between each Phase (§2.1.2, table 3.4) and were accompanied by both epeirogenic episodes and each region's decreasing capacity to accommodate further strain. Clearly the interaction of far-field stresses with the unique structural arrangement of each region individualised Alpine responses. In London, this is illustrated by the evolving reshear behaviour of each basement fault set and more broadly, the London Basin's ongoing formation as the underlying structural domains differentially responded[62] throughout Late Cretaceous-Cenozoic.

Whilst not discussed in §2.1, it is likely that the onset of North Atlantic opening in the earliest Eocene has also contributed by confining the British Isles to present. But it did not alter behaviour temporally since spreading rates have remained relatively uniform following its initial inception (Ellis and Stoker, 2014, fig. 2), unlike Alpine compression.

7.2 Fault-scale

The investigation has characterised major faulting in London from limited direct observations. Structural interpretations have, instead, relied heavily upon multiple lines of indirect evidence, inferences from proxy observations and analogue models, and explicit-driven geological modelling. The findings demonstrate that London's deformation is primarily controlled by the reactivation and inheritance of underlying Variscan strike-slip and post-Variscan normal faults. Their near-surface architectures vary from individual faults to narrow faulted bands to kilometre-scale shear zones (fig. 5.40-42, 5.45) due to set-specific propagation mechanisms and interactions along and between faults.

This section discusses three aspects of fault inheritance in London's near surface identified during this investigation, that are important for London's structural understanding and by extension, its engineering geology. These are the nature of the WSG-Faults (§7.2.1), defining fault propagation and shear zone mechanisms (§7.2.2), and the potential for fault zone misinterpretation (§7.2.3).

[62] Weald Basin: Subhercynian(-Laramide) - Minor inversion. Pyrenean - Progressive inversion. Helvetic - Unclear. ABM: Minimal inversion, localised to individual fault reactivation. Responded to epeirogenic episodes instead.

7.2.1 The nature of the Wimbledon-Streatham-Greenwich Faults (WSG-Faults)

Progressive analysis of the *en échelon* WSG-Faults from initial interpretation (§3.3.3.2, 2.2.2.2) to its internal shear zone characterisation (§6.2.3.1) indicates that they are structurally distinct from London's three inherited fault sets. Its near-continuous, anastomosing Riedel shear zone geometry is comparatively wider (fig. 6.22 vs. §6.1.3.3) with well-developed secondary Riedel shear zones present at points of overlap. These have recurringly reactivated throughout the Alpine Orogeny. It is coincident with a major lineament in cover-stripped Bouguer gravity data (Aldiss, 2013, fig. 11). It demarcates London's two distinct structural domains (fig. 2.31): a succession of periclinal folding in the southeast and block faulting in the north and west of London. Collectively this implies that the WSG-Faults originated from a significant structural weakness in the basement that has regionalised reactivation behaviour.

The origin of the WSG-Faults is unclear and has been further characterised here from Bouguer gravity analysis (fig. 7.5). The gravity contrast it delineates has an arcuate trend that curves eastward, becoming coincident with the Jurassic-preserving Thames Estuary Graben (TEG), an E-W-striking series of *en échelon* reversed normal faults that inverted and exhumed the overlying cover (fig. 3.28-29, §3.2.2.2). Assuming this lineament represents the WSG-Fault's continuation, it is apparent that its geometry mirrors the Variscan Front (fig. 7.5, proxy 'synclinal axes') before curving southeastward.

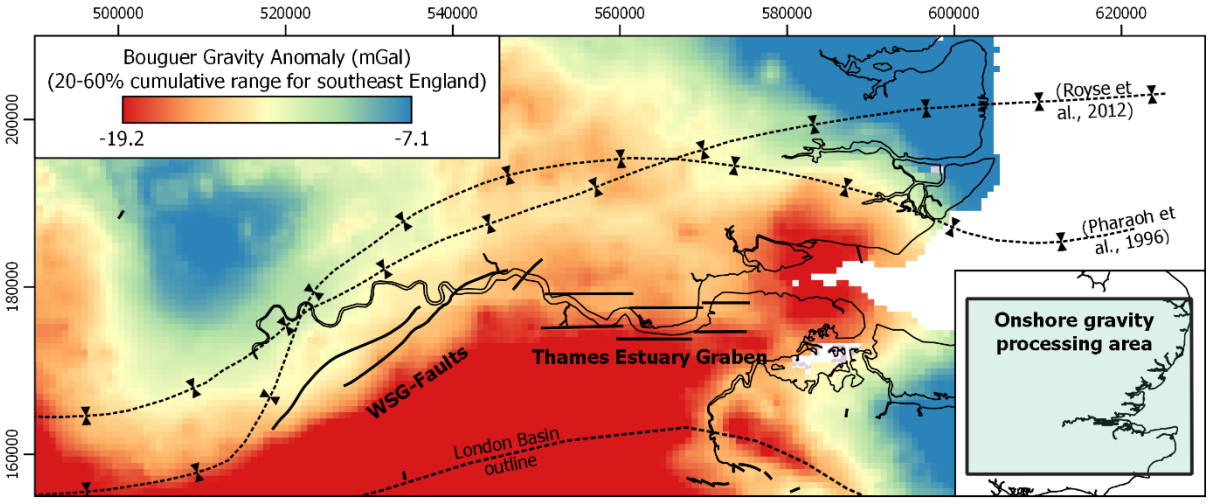

Figure 7.5 – Bouguer gravity anomaly data overlain with positioning of the WSG-Faults and Thames Estuary Graben (TEG). The perceived Basin 'synclinal axes' provide a proxy for Variscan Front positioning. Gravity data processed from BGS point gravity readings in southeast England (inset) using the empirical Bayesian kriging method. Data is graded from the 20-60% cumulative range of values to highlight the contrast that the WSG-Faults and TEG delineate.

Collectively, this indicates that the WSG-Faults and TEG are part of a curving post-Variscan normal fault in the Palaeozoic basement that inverted and reversed into the cover, rather than a distinct structure. This structure must be significantly larger and weaker than other basement faults due to its

unique inheritance architecture, and comparative scale and offset extents in the cover. Its curvature has caused reshear behaviour to vary as obliquity to the Alpine stress axes changes across it: transpressive shearing of the obliquely aligned WSG-Faults with a significant sinistral component, and dip-slip dominant reversal of the sub-perpendicular TEG. This agrees with analogue modelling of oblique and reversed normal fault propagation behaviour (Bonini et al., 2012, Richard, 1991).

Why this fault is distinct from other members in this set is unclear. It is likely the northernmost main listric branch (3.26) that exploited the Variscan thrust sheet based on the contrasting structural domains across it in the cover (fig. 2.31). This boundary demarcates between where post-Variscan normal fault reversal and Variscan strike-slip were preferentially resheared. The periclines (parallel to the WSG-Faults) in the former domain likely cap minor reversed listric fault branches, with their relative scales indicating that they could geometrically accommodate less inversion than the WSG-Faults. Inherited reversed normal faults do occur north of this domain (including suspected basement grabens also (fig. 3.30)), but their near surface behaviour is distinct from the TEG (fig. 3.31 vs. 3.29).

The WSG-Fault was originally attributed to oblique inheritance of the Variscan strike-slip sinistral set based on comparable observations with strike-slip propagation behaviour (fig. 3.33-36 vs. 3.37-39). But reinspection under a broader regional context implies that its unique near surface architecture reflects a significant weakness in the basement associated with the northernmost major listric fault.

7.2.2 Fault propagation and shear zone development

London's basement structures and Alpine reshearing are more complex than envisaged in Chapter 3. Major fault propagation was idealised from analogue models with minimal oblique-slip components (Chapter 3): lateral reshearing of Variscan strike-slips, and dip-slip reversal of post-Variscan normal faults. This is recognised to be unrealistic (§3.2.6) but does explain certain features and behaviours. The WSG-Faults demonstrate that certain inherited faults have sufficient oblique-slip components to significantly alter propagation behaviour away from these two endmembers. Comparisons of differing propagation mechanisms (fig. 7.6.a) show that this will introduce further structural complexities in London's near surface that are dependent on a fault's specific reactivation behaviour in the basement.

The generation of shear zones (§6.2) will be dependent upon both the architecture of the interacting faults and their respective reshearing stresses. The proposed mechanisms are summarised in plan-view in figure 7.6.b, showing both the complex and complicated products that may arise. Except for within-set linkage, shear zone interiors (structures and stress conditions) remain unclear due to a lack of data nor analogue modelling equivalents. For example, transtensive structures present in London are currently unexplained by transpression-favouring mechanisms.

Extensive post-Oligocene denudation of London Platform's cover (~200 m removed) has also partly erased the propagated structures. Therefore, their present-day near-surface structures may not be representative of the free-surface propagation architectures (fig. 3.33) achieved during the main Pyrenean Phase. This will affect their comparability with analogue models of fault inheritance.

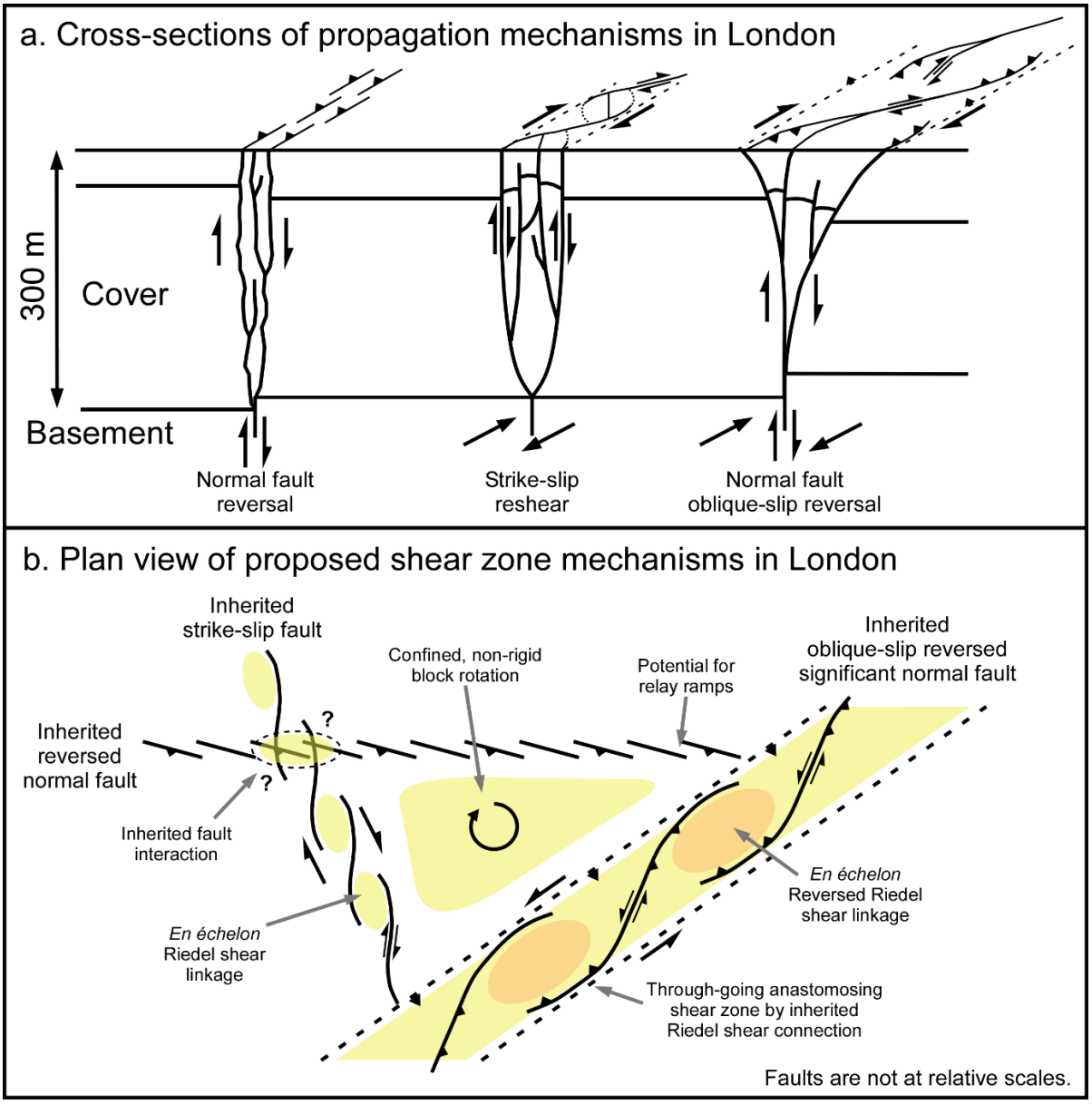

Figure 7.6 – Interpreted major fault inheritance behaviour and shear zone mechanisms in London. a. Proposed propagation mechanisms in London from differing reshear behaviour of basement faults in analogue modelling. Dip-slip dominant normal fault reversal: Comparison of seismic line RG-001 (fig. 3.26) with Miller and Mitra (2011). Lateral-slip dominant strike-slip fault reactivation: Dooley and Schreurs (2012) and Mandl (2000). Oblique-slip reversal of normal faults: Richard (1991), Richard and Krantz (1991), and Richard et al. (1995). b. Proposed shear zone development mechanisms from near surface interactions of propagated basement faults. Shear zones may develop from linkage within and between fault sets, and the rotation of blocks they confine. These mechanisms will likely generate transpressive conditions. It is still unclear how transtensive structures are generated.

7.2.3 Fault zone misinterpretation risks: Folding vs. shear zone

The investigation has focused on Alpine-induced faulting. However, folding is also recognised at varying scales in London's near surface (§2.2.2) and is widespread across London (fig. 7.7), particularly South of the River Thames. The majority are laterally continuous, comprising both gentle, open geometries (Ellison et al., 2004) and periclines (Ford et al., 2010). However, some are short-lived and associated with large inliers (Millwall & Greenwich Anticlines, fig. 2.20).

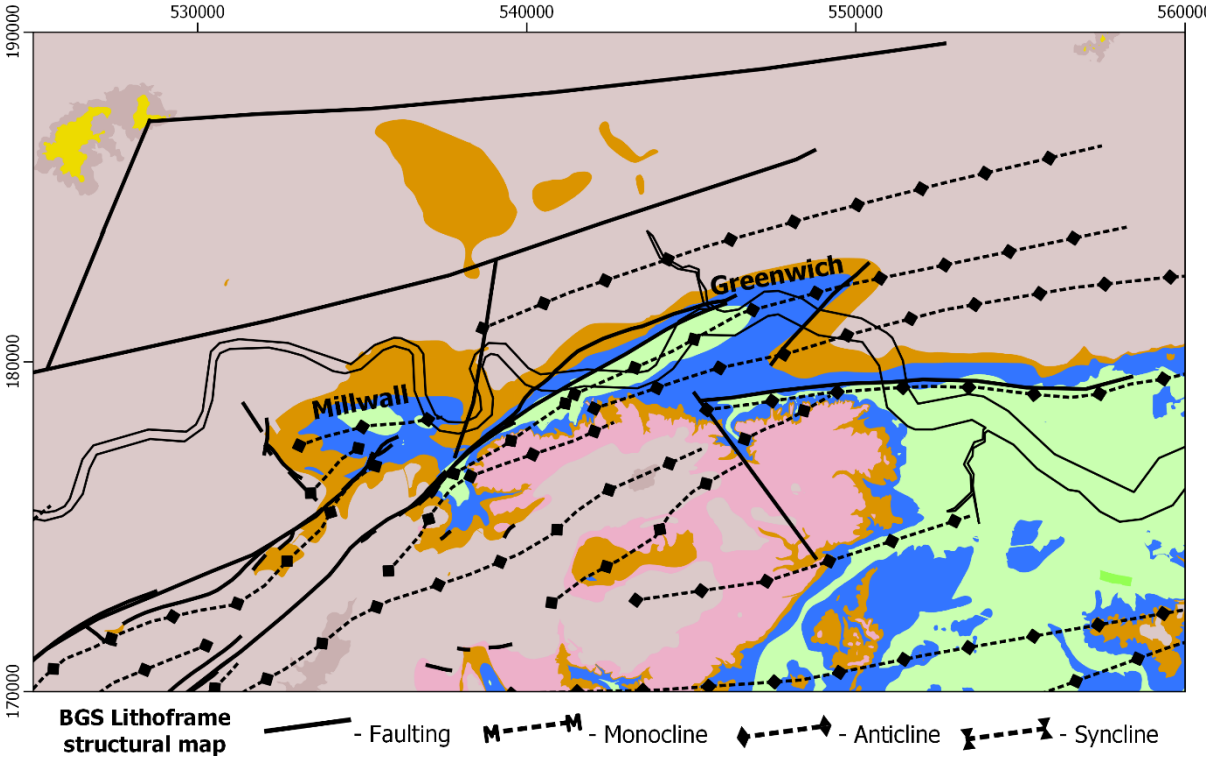

Figure 7.7 – BGS Lithoframe structural interpretation of London. Lithoframe shapefiles provided by Ford (pers comms, 2020).

Internal observations from the Millwall and Greenwich Anticlines demonstrate that they are misinterpreted brittle shear zones (fig. 6.16.b, 6.23). Their historical interpretation as folds reflects low-resolution analysis caused by limited exposure and reliance on poor borehole coverage. To illustrate this, the Greenwich Connection Tunnel Fault Zone (GCT-FZ), coincident with the Millwall Anticline, has an anticlinal-like geometry when interpreted from widely spaced boreholes (fig. 7.8).

These observations do not discredit folding in London since these shear zones uniquely crop out as short-lived lozenge shaped inliers (fig. 7.7), unlike other folds in London. Rather, it highlights the potential risks of misinterpreting fault zones from their fold-like geometries. For example, the anticline interpreted by Davis (1928) (from limited well and tunnel face data, fig. 4.3) is coincident with the overlap of the Wimbledon-Streatham faults and is likely a linkage zone. Similarly, the periclines in southeast London may be capping reversed normal faults (§7.2.2) and likely contain propagated faults.

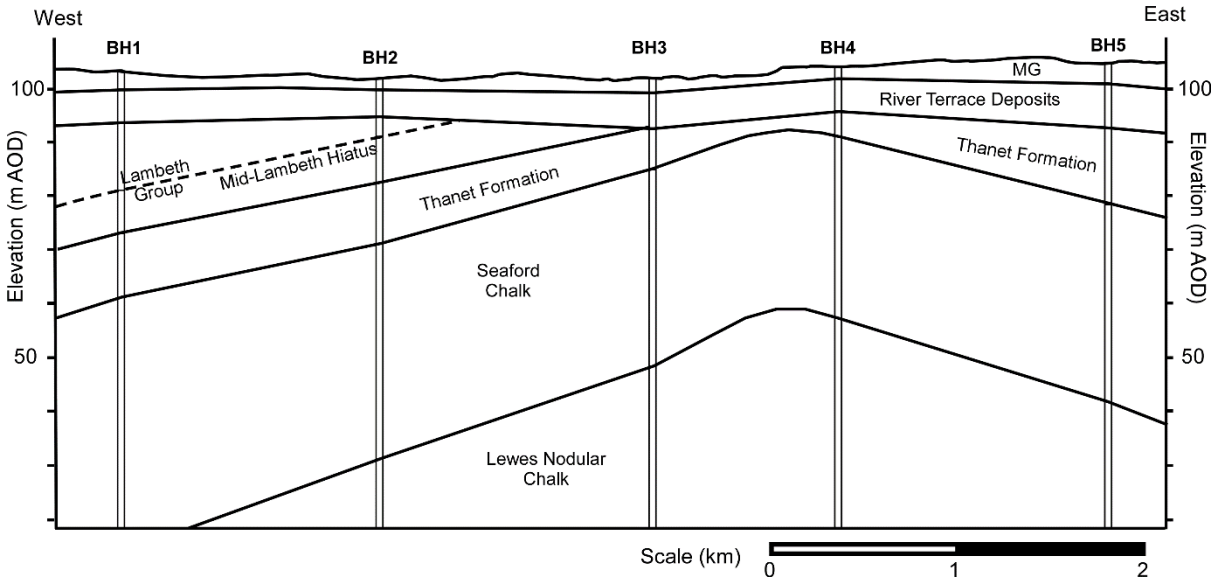

Figure 7.8 – Low-resolution reinterpretation of the GCT-FZ (fig. 6.16.b) as the Millwall Anticline from five widely spaced hypothetical boreholes using stratigraphic positions from the original Thames Tideway cross-section.

Misidentificiation of fault zones has significant geotechnical risk implications as their differing formation mechanisms (brittle vs plastic) strongly affects local ground conditions. For example, increased jointing spacing, enhanced permeability, and unpredictable pore pressures associated with fault zones (Newman, 2009) will not be anticipated onsite if the ground model predicts folding . To overcome this risk for the geotechnical community in London, a criterion is proposed to assess whether a suspected fold onsite may be a misinterpreted fault zone:

- Large amplitude relative to other folding in London (possibly associated with inliers)
- Laterally short-lived
- Elongate to lozenge shape
- Bounded by major faulting
- Enhanced and extensive jointing internally relative to adjacent unfolded rock masses[63].

[63] Jointing is also associated with folding but is restricted to fold hinges.

7.3 How do tectonic-scale processes affect site-scale geology?

The 'ground conditions' of a site are investigated to geotechnically characterise subsurface geological features, parameterise their mechanical behaviour and identify geotechnical hazards. It is a product of the bedrock, its post-depositional alteration, Quaternary processes, and past anthropogenic interactions. Major faulting is recognised as a potential geotechnical hazard in London (Everett and Dewar, 2015) but it is poorly constrained both geologically and geotechnically. This investigation has researched how major faulting can impact ground conditions in London from a geological perspective.

London is structurally more complex than recognised and is conceptually summarised in figure 7.9. Inherited major faults are highly variable and complex due to their specific propagation mechanisms and interactions within and between one another (fig. 7.6): along an individual fault can vary from a narrow brittle fault to a wide shear zone. Their intersection has compartmentalised the subsurface into discrete blocks. The majority are relatively undeformed internally with tectonism restricted to their bounding faulted margins; but some are complex shear zone (fig. 7.6). This behaviour varies across London and is, in part, controlled by the change in dominant basement structures (§7.2.1).

When these 'tectonic-scale' processes are considered at the 'site-scale', major faults deviate the ground away from expected conditions. This reflects the inheritance-related tectonism outlined above (fig. 7.9), offsetting, and their influence on regional sedimentological and hydrogeological processes (§6.1). Overall, major faults can influence the geological features present on site, their elevation, and mechanical properties through deformation and/or lithological changes, and groundwater disruption.

Crucially, modification of the ground is both variable and inconsistent across London, causing their impacts to be both fault- and location-specific. Therefore, accounting for these fault-related ground conditions cannot be achieved by a 'one size fits all' approach to rectifying them. Nonetheless the ways major faults can and do deviate ground conditions and influence engineering geology on site (§7.4) should be appreciated before its ground investigation (§7.5) is undertaken.

Figure 7.9 (next page) – Block model of near surface structures associated with major faulting in East London. The model conceptualises proposed inheritance and shear zone development mechanisms (fig. 7.6), with a simplified geology that does not account for lithological variation nor periglacial features. This collates geological modelling outputs (§5.3-4) with inheritance behaviour (§3.3) and shear zone characterisation (§6.2).

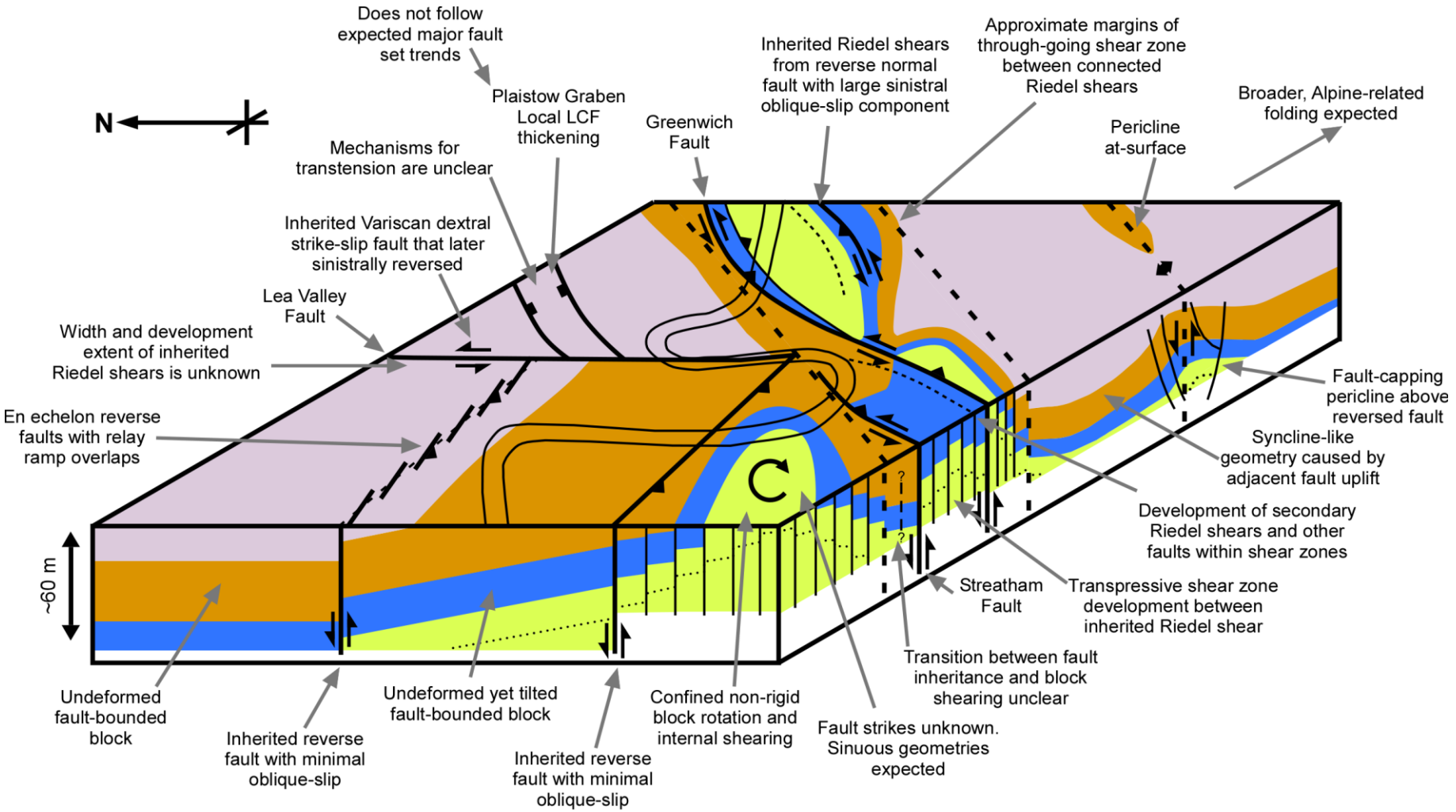
N
Does not follow expected major fault set trends
Plaistow Graben
Local LCF thickening
Greenwich Fault
Inherited Riedel shears from reverse normal fault with large sinistral oblique-slip component
Approximate margins of through-going shear zone between connected Riedel shears
Pericline at-surface
Broader, Alpine-related folding expected
Mechanisms for transtension are unclear
Inherited Variscan dextral strike-slip fault that later sinistrally reversed
Lea Valley Fault
Width and development extent of inherited Riedel shears is unknown
En echelon reverse faults with relay ramp overlaps
Fault-capping pericline above reversed fault
Syncline-like geometry caused by adjacent fault uplift
Development of secondary Riedel shears and other faults within shear zones
Streatham Fault
Transpressive shear zone development between inherited Riedel shear
Transition between fault inheritance and block shearing unclear
Fault strikes unknown. Sinuous geometries expected
Confined non-rigid block rotation and internal shearing
Undeformed yet tilted fault-bounded block
Undeformed fault-bounded block
Inherited reverse fault with minimal oblique-slip
Inherited reverse fault with minimal oblique-slip
~60 m

7.4 Site-scale engineering geology

This section discusses the engineering geology of major faulting and how it manifests on site through offsetting (§7.4.1), rock mass degradation (§7.4.2), minor fault generation within shear zones (§7.4.3), and exploitation by other processes (§7.4.4). These features can all be geotechnically problematic and cause 'unexpected ground conditions' (UGCs) if not identified during the GI stage. Ultimately, this contributes to enhanced uncertainty and risk (§7.4.5) if major faulting is present nearby.

7.4.1 Across-fault layer offsetting

Vertical offsetting is the most obvious impact of faulting on site in London and should be readily identifiable during a GI with high borehole density. It can cause abrupt lithological changes onsite given the limited thickness and variability of certain Palaeogene strata (table 2.1) and the potential offsets (10-30 m, Ellison et al., 2004; fig. 5.35). Offsetting may also introduce further geotechnical issues by allowing water ingress if a perched aquifer or component of the Lower Aquifer is brought into contact with the excavation face.

For example, the Lee Tunnel GI identified that the tunnel alignment would intercept downthrown Thanet Formation within the Plaistow Graben Fault Zone (fig. 2.28, 6.21) rather than the expected White Chalk Group. This was geotechnically problematic because it would introduce difficulties from mixed face conditions, running sands and water ingress (Bellhouse et al., 2015). The impact of fault offsetting was overcome by lowering the tunnel alignment by 10 m, a second GI, and altering the TBM's driving parameters during intersection (Newman et al., 2016).

7.4.2 Fault-related rock mass degradation

Geotechnical appraisal of faulted rock masses in London is limited but they are expected to degrade mass strength and stiffness parameters (Everett and Dewar, 2015) and alter permeability locally. How faulting degrades the rock mass will be dependent upon the extent and style of shearing, positioning along the fault and the material being sheared (Choi et al., 2016, Kim et al., 2004). Variable fault architectures are recognised in London, therefore, an irregular (and potentially unpredictable) impact upon ground conditions should be anticipated.

7.4.2.1 Material-specific responses to faulting

London's near surface lithologies will each respond differently to faulting given the recognised material and mechanical variability between them (table 2.1). Broadly, fault-related shearing will cause fracturing, and possibly fragmentation and comminution, in brittle rocks (fig. 3.10), dilation and grain reorganising in dense sands, and narrow shear zone development within 'cohesive soils'. This will also irregularly affect permeability, promoting isotropic enhancement in sands but anisotropy in clays; the impact on the Lower Aquifer materials has already been outlined in §6.1.3.4.

7.4.2.2 Fault zone deformation

Confined deformation within London's shear zones ('fault zones') will be greater than along individual major faults due to the concentration of shear stresses and resultant strains internally. This will contribute to significant rock mass weakening within fault zones relative to unfaulted rocks, as implied by the London Clay Formation in the Limmo Fault Zone (fig. 7.18). Increased discontinuity frequency, apertures openings, block textures and slickenside surfaces have been observed in the Chalk and London Clay within fault zones (Linde-Arias et al., 2018, Newman, 2009). This implies that deformation is predominantly brittle, but confined shearing may also plastically deform clay-dominant strata.

It is inappropriate to characterise fault zones beyond the general features and expectations above given the identified variability (and uncertainty) in their architectures, extents of internal transpressive or transtensive deformation, and formation mechanisms (§6.2). Instead, GIs should be targeted to account for their individualised impact on the rock mass.

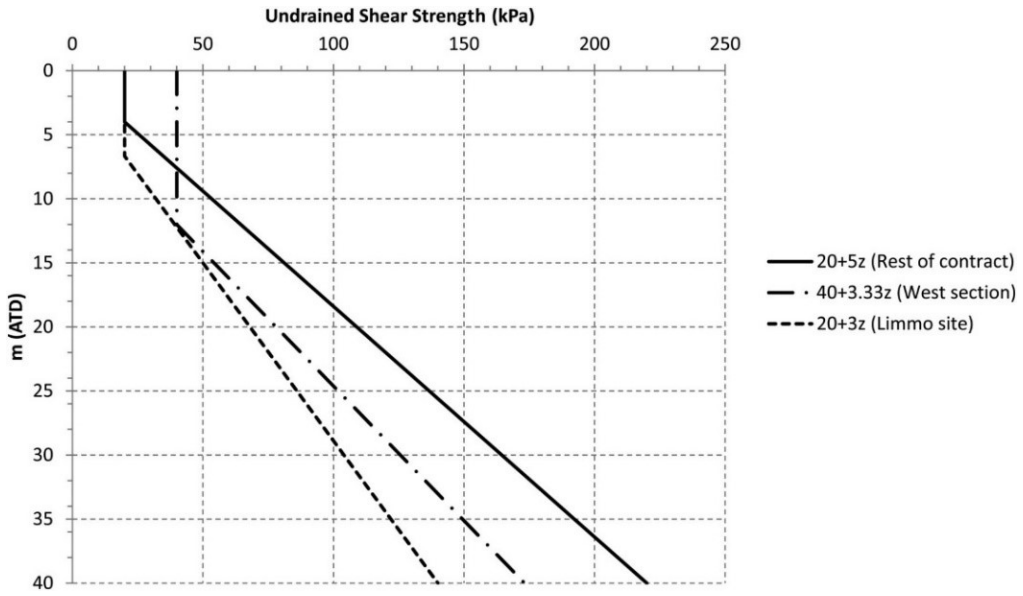

Figure 7.10 – Weakening of the London Clay within the Limmo Fault Zone (L-FZ, fig. 6.21) compared with lower bound undrained shear strength values across the Crossrail tunnel alignment. From Linde-Arias et al. (2018).

7.4.3 Atypical minor fault generation within shear zones

Minor faulting has been attributed solely to low confining stresses in the cover so far (§3.4, §2.2.2.1), but inherited faulting may generate minor brittle structures also (fig. 7.11) by locally distorting stress fields (fig. 3.35.b). This is evidenced in London since both joint set misalignment (Ellison et al., 2004, Bevan and Hancock, 1986) and minor compressive faults are observed near major faults. Both minor thrusting (fig. 2.27) and bedding-parallel shearing are rare in London, but all their observations are proximal to mapped shear zones in London (fig. 6.21) (Crossrail, 2016, Dewey and Bromehead, 1921,

Whitaker, 1889b, De la Condamine, 1852) or proxy inlier/outlier features in the southwestern London Basin (Tudor, 2019, Chandler et al., 1998). These minor fault styles are atypical for London (§2.2.2.1) and demonstrate how further structural complexity can be introduced around shear zones.

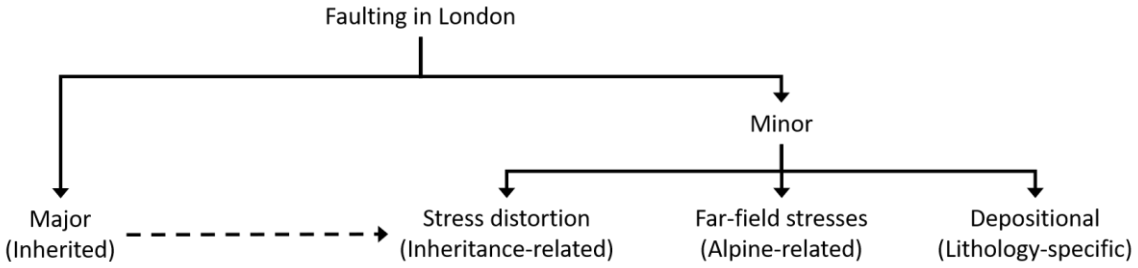

Figure 7.11 – Breakdown of fault origins in London relative to scale (fault definition, §1).

7.4.4 Fault exploitation and associated geotechnical problems

Faults and their extended discontinuity network are susceptible to exploitation by later geological processes due to their enhanced permeability and localised weakness within the broader rockmass. Consequently, the geology around major faults in London may also be indirectly altered around them beyond the direct influences already outlined during this investigation (§6.1-2). Two features suspected of exploiting faults are presented that are both geotechnically problematic and may contribute to UCGs being compounded around major faults.

7.4.4.1 Drift-filled hollows: Quaternary periglacial exploitation

Anomalous rockhead depressions in London (fig. 5.21) infilled with heterogenous, unconsolidated Quaternary and reworked bedrock materials (Ellison et al., 2004) are collectively referred to as drift-filled hollows (DFHs). Multiple periglacial and fluvial mechanisms are apparent from their variable internal architectures (Flynn et al., 2020), and are an area of ongoing debate. But the most significant are attributed to both pingo mechanisms and/or formerly elevated pressures in the Lower Aquifer exploiting vulnerabilities in the overlying strata, including faulted rockmasses, to cause explosive venting (Flynn et al., 2018, Toms et al., 2016, Banks et al., 2015).

An exploitative relationship is supported as many DFHs do cluster near major fault localities (fig. 7.12). The weakened, fractured rock mass around faults provide exploitable hydraulic conduits for elevated fluid pressures to promote these eruptions. Shallower DFHs in West London (fig. 7.12.b; where the London Clay is thicker) indicate that faults enabled groundwater to erupt nearer the surface and overcome the thick impermeable overburden. Not all DFHs are causally associated with major faults. But where they are, it demonstrates how ground conditions around faults can be further deteriorated.

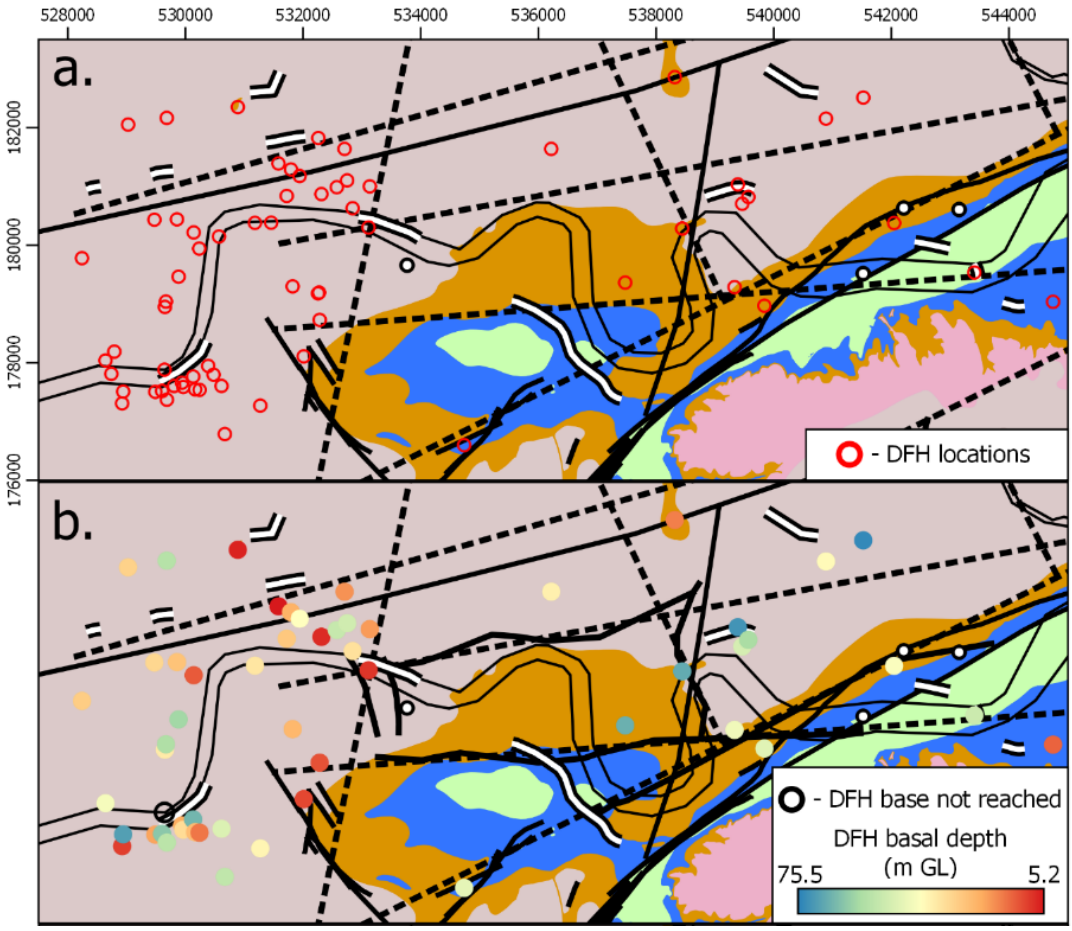

Figure 7.12 – Spatial characterisation of drift-filled hollows (DFHs) in relation to London's major faults and fault zones through GIS analysis of DFH database in Flynn et al. (2020). a. DFH locations. b. DFH basal depth.

7.4.4.2 Harwich Formation cementation: Eocene exploitation

Calcareous concretions and cemented bands throughout the Harwich Formation in London are stronger than uncemented Harwich, have unclear distributions and can be metres in scale (Skipper and Edgar, 2020). Edgar (2021) proposed a causal link with faulting as cementation was consistently coincident with the indirect fault map (fig. 4.28). This is validated at a granular scale in East London by this investigation (§5.4.3). Nearly all interceptions are proximal to major faults (fig. 7.13).

Upwelling calcium-rich groundwater exploited faults since they locally enhanced permeability. Capping by the ~impermeable London Clay Formation likely caused these fluids to concentrate within the underlying Harwich Formation and precipitate to generate these hard bands. Here faulting has indirectly controlled this hydrogeological process, causing ground conditions to further deviate away from expected behaviour locally by strengthening the rockmass rather than weakening it (i.e., §7.4.2).

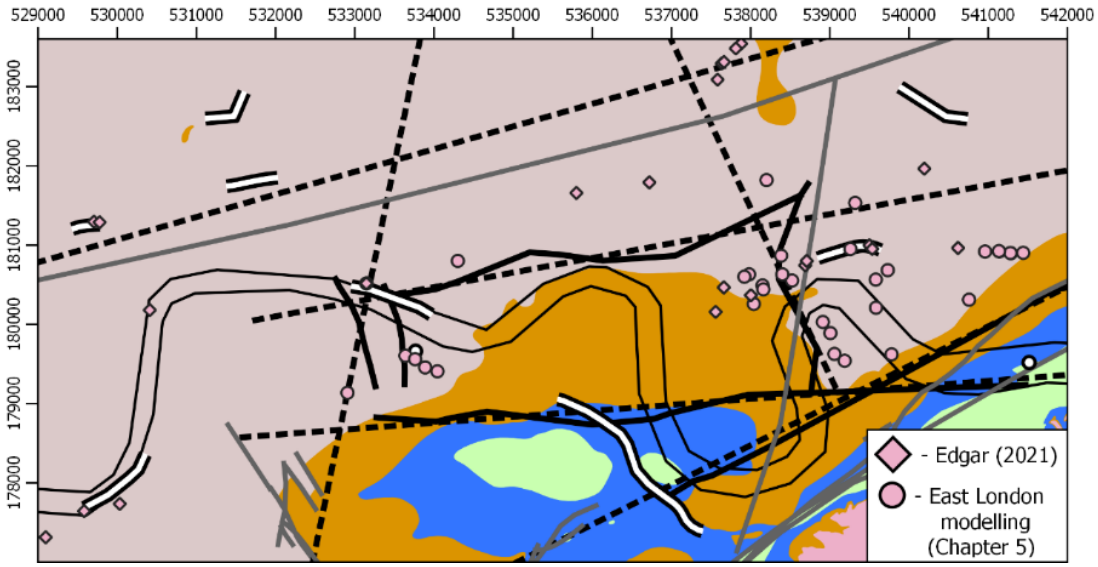

Figure 7.13 – Comparison of Harwich Formation cementation observations with major faulting and fault zones.

7.4.5 Geotechnical uncertainty and risk onsite

The preceding sections in §7.4 have demonstrated how major faulting can alter the rockmass, directly and indirectly, away from expected ground conditions in both a variable and inconsistent manner. This will inhibit their accurate characterisation during the ground investigation (GI) and introduce uncertainty: the degree of confidence in our engineering geological understanding of the ground conditions on site. This uncertainty can be categorised into 'aleatoric' and 'epistemic' (Nadim, 2007), with the 'variable' representing a major fault and associated features on or near site:

- Aleatoric uncertainty – The natural randomness of the variable.
- Epistemic uncertainty – The uncertainty due to lack of knowledge on the variable.

Fault-related UGCs are a product of these uncertainties and reflect their misidentification and/or misinterpretation. The aleatoric uncertainty will be significant given the observed variability of major fault architectures and their associated features. Epistemic uncertainty is currently high and acts at two scales: Firstly, at the fault-scale as their individual architectures (fig. 7.6), influence on other processes (§6.1), and their relationship with other features (§7.3.3-5) are broadly unresolved. Secondly, at site-scale due to potential complexities present and is a function of the aleatoric uncertainty. Both factors will make UGCs more likely and elevate geotechnical risks onsite.

Uncertainty will progressively reduce as the broader epistemic component is overcome by further geological studies, particularly through characterising each fault set and individualising the architecture and geological impact of every major fault. But residual aleatoric and site-scale epistemic uncertainty will both remain high near faults and require targeted GIs (§7.5).

7.5 Tailoring ground investigations near major faulting

Where major faulting is suspected on or near site, problematic ground conditions must be expected until proven otherwise. To mitigate these, the ground investigation (GI) must be targeted to identify them and their associated features. Otherwise, they will not be geotechnically appraised and may become UGCs: "*an assessment of the implications of such faulting can only be made once such faulting has been identified*" (Everett and Dewar, 2015). Whether these are impactful is project-specific but need to be identified regardless.

To aid this, a flow diagram was developed that tailors additional GI requirements depending on a site's positioning relative to a major fault or shear zone (fig. 7.1), represented in two separate tables (tables 7.1-7.2). This will help to account for the varying geotechnical impact of major faulting across London (fig. 7.9) by improving its characterisation on- and near-site. These primarily comprise a combination of borehole log analyses, explicit-driven geological modelling, and lab testing. The recommendations will not directly identify strike-slip faults due to the lack of elevation changes. But possible methods are outlined for collating potential indirect evidence of them (e.g., §4.4.3.1; §5.4.3; §6.1.3.3).

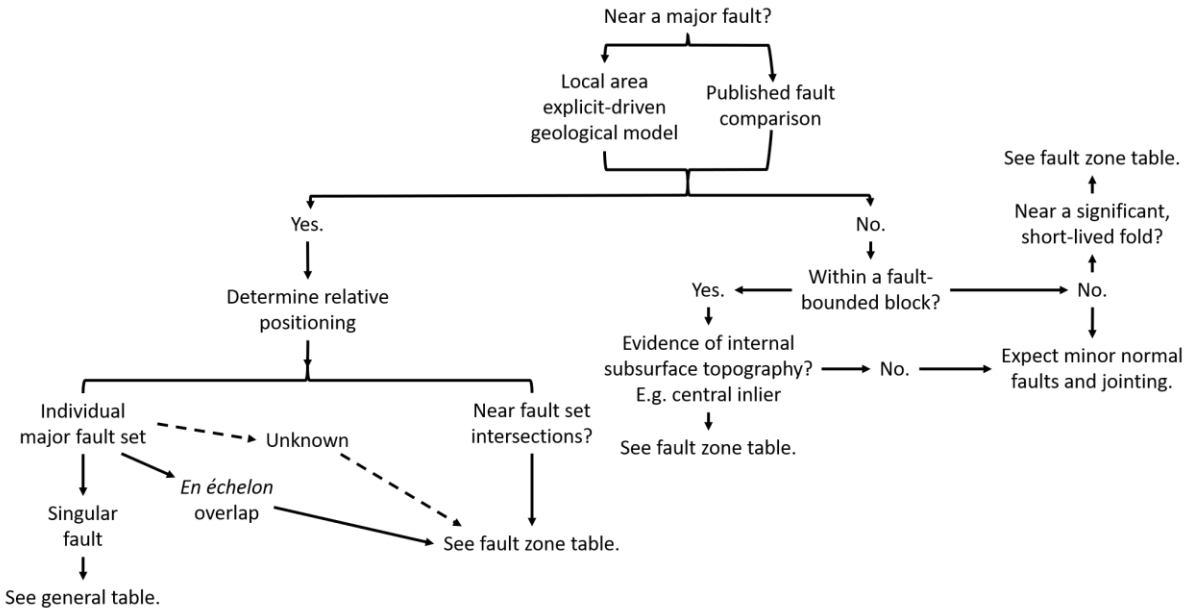

Figure 7.14 – Flowchart for assessing whether targeted ground investigations are necessary for a site in London, depending on its proximity to major faulting. Whilst tailored for faulting only, these methods may also aid characterisation of complications associated with bedrock lithology and periglacial alteration also.

The distance constituting 'near' is intentionally undefined as there is insufficient information to quantify this zone around the major fault at this stage. Instead, it will be site-specific and should be determined during the preliminary desk study (fig. 7.19) by comparing the site with fault maps from this investigation and the BGS Lithoframe, and fault zone locations (fig. 6.21), and by developing a site geological model and (at least) 200 m of the surrounding area and identifying tectonic indicators (§5.4.3; fig. 5.39), both from pre-existing boreholes.

Table 7.1 – General table of ground investigation considerations for the engineering geological appraisal of a singular major fault (fig. 7.19) and potential associated hazards on site.

Characterisation Purpose	Engineering Geology Hazard	Investigative Method(s)	Ground Investigation Input Data
Across-fault lithological changes	Lithological coverage	PSD analysis	Lab testing
		Borehole log analysis	High-density onsite borehole drilling Local boreholes
	Thickness changes	Explicit-driven geological modelling	
	Fault offset		
Fault geometry defining	Fault position(s)		Discontinuity logging Down-hole telemetry & televiewer
	Width/No. of faults		
Structural characterisation	Internal architecture (Damage zone & fault core) (e.g., fig. 5.5.a)	Fracture state	
		Stereographic analysis	
	Slip behaviour		
Deformation characterisation	Geotechnical parameters	Rock mass characterisation	Borehole logs
		Bulk strength and stiffness testing	Bulk sampling Downhole CPTs and SPTs
		Shear plane testing	Intact sampling
	Permeability (Across & along fault)	Down-borehole packer testing	
		Permeability testing	Bulk sampling
Material-specific hazards	Drift-filled hollows	Rockhead analysis (Geological Modelling)	Borehole logs
		Lithological analysis	
	Harwich cementation		

Table 7.2 – Additional criterion for geotechnical appraisal of fault zones and associated hazards (fig. 7.19).

Characterisation Purpose	Engineering Geology Hazard	Investigative Method(s)	Ground Investigation Input Data
To be referred to in addition to the general table (table 7.2) for major fault characterisation			
Shear zone geometry	Shear zone extents	Explicit-driven geological modelling	High-density onsite borehole drilling Local boreholes
	Shear zone type (fig. 7.6.b)		
	Structural characterisation of interior	Stereographic analysis	Discontinuity logging Down-hole televiewer
Shear zone deformation	Enhanced brittle deformation	Fracture state	
		Rockmass characterisation	Borehole logs
		Bulk strength and stiffness testing	Bulk & intact sampling Downhole CPTs and SPTs
		Shear plane testing	
		Permeability testing	Packer testing
	Intact plastic deformation	Shear strength tests	Intact sampling
		Stiffness testing	

8. Conclusion

This research has investigated major faults in London to characterise their origins, architectures, locations, and impact on geological processes and engineering geology (§1.1). London's bedrock geology has been demonstrated to be more complex than recognised (fig. 7.9). Major faults have offset the Late Cretaceous-Palaeogene 'layer cake', regionalised certain geological and hydrogeological processes, and locally distorted the rock mass into complex shear zone structures. Their assessment led to the identification of broader tectonic structures that are critical to our understanding of the London Basin.

The investigative approach and the research outputs are summarised here.

8.1 Research approach

London's geological record is deficient in structural information due to minimal bedrock exposure, limited fault analysis and incomplete subsurface characterisation of both the near-surface and basement-cover relationships. This has caused faults to be under-recognised, since evidence for them is disparate and patchy, and is exacerbated by the historical perspective that London is structurally simplistic, downplaying their documentation (§2.2.2.5).

This research adopts a 'multiple lines of evidence' approach (fig. 1.1) to overcome the information deficiency and characterises major faults across London in a manner could not be achieved by any single method in isolation. This involved the development of two novel methods for fault characterisation that may be applicable in other poorly exposed and/or inaccessible regions:

- Retrospective characterisation of 2D fault reactivation feasibility under palaeostress regimes (§3.2). This couples Sibson's (1985) reshear theory with Alpine Phases stress axes to determine whether London's basement faults could feasibly reactive, but not if they did. The outputs are verified by published observations of Alpine fault reactivation in southern Britain.
- Indirectly mapping faults from spatially coincident lineaments in both long timeframe InSAR and modelled subsurface topography (§4.2.1). The majority of lineaments are validated by the East London geological model (§5.4) and the BGS Lithoframe (fig. 4.25). The method favours dip-slip faults identification because of the reliance on solely vertical data (§4.4.3), but comparisons with lateral E-W InSAR (fig. 4.29) imply applicability for appropriately oriented strike-slip faults.

8.2 London's tectonic framework

The literature review (§2.1.1) shows that the Late Cretaceous-Palaeogene cover in London straddles structurally distinct basement. To determine how this may affect major fault generation, a tectonic framework was developed to outline basement-cover relationships in London for Alpine compression, specifically between basement faults and the unfaulted but weak cover (fig. 3.1). The framework progressed (§7.1.1) to incorporate the outcomes of the fault inheritance analyses (§3.2-3), basement-cover stress distribution (§3.4), fault mapping and extents in the southern London Basin (§4, 5.3-4, 3.4), and observations from seismic profile RG-001 (fig. 3.26). These new insights lead to repositioning of the Variscan Front to account for Variscan faulting in London (§7.1.2), and the tectonic redefining of the London Basin to recognise how the basement controlled its formation (§7.1.3). The outcome is an improved understanding of London's tectonic framework and why it is faulted (fig. 7.4).

The mechanically contrasting basement regions underlying the London Basin are referred to here as 'structural domains'. Previously two domains were recognised (e.g., Sumbler et al., 1996, fig. 2): the Weald Basin and its weak basement; and the rigid London Platform/Anglo-Brabant Massif. In this research, a third domain, the northernmost imbricated Variscan thrust sheet, is inferred under the southern London Basin, which repositions the Variscan Front northwards onto the Massif (§7.1.2). The thrust sheet represents a transitional interface between the basin and platform domains and contains Variscan thrust and strike-slip, and exploitative post-Variscan listric normal faults. Alpine stresses were focused within this domain as the inverting Weald Basin was buttressed against the rigid Massif.

The 'London Basin' has been reinterpreted (fig. 7.4) after evidence contradicting the synclinal model was identified from basement modelling and a critique of its structural interpretation (§7.1.3). The regional structure and the uplift of the Basin's chalk flanks are direct products of differential inversion and epeirogenic responses by the structural domains it straddles. Weald Basin inversion uplifted the region's southern flank to dip northwards whilst south-eastward tilting of the London Platform gently inclined its cover to produce a fold-like geometry (fig. 7.2). Differential cover deformation across the region mirrors the mechanical contrasts of the structural domains. The region is tentatively redefined as the 'London Blanket' because it was formed by the basement it straddles rather than a single discrete mechanism. Comparatively, the London 'Basin' is a strictly geomorphological description.

London is situated above the Variscan thrust sheet domain, which likely extends beyond North London (fig. 7.1). Alpine stresses concentrated here to cause unique inversion characterised by basement fault inheritance but with minimal direct deformation or uplift in the cover (fig. 7.4; §3.4). London's structural geology is, therefore, a product of its crustal positioning.

8.3 Major faulting in London

'Major faults' are defined by this investigation as laterally extensive and mappable faults with metre-to-decimetre scale throws; these are distinct from the short-lived but more prevalent 'minor faults'. Three major fault sets are interpreted in London's near surface, from orientation analysis of faults and indicative lineament features (§4.3.2); these strike ENE, NNE-NE and NW. Their positions are identified to correspond with changes in regional and local subsurface topography (fig. 3.39, 4.12, 5.24-29), strata thicknesses (fig. 5.30-34; §6.1.1-2), at-surface displacement (fig. 4.19; §4.4.6), Lower Aquifer behaviour (§6.1.3), and changes in certain strata (§6.1.1-2). Additionally, fault positions are coincident with certain fluvial, periglacial, and lithological (fig. 4.5; §7.4.4) features.

Major faults are determined to have influenced, to varying degrees, the geological, hydrogeological, and geomorphological processes in London from the Late Cretaceous to present. The key features of the new interpretations presented in this research are summarised here.

8.3.1 Origins and reactivation behaviour

This work has concluded that London's major faults were inherited from three basement fault sets in the shallow, underlying Variscan thrust sheet by coupling kinematic reactivation analyses (§3.2) with propagation evidence from direct observations and indirect near surface evidence (§3.3). The inherited sets comprise a Variscan strike-slip conjugate pair and reversed post-Variscan normal faults. The findings validate the suspected basement origins of significant structures in London (Ellison et al., 2004, Royse et al., 2012).

These basement faults were repeatedly reactivated throughout the Late Cretaceous-Palaeogene in response to Alpine compression. Set-specific reshear mechanisms and obliquity, and favourability are determined to have temporally evolved between each Alpine tectonic phase as the stress field changed to produce characteristic slip behaviour in each set:

- NW-set (strike-slip): Dextral becoming sinistral reshearing with a minimal dip-slip component.
- NNE-set (strike-slip): Sinistral reshearing with a minor dip slip component.
- ENE-set (reversed normal fault): Dip-slip dominant with a minor sinistral slip component.

But reshear preference was also identified to be regionalised, since the dominant fault set changes across London (fig. 2.31). This was attributed to northernmost major listric fault branch (WSG-Fault, §7.2.1) favouring listric normal fault branch inheritance south of it; but this may also reflect practical difficulties in mapping strike-slip faults (§4.4.3).

8.3.2 Major fault architectures: Propagation and interaction in the cover

The inheritance of each fault set was initially determined by comparing their expected reshear behaviour with known propagation processes. Two mechanisms were originally presented, based on their dominant slip component and propagation evidence in the cover and near surface (§3.3): lateral-slip reshear favoured splayed *en échelon* Riedel shear development (fig. 3.33-36), whilst reversed dip-slip dominance caused *en échelon* and branching propagation (fig. 3.27, 3.32). This scheme was revised to incorporate a third mechanism (fig. 7.6.a; §7.2.2) to account for oblique-slip reactivation (§3.2.6) and more complex inheritance indicated by the WSG-Faults (§5.4, 6.1-2, 7.2.1). Two additional observations are made for fault propagation in the southern London Blanket. First, fault curvature causes propagation styles to vary along the length of a fault as the slip sense changes (§7.2.1) (but this is unlikely to be important on the scale of London, fig. 7.5). Secondly, propagation zone widths in the cover are attributed partly to fault development in the basement; the majority are narrow (e.g., Northern Boundary Fault, §6.2.3.3), although weaker but more significant structures have km-wide zones (e.g., WSG-Faults, §7.2.1).

'Fault zones' in London are characterised in §6.2 by compiling structural data and observations from multiple structures (fig. 6.22; table 6.2). They are interpreted to be confined shear zones of oblique-slip Riedel shears with evidence for both transpressive and transtensive conditions (§6.2.1.2). Shear stress concentrations cause significant deformation internally, including the formation of minor faults atypical for London (§7.4.3). Shear zones are demonstrated to be causally linked with major fault interactions (§6.2.2-3), which provide the required bounding faults to generate shear zones through linkage and/or confined block shearing (fig. 7.6.b). However, 'fault zone' characterisation is incomplete and requires additional data to define 3D geometries of internal faulting, transtensional mechanisms, and minor fault zone architectures.

Major fault intersections in the cover are shown to have compartmentalised and offset the bedrock into discrete blocks (fig. 4.22, 4.29, 5.24-29). This partitioning causes irregular subsurface topography through differential offsetting by intersecting faults. Block styles and scales vary across London (fig. 4.28, 2.31), and are attributed here to changes in basement fault dominance under London (§7.2.1). Many blocks are undeformed but may be tilted, with shear zone development only identified in particular one block, the Millwall Anticline (§6.2.3.2, 6.2.3.5).

East London is reinterpreted here to recognise the structural complexity caused by the interplay of fault inheritance, shear zone generation and block compartmentalisation on its subsurface (fig. 7.9).

8.3.3 Major fault coverage and identification in London

Major fault identification in London is inhibited by extensive urbanisation and superficial coverage, and masking within homogeneous strata (Aldiss, 2013). A review of previous mapping contributions (§4.1) and structural interpretations (§2.2.2.5) of London demonstrates that fault identification is also dependent upon both the technique itself and on the perspectives of the investigator, i.e., whether or not they expect faulting to occur. The combination of fault masking by methods and/or data sparsity, and the potential for misinterpretation further contribute to fault underrepresentation.

This investigation demonstrates a more extensive major fault network than previously recognised by undertaking indirect fault lineament mapping (§4.3.1) and explicit-driven geological modelling (§5.2); many faults are independently identified in the BGS Lithoframe (§5.4.1; fig. 4.25). The novel, indirect method presented here (§4.2.1) has identified new structures across London but still lacks the resolution needed to define local, small-scale variation, and so highlights the need for ground truthing. The East London model provides this validation (§5.3), characterising the architectures of major faults and shear zones, as well as demonstrating how they partitioned the subsurface (§5.4). The major fault map of London is still incomplete, however, as demonstrated by isolated fault zones (fig. 6.21), particularly in West London.

Some shear zones have historically been misinterpreted in London. Two major anticlinal outliers in East London are reinterpreted as transpressive shear zones (Millwall and Greenwich) from faulted interiors interpreted during both fault zone analysis (§6.2.3.1-2) and geological modelling (§5.4.4.2). Historical misinterpretation is determined to reflect their comparable fold-like geometries (fig. 7.8) and lack of exposure, with a criterion proposed to improve differentiation (§7.2.3).

The two fault sets with minimal-to-minor dip slip components are likely missed by conventional mapping methods that rely on vertical offsets in unexposed areas (§4.4.3). Several methods have been identified to improve the indirect mapping of strike-slip dominant faults, in order of confidence: long timeframe E-W lateral InSAR analysis (fig. 4.29); in-borehole indicators (fig. 5.39; §5.3.4, §5.1.2); low permeability barriers (fig. 6.14); inlier offsetting (§4.4.3); and linkage zone tracing (§4.4.3).

8.4 Impact on subsurface geology and geological processes

This investigation assesses De Freitas' (2009) proposal that London's subsurface geology and hydrogeology are structurally partitioned by using geological modelling (§5.3), spatial analyses of lithological and groundwater data (§6.1), indirect mapping (§4.2.1, 4.4.4), and comparisons with BGS

Lithoframe outputs (§5.4.1). These demonstrate that major faulting has compartmentalised the ground in London, to varying degrees, from the Late Cretaceous to present.

The intersecting network of inherited faults in London's near surface offset and generate irregular subsurface topography, bound both undeformed and sheared blocks, regionalise both denudation and certain depositional processes, impede Lower Aquifer interactions, and partition at-surface displacement. There is limited indication that certain fault sets were more influential for particular processes. The full extent of fault compartmentalisation is unclear but demonstrates the impact of both their presence and recurring Alpine activity on the ground.

8.5 How tectonic-scale processes affect site-scale engineering

The engineering geological impact of a major fault in London reflects how it alters the expected ground conditions, i.e., its geology, features, and mechanical properties. This investigation identifies that major faults cause alteration at two scales: localised by tectonism-related rockmass degradation, offsetting, the introduction of secondary complications (§7.4) and by shear zone development (§6.2); and regionalised, by block-bounded topographic, sedimentological, and hydrogeological partitioning (§6.1). The presence and scale of these mechanisms are, however, inconsistent and reflect both along-fault structural, and across-fault geological, variation.

8.6 Characterising faulting and its engineering geology effects on site

Major faulting is interpreted to increase uncertainty and geotechnical risk on or near a site (§7.4.5). However, the impact of a particular fault will be unique since the lithological, mechanical, elevational, and hydrological changes caused and their extents will be both fault- and location-specific. Such variation inhibits accurate engineering geological characterisation of major faults during the ground investigation and increases the likelihood of unexpected ground conditions.

A workflow has been designed to target faults and their engineering geological effects through additional investigative measures (§7.5) based on a site's positioning relative to a major fault or shear zone (fig. 7.19). Additionally, a new method for categorising fault zones at the site-scale is also proposed (§6.2.1.3), which should improve and standardise their definition. Collectively, the approaches developed here can improve the engineering geological characterisation of faults to reduce the risk of unexpected ground conditions, and to provide additional structural data.

8.7 Investigation review and research impact

The characterisation of London's major faults is not straightforward. The investigative approach developed here overcomes the information deficiency by collective analysis rather than discrete observations. The extents and mechanisms of individual major faults require further attention because the necessary structural information is broadly incomplete or unavailable. Occasionally limited information led to an overreliance on certain structures that may limit the transferability of some interpretations (e.g., §6.2.3.3). Similarly, it is likely that some faults are not identified in the East London model because the level of structural detail achieved across it is inconsistent, largely due to irregular borehole coverage (§5.5.3, 5.5.5.1). However, the investigation's approach enables the interpretation of London's faults to an unprecedented level of detail, by comparing observations with reasoned inferences and known fault behaviours.

The impacts of these research outputs can be viewed from three perspectives: tectonic, geological, and engineering. Tectonically, the research demonstrates that intraplate regions can respond to far-field tectonic events and undergo complex deformation, reflecting macroscopic strain distributions between mechanically contrasting structural domains, leading to the reinterpretation of the 'London Blanket' (fig. 7.4). Geologically, the work redefines London structurally to demonstrate the greater complexity caused by widespread fault inheritance that has influenced its near surface geology (fig. 7.9). For engineering, the impact of increased structural complexity is to unpredictably alter the ground conditions and rock mass properties through multiple processes, to increase uncertainty and risk near major faults.

The research also develops new methods to structurally analyse faults, and new tools to characterise their engineering geological effects in London. The reshear assessment (§3.2) provides a method for retrospective appraisal of fault reactivation feasibility. This was applied to basement fault sets under London, with its findings broadly verified by proxy evidence. The indirect fault mapping method (§3.3) provides an alternative method to map faults in an urban environment with no exposures. Whilst this method linearises faults and was restricted by data resolution, it identifies both known and unknown faults in London (fig. 4.28). The workflows for targeting major faults during ground investigations and for categorising fault zones are outlined in §8.6, with both providing solutions to standardising fault identification and characterisation in London.

8.8 Recommendations for future works

New research questions have been identified which will continue this research into London geology, Alpine tectonism in southern Britain, and fault reactivation, to verify and develop upon these findings.

8.8.1 Future directions of research on the geology of London

Future research into the structural geology of London should be focussed in four directions: broader, explicit-driven modelling of London; defining the northern limit of fault inheritance; further characterisation of fault zones; and analyses of geotechnical properties near faulting.

The East London model identified new faults and subsurface complexity that require verification. A new modelling programme could be developed to better define faulting and subsurface lithologies within and beyond East London and incorporate the recommendations in §5.5.4. The model should extend to West London and characterise structures along the routes of near-future tunnel alignments (e.g., Crossrail 2, Lower Thames Crossing, Bakerloo Line Extension).

The northern limit of fault inheritance in the southern London Blanket requires further definition (§7.1.2, 3.4) to provide both a proxy for the underlying Variscan Front (fig. 7.1) and define the regional extent of where major faults pose a geotechnical risk.

Fault zone analysis requires higher resolution characterisation to define their 3D internal architectures from a broader range of shear zones and should be focussed towards minor fault zones and contradictory transtensional structures (§6.2.3.3-4). Such development will require greater borehole densities and ideally shallow seismic profiles to generate detailed models.

Data availability has limited the appraisal of the geotechnical impact of faulting in London (§7.4.2) and is an area that needs further attention. An assessment of how faults alter rock mass properties could be achieved by developing material baselines to compare lab testing and fracture logging against, and how these vary between different fault architectures. Fieldwork in proxy locations could also provide direct case studies of faulting in comparable rock masses (e.g., Tudor, 2019, Rhind, 2019).

8.8.2 Future research directions into Alpine tectonism in southern Britain

This investigation shows that southern Britain represents an interplay of far-field Alpine compression and epeirogeny (§2.1.1). As illustrated by the London Blanket (§7.1.3), differential responses to both processes between structural domains demonstrate that intraplate Alpine tectonism in southern Britain was more complex than basin inversion alone. To better understand the interaction of both processes, the exact timings and evolution of each Alpine Phases require further investigation in terms of stress magnitudes and axes orientations. Similarly, regional susceptibility to epeirogenic events requires constraining. This could be approached using to the research steps outlined in §7.1.3.2.

8.8.3 Future research directions into fault reactivation

The Alpine reactivation of pre-existing faults in southern Britain is already established (§3.1). This investigation contributes to that understanding by retrospectively identifying how their reshear feasibility temporally evolved with the stress regime using the method developed in §3.2. It is applicable anywhere where pre-existing faults are reactivated by later stresses. The method itself could be improved by developing it into a 3D mechanism that captures oblique-slip reactivation behaviour (§3.2.6.1).

The approach could become a powerful tool for deducing spatiotemporal variation in reactivation behaviour within a fault set by coupling it with calcite-vein dating of individual reshear events (e.g., Parrish et al., 2018). This would confirm both whether and how a particular fault within a set reactivates to demonstrate regional variation, as the stress field evolved. The exposed Palaeozoic Lustleigh-Sticklepath Fault and its Cenozoic pull-apart structures (fig 3.19; §3.2.3.5) provides a case study to verify this by allowing both timing and kinematic behaviour to be analysed in parallel.

Finally, analogue modelling is recommended to investigate how sinistral reversal of the Variscan dextral strike-slip set (§3.2.3) affected the development of its propagated faults in the overlying cover. Reverse lateral-slip fault inheritance does not appear to have been previously studied, so it is unclear how push-up linkage structures would respond to transtensional conditions. This represents novel research that would also benefit characterisation of cover deformation in London.

8.9 Final remarks

Major faults pose significant geotechnical risks in London but are still a geological uncertainty, requiring further investigations to better characterise them. Two obstacles are identified that may hinder further identification and characterisation of major faults. Firstly, geological perspectives of London need updating to recognise inherited faulting, and that it is a complex product of intraplate Alpine compression and basement tectonism. Secondly, improved data sharing by the geotechnical community is needed from faulted sites to aid investigations such as this, to provide a broader range of structural observations. Collectively, this will lead to an improved expectation and understanding of faulting and help to reduce fault-related uncertainty and the risk of unexpected ground conditions.

Attitudes are now changing towards acknowledging major faulting in London (Aldiss, 2013, Royse et al., 2012), showing their broader coverage (BGS Lithoframe), and describing their structures (e.g., Newman, 2017). This investigation should change perceptions further by characterising the origins, architectures, coverage, geological influences, and site-scale engineering geology of major faults.

9. References

AGAR, S. A., LAWRENCE, J. A., GHAIL, R. C., MASON, P. J. & THOMPSON, S. 2018. PSInSAR remote sensing observations of deformation behaviour at Salisbury Plain, UK. *Engineering in Chalk.*

ALDISS, D., BURKE, H., CHACKSFIELD, B., BINGLEY, R., TEFERLE, N., WILLIAMS, S., BLACKMAN, D., BURREN, R. & PRESS, N. 2014. Geological interpretation of current subsidence and uplift in the London area, UK, as shown by high precision satellite-based surveying. *Proceedings of the Geologists' Association,* 125**,** 1-13.

ALDISS, D., BURKE, H., CHACKSFIELD, B. & TRAGHEIM, D. 2006. Absolute fixing of tide gauge benchmarks and land levels: the BGS contribution to a report on a study of the London and Thames estuary region (CR/07/043N). Unpublished.

ALDISS, D. T. 2013. Under-representation of faults on geological maps of the London region: reasons, consequences and solutions. *Proceedings of the Geologists' Association,* 124**,** 929-945.

ALDISS, D. T. 2014. The stratigraphical framework for the Palaeogene successions of the London Basin, UK, OR/14/008. *British Geological Survey Open Report.* Keyworth, Nottingham: British Geological Survey.

ALDISS, D. T., BLACK, M. G., ENTWISLE, D. C., PAGE, D. P. & TERRINGTON, R. L. 2012. Benefits of a 3D geological model for major tunnelling works: an example from Farringdon, east–central London, UK. *Quarterly Journal of Engineering Geology and Hydrogeology,* 45**,** 405-414.

ALDISS, D. T., FARRANT, A. R. & HOPSON, P. M. 2018. Comments on "Gale, A S., Norman Berry Peake, 1921-2010, a chalk revolutionary" [Proc. Geol. Assoc. 128 (2017), 829-839], and "Gale, A S & Lovell, B., The Cretaceous-Paleogene unconformity in England: Uplift and erosion related to the Iceland mantle plume" [Proc. Geol. Assoc. (2017) doi.org/10.1016/j.pgeola.2017.04.002]. *Proceedings of the Geologists' Association*.

ALLEN, P. 1954. Geology and Geography of the London–North Sea Uplands in Wealden Times. *Geological Magazine,* 91**,** 498-508.

ALLMENDINGER, R. W., CARDOZO, N. & FISHER, D. M. 2011. *Structural Geology Algorithms: Vectors and Tensors,* Cambridge, Cambridge University Press.

ALLSOP, J. & SMITH, N. 1988. The deep geology of Essex. *Proceedings of the Geologists' Association,* 99**,** 249-260.

AMEEN, M. S. 1995. Fracture characterization in the Chalk and the evolution of the Thanet monocline, Kent, southern England. *Geological Society, London, Special Publications,* 92**,** 149-174.

AMEEN, M. S. & COSGROVE, J. W. 1990. Kinematic analysis of the Ballard Fault, Swanage, Dorset. *Proceedings of the Geologists' Association,* 101**,** 119-129.

ANDERSON, H., WALSH, J. J. & COOPER, M. R. 2018. The development of a regional-scale intraplate strike-slip fault system; Alpine deformation in the north of Ireland. *Journal of Structural Geology,* 116**,** 47-63.

ANDREWS, J. N., CHEN, M., DENNIS, F., LONG, J. L. A., PARKER, A., PRICE, M. & RAE, J. E. 1995. Hydrogeology and hydrochemistry of the London Basin. Thames Water Utilities Limited: Postgraduate Research Institue for Sedimentology, University of Reading.

BANKS, V. J., BRICKER, S. H., ROYSE, K. R. & COLLINS, P. E. F. 2015. Anomalous buried hollows in London: development of a hazard susceptibility map. *Quarterly Journal of Engineering Geology and Hydrogeology,* 48**,** 55-70.

BAPTIE, B. 2010. Seismogenesis and state of stress in the UK. *Tectonophysics,* 482**,** 150-159.

BARROW, G. 1906. II. Notes on Recent Excavations in the London area. *Summary of progress of the Geological Survey of the United Kingdom and Museum of Practical Geology for 1905. Memoir of the Geological Survey of Great Britain.* London: HMSO.

BARROW, G. & WILLS, L. J. 1913. *Records of London wells,* London, HMSO.

BARTON, N. 1973. Review of a new shear-strength criterion for rock joints. *Engineering Geology,* 7**,** 287-332.

BARTON, N. 2006. *Rock quality, seismic velocity, attenuation and anisotropy*, CRC press.

BAUERMAN, H., WHITAKER, W., POLWHELE, T. R., TRENCH, R. & BRSTOW, H. W. 1885. *Western part of London, St. Albans, Wendover, High Wycombe, Windsor, Staines, Uxbridge [Solid, 7]*. London: Geological Survey of England and Wales.

BELLHOUSE, M. R., SKIPPER, J. A. & SUTHERDEN, R. N. 2015. The engineering geology of the Lee Tunnel. *Geotechnical Engineering for Infrastructure and Development.*

BERGERAT, F. & VANDYCKE, S. 1994. Palaeostress analysis and geodynamical implications of Cretaceous-Tertiary faulting in Kent and the Boulonnais. *Journal of the Geological Society,* 151**,** 439-448.

BERRY, F. G. 1979. Late Quaternary scour-hollows and related features in central London. *Quarterly Journal of Engineering Geology and Hydrogeology,* 12**,** 9-29.

BEVAN, T. G. & HANCOCK, P. L. 1986. A late Cenozoic regional mesofracture system in southern England and northern France. *Journal of the Geological Society,* 143**,** 355-362.

BEVINS, R. E. H., J. M., EVANS, A. D. & MORGAN, R. 1996. Palaeogene dyke swarm, NW Wales: evidence for Cenozoic sinistral fault movement. *Journal of the Geological Society,* 153**,** 177-180.

BISCHOFF, C., MASON, P., GHAIL, R., GIANNICO, C. & FERRETTI, A. 2020a. Monitoring excavation-related ground deformation in London, UK using SqueeSAR™. *Tunnels and Underground Cities: Engineering and Innovation Meet Archaeology, Architecture and Art: Volume 11: Urban Tunnels-Part 1***,** 5360.

BISCHOFF, C. A., GHAIL, R. C., MASON, P. J., FERRETTI, A. & DAVIS, J. A. 2020b. Revealing millimetre-scale ground movements in London using SqueeSAR™. *Quarterly Journal of Engineering Geology and Hydrogeology,* 53**,** 3-11.

BLACK, M. 2017. Crossrail project: managing geotechnical risk on London's Elizabeth line. *Proceedings of the Institution of Civil Engineers - Civil Engineering,* 170**,** 23-30.

BLUNDELL, D. J. 2002. Cenozoic inversion and uplift of southern Britain. *Geological Society, London, Special Publications,* 196**,** 85-101.

BONÌ, R., CIGNA, F., BRICKER, S., MEISINA, C. & MCCORMACK, H. 2016. Characterisation of hydraulic head changes and aquifer properties in the London Basin using Persistent Scatterer Interferometry ground motion data. *Journal of Hydrology,* 540**,** 835-849.

BONINI, L., BASILI, R., TOSCANI, G., BURRATO, P., SENO, S. & VALENSISE, G. 2015. The role of pre-existing discontinuities in the development of extensional faults: An analog modeling perspective. *Journal of Structural Geology,* 74**,** 145-158.

BONINI, M., SANI, F. & ANTONIELLI, B. 2012. Basin inversion and contractional reactivation of inherited normal faults: A review based on previous and new experimental models. *Tectonophysics,* 522-523**,** 55-88.

BOTT, M. H. P. 1959. The Mechanics of Oblique Slip Faulting. *Geological Magazine,* 96**,** 109-117.

BOYLE, J., STOW, R. & WRIGHT, P. 2000. InSAR imaging of London surface movement for structural damage management and water resource conservation. *ERS-Envisat Symposium 'Looking Down to Earth in the New Millennium'.* Gothenburg, Sweden: European Space Agency.

BRIDGLAND, D. R. & GIBBARD, P. 1997. Quaternary River Diversions in the London Basin and the Eastern English Channel. *Géographie physique et Quaternaire,* 51**,** 337-346.

BRISTOW, C. R., LAKE, R. D., WOOD, C. J., BIGG, P. J., MEDD, A. W., HUGHES, M. J., GREGORY, D. M., EVANS, R. B., HARRISON, R. K., LAWRENCE, A. R., CLARKE, M. R. & SIMMONS, M. B. 1985. *Geology of the country around Chelmsford Memoir for 1:50,000 geological Sheet 241,* London, HMSO.

BRISTOW, H. W., WHITAKER, W. & ETHERIDGE, R. 1862. *The Geology of parts of Berkshire and Hampshire (Sheet 12)*, HM Stationery Office.

BRITISH GEOLOGICAL SURVEY. 1977. *Swansea, England & Wales Sheet 247*. Keyworth, Nottingham: British Geological Survey.

BRITISH GEOLOGICAL SURVEY. 1996. *Romford. Sheet 257. Solid and Drift Geology. 1:50,000.* Keyworth, Nottingham: British Geological Survey.

BRITISH GEOLOGICAL SURVEY. 1998a. *Dartford. Sheet 271. Solid and Drift Geology. 1:50,000.* Keyworth, Nottingham: British Geological Survey.
BRITISH GEOLOGICAL SURVEY. 1998b. *South London. Sheet 270. Solid and Drift Geology. 1:50,000.* Keyworth, Nottingham: British Geological Survey.
BRITISH GEOLOGICAL SURVEY. 2002. *Words Head, England & Wales Sheet 246*. Keyworth, Nottingham: British Geological Survey.
BRITISH GEOLOGICAL SURVEY. 2006. *North London. Sheet 256. Solid and Drift Geology. 1:50,000.* Keyworth, Nottingham: British Geological Survey.
BROMEHEAD, C. E. N., DINES, H. G. & PRINGLE, J. 1925. *The geology of North London: Explanation of one-inch geological sheet 256 new series,* London, HMSO.
BROMEHEAD, C. N. 1922. Excursion to Brockley, Bromley Park and Beckenham: Saturday, July 16th, 1921. *Proceedings of the Geologists' Association,* 33**,** 77-IN4.
BROOKS, M., TRAYNER, P. M. & TRIMBLE, T. J. 1988. Mesozoic reactivation of Variscan thrusting in the Bristol Channel area, UK. *Journal of the Geological Society,* 145**,** 439-444.
BSI 2015. BS5930: Code of practice for ground investigations. British Standards Institution.
BUCHAN, S. 1938. *The water supply of the County of London from underground sources,* London, HMSO.
BUCHANAN, J. G. & BUCHANAN, P. G. 1995. *Basin inversion*, Geological Society London.
BUCKLAND, W. 1826. XI.—On the Formation of the Valley of Kingsclere and other Valleys by the Elevation of the Strata that enclose them; and on the Evidences of the original Continuity of the Basins of London and Hampshire. *Transactions of the Geological Society of London,* S2-2**,** 119-130.
BULLARD, E., GASKELL, T., HARLAND, W. & KERR-GRANT, C. 1940. Seismic investigations on the Palaeozoic floor of East England. *Philosophical Transactions of the Royal Society of London A: Mathematical, Physical and Engineering Sciences,* 239**,** 29-94.
BURKE, H., MARTIN, C. & TERRINGTON, R. 2018. Metadata report for the City of London 3D geological model (OR/18/030) (Unpublished). Nottingham, UK: British Geological Survey.
BURKE, H., MATHERS, S., WILLIAMSON, J., THORPE, S., FORD, J. & TERRINGTON, R. 2014. The London Basin superficial and bedrock LithoFrame 50 Model. British Geological Survey Open Report (OR/14/029). Nottingham, UK: British Geological Survey.
BUSBY, J. P. & SMITH, N. J. P. 2001. The nature of the Variscan basement in southeast England: evidence from integrated potential field modelling. *Geological Magazine,* 138**,** 669-685.
BUTLER, D. E. 1981. Marine faunas from concealed Devonian rocks of southern England and their reflection of the Frasnian transgression. *Geological Magazine,* 118**,** 679-697.
BUTLER, M. & JAMIESON, R. 2013. *UKOGL-RG-001*. UK Onshore Geophysical Library.
BYERLEE, J. 1978. Friction of rocks. *Pure and applied Geophysics,* 116**,** 615-626.
CARDOZO, N. & ALLMENDINGER, R. W. 2013. Spherical projections with OSXStereonet. *Computers & Geosciences,* 51**,** 193-205.
CARTER, D. J. & HART, M. B. 1977. Micropalaeontological investigations for the site of the Thames Barrier, London. *Quarterly Journal of Engineering Geology and Hydrogeology,* 10**,** 321-337.
CAWSEY, D. C. 1977. The measurement of fracture patterns in the chalk of Southern England. *Engineering Geology,* 11**,** 201-215.
CHADWICK, R. & EVANS, D. 2005. A seismic atlas of Southern Britain. British Geological Survey Occasional Publication No. 7. *British Geological Survey, Keyworth*.
CHADWICK, R. A. 1986. Extension tectonics in the Wessex Basin, southern England. *Journal of the Geological Society,* 143**,** 465-488.
CHADWICK, R. A. 1993. Aspects of basin inversion in southern Britain. *Journal of the Geological Society,* 150**,** 311-322.
CHADWICK, R. A. & EVANS, D. J. 1995. The timing and direction of Permo-Triassic extension in southern Britain. *Geological Society, London, Special Publications,* 91**,** 161-192.

CHADWICK, R. A., EVANS, D. J. & HOLLIDAY, D. W. 1993. The Maryport fault: the post-Caledonian tectonic history of southern Britain in microcosm. *Journal of the Geological Society,* 150**,** 247-250.

CHANDLER, R. J. 2000. The Third Glossop Lecture: Clay Sediments in Depositional Basins: the Geotechnical Cycle. *Quarterly Journal of Engineering Geology and Hydrogeology,* 33**,** 7-39.

CHANDLER, R. J., WILLIS, M. R., HAMILTON, P. S. & ANDREOU, I. 1998. Tectonic shear zones in the London Clay Formation. *Géotechnique,* 48**,** 257-270.

CHOI, J.-H., EDWARDS, P., KO, K. & KIM, Y.-S. 2016. Definition and classification of fault damage zones: A review and a new methodological approach. *Earth-Science Reviews,* 152**,** 70-87.

CHROSTON, P. & SOLA, M. 1975. The sub-Mesozoic floor in Norfolk. *Bulletin of the Geological Society of Norfolk,* 27**,** 3-19.

CIGNA, F., JORDAN, H., BATESON, L., MCCORMACK, H. & ROBERTS, C. 2015. Natural and anthropogenic geohazards in greater London observed from geological and ERS-1/2 and ENVISAT persistent scatterers ground motion data: Results from the EC FP7-SPACE PanGeo project. *Pure and Applied Geophysics,* 172**,** 2965-2995.

CLOOS, H. 1928. Experimente zur inneren Tektonik. *Cetralblatt fur Mineralogie,* 5**,** 609-621.

COGNÉ, N., DOEPKE, D., CHEW, D., STUART, F. M. & MARK, C. 2016. Measuring plume-related exhumation of the British Isles in Early Cenozoic times. *Earth and Planetary Science Letters,* 456**,** 1-15.

COLLETTINI, C., TESEI, T., SCUDERI, M. M., CARPENTER, B. M. & VITI, C. 2019. Beyond Byerlee friction, weak faults and implications for slip behavior. *Earth and Planetary Science Letters,* 519**,** 245-263.

CONWAY, B. & MCCANN, D. 1972. A geophysical and geological investigation at Barking Creekmouth, Essex. *Engineering Geology Unit Report EG 7/72.* Institute of Geological Sciences.

COOPER, M. A. & WILLIAMS, G. D. (eds.) 1989. *Inversion Tectonics*.

COPLEY, A. 2017. The strength of earthquake-generating faults. *Journal of the Geological Society*.

COPLEY, A. & WOODCOCK, N. 2016. Estimates of fault strength from the Variscan foreland of the northern UK. *Earth and Planetary Science Letters,* 451**,** 108-113.

CORFIELD, S. M., GAWTHORPE, R. L., GAGE, M., FRASER, A. & BESLY, B. 1996. Inversion tectonics of the Variscan foreland of the British Isles. *Journal of the Geological Society,* 153**,** 17-32.

COSGROVE, J. W. & HUDSON, J. A. 2016. *Structural Geology and Rock Engineering*, Imperial College Press.

COSGROVE, J. W., MORGAN, T. O. & GHAIL, R. C. 2021. The deformation history of southern England, and its implications for ground engineering in the London Basin. *Quarterly Journal of Engineering Geology and Hydrogeology*.

COWARD, M. 1990. The Precambrian, Caledonian and Variscan framework to NW Europe. *Geological Society, London, Special Publications,* 55**,** 1-34.

COWARD, M. P. & SMALLWOOD, S. 1984. An interpretation of the Variscan tectonics of SW Britain. *Geological Society, London, Special Publications,* 14**,** 89-102.

CROSETTO, M., MONSERRAT, O., CUEVAS-GONZÁLEZ, M., DEVANTHÉRY, N. & CRIPPA, B. 2016. Persistent Scatterer Interferometry: A review. *ISPRS Journal of Photogrammetry and Remote Sensing,* 115**,** 78-89.

CROSSRAIL 2005. Appendix E: Analysis of Impacts on Groundwater. *Specialist Technical Report 14: Water Resources Impacts.* London: Crossrail.

CROSSRAIL 2012. Key Plan - 3000 Series drawings - Plans and Geological Sections. *In:* MUSSON, G., DAVIS, J., BOTTERIL, M. & BLACK, M. (eds.) *Crossrail Line 1 Programme.* Geotechnical Consulting Group: Crossrail Limited.

CROSSRAIL 2016. Crossrail Geological Long Section - Post-Construction Update – April 2016: Appendices A & B. *In:* SKIPPER, J. A., SEMERTZIDOU, K., DAVIS, J. & BLACK, M. (eds.) *Crossrail Line 1 Programme.* Crossrail.

CULSHAW, M. G., ENTWISLE, D. C., GILES, D. P., BERRY, T., COLLINGS, A., BANKS, V. J. & DONNELLY, L. J. 2017. Material properties and geohazards. *In:* GRIFFITHS, J. S. & MARTIN, C. J. (eds.) *Engineering Geology and Geomorphology of Glaciated and Periglaciated Terrains – Engineering Group Working Party Report.* London: Geological Society, London, Engineering Geology Special Publications.

DAVIES, N. S., SHILLITO, A. P. & MCMAHON, W. J. 2019. Where does the time go? Assessing the chronostratigraphic fidelity of sedimentary geological outcrops in the Pliocene–Pleistocene Red Crag Formation, eastern England. *Journal of the Geological Society,* 176**,** 1154-1168.

DAVIS, A. G. 1928. The geology of the City and South London Railway Clapham-Morden extension. *Proceedings of the Geologists' Association,* 39**,** 339-IN13.

DE FREITAS, M. H. 2009. Geology; its principles, practice and potential for Geotechnics. *Quarterly Journal of Engineering Geology and Hydrogeology,* 42**,** 397-441.

DE FREITAS, M. H. & MANNION, W. G. 2007. A biostratigraphy for the London Clay in London. *Géotechnique,* 57**,** 91-99.

DE LA CONDAMINE, H. M. 1850. On the Tertiary Strata and their Dislocations in the Neighbourhood of Blackheath. *Quarterly Journal of the Geological Society,* 6**,** 440-449.

DE LA CONDAMINE, H. M. 1852. On a Reversed Fault at Lewisham. *Quarterly Journal of the Geological Society,* 8**,** 193-195.

DECKERS, J. & VAN DER VOET, E. 2018. A review on the structural styles of deformation during Late Cretaceous and Paleocene tectonic phases in the southern North Sea area. *Journal of Geodynamics,* 115**,** 1-9.

DECKERS, J. E. F. & MATTHIJS, J. 2017. Middle Paleocene uplift of the Brabant Massif from central Belgium up to the southeast coast of England. *Geological Magazine,* 154**,** 1117-1126.

DEL VENTISETTE, C., MONTANARI, D., SANI, F. & BONINI, M. 2006. Basin inversion and fault reactivation in laboratory experiments. *Journal of Structural Geology,* 28**,** 2067-2083.

DEWEY, H. & BROMEHEAD, C. E. N. 1921. *The geology of South London: Explanation of one-inch geological sheet 270 new series,* London, HMSO.

DIMOSTHENOUS, M. 2018. *Offshore Geological Disposal Facility for Radioactive Waste.* MSc dissertation, Imperial College London.

DIXON, E. E. L. & STRAHAN, A. 1977. *Pembroke & Linney Head, England & Wales, Sheet 244 & 245*. Keyworth, Nottingham: British Geological Survey.

DOHERTY, P. 2012. *Discontinuities in the London Clay.* MSc Unpublished Dissertation, Imperial College London.

DOOLEY, T. P. & SCHREURS, G. 2012. Analogue modelling of intraplate strike-slip tectonics: A review and new experimental results. *Tectonophysics,* 574-575**,** 1-71.

DUPERRET, A., VANDYCKE, S., MORTIMORE, R. N. & GENTER, A. 2012. How plate tectonics is recorded in chalk deposits along the eastern English Channel in Normandy (France) and Sussex (UK). *Tectonophysics,* 581**,** 163-181.

EDGAR, J. 2021. *Addressing infrastructure challenges posed by the Harwich Formation through understanding its geological origins.* Doctorate, Imperial College London.

EDGAR, J., GHAIL, R. C., LAWRENCE, A. R, Skipper, J., & Mason, P.M. 2021. The impact of facies variability within the Harwich Formation on ground engineering in the London area, UK. *Quaterly Journal of Engineering Geology and Hydrogeology.*

ELLIS, D. & STOKER, M. S. 2014. The Faroe–Shetland Basin: a regional perspective from the Paleocene to the present day and its relationship to the opening of the North Atlantic Ocean. *Geological Society, London, Special Publications,* 397**,** 11-31.

ELLISON, R., BOOTH, S. & STRANGE, P. 1993. Geological mapping in urban areas - The BGS experience in London. *Episodes,* 16**,** 383-388.

ELLISON, R., KNOX, R. O. B., JOLLEY, D. & KING, C. 1994. A revision of the lithostratigraphical classification of the early Palaeogene strata of the London Basin and East Anglia. *Proceedings of the Geologists' Association,* 105**,** 187-197.

ELLISON, R., WOODS, M., ALLEN, D., FORSTER, A., PHARAOH, T. & KING, C. 2004. *Geology of London: Special memoir for 1: 50000 geological sheets 256 (north London), 257 (Romford), 270 (south London), and 271 (Dartford)(England and Wales)*, British Geological Survey.

ELLISON, R. A., ALI, J. R., HINE, N. M. & JOLLEY, D. W. 1996. Recognition of chron C25n in the upper Paleocene Upnor Formation of the London Basin, UK. *Geological Society, London, Special Publications,* 101**,** 185-193.

ELLISON, R. A., LAKE, R. D., BRISTOW, C. R., MERRIMAN, R. J. & HOPSON, P. M. 1986. *Geology of the country around Braintree : Memoir for 1:50,000 geological sheet 223 (England and Wales),* London, HMSO.

ELLISON, R. A., SCHOFIELD, D., ALDISS, D. T., HASLAM, R. B., LEWIS, M., Ó'DOCHARTAIGH, B., BLOOMFIELD, J. P. L., J., BAPTIE, B., SHAW, R. P., BIDE, T. & MCEVOY, F. 2018. National Geological Screening: London and the Thames Valley. *Minerals and Waste Programme Report CR/17/101.* British Geological Survey.

ENTWISLE, D. C., HOBBS, P. R. N., NORTHMORE, K. J., SKIPPER, J. A., RAINES, M. R., SELF, S. J., ELLISON, R. A. & JONES, L. D. 2013. Engineering Geology of British Rocks and Soils - Lambeth Group. *British Geological Survey Open Report.* Keyworth, Nottingham: British Geological Survey.

ENVIRONMENT AGENCY 2018. Management of the London Basin Chalk Aquifer. Revision 6 ed.: Environment Agency.

EUROPEAN ENVIRONMENT AGENCY. 2017. *EEA coastline for analysis* [Online]. European Environment Agency,: European Environment Agency,. Available: https://www.eea.europa.eu/data-and-maps/data/eea-coastline-for-analysis-2 [Accessed 27/02/2020 2020].

EVERETT, C. & DEWAR, A. 2015. Practical experience from the construction industry of anomalous ground conditions in the London Basin. *Geotechnical Engineering for Infrastructure and Development.*

FALCON, N. L. & KENT, P. E. 1960. Geological Results of Petroleum Exploration in Britain 1945-1957. *Geological Society, London, Memoirs,* 2**,** 5-56.

FLYNN, A. L. 2021. *DFHs in the London Basin: chacteristics, origins and assessment of risk.* Doctorate, Brunel University.

FLYNN, A. L., COLLINS, P. E. F., READING, P., BANKS, V. & ANGUILANO, L. 2018. The role of chalk in the development of buried ("drift-filled") hollows. *Engineering in Chalk.*

FLYNN, A. L., COLLINS, P. E. F., SKIPPER, J. A., PICKARD, T., KOOR, N., READING, P. & DAVIS, J. A. 2020. Buried (drift-filled) hollows in London – a review of their location and key characteristics. *Quarterly Journal of Engineering Geology and Hydrogeology***,** qjegh2019-145.

FOOKES, P. G. & PARRISH, D. G. 1969. Observations on small-scale structural discontinuities in the London Clay and their relationship to regional geology. *Quarterly Journal of Engineering Geology and Hydrogeology,* 1**,** 217-240.

FORD, J. 12th May 2020. *RE: Email conversation: BGS Lithoframe Faults in London.* Email to MORGAN, T. O.

FORD, J., BURKE, H., ROYSE, K. & MATHERS, S. 2008. The 3D geology of London and the Thames Gateway: a modern approach to geological surveying and its relevance in the urban environment. *Cities and their underground environment : 2nd European conference of International Association of engineering geology : Euroengeo 2008.* Madrid, Spain: Unpublished.

FORD, J. R., MATHERS, S. J., ROYSE, K. R., ALDISS, D. T. & MORGAN, D. J. 2010. Geological 3D modelling: scientific discovery and enhanced understanding of the subsurface, with examples from the UK [Geologische 3D-Modellierung: Wissenschaftliche Erkenntnisse und vertiefte Einsichten in den Untergrund, mit Beispielen aus Großbritannien]. *Zeitschrift der Deutschen Gesellschaft für Geowissenschaften,* 161**,** 205-218.

FOSSEN, H. 2010. *Structural Geology,* Cambridge, Cambridge University Press.

FOSSEN, H. 2016. *Structural Geology*, Cambridge University Press.

FRESHNEY, E. C., BEER, K. E., WRIGHT, J. E., BURLEY, A. J., CALVER, M. A., EDMONDS, E. A. & HAWKES, J. R. M., R.J. 1979. *Geology of the country around Chulmleigh : Memoir for 1:50,000 geological sheet 309,* London, HMSO.

GAKIS, A., CABRERO, P., ENTWISLE, D. & KESSLER, H. 2016. 3D geological model of the completed Farringdon underground railway station. *Crossrail Project: Infrastructure design and construction.*

GALE, A. S. & LOVELL, B. 2018. The Cretaceous–Paleogene unconformity in England: Uplift and erosion related to the Iceland mantle plume. *Proceedings of the Geologists' Association,* 129**,** 421-435.

GALLOIS, R., MORTER, A. A. & OWEN, H. G. 2016. The stratigraphy of the Gault Formation (Early Cretaceous, Albian) in East Anglia and south-east England. *Proceedings of the Geologists' Association,* 127**,** 606-628.

GHAIL, R., MASON, P. & SKIPPER, J. 2015a. The geological context and evidence for incipient inversion of the London Basin. *In:* WINTER, M. G., SMITH, D.M., ELDRED, P.J.L., TOLL, D.G. (ed.) *Geotechnical Engineering for Infrastructure and Development: XVI European Conference on Soil Mechanics and Geotechnical Engineering.* Edinburgh: ICE Publishing.

GHAIL, R. C., JACQUELINE, S. & MASON, P. J. Identification of Ground Engineering Hazards in London Through the Use of Predictive 4D Geomodelling Tools. 2015b Cham. Springer International Publishing, 907-911.

GHAIL, R. C. & STANDING, J. R. 4th February 2021. *RE: London Clay Slumping.* Email to MORGAN, T. O.

GIBBARD, P. L. & LEWIN, J. 2003. The history of the major rivers of southern Britain during the Tertiary. *Journal of the Geological Society,* 160**,** 829-845.

GIBBARD, P. L. & LEWIN, J. 2016. Filling the North Sea Basin: Cenozoic sediment sources and river styles (André Dumont medallist lecture 2014). *Geologica Belgica*.

GODWIN-AUSTEN, R. 1856. On the Possible Extension of the Coal-Measures beneath the South-Eastern Part of England. *Quarterly Journal of the Geological Society,* 12**,** 38-73.

GREEN, P. F., DUDDY, I. R. & JAPSEN, P. 2018. Multiple episodes of regional exhumation and inversion identified in the UK Southern North Sea based on integration of palaeothermal and palaeoburial indicators. *Geological Society, London, Petroleum Geology Conference series,* 8**,** 47-65.

GREEN, P. F., THOMSON, K. & HUDSON, J. D. 2001. Recognition of tectonic events in undeformed regions: contrasting results from the Midland Platform and East Midlands Shelf, Central England. *Journal of the Geological Society,* 158**,** 59-73.

HADLOW, N. W. 10th June 2020. RE: Fault zone identification through 3D geological modelling for the Thames Tideway Tunnel ground investigation. Email to MORGAN, T. O.

HIGHT, D. 2003. Some characteristics of London clay. *Characterisation and engineering properties of natural soils,* 2**,** 851-946.

HILLIS, R. R., HOLFORD, S. P., GREEN, P. F., DORÉ, A. G., GATLIFF, R. W., STOKER, M. S., THOMSON, K., TURNER, J. P., UNDERHILL, J. R. & WILLIAMS, G. A. 2008. Cenozoic exhumation of the southern British Isles. *Geology,* 36**,** 371-374.

HOLDER, M. T. & LEVERIDGE, B. E. 1986. Correlation of the Rhenohercynian Variscides. *Journal of the Geological Society,* 143**,** 141-147.

HOLLOWAY, S. & CHADWICK, R. A. 1986. The Sticklepath-Lustleigh fault zone: Tertiary sinistral reactivation of a Variscan dextral strike-slip fault. *Journal of the Geological Society,* 143**,** 447-452.

HOPSON, P. M., ALDISS, D. T., SMITH, A., WOOD, C. J., WILKINSON, I. P., WOODS, M. A., ALLSOP, J. M., CHENEY, C. S. & WYMER, J. J. 1996. *Geology of the country around Hitchin : memoir for 1:50000 geological sheet 221 (England & Wales),* London, HMSO.

HOWLAND, A. F. 1989. *An engineering geology database for urban renewal.* PhD, University of London.

HOWLAND, A. F. 1991. London's Docklands: Engineering Geology. *Proceedings of the Institution of Civil Engineers,* 90**,** 1153-1178.

HUBBERT, K. M. & RUBEY, W. W. 1959. Role of fluid pressure in mechanics of overthrust faulting: I. Mechanics of fluid-filled porous solids and its application to overthrust faulting. *GSA Bulletin,* 70**,** 115-166.

HUGGETT, J., ADETUNJI, J., LONGSTAFFE, F. & WRAY, D. 2017. Mineralogical and geochemical characterisation of warm-water, shallow-marine glaucony from the Tertiary of the London Basin. *Clay Minerals,* 52**,** 25-50.

JAPSEN, P. 1997. Regional Neogene exhumation of Britain and the western North Sea. *Journal of the Geological Society,* 154**,** 239-247.

JAPSEN, P. & CHALMERS, J. A. 2000. Neogene uplift and tectonics around the North Atlantic: overview. *Global and Planetary Change,* 24**,** 165-173.

JONES, D. K. C. 1999. On the uplift and denudation of the Weald. *Geological Society, London, Special Publications,* 162**,** 25-43.

JONES, S. M., WHITE, N., CLARKE, B. J., ROWLEY, E. & GALLAGHER, K. 2002. Present and past influence of the Iceland Plume on sedimentation. *Geological Society, London, Special Publications,* 196**,** 13-25.

JORDAN, C. J. & NAPIER, B. 2016. Developing digital fieldwork technologies at the British Geological Survey. *Geological Society, London, Special Publications,* 436**,** 219-229.

JUDD, J. W. 1882. The Possibility of Finding Workable Coal-Seams under the London Area. *Nature,* 25**,** 311.

JUDD, J. W. & HOMERSHAM, C. 1884. On the Nature and Relations of the Jurassic Deposits which underlie London. *Quarterly Journal of the Geological Society,* 40**,** 724-764.

KEAREY, P. & RABAE, A. M. 1996. An interpretation of the gravity anomaly at Warlingham, Surrey. *Geological Magazine,* 133**,** 619-624.

KESSLER, H. & MATHERS, S. 2004. Maps to models - finally capturing the geologist's vision. *Geoscientist,* 14**,** 4-6.

KESSLER, H., MATHERS, S. & SOBISCH, H.-G. 2009. The capture and dissemination of integrated 3D geospatial knowledge at the British Geological Survey using GSI3D software and methodology. *Computers & Geosciences,* 35**,** 1311-1321.

KIM, Y.-S., PEACOCK, D. C. P. & SANDERSON, D. J. 2004. Fault damage zones. *Journal of Structural Geology,* 26**,** 503-517.

KING, C. 1981. *The stratigraphy of the London Clay and associated deposits*, Backhuys.

KING, C. 2006. Paleogene and Neogene: uplift and a cooling climate. *In:* BRENCHLEY, P. J. & RAWSON, P. F. (eds.) *The Geology of England and Wales.* Geological Society of London.

KING, C., GALE, A. S. & BARRY, T. L. 2016. *A revised correlation of Tertiary rocks in the British Isles and adjacent areas of NW Europe*, Geological Society of London.

KIRKPATRICK, I. M. & MCCANN, D. M. 1984. Engineering geological and geophysical investigation of the Barking Creek tidal barrier site. *Quarterly Journal of Engineering Geology and Hydrogeology,* 17**,** 259-268.

KLEY, J. 2018. Timing and spatial patterns of Cretaceous and Cenozoic inversion in the Southern Permian Basin. *Geological Society, London, Special Publications,* 469.

KLEY, J. & VOIGT, T. 2008. Late Cretaceous intraplate thrusting in central Europe: Effect of Africa-Iberia-Europe convergence, not Alpine collision. *Geology,* 36**,** 839-842.

KNOX, R. W. O. B. 1996. Tectonic controls on sequence development in the Palaeocene and earliest Eocene of southeast England: implications for North Sea stratigraphy. *Geological Society, London, Special Publications,* 103**,** 209-230.

KOYI, H. 1997. Analogue modelling: From a qualitative to a quantitative technique — a historical outline. *Journal of Petroleum Geology,* 20**,** 223-238.

KRÉZSEK, C., ADAM, J. & GRUJIC, D. 2007. Mechanics of fault and expulsion rollover systems developed on passive margins detached on salt: insights from analogue modelling and optical strain monitoring. *Geological Society, London, Special Publications,* 292**,** 103-121.

LACK, M. 20th July 2020. *RE: Research enquiry: Access to Environment Agency well data.* Email to MORGAN, T. O.

LAGESON, D. R. 1984. Structural Geology of Stewart Peak Culmination, Idaho-Wyoming Thrust Belt1. *AAPG Bulletin,* 68**,** 401-416.

LAKE, R. D., ELLISON, R. A., HENSON, M. R., CONWAY, B. W., FARR, J. L., MORTER, A. A., HUGHES, M. J., WOOD, C. J., MERRIMAN, R. J., BRISTOW, C. R., GREEN, G. W. & HOLLYER, S. E. 1986. *Geology of the country around Southend and Foulness Memoir for 1:50000 sheets 258 and 259 New Series,* London, HMSO.

LAKE, S. D. & KARNER, G. D. 1987. The structure and evolution of the Wessex Basin, southern England: an example of inversion tectonics. *Tectonophysics,* 137**,** 347-378.

LANE, N. F., WATTS, A. B. & FARRANT, A. R. 2008. An analysis of Cotswold topography: insights into the landscape response to denudational isostasy. *Journal of the Geological Society,* 165**,** 85-103.

LAWRENCE, U. & BLACK, M. 2019. The role of risk and assumption in the engineering geology of Crossrail. *Quarterly Journal of Engineering Geology and Hydrogeology,* 52**,** 425-434.

LE BRETON, E., COBBOLD, P. R. & ZANELLA, A. 2013. Cenozoic reactivation of the Great Glen Fault, Scotland: additional evidence and possible causes. *Journal of the Geological Society,* 170**,** 403-415.

LEE, J., WOODS, M. & MOORLOCK, B. (eds.) 2015. *British Regional Geology: East Anglia*.

LEE, J. R., CANDY, I. & HASLAM, R. 2018. The Neogene and Quaternary of England: landscape evolution, tectonics, climate change and their expression in the geological record. *Proceedings of the Geologists' Association,* 129**,** 452-481.

LEE, J. R., HASLAM, R., WOODS, M. A., ROSE, J., GRAHAM, R. L., FORD, J. R., SCHOFIELD, D. I., KEARSEY, T. I. & WILLIAMS, C. N. 2020. Plio-Pleistocene fault reactivation within the Crag Basin, eastern UK: implications for structural controls of landscape development within an intraplate setting. *Boreas,* 49**,** 685-708.

LEE, M. K., PHARAOH, T. C. & GREEN, C. A. 1991. Structural trends in the concealed basement of eastern England from images of regional potential field data. *Annales de la Société géologique de Belgique*.

LEFORT, J. P. & MAX, M. D. 1992. Structure of the Variscan belt beneath the British and Armorican overstep sequences. *Geology,* 20**,** 979-982.

LENHAM, J., MEYER, V., EDMONDS, H., HARRIS, D., MORTIMORE, R., REYNOLDS, J. & BLACK, M. 2006. What lies beneath: surveying the Thames at Woolwich. *Proceedings of the Institution of Civil Engineers - Civil Engineering,* 159**,** 32-41.

LEWIS, C. L. E., GREEN, P. F., CARTER, A. & HURFORD, A. J. 1992. Elevated K/T palaeotemperatures throughout Nortwest England: three kilometres of Tertiary erosion? *Earth and Planetary Science Letters,* 112**,** 131-145.

LINDE-ARIAS, E., HARRIS, D. & GHAIL, R. 2018. Engineering geology and tunnelling in the Limmo Peninsula, East London. *Quarterly Journal of Engineering Geology and Hydrogeology,* 51**,** 23-30.

LINNEY, L. F. & WITHERS, A. D. 1998. Dewatering the Thanet Beds in SE London: three case histories. *Quarterly Journal of Engineering Geology and Hydrogeology,* 31**,** 115-122.

LISLE, R. J., BRABHAM, P. & BARNES, J. W. 2011. *Basic Geological Mapping*, John Wiley & Sons.

LOCKNER, D. A. & BEELER, N. M. 2002. Rock failure and earthquakes. *In:* LEE, W. H. K., KANAMORI, H., JENNINGS, P. C. & KISSLINGER, C. (eds.) *International Handbook of Earthquake and Engineering Seismology: Part A.* San Diego: Academic Press.

LOCKNER, D. A., MORROW, C., MOORE, D. & HICKMAN, S. 2011. Low strength of deep San Andreas fault gouge from SAFOD core. *Nature,* 472**,** 82-85.

MADDY, D. 1997. Uplift-driven valley incision and river terrace formation in southern England. *Journal of Quaternary Science,* 12**,** 539-545.

MANDL, G. 1988. *Mechanics of tectonic faulting : models and basic concepts,* Amsterdam; New York; New York, NY, U.S.A., Elsevier

MANDL, G. 2000. *Faulting in Brittle Rocks: An Introduction to the Mechanics of Tectonic Faults,* Germany, Springer-Verlag Berlin Heidelberg.

MANSY, J. L., MANBY, G. M., AVERBUCH, O., EVERAERTS, M., BERGERAT, F., VAN VLIET-LANOE, B., LAMARCHE, J. & VANDYCKE, S. 2003. Dynamics and inversion of the Mesozoic Basin of the Weald–Boulonnais area: role of basement reactivation. *Tectonophysics,* 373**,** 161-179.

MARRIOTT, B. T. 2019. *Geotechnical characterisation of the Black Facies of the Blackheath Member in East London.* MSc Dissertation, Imperial College London.

MARTIN, P. I. 1829. XVIII. Observations on the anticlinal line of the London and Hampshire basins, &c. *The Philosophical Magazine,* 5**,** 111-119.

MASON, P. J., GHAIL, R. C., BISCHOFF, C. & SKIPPER, J. A. 2015. Detecting and monitoring small-scale discrete ground movements across London using Persistent Scatterer InSAR (PSI). *In:* WINTER, M. G., SMITH, D.M., ELDRED, P.J.L., TOLL, D.G. (ed.) *Geotechnical Engineering for Infrastructure and Development: XVI European Conference on Soil Mechanics and Geotechnical Engineering.* Edinburgh: ICE Publishing.

MATHERS, S. J., BURKE, H. F., TERRINGTON, R. L., THORPE, S., DEARDEN, R. A., WILLIAMSON, J. P. & FORD, J. R. 2014. A geological model of London and the Thames Valley, southeast England. *Proceedings of the Geologists' Association,* 125**,** 373-382.

MCCLAY, K. & DOOLEY, T. 1995. Analogue models of pull-apart basins. *Geology,* 23**,** 711-714.

MCMAHON, N. A. & TURNER, J. 1998. The documentation of a latest Jurassic-earliest Cretaceous uplift throughout southern England and adjacent offshore areas. *Geological Society, London, Special Publications,* 133**,** 215-240.

MCMAHON, N. A. & UNDERHILL, J. R. 1995. The regional stratigraphy of the southwest United Kingdom and adjacent offshore areas with particular reference to the major intra-Cretaceous unconformity. *Geological Society, London, Special Publications,* 93**,** 323-325.

MEDDENS, F. 1996. Sites from the Thames estuary wetlands, England, and their Bronze Age use. *Antiquity,* 70**,** 325.

MEDDENS, F. & SIDELL, J. 1995. Bronze Age trackways in east London. *Current Archaeology,* 143**,** 412.

MERRIMAN, R. J., PHARAOH, T. C., WOODCOCK, N. H. & DALY, P. 1993. The metamorphic history of the concealed Caledonides of eastern England and their foreland. *Geological Magazine,* 130**,** 613-620.

MEYER, S. M. 2018. *A detailed geological investigation of the City of London region of the London Basin.* MSc dissertation, Imperial College London.

MIDDLETON, T. A. & COPLEY, A. 2014. Constraining fault friction by re-examining earthquake nodal plane dips. *Geophysical Journal International,* 196**,** 671-680.

MILIORIZOS, M. & RUFFELL, A. 1998. Kinematics of the Watchet-Cothelstone-Hatch Fault System: implications for the fault history of the Wessex Basin and adjacent areas. *Geological Society, London, Special Publications,* 133**,** 311-330.

MILLER, J. F. & MITRA, S. 2011. Deformation and secondary faulting associated with basement-involved compressional and extensional structures. *AAPG Bulletin,* 95**,** 675-689.

MOORE, C. 1878. Notes on the Palæontology and some of the Physical Conditions of the Meux-Well Deposits. *Quarterly Journal of the Geological Society,* 34**,** 914-923.

MOORLOCK, B., BOREHAM, S., WOODS, M. & SUMBLER, M. 2003. Geology of the Saffron Walden district–a brief explanation of the geological map. *Sheet explanation of the British Geological Survey,* 1**,** 000.

MORGAN, T. O., GHAIL, R. G. & LAWRENCE, J. A. 2020. Major faulting in London: Evidence for inherited basement faults in the London Basin. *Quarterly Journal of Engineering Geology and Hydrogeology*.

MORTIMORE, R. 2011. A chalk revolution: what have we done to the Chalk of England? *Proceedings of the Geologists' Association,* 122**,** 232-297.

MORTIMORE, R., NEWMAN, T. G., ROYSE, K., SCHOLES, H. & LAWRENCE, U. 2011. Chalk: its stratigraphy, structure and engineering geology in east London and the Thames Gateway. *Quarterly Journal of Engineering Geology and Hydrogeology,* 44**,** 419-444.

MORTIMORE, R. & POMEROL, B. 1997. Upper Cretaceous tectonic phases and end Cretaceous inversion in the Chalk of the Anglo-Paris Basin. *Proceedings of the Geologists' Association,* 108**,** 231-255.

MORTIMORE, R., WOOD, C., POMEROL, B. & ERNST, G. 1998. Dating the phases of the Subhercynian tectonic epoch: Late Cretaceous tectonics and eustatics in the Cretaceous basins of northern Germany compared with the Anglo-Paris Basin. *Zentralblatt für Geologie und Paläontologie,* 11**,** 1349-1401.

MORTIMORE, R. N. 2012. Making sense of Chalk: a total-rock approach to its Engineering Geology. *Quarterly Journal of Engineering Geology and Hydrogeology,* 45**,** 252-334.

MORTIMORE, R. N. 2018. Late Cretaceous tectono-sedimentary events in NW Europe. *Proceedings of the Geologists' Association,* 129**,** 392-420.

MORTIMORE, R. N. 2019. Late Cretaceous to Miocene and Quaternary deformation history of the Chalk: Channels, slumps, faults, folds and glacitectonics. *Proceedings of the Geologists' Association,* 130**,** 27-65.

MORTIMORE, R. N., WOOD, C. & GALLOIS, R. W. 2001. *British upper Cretaceous stratigraphy*, Joint Nature Conservation Committee (JNCC).

MORTON, A. C. 1982. The provenance and diagenesis of Palaeogene sandstones of southeast England as indicated by heavy mineral analysis. *Proceedings of the Geologists' Association,* 93**,** 263-274.

MUSSON, R. & SARGEANT, S. 2007. Eurocode 8 seismic hazard zoning maps for the UK. British Geological Survey.

MYLNE, G. E. 1856. *Map of the geology and contours of London and its environs*. London: Edward Stanford, Charing Cross.

MYLNE, G. E. 1858. *Map of the geology and contours of London and its environs*. London: Edward Stanford, Charing Cross.

NADIM, F. 2007. Tools and Strategies for Dealing with Uncertainty in Geotechnics. *In:* GRIFFITHS, D. V. & FENTON, G. A. (eds.) *Probabilistic Methods in Geotechnical Engineering.* Vienna: Springer Vienna.

NAYLOR, M. A., MANDL, G. & SUPESTEIJN, C. H. K. 1986. Fault geometries in basement-induced wrench faulting under different initial stress states. *Journal of Structural Geology,* 8**,** 737-752.

NEMČOK, M., GAYER, R. & MILIORIZOS, M. 1995. Structural analysis of the inverted Bristol Channel Basin: implications for the geometry and timing of fracture porosity. *Geological Society, London, Special Publications,* 88**,** 355-392.

NEWELL, A. J. 2014. Palaeogene rivers of southern Britain: climatic extremes, marine influence and compressional tectonics on the southern margin of the North Sea Basin. *Proceedings of the Geologists' Association,* 125**,** 578-590.

NEWELL, A. J., WOODS, M. A., FARRANT, A. R., SMITH, H. & HASLAM, R. B. 2018. Chalk thickness trends and the role of tectonic processes in the Upper Cretaceous of southern England. *Proceedings of the Geologists' Association*.

NEWMAN, T. 2008. Ground Modelling for the Lee Tunnel. *Engineering Geology and Experience in the East London and Thames Gateway Area.*

NEWMAN, T. 2009. The impact of adverse geological conditions on the design and construction of the Thames Water Ring Main in Greater London, UK. *Quarterly Journal of Engineering Geology and Hydrogeology,* 42**,** 5-20.

NEWMAN, T. 2017. Engineering geology of the Thames Tideway Tunnel: The Story So Far. *14th Annual BGA Conference.* Institution of Civil Engineers, London, 21 June 2017.

NEWMAN, T. 1st April-3rd July 2019a. *RE: Email correspondence: Chalk exposures and structural observations during the excavation of the Deptford Shaft (DEPCS) for the Thames Tideway project.* Email to MORGAN, T. O.

NEWMAN, T. 23rd July-16th September 2019b. *RE: Email correspondence: Chalk exposures and structural observations during the excavation of the Greenwich Shaft (GREPS) for the Thames Tideway project.* Email to MORGAN, T. O.

NEWMAN, T. 2021. Logging the Lambeth Group Upper Shelly Beds for the Thames Tideway Tunnel in London, UK: More than just "dark grey clay with shells". *Proceedings of the Geologists' Association*.

NEWMAN, T., BELLHOUSE, M., CORCORAN, J., SUTHERDEN, R. & KARAOUZENE, R. 2016. TBM performance through the engineering geology of the Lee Tunnel. *Proceedings of the Institution of Civil Engineers - Geotechnical Engineering,* 169**,** 299-313.

NEWMAN, T. G., GHAIL, R. C. & SKIPPER, J. A. 2013. Deoxygenated gas occurrences in the Lambeth Group of central London, UK. *Quarterly Journal of Engineering Geology and Hydrogeology,* 46**,** 167-177.

NEWMAN, T. G. & WONG, H.-Y. 2011. Sinking a jacked caisson within the London Basin geological sequence for the Thames Water Ring Main extension. *Quarterly Journal of Engineering Geology and Hydrogeology,* 44**,** 221-232.

NEWMAN, T. G., YUAN, L. F. V. & O'KEEFFE, L. C. 2010. Using tunnel boring data to augment the geological model. *Proceedings of the Institution of Civil Engineers - Geotechnical Engineering,* 163**,** 157-166.

OWEN, H. G. 1971. The stratigraphy of the Gault in the Thames Estuary and its bearing on the mesozoic tectonic history of the area. *Proceedings of the Geologists' Association,* 82**,** 187-207.

PAGE, D. & SKIPPER, J. 2000. Lithological characteristics of the Lambeth Group. *Ground Engineering,* 33**,** 38-44.

PAGE, D. P. 1995. Jubilee Line Extension. *Quarterly Journal of Engineering Geology and Hydrogeology,* 28**,** 97-104.

PARRISH, R. R., PARRISH, C. M. & LASALLE, S. 2018. Vein calcite dating reveals Pyrenean orogen as cause of Paleogene deformation in southern England. *Journal of the Geological Society*.

PATTISON, J., BERRIDGE, N. G., ALLSOP, J. M., WILKINSON, I. P., ELLISON, R. A., MILLWARD, D., SMITH, A., HOPSON, P. M., ROBINS, N. S., MORTER, A. A., WOOD, C. J. & MERRIMAN, R. J. 1993. *Geology of the country around Sudbury (Suffolk) : Memoir for 1:50000 geological sheet 206 (England & Wales),* London, HMSO.

PAUL, J. D. 2016. High-resolution geological maps of central London, UK: Comparisons with the London Underground. *Geoscience Frontiers,* 7**,** 273-286.

PEACOCK, D. C. P. 2009. A review of Alpine deformation and stresses in southern England. *Italian Journal of Geosciences,* 128**,** 307-316.

PETROLEUM EXPERTS 2020. MOVE. MOVE 2019.1 ed. Edinburgh: Petroleum Experts (formerly Midland Valley).

PHARAOH, T. C. 1999. Palaeozoic terranes and their lithospheric boundaries within the Trans-European Suture Zone (TESZ): a review. *Tectonophysics,* 314**,** 17-41.

PHARAOH, T. C. 2018. The Anglo-Brabant Massif: Persistent but enigmatic palaeo-relief at the heart of western Europe. *Proceedings of the Geologists' Association,* 129**,** 278-328.

PHARAOH, T. C., MERRIMAN, R. J., WEBB, P. C. & BECKINSALE, R. D. 1987. The concealed Caledonides of eastern England: preliminary results of a multidisciplinary study. *Proceedings of the Yorkshire Geological Society,* 46**,** 355-369.

PHARAOH, T. C., MORRIS, J. H., LONG, C. B. & RYAN, P. D. 1996. *Tectonic map of Britain, Ireland and adjacent areas*. British Geological Survey.

PHARAOH, T. C., WINCHESTER, J. A., VERNIERS, J., LASSEN, A. & SEGHEDI, A. 2006. The Western Accretionary Margin of the East European Craton: an overview. *Geological Society, London, Memoirs*, 32, 291-311.

PHILLIPS, W. 1818. *A Selection of Facts from the Best Authorities: Arranged So as to Form an Outline of the Geology of England and Wales. With a Map and Sections of the Strata*, W. Phillips.
PLINT, A. G. 1982. Eocene sedimentation and tectonics in the Hampshire Basin. *Journal of the Geological Society,* 139**,** 249-254.
PRESTWICH, J. 1847. On the probable Age of the London Clay, and its Relations to the Hampshire and Paris Tertiary Systems. *Quarterly Journal of the Geological Society,* 3**,** 354-377.
PRESTWICH, J. 1850. On the Structure of the Strata between the London Clay and the Chalk in the London and Hampshire Tertiary Systems. Part I - The Basement Bed of the London Clay. *Quarterly Journal of the Geological Society,* 6**,** 252-281.
PRESTWICH, J. 1854. On the Structure of the Strata between the London Clay and the Chalk in the London and Hampshire Tertiary Systems. Part II - The Woolwich and Reading Series. *Quarterly Journal of the Geological Society,* 10**,** 75-138.
PRESTWICH, J. 1858. On the Boring through the Chalk at Harwich. *Quarterly Journal of the Geological Society,* 14**,** 249-252.
PRESTWICH, J. 1878. On the Section of Messrs. Meux & Co.'s Artesian Well in the Tottenham-Court Road, with Notices of the Well at Crossness, and of another at Shoreham, Kent; and on the probable Range of the Lower Greensand and Palæozoic Rocks under London. *Quarterly Journal of the Geological Society,* 34**,** 902-913.
PRESTWICH, J. & MORRIS, J. 1846. On the Wealden Strata exposed by the Tunbridge Wells Railway. *Quarterly Journal of the Geological Society,* 2**,** 397-405.
PRICE, N. J. 1966. *Fault and joint development: in brittle and semi-brittle rock,* Oxford, Pergamon Press.
PRICE, S. J., TERRINGTON, R. L., BUSBY, J., BRICKER, S. & BERRY, T. 2018. 3D ground-use optimisation for sustainable urban development planning: A case-study from Earls Court, London, UK. *Tunnelling and Underground Space Technology,* 81**,** 144-164.
RADLEY, J. D. & ALLEN, P. 2012a. The non-marine Lower Cretaceous Wealden strata of southern England. *Proceedings of the Geologists' Association,* 123**,** 235-244.
RADLEY, J. D. & ALLEN, P. 2012b. The Wealden (non-marine Lower Cretaceous) of the Weald Sub-basin, southern England. *Proceedings of the Geologists' Association,* 123**,** 245-318.
RAINEY, T. P. & ROSENBAUM, M. S. 1989. The adverse influence of geology and groundwater on the behaviour of London Underground railway tunnels near Old Street Station. *Proceedings of the Geologists' Association,* 100**,** 123-134.
REBER, J. E., COOKE, M. L. & DOOLEY, T. P. 2020. What model material to use? A Review on rock analogs for structural geology and tectonics. *Earth-Science Reviews,* 202**,** 103107.
REID, H. F., DAVIS, W. M., LAWSON, A. C. & RANSOME, F. L. 1913. Report of the Committee on the Nomenclature of Faults. *GSA Bulletin,* 24**,** 163-186.
RHIND, O. 2019. *Critical Evaluation of Terrestrial Laser Scanning for Stability Assessment in a Victorian Chalk Mine* MSc, University College London.
RICHARD, P. 1991. Experiments on faulting in a two-layer cover sequence overlying a reactivated basement fault with oblique-slip. *Journal of Structural Geology,* 13**,** 459-469.
RICHARD, P. & KRANTZ, R. W. 1991. Experiments on fault reactivation in strike-slip mode. *Tectonophysics,* 188**,** 117-131.
RICHARD, P. D., NAYLOR, M. A. & KOOPMAN, A. 1995. Experimental models of strike-slip tectonics. *Petroleum Geoscience,* 1**,** 71-80.
RIEDEL, W. 1929. Zur Mechanik geologischer Brucherscheinungen ein Beitrag zum Problem der Fiederspatten. *Zentbl. Miner. Geol. Palaont. Abt.***,** 354-368.
ROBERTS, D. G. 1989. Basin inversion in and around the British Isles. *Geological Society, London, Special Publications,* 44**,** 131-150.
ROSENBAUM, M. S. & WARREN, C. D. 1986. Creating a geological database for planning tunnels under London. *Quarterly Journal of Engineering Geology and Hydrogeology,* 19**,** 413-423.

ROYSE, K., RUTTER, H. & ENTWISLE, D. 2009. Property attribution of 3D geological models in the Thames Gateway, London: new ways of visualising geoscientific information. *Bulletin of Engineering Geology and the Environment,* 68**,** 1.

ROYSE, K. R. 2010. Combining numerical and cognitive 3D modelling approaches in order to determine the structure of the Chalk in the London Basin. *Computers & Geosciences,* 36**,** 500-511.

ROYSE, K. R., DE FREITAS, M., BURGESS, W. G., COSGROVE, J., GHAIL, R. C., GIBBARD, P., KING, C., LAWRENCE, U., MORTIMORE, R. N., OWEN, H. & SKIPPER, J. 2012. Geology of London, UK. *Proceedings of the Geologists' Association,* 123**,** 22-45.

RUFFELL, A. H. & SHELTON, R. G. 2000. Permian to Late Triassic post-orogenic collapse, early Atlantic rifting, deserts, evaporating seas and mass extinctions. *In:* WOODCOCK, N. H. & STRACHAN, R. (eds.) *Geological History of Britain and Ireland.* 1st ed.: Blackwell Science.

SCHOLZ, C. H. 2002. The Mechanics of Earthquakes and Faulting. *The Mechanics of Earthquakes and Faulting, by Christopher H. Scholz, pp. 496. ISBN 0521652235. Cambridge, UK: Cambridge University Press, June 2002.***,** 496.

SCHULTZ, R. A. & FOSSEN, H. 2008. Terminology for structural discontinuities. *AAPG bulletin,* 92**,** 853-867.

SCOTNEY, P. M., CARNEY, J. N. & HARWOOD, M. 2012. New information on Neoproterozoic-Cambrian geology and the Triassic unconformity around Groby, southern Charnwood Forest, UK. *Proceedings of the Yorkshire Geological Society,* 59**,** 37-51.

SCOULAR, J., GHAIL, R., MASON, P., LAWRENCE, J., BELLHOUSE, M., HOLLEY, R. & MORGAN, T. 2020a. Retrospective InSAR Analysis of East London during the Construction of the Lee Tunnel. *Remote Sensing,* 12**,** 849.

SCOULAR, J. M., CROFT, J., GHAIL, R. C., MASON, P. J., LAWRENCE, J. A. & STOIANOV, I. 2020b. Limitations of Persistent Scatterer Interferometry to measure small seasonal ground movements in an urban environment. *Quarterly Journal of Engineering Geology and Hydrogeology,* 53**,** 39-48.

SELWOOD, E. B., EDWARDS, R. A., SIMPSON, S., CHESHER, J. A., HAMBLIN, R. J. O., HENSON, M. R., RIDDOLLS, B. W., WATERS, R. N., HAWKES, J. R., BISSON, G., SCRIVENER, R. C., RIDDLER, G. P., MATTHEWS, S. C., RAMSBOTTOM, W. H. C., WOOD, C. J. & EDMONDS, E. A. 1984. *Geology of the country around Newton Abbott : Memoir for 1:50,000 geological sheet 339 (New Series),* London, HMSO.

SERVAIS, T. & SINTUBIN, M. 2009. Avalonia, Armorica, Perunica: terranes, microcontinents, microplates or palaeobiogeographical provinces? *Geological Society, London, Special Publications,* 325**,** 103-115.

SHACKLETON, R. M. 1984. Thin-skinned tectonics, basement control and the Variscan front. *Geological Society, London, Special Publications,* 14**,** 125-129.

SHERLOCK, R. L. 1947. *London and Thames Valley,* London, HMSO.

SHERLOCK, R. L., CASEY, R., HOLMES, S. C. A. & WILSON, V. 1962. *London and Thames Valley,* London, HMSO.

SIBSON, R. H. 1974. Frictional constraints on thrust, wrench and normal faults. *Nature,* 249**,** 542-544.

SIBSON, R. H. 1985. A note on fault reactivation. *Journal of Structural Geology,* 7**,** 751-4.

SIBSON, R. H. 1990a. Conditions for fault-valve behaviour. *Geological Society, London, Special Publications,* 54**,** 15-28.

SIBSON, R. H. 1990b. Rupture nucleation on unfavorably oriented faults. *Bulletin of the Seismological Society of America,* 80**,** 1580-1604.

SIBSON, R. H. 1994. An assessment of field evidence for `Byerlee' friction. *Pure and Applied Geophysics,* 142**,** 645-62.

SIBSON, R. H. 1995. Selective fault reactivation during basin inversion: potential for fluid redistribution through fault-valve action. *Geological Society, London, Special Publications,* 88**,** 3-19.

SIBSON, R. H. 1998. Brittle failure mode plots for compressional and extensional tectonic regimes. *Journal of Structural Geology,* 20**,** 655-660.

SIBSON, R. H. 2009. Rupturing in overpressured crust during compressional inversion—the case from NE Honshu, Japan. *Tectonophysics,* 473**,** 404-416.
SISMONDI, S., BENG, F. & WEINMAR, W. 2015. Observed differences in the behaviour of the London Clay sub-units during SCL works for Bond Street Station and Tottenham Court Road Station (C300/410). *Crossrail Project: Infrastructure Design and Construction*.
SKEMPTON, A. W., SCHUSTER, R. L. & PETLEY, D. J. 1969. Joints and Fissures in the London Clay at Wraysbury and Edgware. *Géotechnique,* 19**,** 205-217.
SKIPPER, J. 9th April 2019. *RE: Re-naming the 'Lambeth Group Sand Unit'.* Email to EDGAR, J. & MORGAN, T. O.
SKIPPER, J. & EDGAR, J. 2020. The Harwich Formation in London – The legacy of Chris King. *Proceedings of the Geologists' Association,* 131**,** 474-485.
SKIPPER, J. A. 2000. *The stratigraphy of the Lambeth group (Palaeocene) of south east England.* Imperial College London (University of London).
SKIPPER, J. A., SCHOLES, H. E., LAWRENCE, U., PACKER, M. & MENKITI, C. O. 2015. The Lambeth Group in the Crossrail Project of London, UK - the geological model. *Geotechnical Engineering for Infrastructure and Development.*
SMALLEY, S. & WESTBROOK, G. K. 1982. Geophysical evidence concerning the southern boundary of the London Platform beneath the Hog's Back, Surrey. *Journal of the Geological Society,* 139**,** 139-146.
SMITH, A. 2009a. Accuracy of BGS legacy digital geological map data. *Briish Geological Open Report, OR/09/064.* Keyworth, Nottingham: British Geological Survey.
SMITH, A. 2009b. A new edition of the bedrock geology map of the United Kingdom. *Journal of Maps,* 5**,** 232-252.
SMITH, N. 1985. Structure contour and subcrop maps of the pre-Permian surface of the United Kingdom (south). *In:* WHITTAKER, A. (ed.) *Atlas of onshore sedimentary basins in England and Wales: Post-Carboniferous tectonics and stratigraphy.* British Geological Survey.
SOPER, N. J., WEBB, B. C. & WOODCOCK, N. H. 1987. Late Caledonian (Acadian) transpression in north-west England: timing, geometry and geotectonic significance. *Proceedings of the Yorkshire Geological Society,* 46**,** 175-192.
SOPER, N. J. & WOODCOCK, N. H. 1990. Silurian collision and sediment dispersal patterns in southern Britain. *Geological Magazine,* 127**,** 527-542.
STAMP, L. D. 1921. On the Beds at the base of the Ypresian (London Clay) in the Anglo-Franco-Belgian Basin. *Proceedings of the Geologists' Association,* 32**,** 57-IN2.
STAMP, L. D. 1924. Eocene Cycles of Sedimentation. *Geological Magazine,* 61**,** 98-102.
STANDING, J. R. 2020. Identification and implications of the London Clay Formation divisions from an engineering perspective. *Proceedings of the Geologists' Association,* 131**,** 486-499.
STONELEY, R. 1982. The structural development of the Wessex Basin. *Journal of the Geological Society,* 139**,** 543-554.
STRANGE, P. J., BOOTH, S. J. & ELLISON, R. A. 1998. Development of 'rockhead' computer-generated geological models to assist geohazard prediction in London. *Geological Society, London, Engineering Geology Special Publications,* 15**,** 409-414.
SUMBLER, M. G. 1996. *British Regional Geology: London and the Thames Valley,* London, Her Majesty's Stationary Office, for British Geological Survey.
TAYLOR, J. C. M. 1986. Gas Prospects in the Variscan Thrust Province of Southern England. *Geological Society, London, Special Publications,* 23**,** 37-53.
THAMES WATER 2009. London Tideway Tunnels: Thames Tunnel geophysical and hydrographic survey. *Contract no 5LYG/G58 Stage 1 interpretation.* Thames Water.
THOMAS, A. R. A. 2007. Chapter 11 An Integrated Grain-Size and Heavy Mineral Analysis of the Palaeocene Strata of the London Basin. *In:* MANGE, M. A. & WRIGHT, D. T. (eds.) *Developments in Sedimentology.* Elsevier.

TING, C., GILSON, B. & BLACK, M. 2020. Developing the 3D geological model for Crossrail 2, London, UK. *Quarterly Journal of Engineering Geology and Hydrogeology***,** qjegh2020-029.
TOMS, E., MASON, P. J. & GHAIL, R. C. 2016. Drift-filled hollows in Battersea: investigation of the structure and geology along the route of the Northern Line Extension, London. *Quarterly Journal of Engineering Geology and Hydrogeology,* 49**,** 147-153.
TUDOR, D. G. 2019. *Victorian chalk mine stability assessment in Reading, UK: influence of brittle geological structures* MSc, Imperial College London.
TURNER, J. P. 1997. Strike-slip fault reactivation in the Cardigan Bay basin. *Journal of the Geological Society,* 154**,** 5-8.
TURNER, J. P. & WILLIAMS, G. A. 2004. Sedimentary basin inversion and intra-plate shortening. *Earth-Science Reviews,* 65**,** 277-304.
TURNER, J. S. The deeper structure of central and northern England. Proceedings of the Yorkshire Geological and Polytechnic Society, 1949. Geological Society of London, 280-297.
UETA, K., TANI, K. & KATO, T. 2000. Computerized X-ray tomography analysis of three-dimensional fault geometries in basement-induced wrench faulting. *Engineering Geology,* 56**,** 197-210.
VANDYCKE, S. 2002. Palaeostress records in Cretaceous formations in NW Europe: extensional and strike–slip events in relationships with Cretaceous–Tertiary inversion tectonics. *Tectonophysics,* 357**,** 119-136.
WARR, L. N. 2000. The Variscan Orogeny: the welding of Pangaea. *In:* WOODCOCK, N. H. & STRACHAN, R. (eds.) *Geological History of Britain and Ireland.* 1st ed.: Blackwell Science.
WATTS, A. B., MCKERROW, W. S. & FIELDING, E. 2000. Lithospheric flexure, uplift, and landscape evolution in south-central England. *Journal of the Geological Society,* 157**,** 1169-1177.
WEBSTER, T. 1814. VII. On the Fresh-water Formations in the Isle of Wight, with some Observations on the Strata over the Chalk in the South-east part of England. *Transactions of the Geological Society of London,* S1-2**,** 161-254.
WEST, G. 1983. Comparisons between real and predicted geology in tunnels: examples from recent cases. *Quarterly Journal of Engineering Geology and Hydrogeology,* 16**,** 113-126.
WESTHEAD, R. K., MCCARTHY, D. J., COLLIER, J. S. & SANDERSON, D. J. 2018. Spatial variability of the Purbeck–Wight Fault Zone—a long-lived tectonic element in the southern UK. *Proceedings of the Geologists' Association,* 129**,** 436-451.
WHITAKER, W. 1889a. *The Geology of London and of part of the Thames Valley, Volume I: Descriptive Geology,* London, HMSO.
WHITAKER, W. 1889b. *The Geology of London and of Part of the Thames Valley, Volume II: Appendices,* London, HMSO.
WHITAKER, W., BRISTOW, H. W. & HUGHES, T. M. 1872. *The Geology of the London Basin. Part I. The Chalk and the Eocene Beds of the Southern and Western Tracts*, HM Stationery Office.
WHITAKER, W. & DAWKINS, W. B. 1892. *Eastern Part of London, Woolwich, Dartford, Romford [Solid, 1SW]*. London: Geological Survey of England and Wales.
WHITAKER, W. J. 1875. *Guide to the Geology of London and the Neighbourhood,* London, HM Stationery Office.
WILLIAMS, G. A., TURNER, J. P. & HOLFORD, S. P. 2005. Inversion and exhumation of the St. George's Channel basin, offshore Wales, UK. *Journal of the Geological Society,* 162**,** 97-110.
WOOD, S. V. 1866. II.—On the Structure of the Thames Valley and of its Contained Deposits. *Geological Magazine,* 3**,** 99-107.
WOOD, S. V. 1882. The Newer Pliocene Period in England. *Quarterly Journal of the Geological Society,* 38**,** 667-745.
WOODCOCK, N. H. 1991. The Welsh, Anglian and Belgian Caledonides compared. *Annales de la Société géologique de Belgique,* 144**,** 5-17.
WOODCOCK, N. H. 2000a. Late Ordovician to Silurian evolution of Eastern Avalonia during convergence with Laurentia. *In:* WOODCOCK, N. H. & STRACHAN, R. (eds.) *Geological History of Britain and Ireland.* 1st ed.: Blackwell Science.

WOODCOCK, N. H. 2000b. Ordovician volcanism and sedimentation on Eastern Avalonia. *In:* WOODCOCK, N. H. & STRACHAN, R. (eds.) *Geological History of Britain and Ireland.* 1st ed.: Blackwell Science.

WOODCOCK, N. H., MILLER, A. V. M. & WOODHOUSE, C. D. 2014. Chaotic breccia zones on the Pembroke Peninsula, south Wales: Evidence for collapse into voids along dilational faults. *Journal of Structural Geology,* 69**,** 91-107.

WOODCOCK, N. H. & STRACHAN, R. 2000a. The Caledonian Orogeny: a multiple plate collision. *In:* WOODCOCK, N. H. & STRACHAN, R. (eds.) *Geological History of Britain and Ireland.* 1st ed.: Blackwell Science.

WOODCOCK, N. H. & STRACHAN, R. 2000b. Devonian sedimentation and volcanism of the Old Red Sandstone Continent. *In:* WOODCOCK, N. H. & STRACHAN, R. (eds.) *Geological History of Britain and Ireland.* 1st ed.: Blackwell Science.

WOODS, M. A. & CHACKSFIELD, B. C. 2012. Revealing deep structural influences on the Upper Cretaceous Chalk of East Anglia (UK) through inter-regional geophysical log correlations. *Proceedings of the Geologists' Association,* 123**,** 486-499.

WOODS, M. A. & FARRANT, A. R. 5th November 2019. RE: Recent BGS Chilterns Geological Mapping & Structures. Email to MORGAN, T. O.

WOODWARD, H. B. 1909. *The geology of the London District*, HM Stationery Office.

WOODWARD, H. B., BROMEHEAD, C. E. N. & CHATWIN, C. P. 1922. *The geology of the London District*, HM Stationery Office.

WOOLDRIDGE, S. W. 1923. The minor structures of the London Basin. *Proceedings of the Geologists' Association,* 34**,** 175-IN1.

WOOLDRIDGE, S. W. 1926. The structural evolution of the London Basin. *Proceedings of the Geologists' Association,* 37**,** 162-196.

WORSSAM, B. C. 1963. *Geology of the country around Maidstone. Sheet 288.*, HM Stationery Office.

WRIGHT, V., WOODCOCK, N. H. & DICKSON, J. A. D. 2009. Fissure fills along faults: Variscan examples from Gower, South Wales. *Geological Magazine,* 146**,** 890-902.

WU, J. E., MCCLAY, K., WHITEHOUSE, P. & DOOLEY, T. 2009. 4D analogue modelling of transtensional pull-apart basins. *Marine and Petroleum Geology,* 26**,** 1608-1623.

YOUNG, G. W. 1905. The Chalk area of North-East Surrey. *Proceedings of the Geologists' Association,* 19**,** 188-IN1.

ZIEGLER, P. A. 1987. Late Cretaceous and Cenozoic intra-plate compressional deformations in the Alpine foreland—a geodynamic model. *Tectonophysics,* 137**,** 389-420.

ZIEGLER, P. A. 1989. Geodynamic model for Alpine intra-plate compressional deformation in Western and Central Europe. *Geological Society, London, Special Publications,* 44**,** 63-85.

ZIEGLER, P. A. 1990. Collision related intra-plate compression deformations in Western and Central Europe. *Journal of Geodynamics,* 11**,** 357-388.

Appendix A: Private Data Sources

Below is the information and/or data used for this investigation that is not publicly available, outlined in tables according to their associated project. All other information, data and figures used in this document is freely available, and in the public domain or academic literature.

Project/company	Source Originator	Information	Investigation usage(s)
Silvertown Tunnel, (Transport for London) (TfL)	Colin Marshall - Data Control, Silvertown Tunnel; Martin Woodruff - Head of Programme, TfL; [Received 15/03/2019]	Ground Investigation Report (inc. borehole logs and lab data) [PDF format only]	Incorporation into borehole and geospatial databases (Chapter 5)
			East London geological model (Chapter 5)
			Geotechnical spatial variation tester (fig. 5.50)
British Geological Survey (BGS)	Jon Ford - Chief Geologist for England, BGS; Don Aldiss, Honorary Research Associate. [Received 12/05/2020]	BGS Lithoframe structures [shapefiles]	Used throughout for Lithoframe structure illustrations (Chapters 2, 4-7)
Environment Agency (EA)	Martin Lack, Technical Officer, EA [Received 20/07/2020]	Monitoring well data from across East London	Lower Aquifer observation water well analysis (§6.1.3.1)
Thames Water	Mike Jones [Received 07/11/2019]	The 'Reading Report' (Andrews et al., 1995)	Chapter 4 (§4.1.2)
Thames Tideway Tunnel (TTT)	Tim Newman, Project Geologist, TTT; Martin Turner, GIS Manager, TTT/Critigen [Received 06/09/2019]	Ground Investigation Report (inc. borehole logs and lab data) [PDF and AGS format]	Incorporation into borehole and geospatial databases (Chapter 5)
			East London geological model (Chapter 5)
	Tim Newman, Project Geologist, TTT [Received 04-09/2019]	Deptford and Greenwich Shafts exposure notes and structural data	Fault zone analysis (§6.2)
	Tim Newman, Project Geologist, TTT [Received 06/07/2017]	Fault zone cross-sections (Newman, 2017)	
Crossrail	John Davis, Snr Partner, GCG [Received 07/03/2019]	Plan and geological cross-sections (Crossrail, 2012)	
	Jackie Skipper, Snr Geologist, GCG [Received 07/03/2019]	Post-construction update report and appendices (Crossrail, 2016)	Blackwall Facies (§5.1, 6.1.1.2)
			Stress distortion (§7.3.3)
UKOGL	Mark Alldred, Lynx Info Ltd, [Received 11/06.2018]	RG-001 seismic line trace [coordinates file]	Basement analyses (§3.3.2.1; 7.1.2)

Appendix B: Geological modelling cross-sections

Below are the 47 cross-sections constructed during the East London geological modelling programme (Chapter 5). Refer to figure B.1 for their specific locations and B.2 for the lithological key.

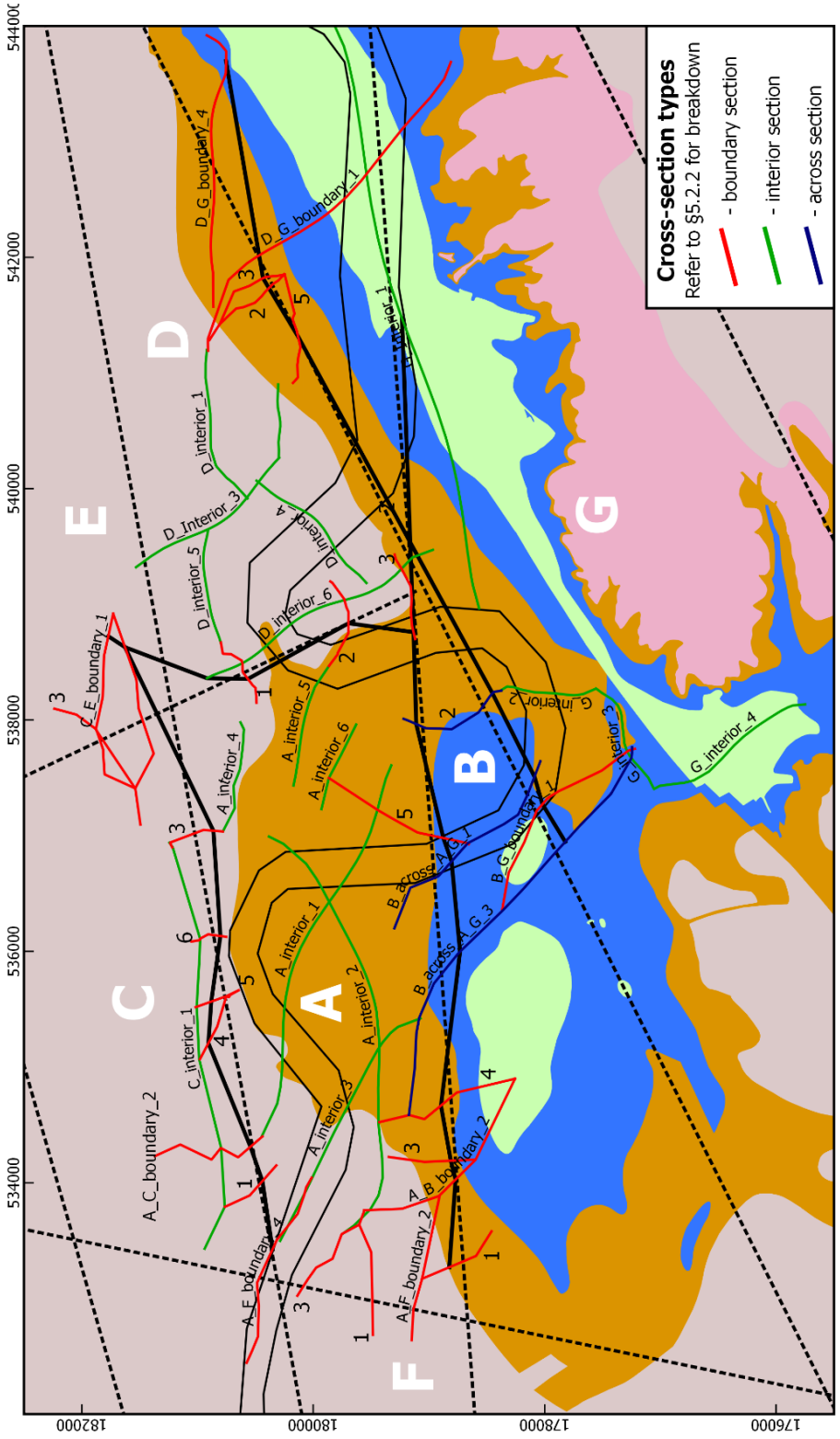

Figure B.1 – Positions of East London cross-sections. Some sections have been labelled with numbers where rendering prevented naming. For these, refer to relative block positioning and section colour for name defining.

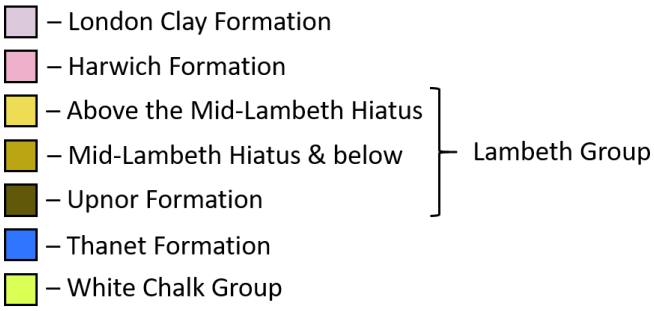

Figure B.2 – Lithological key for geological modelling horizons.

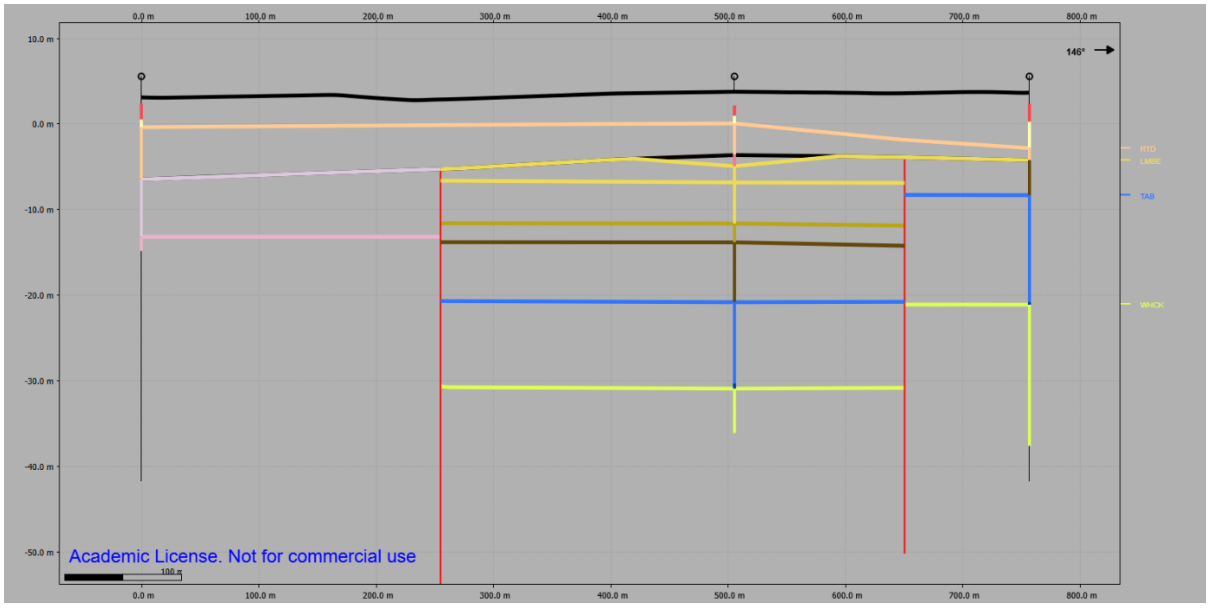

Figure B.3 – Section A_B_boundary_1. Vertical exaggeration: x8.

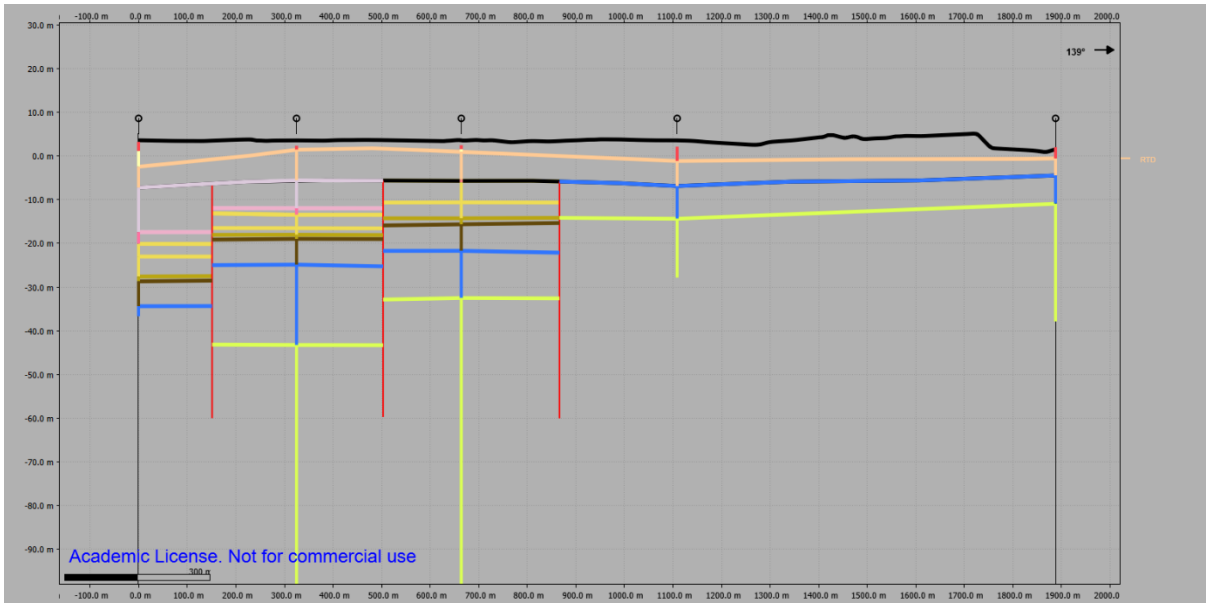

Figure B.4 – Section A_B_boundary_2. Vertical exaggeration: x10.

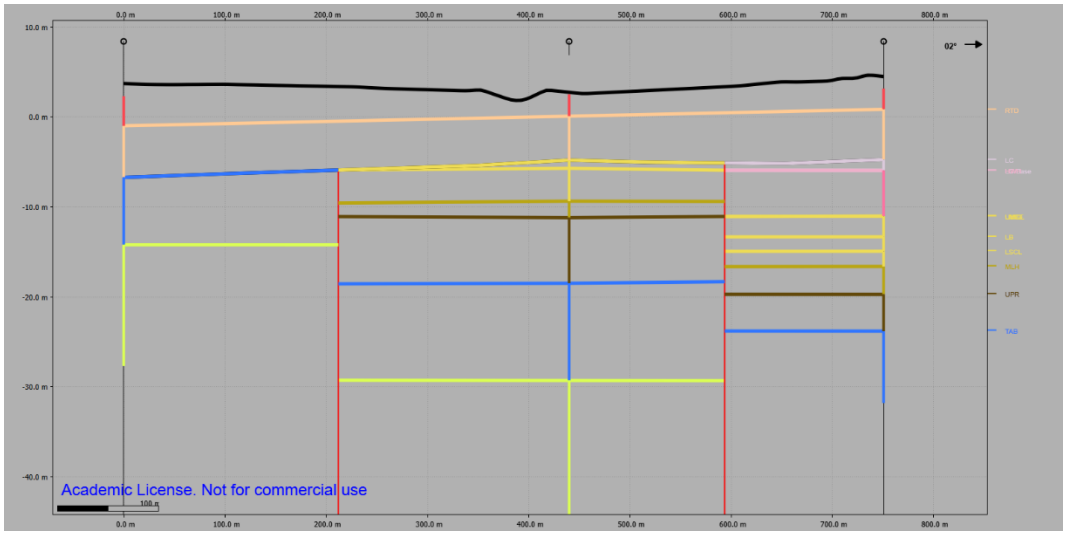

Figure B.5 – Section A_B_boundary_3. Vertical exaggeration: x10.

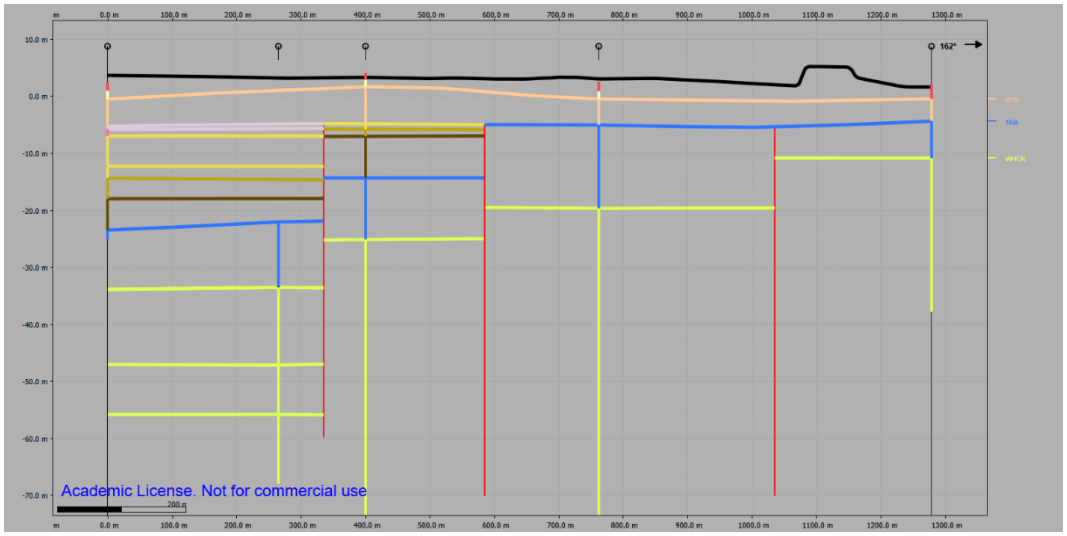

Figure B.6 – Section A_B_boundary_4. Vertical exaggeration: x10.

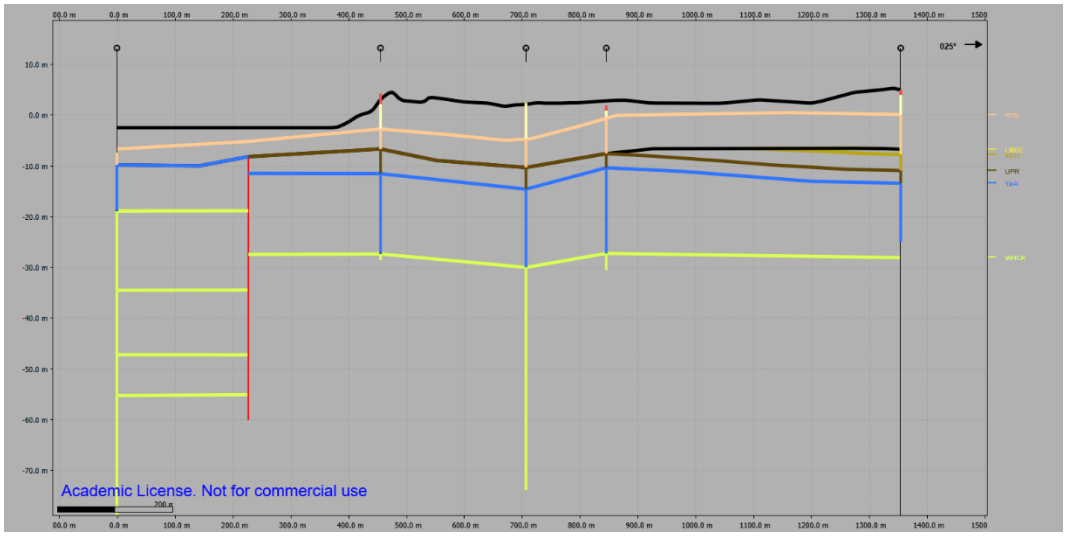

Figure B.7 – Section A_B_boundary_5. Vertical exaggeration: x10.

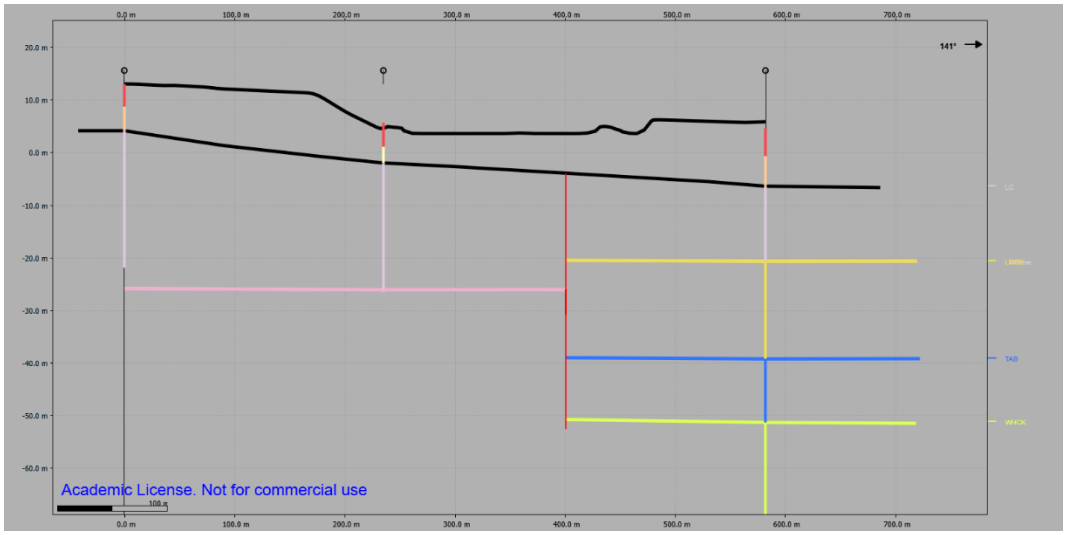

Figure B.8 – Section A_C_boundary_1. Vertical exaggeration: x5.

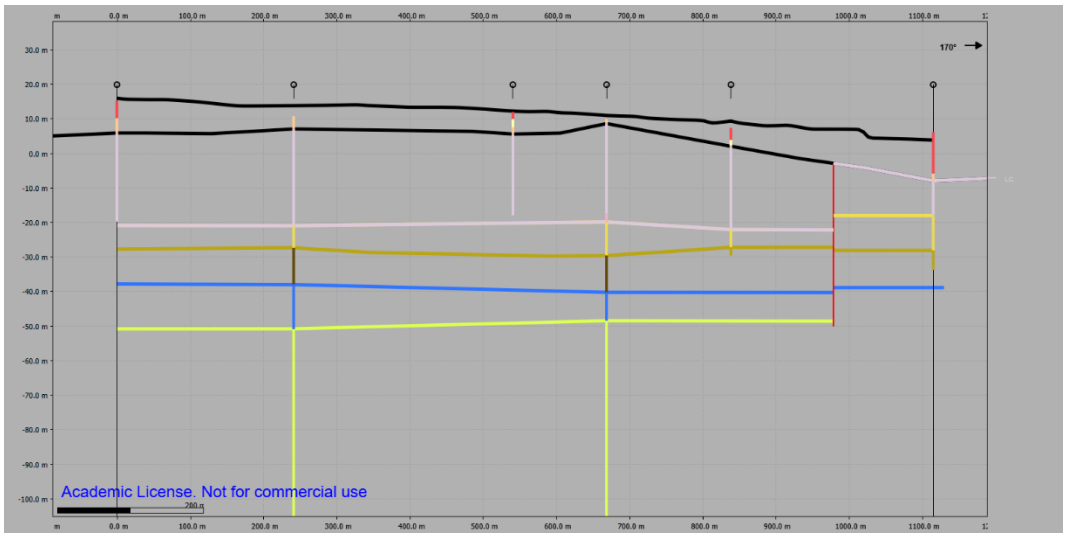

Figure B.9 – Section A_C_boundary_2. Vertical exaggeration: x5.

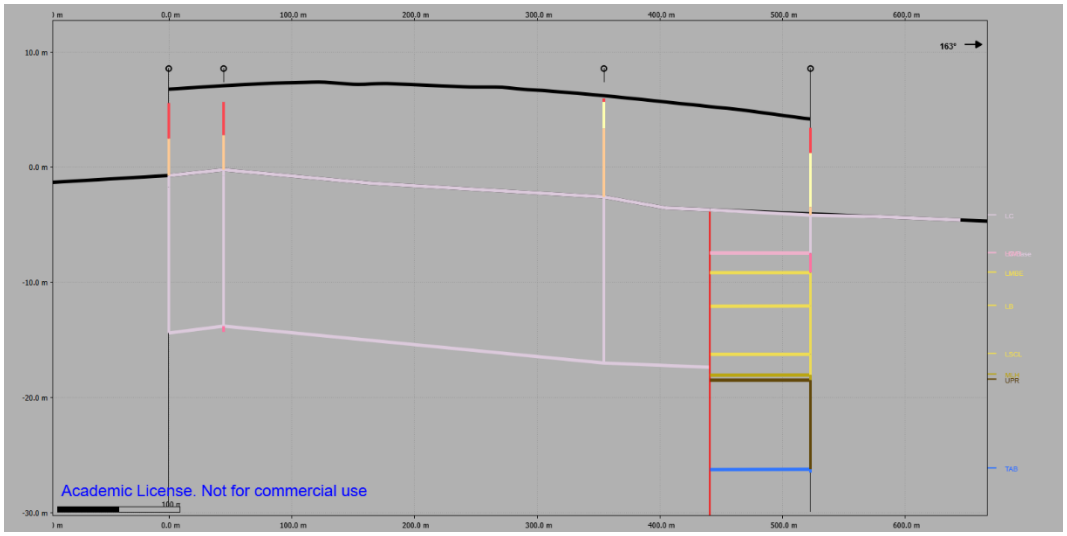

Figure B.10 – Section A_C_boundary_3. Vertical exaggeration: x10.

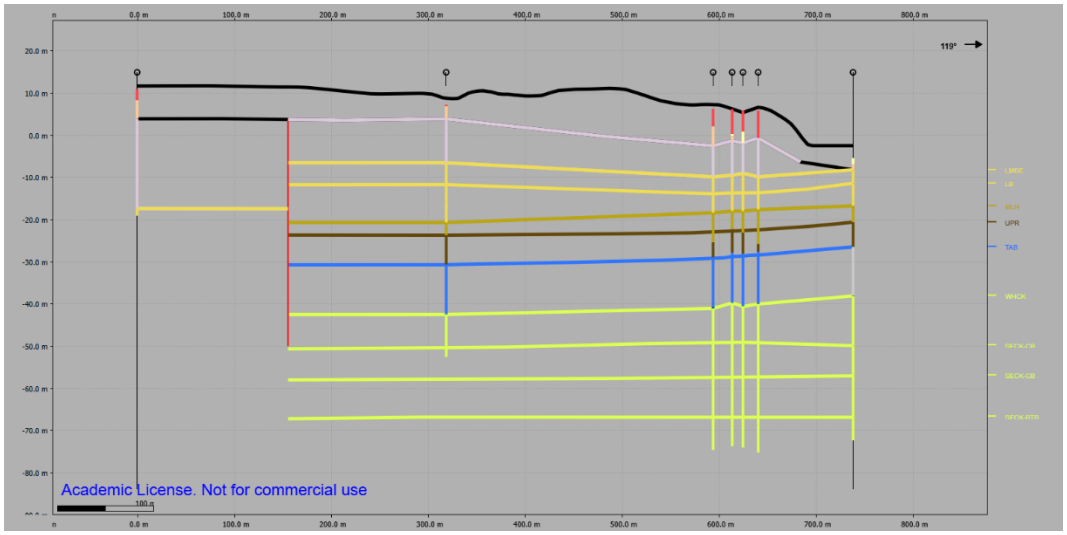

Figure B.11 – Section A_C_boundary_4. Vertical exaggeration: x5.

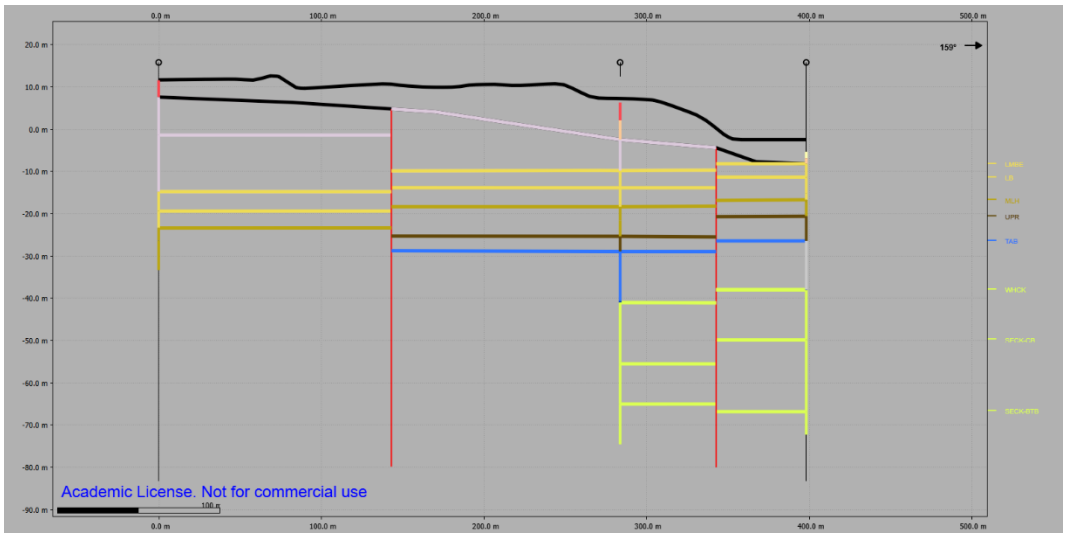

Figure B.12 – Section A_C_boundary_5. Vertical exaggeration: x3.

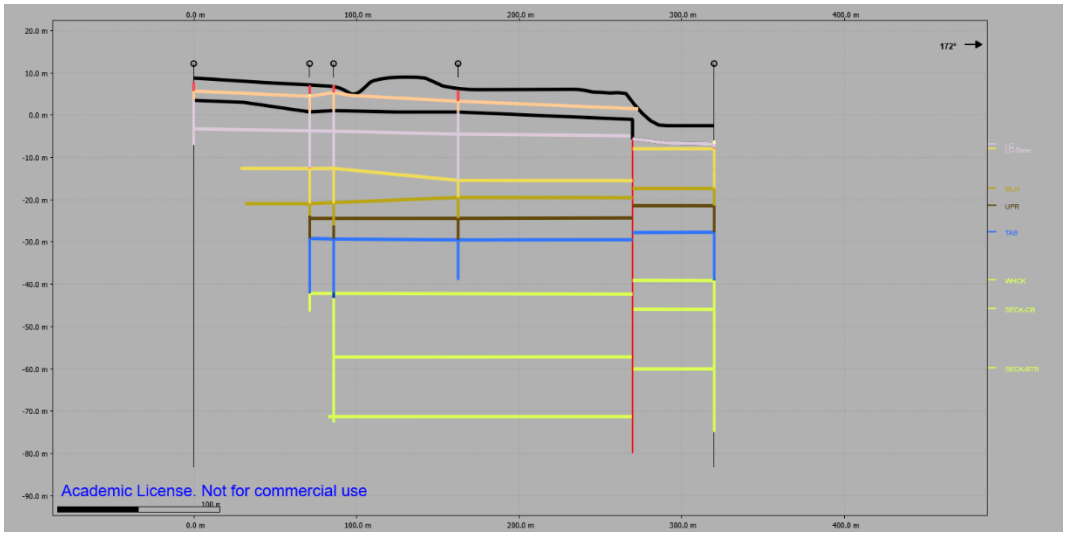

Figure B.13 – Section A_C_boundary_6. Vertical exaggeration: x3.

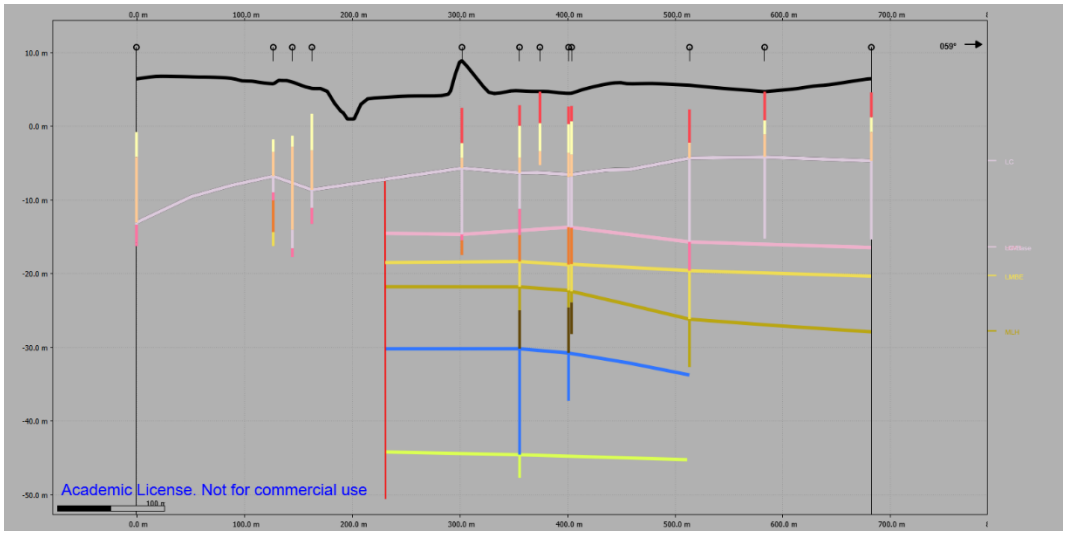

Figure B.14 – Section A_D_boundary_1. Vertical exaggeration: x7.

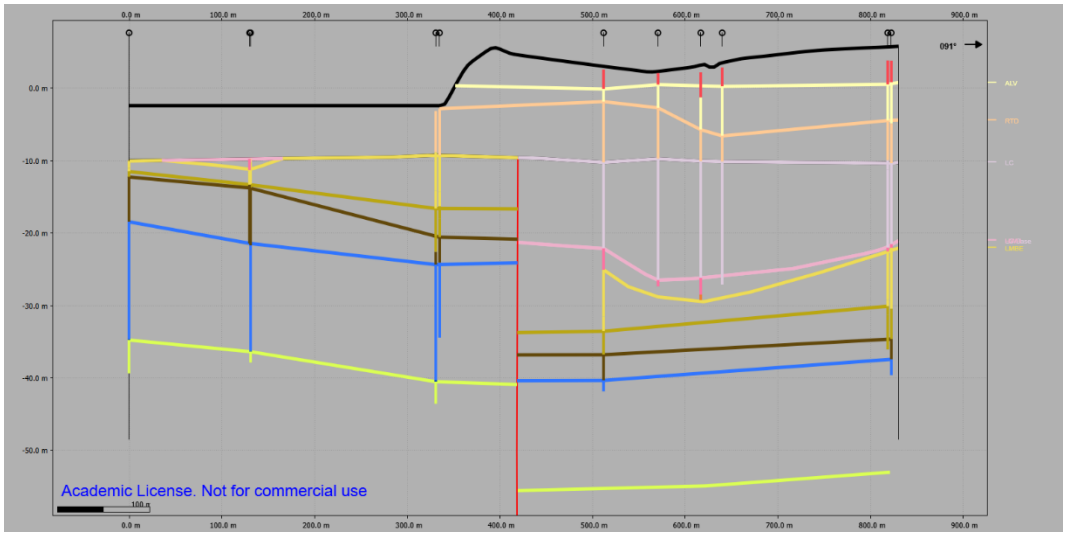

Figure B.15 – Section A_D_boundary_2. Vertical exaggeration: x8.

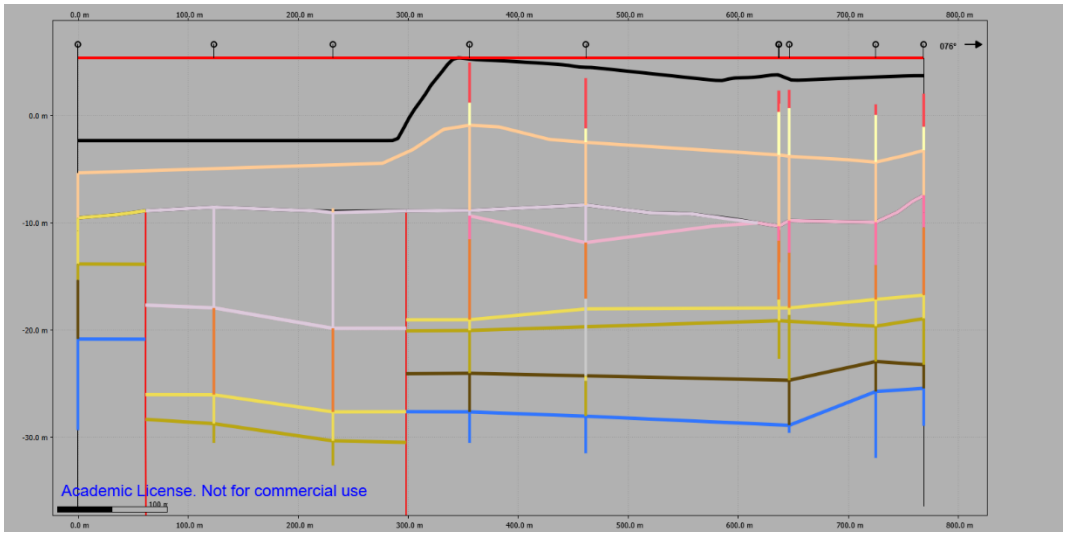

Figure B.16 – Section A_D_boundary_3. Vertical exaggeration: x10.

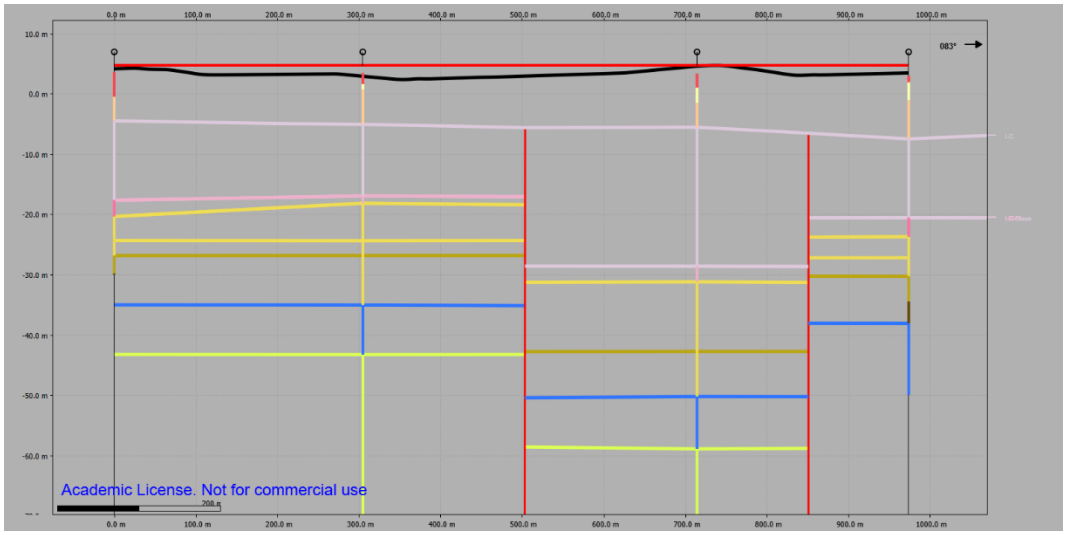

Figure B.17 – Section A_F_boundary_1. Vertical exaggeration: x8.

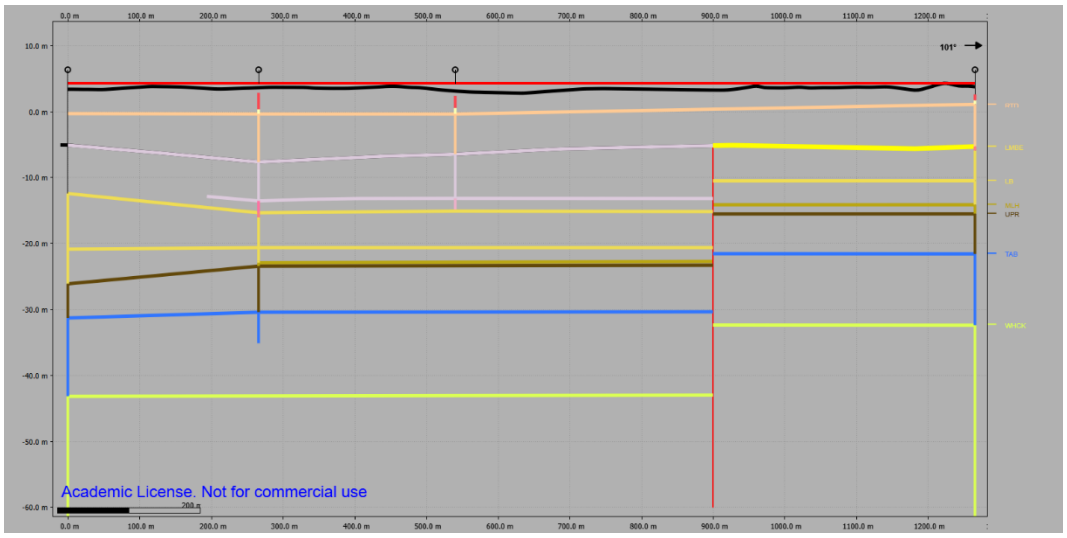

Figure B.18 – Section A_F_boundary_2. Vertical exaggeration: x10.

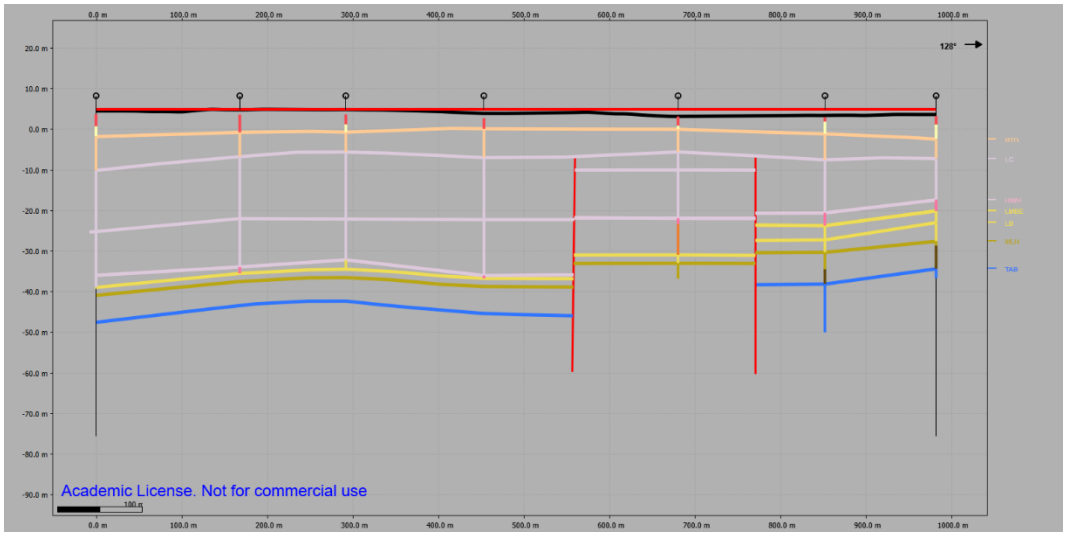

Figure B.19 – Section A_F_boundary_3. Vertical exaggeration: x5.

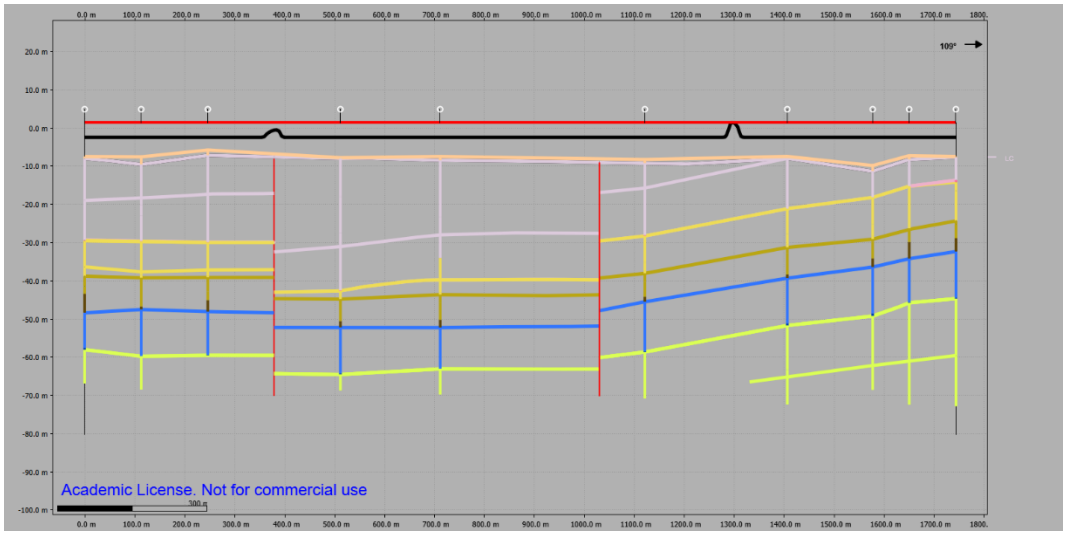

Figure B.20 – Section A_F_boundary_4. Vertical exaggeration: x8.

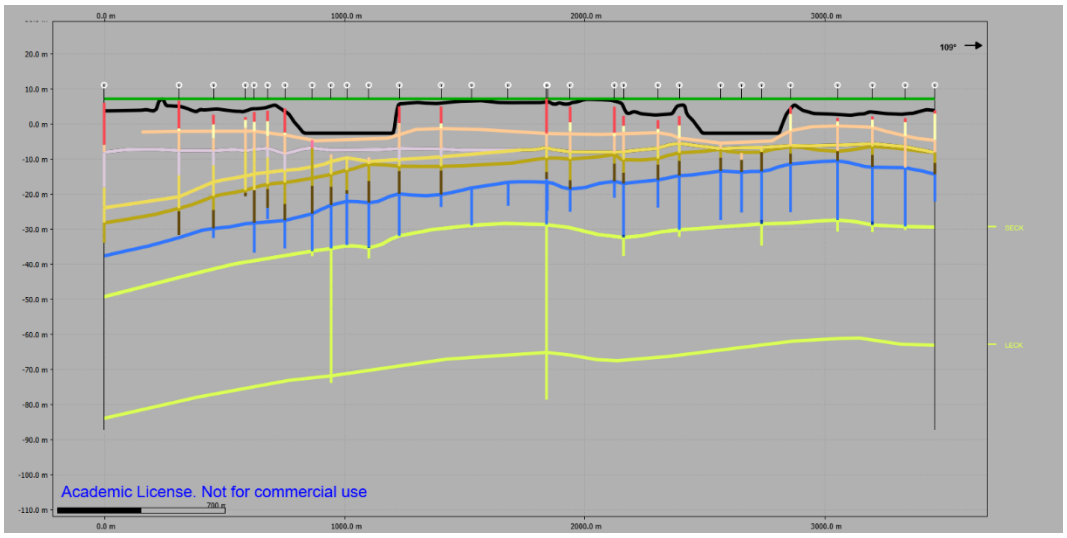

Figure B.21 – Section A_interior_1. Vertical exaggeration: x15.

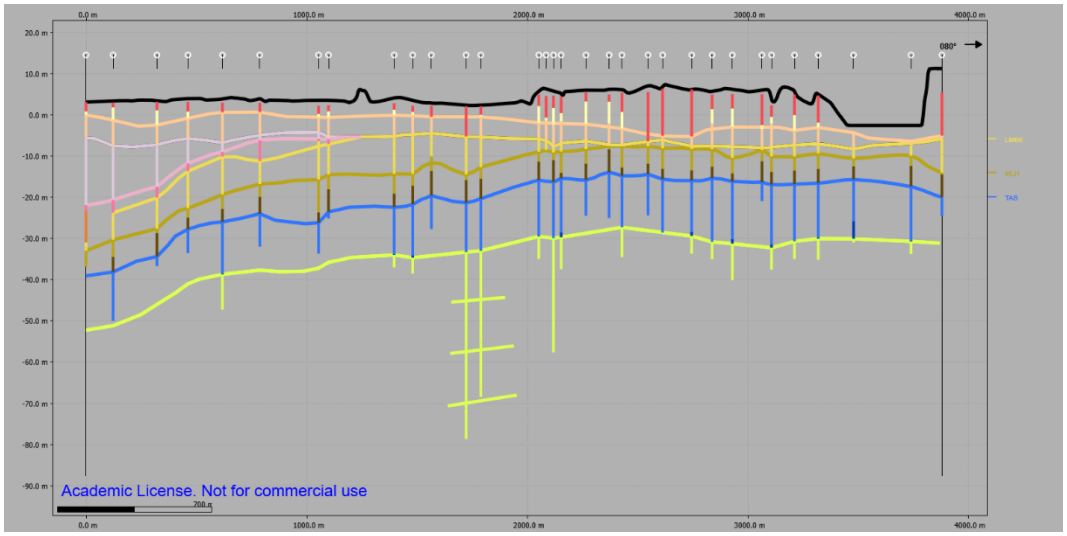

Figure B.22 – Section A_interior_2. Vertical exaggeration: x20.

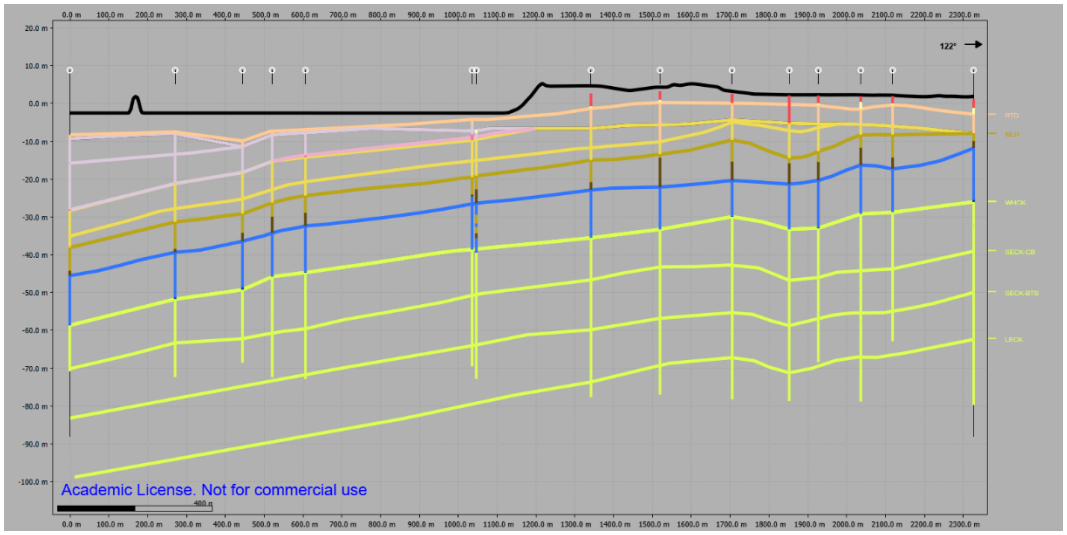

Figure B.23 – Section A_interior_3. Vertical exaggeration: x10.

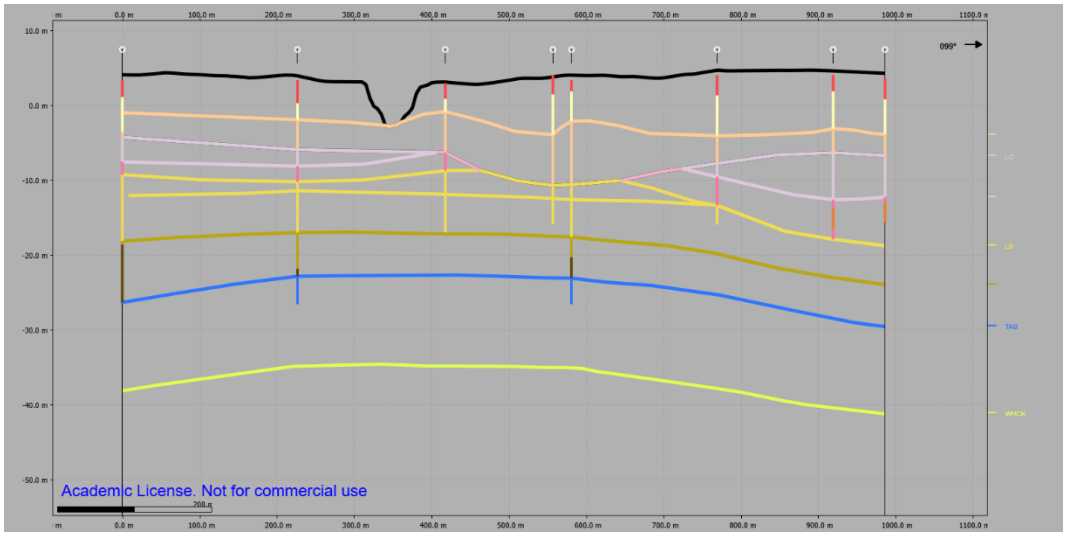

Figure B.24 – Section A_interior_4. Vertical exaggeration: x10.

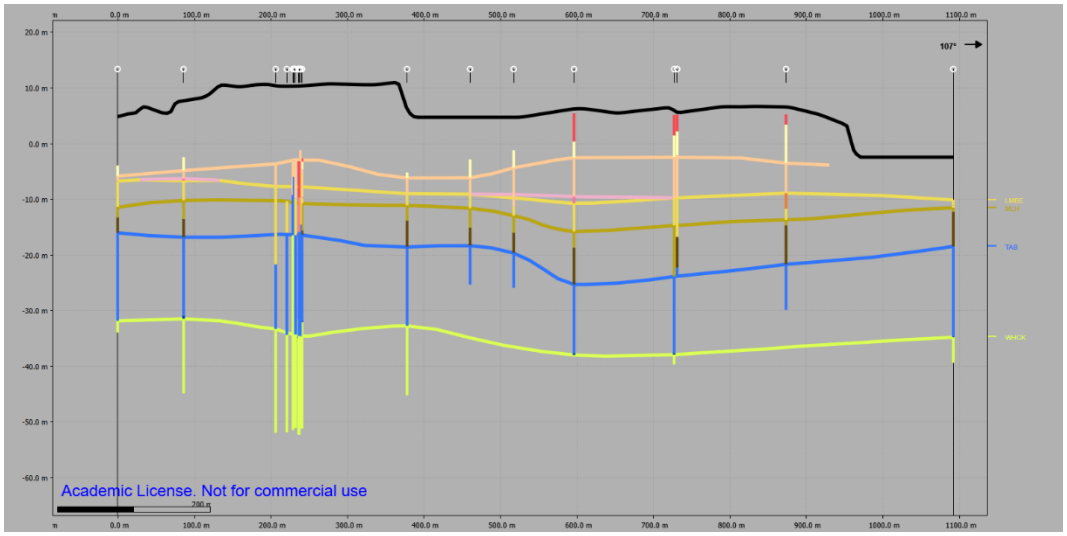

Figure B.25 – Section A_interior_5. Vertical exaggeration: x8.

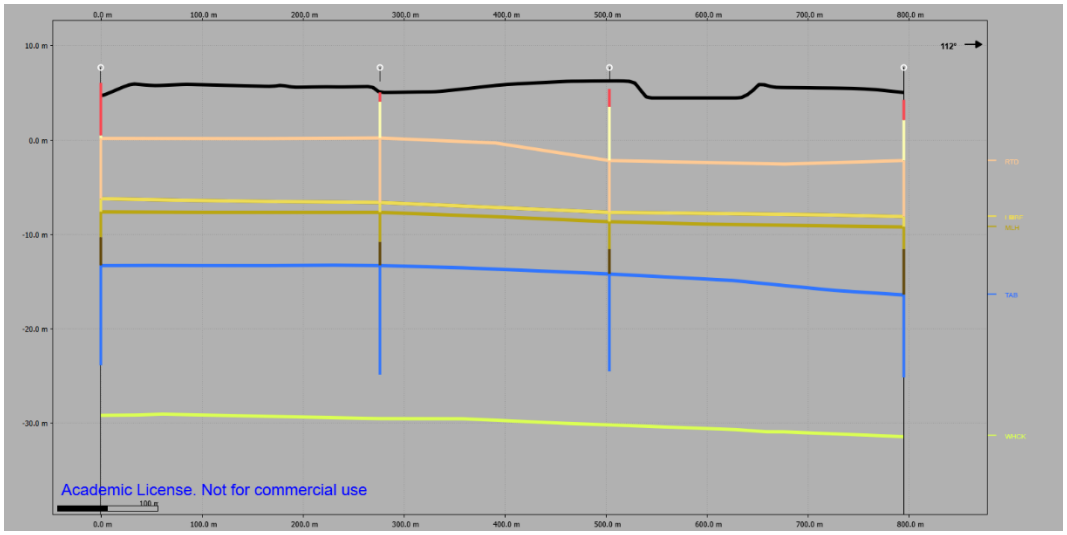

Figure B.26 – Section A_interior_6. Vertical exaggeration: x10.

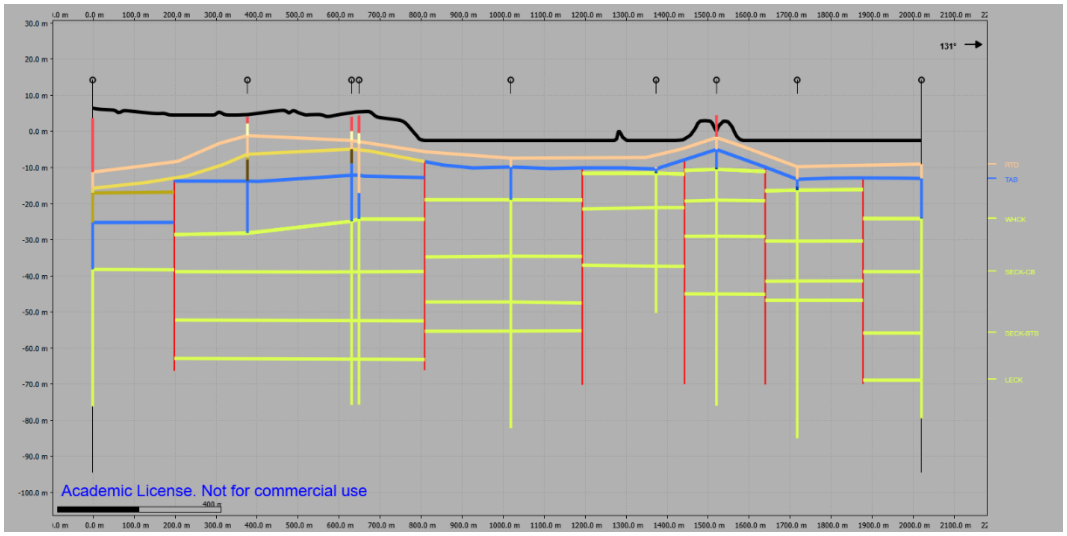

Figure B.27 – Section B_across_A_G_1. Vertical exaggeration: x10.

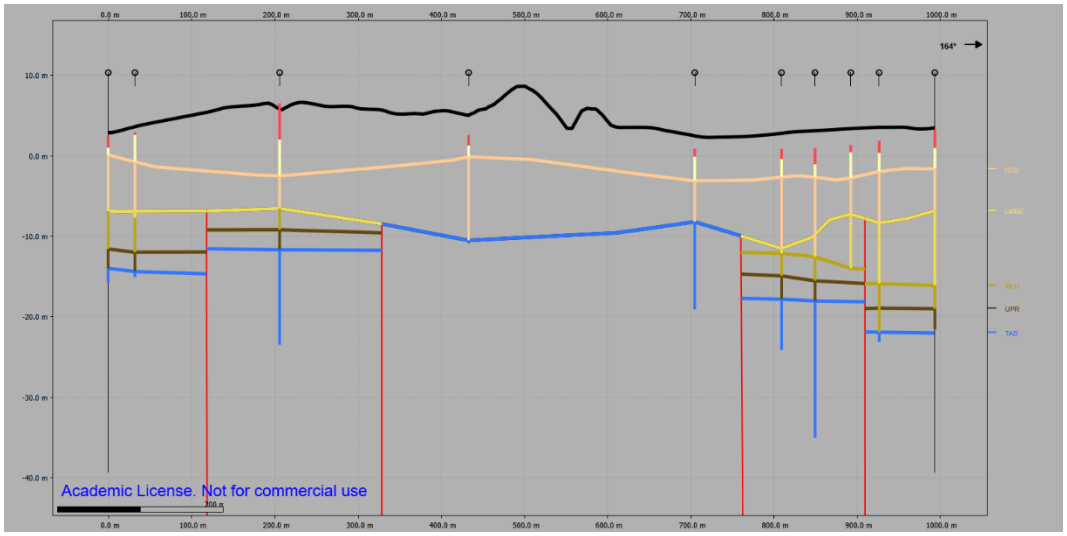

Figure B.28 – Section B_across_A_G_2. Vertical exaggeration: x10.

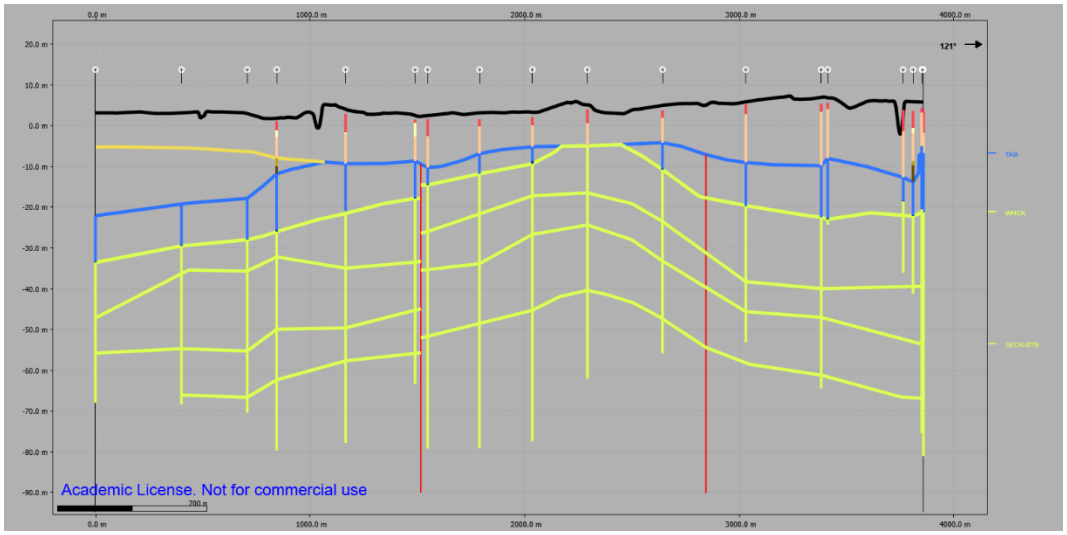

Figure B.29 – Section B_across_A_G_3. Vertical exaggeration: x20.

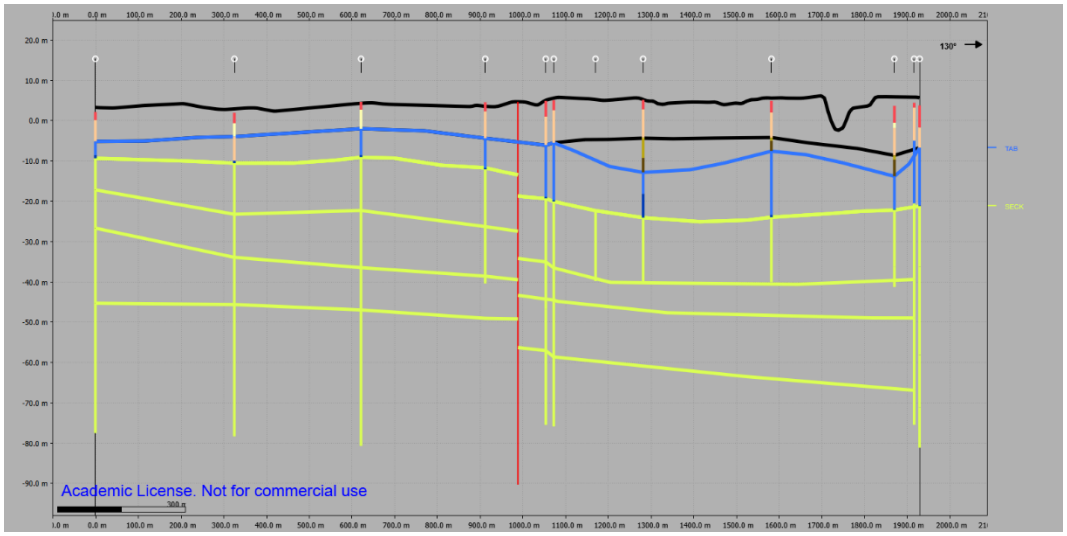

Figure B.30 – Section B_G_boundary_1. Vertical exaggeration: x10.

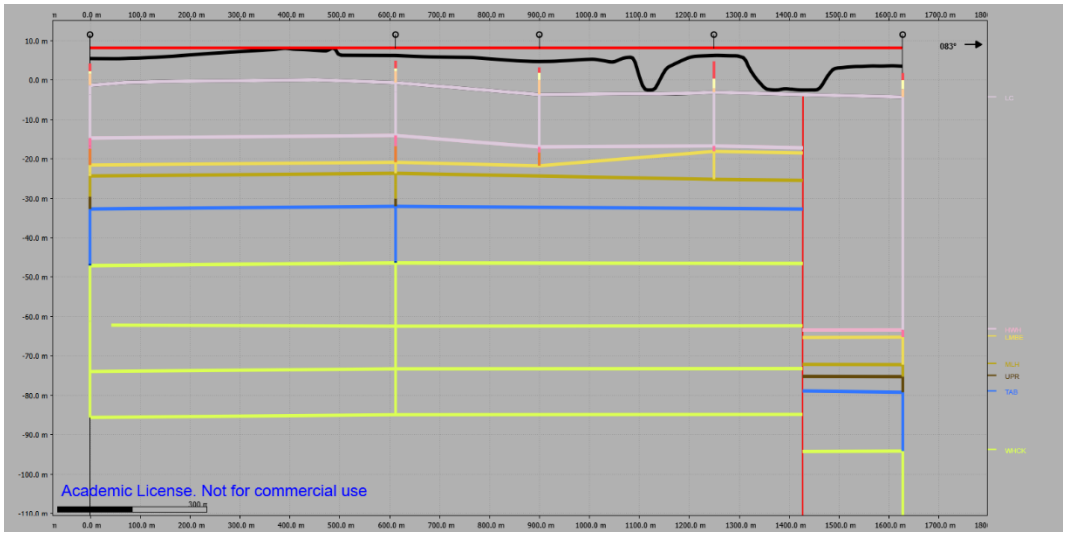

Figure B.31 – Section C_E_boundary_1. Vertical exaggeration: x8.

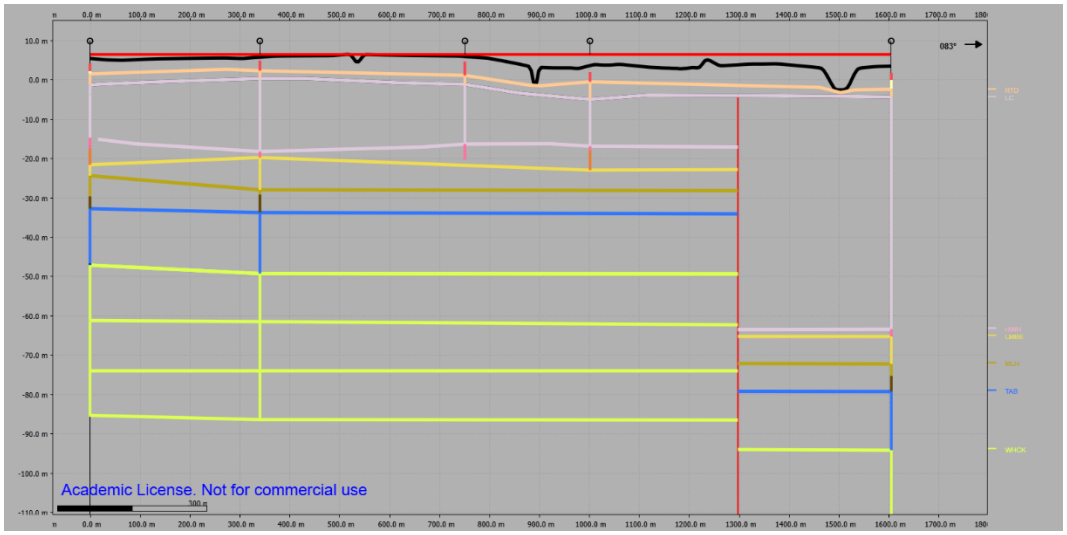

Figure B.32 – Section C_E_boundary_2. Vertical exaggeration: x8.

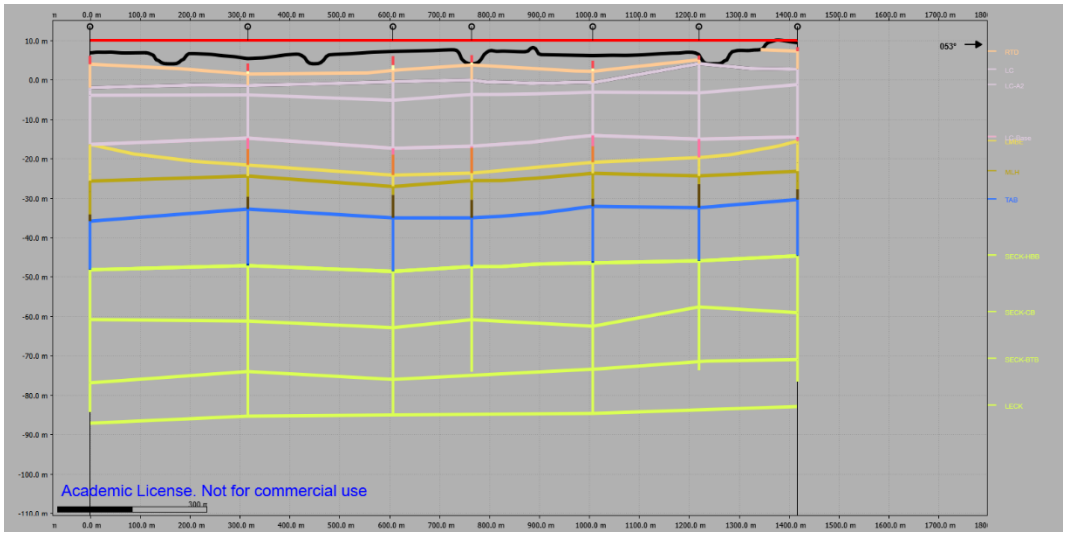

Figure B.33 – Section C_E_boundary_3. Vertical exaggeration: x8.

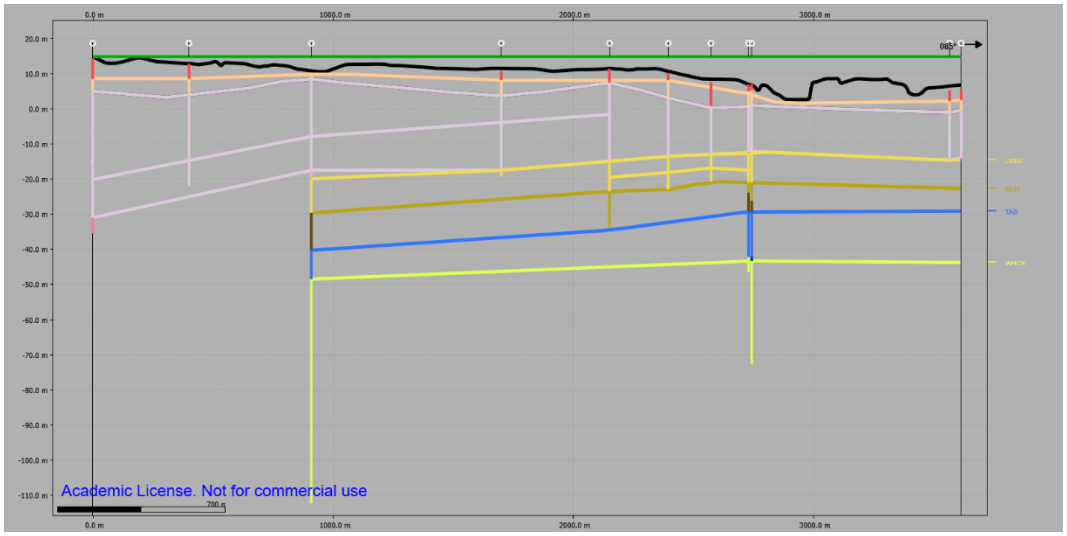

Figure B.34 – Section C_interior_1. Vertical exaggeration: x15.

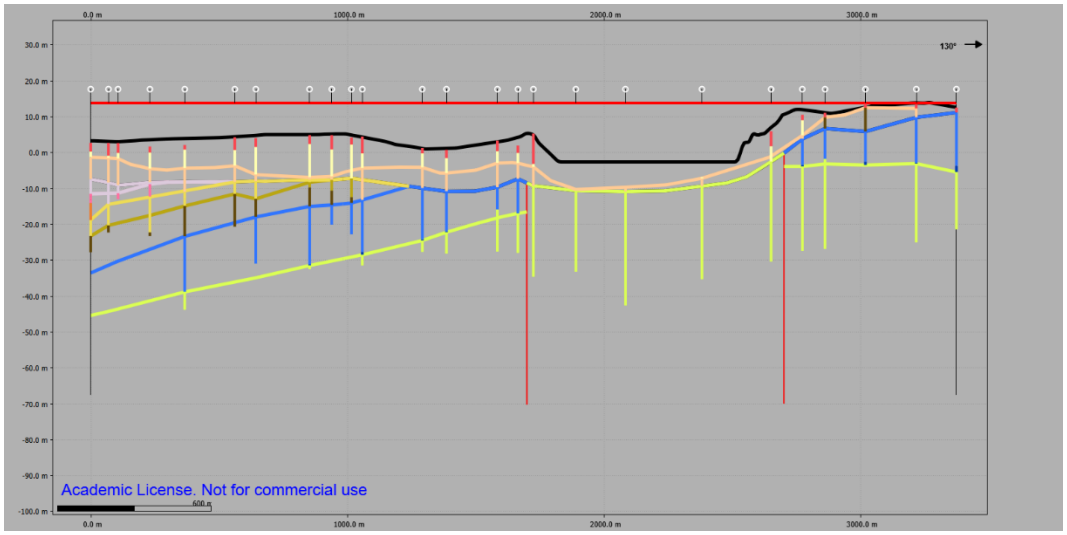

Figure B.35 – Section D_G_boundary_1. Vertical exaggeration: x15.

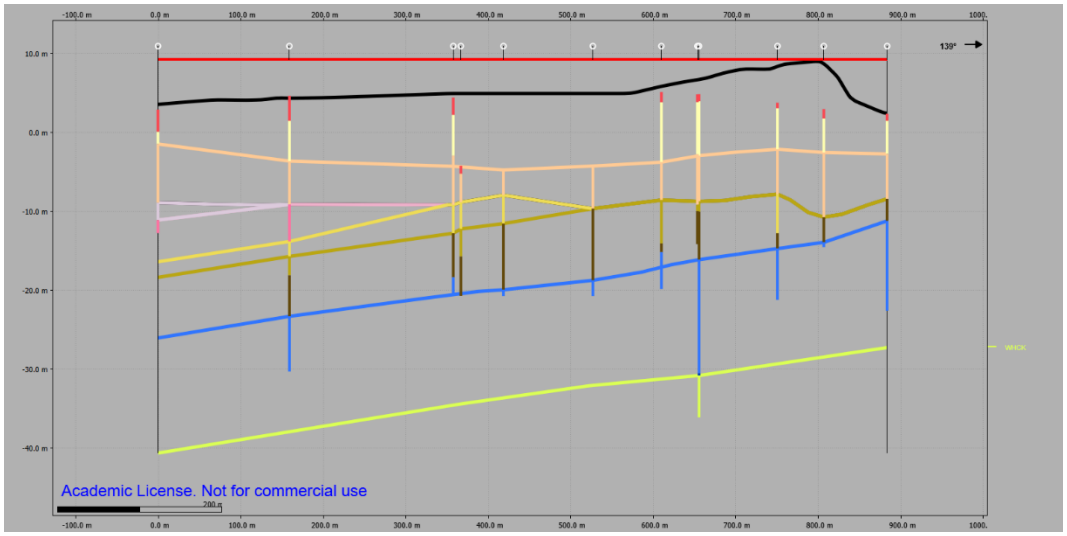

Figure B.36 – Section D_G_boundary_2. Vertical exaggeration: x10.

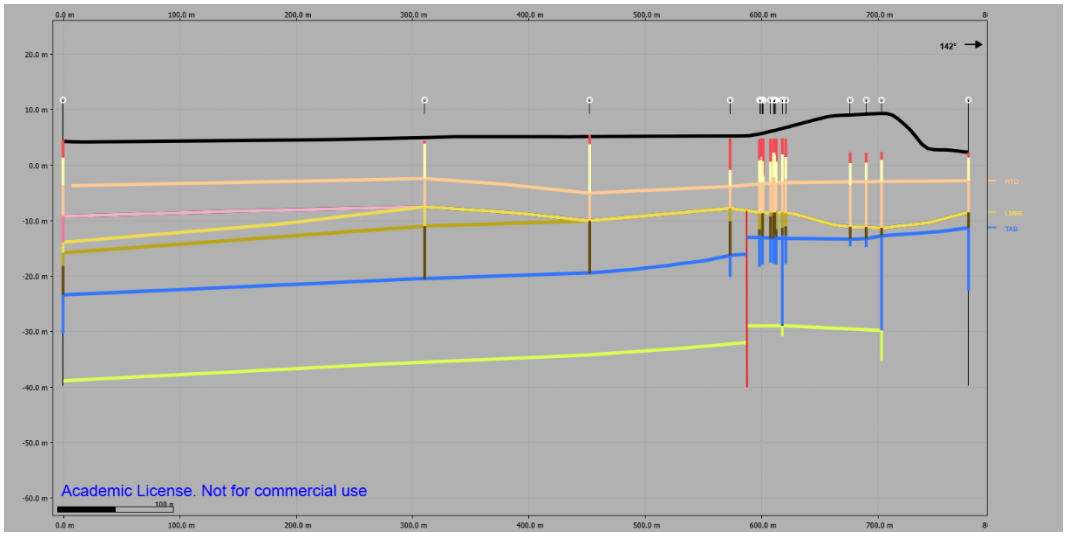

Figure B.37 – Section D_G_boundary_3. Vertical exaggeration: x5.

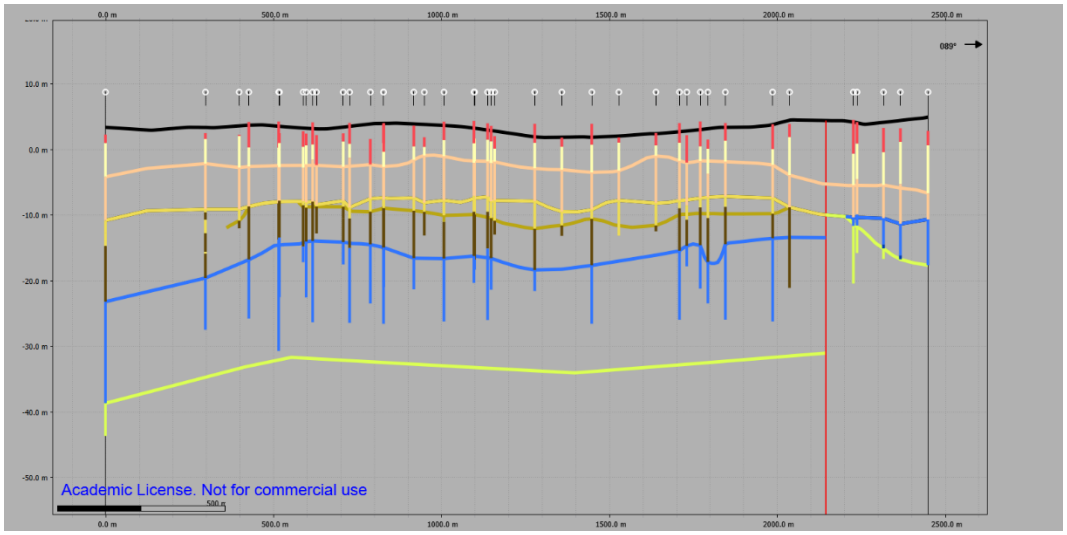

Figure B.38 – Section D_G_boundary_4. Vertical exaggeration: x20.

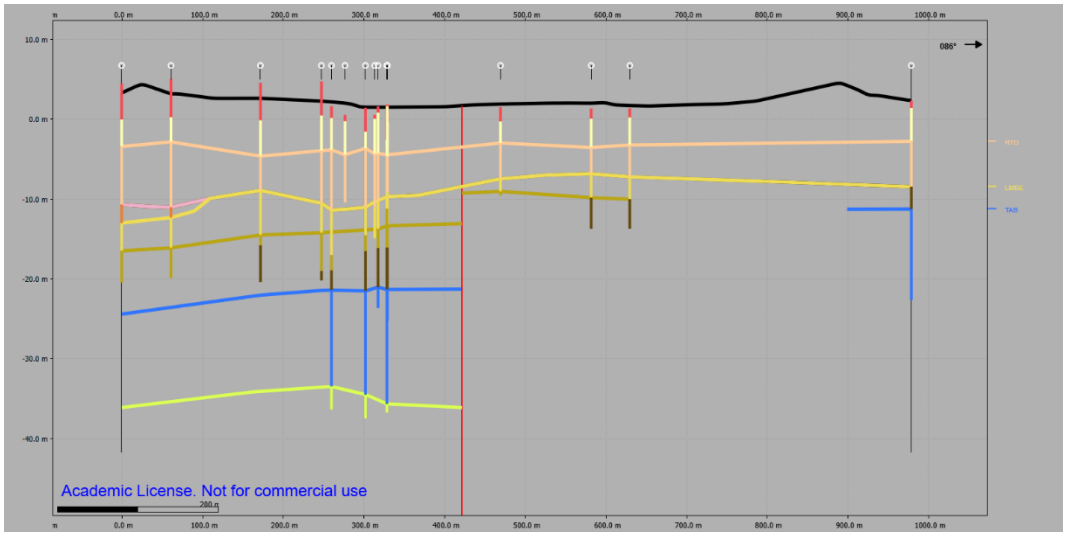

Figure B.39 – Section D_G_boundary_5. Vertical exaggeration: x10.

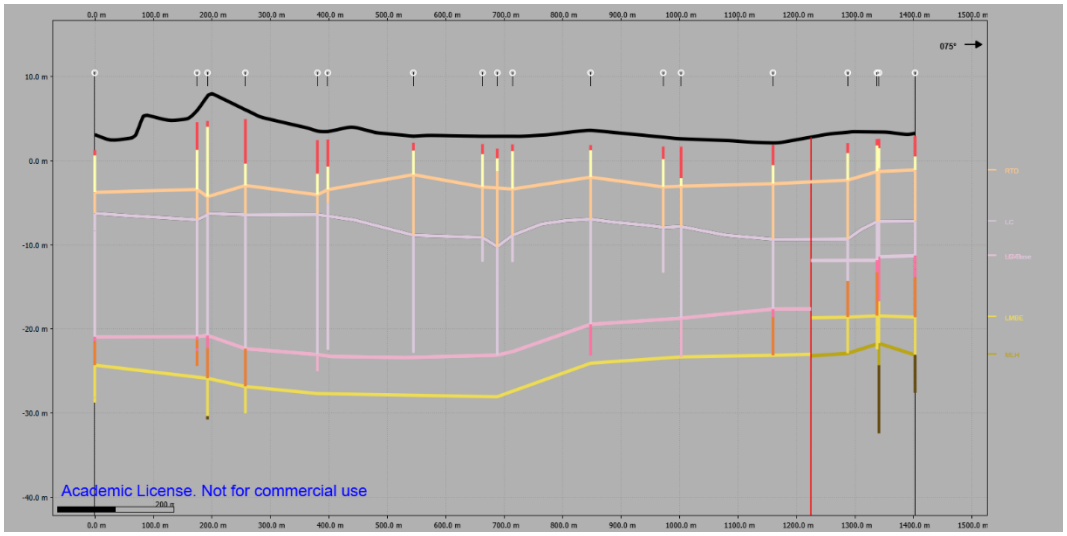

Figure B.40 – Section D_interior_1. Vertical exaggeration: x15.

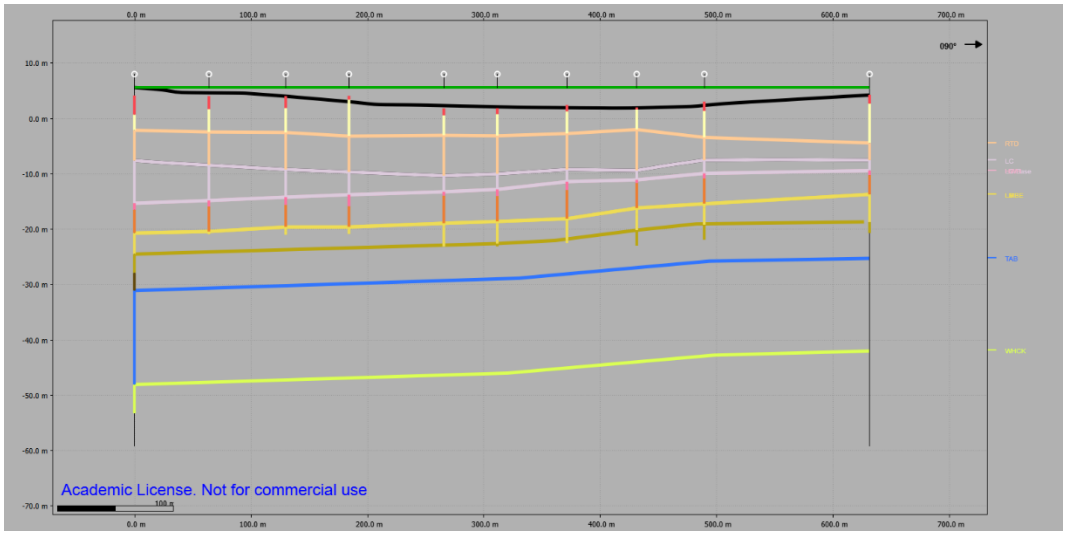

Figure B.41 – Section D_interior_2. Vertical exaggeration: x5.

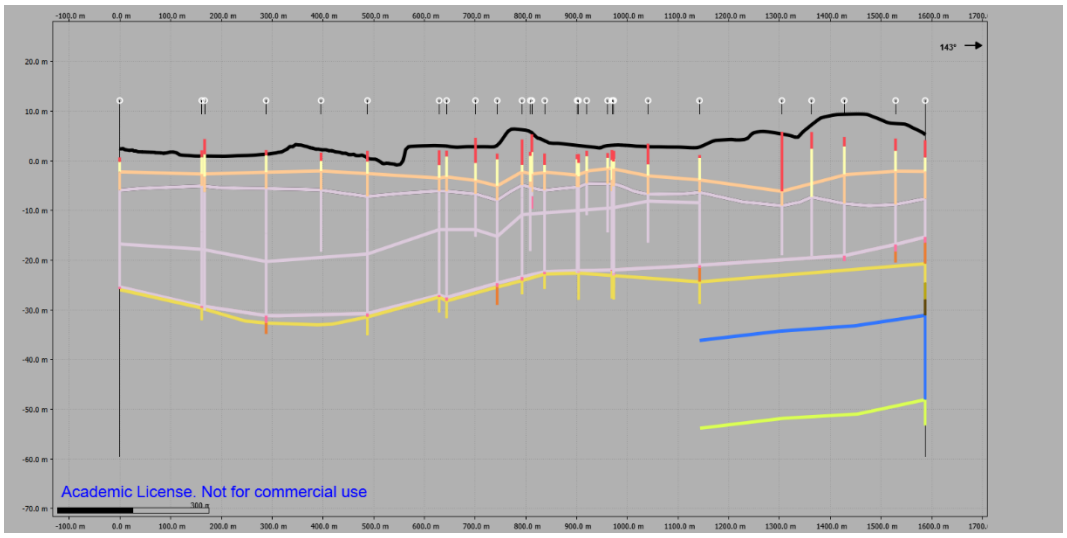

Figure B.42 – Section D_interior_3. Vertical exaggeration: x10.

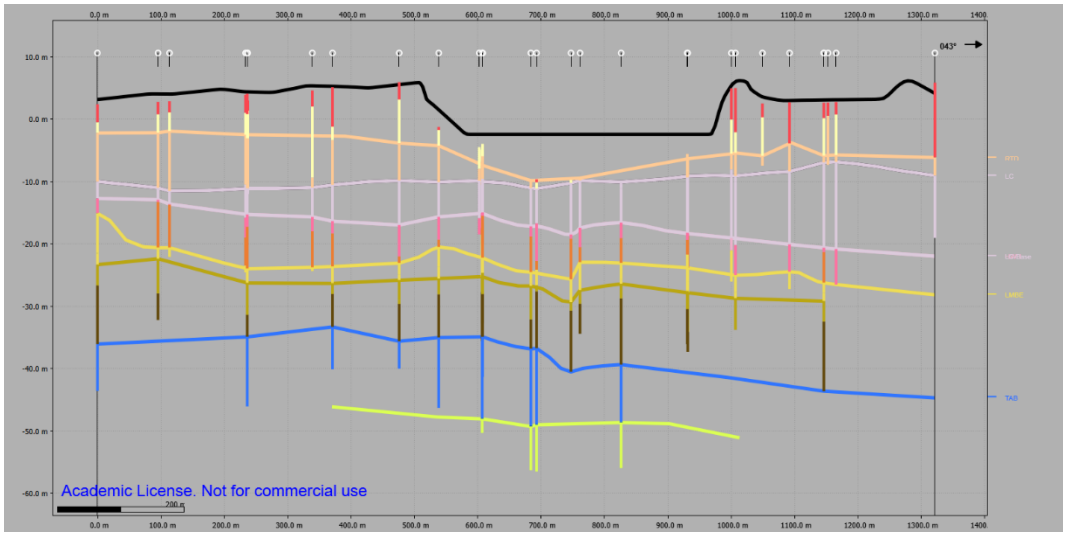

Figure B.43 – Section D_interior_4. Vertical exaggeration: x10.

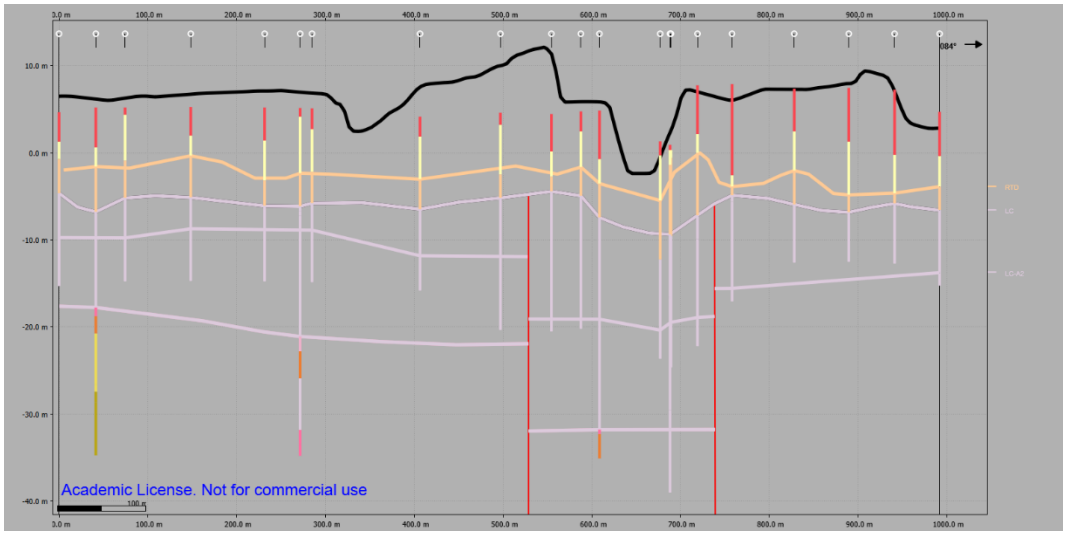

Figure B.44 – Section D_interior_5. Vertical exaggeration: x10.

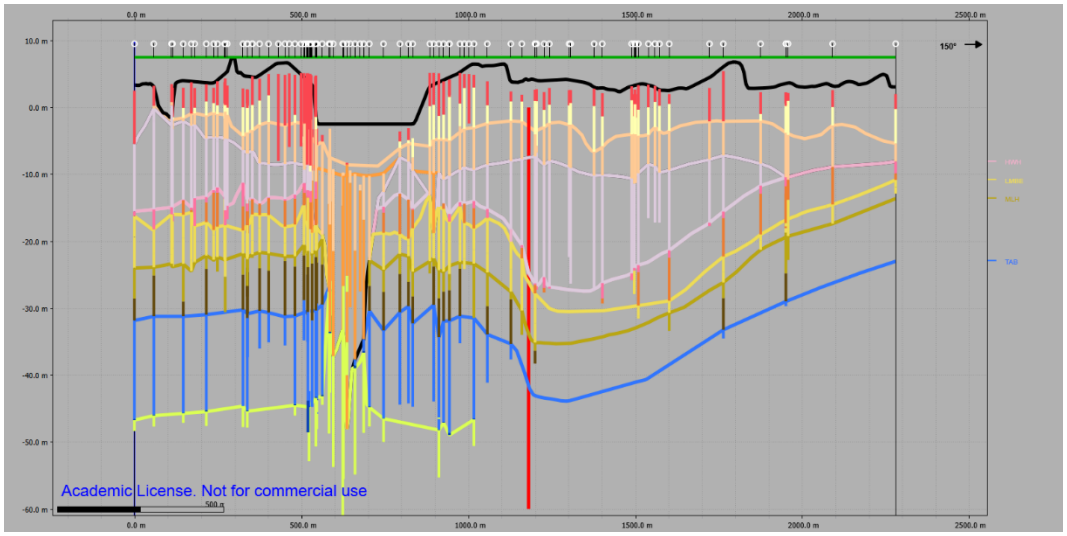

Figure B.45 – Section D_interior_6. Vertical exaggeration: x20.

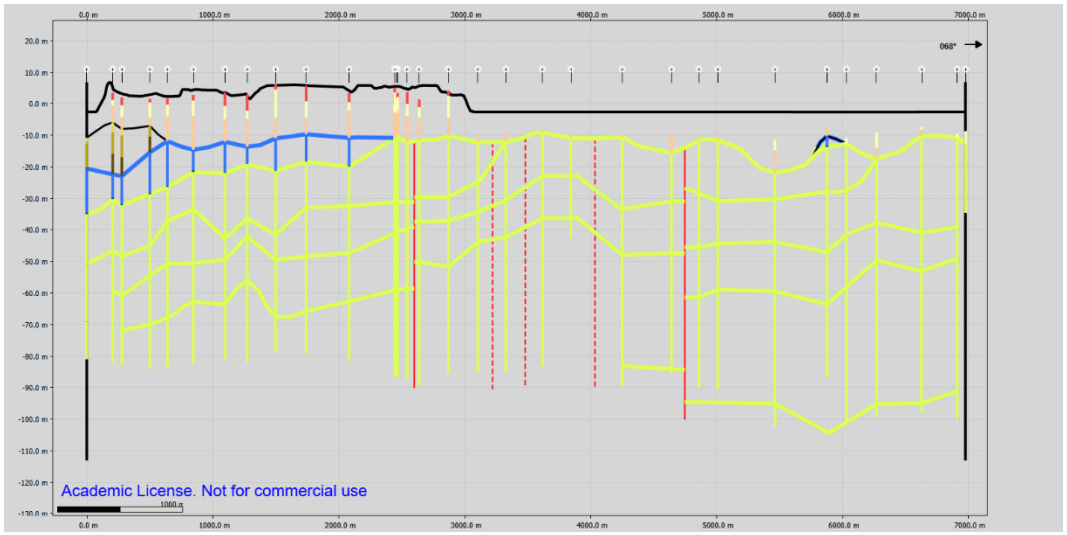

Figure B.46 – Section G_interior_1. Vertical exaggeration: x25.

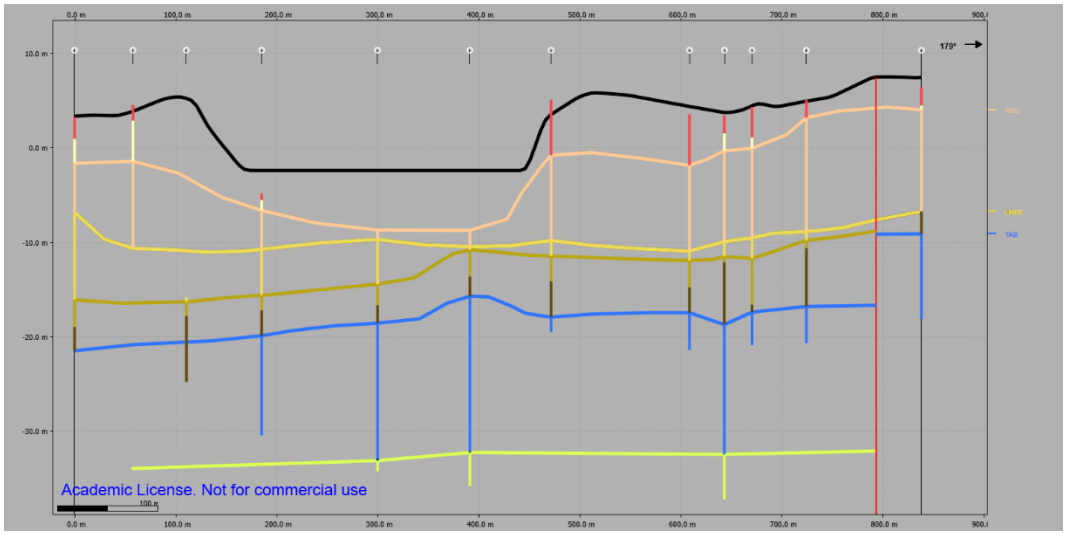

Figure B.47 – Section G_interior_2. Vertical exaggeration: x10.

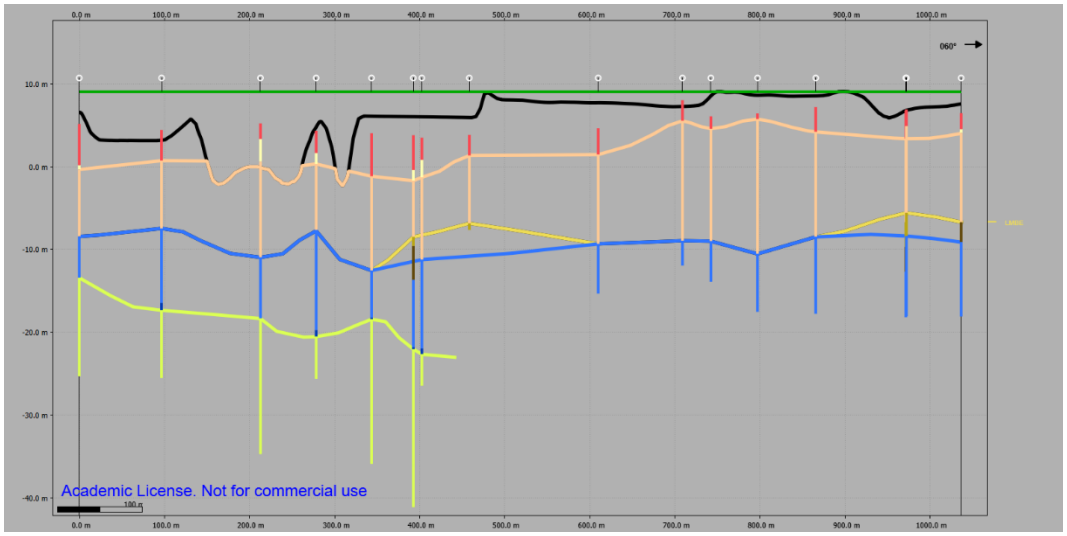

Figure B.48 – Section G_interior_3. Vertical exaggeration: x10.

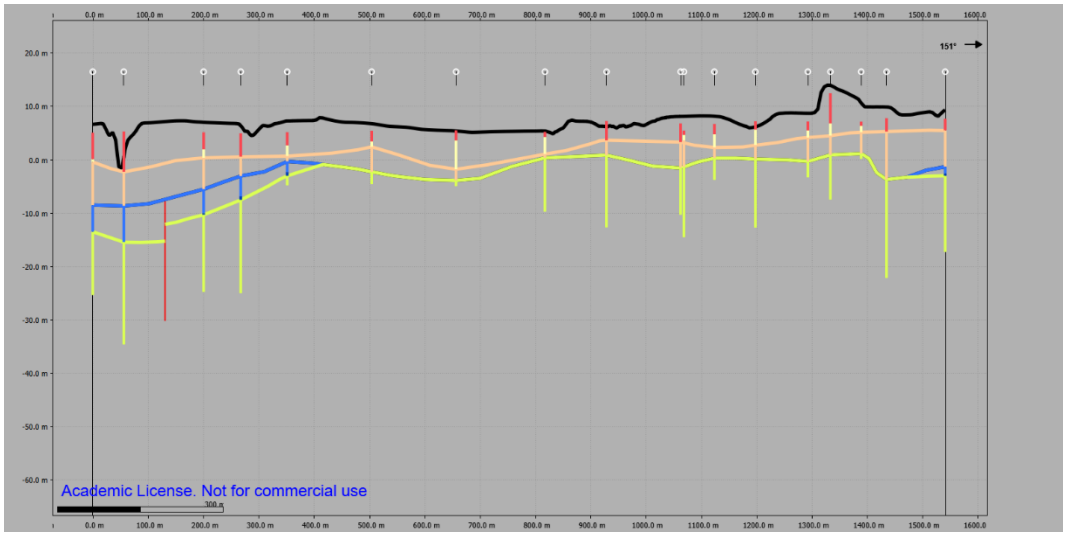

Figure B.49 – Section G_interior_4. Vertical exaggeration: x10.